Title

PROCEEDINGS OF THE INTERNATIONAL SYMPOSIUM ON COUPLED PROCESSES AFFECTING THE PERFORMANCE OF A NUCLEAR WASTE REPOSITORY, BERKELEY, CALIF., SEPT. 18-20, 1985.

Author

Tsang, C-F.

Publication Date

1985-09-01

Lawrence Berkeley Laboratory
UNIVERSITY OF CALIFORNIA

EARTH SCIENCES DIVISION

PROCEEDINGS OF THE INTERNATIONAL SYMPOSIUM ON COUPLED PROCESSES AFFECTING THE PERFORMANCE OF A NUCLEAR WASTE REPOSITORY

Berkeley, California, September 18-20, 1985

September 1985

Prepared for the U.S. Department of Energy under Contract DE-AC03-76SF00098

DISCLAIMER

LBL-21850

Proceedings of the International Symposium on Coupled Processes Affecting the Performance of a Nuclear Waste Repository

Berkeley, California
September 18-20, 1985

Program and Papers

Chin-Fu Tsang, Symposium Chairman

Earth Sciences Division
Lawrence Berkeley Laboratory
University of California
Berkeley, California 94720

Sponsored by

The U.S. Department of Energy
and
The U.S. Nuclear Regulatory Commission

In Cooperation with

The OECD Nuclear Energy Agency
and
The Commission of the European Communities

This work was supported by the Office of Nuclear Regulatory Research, U.S. Nuclear Regulatory Commission, and the Office of Civilian Radioactive Waste Management, U.S. Department of Energy, through U.S. Department of Energy Contract No. DE-AC03-76SF00098.

PROCEEDINGS OF THE INTERNATIONAL SYMPOSIUM ON COUPLED PROCESSES AFFECTING THE PERFORMANCE OF A NUCLEAR WASTE REPOSITORY

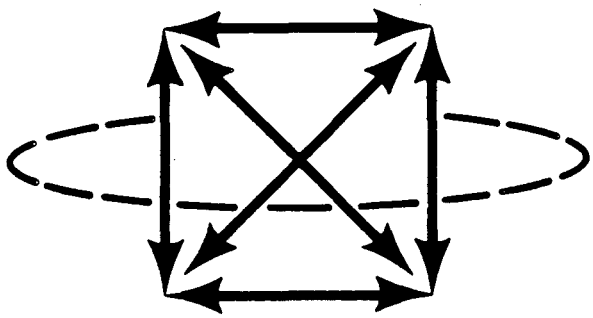

Lawrence Berkeley Laboratory
September 18–20, 1985

PROGRAM

Wednesday, September 18

6:00 pm	Symposium Banquet at Lawrence Hall of Science		
	G.T. Seaborg Lawrence Berkeley Laboratory	The New Elements	

Thursday, September 19

Coupled Thermomechanical-Hydrochemical Processes for a Nuclear Waste Repository

9:00 am	G. de Marsily Ecoles des Mines, Paris	An Overview of Coupled Processes with Emphasis in Geohydrology	68
	N.G.W. Cook U.C. Berkeley	Coupled Processes in Geomechanics	73
	D. Langmuir Colorado School of Mines	Overview of Coupled Processes with Emphasis in Geochemistry	—
12:00 noon	Lunch		
1:00 pm	Film: Progress of Stripa Project		
1:30 pm	**Review of Contributed Papers**		
	Rapporteurs:		
	K. Pruess Lawrence Berkeley Laboratory		
	B.R. Clark Leighton and Associates		
	C.L. Carnahan Lawrence Berkeley Laboratory		
3:30–5:00 pm	**Poster Session for All Contributed Papers**		

Friday, September 20

9:00 am **Discussion of Contributed Papers**

Discussion Leaders:

K. Pruess
Lawrence Berkeley Laboratory

B.R. Clark
Leighton and Associates

C.L. Carnahan
Lawrence Berkeley Laboratory

12:00 noon Lunch

1:00–5:00 pm **Panel Discussion on Coupled Processes for a Nuclear Waste Repository**
(including short presentations by the panel members)

Panel Members

C. Fairhurst
University of Minnesota
Minneapolis, Minnesota

R.O. Fournier
U.S. Geological Survey
Menlo Park, California

K. Kovari
Federal Institute of Technology
Zurich, Switzerland

I. Neretnieks
Royal Institute of Technology
Stockholm, Sweden

S.P. Neuman
University of Arizona
Tucson, Arizona

T.H. Pigford
University of California
Berkeley, California

P.A. Witherspoon
Lawrence Berkeley Laboratory
Berkeley, California

Chin-Fu Tsang, Moderator
Lawrence Berkeley Laboratory
Berkeley, California

5:00 pm C.-F. Tsang
Lawrence Berkeley Laboratory
Concluding Remarks

PROCEEDINGS OF THE INTERNATIONAL SYMPOSIUM ON COUPLED PROCESSES AFFECTING THE PERFORMANCE OF A NUCLEAR WASTE REPOSITORY

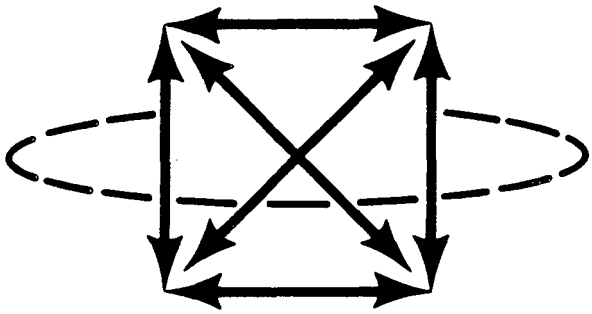

Lawrence Berkeley Laboratory
September 18–20, 1985

CONTRIBUTED PAPERS

GEOCHEMISTRY

COUPLED PROCESSES IN NRC HLW RESEARCH

Frank A. Costanzi
Office of Nuclear Regulatory Research
U.S. Nuclear Regulatory Commission

Ladies and Gentlemen:

I would like to add my welcome to that of Dr. Rosenblatt and to thank you for your interest in the area of coupled processes. My Branch in the NRC's Office of Nuclear Regulatory Research has the responsibility of managing the NRC research effort in support of evaluating license applications for disposal of nuclear waste, and promulgating regulations and issuing guidance documents on nuclear waste management. In order to do this we fund research activities at a number of laboratories, academic institutions, and commercial organizations. One of our research efforts is the coupled processes study here at Lawrence Berkeley Laboratory under Dr. Chin-Fu Tsang. We also participate in meetings such as the one we are attending today, as an effective method of assuring that a free interchange of information occurs among various scientific disciplines so that a sound technical basis is established for regulatory decisionmaking.

Before telling you why we are interested in coupled processes I would like to describe the areas toward which my group is directing our research efforts in the next few years. Our program is grouped under three general headings: Materials and Engineering, Hydrology and Geochemistry, and Compliance Assessment and Modeling. The specific research activities in each area relate to the performance objectives of NRC's HLW regulation and the EPA HLW standard. The general objective of our research program is to assure that the NRC has a sufficient independent technical base to make sound regulatory decisions. In other words, that we at NRC not only understand how a geologic repository is supposed to work, but that we understand the nature of the demonstration that it does work. I would appreciate any comments as to the utility of these research activities, and any suggestions for additional research and/or changes in emphasis.

MATERIALS AND ENGINEERING:

Our material and engineering program is focused on the waste package and its environment. The research is keyed to the containment and controlled release requirements of Part 60

Objective:

- Identify waste package failure mechanisms. Learn how to make confident extrapolations of short-term waste package tests to the 300-1000 year containment period required by Part 60. Develop techniques to assess the stability of waste emplacement areas in the evaluation of the engineered barrier system.

Activities:

- Identify corrosion properties of DOE candidate waste package materials, including: susceptibility to sensitization and stress corrosion, general corrosion, the initiation and growth of pits, and the statistics of pitting corrosion.

- Assess suitability of electrochemical predictive techniques for early detection of pitting corrosion.

- Assess the potential for hydrogen embrittlement of waste package materials.

- Identify and quantitatively assess the

effects of waste package manufacturing techniques on waste package performance.

- Characterize properties of spent fuel as a HLW waste form.

- Identify the key interactions of host rock and backfill materials with waste package and its expected environment.

- Evaluate the effectiveness of rock mass sealing techniques in basalt, salt, tuff, and granite.

HYDROLOGY AND GEOCHEMISTRY

The Hydrology and Geochemistry research is focused on the movement of radionuclides beyond waste package to the environment. The research is keyed to the controlled release requirement in Part 60 and the overall EPA HLW standard.

Objective:

- Identify and quantitatively describe (1) ground-water interactions with waste packages, (2) radionuclide transport and (3) uncertainties inherent in the quantitative description of the above.

Activities:

- Conduct field experiments to assess results of previous theoretical and laboratory research into groundwater flow in fractured media.

- Model multi-phase fluid flow and contaminant transport in unsaturated fractured media. Conduct field evaluations of measurement methods and data analysis techniques suitable for modeling flow and transport in unsaturated media.

- Assess the role of geochemistry in the thermally disturbed area near a repository, focusing on coupled interactions including those between the waste package and its environment.

- Assess the importance of valence state on radionuclide solubility, speciation, and sorption in basalt and tuff.

- Evalute the use of groundwater dating techniques for identifying hydrostratographic units.

COMPLIANCE ASSESSMENT AND MODELING

The Compliance Assessment and Modeling portion of our program is focused on the "mechanics" of technical licensing review. That is, these activities deal with the structure and formalism of the demonstration that the repository works. Hence, the research is keyed to the requirement of reasonable assurance of repository performance contained in Part 60.

Objective:

- Develop regulatory confidence in DOE's ability to demonstrate long term extrapolation of radionuclide transport and natural system stabilities. Develop regulatory confidence in the use of performance assessment techniques.

Activities:

- Conduct laboratory studies assessing heat transfer from emplaced HLW.

- Develop computational methods for evaluating DOE compliance with EPA release standards.

- Conduct natural analog studies to improve understanding of "normal" repository performance, and develop systematic approach to identify and study the most promising natural analog systems as means of validating performance assessment models.

- Develop a method to identify systems and components important to safety during the pre-closure phase of repository development.

ADDITIONAL AREAS:

Other areas are under active consideration for inclusion in our program at a later time.

- behavior of a repository under "off-normal" conditions
- formal validation of models
- study of natural analogs to validate predictions
- formal peer review of science used in developing the technical basis for repository licensing

As you can see, our research activities are broad and varied. However, there is a common element. Each research question demands some assumption about the conditions of the repository at some point in time. Our interest in coupled processes arises from the recognition that, in fact, none of this research truly can be undertaken in a vacuum. It is precisely the study of coupled processes and phenomena that not only enables us to assess whether we have made reasonable assumptions about repository conditions, but also provides the context for both performing the research and interpreting the results.

Our coupled processes work here at LBL is directed at identifying and characterizing the significance of coupled processes for HLW isolation, assessing the current state of knowledge of coupled processes, and considering how to address coupled processes in the license review. We regard this bringing together of U.S. workers and workers from other countries on coupled processes to discuss recent results of field, laboratory, and theoretical studies as an opportunity to complement that work. What we would like to gain from this symposium is further insight into how coupled processes and phenomena evolve over time, as evidenced from the field and laboratory tests, natural analogue studies, and the mathematical modeling studies which have been done by participants in this symposium. Also, we would like to get some idea of the state of verification or validation of the work presented.

Over the next three days, we of the NRC would like you to help us reach a goal of putting the various coupled processes into some sort of time/sensitivity context. Specifically, we seek to answer following questions. When in the evolution of the repository system is the phenomenon or process under consideration important? Which of the processes or phenomena is relatively unimportant to repository performance and can thus be studied less intensively? Which of the important processes brings with it the greatest uncertainties?

Again, I welcome the participation of each of you at this symposium.

IMPLEMENTATION OF THE NUCLEAR WASTE POLICY ACT OF 1982

Cyrus Klingsberg

Office of Civilian Radioactive Waste Management
U.S. Department of Energy
Washington, D.C. 20585

A major milestone in the nation's management of nuclear waste was met when the President signed the Nuclear Waste Policy Act (NWPA) into law on January 7, 1983. The NWPA established a national policy for safely storing, transporting, and disposing of spent nuclear fuel and high-level waste. Under the Act, the U.S. Department of Energy (DOE) has the primary responsibility to:

- Perform research and development, and demonstrate the disposal of spent fuel and high-level waste;
- Design, schedule, site, construct, and operate deep-mined geologic waste repositories.

The NWPA authorizes a number of activities which, taken together, can meet the objectives of providing safe and permanent disposal of spent fuel and high-level waste:

1. Protection of public health and safety, along with environmental acceptability;
2. Acceptance of waste for disposal starting not later than January 31, 1998;
3. Safe transportation of waste to the repository;
4. Provisions for limited interim storage of spent fuel for utilities, as approved by the Nuclear Regulatory Commission (NRC);
5. Examination of existing storage by nuclear utilities to assure that facilities are used effectively at reactor sites until the waste is accepted for disposal;
6. Involvement of the States and Indian tribes, and full and open public participation;
7. Full cost recovery, with costs borne equitably by the waste generators.

In December 1984, DOE issued its General Guidelines for the Recommendation of Sites for Nuclear Waste Repositories. These guidelines are compatible with regulations issued by the NRC (and have NRC concurrence) and with standards established by the U.S. Environmental Protection Agency (EPA).

In June 1985, a second important policy document required by the NWPA, the Mission Plan for the Civilian Radioactive Waste Management Program, was submitted to Congress. The two parts of this plan discuss the goals, objectives, and strategy for disposing of spent fuel and high-level waste and summarize other aspects of the waste management program: monitored retrievable storage, Federal interim storage, transportation, and systems integration activities and institutional plans and activities. In its second section the plan discusses key issues and information needs and plans for building a nuclear waste repository. The document also summarizes information on site investigation and characterization, the nuclear waste package, a possible test and evaluation facility, schedules, and costs.

Studies for isolating high-level radioactive wastes have been going on since 1957 when the National Academy of Sciences first recommended deep geologic disposal. When the NWPA was passed, DOE had underway field and laboratory testing at nine sites: one in Louisiana, two in Mississippi, one in Nevada, two in Texas, two in Utah, and one in Washington.

Based on its General Siting Guidelines and on Draft Environmental Assessments required by the NWPA, DOE proposed three of the nine potentially acceptable sites for recommendation to the President for possible site characterization. In addition to environmental and socioeconomic studies, the detailed site characterization process will involve constructing exploratory shafts between 1,000 and 3,500 feet deep to determine potential host rock conditions at the proposed repository level. It is expected that the site for the first repository will be recommended by DOE and approved by the President in 1991, based on the results of site characterization. DOE will ask the NRC for authorization to construct a repository at that site, and for authorization to operate the repository beginning in 1998.

The method for selecting the second repository site will follow the screening process that was developed for the first repository. The second repository is scheduled to begin operation in 2006.

A nuclear waste repository will resemble a relatively large mine with surface facilities that will cover about 400 acres. Vertical shafts will descend thousands of feet from the surface. Here, in a stable rock formation, a network of horizontal tunnels will be constructed for emplacing the waste. The waste will be in solid form in thick-walled cylindrical containers which will be placed in prepared holes.

Before the DOE can apply to the NRC for a license to operate its first radioactive waste repository, it will be necessary to characterize the recommended site in considerable detail and with sufficient accuracy and precision to justify the issuance of a license to operate the repository.

Because of this need to characterize a repository site adequately, the DOE continues its efforts to improve its understanding of the kinds of tests that will best serve that purpose.

This brings us to the subject at hand today. The DOE has not, at the present time, established a position with respect to coupled testing. However, in furthering the development of its site characterization program, the DOE and its field projects, three of which are represented in this symposium, welcome you, and look forward to benefiting from the deliberations of this Symposium.

OPENING PRESENTATION BY THE OECD NUCLEAR ENERGY AGENCY TO THE INTERNATIONAL SYMPOSIUM ON COUPLED PROCESSES AFFECTING THE PERFORMANCE OF A NUCLEAR WASTE REPOSITORY

S.G. Carlyle, OECD/NEA

The OECD Nuclear Energy Agency is particularly pleased to be able to cooperate with the sponsors of this Symposium on Coupled Processes, as the subject is complementary to several recent activities of the NEA; in particular those of the Co-ordinating Group on Geological Disposal and the International Information Retrieval System (ISIRS) group. The Co-ordinating group was established in 1975 by the Radioactive Waste Management Committee to, as the name suggests, help coordinate research and advise the RWMC. The coordination covers three main activities: (i) the consideration of progress of NEA projects that fall under the heading of geological disposal; (ii) organising workshops to address topical issues; and (iii) provision of a forum for the exchange of scientific information arising from national research programmes in OECD Member countries.

The scope of these activities cover two general headings: (a) the development of performance assessment methodologies and (b) the acquisition of field and laboratory data. The recently established User's Group for Systems Variability Analysis Codes provides an international forum for those actively developing probabilistic codes to:

(a) exchange codes, information and experience;

(b) provide for mutual peer review;

(c) discuss topical technical issues; and

(d) identify aspects of code development and plan intercomparisons of mutual benefit.

The NEA is also taking an increasingly active role in the Swedish HYDROCOIN exercise, which addresses the modelling of groundwater flow mainly by comparing the capabilities of different models to describe field measurements and the impact on groundwater flow calculations of various physical phenomena.

In addition, the NEA Data Bank is building-up a library of various waste management codes, used in carrying out performance assessments to provide a service to OECD Member countries. Here tested and documented codes are available on request.

The NEA Data Bank is also involved in the International Sorption Information Retrieval System (ISIRS). This data base system, originally developed by PNL, stores and handles data related to the sorption of radioelements from solution onto geologic media. The objective of the project is to advance the understanding and prediction of the migration of radionuclides through geological media in support of performance assessments for radioactive waste disposal. In addition, a similar data base of chemical thermodynamic data is currently being developed by the NEA to provide comprehensive, internally consistent, CODATA compatible data for use in predictive mathematical models.

The NEA is also involved in the acquisition of field and laboratory data aimed at acquiring a detailed understanding of geological disposal systems. Currently, this focuses on the International Stripa Project which will be discussed later in the Symposium.

Perhaps the most important activities of the NEA in relation to this Symposium are the findings of several recent workshops held by NEA on geological disposal; with particular emphasis being placed on near field and geosphere studies. I can mention several of direct relevance to this Symposium:

In 1981:

Near Field Phenomena in Geological Repositories for Radioactive Wastes, Seattle

In 1982:

Geochemical Processes and the Geological Disposal of Radioactive Waste, Paris

In 1983:

Sorption - Modelling and Measurement for Nuclear Waste Disposal Studies, Paris

Source Term for Radionuclide Migration from High-Level Waste or Spent Nuclear Fuel Under Realistic Repository Conditions, Albuquerque

In 1985:

Effects of Natural Organic Compounds and Microorganisms on Radionuclide Transport, Paris

Symposium on In Situ Experiments in Granite, Stockholm.

The proceedings from each of these workshops reveal certain insights into the treatment of coupled processes but perhaps the most directly relevant to this Symposium are the conclusions of the Workshop on Coupling Geochemical and Hydrologic Models held in Paris in June 1984. These inter-alia declared that:

(1) There is a definite need for some coupling between geochemical and hydrologic models in radioactive waste performance assessment. This need arises from the inherently coupled nature of radionuclide migration. There is no, and there need not be, a unique method to perform this coupling;

(2) Coupling in this context is not limited to mean exclusively the co-execution of geochemical and hydrologic computer codes, but it intended to encompass all methods of passing data and merging geochemical and hydrologic understanding in performance assessment modelling;

(3) The development of "megacodes" (i.e., large directly coupled hydrochemical-geologic computer codes) is practically unrealistic. Indirect coupling methods and the coupling of limited submodels should provide useful tools for helping to answer a number of specific questions. Since comprehensive megacodes are impractical, an understanding of where simplifications can be made is desirable;

(4) Coupled models are only one among a wide variety which may be used to predict potential radionuclide migration. These simplified coupled models must be used in conjunction with larger thermodynamically-based codes with laboratory work and with observation of nature;

(5) Basic to the use of any of these predictive techniques is the detailed understanding of the physical and chemical processes involved. This understanding must be developed in order to maximize confidence in the predictions.

The use of coupled models developed in this perspective was found to be an important contribution to assure that the major interactions in water and nuclide transport are considered in disposal system performance analyses.

It is clear that at the present time, coupled processes are one of the principal issues in the development of realistic performance assessment methodologies and in developing confidence in proposed disposal solutions. I am sure that this Symposium will make a major contribution to resolving this issue. Finally, I would like to thank you on behalf of NEA for this opportunity to address the Symposium.

OUTLINE OF SOME EUROPEAN COMMUNITY ACTIVITIES ON COUPLED PROCESSES

P. F. Venet
COMMISSION OF THE EUROPEAN COMMUNITIES
Rue de la Loi 200, B-1049 Bruxelles

In these few words of introduction, I would like to give you an outline of some of the European Community activities in the field of coupled processes linked with radioactive waste geological disposal. This is an example, a succesful one I think, of what can be realised at international level.

We have greatly appreciated the work realised during the first panel which was organised in Berkeley in January 1984 on coupled processes. Taking into account the importance we attach to this question and added to the fact that these problems are so comprehensive that they cannot be efficiently dealt with in a strictly national framework, we took pleasure in accepting the co-sponsorship of the symposium which opens today.

Some people may need a very short presentation about the European Community. At the moment, ten countries of the old Europe belong to it : from Denmark to Italy and from Ireland to Greece, including the Federal Republic of Germany, Belgium, the Netherlands, France and the United Kingdom. Two more countries, Spain and Portugal, will join us on the 1st of January next year. By signing the European Treaties, the European Community countries recognised that certain fields, such as agricultural policies, commercial relations or the Energy sector could be treated more efficiently by pooling their resources.

About ten years ago, the Commission started up important research programmes in the field of management and storage of radioactive waste. It can be said that at present, most of the work realised by the Community countries on high-level waste and its disposal is done within the Community programmes. This work is either led by organisations and firms of these countries in the framework of contracts co-financed by the Commission, or realised in the Commission laboratories, the most well-known being the Joint Research Centre at Ispra in North Italy.

The propagation of heat in the waste environment initiates a certain number of interactive disturbances. All these phenomena overlap. The problem of coupled processes is inevitably dealt with in-depth in the Community programme, taking into account its actual nature.

The following three slides show some work aiming at recognising and modelling the coupled processes. The processes have been regrouped in the main geological media at present considered in Europe, namely, salt, granite and clay. In fact, the properties of these media are very different from each other and the borderline between the processes is often imprecise. For this presentation, I have retained four types of coupled processes : thermo-mechanic, thermo-hydraulic, hydraulic-mass transfer and finally, thermo-geochemical and mineralogical. The studies have been classed accordingly as realised at laboratory scale or in situ or as they concern simulation by calculation.

The first slide concerns salt rocks. I will only specify what is realised by Utrecht University in the Netherlands. It concerns a little known aspect for the scientists but nevertheless a crucial one. In this study, the influence of brine on the creep behaviour of salt is being investigated. Samples of salt were creep-tested under uniaxial compression at various stress levels. During testing, saturated brine was poured around the samples. It could be seen that the adjunction of brine resulted in a clear increase of creep rate : the higher the stresses, the stronger the influence. A comparative test was made by adding volatile oil, which did not cause any increase in creep rate. It could be concluded that there is a marked interaction between the presence of brine in salt and its creep rate under compression.

The second slide is devoted to clay. We were surprised that clay, as a geological formation to be considered for disposal, did not appear in the report established by the Lawrence Berkeley Laboratory following the first panel. A certain number of European countries are however interested in this, for example, Belgium, Italy and more recently the United Kingdom and France.The example selected is a little anecdotal. It concerns the study of a thermo-chemical process, studied on a large scale and in-situ. This study was undertaken by ENEA in Italy. A magmatic body intruded a pliocenic clay layer at ORCIATICO, Italy, about 2 million years ago. The size of the intrusion was several hundred meters in diameter and its maximum temperature was estimated at 800°C.

At the interface, the clay was turned into hard stone. The investigations showed that the effect of dehydration in clay appeared at a distance of 10 to 20 metres from the interface. However, mineralogical changes could be found only up to 2 to 4 metres away from the interface.

The last slide concerns granite. The example considered corresponds to a new approach as regards the safety aspects. It concerns a computer code simulating a hydromechanical process. In the framework of the "geo-prospective" methodology, the BRGM in France has developed a computer code, CASTOR, which allows the interaction of geological factors to be predicted on a specified site. An

initial application of this code was carried out in a generic way on a granite site, assuming that an ice cap, 1000 m thick, would develop in 2000 years and last about 100.000 years. The coupled influence of sea-level change and ice weight on the ground water flow patterns was calculated. It could be seen that these factors resulted in a 50 times reduction of the groundwater flow velocity at the location of a hypothetical repository. Such effects therefore need to be considered for predictive evolution scenarios.

At the end of these introductory remarks, I would like to wish you, Mr. Chairman, Ladies and Gentlemen, in the name of the Commission of the European Communities, most fruitful discussions and exchange of views during these next three days. Such a symposium can only strengthen international co-operation which is so necessary in these fields.

The European Community

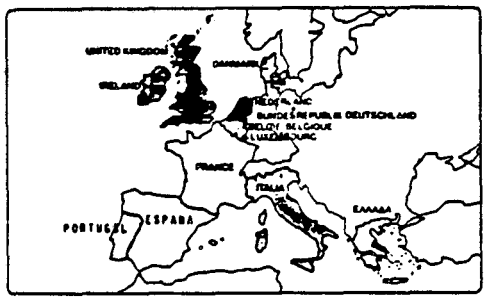

COUPLED PROCESSES IN CLAY (CEC-PROGRAM)

COMMISSION
EUROPEAN COMMUNITIES

PROCESSES	THERMO-MECHANICAL	THERMO-HYDRAULIC	HYDRAULIC-MASS TRANSFER	THERMO-CHEMICAL
LABORATORY TESTS	INFLUENCE OF FREEZING AND HEATING ON STRENGTH OF CLAY (CEN/SCK)		INTEGRAL MIGRATION EXPERIMENTS IN SAND COLUMNS (CEA, JRC-ISPRA)	
IN-SITU TESTS	INFLUENCE OF FREEZING ON CLAY BEHAVIOUR AT MOL (CEN/SCK, FORAKY)	HEATING TESTS AT : - MONTEROTONDO (ENEA) - TERNAGEN (CEN/SCK)	TRACER TEST AT DRIGG (BGS) NATURAL MIGRATION ANALOGUES AT LOCH LOMOND (BGS)	STUDY OF NATURAL VOLCANIC INTRUSION IN CLAY AT ORCIATICO (ENEA)
COMPUTER CODES	TRAITEME (ISMES)	MAPPU FOR CONVECTIVE FLOW (UKAEA)	METROPOL (RIVM)	WHATIF (RISØ NAT. LAB.)

COUPLED PROCESSES IN SALT (CEC-PROGRAM)

COMMISSION
EUROPEAN COMMUNITIES

PROCESSES	THERMO-MECHANICAL	THERMO-HYDRAULIC-MECHANICAL	HYDRAULIC-MASS TRANSFER	THERMO-GEOCHEMICAL AND MINERALOGICAL
LABORATORY TESTS	CREEP TESTS AT ELEVATED TEMPERATURES (GSF, BGR)	INFLUENCE OF BRINE ON SALT CREEP (UNIV. UTRECHT)	BRINE SEGREGATION AND PRECIPITATION OF MINERALS (GSF) COLUMN INTEGRAL EXPERIMENTS (F.U. BERLIN)	INFLUENCE OF HEAT ON THE MINERALOGY OF SALT (GSF)
IN-SITU TESTS	HEATING TESTS NR. n. 5, 6 AT ASSE (GSF) SALT CONVERGENCE IN THE 300 METER BOREHOLE AT ASSE (CEN)	FLUID LIBERATION IN HEATED SALT AT ASSE (GSF)	FLOODING OF GALLERIES AT ASSE (GSF)	RESEARCH ON CONTACTS BETWEEN SALT AND VOLCANIC INTRUSION (GSF)
COMPUTER CODES	CALCULATION CODES (GSF, ECN, KFK RWTH AACHEN) INTERCOMPARISON EXERCICE COSA	FLUID AND GAS MOVEMENTS INCLUDED IN SALT (RWTH AACHEN)	INFLUENCE OF BRINE DENSITY ON FLOW IN AQUIFERS (RIVM)	

COUPLED PROCESSES IN GRANITE (CEC-PROGRAM)

COMMISSION
EUROPEAN COMMUNITIES

PROCESSES	THERMO-HYDRO MECHANICAL	THERMO-HYDRAULIC	HYDRAULIC-MASS TRANSFER	THERMO-CHEMICAL
LABORATORY TESTS	TESTS ON GRANITE SAMPLES AT HIGH TEMPERATURE (CEA)	VARIATION OF FISSURES PERMEABILITY IN HEATED SAMPLES (ENP)	COLUMN INTEGRAL EXPERIMENTS (CEA, JRC-ISPRA)	DISSOLUTION-REPRECIPITATION OF SILICA IN FRACTURES (BRGM)
IN-SITU TESTS	HEATING EXPERIMENTS AT FANAY-AUGERES (CEA, BRGM)	HEATING EXPERIMENTS AT TROON (UKAEA)	"SCALE EFFECT" AT FANAY-AUGERES (CEA) FRACTURE TEST AT TROON (UKAEA)	STUDIES ON NATURAL HYDROTHERMAL PHENOMENA (BRGM)
COMPUTER CODES	CASTOR GEOPROSPECTIVE CODE APPLIED TO GLACIATION (BRGM)	METIS (CEA, ENP)	COUPLING OF FLOW AND GEOCHEMICAL CODES (BGS, ENP)	CODE ON DISSOLUTION-REPRECIPITATION OF SILICA IN FRACTURES (ENP)

BASALT WASTE ISOLATION PROJECT OVERVIEW

David H. Dahlem
Basalt Waste Isolation Division
U. S. Department of Energy
P. O. Box 550
Richland, WA 99352

INTRODUCTION

The proposed candidate basalt site for a high level nuclear waste repository is located beneath the Hanford Nuclear Reservation in southeastern Washington State (Figure 1). At this point, the Hanford Reservation has been selected as one of three preferred candidates in the draft Environmental Assessment. Project activities have concentrated on (1) understanding the site location with respect to the 10CFR60, 40CFR191, and 10CFR960, (2) identifying critical parameters for design of waste package and repository seals, and (3) identifying parameters for repository design. This paper describes the program to evaluate the site and identify the natural processes that would effect isolation.

The viability of the reference repository location (RRL) depends on findings in several important areas; (1) the groundwater circulation system, (2) the nature and complexity of the basalt horizons and inhomogeneities, and (3) the structural stability of the repository environment relating to vulcanism and seismicity. Other issues are subordinate.

The Repository Site program has two major testing and data collecting phases: (1) an early reconnaissance activity to locate a site and to assess site suitability, and (2) site characterization to evaluate performance uncertainties. The emphasis in all studies is on identifying system baseline conditions and processes of change. Data collection originally started with surface-based exploration and will continue in in situ measurements in subsurface facilities such as the exploratory shaft facility and in special boreholes to confirm surface work and to collect unique data.

Geologic Program Status

The following sections present the current understanding of the geologic and geophysical properties of the basalt site. Areas that significantly influence the testing program (described in a later section) are highlighted.

Geomorphology

The Hanford site is located within the Columbia Plateau geologic province between the Yakima Fold Belt to the west, the Blue Mountains to the south, and the Palouse. It is at the point where ridges of the Yakima Fold Belt dip east beneath the west dipping Palouse Slope.

The principal geomorphic processes affecting the area during Quaternary time were degradation of bedrock ridges and scouring associated with late Pleistocene cataclysmic floods, and sedimentation associated with wind and water redistribution of glacial outwash of the above materials. The most recent flood was about 13,000 yrs B.P., associated with the last ice advance.

On the basis of paleoclimatic information, only two ice advances are expected in the next 100,000 years; beginning at 15,000 and 35,000 years.

Stratigraphy and Lithology

The Reference Repository area is underlain by three rock sequences (Figure 2): the basalt group is pre-Tertiary epiclastic sedimentary rocks from 6,000 to 18,000 feet thick. This, in turn, is overlain by the Columbia Basalt Group, from 10,000 to 16,000 feet, and by about 500 feet of post basalt sediments.

In the RRL area, the Yakima Subgroup of the Columbia Basalt group is divided into the Grande Ronde, overlain by the Wanapum, and in turn by the Saddle Mountain flow sequences. Within the Grande Ronde sequence, the Cohassett flow is the current reference horizon.

The Cohassett flow is mid-way in the Sentinel Bluffs sequence. From systematic studies of the Cohassett flow, internal or intraflow structural features have been defined allowing a modicum of prediction of mechanical characteristics. Intraflow structural domains differ in strength and mechanical properties, and therefore are of interest in assessment. Fracture (or joint) density has been evaluated for the candidate flows with the Cohassett the most intact, least fractured flow of those studied.

The Grande Ronde, Wanapum, and Saddle Mountains sequences are each separated by sedimentary interbeds of the Ellensburg Formation. The lowest of the interbeds is the Vantage, separating the Grande Ronde and Wanapum basalts. From this point upward in the basalt

section, volcaniclastic sedimentary interbeds become an important part of the geohydrologic control. The Mabton interbed is the thickest unit separating the Wanapum from overlying Saddle Mountains basalts, but each flow in the latter two sequences is overlain by an interbed.

The principal uncertainties in the stratigraphy and megascopic lithology are focused on the need to identify and characterize individual flows and to predict variations. Elements in this area consist of flow thickness, intraflow structures, fractures, and textural discontinuities such as zones of vesiculation and brecciation.

Structural Geology and Tectonics

The structural geology of the RRL area is characterized by compressional features comprised of sharp east-west trending anticlines and shallow intervening synclinal valleys. In general the anticlines are asymmetrical and overturned on the north limbs. Second and third-order folds are common on first-order anticlines.

Thrust and high-angle reverse faults are common along the steeper limb of anticlines. Estimated displacements range from several meters to 2.5 km such as along the Saddle Mountains fault at Sentinel Gap. Fault dips vary from 45° to vertical. Northeast- to Northwest-trending cross faults with up to several tens of meters dip-slip and postulated strike-slip displacement transect the anticlined folds. In addition, fold trends commonly display abrupt bends along strike.

Several large-scale features provide the regional structural framework. The Olympic-Wallowa lineament (OWL) and Hog Ranch-Naneum Ridge anticline trend into the Columbia Plateau and transect the Yakima Fold belt. The OWL is 400 km long topographic lineament extending from the Olympic Mountains in northwestern Washington to the Wallowa Mountains of northeastern Oregon. The Cle Elum-Wallula lineament (CLEW) is the central third of the OWL feature, in which area occur northwest-trending faults. In the Pasco Basin, the CLEW is the series of features including Rattlesnake Mountain, and several doubley-plunging anticlines to the southeast. This local feature is referred to as the Rattlesnake-Wallula lineament (RAW). East of Wallula Gap the CLEW is defined by west northwest trending faults of the Wallula fault system.

Evidence for possible Quaternary faulting within the Yakima Fold Belt occurs 75 km west of the site at Toppenish Ridge. Five hundred year old sag ponds at that location are similar to features on Gable Mountain.

The Pasco Basin, in which the site is located, is one of four structural and topographic basins in the Yakima Fold Belt. It is defined on the north by the Saddle Mountains and on the south by the RAW structure. The Hog Ranch structure and Palouse Slope are the western and eastern boundaries. The main trends within the basin are easterly to southeasterly from northwest to southeast. Structural and topographic relief lessens to the southeast, with several of the Yakima folds receding into the subsurface.

Four anticlinal structures define the immediate structural environment of the site: the Saddle Mountains, Umtanum-Gable Mountain, Yakima Ridge and Rattlesnake Mountain, and anticlines along the RAW to the southeast. The intervening synclines are the Pasco Basin on the east, Wahluke syncline, Cold Creek syncline, and Benson Ranch syncline from north to south.

The Cold Creek syncline is a broad southeasterly plunging fold with a relatively steep southern limb toward Yakima Ridge. The structure is interpreted to have been a thick basalt section controlled north and south by anticlinal ridges.

Structural analysis indicates that tectonic forces have been accomodated by folding and closely parallel faulting above the northern limbs of anticlines. These features consist of steep reverse faults and pronounced brecciation parallel to fold axes. Rate of deformation has been assessed from the thinning of flows over ridges and current leveling and trilateration surveys.

The eruption of tholeiitic flood basalts from 7 to 8.5 m yrs B.P. is the most significant volcanic event to effect the Pasco Basin. Feeder dikes for these eruptions have been iden-

tified on the eastern basin margin. The only volcanic events subsequent to these are from the Cascade Range, west of the site.

The principal uncertainties in the area of structural geology center around the nature, mechanism, and timing of tectonic deformation effecting long term stability of the site and effect on groundwater circulation in the Pasco Basin.

Seismology

The Columbia Plateau is an area of moderate seismicity based on the historical record. The seismicity of the RRL is low as compared with that of the Columbia Plateau. The seismicity can be grouped into two types of events: deep events and shallow swarms.

The earthquake swarm is the predominant activity of the site area. Swarms typically occur over periods of a few days to several months, are constrained to a rock volume typically 2 km X 5 km X 3-5 km deep, and may contain several hundred earthquakes from magnitude 1.0 to 3.5.

Centers of swarm activity have been recorded near the site at Wooded Island, Coyote Rapids, and northeast of the site between the Saddle Mountain and Frenchman Hills anticlines. The evolution of these events indicates no specific probable structural relation.

The principal uncertainties on the site seismicity include the nature of the mechanism and potential ground motion related to swarm events and the nature of surface wave transmission within the area to the repository rock volume.

Engineering Geology

The engineering properties of concern are those that bear directly on the excavation characteristics of the basalt. The data now available have come from the analysis of outcrops, borehole cores, and in situ measurements from the Near Surface Test Facility (NSTF) constructed in Gable Mountain, northeast of the RRL. A central concern in the data collection effort has been understanding and predicting the in situ response of the rock mass to changes imposed by excavation and from thermal simulations of waste loading.

Intact basalt from the flow interiors is hard, brittle rock that is insensitive to temperature change at 150-200°C and has little definable mechanical change up to 500°C. The intact basalt shows a significant increase in strength with confining stress. Uniaxial comprehensive strength differs between Grande Ronde flows, with typical values for the Cohassett interior and flow top breccias of 290 MPa (42,000 psi) and 1,000 MPa (15,000 psi), respectively.

Jointing is common in the flows and is typically characterized as tight with pervasive filling by secondary minerals. Testing of jointed samples under triaxial loading and direct shear indicates the secondary minerals do not dominate the joint properties. Joint friction angles measured in the NSTF were 35° for the Pomona flow. A value of 42° was obtained for Grande Ronde basalt. Normal and shear stiffness tests on core from the NSTF indicate relatively high stiffness reflecting the competent nature of the joint surfaces and thin joint fillings.

Under low stress conditions, the joint frequency is sufficiently high to significantly influence the rock mass modulus and rock mass strength. Under high stress conditions at the repository depth, joints are expected to be tighter and have less effect on rock mass modulus.

No reliable data on deformation moduli are available at this time.

Thermal properties at the repository horizon probably can be estimated with sufficient accuracy from laboratory tests. This is based on the agreement between lab and NSTF measurements. Thermal properties are expected to be influenced by rock porosity and moisture conditions. Jointing does not appear to have a pronounced effect on thermal or thermomechanical properties and no thermal anisotropy was observed in current testing.

Stress measurements by hydraulic fracturing in three holes within the reference repository location in all four potential repository hori-

zons have produced a consistent pattern of in situ stresses that are oriented with the maximum stress essentially north-south and the minimum stress vertical. The maximum horizontal stress does not show any significant increase with depth within the flows or between the four flows tested. The maximum horizontal stress is estimated to be 61.5 MPa (8,900 psi) in the Cohassett flow. In the Cohassett flow, the intermediate horizontal stress is 32.4 MPa (4,700 lb/in^2) with a minimum (vertical) stress of 24.1 MPa (3,500 lb/in^2). These stress levels are high and are compatible with the observed borehole spalling, core disking, and seismic activity in the area.

Rock spalling and small rock bursts can be anticipated given the stress field and brittle nature of basalt, however, the jointed nature of basalt may mitigate the spalling potential by relieving the high stress concentrations around openings.

Geohydrology

Since 1977, reconnaissance hydrologic studies have been conducted in and around the Cold Creek syncline to identify stratigraphic intervals of high and low hydraulic conductivity, areal and stratigraphic hydraulic head distributions, geochemical trends and the influence of geologic structures on circulation patterns. In this program, testing has become progressively sophisticated as new facilities have been constructed. To date, the emphasis has centered on understanding the circulation systems, which in turn requires hydraulic stress testing of discrete horizons. A reference piezometric baseline for this testing is an integral part of the program.

Preliminary studies indicate that basalt flow-brecciated tops and interflow sedimentary units have higher hydraulic conductivity than flow interiors. For flow tops and interbeds, conductivity ranges from 10^{-12} to 10^{-1} m/s with a geometric mean of 7 X 10^{-6} m/s. For the flow interiors, the range is 10^{-15} to 10^{-8} with a geometric mean of 1 X 10^{-12} m/s. The hydraulic conductivity of interflow zones differs between basalt sequences and generally decreases with depth. Hydraulic gradient for the Grande Ronde has been estimated to be 2X10^{-4} m/m with direction of flow within the RRL toward the south-southwest. The direction of regional flow appears to be southeast. The local influence of synclinal structural dip is presumed to be the reason for the discrepancy. Vertical hydraulic gradient in the Grande Ronde appears to be upward at 1X10^{-3} m/m.

Hydrochemical data have been used to interpret the circulation systems. These data suggest that two flow systems exist beneath the Hanford site; one in the Grande Ronde and one in the Saddle Mountain and near-surface sediments. Within the Wanapum basalts, limited mixing occurs. Chemical signature data suggests waters of the Grande Ronde are probably part of regional circulation systems in contrast to the more locally circulating waters of the Saddle Mountain basalts.

Possible boundary conditions which may influence geohydrologic conditions at the site are listed below.

- The postulated "Cold Creek Barrier" located just west of the RRL. Hydrologic evidence suggests that this geophysical anomaly may act as an impermeable boundary to groundwater flow.

- The anticlinal ridges to the north and south of the RRL. However, it is not known at this time whether these structures may act as impermeable boundaries, constant head boundaries, or what the extent of such boundaries may be.

- The Columbia River may act as either a source or sink to groundwater in the deep basalts. Hydrologic data collected to date do not confirm either suggestion. The Columbia River is a sink (discharge area) for the unconfined aquifer.

Geochemistry

An understanding of the rock-fluid system environment of the repository is essential to predict repository isolation-containment characteristics. To date, information includes phase definition and distribution of components from petrologic and geologic studies. Reconnaissance geochemical sampling in these studies provides

gross system characterization. Limited experimental work identifies the behavior of radionuclides in this system and provides detail on phase stability and reactions.

The major mineral composition of the dense interiors of Grande Ronde basalts ranges from 0 to 35% pyroxene, 25 to 48% plagioclase, 0 to 6% Fe-Ti oxides, 0 to 3% olivine, and 20 to 65% mesostasis. Less abundant phases include apatite, orthopyroxene, pigeonite, and sulfides. The mesostasis is primarily glass.

The concentrations of most major element oxides and trace elements are relatively consistent throughout the Grande Ronde section. The ratio of $FeO/(FeO+Fe_2O_3)$ varies from about 0.76 to 0.79 in the dense interiors of candidate basalt flows. Therefore, the rock mass is highly reduced in the flow interiors. Hematite blebs are disseminated in the groundmass. Secondary phases in fractures, vesicles, and vugs include smectitic clays, zeolites, and silica. Other secondary minerals have been identified but are present in much lower amounts. The presence of secondary pyrite in these basalts provides strong evidence for reducing conditions in the site system.

The sedimentary interbeds consist of tuffaceous siltstone with lesser amounts of quartz sandstone, conglomerate, and well-sorted vitric tuff. Most of these sediments are friable but some are cemented with calcite, clay, opal, and zeolite.

The primary phases of the basalts are not in equilibrium with the present physiochemical environment. They are metastably persistent, however, because the kinetics of alteration are slow at the ambient low temperatures of the basalts. The lack of reliable thermodynamic data on secondary minerals prevents a rigorous evaluation of their stability.

Major inorganic components of deep basalt groundwaters are sodium (50 to 450 mg/L), potassium (4 to 36 mg/L), calcium (2 to 18 mg/L), magnesium (2 to 12 mg/L), silicon (25 to 175 mg/L), chloride, (50 to 550 mg/L), fluoride (5 to 55 mg/L), and sulfate (25 to 250 mg/L). Measured pH values range from 7.2 to 10.8 (most are in the range of 9.2 to 9.8). Alkalinity (as CaCO3) ranges from 75 to 225 mg/L. Both vertical and lateral major element compositional variations are observed.

Methane is the major dissolved gas found in groundwaters. Minor amounts of nitrogen, argon, and carbon dioxide are also present. Estimates of methane concentrations range from 350 to 700 mg/L for groundwaters in Grande Ronde basalts.

RADIONUCLIDES

Sorption of key radionuclides occurs by chemisorption and ion exchange reactions with minerals in the groundwater flow path. Actinides are strongly sorbed by each of the geologic solids studied (basalt, secondary minerals, and interbed materials), as are radionuclides that exist in solution as hydrated metal ions. Non-metallic radionuclides such as iodine-129, carbon-14, and selenium-79 exist only as anions in solution and are weakly sorbed.

Most radionuclide sorption reactions are at least partially irreversible under conditions expected in basalt groundwaters. Sorption and desorption isotherms for a given radioelement are non-single-valued and show a significant degree of sorption hysteresis. This hysteretic effect is important to radionuclide transport calculations since it can lower peak radionuclide concentrations in groundwater and delay transport. Migration of radionuclides as particulates suspended in groundwater must also be considered as a possible transport mechanism.

The chemical species of radionuclides in the site system will influence their retardation behavior. Speciation, in turn, depends on the oxidation state of the radionuclide and on the presence of complexing ligands. The preponderance of evidence indicates that conditions in the site system are reducing. It is expected, therefore, that radionuclides will be present in lower oxidation states.

A large quantity of radionuclide sorption and desorption data have been obtained. A wide range of experimental conditions have been examined in these measurements in an attempt to duplicate the variety of possible conditions expected in the site system. Because of uncertainties in groundwater composition, oxidation states of some radionuclides, and composition of geologic solids in groundwater flow paths,

attempts have been made to determine the sensitivity of radionuclide sorption to these parameters. As a result of these efforts, most existing sorption information was obtained at the extremes of expected conditions (oxidation states, groundwater compositions, etc.). Although this may be adequate for certain radionuclides, additional data is needed for radionuclides that are highly sensitive to these sorption parameters.

ENGINEERED BARRIERS

The development of engineered barriers, (i.e., the waste package and repository seals) has been proceeding in parallel with site exploration. The BWIP waste package concept incorporates the waste into a low-carbon steel, thick-walled cylindrical container which is designed for at least 1,000 years containment in accordance with the NRC containment requirement. A six-inch layer of crushed basalt-bentonite clay packing material is placed between the container and host rock to retard groundwater flow and to buffer groundwater oxygen concentrations to extremely low levels, thereby promoting conditions favorable to container life, and lower solubilities and higher sorptivities for many radionuclides. Thus the packing material is expected to play an essential role in meeting the NRC requirement for controlled release and the EPA cumulative mass flux requirement during the isolation period The current waste package program addresses characterization of the waste package environment, testing of waste package components under repository-relevant conditions, waste package design, and performance analyses. In the environmental area, studies include alpha/gamma radiolysis, natural analogs, redox sensitivity, and geochemical modeling. In the testing area, studies include degradation of iron-base and copper-base container materials, static and flow-through release testing of spent fuel and glass waste forms, and a variety of packing material physical and chemical tests. In the design and performance analysis areas, the advanced conceptual design of the waste package and a reliability analysis are nearly complete.

Repository seal development activities involve testing to understand site conditions and material behavior, testing to demonstrate emplacement techniques and component performance, modeling and analysis to assess seal system performance and predict repository conditions which affect performance, and design. All these activities support the selection of materials and evolution of sealing concepts to assure that excavated openings do not become pathways to compromise the ability of the site to isolate wastes.

The principal activities through the initial part of site characterization involve laboratory testing of candidate backfill materials, modeling and performance analysis of alternative shaft and borehole sealing concepts to provide a basis for design optimization relative to performance criteria, and performing conceptual and advanced conceptual design of shaft and borehole seals.

TESTING PROGRAM

The objectives of the testing program include (1) providing a data base for license application, (2) providing assurance on performance issues, and (3) providing data for engineering and design of the repository and dependent operations. At Hanford, the testing effort is oriented toward answering questions on the groundwater system, rock complexities, and stability with respect to demonstrating containment and isolation. (Table 1)

In the event Hanford is selected for site characterization, the testing program will be outlined in the Site Characterization Plan. Central to activities during characterization is providing an understanding of site geologic heterogeneities. As a result, this data collection and testing effort is strongly flavored by classical exploration and engineering geologic studies. Major elements of this program are described below.

Geology

Uncertainties in the current knowledge of the site stratigraphy and lithology are based on the paucity of subsurface data, and show up in lower confidence level estimates of basalt flow thickness, variation in intraflow structure, fracture characteristics, and petrology, both of the flows and interbeds. The work to be conducted on surface outcrop and from boreholes will include

field mapping, surface and subsurface geophysics, laboratory analysis of chemistry and petrology.

In the area of structural geology, current information concentrates on the geometric characteristics of folds and faults. The data are incomplete and uncertainties exist on the nature, mechanisms, and timing of tectonic deformation. Significant work remains in characterizing the large-scale regional structures like the RAW, and evaluating the possible influence of regional tectonic forces on repository stability.

Groundwater Hydrology

The principal activities in groundwater hydrology include characterizing the regional groundwater flow system, providing a baseline for flow system interpretation, and determining the value of hydraulic properties for the repository rock volume. System uncertainties will be identified through numerical modeling which will require evaluating boundary conditions for the Cold Creek syncline.

Key to the evaluation of the hydrologic system are data obtained from a monitoring system of over 35 monitoring wells at and surrounding the RRL. From these facilities, water level and pressure data are being monitored; first, to establish a baseline and second, in response to formational responses during nearby drilling and pumping activities. A specific phase of testing (large hydraulic stress testing or LHS) will consist of pumping selectively from wells in this system and observing responses in neighboring nested piezometers up to kilometers from the test point.

Pump tests are planned for both local and remote testing, involving scales of hours and days up to a month or more of pumping.

Three types of tests will be conducted from the Exploratory Shaft facility (Table 2): borehole, chamber, and tracer breakthrough between boreholes. Borehole testing procedures will include constant head injection, pulse, and cross hole techniques.

Both surface and subsurface boreholes will be used as monitoring points during all subsequent testing and construction activities.

Rock Mechanics Testing

A key area in demonstrating a viable rock environment is demonstrating stability of underground openings at depth and facility of construction and operations methods. The available data on rock properties provide a basis for evaluating these items but in situ observation, mining, and underground testing are needed. Specific underground tests will be based on the first in situ observations during shaft sinking and facility breakout. Table 2 shows elements in the testing program. Figure 3 shows the exploratory shaft test facility layout with the location of individual tests in the geomechanical testing program. Integrated thermo-mechanical and hydrological testing may be required to establish that mechanical performance will not impact waste isolation. The nature of such tests can only be proposed at this point. In situ test data will provide guidelines for such tests.

REFERENCES

U. S. Department of Energy, 1982, Site Characterization Report for the Basalt Waste Isolation Project, DOE/RL 82-3, 3 Vols., Rockwell Hanford Operations for the U. S. Department of Energy, Washington, D. C.

U. S. Department of Energy, 1982, Test Plan for Exploratory Shaft Phase I and II Testing, SD-BWI-TP-007

U. S. Department of Energy, 1984, Draft Environmental Assessment for the Basalt Waste Isolation Project, DOE/RW-0017

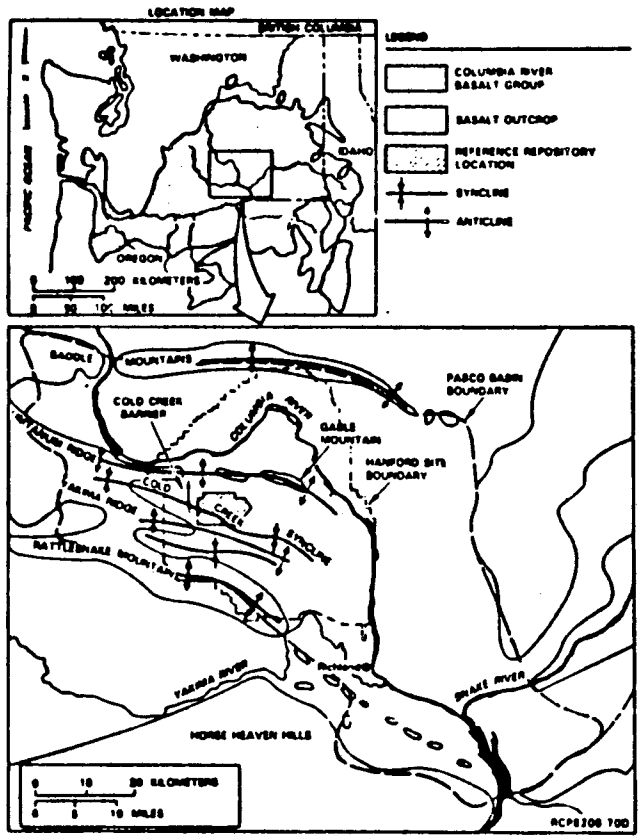

Figure 1. Extent of the Columbia River Basalt Group, the Pasco Basin, and the proposed site for a repository in basalt.

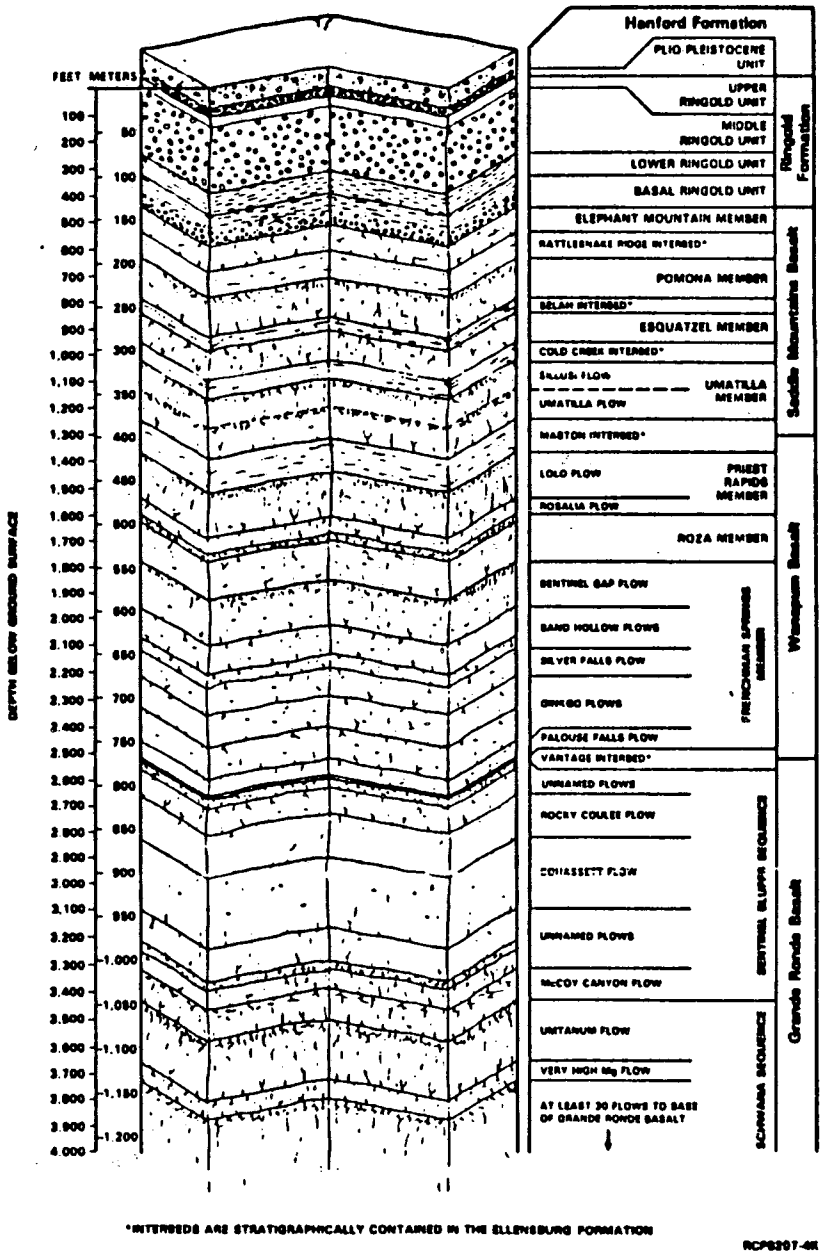

Figure 2. Reference Repository Location Stratigraphy.

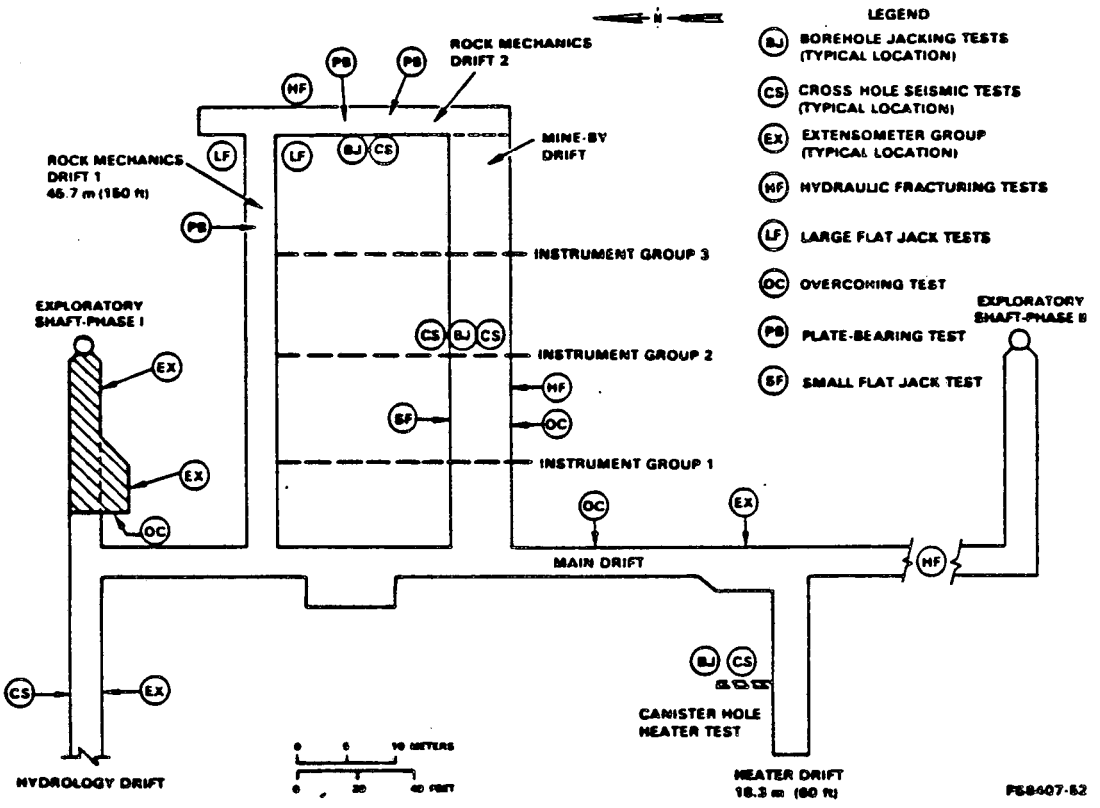

Figure 3. Plan View of ES-11 Facility Showing Rock Mechanics Test Location.

TECHNICAL OBJECTIVES / PLANNED TESTS	PHASE I						PHASE II				REFERENCE SECTION	
	I-1 PRINCIPAL BOREHOLE	I-2 SHAFT CONSTRUCTIBILITY	I-3 SHAFT LINER BEARING	I-4 SHAFT STATION GEOHYDROLOGY	I-5 SHAFT STATION GEOMECHANICS	I-6 SHAFT STATION CONSTRUCTIBILITY	II-1 GEOLOGIC CHARACTERIZATION	II-2 HYDROLOGIC CHARACTERIZATION	II-3 GEOMECHANICS CHARACTERIZATION	II-4 UNDERGROUND CONSTRUCTIBILITY	EXPLORATORY SHAFT TEST PROGRAM VOLUME I	PRELIMINARY TEST DESCRIPTION VOLUME II
GEOLOGIC CHARACTERIZATION												
PRINCIPAL BOREHOLE TESTS	●										8.2.4	APPENDIX A
BOREHOLE TESTS				●	○		●	○	○		8.3.1	2.3.1
FACILITY TESTS					○	●	●	○	○	●	8.3.1	3.2.3
HYDROLOGIC CHARACTERIZATION												
PRINCIPAL BOREHOLE TESTS	●										8.2.4	APPENDIX A
BOREHOLE HYDROLOGY TESTS				●				●	○		8.3.2	3.3
CHAMBER TESTS								●			8.3.2	3.4
TRACER TESTS								●			8.3.2	3.5
GEOMECHANICS CHARACTERIZATION												
PRINCIPAL BOREHOLE TESTS	●										8.2.4	APPENDIX A
OPENING DEFORMATION MONITORING					●				●		8.3.3	4.3.3
OPENING SUPPORT MONITORING					●				●		8.3.3	4.3.3
ACOUSTIC EMISSION MONITORING					●				●		8.3.3	4.3.4
BOREHOLE JACKING TEST									●		8.3.3	4.3.5
CROSS HOLE SEISMIC TEST									●		8.3.3	4.3.6
PLATE BEARING TEST									●		8.3.3	4.3.7
LARGE FLAT JACK TEST									●		8.3.3	4.3.8
ROOM SCALE ENLARGEMENT									●		8.3.3	4.3.9
CANISTER HOLE DRILLING TEST									●		8.3.3	4.3.10
HEATER TEST									●		8.3.3	4.3.11
SMALL FLAT JACK TEST									●		8.3.3	4.3.12
OVERCORING TEST					●				●		8.3.3	4.3.13
HYDRAULIC FRACTURING TEST									●		8.3.3	4.3.14
CONSTRUCTIBILITY REPORTING		●	●			●				●	8.4	5.0

PS8310 77

LEGEND
● PRIMARY DATA ○ SUPPORTING DATA

---- Table 1 - Exploratory Shaft Objectives and Planned Tests.

Table 2

SWIP HYDROLOGIC TEST ACTIVITIES

TEST ACTIVITY	TEST OBJECTIVES	PRIMARY FACILITIES	TEST MECHANICS
PIEZOMETRIC BASELINE MONITORING	• DEFINE WATER-LEVEL TRENDS FOR TESTING PURPOSES • GROUNDWATER FLOW CONCEPTUALIZATION DIRECTION OF FLOW HEAD DISTRIBUTION • REGIONAL GROUNDWATER FLOW MODEL CALIBRATION	• DC-19, DC-20, DC-22, RRL-2A, HANFORD MONITORING WELLS (SEE ATTACHMENTS)	• WATER-LEVEL MEASUREMENTS IN ALL AVAILABLE DEEP BOREHOLES • PRESSURE MEASUREMENTS IN DC-19 DC-20, & DC-22 • NO WITHDRAWALS OF GROUNDWATER AT HANFORD FOR A 1-YEAR PERIOD
GRANDE RONDE LARGE-SCALE HYDROLOGIC STRESS TESTS (LHST)	• AREAL HYDRAULIC PARAMETRIC EVALUATION • IDENTIFY BOUNDARIES WITHIN GRANDE RONDE (LIMITED AREA) • VERTICAL CONDUCTIVITY • LITHOLOGIC CONTINUITY • PRESENCE/ABSENCE OF HIGHLY TRANSMISSIVE ZONES	• RL-2B - PUMPING WELL • RRL-2C - MONITORS DENSE INTERIORS OF GRANDE RONDE • DC-19, DC-20, DC-22 • DC-1, DC-2, DC-4, DC-6, DC-7, DC-8, DC-12, DC-19, DC-18, RRL-6B, RRL-14, McGEE	• PUMP SEQUENTIALLY ROCKY COULEE FLOW TOP, COHASSET FLOW TOP, COHASSET FLOW BOTTOM, AND UMTANUM FLOW TOP • MEASURE DRAWDOWN AT NESTED PIEZOMETERS AND OTHER WELLS • "PIGGYBACK" TRACER TESTS • ANALYTICAL AND INVERSE NUMERICAL SOLUTIONS
WANAPUM LARGE-SCALE HYDROLOGIC STRESS TESTS (LHST)	• LARGE-SCALE STRESS OF WANAPUM AQUIFERS TO ADDRESS BOUNDARY CONDITIONS, NEAR TO FAR FIELD	• DC-18, DC-20, DC-22 • DB-1, DB-2, DB-11, DB-12, DB-16, DC-18C, ENYEART, FORD, O'BRIEN, McGEE	• PUMP PRIEST RAPIDS • MEASURE DRAWDOWN • ANALYTICAL AND INVERSE NUMERICAL SOLUTIONS
SMALL-SCALE TESTS	• HYDRAULIC PARAMETER EVALUATION • PRE-LHST EVALUATION TO SIZE TESTS	• AS NEEDED	• PULSE, INJECTION, ETC.

COUPLED PROCESSES ADDRESSED BY UNDERGROUND TESTING FOR THE SALT REPOSITORY PROJECT

H. Kalia[1*], W.J. Roberds[2], and R.J. Byrne[2]

ABSTRACT

As part of the licensing process, various aspects of performance of a repository system must be assessed in order to demonstrate compliance with the pertinent federal regulations (e.g., 10CFR60, 40CFR191, etc.). Such performance will be a function of the site characteristics (which require definition) and the design variables (which can be specified), i.e., the system parameters. The relevant system parameters derive from a consideration of the processes taking place within the system. These processes can be categorized as thermal, mechanical, hydrological, and chemical, or as combinations of these. Uncertainties in the understanding of the processes, in their representation by models, and in the system parameters lead to uncertainties in performance prediction. The basic objective of underground testing, as well as other testing, is to sufficiently reduce these uncertainties.

A tentative set of information needs, which derives from current uncertainties in both the relevant system parameters and the modeling of processes (coupled and uncoupled), has been developed for the Salt Repository Project (SRP). A program of underground testing to be conducted in an Exploratory Shaft Facility (ESF) has then been developed to satisfy, in conjunction with other test programs, these (SRP) information needs. This activity is discussed in this paper, with emphasis on coupled processes.

1 Office of Nuclear Waste Isolation, Battelle Project Management Division; Columbus, Ohio

* Presenter of Paper

2 Golder Associates, Inc.; Redmond, Washington

INTRODUCTION

As established by the Nuclear Waste Policy Act of 1982 (NWPA), the U.S. Department of Energy (DOE) will select and investigate potential site(s), and design, construct, operate and decommission the repository, as approved by the U.S. Nuclear Regulatory Commission (NRC) through the licensing process. Currently, sites in various media, including salt, are being considered for repository development. The Office of Nuclear Waste Isolation (ONWI), administered by the Battelle Project Management Division (BPMD) of Columbus, Ohio, has the responsibility for repository development for the Salt Repository Project Office (SRPO) of the DOE. If, based on available information, a salt site is recommended and approved as one of three sites for further consideration, then that site will be characterized in detail to provide the additional information necessary for recommending a single site for repository development and license application, and for repository design and performance assessment (as required by the licensing process). Such detailed site characterization will include additional surface-based site investigations and testing, laboratory studies, and underground tests and investigations conducted in an exploratory shaft facility (ESF). In preparation for this work, Golder Associates, Inc. of Redmond, Washington has been retained by BPMD to develop and subsequently perform (if necessary) an underground test program (UTP) in the ESF for the SRPO. Other contractors are currently developing other aspects of the program, e.g., laboratory test program, performance assessment, etc.

The general approach taken in the development of the test programs is as shown in Figure 1. First, a set of information needs, i.e., the additional information needed to determine compliance with the regulations, must be identified. These information needs should be derived explicitly from the pertinent regulations, although until sensitivity studies,

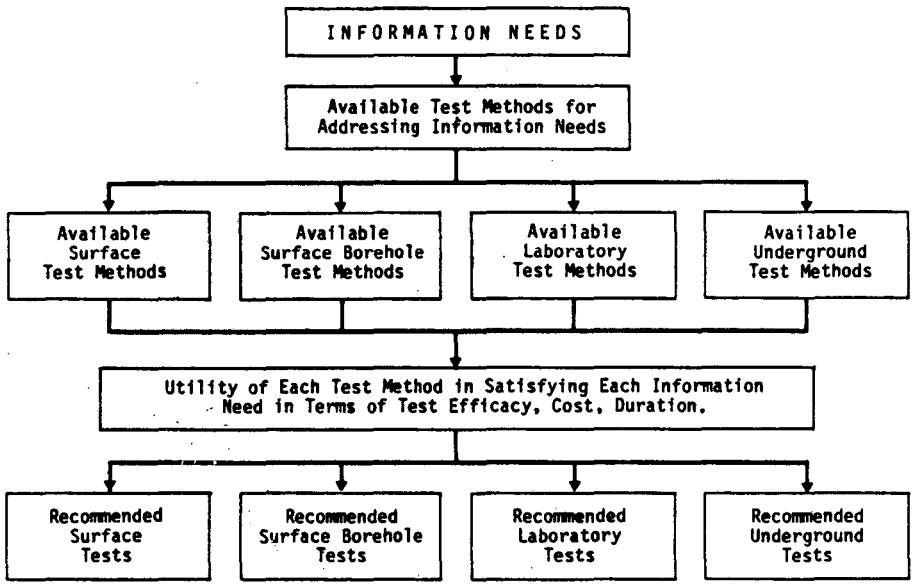

Figure 1 APPROACH TO DEVELOPMENT OF TEST PROGRAMS

uncertainty analyses, and compliance threshold decisions are completed, they may have to be qualitative in nature. As will be discussed in more detail in the following section, these information needs include, but are not limited to, the consideration of coupled processes.

Once the set of information needs has been identified, then all of the test methods available for addressing each can be identified and evaluated with respect to how well it addresses that information need, as well as the cost and duration of such testing. Based on these evaluations, programs of testing would then be recommended as the suite of tests which satisfies the information needs, at reasonable cost within schedule. As noted in Figure 1, test methods have been categorized in terms of whether they are conducted from the ground surface (non-borehole), within surface-based boreholes, in the laboratory on design elements or on samples obtained from on- or off-site, or from underground in an ESF. The development of the testing programs, especially the underground testing program, in response to these information needs will be subsequently discussed in more detail in a following section.

INFORMATION NEEDS

At License Application (LA), it will be necessary to demonstrate compliance with all of the pertinent regulations (e.g., 10CFR60, 40CFR191, etc.). Many of these regulations are performance-based, i.e., performance of the system or component must meet or exceed some specified value. Hence, in order to demonstrate compliance with such performance-based regulations, it will be necessary to defensibly assert, with reasonable assurance, that performance will satisfy the regulatory requirements. There is often significant uncertainty in such performance predictions, especially over the long term and for systems as complex and unique as a repository. Such uncertainty in the performance prediction is a function of the inherent uncertainties in:

- The understanding of the processes at work when the system is perturbed, i.e., the conceptual model which describes the processes;
- The numerical representation of the processes as functions of parameters and the solution procedures, i.e., the numerical model;
- The parameters which describe the geometry, nature and behavior of naturally occuring materials at the site and the nature of naturally occurring perturbations to the system (e.g., tectonics, climatic changes, etc.), i.e., site characteristics; and
- The parameters which describe the geometry, nature and behavior of designed elements, procedures and events, i.e., design variables.

In order to achieve a given level of confidence in a performance prediction, and therefore to determine compliance with performance-based regulations, specific combinations of uncertainty in the models and parameters must not be exceeded. Such a combination of types of information and associated levels of confidence in each, which is intended to be necessary and sufficient to determine compliance, is termed the "information requirements". These information requirements are determined in part by sensitivity studies, e.g., the sensitivity of the uncertainty in the

performance prediction to the uncertainty in each of the various models and parameters. These information requirements must be satisfied in order to determine compliance with the performance-based regulations, otherwise the uncertainty in the performance prediction will be too large to determine compliance, i.e., reasonable assurance will not be achieved.

Much data relevant to the information requirements currently exist, both site specific and generic. In most cases, however, the uncertainties in the currently available information are still too large (i.e., the information requirements are not satisfied) due to insufficiencies in the data base. These data base insufficiencies might include at the present time:

- Data uncertainties due to possible measurement errors (random or systematic);
- Nonrepresentative sampling of data, i.e., the statistics of the data do not represent the statistics of the population;
- Absence of enough data to be statistically significant; and
- Uncertainty in the correlation between the data and the information required, e.g., the relationship between hard measured data and an inferred parameter.

In order to correct these data base insufficiencies, a program of site characterization must be implemented.

The "information needs" consist of the additional information needed to satisfy the information requirements and thus determine compliance. Once the information needs have been identified, as discussed above, a testing program can be developed to produce the data which are necessary and sufficient to satisfy these information needs (Figure 1).

Consistent with the above discussions and with previous generic treatments (e.g., as contained in the DOE Mission Plan), a tentative set of information needs has been identified for the SRP, particularly to guide the development of the underground test program in the ESF at a salt site. This tentative set of information needs, and the coupling of physical (i.e., thermal, mechanical, and hydrological) and chemical (including radiological) processes which must be considered in satisfying each information need, is summarized in Table 1. Specifically, this identification of the information needs was done as follows:

(1) A comprehensive hierarchy of performance issues was developed, starting with broad issues and progressing in increasing levels of detail until the issue was stated at or below the level of those specified in the regulations.

(2) The pertinent sections of the regulations (i.e., Nuclear Waste Policy Act of 1982, 10CFR60 - Disposal of High-Level Radioactive Wastes in Geologic Repositories (NRC), 40CFR191 - Environmental Standards for the Management and Disposal of Spent Nuclear Fuel, High-Level and Transuranic Radioactive Wastes (EPA), 10CFR960 - General Guidelines for the Recommendation of Sites for Nuclear Waste Repositories (DOE), 10CFR20 - Standards for Protection Against Radiation (NRC), and 30CFR Ch.I - Mine Safety and Health Administration (Dept. of Labor) - Subch.D,E,N) were cited and categorized as specifying performance, information, testing, or other regulatory requirements. The regulatory performance requirements were then stated in terms of the appropriate performance issues.

(3) The methods which are available to resolve each of the most detailed performance issues were identified, and the type of information required by each method listed. These methods include:

(a) Demonstration, where an element of the repository is physically constructed, the performance measured or observed, and the results used directly to predict repository performance (without determining parameter values or developing models);

(b) Empirical analysis, where past experience under similar conditions is quantified and transferred to repository performance (without a formal theoretical basis); and

(c) Numerical analysis, where conceptual and then numerical models which represent the perceived physical processes are developed, input parameters assessed, and performance predictions calculated.

(4) The information required for resolving the performance issues by the various methods, in conjunction with the regulatory information requirements, was then compiled into a single list of information requirements (Table 1). These information requirements were then related back to the pertinent regulations through the performance issues. Because the level of confidence defining compliance at LA has not yet been specified and because sensitivity studies on the uncertainty in performance predictions to uncertainties in models/parameters have not yet been conducted, these information requirements are necessarily qualitative in nature (i.e., the maximum acceptable level of uncertainty in each type of information has not been determined).

(5) The current status of satisfying the information requirements was summarized, based on the available data base (both site specific and generic).

(6) The additional information needed to satisfy each of the information requirements,

and thus determine compliance at LA, was then determined (Table 1). These information needs were then related back to the pertinent regulations in the same way as the information requirements. Again, because the information requirements are currently qualitative in nature, these information needs are also qualitative.

PROGRAM OF UNDERGROUND TESTING

Test programs are being developed to provide the data which are necessary and sufficient to satisfy the set of information needs and thus determine compliance with the regulations.

Data relevant to satisfying the information needs can be obtained in a variety of ways. Such data may be site specific or generic in nature, although the interpretation of generic data will generally result in greater uncertainty in the assessment of information for site specific performance predictions than will the interpretation of otherwise identical site specific data. The methods available for obtaining these data can be categorized as testing conducted from the ground surface (non-borehole), within surface-based boreholes, in the laboratory on design elements or on samples obtained on- or off-site, or from a subsurface test facility. Each of the test methods provides different quality data due to the scale of the test sample, the degree of sample disturbance, the accuracy and reliability of the test, and the parameters incorporated by the test. The uncertainty in the assessment of the information decreases as both the relevance and the number of tests increases. However, the cost of testing increases with the number of tests and generally also with the complexity of tests. Hence, the optimum test program consists of that number of each type of test which is sufficient to satisfy the information needs at the lowest cost and within schedule.

The various test methods available for addressing each tentative SRP information need have been identified, and each test method subjectively and qualitatively evaluated with respect to its relevance to the information need and to its cost and duration. Generally speaking, surface testing, surface borehole testing, and laboratory testing, with some exceptions, do not address either model validation or design evaluation; rather underground testing is required. In addressing site characteristics, the tests in each of the categories have the following general attributes:

Surface Testing, i.e., tests conducted at the site from the surface, excluding surface boreholes,

- Allows for relatively continuous areal coverage.
- Can provide large-scale (regional) characterization.
- Utilizes a test volume which is sometimes too large (e.g., in seismic, magnetic, gravity surveys), averaging the effects of different rock types or discontinuities.
- Results in minimal sampling disturbance.
- Typically offers poor resolution and limited penetration depths.
- Cannot assess response characteristics for a range of, or changes in, environmental conditions.

Surface Borehole Testing, i.e., tests (including drilling) conducted at the site in and between boreholes drilled from the surface,

- Is a function of the number, location, and depth of boreholes.
- Can provide large-scale (regional) characterization by multiple boreholes.
- Typically in a single borehole test, utilizes a test volume which is unrepresentatively small.
- Utilizes samples for which disturbance due to drilling may be significant.
- Results in additional uncertainty from poor control or accuracy due to remoteness from the test zone.
- Cannot typically assess response characteristics for an appropriate range of environmental conditions.

Laboratory Testing, i.e., tests conducted in the laboratory on samples obtained at the site (from the surface, from surface-based boreholes, or from the ESF),

- Is limited to samples obtained from boreholes or from underground.
- Utilizes a test volume which may be too small to represent the rock mass.
- Allows for tight control of test conditions.
- Utilizes samples for which disturbance (mechanical, geochemical) due to drilling activities and stress relief may be significant.
- Can assess response characteristics for a wide range of environmental conditions, although the actual in situ conditions may not be known.
- Can perform scaled-down simulation testing.

Underground Testing, i.e., tests (including drilling) conducted within the ESF,

- Does not allow for broad spatial coverage, except by extensive drifting and subsurface drilling.
- Can often test representative volumes.
- Does not allow for as tight control of test conditions as for laboratory testing.

- Utilizes samples for which there will be some disturbance (e.g., stress relief) associated with excavation; however, this disturbance will be analogous to that which will occur in the actual repository if similar excavation methods are utilized.
- Can theoretically assess response characteristics for a wide range of environmental conditions, although this may be impractical (in terms of complexity, cost, and duration) in many cases.
- Can perform direct simulation testing.

In addition to the above considerations which affect the correlation of the test data to the information needed, there are also significant differences between the tests in terms of duration and cost. In assessing response characteristics and validating models, the time required to achieve meaningful test results for time-dependent processes (e.g., creep, heat flow, fluid flow, geochemical alteration) increases dramatically with scale. Hence, large-scale underground testing which incorporates such processes may have significant schedule impacts. Similarly, the costs of tests typically increase with scale, duration, and complexity. Hence, large-scale underground tests of long duration also tend to have significant cost impacts.

By considering the information needs to be satisfied by testing, and the efficacy, cost and duration of the available test methods for addressing the information needs, the integrated test program (surface, surface borehole, laboratory and underground) can be selected. The underground tests which are considered to be needed to supplement the other anticipated tests to satisfy the information needs are summarized in Table 2. This suite of tests forms the basis of the proposed program of underground testing for a salt site. As the information needs and the test method evaluations are currently qualitative in nature, the selected suite of tests is based on subjective assessments. Hence, as the information needs are quantitatively defined and the other test programs finalized, the program of underground testing may be revised somewhat, although major revisions are not anticipated.

In the evaluation and selection of the test methods, coupled processes were considered, specifically in the incorporation of the various test parameters by each test and in the related relevance of each test to the information needs. The coupling of physical (i.e., thermal, mechanical, and hydrological) and chemical processes which are incorporated in each selected underground test is presented in Table 2. It should be noted that the coupled processes which must be considered in each information need (Table 1) are not completely covered by the proposed program of underground testing (Table 2). This is because coupled processes can often be more efficiently investigated in the laboratory. The laboratory generally offers more control and precision than does underground testing, but at smaller scale, under assumed (rather than actual) environmental conditions, and on disturbed samples. The disadvantages of laboratory testing relative to underground testing can be overcome to a large extent by performing similar but less complicated underground tests (incorporating fewer coupled processes) to validate or calibrate specific aspects of the laboratory test. These aspects of the other testing programs have been considered in the development of the proposed program of underground testing for a repository in salt. The underground test program does not satisfy all the information needs but is one element of the overall site characterization and testing effort.

SUMMARY AND CONCLUSIONS

A tentative set of information needs has been identified for the Salt Repository Project, specifically for guiding the development of the underground testing program in an ESF in salt. These information needs must be satisfied in order to determine compliance with the regulations. These information needs have been explicitly derived from the regulations and take credit for currently available information, but are currently qualitative in nature. Specific coupled processes must be considered in satisfying each information need (Table 1).

To satisfy the identified set of information needs, a program of underground testing has been proposed for the Salt Repository Project, in conjunction with the other anticipated test programs (i.e., surface (non-borehole), surface-based boreholes, and laboratory). The program has been developed by first identifying the test methods available for addressing the information needs, and then evaluating each with respect to the relevance of the test results to the information need (i.e., the post-test uncertainty in the model or parameter), as well as to the cost and duration of the test. The coupled processes incorporated in each test method (Table 2) are a major factor in this evaluation. The proposed program of underground testing consists of those underground tests which are necessary and sufficient, in conjunction with the other anticipated test programs, to satisfy the tentative set of information needs.

TABLE 1 TENTATIVE SET OF INFORMATION NEEDS: CONSIDERATION OF COUPLED PROCESSES

INFORMATION NEEDS	PROCESSES			
	Thermal	Mechanical	Hydrological	Chemical*
SITE CHARACTERISTIC ASSESSMENT				
Geology				
Stratigraphy/Lithology				
Structure				
Tectonic Activity				
Man-Made Disturbance				
Geomechanics				
In Situ Stress				
Strength	o	●		o
Deformation Moduli	o	●		o
Creep/Fusing	o	●		o
Thermomechanics				
In Situ Temperature				
Thermal Conductivity	●			
Specific Heat	●			
Thermal Expansion	●	●		o
Geohydrology				
In Situ Hydraulic Pressure				
Hydraulic Conductivity	o	o	●	o
Effective Porosity		o	●	o
Specific Storage		o	●	
Dispersivity/Diffusion	o		●	●
Brine Migration	●	o	●	o
Geochemistry				
Mineralogy/Petrology				
Hydrochemistry				
Gas Content				
Adsorption/Retardation	o		o	●
Alteration/Solubility	o	o	o	●
DESIGN/MODEL VALIDATION				
Shaft				
Construction Procedures				
Construction Affected Zone				
Strength	o	●		o
Deformation Moduli	o	●		o
Creep/Fusing	o	●		o
Thermal Conductivity	●			
Specific Heat	●			
Thermal Expansion	●	●		o
Hydraulic Conductivity	o	o	●	o
Effective Porosity		o	●	o
Specific Storage		o	●	
Dispersivity/Diffusion	o		●	●

TABLE 1 TENTATIVE SET OF INFORMATION NEEDS: CONSIDERATION OF COUPLED PROCESSES-Continued

INFORMATION NEEDS	PROCESSES			
	Thermal	Mechanical	Hydrological	Chemical*
Mechanical Response		●		
Thermal/Thermomechanical Response	●	●		
Hydrologic Response			●	
Radionuclide Transport			●	●
Hydrochemical/Geochemical Response				●
Room				
Construction Procedures				
Construction Affected Zone				
Strength	o	●		o
Deformation Moduli	o	●		o
Creep/Fusing	o	●		o
Thermal Conductivity	●			
Specific Heat	●			
Thermal Expansion	●	●		o
Hydraulic Conductivity	o	o	●	o
Effective Porosity		o	●	o
Specific Storage		o	●	
Dispersivity/Diffusion	o		●	●
Mechanical Response		●		
Thermal/Thermomechanical Response	●	●		
Hydrologic Response			●	
Radionuclide Transport			●	●
Hydrochemical/Geochemical Response				●
Emplacement Hole				
Construction Procedures				
Construction Affected Zone				
Strength	o	●		o
Deformation Moduli	o	●		o
Creep/Fusing	o	●		o
Thermal Conductivity	●			
Specific Heat	●			
Thermal Expansion	●	●		o
Hydraulic Conductivity	o	o	●	o
Effective Porosity		o	●	o
Dispersivity/Diffusion	o		●	●
Mechanical Response		●		
Thermal/Thermomechanical Response	●	●		
Hydrologic Response			●	
Radionuclide Transport			●	●
Hydrochemical/Geochemical Response				●

TABLE 1 TENTATIVE SET OF INFORMATION NEEDS: CONSIDERATION OF COUPLED PROCESSES- Continued

INFORMATION NEEDS	PROCESSES			
	Thermal	Mechanical	Hydrological	Chemical*
Waste Package				
Mechanical Response		●		
Thermal/Thermomechanical Response	●	●		
Corrosion				●
Dissolution				
Backfill/Seal**				
Construction Procedures				
Backfill/Seal Material:				
Strength	o	●		o
Deformation Moduli	o	●		o
Creep/Fusing	o	●		o
Thermal Conductivity	●			
Specific Heat	●			
Thermal Expansion	●	●		o
Hydraulic Conductivity	o	o	●	o
Effective Porosity		o	●	o
Dispersivity/Diffusion	o		●	●
Chemistry				
Adsorption/Retardation	o		o	●
Alteration/Solubility	o	o	o	●
Consolidation/Mechanical Response		●		
Thermal/Thermomechanical Response	●	●		
Hydrologic Response			●	
Radionuclide Transport			●	●
Hydrochemical/Geochemical Response				●
Repository Operating Systems				
Ventilation/Cooling				
Dewatering				
Hoisting				
Underground Transport				
Safety and Health Procedures				
Emergency Procedures				
Repository Operations				
Waste Handling/Emplacement Procedures				
Waste Retrieval Procedures				

● The fundamental process(es) which define the information need and thus must be considered in satisfying that information need.
o The secondary process(es) which, although not fundamental, affect the satisfaction of the information need in a less significant manner and thus should also be considered in satisfying that information need.
* Chemical processes include radiological effects.
** Backfill seal includes consideration of operational and permanent shaft and borehole seals, room seals and backfill, and emplacement hold backfill.

TABLE 2 PROPOSED UNDERGROUND PROGRAM: CONSIDERATION OF COUPLED PROCESSES

TEST	PROCESSES			
	Thermal	Mechanical	Hydrological	Chemical**
Geology				
Geologic Mapping				
Drilling*	●	●	●	●
Geophysical Borehole Logging				
Electrical Surveys				
Gravity Surveys				
Radar Probing				
Seismic Surveys				
Seismic Monitoring		●		
Block Sampling*	●	●	●	●
Geomechanics				
Stress Measurement	o	●		
Borehole Pressuremeter/ Jacking Test		●		
Borehole Condition/ Convergence Monitoring	o	●		
Torsional Shear Test		●		
Mine-by Test		●		
Rock Bolt Pullout Test		●		
Facility Mechanical Response Monitoring	o	●		
Thermomechanics				
Thermal Conductivity Probe Testing	●			
Waste Package Heater Test	●	●		o
Room Heater Test	●	●		o
Room Backfill Test	●	●		o
Facility Thermal Response Monitoring	●			
Geohydrology				
Single Borehole Hydraulic Conductivity Test		o	●	
Cross-hole Hydraulic Conductivity Test		o	●	
Cross-hole Tracer Test		o	●	
Tracer Diffusion Test			o	●
Underground Borehole Seal Test		o	●	
Room Seal Test		o	●	
Brine Migration Test	●	o	●	o
Grout Injection Test		o	●	o
Facility Hydrological Response Monitoring	o	o	●	
Geochemistry				
Formation Fluid Sampling*	●	o	●	●

● The fundamental process(es) incorporated by the test method.
o The secondary process(es) which, although not the primary focus of the test method, affect the test results and are incorporated by the test method.
* Samples are tested in the laboratory (i.e., thermal, mechanical, hydrological, and chemical tests are performed in the laboratory on core obtained from drilling and on block samples, while especially chemical analyses are performed on formation fluid samples).
** Chemical processes include radiological effects.

EXPERIMENTS PERFORMED ON GRANITE IN THE UNDERGROUND RESEARCH LABORATORY AT FANAY-AUGERES, FRANCE

A. Barbreau*, B. Come**, S. Derlich*, E. Durand***
G. de Marsily****, P. Peaudecerf***, G. Vouille****

* CEA, Institut de Protection et de Sûreté Nucléaire, DPT
B.P. n° 6, 92260 FONTENAY-AUX-ROSES, France

** Commission des Communautés Européennes, DG XII
200, rue de la Loi, B-1049 BRUXELLES, Belgique

*** Bureau de Recherches Géologiques et Minières
B.P. 6009, 45060 ORLEANS CEDEX, France

**** Ecole Nationale Supérieure des Mines de Paris
35, rue Saint-Honoré, 77305 FONTAINEBLEAU, France

ABSTRACT

The "Département de Protection Technique" (DPT), of the "Institut de Protection et de Sûreté Nucléaire" (IPSN) of the "Commissariat à l'Energie Atomique" has developed in the FANAY-AUGERES uranium mine, near Limoges, in a granitic formation of the Massif Central, an underground research laboratory in order to improve the knowledge of the properties and behaviour of the fractured medium. Two main programmes are at present underway in this laboratory with the participation of the "Bureau de Recherches Géologiques et Minières" (BRGM) and the "Centre d'Informatique Géologique" of the "Ecole Nationale Supérieure des Mines de Paris", in the framework of cost shared contracts with the CEC : the study of the influence of the scale effect on the measured value of the permeability and dispersion coefficients, and an hydro-thermo-mechanical experiment. This paper is devoted to the review of the preliminary results of the first experiment and to the description of the second one which is now being initiated.

The first study, the scale effect experiment, is carried out in a test section 100 m in length of a drift of the mine, situated 170 m below ground. Six 10 to 20 m long boreholes were first drilled from the drift to test the suitability of the site for the experiment ; then ten 50 m long radial boreholes were fully cored, and equiped with 68 inflatable packers isolating 68 measurement chambers, where the hydraulic pressure is recorded. In the same time, the flow of water arriving in the test section of the drift is measured. As the order of magnitude of the hydraulic conductivity of the Fanay granite is 10^{-8} m/s, the flow rate for the 100 m section of the drift is large enough (6 l/mn) to be measurable in liquid form, the moisture carried away by ventilation being negligible. In addition to the pressure measurements, 250 injection tests were carried out in the boreholes, and the fracture network geometry and properties were recorded both on the drift walls and on the cores. Stress measurements will also be made, and, in a later phase, injection of tracers in the radial chambers of the boreholes, with a monitoring of the concentration of the tracer in the water arriving in the drift. The preliminary results obtained and the methodology used to interpret them are described.

The second study, the hydro-thermo-mechanical experiment, is carried out in another drift of the same mine. Only the preliminary investigations are now in progress. The purpose is to perform a simulation on a reduced scale in time and space of the different physical phenomena linked to the thermal loading of radioactive waste. A chamber with a 10 m x 10 m floor is now being excavated in the granite. The rock mass will be heated by means of electrical resistors placed in boreholes two meters below the floor. Temperatures, fluid pressure and mechanical deformations will be observed in the rock mass and in the surface of the chamber floor. Particular attention will be paid to the behaviour of fractures and to the modifications in rock mass permeability induced by the thermal effect. The different thermal, mechanical and hydraulical data obtained during a six months experiment including a heating phase of about one month will be interpretated using different models that will be compared to each other.

1. THE SCALE EFFECT EXPERIMENT

1.1 Objectives

Two separate objectives are assigned to this experiment. The first one is to develop a methodology for evaluating the hydraulic properties of a fractured crystalline rock from an underground opening. The second is to understand how these hydraulic properties at large scale, representative of a real repository, can be inferred from relatively small scale measurements.

On the first goal, it may be of interest to recall that the French Radioactive waste disposal program recommends the selection of several potentially favorable HLW disposal sites, in various formations (crystalline rocks, clays, shales, and perhaps bedded salt). On these sites, detailed surface investigations will be performed (mapping, structural analysis, geophysics, several boreholes and tests...) until one (or perhaps several) site(s) will be selected for the sinking of a shaft and the excavation of an underground research laboratory,

where the properties and behaviour of the formation will be studied in detail to provide data for a preliminary safety analysis. At this time, the screening process of the potential favourable sites has been initiated, but the opening of an underground research laboratory is still far along the road.

It is also clear that, for a crystalline rock, the hydraulic properties of the fracture network is one of the key issues that will be determinant in the assessment of the suitability of the site for HLW disposal. In a recent review of the French Radioactive Waste Disposal Program (Castaing et al., 1984), published by the Ministry of Industry, the issues considered of importance for a crystalline disposal site were (i) the hydrology of the fracture network and it spatial predictibility (ii) the evolution of these properties with time due to the excavation, to coupled thermo-mechanical processes and to natural geodynamic processes (iii) matrix diffusion as a potential retardation mechanism, the behaviour of colloïdal matter being taken into account (iv) the backfilling and sealing of holes, drifts and shafts (v) and finally the importance to be given to a "well scenario", when drinking water is withdrawn directly from a shallow well above a deep repository. Recent experience in France with the hydraulic testing of deep boreholes in granite of low hydraulic conductivity has indeed shown that, when the connectivity of the network is low, surface measurements are inefficient to understand the flow properties of the medium, and underground testing is necessary. It is therefore necessary to develop a methodology for hydraulic testing in an underground laboratory.

To this end, the Fanay-Augères Uranium mine was selected. Alike the Stripa site, Fanay-Augères is not a potential repository site, but appeared suitable for carrying the experiment. On the one hand the hydraulic conductivity of the fractured medium is rather high (10^{-8} m/s), which makes it possible to measure significant inflows of water easily, and to perform tracer tests with long travel distances in relatively short time periods. On the other hand, extensive studies of the fracture pattern in a large number of drifts in the mine, and of outcrops at the surface, were available, making it a rather unique facility for studying the geometry of the fracture network and its evolution with depth or at the vicinity of a major tectonic structure.

At this stage, we are already adressing the problem of the second goal of the experiment : relating the large scale hydraulic properties of the medium with small scale measurements. The basic idea behind the setting up of the experiment is (i) to relate the large scale flow rate in a fractured medium to small scale observations of the geometry and properties of the fracture network, and to the results of local injection tests, and (ii) to study the hydrodynamic dispersion in a fracture network for increasing travel distances of the tracer, to observe if an asymptotic diffusive behaviour can be reached and characterized by geometric properties of the fracture network, or if a different type of large scale behaviour must be used for predicting radionuclide transport. In a "real" underground research laboratory, it is believed that only small scale measurements will be feasible, from which large scale properties will have to be infered. Providing tools to make this inference is the goal of the scale effect experiment.

1.2. Data collection

The following data have been collected :

1.2.1. Fracture network description. A systematic survey of the eastern wall of the drift of the test section was made, where each fracture was numbered and the following properties determined : (i) type of element (diaclase, fracture, fault, dyke, fracture zone) (ii) aperture (iii) fracture filling (iv) presence of water (v) decompression (vi) rugosity (vii) length, position, and orientation in space of the element. A statistic over more than 1,000 fractures shows that, on the average, they are fairly short (only 6 % exceed 3.5 m). Two thirds of them do not have any noticeable aperture, and 44 % seem moist on observation.

The structural characteristics of all the discontinuities encountered by the exploration holes were studied on core samples and their spatial orientation determined partly by a core orientator, partly by taking prints of the boreholes. The various data gathered in these different ways (orientation, distance between fractures,...) were treated statistically. The average fracture density if high : around 6 fractures per linear meter in large-grain granite and 10 in a fine-grain one contiguous to the first (see example, figure 3).

1.2.2. Small scale hydraulic tests. These tests were performed on the 16 radial boreholes available in the drift. Their location is shown in figures 1 and 2.

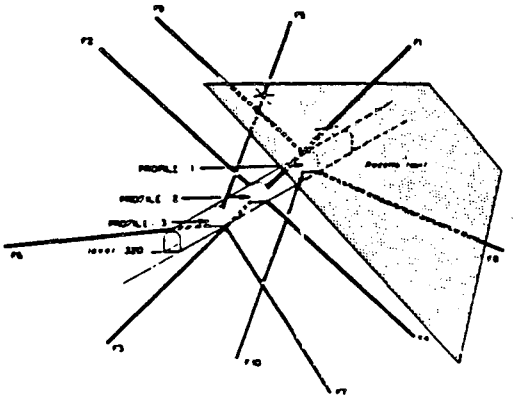

Figure 1. Perspective view of the experimental gallery at Fanay-Augères and of the three sections of the radial exploration boreholes.

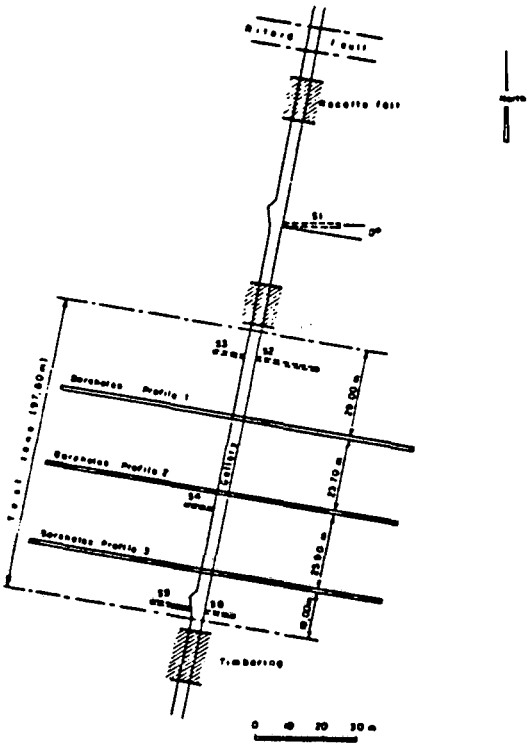

Figure 2. Plan view of the test zone
Fanay-Augères mine, Level 320
(175 m below ground)

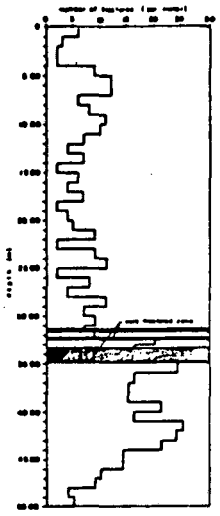

Fig. 3

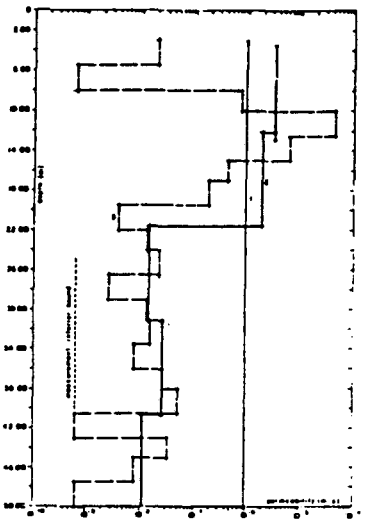

Fig. 4

Figure 3. Fracture density along the F9 borehole

Figure 4. Permeability log of borehole F4
curve 1 : global measurements
curve 2 : measurements on around 10 m chambers
curve 3 : measurements on 2 or 2.5 m chambers

The study of the inflow of water into the 6 short exploration wells was done with the help of a single packer moved in successive, 2 m steps and showed that the inflow points were generally localized in certain well-defined areas. The permeability in the ten 50 m boreholes was determined by injection of water at several prescribed pressures either behind a single packer of between double packers. Three lengths were chosen for the chambers : around 50 m, 10 m and 2 m (or 2.5 m). The permeability values obtained by these tests range from 1.10^{-6} to 3.10^{-8} m/s for the 50 m tests, from 8.10^{-6} and a value lower than 2.10^{-10} m/s (which corresponds to the lower limit of the capacity of the equipment) for the 10 m tests and from 5.10^{-5} to a value lower than 6.10^{-10} m/s for the 2 m and 2.5 m tests. Figure 4 shows the results obtained from the F 10 borehole in the form of a permeability log. The formation presents a strong permeability heterogeneity, which suggests localized outflows.

From a structural point of view, there is no direct relation between the fracture density in the formation and the measured permeability. In particular, it should be noted that the most highly fractured zones do not have the highest permeability. The main factors governing the hydraulic conductivity are the degree of aperture of the fractures and their interconnection.

1.2.3. Flow rate in the drift. Three small dams have been build above, in the middle, and below the experimental section ; the water coming from above is by-passed in a pipe connected donwstream ; the water collected in the test section is collected and measured with a flow meter. The total flow rate is close to 6 l/mn.

1.2.4. Pressure measurements. The six short boreholes have a single measurement chamber at their extremity ; the ten 50 m long boreholes have been equiped with 68 2 m long inflatable packers isolating 68 measurement chambers of 5 m in length in the average. Each chamber is connected to the drift by two rilsan tubing, to record the pressure, and also to permit flushing of the chamber or injection of a tracer. All this equipment has been in place since January 1985. A preliminary example of the pressure readings in the four boreholes of the 2nd profile is given in figure 5, for May 1985, in a transient situation and will be discussed in section 1.3. These pressures are expressed as m of water above the drift floor, and tend to fluctuate with rainfall or with external disturbances in the mine.

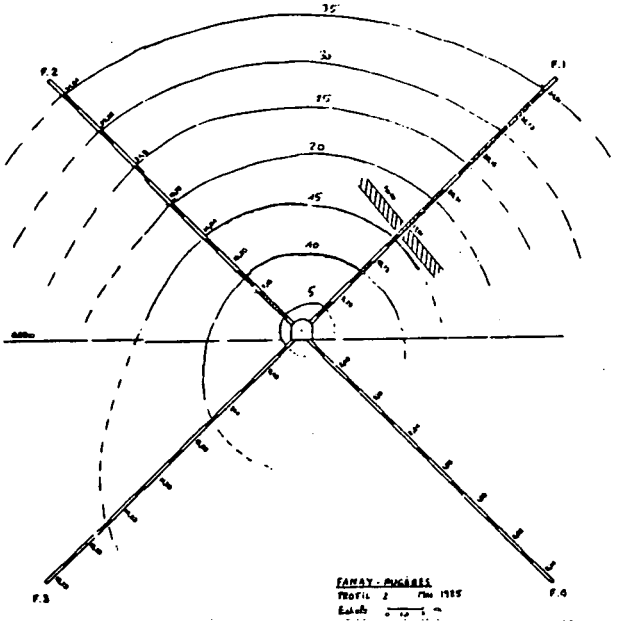

Figure 5. Measurements in the pressure chambers on the 2nd profile (4 boreholes) of the test section, and tentative map of hydraulic head (the head is measured from the floor of the drift).

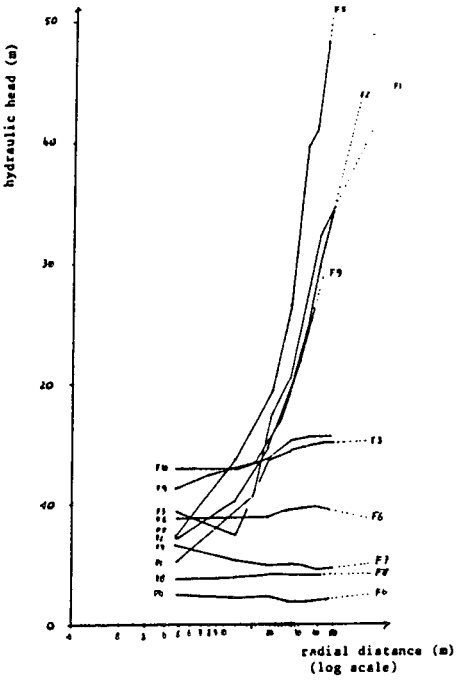

Figure 6. Hydraulic head in the pressure chambers as a function of the radial distance to the center of the drift, in the ten 50 m boreholes of the test section (log scale for the distance).

1.3. Interpretation of the measurements

1.3.1. Global interpretation. From the fracture density measurements and the estimated fracture length, one can show that the fracture network has a connectivity well above the percolation threshold. This threshold is approximately defined by $Nr^3 \geq 0.15$ to 0.30, where N is the fracture density, and r the average radius of the fractures, taken to be disks in three dimensions with random orientation. (For a discussion on the percolation threshold, see Long et al., 1982, Long, 1983, Schwartz et al., 1983, Engelman et al., 1983, Robinson, 1984, Guyon et al., 1984, Charlaix et al., 1984, Wilke et al., 1985, Marsily, 1985). The pressure pattern as shown on figure 5 is also an evidence that the fracture network is well connected : the pressure increases gradually with distance from the drift, especially in the upper holes. For such well connected systems, an equivalent continuous medium can be defined, and an average hydraulic conductivity estimated. The flow being essentially radial towards the drift (at least for the upper part of figure 5), one can see by plotting the head versus the log of the distance (figure 6) that a similar average behaviour for all radial holes oriented upwards is obtained after approximately 20 m in this case. This seems thus to be the scale at which a "Representative Elementary Volume" could be approximately defined, for flow problems, in this drift. This figure is interesting as earlier hydraulic tests performed elsewhere in the same mine with a length scale of 10 m had shown that it was not possible to define any average behaviour at such scale. Given the measured flowrate collected in the drift, the average equivalent hydraulic conductivity at this scale is in the order of 10^{-8} m/s.

It is necessary to explain, however, the pressure pattern observed in the holes oriented downwards. Although some perturbation by transient effects or by drilling done elsewhere in the mine is possible, we believe that the observations show the effect of the rather long length of the measurement chambers (5 m) relative to that of the packers (2 m). These chambers are by definition volumes of equal pressure, and can thus provide a preferential path for water flowing towards the drift. It is interesting to see that this effect is very different towards the east or the west of the drift (the same phenomenon is observed in the 2 other profiles), thus showing an effect of the anisotropy of the fracture pattern. Such an effect is not observed in the boreholes oriented upwards, as the chambers in these boreholes are not volumes of equal pressure : as the hydraulic gradient towards the surface in the medium is close to one, most of the measurement chambers are not filled up with water. They impose a seepage face condition which preserves the hydraulic gradient, and therefore they do no provide a preferential pathway for the flow to the drift. Incorporating this feature in the interpretation of the results is essential and will be done at the small scale.

1.3.2. Small scale interpretation leading to large scale behaviour. This work is presently underway, and no results are yet available. We will only briefly describe the three-step approach that will be used. The first step is to describe in detail the connectivity of the fracture network, using the fracture geometry data. The second step is to assign to each family of fractures an average directionnal hydraulic conductivity, expressed as a semi-

empirical formula involving all the observations made on the walls of the drift or on the cores. This formula will depend on a limited number of adjustable parameters, eg. 4 or 5 per family of fractures. The third step is to calibrate these adjustable parameters by fitting simultanously all the hydraulic measurements made in the drift using a network model of the fracture system. This fitting will be done automatically using an inverse minimization algorythm. The key assumption in this procedure is that the properties of the fractures can be described, in the average, family per family. In Fanay-Augères, approximately 5 families of fractures can be defined, based on the tectonic history of the formation. It is believed that these families have different hydraulic properties, which cannot be lumped into a single "average" fracture representing the global behaviour of the medium. Now for each family, the "average properties" are defined as an ensemble average, over all possible realisations of the fracture network, considered to be a random process. But using the assumption of ergodicity, this ensemble average is determined by spatial averaging the discrepancies between the local hydraulic measurements and the calculated ones using the global model, and not by spatially averaging the hydraulic properties themself. This ergodic hypothesis is seen as the basic tool to use small scale measurements for the determination of large scale behaviour. We will now briefly expand on these three steps.

Step 1. Fracture Network connectivity. This step is considered essential, as fractures can definitly not be considered as always infinite and connected. A 2-D or 3-D fracture network is generated randomly as in Long (1983), Robinson (1984), Rouleau (1984) or taking into account the spatial variability of the fracture density, as in Long and Billaux (1985). Conditionnal simulations of the fracture network (conditionned by the observations, as in Anderson (1985) will also be considered. The fracture shapes considered will be disks or parallelograms. From the geometrical description of the fracture system, a "connectivity" matrix will be determined : if two fractures intersect, their "centers" are connected : a non-zero entry will represent the direct link between the two nodes of the system. A zero value will be used otherwise.

Step 2. Hydraulic resistance to flow between two nodes of the network. We intend to use here a different approach than what has been done so far ; we believe that trying to solve the exact flow equations within each fracture plane is both too complex and unrealistic, since many totally arbitrary assumptions have to be made to correctly represent the flow : parallel plane, specified aperture, geometric shape of fracture (e.g. disks...), absence of fracture filling... We will therefore use here a Bayesian approach to determine the hydraulic resistance to flow between nodes in the connectivity matrix. An "a priori" estimate of this resistivity will be based on the descriptive properties which have been collected on the fractures by observation on the wall of the gallery or on the cores of the boreholes. These are defined as averages for each family of fractures and are : (i) type of element (diaclase, fracture, fault, dyke, fractured zone) ; (ii) aperture ; (iii) fracture filling ; (vi) presence of water ; (v) decompression ; (vi) rugosity. An empirical relationship between the hydraulic resistivity and these parameters for each fracture plane will be established, based also on the length of the connection between two nodes in each fracture plane ; the two resistivities forming the connection between two nodes (one for each fracture plane) are of course put in series to determine the unique resistivity between two nodes in the connectivity matrix. The empirical relationship between fracture properties for each family of fractures and hydraulic resistivity will be based on a limited number of linear coefficients weighing the importance of each factor.

Step 3. Calibration of the coefficients. Both the large scale permeability tests (with the prescribed geometry of the chambers and the small scale injection tests can be used for the calibration. Each steady state test will be defined by its boundary conditions, and the flow problem will be solved by inverting the "connectivity" matrix ; this assumes that the flow problem is simply defined by applying Kirchoff's law at each node, i.e. the principle of mass balance in each fracture plane ; note in this respect that the precise determination of what is really the "center" or "node" of each fracture is unimportant : since the flow equations are assumed linear, and since the resistivities between nodes are only parameters, any location within the fracture plane can be selected as node.

A calibration criterion will be defined, e.g. based on the differences between calculated and observed pressures (for the large scale tests) or calculated and observed flow-rates (for the injection tests). The calibration will consist in minimizing the criterion with respect to the unknowns of the empirical relationship between hydraulic resistivity and fracture properties. Given that a very limited number of unknowns will be determined in this way (4 or 5 per family or fractures) the computationnal time is expected to remain reasonnable.

The calibration criterion being based on a large number of measurements, the objective of this approach is to determine an "average" behaviour of each family of fracture, and thus the average large scale flow properties of the medium ; but the use of the connectivity matrix, which is totally based on the geometric description of the fracture network, and can be conditionned on small scale observations (wall of gallery, fractures of cores...), make it possible to also use local hydraulic measurements, like the injection tests between packers, for calibration in the same model : it represents both the large scale and the small scale features of fractured media, and nowhere makes any assumptions on the existence of a continuous equivalent medium, or a representative elementary volume. Once it has been calibrated, it can be used on a predictive mode to define average properties (to be used on another continuous equivalent model) and the local variability of the flow in local fracture systems.

The expected proof of the validity of this approach will be that the model calibrated independently on the large scale pressure measurements and then on the small scale injection tests will yield the same results : although preliminary tests have been started, this is yet entirely to be done. It is worthwhile noting that this type of approach can easily be extended to include any new type of measurements which can be made on fractured systems, e.g.

geophysical measurements, stress field, new interference tests (e.g. sinusoïdal) new parameters recorded, etc...

1.4. Hydrodynamic dispersion experiment

As indicated earlier, tracer tests will be carried out by injecting various tracers in several of the 68 injection chambers isolated in the ten boreholes of the test zone. The sampling of the water will be made in the flowing water arriving in the gallery, and not inside the formation. In a first phase, only conservative tracers will be used, but later on sorbing tracers or even colloids may be used.

The essence of the interpretation of this experiment will be very similar to what is planned for flow. Given the calibrated flow model, only a longitudinal dispersion mechanism will be determined, for each family of fracture. From the flow model, the flow path from any injection point will be determined, i.e. the proportion of the flow between each of the nodes of the connectivity matrix, from the injection point to the walls of the gallery. Between each connected node of the system, the flowpath will be decomposed into its two components, one in each fracture plane of the link. Inside one given plane, the transfer of solute will be represented by an empirical analytical transfer function, depending (through a limited number of linear coefficients) on the principal characteristics of each family of fractures. Between two nodes, the transfer of solute, for a pulse injection of tracer, will be given by the convolution of the two transfer functions for each of the two fractures which are interconnected. Between a series of interconnected nodes, the transfer is again given by the convolution of the transfer functions between two nodes. Finally, the arrival at the boundary (the walls of the gallery) is given by the weighted sum of all the transfer functions between the injection point and nodes at the gallery, all flowpath being considered, the weights being the relative flowrates (from the flow model) along each flowpath. The calibration of the unknowns (the linear coefficients of the transfer functions, for each family of fracture) will be made by minimizing a criterion based on observed and calculated concentrations, for a number of tracer tests. Similarly, the validation of this approach will be obtained if it is possible to calibrate the model with a first set of tracer tests, and obtain the same degree of calibration for another set, independently of the distance from the gallery at which the injection was made. If this validation proves successfull, the problem of the scale effect in fractured media will perhaps be better understood.

2. THE HYDRO-THERMO-MECHANICAL EXPERIMENT

2.1. Objectives

In the french HLW disposal program, the decision has been made that the maximum temperature which can be reached in any point of the rock formation must remain below 100°C. Two reasons contributed to this decision : (i) if the temperature is increased above 100°C, the level of complexity and uncertainty in the behaviour of the host rock is increased, as our knowledge and data base on mechanical and geochemical behaviour at high temperatures (both for the rock itself and for the backfill) becomes vanishingly small ; (ii) the economics of disposing early of heat-emitting waste is not favourable ; for reprocessed HLW, even if a temperature of e.g. 200°C was acceptable, the cost of building a repository accepting 20 years old waste is much higher than that for an older waste, with a maximum temperature of 100°C : interim surface storage is economically a better alternative. A period of interim storage on the order of 50 years is therefore considered, which makes it easier to keep the temperature in the repository below 100°C.

Nevertheless, the influence on the confinement of the large amount of heat which will be released by the wastes is considered determinant, and thus requiring experiments. The integrated amount of heat released by one canister of waste is estimated to $6\ 10^6$ kWh between year 50 and infinity, most of which is released in the first 1,000 year. It is unfortunately not possible at this stage to study this influence at the real scale, because the time frame (hundred of years) and the length scale (kilometers) is too large ; one must therefore restrict the study to a scaled experiment. At Fanay-Augères, the following choices have been made : (i) both the heating and the cooling phase of the heat load of waste must be studied ; (ii) the duration of the experiment is to be kept relatively short (less than one year, for this first phase) in order to avoid problems with the degradation of the measurement probles ; (iii) the coupled phenomena which will be studied are :

- the opening and closing of individual existing fractures
- the global hydraulic conductivity variation
- the deformation of the rock mass
- the generated stress field and residual stress field after cooling

(iv) modelling of the small scale behaviour to interpret the measurements should be used to extrapolate the results at the full scale of a HLW disposal vault ; therefore the geometry of the scaled experiment should be, if possible, representative of a real repository. With these goals in mind, the following plans have been made.

2.2. Design of the experiment

If a deep repository in a rock formation can be approximated by a point source in a spherical coordinate geometry, then the dimensionless parameters for heat conduction on such a system vary as t/R^2. This ratio was taken as the scaling factor. Using a time scaling factor of 10^{-5}, a 1,000 m deep repository is represented by a source 3.3 m below a planar surface. It was therefore decided to excavate a room 10 x 10 m in the Fanay mine, at a depth of 100 m below ground to represent the ground surface, and to use a planary heat source of approximately 1 m^2, 2 to 3 m below the floor of the room, to represent the repository. Several numerical calculations were then made to determine the heat source power as a function of time, with this geometry, with the following constraints : (i) the maximum temperature should be in the order of 100°C, reached in approximately 3 months ; (ii) in one year, the temperature should essentially return to the original value ; (iii) the thermal expansion of the rock mass should be larger than what is needed to close the fractures of the system ; (iv) the stress and strain field should be large enough to be measurable, particularly at the floor of

the room representing the ground surface.

A large number of preliminary calculations were made using a finite element code calculating the thermal field as a function of the heat output, then the thermal expansion and the stress and strain fields ; calculations were made in two-dimensions assuming an axy-symetric geometry along a vertical line orthogonal to the floor of the excavated room and a continuous equivalent medium. The following parameters were assumed for the granite thermal conductivity 2.5 $Wm^{-1}K^{-1}$; heat capacity 2.19 x 10^{6} $Jm^{-3}K^{-1}$; Young's Modulus 10^{10} Pa ; Poisson ratio 0.25 ; thermal expansion 8 x $10^{-6}K^{-1}$. Initially, a decaying heat source was considered, to represent a scaled equivalent to the real heat output of HLW. But it was found that a better stress field was generated using a constant heat output during 50 days, then shutting off the heater and monitoring the return to ambient temperature. The selected heat source is made up of fine parallel horizontal boreholes 0.146 m in diameter, 1.50 m in length and at 0.30 m from each other, with a total heat output of 1 KW. They are situated 3 m below the floor of the room (figure 7).

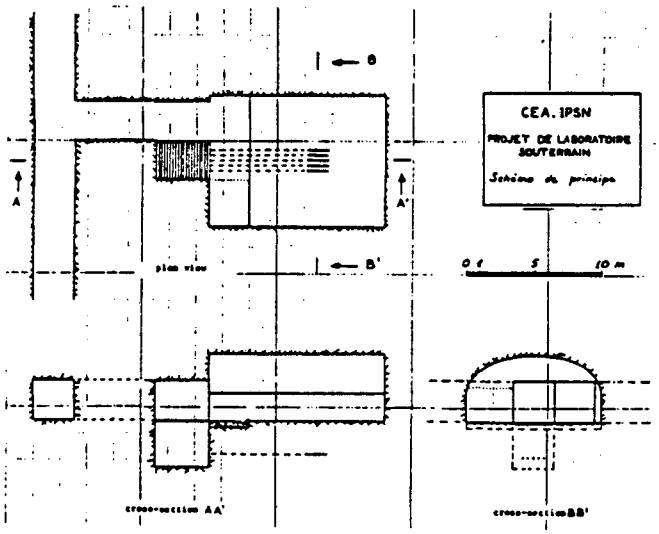

Figure 7. General lay-out of the hydro-thermo-mechanical experiment (excavated chambers and heated zone).

The maximum temperature obtained in 50 days is 103°C, and the temperature of the floor of the excavated room increases by 9°C only (figure 8). The deformation of this floor and the stress were found measurable.

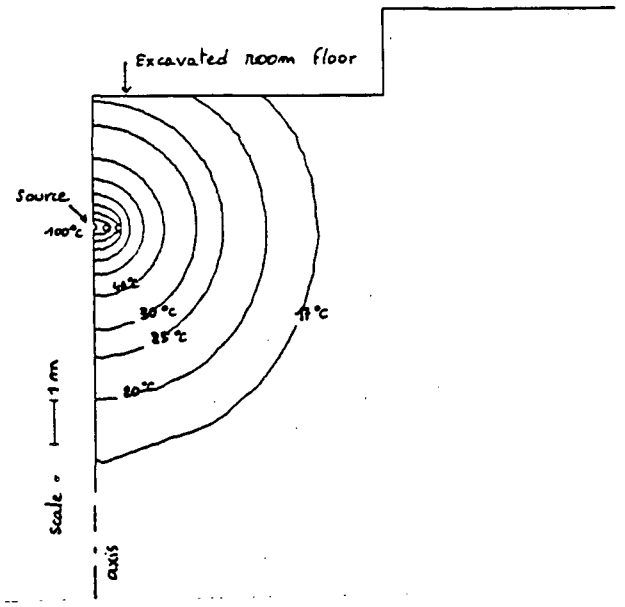

Figure 8. Vertical cross-section of the heated zone after 50 days, with the temperature isotherms °C.

2.3. Experimental program

During and after the heating phase (50 days at 1 kW) the following measurements will be made.

- Temperature distribution in the rock : 50 probes will be installed inside 10 small diameter boreholes, and 12 probes near the floor of the excavated room.

- Strain distribution : this will include 3 borehole extensiometers, and also a detailed survey of individual fractures, either on the floor (normal and tangential displacement), or within boreholes, for fractures orthogonal to the hole with a measurement of the normal displacement. The floor of the excavated room will also be levelled periodically.

- Stress distribution : 4 flat jacks will be installed at the floor, as no satisfactory equipment is available for boreholes. 38 pressure transducers will be used to monitor stress and strain in the locations of the flat jacks.

- Hydraulic pressure : 9 boreholes with 2 or 3 pressure measurements each, in very small chambers, will be installed at the boundary of the system, and inside the heated zone.

- Hydraulic conductivity : 10 boreholes will be used to access individual fractures, where hydraulic tests will be performed periodically.

- Flow rate : in the excavated chamber, the flow coming from the floor will be separated from that coming from the ceiling and the walls. Both will be monitored.

- Miscellanous parameters : the moisture content of the air, the temperature of the air and of the water arriving in the room will be monitored.

A total of approximately 150 parameters will thus be measured ; the data acquisition system will consist of a local measuring and recording device, connected to a minicomputer with large storage and ploting capacities, installed at the ground surface in a clean environment. At present, the equipment of the site is progressing, and the measurements should start in 1986.

2.4. Interpretation of the results

The major issue which will be studied with the proposed measurements is the variation of the hydraulic conductivity of the fracture network with the temperature and stress variations. Various coupled hydro-thermo-mechanical models will be used, incorporating the relationships which will be observed at a small scale (e.g. individual fracture properties) to reproduce the global behaviour. These models will in turn also be used to extrapolate the results to a real repository, using the flow model which has been described in the first section, for the scale effect experiment, but then modifying the fracture properties as a function of the temperature and stress distribution.

3. CONCLUSION

Both the scale effect and the hydro-thermo-mechanical experiments underway in the Fanay-Augères granitic mine are aiming at establishing a methodology which can further be applied to a potential HLW repository site, in a crystalline environment.

The large scale hydraulic conductivity measurements have already given significant results in term of the average behaviour ; the point of interest is now the feasability of relating this large scale behaviour to the small scale measurements. To this end, a model has been proposed, based on ergodic assumptions and on the distinction of the properties of each family of fractures. The hydrodynamic dispersion experiment is planned for late 1985.

The hydro-thermo-mechanical experiment has been planned to take place at a scale of ten meters, with a one year duration. The equipment of the facility is now underway, and tests will be conducted in 1986. It may be necessary, however, to consider in a later phase an experiment at a larger scale and for a longer time, if a scale effect is found which would preclude the extrapolation from the small scale to the real scale of a repository. But such a large scale test should then take place in a potential disposal site, not in a methodological laboratory.

REFERENCES

Anderson, J. (3-7 Juin 1985). Predicting mass transport in fractured rock with the aid of geometrical field data, Symposium International sur l'Approche Stochastique des Ecoulements Souterrains, AIRH, Montvillargenne.

Castaing, R. et al. (1984). Conseil Supérieur de la Sûreté Nucléaire. Rapport du Groupe de Travail sur les recherches et développements en matière de gestion des déchets radioactifs. Rapport Ministère du Redéploiement Industriel et du Commerce Extérieur, Paris.

Charlaix, E., Guyon, E., Rivier, N. (1984). A criterion for percolation threshold in a random array of plates, Solid State Comm., 20, 11, p. 999-1002.

Durand, E., et al. (Avril 1984). Etude de l'effet d'échelle en milieu fissuré. Phase pilote : certification du site de Fanay-Augères, Rapport CEA-BRGM-ENSMP, BRGM 84 SGN 237 STO.

Engelman, R., Gur, Y., Jaeger, Z. (1983). Fluid flow through a crack network in rocks. J. Appl. Mech., 50, p. 707-711.

Guyon, E., Hulin, J.P., Lenormand, R. (1984). Application de la percolation à la physique des milieux poreux, Annales des Mines, n° 5-6, p. 17-40.

Long, J.C.S., et al. (1982). Porous media equivalents for networks of discontinuous fractures. Water Resour. Res., 18, 3, p. 645-658.

Long, J.C.S. (1983). Investigation of equivalent porous medium permeability in networks of discontinuous fractures, Ph.D thesis, Lawrence Berkeley Laboratory, Univ. of California.

Long, J.C.S., Billaux, D. (3-7 Juin 1985). La génération aléatoire de champs de fractures : prise en compte de la variabilité spatiale de certains paramètres, Symposium sur l'Approche Stochastique des Ecoulements Souterrains, AIRH, Montvillargenne.

Marsily, G. de (Jan 7-12 1985). Flow and transport in fractured rocks : connectivity and scale effect, IAH International Symposium on the hydrogeology of rocks of low permeability, Tucson, USA.

Robinson, P.C. (1984). Connectivity, flow and transport in network models of fractured media, Ph.D thesis, Oxford, Theoretical Physics Division, AERE Harwell TP 1072.

Rouleau, A. (1984). Statistical characterization and numerical simulation of a fractured system. Application to a groundwater flow in the Stripa granite, Ph.D thesis, Univ. of Waterloo.

Schwartz, F.W., Smith, L., Crowe, A.S. (1983). A stochastic analysis of macroscopic dispersion in fractured media, Water Resour. Res., 19, 5, p. 1253-1265.

Wilke, S., Guyon, E., Marsily, G. de (1985). Water penetration through fractured rock : tests of a tridimensional percolation description, Mathem. geology, 17, 1, p. 17-27.

Wilson, C.R. et al. (1983). Large scale hydraulic conductivity measurements in fractured granite, Int. J. Rock Mech. Min. Sci. Geomech. Abst., 10, 6, p. 269-276.

RECENT PROGRESS OF THE NEA STRIPA PROJECT ON IN SITU EXPERIMENTS IN GRANITE ASSOCIATED WITH THE DISPOSAL OF RADIOACTIVE WASTES

Mr. S.G. Carlyle, OECD/NEA, 38 Bd. Suchet, 75016 Paris, France
and Dr. H. Carlsson, KBS/SKB, Box 5864, S-102 48 Stockholm, Sweden

ABSTRACT

The NEA Stripa Project has devoted considerable effort to the measurement and assessment of the hydrogeology, hydrogeochemistry and migration phenomena of the stripa granite and to the simulation of conditions likely to be found within an engineered repository in granitic rock. These include (i) the refinement of existing and the development of new, geophysical and hydraulic techniques for the mapping and characterisation of fractures in crystalline rocks; (ii) conducting field experiments to assess the migration of tracers in single and multiple fracture systems; and (iii) studying the behaviour of bentonite clay as a backfilling and sealing material in a granitic environment. The results and conclusions from Phase 1 of the project, and early results from Phase 2, were presented at a Symposium held in Stockholm, Sweden, in June 1985. This paper summarises the most important findings and outlines the main aims of possible future research under any Phase 3 of the project. The latter may well include making mathematical predictions of the hydrogeological behaviour of the stripa granite and their subsequent validation by field measurements.

INTRODUCTION

Granite rock is considered by many experts to possess properties which make it a suitable candidate for the isolation of radioactive wastes; in particular the highly active heat generating wastes that arise from nuclear power generation. Granites are typically very hard, massive, crystalline, igneous rocks. Their crystallinity means that the rock itself has a low permeability with any significant groundwater flow being restricted to joints and fissures within the rock mass. The latter characteristic is important when considering granite as a potential host for a radioactive waste repository, as the most probable mechanism by which radioactivity could return to man is via groundwater flow. In addition, the inherent stability of granite masses means that they are resistant to earth movements and the forces of erosion and weathering, and therefore a repository placed deep (300-700 metres) within a granite rock mass is very unlikely to be disturbed by climatic or geological events.

It is primarily these properties that have led to considerable research effort to be orientated towards the evaluation of hydrogeological and geochemical behaviour of granite with respect to its ability to contain radioactive wastes. Groundwater flow through granite is closely linked to the complex distribution and nature of fissures. This fact, coupled with the need to assess the potential impact of heat generating wastes on surrounding rocks, means that it is necessary to carry out in situ experiments under conditions which closely resemble those of an actual repository. It was this need that led to a major research programme being established based on experiments carried out at the Stripa Mine in Sweden. This was an abandoned iron ore mine in central Sweden where 400 metres of new drifts were driven, at a depth of 360 metres below ground, using "smooth wall" blasting techniques to provide a realistic repository-like environment.

Between 1977-80, a series of initial experiments were carried out at Stripa under the Swedish American Cooperative (SAC) Programme [1,2]. This was an exercise carried out jointly between Lawrence Berkeley Laboratory of the University of California under the sponsorship of the Department of Energy and the Division KBS of the Swedish Nuclear Fuel Supply Company (now known as the Swedish Nuclear Fuel and Waste Management Company, SKB). The main thrust of work under the SAC programme was to develop techniques to measure certain properties and phenomena including thermomechanical, hydrogeological, geophysical and geochemical aspects.

The NEA International Stripa Project began in May 1980 on the strength of the results of the SAC programme and the wide interest shown in other OECD Member countries. At the present time nine countries participate in the project: Canada, Finland, France, Japan, Spain, Sweden, Switzerland, United Kingdom and the United States. Co-ordination is provided by the OECD/NEA and project management is carried out by SKB. Two phases of research have been agreed: Phase 1 was carried out from 1980-85 and Phase 2 started in 1983 and is planned to be completed in 1986; under each phase research was carried out under five headings:

-- Hydrogeological investigations of the Stripa granite;

-- Migration within single and multiple fracture systems;

-- The detection and characterization of fracture zones in granite by cross-hole investigation techniques;

-- The hydrogeochemistry of groundwaters at the Stripa Mine;

-- The behaviour of bentonite clay as a backfilling and sealing material under field conditions; and

This paper summarises the results and conclusions from Phase 1 of the Stripa Project and the early results from Phase 2 as presented at a Symposium on the project held in Stockholm on 4th-6th June 1985.

HYDROGEOLOGICAL INVESTIGATIONS

Hydrogeological studies are carried out in order to test and develop techniques for hydrogeological investigations of an underground granitic environment and have included adapting and further developing available methods for determining hydraulic conductivity *in situ* using single, vertical and horizontal boreholes and between successive boreholes [3]. Three different types of hydraulic testing have been performed: pressure build-up tests; constant pressure injection tests; and interference tests. The pressure build-up tests have been performed in sections two metres long isolated by borehole packers. The sections being tested are selected on the strength of results from single hole geophysics and core logging. The evaluation was based on various types of cross-plotting techniques and subsequent comparison of results with theoretical models. It has been found that very careful evaluation is required in order to avoid misinterpretation. In order to obtain reliable results, especially in sections with low hydraulic conductivity, it is essential to take into account wellbore storage and skin effects. Provided this is done, it is possible to describe the hydrogeological conditions in terms of discrete flow regimes. One disadvantage of the pressure build-up tests is that they are time consuming. For example, in order to measure conductivities in the order of 10^{-12} m/s a total testing time of about two weeks is required.

Constant pressure injection tests have been performed in 10 metre sections along the entire length of four boreholes. The injection time for each test is two hours which has been found sufficient to measure hydraulic conductivities greater than 3×10^{-12} m/s. However, problems have been encountered where tests are affected by the build-up of formation pressure. This is most evident in horizontal boreholes where the formation pressure can become higher than the maximum injection pressure. Nevertheless, constant pressure injection is a comparatively fast testing technique; it gives fairly reliable data which is evident from the consistent results achieved by using different evaluation procedures.

Interference tests focus on the interconnections between highly conductive zones in one borehole and parts of other boreholes. The measurement starts as a pressure build-up test but a much longer build-up period up to three months is used. After the build-up period, the pressure in the selected source section is released and the resultant pressure changes are recorded in the receiver sections.

Investigation of the hydrogeological characteristics of the ventilation drift area of the mine has involved the collection of detailed information on the geometry and flow characteristics of the fracture system in the granite at Stripa. Fracture data collected in the vicinity of the ventilation drift has been analysed in detail to yield distinct fracture sets and fracture networks [4]. Flow rates predicted for these networks agree closely with the measured flow rates when the mean aperture used in the fracture network flow model is approximately equal to the mean aperture determined from borehole packer injection tests.

Hydrogeological research carried out in Phase 1 has demonstrated the need for co-ordinated surface and underground hydrogeological investigation of repository sites in granite in order to fully characterise the flow regime. No single method can be used in isolation if a thorough understanding is to be obtained.

MIGRATION STUDIES

Studies of migration within fractures began with an investigation of the flow within a single fracture and then progressed to a large-scale three-dimensional experiment. The aim of the study of flow within a single fracture was to observe the movement of non-sorbing (eg. Iodide and Uramine) and sorbing tracers (eg. Ceasium and Strontium) in situ and to interpret these movements in terms of the likely migration of radionuclides. Figure 1 gives a schematic view of the test site for this study. The results show that flow in the two fractures examined was unevenly distributed and it is estimated that flow takes place in channels making up between 5-20 per cent of the fracture surface [5]. Figure 2 gives a diagramatic representation of this concept for flow within a fracture. The sorbing tracers did not reach the sampling holes which was found to be due to sorption on the fracture surface. Examination of the rock matrix revealed that in some instances tracers had migrated several millimetres into the rock matrix which confirmed similar measurements made in the laboratory.

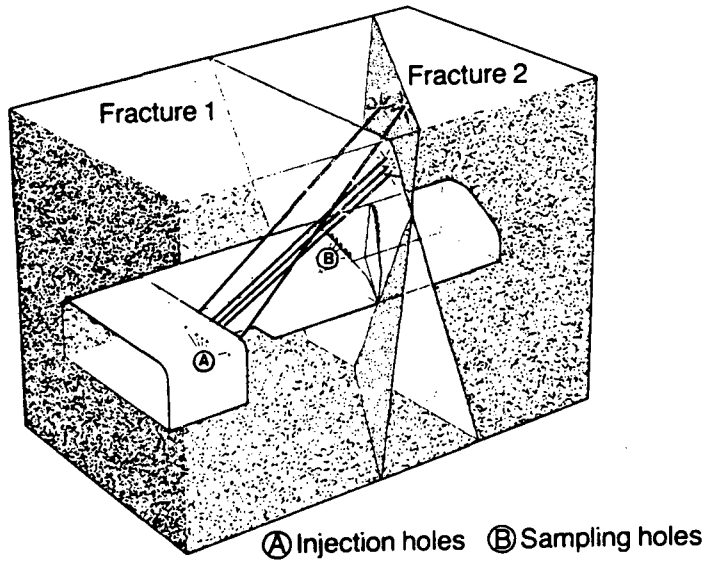

Figure 1. Schematic representation of the test site for the migration in a single fracture study [5]

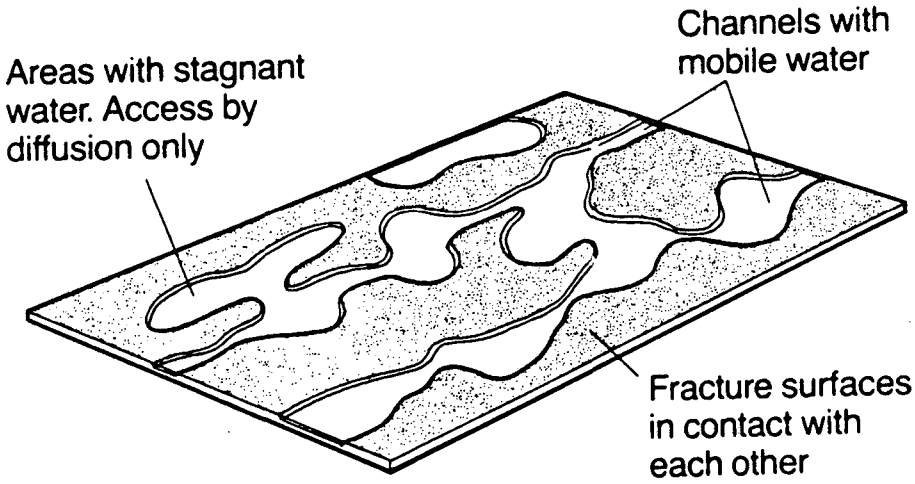

Figure 2. Diagramatic representation of flow in a single fracture [5]

The results and experience gained from the single fracture study were utilised in planning a three-dimensional migration test being performed in Phase 2 of the project. The objective of this study is to obtain an understanding of the spacial distribution of water flow pathways in crystalline rock over distances up to fifty metres. Figure 3 shows the layout of the 3-D test facility. A series of tracers have been injected from three vertical boreholes and Figure 4 shows the pre-test high water flow points and early results of tracer emergence. These preliminary results indicate that water does not flow uniformly within fractures but seems to be localised to wet areas with large regions of very low water flow in between [6]. In addition, it is now thought that flow on this small scale cannot be described by a homogeneous porous media flow model.

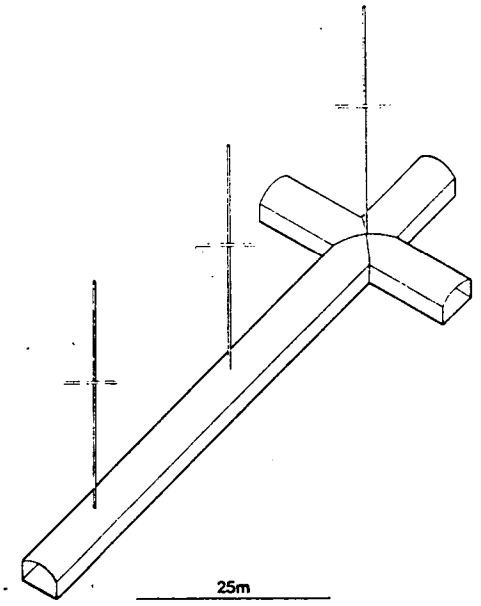

Figure 3. Layout of the 3-D test site with the three vertical injection holes [6]

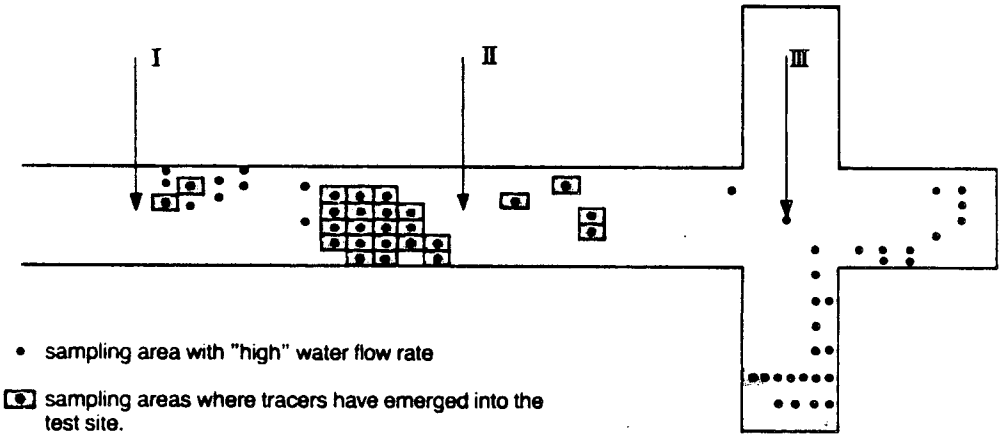

Figure 4. Sampling areas that have "high" water flow rates and in which tracers have been found [6]

CROSS-HOLE INVESTIGATIONS

From the point of view of disposal there is need to have an adequate understanding of the hydrological characteristics of the rock surrounding a repository in order to predict its performance as a medium for containing radioactive wastes. The primary purpose of the cross-hole investigations is to develop methods and procedures for determining the location, extent, thickness and dominant physical properties of fracture zones. These developments are necessary due to the highly complex distribution and characteristics of fractures within granite rock masses.

To date much of the work carried out has been concentrated on the development of reliable tools to carry out measurements. Again no single tool is regarded as having the capability to furnish sufficiently reliable hydrological information, and so seismic, radar and hydraulic testing methodologies are being examined. Conventional

seismic investigation tools are being used in conjunction with a newly developed tomographic analytical method which can provide a 2D or 3D picture of the area being investigated [7,8]. Investigations have been carried out at a regional scale site at Gidea and on a smaller scale in the Stripa Mine. Single hole reflection measurements have now been performed in several boreholes in the Stripa Mine with a radar system developed within the Stripa Project [9,10]. Figure 5 shows the principle of borehole radar reflection measurements and the patterns generated by plane and point reflectors. The reflection measurements show good resolution indicating major fracture zones. It has been found possible to identify reflections from the larger fracture zones up to a distance of 115 metres from the boreholes. Tests made with a high frequency version of the system (50 MHz) have given reflections from water filled boreholes which have a diameter of only 76 millimetres. Cross-hole radar measurements have recently begun and work is continuing on the use of tomographic analytical techniques to aid the analysis of the data.

Cross-hole investigations using hydraulic techniques are also under development at Stripa [11]. Initially single hole hydraulic measurements were carried out involving the determination of hydraulic conductivity and head along 10 metres sections. At first, there was generally a poor correlation between single hole geophysics and geology and the results from hydraulic conductivity. It was thought that improvements could be made by conducting cross-hole measurements between boreholes spaced up to 45 metres apart. This was carried out using hydraulically conductive sections of the holes as source zones. Sinusoidal tests are used where low frequencies (long periods) are measured first and then the frequency is increased until no further data is received. The results indicate that fissure - rock matrix interactions occur and groups of fissures have been delineated [12]. Work is now in hand to correlate the hydraulic measurements to those from seismic and radar studies.

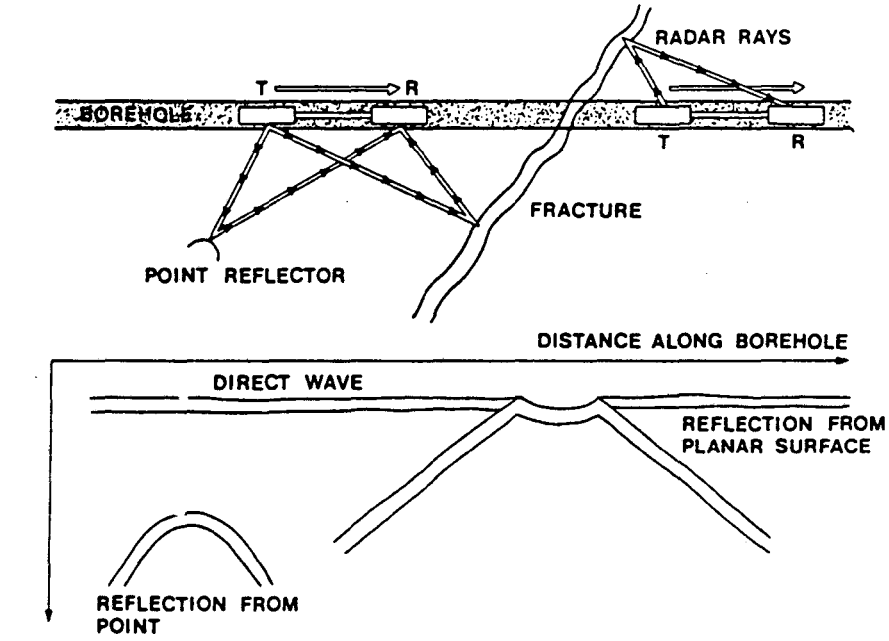

Figure 5. Principle of the borehole reflection radar and the patterns generated by plane and point reflectors [10]

HYDROGEOCHEMICAL INVESTIGATIONS

Hydrogeochemical investigations are carried out at Stripa in order to gain an understanding of the origin and evolution of the groundwater and to develop procedures and methodologies for hydrogeochemical investigations at potential radioactive waste disposal sites [7,8]. The geochemical data obtained at Stripa are consistent with the hydraulic conductivities inferred from hydraulic tests. The groundwater at Stripa is thought to have originated as fresh meteoric water that infiltrated during a cooler climate and reacted to a considerable extent with the crystalline bedrock. The water-rock interactions are still in progress and the water chemistry is heavily influenced by present-day reactions (e.g. precepitation-dissolution reactions, redox processes and subsurface radionuclide production). The high salinity of the deep Stripa groundwater is thought mainly due to fluid inclusions. The Total Dissolved Solids (especially chloride) indicates that there is little or no mixing of water between fracture zones.

It is concluded that it is not meaningful to speak of the "age" of groundwater. It is considered relevant to speak instead of the mean residence time of a specific constituent in the groundwater. The ^{14}C data suggest mean residence times greater than 20 000 years for water in the deeper zones. Younger water (less than 50 years) has infiltrated in parts of the mine.

Phase 1 of the hydrogeochemistry programme has given a much improved understanding of the general processes that control the chemical and isotopic composition of deep groundwaters in crystalline bedrock. The usefulness of techniques for groundwater sampling and analysis, some of them applied for the first time, have been evaluated. The work also included the development of a general geochemical concept and model for groundwater processes in crystalline rock. The hydrogeochemistry of the groundwaters of Stripa cannot be considered unique, for example, they show similarities with the saline groundwaters in the crystalline rocks of the Canadian Shield.

INVESTIGATIONS OF BENTONITE AS BUFFER, BACKFILL AND SEALING MATERIAL

The large scale Buffer Mass Test at Stripa was designed to test predictions of the behaviour of certain bentonite-based buffer materials when heated under field conditions. Blocks of sodium bentonite were placed in a series of six large diameter boreholes containing heaters to simulate the heat output from a spent fuel canister. In addition, the tunnel above two of the heater boreholes was backfilled with a sand/bentonite mixture. Figure 6 outlines the main features of the Buffer Mass Test. During the test, temperatures, moistering of the buffer materials and the associated build-up of swelling pressures and piezometric head were measured. The results compared very well to the predicted behaviour of the buffer materials [9]. It was therefore concluded from the Buffer Mass Test that the main physical processes are understood and can be predicted for various repository geometries. The dominant process is the uptake of water from the surrounding rock mass since it governs the build-up of temperature and swelling pressures. This uptake is primarily related to the water-bearing capacity of the surrounding rock, i.e. through the presence of one or a few hydraulically active joints or fractures. The inference from the validation of the predicted behaviour of bentonite-based buffer materials by realistic field measurements, is that the material performs the task of isolating a heated canister very well and that the techniques used for its preparation and application are more than adequate.

The Borehole, Shaft and Tunnel Sealing Project, which began in 1983 and will be completed in 1986, consists of four individual plugging tests using sodium bentonite [10]. Two of the tests deal with borehole sealing, with the aim of assessing techniques used for inserting bentonite plugs in boreholes of varying length and to study the maturation rate of bentonite. In the shaft plugging test, bentonite/rock interactions are investigated to assess the sealing capabilities of bentonite. The difference in behaviour with blasted and slot-drilled rock are being assessed with particular emphasis on the influence of water-bearing structures. Finally, the tunnel plugging test is designed to demonstrate the construction phase and general isolating power of a full-scale backfilling and sealing exercise. It can be seen that each of these tests are designed to test the sealing ability of sodium bentonite by exposing the plugs to hydraulic gradients of varying magnitude. This ability is due to the very low hydraulic conductivity of sodium smectite, the major constituent of the bentonite, and the high swelling pressure exerted on the surrounding rock mass. The swelling creates a tight contact with the rock and tends to close certain joints and fractures in the rock adjacent to the bentonite plugs.

FUTURE EXPERIMENTAL INVESTIGATIONS AT STRIPA

The majority of work carried out under Phase 1 and 2 of the project involved the development of tools and methods for comprehensive site investigations. It is considered that any Phase 3 of the project should concentrate on the detailed assessment of an

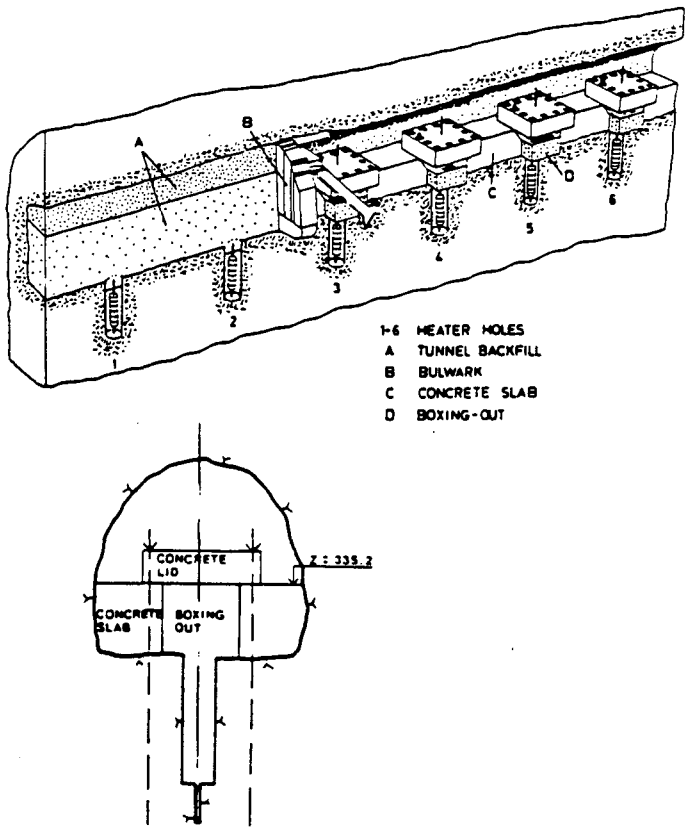

Figure 6. Main features of the Buffer Mass Test [15]

undisturbed area of granite using available tools and in particular those methods and procedures developed during Phases 1 and 2. An interdisciplinary approach would be used where the needs of those carrying out safety analyses would largely guide the search for information. For example, the hydrological characteristics of the research area would be modelled based on information gained during an initial general hydrological investigation and the model would then be validated by further investigations or experiments. If the model is not validated then further improvements would be made. Concurrent with this primary study would be the necessary continuation of existing studies in order to examine specific aspects of the behaviour of a repository in granite.

Also suggested for study in any Phase 3 under the heading of engineering design studies, are the behaviour of alternative sealing materials that could be used in a repository. With a view to possible licensing requirements, the longevity of sealing materials is thought particularly important. Particular emphasis would be given to testing methods and procedures. In addition, research into methods of treating the rock surface to improve sealing or isolation properties was also suggested as a possible topic for study.

CONCLUDING REMARKS

Although much of the work to date under the Stripa Project has involved the development of techniques for the detailed investigation of a repository site, a number of conclusions can be drawn regarding the measurement and mathematical modelling of coupled processes in granitic rocks. The main conclusion must be that there is great difficulty in measuring detailed hydrogeochemical processes, due to the natural heterogeneity of flow patterns in granite. Flow has been found to be extremely variable and hence any predictions of likely flow regimes would at the present time have a high degree of uncertainty. It must be emphasised, however, that the large scale behaviour of granite as a barrier to migration can be predicted to be very effective.

A further conclusion can be reached on the necessity to use an integrated approach to detailed investigations. A combination of standard hydrological tests and cross-hole measurements, including seismic, radar and hydraulic techniques, together with hydrogeochemical analyses and migration studies, needs to be used in order to develop a comprehensive picture of the processes operating at a specific site. No single technique can be used to yield sufficient information. Finally, it is only by developing a detailed understanding of the hydrogeochemical processes operating at a particular site that existing predictive flow models can be adapted to that site. It is on these broad lines that any Phase 3 of the Stripa Project will be orientated.

REFERENCES

[1] Proceedings of the NEA Workshop on Geological Disposal of Radioactive Wastes - In Situ Experiments in Granite, OECD/NEA, Paris 1983

[2] Robinson R.A. (1985), "Summary of Results and Conclusions From the Cooperative Project at Stripa Between Sweden and the United States During 1977-1980", Proceedings of an NEA Information Symposium on In Situ Experiments in Granite Associated with the Disposal of Radioactive Waste, Stockholm, Sweden, 4-6 June 1985, OECD/NEA (In press)

[3] Carlsson L., Olsson T. (1985), "Hydrogeological Investigations, Results and Conclusions", Proceedings of an NEA Information Symposium on In Situ Experiments in Granite Associated with the Disposal of Radioactive Waste, Stockholm, Sweden, 4-6 June 1985, OECD/NEA (In press)

[4] Gale J.E., Rouleau A. (1985), "Hydrogeological Characterization of the Ventilation Drift Area", Proceedings of an NEA Information Symposium on In Situ Experiments in Granite Associated with the Disposal of Radioactive Waste, Stockholm, Sweden, 4-6 June 1985, OECD/NEA (In press)

[5] Abelin H., Moreno L., Tunbrant S., Gidlund J., Neretnieks I. (1985), "Flow and Tracer Movement in Some Natural Fractures in the Stripa Granite, Results From the Stripa Project Phase 1", Proceedings of an NEA Information Symposium on In Situ Experiments in Granite Associated with the Disposal of Radioactive Waste, Stockholm, Sweden, 4-6 June 1985, OECD/NEA (In press)

[6] Birgersson L., Abelin H., Gidlund J., Neretnieks I. (1985), "Water Flow Rates and Tracers Transport to the 3-D Drift in Stripa", Proceedings of an NEA Information Symposium on In Situ Experiments in Granite Associated with the Disposal of Radioactive Waste, Stockholm, Sweden, 4-6 June 1985, OECD/NEA (In press)

[7] Cosma C. (1985), "Detection of Fractured Zones by Cross-Hole Seismics", Proceedings of an NEA Information Symposium on In Situ Experiments in Granite Associated with the Disposal of Radioactive Waste, Stockholm, Sweden, 4-6 June 1985, OECD/NEA (In press)

[8] Pihl J., Gustavsson M., Ivansson S., Morén P. (1985) "Tomographic Analysis of Cross-Hole Seismic Measurements", Proceedings of an NEA Information Symposium on In Situ Experiments in Granite Associated with the Disposal of Radioactive Waste, Stockholm, Sweden, 4-6 June 1985, OECD/NEA (In press)

[9] Olsson O., Forslund L., Lundmark L., Sandberg E., Falk L. (1985), "The Design of a Borehole Radar System for Detection of Fracture Zones", Proceedings of an NEA Information Symposium on In Situ Experiments in Granite Associated with the Disposal of Radioactive Waste, Stockholm, Sweden, 4-6 June 1985, OECD/NEA (In press)

[10] Olsson O., Falk L., Sandberg E., Carlsten S., Magnusson K.A. (1985), "Results from Borehole Radar Reflection Measurements", Proceedings of an NEA Information Symposium on In Situ Experiments in Granite Associated with the Disposal of Radioactive Waste, Stockholm, Sweden, 4-6 June 1985, OECD/NEA (In press)

[11] Holmes D.C., Sehlstedt M. (1985), "Cross-Hole Investigations - Design of the Hydraulic Testing System", Proceedings of an NEA Information Symposium on In Situ Experiments in Granite Associated with the Disposal of Radioactive Waste, Stockholm, Sweden, 4-6 June 1985, OECD/NEA (In press)

[12] Black J.H., Barker J.A. (1985), "Cross-hole Investigations - Preliminary Results of Single-Borehole Hydraulic Tests and Early Cross-hole Sinusoidal Measurements", Proceedings of an NEA Information Symposium on In Situ Experiments in Granite Associated with the Disposal of Radioactive Waste, Stockholm, Sweden, 4-6 June 1985, OECD/NEA (In press)

[13] Nordstrum D.K., Andrews J.N. (1985), "Progress on Geochemical Investigations of Water-Rock Interactions at Stripa", Proceedings of an NEA Information Symposium on In Situ Experiments in Granite Associated with the Disposal of Radioactive Waste, Stockholm, Sweden, 4-6 June 1985, OECD/NEA (In press)

[14] Fritz P., Fontes J.C., Frape S.K. (1985), "Stable Isotope and Radiocarhon Analyses at the Stripa Test Site - Phase 1, Proceedings of an NEA Information Symposium on In Situ Experiments in Granite Associated with the Disposal of Radioactive Waste, Stockholm, Sweden, 4-6 June 1985, OECD/NEA (In press)

[15] Pusch R. (1985), "The Buffer Mast Test", Proceedings of an NEA Information Symposium on In Situ Experiments in Granite Associated with the Disposal of Radioactive Waste, Stockholm, Sweden, 4-6 June 1985, OECD/NEA (In press)

[16] Pusch R. (1985), "The Borehole, Shaft and Tunnel Sealing Test", Proceedings of an NEA Information Symposium on In Situ Experiments in Granite Associated with the Disposal of Radioactive Waste, Stockholm, Sweden, 4-6 June 1985, OECD/NEA (In press)

AN OVERVIEW OF SOME GEOTECHNICAL EXPERIMENTS WITHIN THE CANADIAN NUCLEAR FUEL WASTE MANAGEMENT PROGRAM

K.W. Dormuth

Atomic Energy of Canada Limited
Whiteshell Nuclear Research Establishment
Pinawa, Manitoba R0E 1L0

ABSTRACT

Within the Canadian Nuclear Fuel Waste Management Program, extensive geotechnical experimentation is being carried out on processes of significance to the safe disposal of nuclear fuel waste in fractured plutonic rock. Examples of experiments conducted in the program illustrate the relationship between mathematical models and field information.

INTRODUCTION

An extensive program of geoscience research is being conducted as part of Canada's Nuclear Fuel Waste Management Program. The purpose of this research is to establish the technology for safely disposing of nuclear fuel waste deep within plutonic rock of the Canadian Shield. The focus on plutonic rock arises from consideration of probable suitability of the rock type in the Canadian context (Dormuth and Scott, 1984).

The experimental program is designed to develop the necessary understanding of processes that may significantly affect the performance of a disposal vault, and to develop a methodology for characterizing a plutonic rock mass to evaluate its suitability for isolating nuclear fuel waste.

An important aspect of the program is that results must be "transportable" to sites other than those at which the research is carried out, because the current program calls for an assessment of the concept of disposal in plutonic rock in generic (as opposed to site-specific) terms. This leads to an emphasis on the use of site-specific research to develop a methodology that has a broad application. In particular, the development and validation of mathematical models, soundly based on field observations, are major objectives of the experimental program.

The following sections briefly discuss the experimental program in the disciplines of geophysics, geology, geomechanics and hydrogeology. Examples are given of experiments in each of the areas. No attempt is made to be comprehensive. Instead, emphasis is placed on a few examples that indicate the use of experimental procedures in the development of models having broad application.

GEOPHYSICS

Research in geophysics is directed at developing an exploration technology to detect and evaluate the structural characteristics of rock masses of relatively high integrity and uniformity. The program consists of (i) testing previously existing and newly developed exploration techniques for the evaluation of rock masses and (ii) through application of these airborne, surface and subsurface techniques, providing the field data necessary for the development of concepts and models that form the basis for site-selection criteria and safety analyses.

An experiment conducted at the site of a gabbro-anorthosite pluton at East Bull Lake near Massey, Ontario, was used to test the ability of gravity surveys to determine the size of a plutonic rock body (Niblett et. al, 1985). A detailed residual gravity map of a 12-km^2 area including the body was prepared from gravity surveys of Reford (1982, 1983) and Watson (1982). Densities of rocks in the area were determined from measurements of over 1900 rock samples collected from the pluton and surrounding rocks. The mean density of gabbro samples from the pluton is 2.93 g/cm^3 and that of the anorthosite samples is 2.85 g/cm^3. The mean density of samples of the surrounding granitic basement rocks is 2.65 g/cm^3. This information was used by Reeves (1983) to produce two- and three-dimensional models of the pluton. Both models indicated the maximum vertical thickness of the pluton to be about 400 m.

A cored borehole was drilled near the location of maximum residual gravity to determine the thickness of the pluton and test the gravity models. It penetrated granitic basement rocks at 773 m, indicating that the gravity models underpredicted the maximum depth of the pluton by 50%.

It has been conjectured that the discrepancy may have been caused by failure to account for significant amounts of diabase (density 3.03 g/cm^3) encountered during drilling, or by surface samples having densities that are not representative of the basement rock at depth.

Regardless of the explanation for the discrepancy, the experiment gives an indication of the accuracy that can be expected from this method in determining the depth of a gabbroic body without drilling. The accuracy is quite adequate for use in initial surveys in site screening. It is interesting that earlier simpler models by Watson (1982) indicated a maximum thickness of 500 m to 770 m. This would imply that simpler survey models are adequate for initial field surveys.

GEOLOGY

In the geological research program, great emphasis is placed on the determination of structural features that could affect the structural stability of the rock and its ability to conduct groundwater. The extent to which surface observations may be used to make inferences about structural features at depth is considered to be an important subject for investigation. Effective

methods of making such inferences would minimize the number of boreholes needed in site investigations, thereby decreasing the cost and maintaining maximum possible integrity of the rock.

An experiment was conducted on a pluton, during the summer of 1984, near Atikokan, Ontario, to test a methodology for integrating surface geological and geophysical data from one area (the prediction area) of the pluton with surface and subsurface data from elsewhere on the pluton (the control area), to predict subsurface fracture conditions, to a depth of 1 km, at the prediction area (Brown and Rey, 1985). The prediction area selected was expected to have relatively few fractures (an intrablock) on the basis of regional geological and geophysical data, confirmed by subsequent detailed ground work. This intrablock is bounded by major faults.

A borehole was sited in the intrablock area so that it would avoid major structural discontinuities on the basis of information available before drilling. However, it was recognized that, at depth, the borehole might intersect one of the major faults bounding the intrablock.

The predictions made of fracture conditions to be encountered in the borehole took the form of probability distributions of smaller scale fractures. Fracture data from an existing set of five cored boreholes at the control area were used to establish a relationship between surface fracture data and subsurface data at that location. For the control area, the distributions of fracture orientations derived from the subsurface data were similar to those derived from surface data, except for those orientations that could not be sampled properly in the subsurface because of the trend of the boreholes. Examination of the depth dependency indicated that the fracture population below about 180 m is statistically different from that of the upper 180 m. This difference was accounted for in the predictive analysis.

It was expected that the subsurface environment at the prediction area would differ from that at the control area, since the latter contains major structural discontinuities, whereas none were indicated by surface data within the intrablock. On examining data from sections of the boreholes at the control area that were intersected by faults and comparing them with sections not near faults, it was concluded that there is a strong decrease in fracturing with depth in intrablock areas, whereas in fault environments there need not be a strong decrease and, in fact, in a faulted environment fracturing can increase with depth. That a strong decrease in fracturing should occur in an intrablock area is borne out by analysis of data taken from boreholes in an intrablock of the Lac du Bonnet Batholith, some 300 km away. The less systematic behaviour of the fault environment precluded a prediction of these environments at depth.

Also, moderate dipping to subhorizontal fracture zones may occur in the subsurface, which cannot be predicted on the basis of surface mapping. In fact, a detailed seismic survey of the prediction area revealed a minor reflector at a depth of ~ 210 m, which might indicate such a zone. The prediction included a suggested modification to be applied to the distribution if such a zone were encountered, based on analysis of fracture data from similar environments in other boreholes. The seismic survey also indicated that the borehole would intersect one of the major boundary faults at a depth of 800-1000 m. No attempt was made to predict the fracture environment related to this fault.

On the basis of these observed relationships, fracture data from surface mapping at the prediction area were used to predict fracturing patterns in a borehole drilled at that area. The borehole was drilled and data from it were compared with the predictions.

The observed frequency distribution in the upper 150 m agreed well with the predicted distribution. The borehole fracture frequency distribution appears to be bimodal, which was not predicted. However, observed and predicted median values and standard deviations are in good agreement.

A subvertical fracture zone was encountered at 270 m to 300 m downhole that was not predicted. If this fracture zone is excluded from the data, the predicted distribution approximates the observed distribution well from 150 m to 400 m downhole. As in the case of the near-surface data, the major difference between the predicted and observed distributions is that the subsurface data show a bimodal distribution. The median values and standard deviation of the two distributions are similar.

Four small fracture zones with moderate to subhorizontal dip were intersected between 400 m and 650 m. The possibility of occurrence of this type of zone was stated in the prediction, and the effect on the predicted fracture distributions defined. The predicted distributions, when modified to account for the zones agree, fairly well with the observed distributions, although the agreement is not as good as in the previous two cases.

From 650 m to 800 m the borehole intersected a contact zone between the central core of the granite and a marginal monzodiorite phase. The contact was recognized at surface, but not predicted to intersect the borehole at depth.

From 900 m to the bottom of the borehole at 1206 m, a fault environment was encountered. This intersection of the boundary fault with the borehole was predicted on the basis of information from the seismic survey. No attempt was made to predict the fracture distributions associated with the fault.

Overall, there appears to be a good basis for inferring subsurface fracture orientation and frequency distributions from surface data and limited borehole information, at least to depths of about 400 m. However, major anomalies did occur, i.e. the subvertical zone at 270 m and the lithological contact from 650 m to 800 m, which were not predicted. Allowance must be made for such occurrences in evaluating potential sites for disposal.

HYDROGEOLOGY

The objective of hydrogeological research is to define the physical and chemical characteristics of groundwater flow systems at scales relevant to the analysis of potential radionuclide migration from a disposal vault. The research program began by developing methods to measure physical and chemical properties of groundwater within individual boreholes and individual fractures. It has progressed toward developing methods to determine these parameters for the larger site and regional scales.

The construction of the Underground Research Laboratory (URL) near the town of Lac du Bonnet in Manitoba, Canada, has been used to perform an experiment to test our ability to use information obtained from the surface and from boreholes to model the hydrogeological behaviour of a plutonic rock mass on the kilometre scale. The laboratory is being excavated in a large granitic batholith. The experiment serves as a validation of theoretical methods employed as well as of methods of generating model parameters from field observations.

The experiment (Davison and Guvanasen, 1985) consists of four phases: (i) geological and hydrogeological characterization of the URL site before excavation of the shaft, (ii) development and calibration of hydrogeological models of the site based on pre-excavation observations, (iii) prediction of the changes in the groundwater regime that will occur due to excavation of the URL, and (iv) comparison of predictions with observations of the changes in the groundwater conditions during and subsequent to excavation. The first three phases are complete, and preliminary results are available from the fourth phase.

Subsurface information is provided by an extensive program of borehole drilling, logging, testing, instrumentation and monitoring. The borehole array consists of 58 water-table wells in unconsolidated overburden, 41 shallow bedrock holes (10 to 60 m long), and 25 deep boreholes (about 100 m to 1100 m long). Fracture information, from the entire network of boreholes, and hydraulic testing were used to develop a conceptual model of the structural controls and boundary conditions affecting groundwater flow at the site. The conceptual model was used as a basis for the development of numerical models for predicting the changes that would occur to the hydrogeological conditions during and after excavation.

Several groups of mathematical modellers were given the information from the characterization program and asked to independently make the prediction. Two modelling teams, AECL and INTERA, have completed the exercise to the point of making predictions of the rate of inflow of groundwater to the excavation and the drawdown of piezometric levels surrounding the excavation. INTERA used the three-dimensional finite-difference program SWIFT and AECL used the three-dimensional finite-element program MOTIF. Both models were calibrated using long-term head measurements and inter-borehole pumping tests, and the calibrated models were used to predict the transient.

Preliminary comparisons of model predictions with observed changes in the hydrogeologic conditions have thus far been completed only for the AECL model. The change in piezometric conditions in the rock mass with time is in general, predicted well by the model. Discrepancies do occur very near the excavation where the model under predicted the drawdown. However, at most observation points, the predicted spatial and temporal distribution of the drawdown is in good agreement with observation. The overall trend in predicted rate of inflow into the excavation also agrees well with observation. The magnitude of the inflow is, in general, over-predicted by a factor of three. Discrepancies are thought to be contributed to by several factors, including deviations of actual excavation rates from assumed rates, the existence of vertical fractures connecting the shaft with a highly conductive subhorizontal fracture zone, and the effect of stresses caused by excavation on the local hydraulic conductivity of the rock. It should be emphasized that the discrepancies are very small in comparison with the variability in values of hydraulic parameters in the rock mass. The overall agreement between observation and prediction is considered to be extremely good.

GEOMECHANICS

Geomechanics research is being carried out to elucidate the response of a jointed plutonic rock mass to stresses imposed by mechanical and thermal phenomena that would be associated with a disposal vault. Experiments are carried out both in the laboratory and in the field. The Underground Research Laboratory is a major focus of field activity.

The shaft of the URL has been excavated to a depth of 255 m, and its construction has been used to study the mechanical response of jointed granite (Chan, Lang and Thompson, 1985). During the excavation, rock displacements were measured by instruments placed in boreholes drilled in four arrays at depths of 15 m, 62 m, 185 m and 218 m. Instruments in each array included sonic probe extensometers installed in horizontal boreholes, CSIRO, hollow inclusion triaxial strain cells, and convergence pins to monitor shaft convergence as excavation progressed. The layout of the instrumentation was determined by the use of borehole geological information, numerical scoping calculations and practical constraints on implementation.

Before beginning shaft sinking, the displacements and stress changes expected at all instrumentation points in the rock were predicted by three-dimensional, linear elastic continuum analysis. The rock was assumed to have a Poisson's ratio of 0.26 on the basis of laboratory tests on cores. The rock-mass deformation modulus was taken to be 40 GPa, which was determined through use of the NGI (Barton et al., 1974) and CSIR (Bieniawski, 1976) rock-mass classification schemes. In situ stress values were determined from hydraulic fracture tests and preliminary data from overcoring measurements in the shaft collar excavation. The maximum horizontal principal stress was taken to be 10.6 MPa and the minimum horizontal principal stress was taken to be 6.0 MPa. Below 86.5 m both horizontal principal stresses increased linearly with depth. The vertical stress was taken to be the lithostatic pressure of the overlying rock.

So far, only results from measurements at the 15-m depth have been analysed. In general, the predicted displacements fell well below the measured displacements. The rock-mass deformation modulus input to the model was then adjusted to achieve a best fit, giving a value of 31.5 GPa. The calibrated model agrees well with measurements until the shaft bottom advances to a depth of about 22.5 m. Subsequently, calculated displacements are below measured displacements by about 30%. It is conjectured that at least part of the discrepancy is caused by thermal expansion of the rock by the warm air in the shaft. This possibility is being investigated.

Comparison of model results with experiments strongly suggests that the rock mass at a depth of 15 m behaves, to a good approximation, as a linear elastic continuum.

CONCLUSION

Experimental programs to date give a strong indication that fractured plutonic rock is amenable to the characterization and analysis necessary to qualify it as a suitable disposal medium, and to evaluate and inter-compare potential disposal sites. The experiments summarized illustrate that a strong link is being developed between mathematical models and actual situations encountered in the field. This link is vital to placing safety assessments on a firm scientific basis.

REFERENCES

Barton, N., R. Lien and J. Lunde (1974). "Engineering classification of rock masses for the design of tunnel support." Rock Mechanics, Vol. 6, pp. 189-236.

Bieniawski, Z.T. (1976). "Rock mass classification in rock engineering." Proceedings of the Symposium for Rock Engineering, Vol. 1, pp. 97-106, Rotterdam: Balkema.

Brown, P.A. and N.A.C. Rey (1985). "The characterization and discrimination of fracture environments within the Eye-Dashwa Pluton, Atikokan, Ontario." Proceedings of the American Nuclear Society meeting on High Level Nuclear Fuel Waste Disposal Technology and Engineering, Pasco, WA., 1985 September 24-26.

Chan, T., P.A. Lang and P.M. Thompson (1985). "Mechanical response of jointed granite during shaft sinking at the Canadian Underground Research Laboratory." Proceedings of the 26th U.S. Symposium on Rock Mechanics: Research and Engineering Applications in Rock Masses, Rapid City, SD., 1985 June 26-28.

Davison, C.C. and V. Guvanasen (1985). "Hydrogeological characterization, modelling and monitoring of the site of Canada's Underground Research Laboratory." Proceedings of the 17th International Congress of the International Association of Hydrologists on Hydrogeology of Rocks of Low Permeability, Tuscson, AZ., 1985 January 7-9.

Dormuth, K.W. and J.S. Scott (1984). "Research and development for a plutonic rock radioactive waste disposal vault." Proceedings of the IAEA conference on Radioactive Waste Management, Vol. 4, pp. 221-242, Seattle, WA., 1984.

Niblett, E.R., R.A. Gibb, R.D. Kurtz, P. Lapointe, W.A. Morris, J.A. Ostrowski and A.K. Sinha (1985). "Ground geophysics results from the East Bull Lake pluton." Proceedings of the Seventeenth Information Meeting of the Nuclear Fuel Waste Management Program, Atomic Energy of Canada Limited Technical Record, TR-299.**

Reeves, C.V. (1983). "Interpretation of airborne magnetic gradiometer survey and integration with other geophysical data, East Bull Lake research area RA 7, Algoma District, Ontario." Unpublished Report RW/GPH-138-82.*

Reford, S.W. (1982). "Density profiling over the East Bull Lake gabbro intrusion, Research Area RA 7." Unpublished Report RW/GPH-138-82.*

Reford, S.W. (1983). "A detailed gravity survey of the East Bull Lake intrusion, Research Area RA 7, Algoma District, Ontario," Unpublished Report RW/GPH-176-82.*

Watson, R.K. (1982). "A gravity survey of the East Bull Lake intrusion, Research Area RA 7, Algoma District,Ontario." Unpublished Report RW/GPH-124-82.*

---

* Unpublished report available from Gravity Data Centre, Earth Physics Branch, 1 Observatory Crescent, Ottawa, Ontario K1A 0Y3, Canada.

** Unrestricted, unpublished report, available from SDDO, Atomic Energy of Canada Limited Research Company, Chalk River, Ontario K0J 1J0, Canada.

GEOLOGICAL DISPOSAL IN THE BELGIAN CONTEXT

R.H. Heremans
National Agency for Radioactive Waste and Fissile Materials Management
ONDRAF/NIRAS
Bd. du Régent 54, Brussels, B-1000 Belgium
L.H. Baetslé
Belgian Nuclear Research Centre
SCK/CEN
Mol, B-2400 Belgium

ABSTRACT

The way of tackling the high level and α bearing waste burial problem can vary from one country to another. In Belgium, if the electro-nuclear power represents about 60% of the total electricity production, the installed capacity is however limited to 5500 MWe. Furthermore, Belgium is a small country, densily populated, and its geology does not allow a large choice of underground formations acceptable for safe waste disposal.

In 1974 site specific investigations were started on a 700 hectares area in the NE part of the country where Belgium's main nuclear research centre and some nuclear fuel cycle facilities are located. The formation considered is a tertiary age clay layer underlaying the Mol-Dessel area.

Study and research works were organized in the frame of successive five year programs. During the first five years the main objectives were

- to collect informations on the clay's various characteristics and possible interactions with the waste package;
- to perform some field works in order to explore and define the litho-stratigraphy of the underground;
- to assess the technical feasibility and the long term safety of a burial system in clay.

For the second five year period it was aimed

- to set up an extended hydrological measurement network at regional scale
- to carry on thoroughly the studies on the physico-chemical aspects of the clay-waste interactions and on the long term safety of the system.

After 10 years of intensive field, laboratory and desk works the obtained results allowed to start the drafting of a "Preliminary Safety and Feasibility report" in view of the construction of a demonstration facility.

The project is performed by the CEN/SCK in the frame of shared financing contracts with the CEC and ONDRAF/NIRAS.

INTRODUCTION

The first nuclear power stations in Belgium (2 PWR units of 390 MWe and 1 of 870 MWe) were put into operation in 1975. At that time, an option was already taken to build a nuclear reactor park of 5500 MWe. However a maximum of 10.000 MWe capacity was not expected to be exceeded before the end of the present century.

On the basis of such a nuclear power equipment and spent fuel supposed to be reprocessed, the Belgian Nuclear Research Centre (CEN-SCK) decided in the early seventies to start investigations on the geological disposal of high level and α bearing waste.

Presently 5500 MWe are installed and the 7 PWR units in operation produce about 60% of the total electricity consumption in our country. No other plants are under construction, and even if the installation of a supplementary 1200 MWe unit is envisaged in the near future, the 10.000 MWe will not be reached in the year 2000. Anyway the scale for an underground burial facility, foreseen in the very beginning still prevails, especially since the Belgian Authorities have also committed themselves in the mean time to dispose off the high level and α bearing waste arisen from the previous EUROCHEMIC reprocessing plant.

A small electro-nuclear power plants park (equivalent to 10 GWe during 30 years) constitutes the first particularity which characterises the Belgian program on geological disposal.

The initial task the CEN/SCK undertook together with the Belgian Geological Service was to draw up a catalogue of geological formations having potentially favourable characteristics for waste disposal. Belgium being very small, only 30.500 km^2, and its hydrogeology at medium depth being well known, this survey brought us rapidly to the conclusion that neither rock-salt formations nor interesting hard rock massifs were existing at accessible depth and that only pelitic (clays and shales) formations could be considered as possible host media.

A choice of a host medium limited to one variety of rock in a small country (with a high population density) is a second particularity of the Belgian situation.

For various technical and socio-political reasons, the investigations started directly on a potential disposal site located in the N.E. part of the country and situated within the Boom clay formation. This site covers about 700 hectares of the Mol and Dessel villages; the

Nuclear Research Centre and some fuel cycle facilities are implanted there.
This Oligocene plastic clay was known from previous drillings or quarry exploitations in nearby areas. It was supposed to be present at the selected site under a compact and homogeneous facies, with a thickness of about 100 m at an average depth of about 230 m and sandwiched between two water bearing sandy formations.
Tunneling experience in such a type of argillaceous material at depths greater than 100 m was never gained anywhere.

The general hydrogeological context of the site and the uncertainties concerning minability of the Boom clay are other particularities which at the outset made the Belgian program looking different from many others.

At the time we had to start our activities the particularities were such that the R&D program planned had, at least in Europe, a certain character of originality, even of audacity.

ORGANISATION AND FINANCING OF THE PROJECT

Such a project is also characterized by its multidisciplinary aspect (geology, chemistry, mining, physics...), its various investigation scopes (field, laboratory, desk...), its cost and forecast duration. All these were taken into consideration in organizing the project management.

It was decided to work within successive five year programs including an annual revision of the objectives and the corresponding financial means. Highly specialized research or control laboratories, experimented companies or engineering offices, public or private, were involved and are charged of specific activities each time their capabilities were recognized, the CEN/SCK being the project coordinator.
Once the program approved by the board of directors of the CEN/SCK it had to be financed by its endowment and eventually by an additional non-recurring budget allowed by the Ministry of Economic Affairs.

In 1976 the Commission of the European Communities launched its R&D program on waste management and since that time the Belgian project is financially supported by the Commission in the frame of a shared cost contract. Moreover in august 1980 a law was voted in Belgium establishing the National Agency for Radioactive Waste and Fissile Materials Management (ONDRAF/NIRAS) and the waste producers are presently financing the R&D through this national body. The programs are discussed and defined by a technical committee composed of representatives of CEN/SCK, the waste producers and ONDRAF/NIRAS.

As a member state of the European Communities and as a member of other multinational organisations as the NEA/OECD or the IAEA/UNO, Belgium participates since the early beginning to the various working parties organized in the field of final waste disposal. These most interesting worldwide contacts with experts of other organisations involved in the same type of research contributed and still are contributing to the rational and equilibrated development of our program.

THE FIRST FIVE YEAR PROGRAM

In summary, the objectives of the 1975-1979 program were to give a preliminary answer to the two following questions :

- is clay an acceptable host medium for the disposal of conditioned high level and α bearing waste and which are its main limitations ?
- can the Mol-Dessel site be integrated in a global long term safe and economical acceptable waste disposal system and which are in that case the main constraints ?

The laboratory analyses and investigations were performed mostly on core-samples taken at different depths on the site. Some comparative work was also done on samples directly taken from a quarry excavated in the same formation and situated in the Boom clay outcrop zone, about 30 km S.W. of Mol.

It was demonstrated that the petrographical, mineralogical and chemical compositions of the Boom clay as well as its chemical, physical and geomechanical properties vary not much in function of depth.

At the Mol site location, the formation could be considered as being quite homogeneous throughout its whole thickness.

The main strong point investigated in the laboratory concerns the retention capacity for radionuclides. During a first series of tests, distribution coefficients (Kd) were determined in a classical way and the sensitivity of this coefficient to different parameters has been tested. It soon appeared however that the experimental conditions used for measuring the Kd were not representative at all of the real conditions prevailing in the clay at depth, moreover that the ion exchange phenomenon alone, or the Kd notion, could not explain the retention capacity of the clay.

At the end of 1979, even if a full scientific explanation of the results could not be given, the data although allowed to conclude that the Boom clay had an excellent retention capacity for most toxic radionuclides and plans were made to extend the basic scientific work on this clay trump.

Laboratory results obtained during clay compatibility tests indicated that some materials such as Hastelloy C, titanium, UHB 904L and others have a good corrosion resistance even at higher temperatures. The tests on corrosion resistance of waste matrices such as glass, concrete, etc., were at the end of the first five year program not sufficiently advanced to provide conclusions, but there was no indication that particular difficulties could be expected.

Orientation experiments on the effects of intense γ irradiation were at that time essentially qualitative and have shown formation of hydrogen, methane and CO2. However it was considered that, an adequate geometrical configuration of the buried waste might reduce to within acceptable safety limits, a possible impact of radiation on the geological environment.

The geomechanical properties of clay samples taken in various conditions and at different depths and locations were extensively studied in order to gain enough information to assess the minability of the clay and to start a technical feasibility study of a disposal facility at about 250 m depth.
Laboratory tests completed by a heat transfer experiment performed in a Boom clay quarry using an electrical heater simulating a HLW source gave some realistic information about the thermal conductivity and thermal diffusivity in clay.

From the various field works, including lineament location on space and aerial imagery, geological drillings, borehole logging and seismic prospection it was possible

- to define precisely the stratigraphic column under the site up to -600 m;
- to confirm that the clay formation spreads out subhorizontally under the prospected area with a thickness of about 100 m;
- to conclude that the clay layer is free of flexures or faults, and that its slope is about 1% in the N.NE direction.

Figure 1 shows a NNW-SSE cut through the Mol-Dessel site.

Table 1 gives some information on the Boom clay composition and properties.

CHEMICAL COMPOSITION OF DRY MATERIAL (∿%)	63.72 SiO_2, 14.50 Al_2O_3, 5.88 Fe_2O_3 2.24 K_2O, 1.37 Na_2O, 0.64 CaO 0.50 TiO_2, 0.70 MgO weight loss at 1000° C : 9,8 organic content : 2.3 to 6.5
MINERALOGICAL COMPOSITION (∿%)	25 illite, 20 smectite, 30 vermiculite-like, 15 illite-montmorilonite interstratified, 10 chlorite-vermiculitelike interstratified.
GRANULOMETRIC COMPOSITION (∿%)	49 : d <2μ , 47 : 2μ < d <60 μ , 3.5 : 60μ < d< 200 μ 0.5 : d >200
PETROGRAPHICAL COMPOSITION	pyrite, calcite, quartz, gypsum
NATURAL WATER CONTENT (∿%)	22.3
NATURAL VOLUME WEIGHT (kN/m^3)	19.6
POROSITY (%)	38.5
SATURATION DEGREE (%)	95-100
PERMEABILITY (m/s)	10^{-10} - 5.10^{-12}
THERMAL CONDUCTIVITY "IN SITU" (W/m°C)	1.69
THERMAL DIFFUSIVITY (m^2/y)	18.8
SPECIFIC HEAT (J/kg°K) AT 25°C	7.22
ATTERBERG LIMITS (%) Wp	26.5
Wl	77.5
Ip	51.0
TRIAXIAL C.U Ccu (MN/m^2)	0.127
Pcu (°)	17.5
TRIAXIAL U.U Cu (MN/m^2)	0.588

TABLE 1 BOOM CLAY COMPOSITION AND SOME OF ITS PROPERTIES.

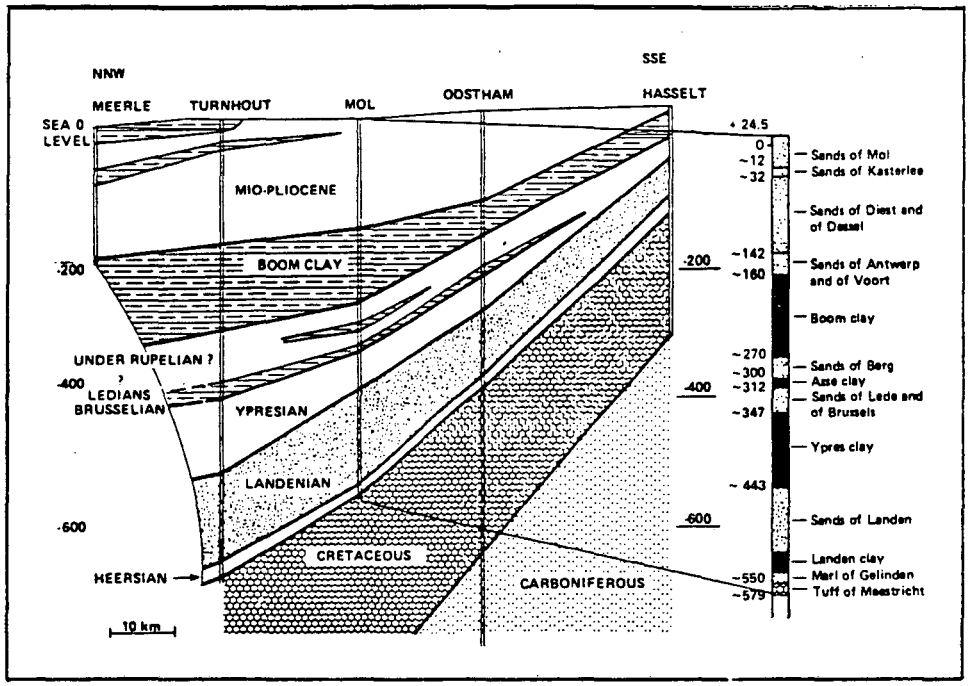

FIGURE 1 - NNW - SSE CUT THROUGH THE MOL-DESSEL SITE.

During the feasibility study a first conceptual design for a repository, adapted to the site conditions and taking into account the geotechnical and thermal properties already determined for Boom clay was developed. Such a facility would be constituted of full lined circular galleries having a useful diameter of 3 to 4 m. While the low heat emitting waste drums could be stacked in the main galleries, the HLW canisters could be emplaced in some 20 m long inclined pits grafted at regular intervals on the main gallery walls. This configuration is presented schematically in figure 2.

The evaluation of the long-term risks associated with the disposal of waste at the Mol-Dessel site has been undertaken in co-operation with the Joint Research Centre of the Commission of the European Communities at Ispra. In á first approach the realized studies dealt with the possible occurence of disruptive events of geological and other origins and made more particularly use of the Fault Tree Analysis technique; in a second approach, the normal evolution of the site has been studied.

The results obtained during these various exercises were judged to be satisfactory. The occurrence probability of catastrophic events involving rupture of the geological barriers is limited. First calculations on radionuclide migration in clay indicated extremely slow movements in most cases.

The main conclusions of the research and study work performed during the first five year program are summarized in table 2.

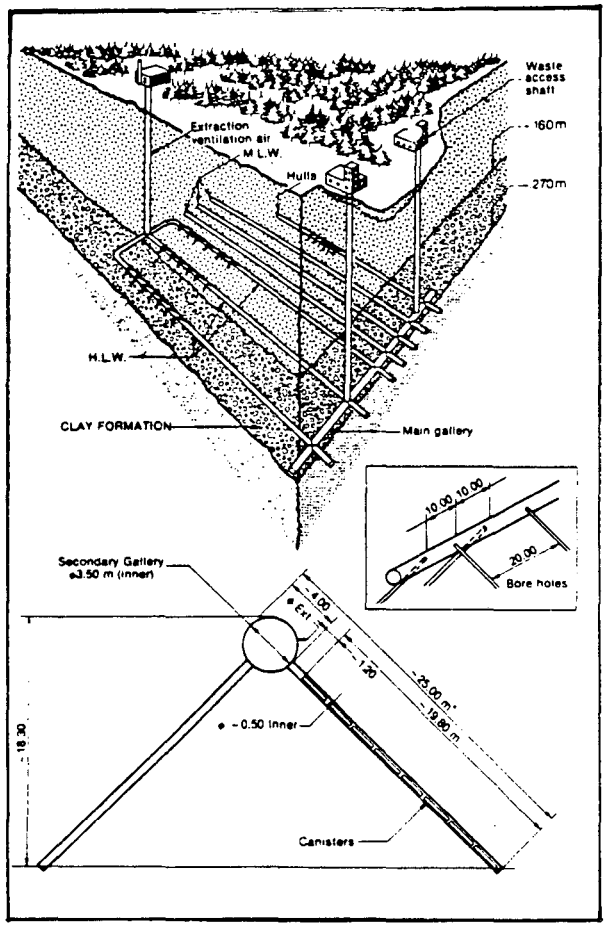

FIGURE 2

CONFIGURATION OF A DISPOSAL FACILITY IN CLAY.

LABORATORY INVESTIGATIONS	- clay characteristics quite constant along the total thickness of the layer - excellent radionuclide retention capacity - corrosion resistant materials available - poor geotechnical properties
FIELD INVESTIGATIONS	- local geological sequences confirmed - "homogeneity" of the layer proved (no faults, no flexures > 5 m) - slope of the layer ± 1%NNE
STUDY WORK	- feasibility - yes but - cooling time 50 years - minability to be demonstrated - safety analysis first approach : favourable results

TABLE 2 DIGEST OF THE MAIN RESULTS FROM THE FIRST FIVE YEAR PROGRAM

THE SECOND FIVE YEAR PROGRAM

On these bases the decision was taken to carry on with the project for another five years, emphasis being given to minability aspects and a better understanding of the local and regional hydrology.
In practice, and besides further laboratory investigations and long-term safety analysis studies, the two main objectives were :

- the construction into the Boom clay of an underground experimental facility at 225 metres below ground level for "in situ" experimentation and reconnaissance. The construction of a shaft and a gallery was intended to prove the technical possibility of building underground structures in a plastic argillaceous medium and to scale up the feasibility of digging at this depth to real dimensions

- the deployment of a large network of hydrogeological observation wells in the main aquifers over- and underlying the Boom clay. By this regional hydrological survey it was intended to get a picture of the ground water flow system around the Mol-Dessel site and to evaluate by modelling the impact of some possible future evolution scenario on the flow system.

The construction of the facility started, in artificially frozen soil, in summer 1980 and was completed in summer 1984 by the digging, in unfrozen clay, of a 20 m deep vertical shaft and a 6 m long horizontal gallery, both with a 1.4 m useful diameter. These last works were the most relevant and successful experiments in this part of the program. Figure 3 gives a scheme of the as built underground laboratory.

From the last quarter of 1984 on, various other "in situ" experiments were launched progressively starting with corrosion tests on metals, alloys and waste matrices, and followed by heat transfer, hydraulic and migration tests, etc.

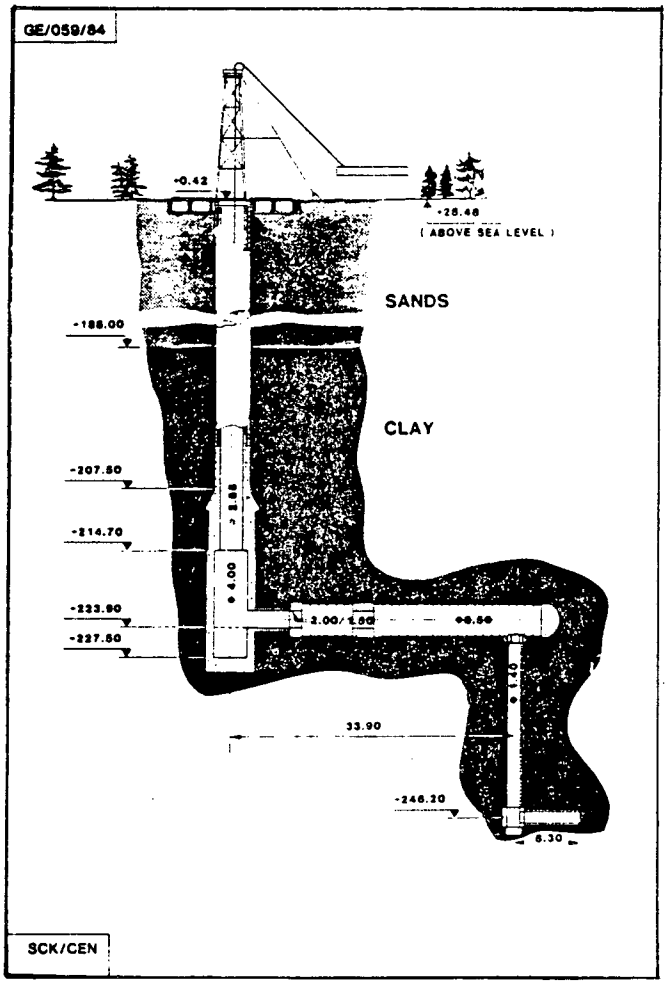

FIGURE 3

UNDERGROUND LABORATORY IN CLAY - AS BUILT -

In 1984 the regional hydrological observation network was completed. One hundred and thirty-two piezometers are now included in this network and installed at thirty-two locations. A total area of about 2,500 km^2 is thus surveyed.
During the drilling of the wells and before bringing in the piezometers, borehole loggings were systematically performed. This allowed to make, together with the visual examination of the cuttings, fairly good and detailed correlations between wells. In these wells, piezometric water levels are regularly measured. Sampling of ground water is made all along and numerous water quality data are determined : e.g. chemical composition, temperature, physico-chemical properties, ^{14}C-content (for reckoning transit and residence times), etc. At some locations also precipitation is measured.
Slug or pumping tests are performed in order to determine hydraulic characteristics of the surveyed aquifers. All these data feed a data bank, which can be consulted for modelling the ground water flow regime.

The field measurements combined with numerous results from various laboratory investigations give now a clear pattern of the water movement and residence time within the different aquifers and aquicludes on and around the site. It could be shown that the general groundwater flow regime is relatively insensitive to slow changes in the overall hydrogeology resulting from possible future climatic modifications and their consequences, e.g. erosion, sea level fluctations, etc.

As planned, the physico-chemical properties of the Boom clay were sift to the very bottom. Two teams, one of the CEN/SCK and one of the University of Leuven are working on the subject. The solid phase composition of the material, the interstitial water properties and the redox potential of the medium were analysed. It is now demonstrated that the interstitial solution contains essentially HCO^-_3, "in situ", in equilibrium with the solid phase compounds at pH 8.5 and Eh = -260 mV (she) determined by the presence of FeS_2.

The organic carbon content of the Boom clay is due to the present humines and humic acids. In alkaline conditions the latter are also very reducing and contribute to the total ion exchange capacity of the soil. These elements being known it became easier to describe the excellent radionuclide retention capacity of the Boom clay and to introduce the obtained data into modelling. Some important findings to be confirmed by complementary laboratory and "in situ" experiments are summarized here :

- the solubility of Sr is controlled by the carbonate excess present in the clay. The residual dissolved Sr is partitioned between the interstitial water and the absorbing mineral phases, according to ion exchange laws. For this case a Kd value approaching 300 ml g^{-1} is obtained over the whole thickness of the Boom clay layer;
- the fate of Cs in the clay on the contrary is determined by the illite fraction present in it, a mineral which has a very selective affinity for Cs.
  In situ Kd values of about 3,000 ml g^{-1} have been obtained for samples of all levels of the Boom clay.

Worth to be mentioned are the last results obtained for diffusion coefficients (Df) in very representative "in situ" conditions and which are worse than those obtained previously. This phenomenon could be interpreted in terms of hindered accessibility of the sorption sites when the clay particles are close together.

- Eu, Tc, Pu and their analogues are all displaced from their carbonate complexes, and are quantitatively complexed by the organic matter. The mobility of each nuclide is controlled by the mobility of the organic molecules. The high molecular weight of the humic acids strongly impedes any substantial radionuclide migration.

Other reactions presently studied concern for instance the reduction capacity of the organic material for Tc and Pu, the influence of oxygen on clay properties and the consequences for retention; pH, Eh variations, formation of Fe and Al sesquioxydes and their scavenging effects on some nuclides e.g. Eu.

Corrosion experiments in clay, impact of α and γ irradiation on clay, influence of temperature cycles on geomechanical properties of clay are some other subjects which were further investigated on a routine basis during the 2d five year program.

A new study subject concerns sealing and backfilling materials and their emplacement techniques. Up to now good results were obtained from bentonite, cement, Boom clay and epoxy resin mixtures the latter one improving the imperviousness.

As far as safety analysis is concerned a couple of scenarios have been selected for the assessment of the consequences and the risks to man associated with the failure of the geological barrier : a tectonic displacement through the clay and the repository and a glacial erosion scenario were thoroughly studied.

The methodology followed for assessing the consequences and risks for these disruptive scenarios is the probabilistic approach developed by the JRC-Ispra team. In this approach and with existing computational tools (LISA-code) the uncertainty and sensitivity analysis were strongly developed.

Along with this probabilistic assessment for the long-term safety, the performances of a geological disposal system in Boom clay at the Mol site were also evaluated on the basis of a normal evolution scenario, based on the natural degradation of its engineered components.
In the latter the results of the various laboratory tests and experiments are of course of prime

importance.

In the natural evolution scenario the only release path for the radionuclides is by migration through the Boom clay and hence this puts in evidence the importance given in the program to the study of the geochemical buffering capacity of the Boom clay and the modelling radionuclides migration.

A computer program based on the analytical solution of the diffusion equation permits to calculate now the expected migration distances of the most important radionuclides. Coupling of this model with others such as thermal and water flow ones is now currently studied and some preliminary results will be presented by M. Baetslé during the present symposium.

It should be mentioned here too, that Belgium is participating in the PAGIS-action of the Commission of the European Communities (PAGIS stands for Performance Assessment of Geological Isolation Systems). Within that action the CEN/SCK is in charge of the co-ordination of the studies related to clay option. The Mol-Dessel site and the repository design developed by the CEN/SCK are taken in these studies as reference case.

At the end of 1984 a new balance of the acquired knowledge was drawn up, it is briefly summarized in table 3.

ment of some investigation techniques and accompanying modelling tools is also required.

Besides these R&D goals a very important objective for the future is the construction of a demonstration facility. The demonstration program on the reliability of the conceived disposal system in clay itself will outlast the third five-year program.

This project involves the design and construction and gradual operation with representative waste forms of the underground demonstration facility. It is however already clear that two aspects of the system's reliability demonstration will be dealt with :

1) the direct demonstration of the technical feasibility, by proving with selected candidate construction materials and techniques that an underground disposal facility in clay can be built, and that waste can be conveyed and emplaced in it according to the regulations and rules and without incidents. The waste materials used in the demonstration facility will be emplaced in a retrievable manner;

2) the indirect demonstration of the safety by extensive monitoring and of the system performances by optimization of its components. The demonstration of the validity of the mathematical models and confidence in the long term predictions about the safety and performances of the system will be incremented.

LABORATORY INVESTIGATIONS	- physico-chemical properties of the clay's solid and liquid phase well known - excellent retention capacity for various radionuclides confirmed - geomechanical properties more extensively and thoroughly known - limited corrosion for selected metallic materials and waste matrices confirmed
FIELD INVESTIGATIONS	- minability in unfrozen clay proved during construction of underground laboratory - "homogeneity" of clay layer confirmed by visual inspection and sampling during same construction works - hydrogeological investigation scope at regional scale made available
STUDY WORK	- safety analysis - further studies tend to confirm the long term safety - cost evaluation started

TABLE 3 DIGEST OF THE MAIN RESULTS FROM THE SECOND FIVE YEAR PROGRAM

THIRD FIVE YEAR PROGRAM AND FUTURE ACTIVITIES

The fact that the objectives, fixed in 1980 were matched at the end of the second five year program does not mean that the research did get its final goals. In the future program a large number of results obtained from laboratory and desk studies need to be confirmed by "in situ" experiments, complementary field studies and even other laboratory investigations. Improve-

At the onset of the third five year program (1985-1989) an interim safety and feasibility report, based on the present knowledge and already acquired experience has to be prepared. This report will constitute one of the most important cornerstones of the procedure for obtaining the necessary authorizations in view of

the construction of an underground demonstration facility.

x

x x

SWISS FIELD INVESTIGATIONS FOR RADIOACTIVE WASTE REPOSITORIES

C. McCombie, A.L. Nold, M. Thury
National Cooperative for the Storage of
Radioactive Waste (Nagra)
Parkstrasse 23
5401 Baden, Switzerland
056/20.55.11

ABSTRACT

The Swiss National Cooperative for the Storage of Radioactive Waste, Nagra, plans two types of repositories, one for high level waste and possibly certain alpha-containing intermediate level wastes (Type C repository) and one for low and intermediate level wastes (Type B repository). For the Type C repository, a regional field investigation program was started in 1980 with geophysical, hydrogeological and neotectonic investigations and a deep drilling program, in which to date 6 deep boreholes of a total length of more than 10 km have been drilled and investigated. For the Type B repository, preliminary field investigations have been carried out at 20 potential sites and a detailed site investigation program at 3 sites is ready to start as soon as the needed permits from the authorities are granted. At Grimsel, an underground test facility (FLG) has been excavated and several test programs are in progress.

1. INTRODUCTION

Nagra (Swiss National Cooperative for the Storage of Radioactive Waste) is responsible for planning the final disposal of all active wastes arising from power production as well as from medicine, industry and research applications. The current display concept involves two types of repositories.

- **Type C repository** for high-level waste and certain alpha-containing intermediate-level wastes
- **Type B repository** for all remaining intermediate and low-level wastes

The Type C repository is planned in mined galleries with vertical access shafts at a depth of about 1200 m. The host rock of first priority is the crystalline basement in northern Switzerland, which is covered by a few hundred meters of sediments. The first stage of a site selection program was initiated in 1980 with regional investigations of an area of about 1000 km^2. Six deep boreholes of a total length of more than 10 km have been drilled and investigated. A regional geophysical program, a regional hydrogeological program and a neotectonic program are under way. The Type C field program is described in more detail in part 3 of this paper.

The Type B repository is planned as a horizontally accessed mined cavern system with an overburden of a few hundred meters. Three potential sites have been selected in the Swiss Alps in different host rocks: marl, gneiss and anhydrite. The Type B site selection program, described in part 2 of this paper, was started in 1978. In 1983 Nagra has applied to the federal government for the permission to carry out site investigations at the three sites.

In 1984, Nagra built in the Swiss Alps near the Grimsel Pass an underground rock laboratory in crystalline rock. Several tests are in progress or in the planning stage for the improvement of measurement techniques, and for investigation of specific questions relevant to the Swiss repository concepts for both types of repositories.

The Federal Government Ruling of 6th October 1978 on the Atomic Act designates the guaranteeing of "permanent safe management and final disposal" of radioactive waste as a prerequisite to future development of use of nuclear energy in Switzerland. Nagra therefore presented to the Federal Government at the beginning of 1985 a report on technical feasibility and achievable safety of final repositories for radioactive wastes in Switzerland (the so-called Project Gewähr 1985). A complete safety analysis had to be carried out, based on the data and on the results already available from the ongoing regional investigation program. This safety analysis allowed identification of the critical geological factors and emphasis can therefore be given to these factors during further data analysis and investigations.

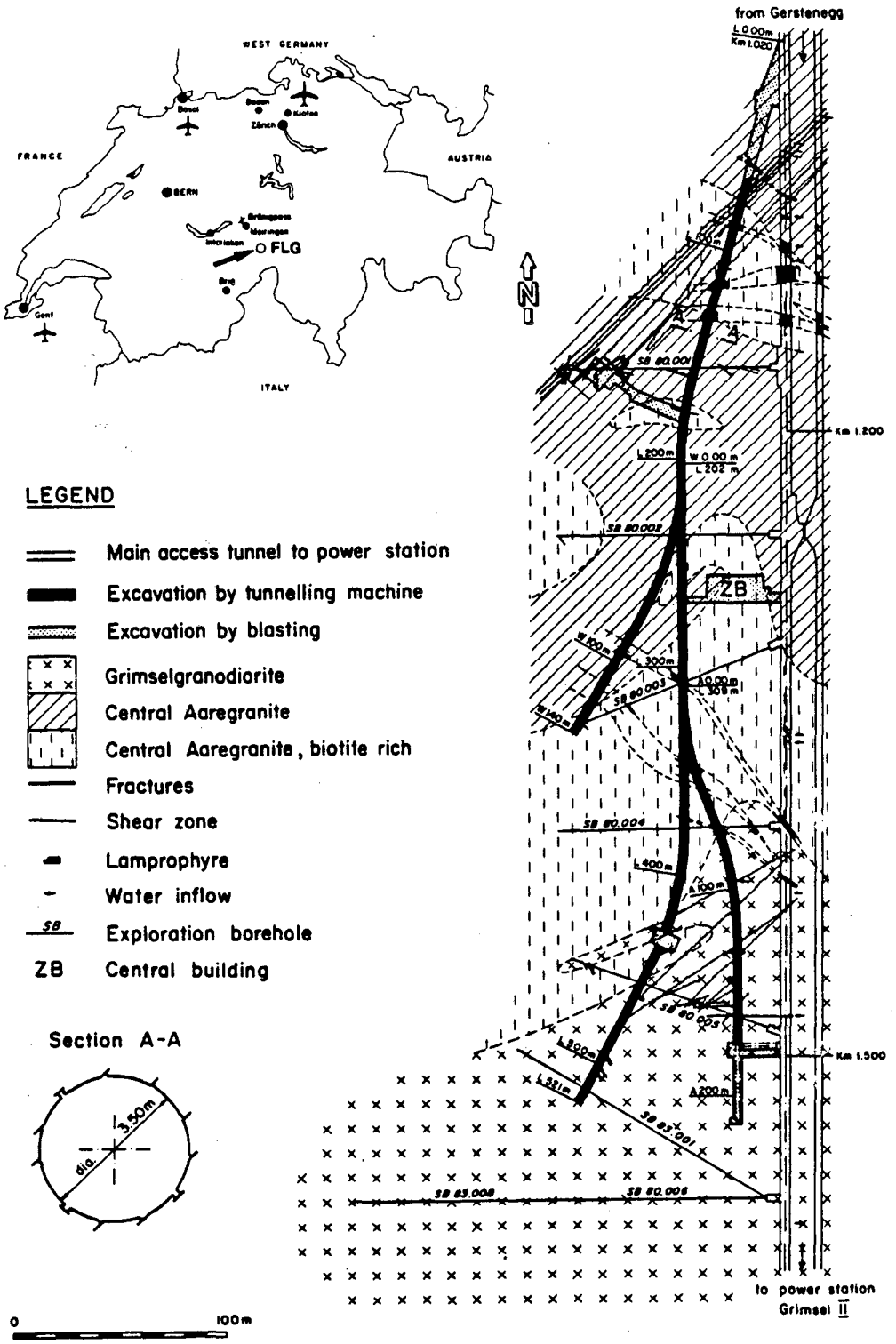

Figure 1. Grimsel underground test facility (FLG), situation map and geological overview

2. FIELD PROGRAM AT THE GRIMSEL UNDERGROUND TEST FACILITY (FLG)

Development of FLG Project

Although Nagra participates at the Stripa Project in Sweden, already in 1979 it was decided that Switzerland should have its own underground test facility:

- to gain practical experience in the development, testing and use of instruments and measurements techniques in underground laboratories,
- to carry out specific experiments relevant to Swiss repository concepts, and
- to assess the extent to which foreign research results can be applied to the geological conditions in Switzerland.

The 1980/81 investigations in the Grimsel area proved the site to be suitable for an underground test facility and gave the necessary information to plan the experimental program outlined below.

The FLG is located in the Swiss Alps and situated about 1200 m from the entrance to an underground power station. The crystalline rock overburden is between 400 and 500 m. The lab was built between May 1983 and April 1984 using a fullface tunnelling machine to excavate the tunnel system shown in Figure 2.

The experiments are carried out in close cooperation between Swiss experts and German experts from the Bundesanstalt für Geowissenschaften und Rohstoffe (BGR) and the Gesellschaft für Strahlen- und Umweltforschung mbH (GSF). The cooperation with BGR and GSF is based on a bilateral letter exchange between Swiss and German authorities and individual contracts between Nagra and BGR/GSF. The basic design and construction was performed by Nagra, which is further responsible for the project management and the provision of the necessary logistics.

FLG Experimental Program

Some investigations within the Grimsel program began during construction of the lab. For the main investigations a 5 years program has been formulated, starting in 1984 and ending in 1988.

The basic goals for the individual scientific investigations are outlined below:

Excavation effects: Testing the rock mass surrounding man-made openings in crystalline rock, in order to assess the influence of these cavities on the hydrogeological conditions.

Geophysics: Testing and further development of nondestructive methods for locating hydrogeologically important rock discontinuities and weaknesses from exploratory boreholes and underground openings, at short ranges of up to approx. 50 m as well as in the far field.

Heat-induced reactions: Investigations which lead to an understanding of heat-induced reactions in fractured crystalline rocks.

Hydrogeology: The acquisition of additional hydrogeological data which can help in developing a general hydrogeological model, adaptable to specific field situations, in fractured crystalline rock of low permeability.

Laboratory experiments: Complementing the in-situ tests by laboratory experiments which are also needed for the development of mathematical models.

Migration: The acquisition of additional chemical and physical data necessary for understanding the transport of nuclides in the fractures of crystalline rock.

Neotectonics: Testing and further development of methods for locating neotectonically active disturbed zones.

Rock stress measurements: Testing and further development of existing methods used in shallow boreholes in order to determine the rock stresses in deep boreholes.

3. FIELD PROGRAM FOR HLW DEEP DISPOSAL PROJECT (TYPE C)

The investigation area (Fig. 2) was selected along the northern border of Switzerland in a region where the top of the crystalline basement was expected at maximum depth of 1'500 m. The investigation area lies in an area of relatively low seismic activity between the two more active areas around Basel and Schaffhausen.

Figure 3 shows a geological section through the investigation area, from the Kaisten borehole to the Schafisheim borehole. The section is based on an interpretation of a seismic reflection survey. A large Permocarboniferous trough which trends west-east through the investigation area has been discovered below the mesozoic sediments.

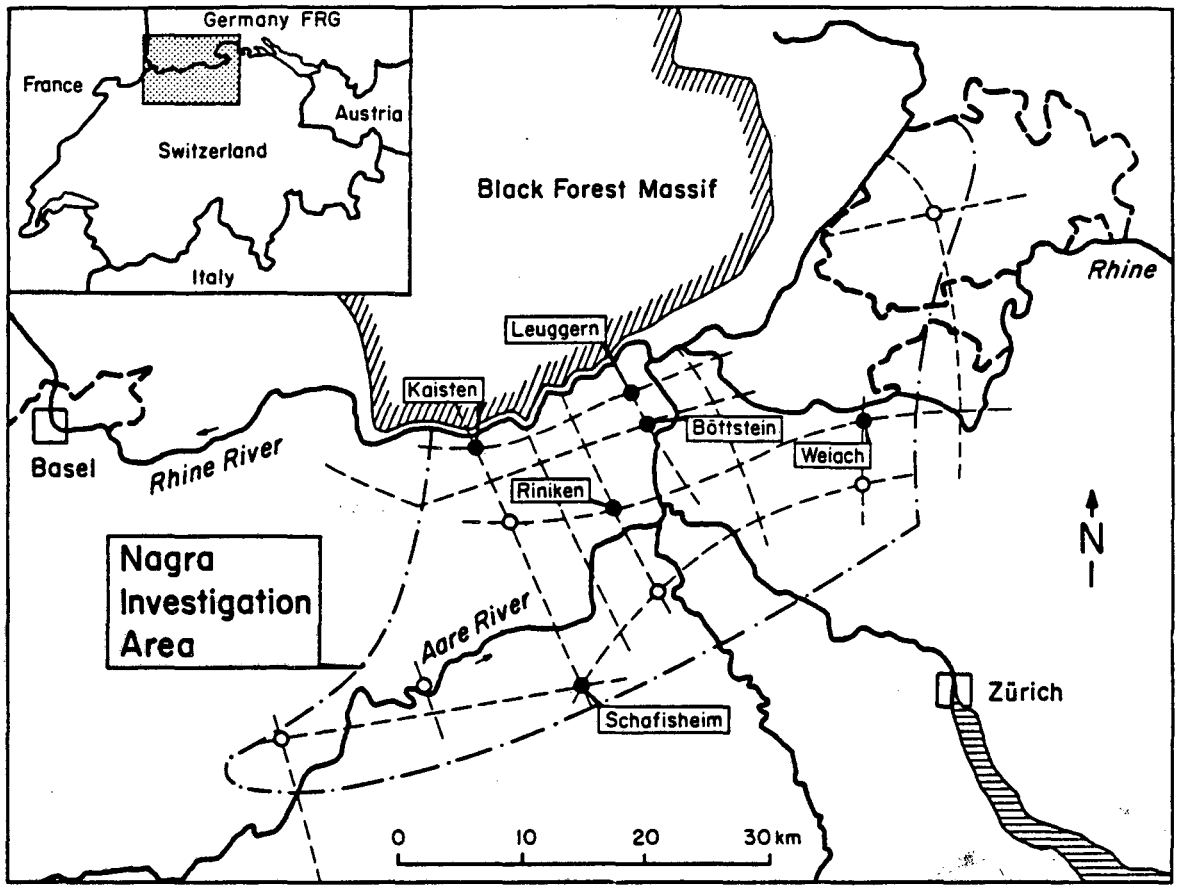

Figure 2. Nagra investigation area with drilled deep boreholes (black cercles), and reflection seismik lines (dashed lines).

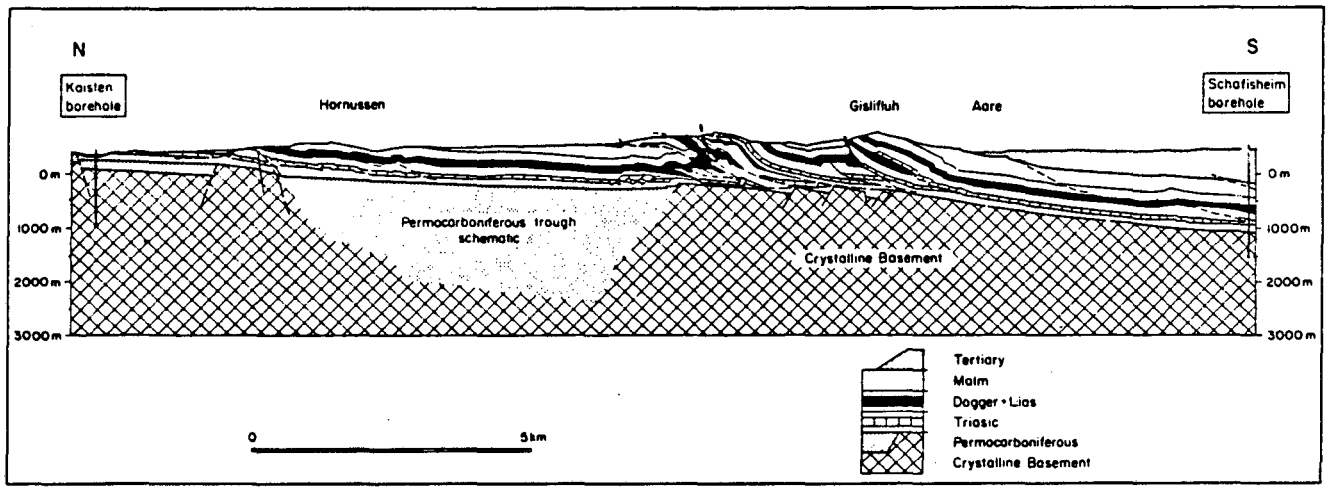

Figure 3. Geological section through the Nagra investigation area

The aim of the Type C program is to ensure that a Swiss repository, if needed, can be operational by the year 2020. The program is divided into 4 phases:

1980-1989 Phase 1	Regional investigation and site selection
1989-1995 Phase 2	Detailed site investigations at 1-3 locations and selection of one site
1995-2005 Phase 3	Detailed site investigation at 1 location with test shafts and underground laboratory
2005-2020 Phase 4	Repository preparation

Phase 1 includes four technical programs, which are described below:

- Deep drilling program
- Geophysical investigation program
- Regional hydrogeological program
- Neotectonic program

The program is managed by Nagra. More than 50 university institutes, consulting companies, consultants and contractors with more than 200 scientists from 8 countries work in the program. The costs involved to date are approximately 50 Mio US$.

The results of the geological investigations are published in the Nagra Technical Report series. About 50 geologic reports are presently available and a further 20 are in preparation.

Deep Drilling Program

A series of 12 deep boreholes spread over the investigation area was planned to explore the geological structure of the subsurface with emphasis on detailed investigation of the practically unknown crystalline basement below the sedimentary cover. Investigation of water flow systems in the basement as well as their hydraulic and hydrochemical characterization provide the input data needed for a hydrogeological model of the area.

To date, six boreholes have been drilled with depths between 1300 and 2500 m. Figure 4 shows an overview of the geology of these boreholes. The main parts of the scientific investigation program were:

- Coring over about 90 % of the boreholes and detailed laboratory analysis of the cores.
- Core orientation (very successful with a sonic televiewer) and detailed fracture orientation statistics.
- Geophysical logging with practically all tools available today. For the granite of the Böttstein borehole, a synthetic faciolog was developed, which corresponds remarkably well with the observed petrography.
- Fluid logging to detect water inflow zones. Very small inflow zones were detected by the logging of the electrical conductivity of the borehole fluid during pumping. In order to obtain a maximum conductivity contrast between borehole fluid and inflowing ground water, the borehole fluid was replaced by deionized water.
- Hydraulic testing. Systematic double packer tests with intervals of 12 - 25 m have been carried out to obtain a continuous profile of the hydraulic conductivity of the crystalline basement. Figure 5 shows the conductivity profile from the Böttstein hole.
- Water sampling of ground water of the sedimentary aquifers and of flow zones in the crystalline basement was carried out, mostly during the drilling operations which were interrupted when a promising flow zone was observed. The crystalline sections of the boreholes were drilled either with deionized water or inflowing deep ground water, without any additives except two tracers to allow in-situ analysis of residual contamination of the water samples. Water samples were taken at the surface when the flow was sufficient and also downhole with pressure vessels. The analysis program is described in the hydrogeology section below.

At the beginning of 1984, a multipacker system was installed in the Böttstein borehole with 8 packers, allowing long-term observation of the hydraulic head of 8 different zones of the crystalline section. The system has worked perfectly until now. During this year, a similar multipacker system was installed in four other boreholes. Some packer failures have occurred so that data from the long-term observation program is still limited.

Borehole :	BOETTSTEIN		WEIACH		RINIKEN		SCHAFISHEIM		KAISTEN		LEUGGERN	
Geology :	m	d	m	d	m	d	m	d	m	d	m	d
Quaternary	18	0	37	0	25	0	244	0	45	0	48	0
Tertiary	–		149	37	–		332	244	–		–	
Jurassic	–		518	186	464	25	529	576	–		–	
Triassic	297	18	285	704	327	489	385	1105	80		175	
Permian	–	–	461	989	985	816	–	–	172	125	–	–
Carboniferous	–	–	570	1450		1801	–	–	–	–	–	–
Crystalline Basement	1186	315 Granite 1501	462	2020 Gneis 2482			516	1490 Granite Syenite 2006	1009	297 Gneis 1306	1466	223 Gneis Granite 1689

core 1501 final depth m : thickness (m) d : depth of top formation (m)

Figure 4. Geological overview of the Nagra deep boreholes

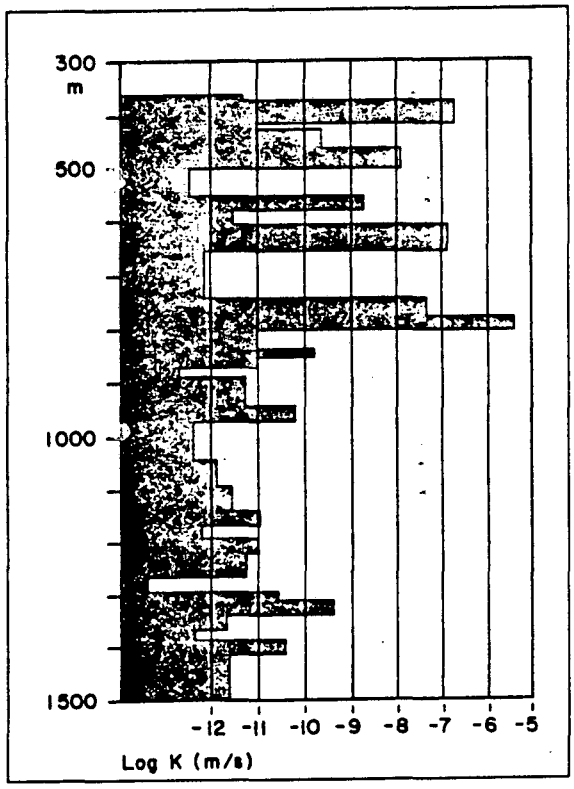

Figure 5. Profile of hydraulic conductivities of the granite section of Böttstein borehole, measured with double packer tests

Geophysical Investigation Program

A geophysical program has been carried out over the whole investigation area with the aim of mapping the regional structural geology, using also the observations from the drilling program. The field work of the geophysical program was finished early this year. Interpretation work is still continuing.

In 1981/1982 a gravity survey with about 5'000 stations was carried out. A significant mass deficit was observed in the area of the Permocarboniferous trough. In 1981 an aeromagnetic survey with more than 6'000 km of lines was carried out. No significant magnetic anomalies have been detected. In 1981 a magnetotelluric survey was carried out along the line Kaisten-Schafisheim (Fig. 2). The measurements were disturbed by surface effects and are therefore not conclusive.

In 1981/1982 a first seismic refraction survey with about 200 km of lines was carried out, giving the first indication of the existence of the Permocarboniferous trough. In 1984 an additional seismic refraction survey was carried out along the axis of the Permocarboniferous trough. Interpretation work is still going on.

In 1982/1983 a first seismic reflection survey with about 180 km of lines was carried out. These lines allowed a detailed interpretation of the regional structural geology of the mesozoic sediments. In some parts of the area of the Permocarboniferous trough, series of horizontal or inclined reflection bands indicate the presence of paleozoic sediments. However, the top of the basement below these paleozoic sediments does not reflect significantly and mapping of the top of the basement is therefore rather difficult. Within the crystalline basement, some series of reflections have been observed down to a depth of about 7 km. Detailed interpretation of the structural geology below the mesozoic is still continuing. In 1983/1984 and 1984/1985, two additional seismic reflection surveys were carried out to provide a more detailed network of profiles. Interpretation is still going on.

Regional Hydrogeological Program

A proper understanding of the deep groundwater flow regime is needed to predict flow paths, travel times and dilution effects of ground water moving between a repository location and the biosphere. In addition, the assessment of the chemical composition of ground water in the near-field of a repository is very important.

The flow regime in the Nagra investigation area is rather complicated: the mesozoic sedimentary cover contains some important limestone aquifers separated by impermeable formations of clay, anhydrite and rock salt. As shown on Figure 3, the mesozoic sediments are folded and overthrusted in some areas, allowing potential water flow through fault zones and thrust zones connecting different sedimentary aquifers. The sedimentary filling of the Permocarboniferous trough is, in general, of fairly low permeability; however, some open fractures with large mud losses during drilling have been observed. The crystalline basement conducts ground water in crushed zones and fracture systems. Based on the information from the first 6 deep boreholes, the upper 500 m of the basement have an average hydraulic conductivity of about 10^{-7} m/s. Below, the hydraulic conductivity is about 10^{-11} m/s, except in fault zones which can have high conductivities, as observed, down to a depth of at least 1'700 m.

The Nagra investigation concept is as follows:

- to prepare a hydrodynamic model for the assessment of the flow field
- to investigate the hydrochemistry and isotopic composition of the ground waters of the different aquifers
- to validate the hydrodynamic model with the results of the hydrochemistry of the different water types and with the hydraulic head observations at different depths in the deep boreholes.

In 1981, the preparation of a regional hydrodynamic model was started. It covers a surface area of about 25'000 km^2 including the infiltration areas in the Swiss Alps and in the Black Forest massif in Germany. The model contains about 5'600 finite elements. Up to now more than 25 runs have been carried out, mainly with different sets of parameters for hydraulic conductivities of the various aquifers and aquitards.

In 1984 a local hydrodynamic model was prepared for the most relevant part of the investigation area, covering about 1'000 km^2. With about 6'000 elements, it allowed a more detailed representation of the geometry of the different aquifers. The lateral water inflow into the model was derived from the results of the regional model. More than 10 runs have been carried out with different sets of input parameters, resulting in a set of possible flow paths from potential repository locations to the biosphere.

A first validation of the two hydrodynamic models has been carried out with the preliminary results of the hydrochemistry of the aquifers and hydraulic head observations of the deep boreholes. During the next year, improvements on the representation of the geometry of the aquifers of the models, as well as a detailed validation of the hydrodynamic models are planned.

The hydrochemical program started in 1981 with the collection of waters from about 100 springs and wells of different aquifers in the investigation area and its surroundings. Detailed hydrochemical and isotope analyses have been carried out. In the deep boreholes, about 60 water samples have been collected and analysed. It was possible to define several different water types in the sedimentary aquifers as well as in the crystalline basement. A detailed study is presently being carried out for a better understanding of the rock-water interaction and the evolution of the ground waters of the different aquifers.

Neotectonic Program

The main aim of the neotectonic program is to detect fault zones capable of tectonic reactivation in order to avoid these zones within repository sites. The program was started in 1981 with various approaches:

Lineaments detected on satellite imageries have been checked on aerial photos and in the field without finding clear indications of active faults.

Along the main rivers of the investigation area, a detailed analysis of morphology of bedrock below the quaternary alluvials was carried out, based on information from numerous shallow ground-water wells. Along the Rhine several fault zones seem to be active. These zones are at distances of 3 - 8 km, the movement rate is about 0.1 - 0.2 mm per year.

The dip of the present surface of quaternary alluvials of the main river plains has been analysed to find dip anomalies which could be caused by recent fault movements. Some small anomalies were found.

A detailed re-analysis of the high accuracy levelling of the Swiss Topographical Survey was carried out and 2 areas of relative uplift and sink were detected, with movement rates of 0.1 - 0.3 mm per year.

The investigation area is well known as a seismically relatively quiet area, based on records from the 14th century. However in 1983 Nagra installed a network of 9 seismographs for a long-term microseismic survey. With this network, events of Magnitude 1 can be detected with an accuracy of less than 1 km horizontally and vertically. During the last two years of records, three events of magnitude 1 have been registered in the investigation area.

The neotectonic program continues with detailed analysis of the potentially active fault zones detected.

4. FIELD PROGRAM FOR L/ILW REPOSITORY (TYPE B)

Program and Time Table

The site selection program for type B repository, which is planned as a horizontally accessed mined cavern system with an overburden of a few hundred meters of rock, was started in 1978 with the selection of host rock formations. The following geologic formations were selected:

- anhydrite
- marl (mesozoic marl formations in the sediments of the alpine region)
- clay (Opalinuston, Dogger, in the region of the Jura mountains)
- crystalline rock (gneiss and granite in northern Switzerland and in the Alps)
- limestone formations (above the groundwater table) where they are covered by impermeable clay layers.

Based on a careful literature survey, 100 sites were identified in 1981, 20 sites were preselected, based mainly on the following criteria:

- geometry and size of volume of host rock
- hydrogeologic conditions
- predictability of detailed structural geology and hydrogeology
- current state of knowledge on geology and hydrogeology.

In 1983, a further selection was carried out after detailed desk studies and field inspections. In addition to the above mentioned criteria, the environmental and public impact and the general access possibilities were considered. Three sites have been selected for site investigations, six further sites are in reserve. Site investigation programs have been prepared and applications for permission for investigations have been submitted to the federal government.

The permission of the federal government is expected late in 1985, further permits from cantonal and communal authorities are then needed, which might cause further delays for the start of the 3 site investigation programs.

The time table for further work is as follows:

1985	Phase 1A	Preparation of detailled investigation programs, field inspections
1986-1987	Phase 1B	Investigation of three sites by boreholes and geophysical surveys
1987-1989	Phase 2	At least at one site, excavation of a gallery into the repository area, geologic and hydrogeologic investigations and in-situ tests
1989/90		Application for a license for the repository site
from 1995		Start of operation of the repository

This time table does not allow for delays of investigation permits due to political opposition.

Strategy for Site Characterisation

The strategy for site characterization is to carry out parallel site investigations (in different phases) and safety analysis with a gradually improved geological and hydrogeological data-set, in order to assure optimiziation of field work and to avoid delays.

For the Oberbauenstock Site, a complete safety analysis was carried out in 1984 for Project Gewähr. For the two other sites, safety analysis is underway.

The procedure can be summarized as follows:

- Safety analysis, based on geological and hydrogeological data-sets with parameter variations
- Identification of critical geological and hydrogeological parameters
- Phase 1 investigations (boreholes and geophysical surveys) with emphasis on determination of critical parameters with sufficient accuracy
- Revised safety analysis based on measured parameters
- Phase 2 investigations: gallery and in-situ tests
- Safety analysis report and application for site license.

Oberbauenstock Site

The Oberbauenstock Site is located in central Switzerland, 24 km southeast of Lucerne. The host rock is cretaceous marl (Valanginian) of the sedimentary sequence of the helvetic nappes. Figure 6 shows a geological profile through the site. A recently constructed highway tunnel 9 km long crosses the host rock formation and investigations for this tunnel allowed characterization of the host rock and definition of a geological and hydrogeological data set for the safety analysis which was carried out in 1984 for Project Gewähr.

The main areas to be investigated are:

- geometry of the host rock and structural geology of the site
- permeability of the host rock
- permeability of the disturbed zone around galleries and caverns.

The main investigations in phase 1 are:

- reflection seismic surveys along the existing highway tunnel
- one or more boreholes of length about 300 m from an existing auxiliary tunnel of the highway tunnel
- hydraulic tests and water sampling in short boreholes in the auxiliary tunnel.

Bois de la Glaivaz Site

The Bois de la Glaivaz Site is located in the western part of the Swiss Alps, 40 km southeast of Lausanne. The host rock is a tectonically accumulated anhydrite body to extend to expected a few km^3. At the surface, the anhydrite is transformed into gypsum.

The main areas to be investigated are:

- geometry of the anhydrite rock mass
- depth of gypsification of the anhydrite
- detection of potential water-bearing strata and lenses of sandstones and limestones.

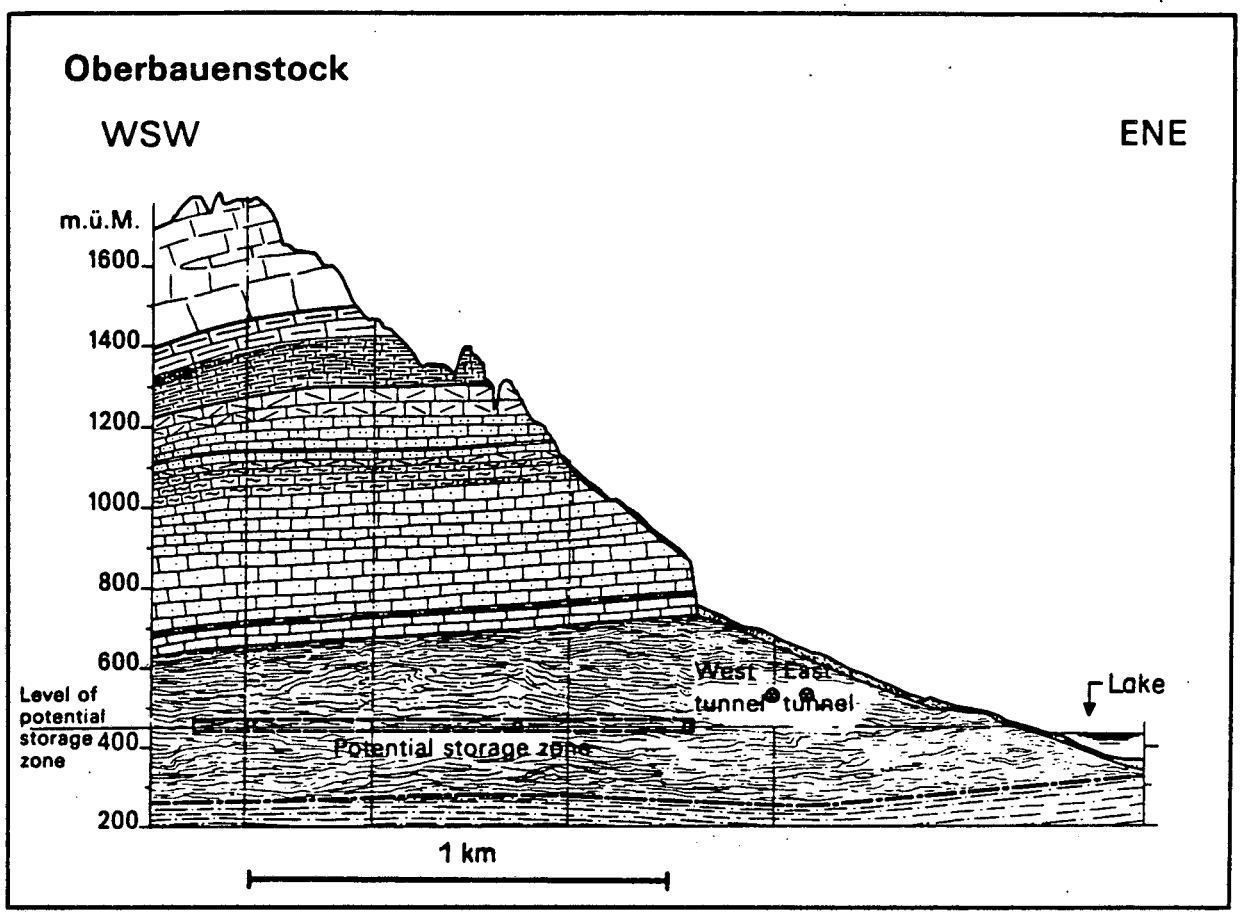

Figure 6. Oberbauenstock Site, geological profile through the planned repository zone

The main investigations in phase 1 are:

- one or more deep boreholes (about 1000 m long) with detailed hydraulic testing and water sampling
- seismic reflection surveys from the surface and seismic tomography between borehole(s) and surface.

Piz Pian Grand

The Piz Pian Grand Site is located in the eastern part of the Swiss Alps, 55 km south-southwest of Chur. The host rock is Gneiss of the penninic Adula-nappe. In the vicinity of the planned repository area, there is a water conduit for a hydropower station where, during construction, there was no water inflow over a distance of about 800 m.

The main area to be investigated is:

- determination of water flow systems and water flow field in a highly anisotropic fractured medium.

The main investigations in phase 1 are:

- geophysical surveys from the existing tunnel
- in the tunnel: short boreholes with hydrotests and water sampling.

AN OVERVIEW OF COUPLED PROCESSES WITH EMPHASIS IN GEOHYDROLOGY

G. de Marsily

Ecole des Mines de Paris
35 rue Saint-Honoré
77305 Fontainebleau, France

1. ABSTRACT AND INTRODUCTION

In the underground, fluids are always present ; most of the time, water is saturating the medium, but in some cases unsaturated media can be found even at great depth. These fluids are in general moving because of pressure gradients imposed by a complex function of the topography and of infiltraton (thus of the climate). The outlets of these movements are generally very localized (e.g. streams, springs) because again of topographical effects and/or of natural discontinuities which act as drains of the system. The fluid velocity and pathways in the underground are governed by the distribution of the hydraulic conductivity throughout the system, from the recharge zones to the outlets. This general circulation is in most cases slow enough for the water to reach equilibrium (or pseudo-equilibrium) with each of the successive types of rocks along its flowpath at their respective pressure and temperature. These successive equilibriums mean changes in chemical composition of the water, thus reactions with the medium (precipitation, dissolution, etc...) which in turn modify the hydraulic conductivity and flow path. Natural geodynamic processes (e.g. stress distribution variations, tectonic activity) on the other hand also modify the hydraulic conductivity and the flow path. These two mechanisms of natural modification of the flow system are generally negligible at the human time scale, but very significant at the historic time scale and the geologic time scale. The natural circulation field is thus a fully coupled thermal-hydrological-mechanical-geochemical system, and numerous evidence are available to study this coupling.

When wastes will be disposed of in the underground, will these coupling effect (i.e. the modification of the flowsystem) be increased ? It is necessary to distinguish between the non heat-emitting wastes and the heat emitting ones. For the former, the flow system will be essentially modified by the excavation and later backfilling of the rock, with the corresponding stress variations, and by the chemical anomaly introduced by the waste package and backfill, with which the water will have to equilibrate. In addition, for heat emitting wastes the heat load constitutes a major energy source for activating a series of complex coupled processes, which will have a time constant much shorter than most of the ones observed naturally, because of this intense energy source. The integrated heat released by 2000 m^3 of reprocessed glass cooled 50 years at the surface is 8 x 10^9 kWh after their disposal, most of which is produced in the first 1,000 years.

In this paper, we will try to review these processes, and mention, when possible, the similar coupled processes which can be observed in nature.

2. MODIFICATION OF THE FLOW FIELD

2.1. Mechanical coupling occurs with the stress modifications induced by the excavation, which extend several diameters of the galleries into the rock mass. Together with the backfill, which has different properties than the host rock, these zones can constitute a preferential new flowpath in the system (e.g. a short circuit between two water conducting fractured zones with different hydraulic heads). Preferential flow path are often observed in nature, when doing tracer tests for instance.

In addition, the later natural tectonic movements of the zone will be modified by the "weakness" introduced by the excavation, as major faults are observed to take place in zones where the minor fractures had a higher density. The differential composition of the backfill (e.g. in seismic events) can also create such flow paths. Field experiments and modelling studies are required here.

2.2. Thermo-mechanical coupling results from the thermal stresses imposed to the rock by the heat load ; this effect is important both for the heating and for the cooling phase of the wastes. In fractured rocks, the closing and opening of a network of joints with the stress field variation is not well predictable, nor the hydraulic conductivity variation occuring with these changes in opening (both at the single fracture or fracture network level). In nature, thermo-mechanical coupling is observable around magmatic phenomena (plutons, dykes, lava flows...). Intense fracturing and hydro-thermal circulations at the contact between the heat source and the existing rock is always observed. But the temperature level being different, large scale test are needed here, especially in fractured systems.

For clays, modelling work is presently done at ISMES in Italy to represent the flow field which is generated when heating the clay. The thermal expansion of the clay squeezes out significant amounts of water which is carried away in the general circulation of the system, influenced by the thermal currents ; the hydraulic conductivity of the clay is also affected by this expansion. Tests in the laboratory to measure the relevant properties of the clay, and choose the appropriate constitutive model, are done in Italy, Belgium and the UK.

2.3. Thermal coupling in the saturated zone is one of the first coupled mechanism which was mentionned and studied in waste disposal. This concerns thermal currents generated by density differences of hot water. This mechanism is well understood, and probably reasonnably well quantified, both in porous media

and in a single fracture. Additional work is however needed for predicting thermal currents in a complex fracture network, and for the coupling of thermal currents with natural field pressure gradients or natural salinity and density variations in the media, especially around salt structures. Thermal currents are observed (but difficult to measure) in most natural geothermal systems.

2.4. Thermal coupling in the unsaturated zone is an order of magnitude more complex. In tuffs, a thermal loop is created, with a liquid phase flow towards the canisters, and a vapour phase flow outwards, with successive condensation of the vapor. In fractured tuffs, complex capillary and relative permeability phenomena can take place between the fractures and the pores, involving extreme non linearities in phase transition, component disappearances and capillary discontinuities in fracture faces. Modelling studies are underway on this problem at Lawrence Berkeley, at Sandia, etc... and experimental studies are also required. Exact natural analogs are difficult to find, if any. Phreatic explosions which occur in volcanic systems are however natural examples of thermally induced two-phase flow systems which leed to explosive behaviour because of the mentionned non linearities.

Another two-phase flow system occurs in the resaturation of a repository after closure, in the thermal field of the wastes. Relative permeability and capillary effects are to be considered, as well as the dissolution or adsorption of air, or the leakage of air through particular pathways.

2.5. Chemical and thermo-mechanical coupling with the flow field is linked to precipitation, dissolution of material, which will clogg the system or enhance its hydraulic conductivity. As they occur naturally and can be observed in many systems (e.g. geothermal vents which seal, or on the contrary karstic systems which develop) they are bound to occur in wastes disposal, and be enhanced by the thermal gradients in the near field. Both the backfill and the host rock are concerned by such processes. One can mention :

- increase in hydraulic conductivity of the backfill by Na to Ca Bentonite transformation, or Bentonite to Illite transformation. Such transformations do occur in nature.
- total clogging of a portion of the system by precipitation, which can be the cause of a subsequent hydraulic fracturing because of pressure build-up, thus creating a short circuit in the flow system. Such phenomena are observed in geothermal systems.
- partial clogging of a system, where only narrow channels are left open for fluid flow (piping effect). In such channels, the fluid velocity becomes high, and the contact area with the rock for sorption of radionuclides becomes small, which both result in a enhanced migration towards the biosphere. Such channels are observed in nature, for instance the "veins" (open channels one inch in diameter) observed by Nagra in Switzerland in some cores of the crushed zones in the granite ("kakirites").

- Fractures in natural systems are also found to be most of the time sealed by precipitation of silica, of calcite, or of weathering products of unstable minerals (e.g. Feldspath generating clays). The rate of sealing of natural system is very poorly known, but could be rather fast (e.g. tens of thousands of years or less). This sealing can be greatly enhanced by the localized heat source provided by the wastes.

- Dissolution can also be the cause of such piping effects.

- For tuffs, the two-phase counter current flow (heat-pipe effect) will generate precipitation towards the canister, and dissolution by the condensing vapor phase and/or the capillary attracted liquid phase, with possible chemical reactions (e.g. acid formation in the presence of chloride).

All these effects need to be investigated in carefully designed in situ field experiments and also analog studies.

3. MODIFICATION OF THE TRANSPORT MECHANISMS

So far we have only reviewed some coupled processes which may affect the flow field in the system. We will now turn to coupled processes affecting the transport of the radionuclides towards the environment. This is somehow an artificial distinction, since the modification of the flow is of course the first major process affecting transport.

3.1. Chemical and thermo-chemical coupling is perhaps the problem of major concern. It will essentially be delt with in the review of chemical processes, since it concerns the change in the chemical nature of the species, with the corresponding retardation effects, which may take place along the flow path. We will only focus here on two issues.

- The possible sealing of the pores of the matrix in a dual fractured-porous system, by precipitation occuring in the fractures. If the surface of the fractures becomes coated with precipitated material, this may reduce or even anihilate the favorable role of matrix diffusion for radionuclide retardation. This clogging of the pores can be produced by non-radioactive elements either naturally occuring, or coming from the backfill (erosion of bentonite, or dissolution and reprecipitation in the thermal field). The existence of such sealing of pores may be the reason for the differences observed between Swiss and Swedish samples of granite, in analog studies of uranium series disequilibrium.

- The formation of real colloïds or pseudo-colloïds (i.e. sorption of radionuclides on existing colloïds) after the leaching of the wastes. Glass is known to liberate colloïds during dissolution, and colloïds are formed if a redox-front exist at some distance from the waste. The stability and transport of these colloïds, especially in fractured systems, is of major concern. They may be neutral, and therefore not be retarded by sorption mechanisms ; they may be negatively charged, and then be transported at a velocity larger than the average water velocity (this phenomenon, known as hydrodynamic chromatography, is explained by the fact that the particles being expelled from the walls always travel in the microscopic water veins having the largest velocity : the particle velocity can be 1.2 to 1.4 times the average water velocity). In porous media, colloïds are found to be in general filtrated by the medium (at least if their diameter is larger than 1/100 that

of the grains). But in fractures, there is very little evidence of any filtration of colloïdal material. The role of colloïds is known to be of large importance in the natural mobility of elements in soil profiles ; in fractured systems, very little is known on the mobility of the weathering products of the minerals (e.g. clays), which are found ubiquously : are they formed where they are found, or have they travelled in colloïdal form ?

3.2. Thermal coupling may have an indirect impact on the transport processes in at least the two following ways :

- the thermal currents (§ 2.3.) which modify the flow field can in turn modify the geochemical composition of the water, thus the chemical speciation of the leached and transported radionuclides. For instance, the thermal loops may bring oxydated water from the surface towards the repository, or bring up deep waters from below with a different salt content.

- In salt, the fluid inclusions which are mobile in the thermal field may bring towards the waste fluids capable of corrding or interacting with the canisters or the wastes itself. Such phenomena are receiving much attention in the Federal Republic of Germany.

3.3. Thermodynamical coupling effects on transport processes

In the classical theory of irreversible thermodynamic processes, the existence of coupling effects are well known. If we consider for instance the four major gradients which can be applied to a porous system (gradient of head, of concentration, of temperature, of electric potential), their major influence on the system are given the names of Darcy's law, Fick's law, Fourier's law and Ohm's law and create fluxes of water, elements, heat or electricity respectively. But if we look at these gradients and fluxes as a 4 x 4 matrix, these major influences are only the diagonal terms and the off-diagonal terms, which are all known to occur, are refered to as "effects". The following table describe the names which have been given to these processes.

fluxes of / gradients of	head	concentration	temperature	electric potential
water	DARCY	chemical osmosis	thermal osmosis	electro osmosis
elements in solution	ultra filtration	FICK	Soret	electro phoresis
heat	thermal filtration	Dufour	FOURIER	Peltier
electric current	Benoo	sedimentation current	Seebeck or Thompson	OHM

The importance of these effects in the near field are probably not negligible. Based on data collected from the litterature, C.L. Carnahan at LBL was able to show that for early times and reasonable assumptions of repository conditions, thermal-osmotic and chemical-osmotic flows of water and solutes in semi-permeable packing may exceed flows predicted by advection and diffusion alone by two to three orders of magnitude. In permeable materials, thermal diffusion may contribute to solute flows to a smaller but still significant extent.

The role of electric potential also needs to be investigated. Natural potentials are known to occur in the ground, e.g. the spontaneous potential, which is systematically measured when logging an oil well, or the teluric currents, which are highly variable, but have been used as natural sources for electric geophysical surveys. Artificial electric potentials can also result from the presence of different metals in a repository, e.g. various steels, cast iron, coper... or directly from radiolysis. All these electric potential sources may have an effect on elctro-osmosis flow of water, or electro-phoretic transport of solutes or colloïds. All these effects need to be investigated, first in the laboratory, in order to evaluate the value of the so-called "phenomenological coefficients", i.e. the proportionality constants between the gradients and the fluxes for the off-diagonal effects. Then numerical simulations and sensitivity studies will help evaluate the significance of these effects in relation to the direct (diagonal) terms.

In nature, the Soret effect has been suggested as the possible cause of occurence of some ore deposits, and osmotic membrane effects are observed in sedimentary basins with clays layers and brines. Electro-osmosis has been used industrially to drain low permeability clay layers and accelerate compaction.

3.4. Effects of gas emission on transport mechanisms

In saturated media, several mechanisms can produce gases : corrosion of the canister, biochemical decomposition of the waste in the environement (e.g. intermediate level wastes with organic matter, bitumen...), γ-radiolysis and α-radiolysis. In a salt formation, gas profuction by γ-radiolysis is estimated in the Federal Republic of Germany at the following rate , in liter per year, per meter of hole containing thin-walled steel canisters : O_2, 2 l ; H_2, 7 l ; CO_2, 1 l ; HCl, 0.1 l. These volumes are expressed at ambient temperature and pressure conditions, for a dose rate of 10^5 rad/h. Gas production by α-radiolysis is estimated at a few cubic meters per year per canister. This volume is expressed at a pressure of 9 MPa, not at ambient conditions. It assumes that, in an accident scenario, water has invaded the repository, and that all the wastes is put into soluble form, in order to maximize the α-radiolysis, as any layer of protective material will present the α particles to interact with the water. In any case this gas production can perhaps pressurize and hydraulically fracture an impervious buffer surrounding the wastes ; the movement of the gas bubbles, in a two-phase flow system, has also been shown in the FRG to enhance the transport of solutes. This is presently simulated with an apparent diffusion coefficient, larger than the effective one. This effect clearly needs additionnal testing in the laboratory and later in situ. In nature, complex two-phase flow systems occurs in geothermal geysers, or in natural mineral springs with high carbonic acid content.

In unsaturated conditions, gas production can take the form of vigourous boiling in the vicinity

of a high-level waste package. This could eject small liquid droplets into the gas phase. An aerosol may then form which can be transported along with the gas phase, and could carry liquid soluble contaminants towards the biosphere. This mechanism should be studied in the laboratory and theoretically.

4. A SPECIAL NOTICE FOR FLOW AND TRANSPORT IN FRACTURED MEDIA

Most natural formations are fractured, even when they are said to be plastic (e.g. clays, salt). The role of these fractures may be minor, or on the contrary very important. We have seen that many coupled processes discussed above are related to the existence of fractures (e.g. matrix diffusion, colloïd transport, hydraulic fracturing, thermal expansion...). One must however realize that the basic phenomena of flow and transport in fractured systems are still very poorly understood and represented. Most of the applied work has been done so far using the continuous equivalent porous medium assumption, and only in the last five years has a new approach, based on percolation theory and connectivity concepts, been suggested. But field applications and verifications of these concepts are extremely scarce. It is therefore clear that any in situ work on coupled processes in a fractured medium first needs to adress and answer the question of predicting flow and transport in a network of fractures. And for this, large-scale in situ experiments are urgently required.

5. CONCLUSION

There is a natural tendency among scientists to put forward our uncertainties, and to list all the problems which need to be studied before a final answer to a complex question can be given. As time goes by, the list of new problems may even grow faster them the list of resolved issues. In the late fifties, France was studying the possibility of testing nuclear weapons in the underground. At one point, the decision had to be taken wether the test should go on or not. A bunch of scientist then drew the attention of the decision makers on the possible detrimental role of radiations on one of the constituants of the host rocks, namely the pyroxenes. The decision went as high as President Charles de Gaule, who had this final word : "France will not wait for the Pyroxenes !". And the test went on.

Is nuclear waste disposal going to wait for the coupled processes ? I personnaly believe that it should, because (i) some coupled processes are not minor effects, they can be of major consequences. One could talk about synergetic effects, which emphasizes this aspect ; (ii) time is not running short ; we know how to do interim storage, and we know we do not loose money by doing so, on the contrary interim storage is economically beneficial, at least for high level wastes. There is therefore no scientific argument to deliberately neglect potentially important mechanisms which may effect safety.

It is however the role of scientists to give priorities to the various problems they suggest to consider. The following list of priorities has been agreed upon at the LBL coupled processes meetings, for hydrological phenomena :

a. Large sclae thermo-hydro-mechanical effects
b. Colloïd transport
c. Thermochemical (precipitation/dissolution)
d. Thermo-hydrological currents (for tuff)
e. Dispersion effect (channeling) in fractured media

6. REFERENCES

Avogadro, A., and de Marsily G. de (1983). The role of colloïds in nuclear waste disposal, in Scientific Basis for Nuclear Waste Management VII, G.L. McVay, ed., Materials Research Society Symposia Proceedings 26, Elsevier Science Publ. Co., 495-505.

Benet, J. (1981). Contribution à l'étude thermodynamique de milieux poreux nonsaturé avec changement de phase, Thèse de Docteur Science, Univ. Montpellier, France.

Bertrands, L., Beucher, H., Creutin, D., Feuga, B., Landry, D., and Thiery, D. (1982). Essai de détermination de la distribution régionale du tenseur de perméabilité du "Milieu poreux équivalent", Colloque G. Castany, Nov. 16-17, Orléans, published by BRGM, Orléans, France.

Beucher, H. (1983). Contribution de la Géostatistique à l'étude d'un milieu fracturé et mise au point d'un modèle hydraulique sur le site de la Mine de Fanay-Augères, rapport LHM/RD/83/10, Ecole des Mines de Paris, Fontainebleau, France.

Beucher H., Marsily, G. de (1984). Approche statistique de la détermination de perméabilités d'un massif fracturé. Rapport LHM/RD/84/16, Ecole des Mines de Paris, Fontainebleau, France.

Bories, S., Bacon, J., and Monferran, M. (1980). Influence de la teneur en eau et de la température sur la conductivité thermique des milieux poreux non saturés. Proceedings, 7th Int. Symp. IAHR, Toulouse, France.

Bories, S., Crausse, M., and Bacon, J. (1980). Etude fondamentale des transferts couplés chaleur-masse en milieu poreux. Rapport GE 16, Institut de Mécanique des Fluides, Univ. de Toulouse, France.

Combarnous, M.A., and Bories, S. (1975). Hydrothermal convection in saturated porous media, Adv. in Hydroscience 10, 232-307.

Commission of the European Communities (1982). Nuclear Science Technology, Admissible Thermal Loading in Geological Formations. Consequences on a radioactive waste disposal methods. Report EUR 8179, Luxembourg, 4 volumes.

Creutin, D. (1981). Analyse statistique de la distribution spatiale de la fracturation dans un massif cristallin. Rapport LHM/RD/81/10, Ecole des Mines de Paris, Fontainebleau, France.

Delhomme, J.P. (1978). Kriging in the hydrosciences. Adv. in Water Resources 1(5), 251-266.

Dieulin, A. (1982). Filtration de colloïdes d'actinides dans une colonne de sable argileux. Rapport LHM/RD/82/23, Ecole des Mines de Paris, Fontainebleau, France.

Dodds, J. (1982). La chromatographie hydrodynamique

analysis, Analysis 10(3), 109-119.

Dunand, M., Vauclin, M., and Vachaud, G. (1980). Simulation du comportement thermique du sol autour d'un échangeur enterré de pompe à chaleur. Proceedings, 7th, Int. Symp. IAHR, Toulouse, France.

Hodgkinson, D.P., and Bourke, P.J. (1979). Assessment of effects of thermally induced water movement on leakage from a radioactive waste repository. Note, OECD/NEA, Paris, France.

Hosanski, J.M. (1980). Contribution à l'étude de transferts thermiques en milieu fissuré. Thèse de Docteur Ingénieur, Ecole des Mines de Paris, Fontainebleau, France.

Jouana, P., and Louis, C. (1984). Ecoulement dans les milieux fissurés, méthodologie d'étude et modélisation. Les Annales des Mines.

Journel, J.A., and Huijbrecht, C. (1978). Mining geostatistics, Academic Press, New-York.

Long, J.C.S. (1983). Investigation of equivalent porous medium permeability in networks of discontinuous fractures, Ph.D. Thesis, Lawrence Berkeley Laboratory, Report LBL-16259.

Matheron, G. (1971). The theory of regionalized variables and its application. Cahier 5, Centre de Morphologie Mathématique, Ecole des Mines de Paris, Fontainebleau, France.

Person, J. (1981). Caractérisation de propriétés thermo-hydrauliques d'un sol non saturé. Application au stockage d'énergie par systèmes internes. Thèse de Docteur Ingénieur, Univ. Grenoble, France.

Pusch, R. (1983). Stability of deep-sited smectite minerals in crystalline rock-chemical aspects, SKBF KBS Tek. Rap. 83-16, Stockholm, Sweden.

Pusch, R. (1983). Use of clays as buffers in radioactive repositories, SKBF KBS Tek. Rap. 83-46, Stockholm, Sweden.

Quintard, M. (1984). Convection naturelle en milieu poreux : systèmes non stationnaires. Déplacement. Les Annales des Mines.

Ribstein, A. (1983). Contribution à l'étude des massifs rocheux fissurés : transfert de fluide, de chaleur et de matière dissoute associés. Thèse de Docteur Ingénieur, Ecole des Mines de Paris, Fontainebleau, France.

Runchal, A.K., and Maini, T. (1979). The impact of a high level nuclear waste repository on the regional groundwater flow, Principia Mechanica, Ltd. Report, London, England.

COUPLED PROCESSES IN GEOMECHANICS

Neville G. W. Cook

Department of Materials Science and
Mineral Engineering, University of
California, Berkeley
and
Earth Sciences Division,
Lawrence Berkeley Laboratory
Berkeley, California 94720

ABSTRACT

The safe operation of an underground repository for the disposal of nuclear wastes and the isolation of these wastes from the accessible environment, may be affected adversely by the formation of new fractures in the rock close to these excavations or by movements across pre-existing fractures. Both phenomena may so enhance the permeability of the rock as to allow possibly contaminated groundwater to reach the accessible environment. For hard rocks, the formation of new fractures in the regions of high stress concentration adjacent to excavations is analyzed in terms of "breakouts" or "spalling". In rocksalt, creep may allow the stress adjacent to excavations to decrease below the hydrostatic pressure so that hydraulic fractures may form, or the extension of layers other than salt may produce new hydraulic conduits. The deformation of fractures in response to changes in stress pore pressure, and temperature are analyzed for pre-existing fractures, as is also the shear stability of the fractures. Experience and in situ testing are seen to be of the greatest importance in identifying and understanding coupled phenomenon in geomechanics.

INTRODUCTION

The overall geomechanical requirements for a waste repository are to ensure safety during repository excavation, waste emplacement and backfilling, and to obviate disturbances to the rock mass that could result in the release of radioactive material to the accessible environment after closure. To meet these requirements it is necessary to demonstrate that

- the deformation of canister holes will be acceptable and stable;
- the deformation of rooms will be acceptable and stable;
- any new rock fractures which may be produced wil' not lead to unacceptable seismicity or unacceptable increases in hydraulic, or decreases in thermal, conductivities;
- the opening and, perhaps, closing of pre-existing and, new joints and fractures will not lead to unacceptable increases in hydraulic conductivity;
- the shearing of pre-existing joints and fractures will not produce unacceptable seismicity or unacceptable increases in hydraulic conductivity;
- backfilling and sealing of holes, rooms and shafts will provide adequate containment of, possibly contaminated, groundwater.

HOLES AND ROOMS

Hard Rock

It is obvious that the excavation of boreholes, for canister emplacement, and drifts, for the repository access ways and rooms, will result in a redistribution of the rock stresses adjacent to these excavations. At the depths of most proposed repositories, say 500 m to 1000 m below surface, the vertical stress will result essentially from the weight of the overburden and will, therefore, have values between 12 MPa and 25 MPa. Horizontal stresses in the shallow crust have values that range from as little as a third of the value of the vertical stress to more than three times its value (Hoek and Brown, 1980). The uniaxial compressive strengths of rocks at proposed repository sites range from essentially zero for salt, up to 250 MPa or more for basalt or granite. These strengths are typical mean values from laboratory measurements on small specimens of rock. The statistical spread of values from individual specimens may be as great as 50 percent. Furthermore, the strengths of small samples are considered to be significantly greater than those of rock masses *in situ* (Goodman, 1980; Hoek and Brown, 1980). Accordingly, it is not improbable that the concentration of tangential stress in the wall of an excavation may be sufficient for the tangential stress to exceed the strength of the rock. Indeed, there is already clear evidence from potential repository sites that this will occur. For example, the walls of exploratory boreholes in the basalts at Hanford have been found to be "broken out" (Kim, *et al.*, 1984), as have large diameter boreholes at the Nevada Test Site, (Springer, *et al.*, 1984).

Ordinarily, well bore breakouts and the analogous spalling of the walls of larger excavations would not be viewed as a phenomenon involving coupling. However, the maximum elastic stress concentration around openings depends upon the shape of the excavation. Specifically, the stress concentrations at the ends of the major and minor diameters parallel to the axes of the principle stresses for holes with ellipitical cross sections are given by:

$$\sigma_{\theta x} = \left[1 + 2\left(\frac{a}{b}\right)\right]\sigma_y - \sigma_x \qquad (1)$$

$$\sigma_{\theta y} = \left[1 + 2\left(\frac{b}{a}\right)\right]\sigma_x - \sigma_y \qquad (2)$$

where

σ_x and σ_y are the maximum and minimum principal stresses in the plane of the hole;

a = semi axis of the elliptical hole in the x-direction,

b = semi axis of the elliptical hole in the y-direction. (Jaeger and Cook, 1979).

In general, the maximum horizontal stress concentration around an opening in an elastic material increases approximately as the square root of the ratio between the distance of the hole surface from its center and the local radius of the curvature of that surface (Jaeger, 1979). The sketch in Figure 1 illustraste how the shapes of a circular borehole change as a result of "break out". A drift with a circular cross section "spalls" in much the same way. It can be seen that the change in cross section of the hole brought about by breakout or spalling accentuates the tangential stress concentration in the region adjacent to the breakout, causing further degradation. There is, thus, a powerful coupling between the geometry of a hole and its stability.

In practice, it would be very difficult to drill and keep open large numbers of boreholes for canister emplacement under conditions where breakout occurs. Likewise, it would be onerous and,

perhaps, dangerous to excavate drifts and rooms where spalling occurs. Breakouts and spalling also make it very difficult to plug or seal boreholes and drifts or shafts effectively, because the cracking and dilatation associated with breakout and spalling creates conduits through the rock by which groundwater can bypass the seals.

The conditions under which breakout and spalling occur can be analyzed using the theory of elasticity. Assume that the rock adjacent to an excavation begins to fail when the tangential stress becomes equal to the uniaxial compressive strengths, C_o , that is;

$$\sigma_\theta \geq C_o \tag{3}$$

Let

$$\frac{\sigma_z}{\sigma_y} = R$$

$$\frac{(\sigma_z - \sigma_y)}{C_o} = S$$

For a circular cross section of excavation, a = b, and this criterion becomes

$$3\sigma_z - \sigma_y \geq C_o$$

or

$$3\sigma_z - \frac{\sigma_z}{R} \geq \frac{(\sigma_z - \sigma_y)}{S}$$

that is,

$$S \geq \frac{(R - 1)}{(3R - 1)} \tag{4}$$

From equations (9) and (2) it can be seen also that the tangential stress around an excavation of elliptical shape is constant if $a/b = R$. In this case, the criterion becomes

$$\left[1 + 2\left(\frac{b}{a}\right)\right]\sigma_z - \sigma_y \geq C_o$$

or

$$\left[1 + 2\left(\frac{b}{a}\right)\right]\sigma_z - \frac{\sigma x}{R} \geq \frac{(\sigma_z - \sigma_y)}{S}$$

that is

$$S \geq \frac{(R - 1)}{(R + 1)} \tag{5}$$

These criteria are plotted also in Figure 1. Above the upper curve excavations with circular cross sections are stable. Between the upper and lower curves, excavations with ellipital cross sections and semi axes in the same ratio as the stresses are stable. Below the lower curve excavations will fail by breakout and spalling. Note that between the upper and lower curves initially circular excavations will fail to stable breakout shapes with their long diameter oriented perpendicular to the long semi axes of a stable elliptical cross section, that is, the stability criterion bifurcates. Below the lower curve, excavations with initially elliptical cross sections would enlarge to stable breakout shapes with a long axis perpendicular to the long semi axis of the ellipse, that is, a large volume of rock would fail.

The concept of effective stress has proved to have such wide applicability that it probably can be used also in the analysis of breakouts and spalling. In the presence of pore pressure, p, the effective stresses becomes $\sigma_z' = \sigma_z - p$ and $\sigma_y' = \sigma_y - p$. Pore pressure changes the ratio R to $R' = (\sigma_z - b/\sigma_y - p)$ but not the ratio S. Therefore, pore pressure can be expected to inhibit breakout and spalling.

As a result of the excavation of a repository, pore pressures can be expected to decrease, thereby enhancing breakout and spalling. Increase in pore pressure, such as may occur after closure, would enhance stability.

Thermoelastic stresses can be expected to exacerbate spalling. The tangential stress around an excavation with a surface temperature T_s is increased by

$$\Delta\sigma_\theta = \frac{\alpha E T_s}{(1-\nu)} \tag{6}$$

where

α = linear cofficient of thermal expansion

E = Young's modulus

ν = Poisson's ratio (Timoshenko and Goodier, 1951).

If the interior surface of an excavation is at a constant temperature, breakouts and spalling can be analyzed as described above by substituting $C_o' = C_o - \Delta\sigma_\theta$ for the uniaxial compressive strength, that is,

$$S = \frac{(\sigma_z - \sigma_y)}{(C_o - \Delta\sigma_\theta)} \tag{7}$$

Should thermally exacerbated spalling occur in a canister hole, an annulus of broken rock with diminished thermal conductivity will be created around the canister. This will lead to greater canister temperatures in order to maintain the flow of heat through the rock equal to that generated by radioactive decay in the canister. While this increase in temperature could prove damaging to a canister, the temperature of the rock at the new boundary of the solid rock will diminish as the reciprocal of the logarithm of the diameter of solid boundary. This decrease in temperature will reduce the thermally induced stress until spalling ceases. Alternatively, if the annular space between the canister and the hole is limited, this space will fill with spalled rock and the dilatation associated with further spalling will compress it, eventually generating a normal stress sufficient to prevent any new spalling from occurring.

This sequence of events was predicted and observed in one of the experiments at Stripa in which a full scale electrical heater with a power output of 5 kW simulated a caniste. of spent fuel 3 years out of the reactor, (Cook and Meyer, 1980), Fi ure 3. In this particular experiment, the rock mass in which the canister hole was drilled was heated also by a ring of peripheral heaters to simulate the thermal field in an actual repository that would result from adjacent canisters of waste.

The phenomenon of wellbore breakouts has attracted considerable attention recently as a method for determining stresses in rock at depth. Gough and Bell (1981, 1982) have analyzed breakouts in terms of elastic stress distributions and a Mohr Coulomb failure criterion. Zoback *et al.* (1985) making similar assumptions, show that breakouts result from shear failure of the rock where the compressive stress concentration is greatest around the hole. However, Fairhurst and Cook (1966) observed that spalling of the walls of the drifts occurs by rock splitting parallel to the direction of maximum tangential compression, and used a fracture mechanics model for the growth of Griffith cracks in compression to explain their observations. Freudenthal (1977) on the basis of a shear dilatancy model suggests that extensile fracturing may occur adjacent to excavations in rock subject to compression. In hard rock, spalling is characterized by extensive planar fractures, sometimes with dimensions of meters, that break the rock adjacent to the walls of excavations into sheets with thicknesses of the order to centimeters. The fractures follow the direction of the maximum horizontal stress with remarkable fidelity. Horii and Nemat Nasser (1985) have developed a numerical fracture mechanics model for the propagation of Griffith cracks in compression which results in spalling adjacent to a free surface.

Breakouts and spalling could make repository construction difficult and hazardous and may make retrieval very difficult, but the effect of this phenomenon may be most significant in terms of repository performance. The rooms and access ways of a repository constitute a network of interconnected hydraulic conduits, which did not exist in the natural state prior to repository excavation. Even filling these excavations with an uncemented backfill will reduce

their hydraulic conductivity to a negligible extent. To insure isolation of the wastes, these conduits will have to be interrupted at many points in the repository by the installation of cemented plugs and seals. If breakouts and spalling are dilatant phenomena, the cracks and fractures associated with them will produce permeable zones in the rock adjacent to breakouts and spalling. These permeable zones constitute paths by which possibly contaminated groundwater can be pass seals and plugs.

The strengths of even hard rocks are time dependent and decrease also with temperature and in the presence of water. Therefore, even where breakouts and spalling are not a problem in the short term of repository construction, they may become so in the longer term. Tapponier and Brace (1976) observed that virtually all stress induced cracks in Westerly granite at 23°C, a strain rate of 10^{-5} s^{-1} and confining stress of 50 MPa were extensile. Kranz (1979) showed that confining pressure strongly inhibits crack growth and time to failure in constant stress creep tests on dry Barre granite. For example, at a stress difference of 87 percent of the short term strength, the time to failure at a confining stress of 53 MPa was about 15 x 10^3 s whereas at a confining pressure of 0.1 MPa the time to failure was only about 400 s. Friedman *et al.* (1979) showed that the strength of charcoal granodiorite decreased from about 350 MPa at room temperature to only 140 MPa at a temperature of 400°C at zero confining pressure but that at a confining pressure of 50 MPa the strength decreased from about 630 MPa to 540 MPa, over the same temperatures. All the evidence seems to show that over extended period of time, say decades, breakout and spalling are likely to occur adjacent to repository excavations, where the confining stress is virtually zero. This may produce sones of enhanced hydraulic conductivity in the rock. The only effective way to inhibit breakout and spalling is through the early application of a confining stress, that is, this stress must be applied within hours, preferably minutes, of excavation to take advantage of the higher, short term strength of the rock.

Rock Salt

Rocksalt has negligible shear strength. Breakout and spalling are not expected to be major problems. Indeed, the creep deformation of rocksalt is expected ultimately to encapsulate the wastes completely. However, the closure of excavations may occur much more slowly than laboratory tests would lead one to expect. Steady state creep of rocksalt under isothermal, triaxial compression in laboratory tests is a power function of the stress difference.

$$\dot{\epsilon} = A \left[\frac{(\sigma_1 - p)}{K} \right]^n \tag{8}$$

where

$\dot{\epsilon}$ = strain rate;
A = constant that depends upon the temperature;
σ_1 = maximum principal stress;
$\sigma_2 = \sigma_3 = p$ = confining pressure;
K = normalising factor, say, the bulk modulus;
n = a hardening exponent with a value of typically of 4 or 5.

For multiaxial stress states, equation (8) can be written as

$$\dot{\epsilon}_{ij} = \frac{3}{2} A \left(\frac{\sigma_e}{K}\right)^{n-1} \left(\frac{S_{ij}}{K}\right), \tag{9}$$

where S_{ij} are the deviator stresses, that is,

$$S_{11} = \frac{(2\sigma_r - \sigma_\theta - \sigma_2)}{3}$$

$$S_{22} = \frac{(2\sigma_\theta - \sigma_2 - \sigma_r)}{3}$$

$$S_{33} = \frac{(2\sigma_2 - \sigma_r - \sigma_\theta)}{3}$$

and

$$\sigma_e = \left[\frac{3(S_{11}^2 + S_{22}^2 + S_{33}^2)}{2} \right]^{1/2} \tag{10}$$

Equation (9) can now be written conveniently as:

$$\dot{\epsilon}_{ij} = \frac{1}{2\eta} \sigma_e^{n-1} S_{ij}, \tag{11}$$

where

$$\eta = \frac{K^n}{(3A)}.$$

Consider now the creep deformation of a long, cylindrical hole in plane strain subjected to lithostatic stresses at infinity. Let the radius of the hole be r_o and the radial displacement of this boundary be u_o . When the creep strain is larger than the elastic strain, the deformation of the rocksalt will be almost incompressible, that is

$$\dot{u}_o \; r_o = \dot{u} \; r, \tag{12}$$

where u = the radial displacement at any radius r and the dot signifies the time derivative.

The stress equation of equilbrium in cylindrical coordinates is:

$$\frac{\partial \sigma_r}{\partial r} = \frac{\sigma_\theta - \sigma_r}{r}, \tag{13}$$

and the radial, tangential and axial strain rates are, respectively,

$$\dot{\epsilon}_r = -\frac{\dot{u}}{r} = -\frac{\dot{u}_o \; r_o}{r^2} \tag{14}$$

$$\dot{\epsilon}_\theta = \frac{\dot{u}}{r} = \frac{\dot{u}_o \; r_o}{r^2} \tag{15}$$

$$\dot{\epsilon}_2 = 0$$

so that, from equations (11) and (14) and (15)

$$(\sigma_r - \sigma_\theta) = 2\eta \; \sigma_e^{1-n} (\dot{\epsilon}_r - \dot{\epsilon}_\theta) \tag{16}$$

$$= -4\eta \left(\frac{\dot{u}_o \; r_o}{r^2}\right) (3\eta \; \dot{\epsilon}_e)^{1-n/n}$$

where

$$\dot{\epsilon}_e \equiv \frac{(2 \; \epsilon_{ij} \; \epsilon_{ij})}{3})^{1/2} = \left(\sqrt{\frac{4}{3}} \frac{\dot{u}_o \; r_o}{r^2} \right)$$

and, from equation (13),

$$\sigma_r = \int \left[\frac{(\sigma_\theta - \sigma_r)}{r} \right] dr$$

$$= 4\eta \left(\frac{\dot{u}_o \; r_o}{r^2} \right) \left(3\eta \sqrt{\frac{4}{3}} \frac{\dot{u}_o \; r_o}{r^2} \right)^{(1-n)/n} r^{-1} \, dr$$

$$= (3\eta \; \dot{u}_o \; r_o)^{1/n} \left(\frac{4}{3}\right)^{(1+n)/2n} \int r^{(-2-n)/n} \, dr$$

$$= -(3\eta)^{1/n} \; (\dot{u}_o \; r_o)^{1/n} \left(\frac{4}{3}\right)^{(1+n)/2n} \tag{17}$$

$$\frac{n}{2} r^{-2/n} + C$$

At $r = \infty$, $\sigma_r = \sigma_H$ the lithostatic stress, so that

$$\sigma_r = \sigma_H - (3\eta)^{1/n} \; (\dot{u}_o \; r_o)^{1/n} \tag{18}$$

$$\left(\frac{4}{3}\right)^{(1+n)/2n} \frac{n}{2} + r_o^{-2/n},$$

and at $r = r_o$, $\sigma_r = 0$, so that,

$$\sigma_H = (3\eta)^{1/n} \ (\dot{u}_o \ r_o)^{1/n} \ (\frac{4}{3})^{(1+n)/2n} \ \frac{n}{2} \ r_o^{-2/n},$$

that is,

$$\frac{\dot{u}_o}{r_o} = \frac{(2\sigma_H/n)^n}{[3\eta \ (\frac{4}{3})^{(1+n)/2n}]} \tag{19}$$

but $\dot{u}_o/r_o = \dot{\epsilon}_r$ and, comparing equation (19) with equation (8), it can be seen that the effect of the axisymmetric geometry is to diminish the effective magnitude of the stress difference reducing creep by a factor of $(2/n)^n$.

The tangential stress can be found from equations (13) and (18), and is given by,

$$\sigma_\theta = (3\eta)^{1/n} \ (\frac{4}{3})^{1+n/2n} \ (\dot{u}_o \ r_o)^{1/n} \ (1 - \frac{n}{2}) \ r^{-2/n} + \sigma_H \tag{20}$$

Finally, the axial stress can be found from equations (9) (19) and (20). The axial strain rate $\dot{\epsilon}_2 = 0$, σ_e cannot be zero so that, from equation (9) the deviator stress S_{33} must be zero, that is,

$$\frac{(2\sigma_2 - \sigma_r - \sigma_\theta)}{3} = 0$$

or

$$\sigma_2 = (3\eta)^{1/n} \ (\dot{u}_o \ r_o)^{1/n} (\frac{4}{3})^{1+n/2n} \left(\frac{1}{2} - \frac{n}{2}\right) r^{-2/n} + \sigma_H \tag{21}$$

It follows that at $r = r_o$

$$\sigma_r = 0$$
$$\sigma_\theta = \frac{2\theta_H}{n} \tag{22}$$
$$\sigma_2 = \frac{\sigma_H}{n}$$

Equations (22) show that the tangential and axial stresses around a circular excavation in rocksalt become less than the hydrostatic stress if $n \geq (\overline{\rho}/\rho_w)$ where $\overline{\rho}$ = the mean density of the overburden and ρ_w is the density of water or brine.

In reality, repositories will not be isothermal so that η, which is a function of temperature, will become a function of r. This will affect the preceding result quantitatively, but not qualitatively, except to diminish the stresses adjacent to the excavation to an even greater extent when the highest temperatures correspond to the smallest radii.

The creep deformation of rocksalt produces large extensile strains in a radial direction. Many rocksalt deposits are interbedded with layers of shale, clay and anhydrite. Most of these layers are much more brittle than rocksalt so that they may be broken intensively by extension.

Consider a layer of brittle rock, embedded in rocksalt, at a height h above an excavation with a circular cross section. If u_o is the radial displacement at the surface of this hole with radius r_o, then the radial displacement for incompressible flow at any other radius is given by:

$$u = \frac{u_o \ r_o}{r} \tag{23}$$

and the displacement parallel to any layer at $y = h$ is

$$\delta = \frac{u_o \ r_o}{r} \cos\theta = \frac{u_o \ r_o \ x}{(x^2 + h^2)} \tag{24}$$

The strain parallel to the layer is, therefore,

$$\epsilon_x = \frac{\partial \delta}{\partial x} = \frac{u_o \ r_o \ (h^2 - x_2)}{(x^2 + h^2)^2} \tag{25}$$

so that extension of the layer occurs for all $x > h$. Brittle layers easily break in extension. The resulting void space may, therefore, increase their hydraulic conductivity significantly.

FRACTURES

Fracture Aperture and Hydraulic Conductivity

In rocks of intrinsically low permeability, joints, faults and fractures constitute the principal conduits for the transport of groundwater. Essentially, the conductivity of these features, collectively referred to as fractures, arises from the fact their opposing surfaces are not completely flat, so that contact occurs between the surfaces across the asperities and voids exist between the surfaces elsewhere. The geometry of these contacts and voids varies with the stress normal to the fracture plane and the pore fluid pressure within it. The hydraulic conductivity of fractures depends upon the apertures of the voids and the manner in which they are interconnected. Under some conditions, shear displacements between the two surfaces may be expected to result in major changes in the geometry of contacts and voids.

It has been shown that, when the contact areas comprise a small fraction of the fracture surface area, fluid flow in a fracture is similar to that between parallel plates and the hydraulic conductivity of the fracture increases as the cube of the mean void aperture, (Iwai, 1976; Gangi, 1978). Experiments (Goodman, 1976; Bandis *et al.*, 1983) and theory (Walsh, 1981; Brown and Scholtz, 1985) based on the topography of the fracture surfaces show that this mean void aperture is a non linear function of the effective normal stress across the joint, that is, the difference between the total normal stress and the pore fluid pressure. As the normal stress increases so do the areas of individual contacts as well as the numbers of contacts. In principle, the hydraulic conductivity of a fracture can be derived from the mean joint aperture using the cubic relationship between these quantities.

However, experiments by Iwai (1976), Engelder and Scholtz (1981) and Raven and Gale (1985) have shown that the cubic relationship between fracture aperture and hydraulic conductivity breaks down at high stresses and small apertures, Figure 3. For apertures of less than about $10\mu m$ increases in the effective stress, to more than 10 MPa or 20 MPa, reduce the fracture aperture with little or no effect on the fluid flow. This means that under these conditions major void spaces in the fracture must close with virtually no change in the hydraulic resistance of the fracture. This can occur only if major void spaces are either isolated from the flow path or if the principal resistances to fluid flow occur in restricted connections between these voids. It follows that the hydraulic resistance of such restrictions must be comparatively insensitive to the normal stress, which would be the case if these restricted pathways resembled little pipes or tubes.

Actual curves showing the deformation of a fracture in basalt (Tsang and Witherspoon, 1981) and one in granite (Sun *et al.*, 1985) are shown in Figure 4. Note that these curves are fitted quite well by the hyperbolic relationship proposed by Bandis *et al.*, (1983).

$$\sigma = \frac{DK_i}{(1 - D/D_m)} \tag{26}$$

where

D = volumetric closure of the fracture;
D_m = maximum volumetric closure of the fracture;
$K_i = \frac{\partial \sigma}{\partial D}$ at σ=0 that is, the intial specific stiffness of the fracture.

The specific stiffness at any stress, K, can in principal be measured seismically (Chen, *et al.*, 1985), is given by

$$K = \frac{K_i}{(1 - D/D_m)^2} \tag{27}$$

Consider first how a change in the pore pressure, Δp, at constant applied stress, σ, changes the aperture of a fracture and hence its hydraulic conductivity. The aperture of a fracture depends virtually on the effective stress so that the aperture merely changes to that corresponding to a new effective stress $(\sigma - \Delta p)$. Of course, the reduction in effective stress reduces the frictional resistance to sliding between the fracture surfaces without changing the shear stress, so that the fracture may become unstable or less stable.

Second, consider a change in the pore pressure, Δp, when the total displacement of the fracture and the adjacent solid rock is held constant, as in plane strain. Let the change in pore pressure occur first. This would result in dilatation of the fracture and an equal displacement between any two planes parallel to the fracture in the solid rock adjacent to the fracture. Next change the applied stress by an amount $\Delta\sigma$. This will partially close the fracture and compress the solid rock one each side of the fracture by an amount $\Delta\sigma L/E'$ where L is the spacing between fractures, or the amount of solid rock on each side of the fracture, and E' is the plane strain modulus, that is,

$$E' = E \frac{(1-\nu)}{[(1+\nu)(1-2\nu)]}$$

The correct value of $\Delta\sigma$ is that which produces compression of the solid rock one each side of the fracture that equals exactly the change in fracture aperture brought about by $(\Delta\sigma - \Delta p)$, as is illustrated in Figure 5.

The effective normal stress across fractures is expected to change as a result of the redistribution of stresses around excavations, thermally induced stresses and pore pressures.

Effect of stress

In general, the excavation of openings always results in a decrease in the stress radial to the walls of the excavation. The stress in a tangential direction may increase or decrease depending upon the shape of the excavation and the ratios of the far field stresses. A criterion that the tangential stress should always exceed the original stress in any direction is most difficult to satisfy for a tangential stress parallel to the original maximum stress, that is,

$$\sigma_\theta \geq \sigma_z$$

If a is the major semi axis of an excavation with an elliptical cross section then

$$\left[1 + 2\left(\frac{b}{a}\right)\right]\sigma_z - \sigma_y \geq \sigma_z$$

or

$$\frac{b}{a} \geq \frac{R}{2}$$

For maximum stability, $b/a = 1/2$, so that the maximum ratio of the stresses that satisfies both the stability and tangential stress criteria is $R = \sqrt{2}$.

One of the experiments at Stripa (Wilson *et al.*, 1983) involved the measurement of the flow of groundwater into a drift with a cross section of 5 m square and a length of 30 m, and of the pressure gradients in the rock out to radial distances of up to 40 m. Plots of the hydraulic head in the rock around this drift at different radial distances against the logarithm of distance, Figure 6, were linear, as would be expected. However, the lines fitting these data do not intersect the wall of the drift at zero head, indicating that the head loss through an annulus of rock about 2 m thick around the drift was relatively much greater than that in the rock further away from the drift. Whereas the hydraulic gradient between radial distances of 4 m to 40 m showed the permeability of the rock mass around the drift to be about 10^{-10} m/s, the hydraulic gradient through the annulus showed the permeability of the rock immediately around the drift to be about 3×10^{-11} m/s. This reduction in permeability could easily be the result of the closure of fracture apertures by the tangential stress concentration in the rock adjacent to the drift.

Measurements of the stresses in the rock at Stripa indicated that the vertical stress was only about 5 MPa whereas the two horizontal stresses were about 20 MPa (Doe, *et al.*, 1981). This would result in the tangential stress in the roof and the floor of the drift being considerably greater than the original rock stress while that in the walls would actually be in tension. Very careful mapping showed that three of the four principal sets of joints dipped at more than 50° while the forth set was sub horizontal (Gale *et al.*, 1982). The near vertical joints would have been closed under the high tangential stress which may account for the observed decrease in flow.

Effects of temperature

Increases in the temperature of the rock around a repository will produce thermal expansions that result in changes in stress. In general, within the volume of rock through which temperatures increase there will be an increase in compressive stress. In order to maintain overall equilibrium, it follows that outside the heated volume there must be exactly compensatory decreases in compressive stress. While increases in stress will tend to close fractures and therefore decrease the permeability of the volume of heated rock, the corresponding decreases in stress will enhance permeability outside the heated volume. In total, the net effect of changes in temperature must be to increase the overall permeability of the rock mass, because of the highly non linear relationship between the hydraulic conductivity of a fracture and the normal stress across it.

Porous materials have the same coefficient of linear expansion as the material of their solid matrix. However anomalously low values for thermally induced displacements and stresses were measured in the Stripa heater experiments (Chan *et al.*, 1980). These values have been shown (Cook, 1983) to result from the deformation across fractures. Imagine a column of rock of length L that is subject to stress, σ, contains a fracture normal to its axis, and is constrained at its ends from expansion, so that an increase in temperature produces also an increase in the stress across the fracture. Let $\Delta\overline{T}$ be the mean increase in temperature of a heated length l of this column. In the absence of the fracture, the thermally induced increment of stress would be

$$\Delta\sigma = \frac{l\ \alpha\ \Delta\overline{T}}{L} E \tag{26}$$

where

α = coefficient of linear thermal expansion of the intact rock;
E = Young's modulus.

In the presence of the fracture with a specific stiffness K at a stress σ, the thermal expansion would partly be taken up by closure of the fracture aperture so that the increment in stress would be

$$\Delta\sigma' = \frac{l\ \alpha\ \Delta\overline{T}}{\left[\frac{L}{E} + \frac{1}{K}\right]}$$

The thermally induced displacements of any points on each side of the fracture are shown in Figure 7 as are the corresponding displacements that would exist in the absence of a fracture. From this figure it can be seen that the thermally induced displacements are altered so much by the fracture that no predictions about stress or displacements can be made without at least knowing the specific stiffness of the fracture and its location relative to the temperature field and the measuring points.

Effect of pore pressure

Probably the largest change in stress across a fracture will result from changes in pore pressure that can be expected as a consequence of the thermal expansion of water. For some period after excavation and before closure, the repository excavations will act as an hydraulic sink so that pore pressures in the rock around a repository will decrease from their original values, and this decrease will result in further closure of most fractures. Most repositories are expected to experience a thermal pulse as a result of the radioactive decay of the wastes. In many cases the peak temperature of this pulse will be reached within a few decades of waste emplacement (Wang *et al.*, 1980). After the repository excavations have been closed, any repository below the water table will begin to resaturate. Some idea of the order of magnitude of this resaturation time can be gained from the large scale permeability experiment at Stripa. In this experiment the total inflow of groundwater into a drift measuring 30 m in length by 5 m square cross section, was 50 ml/min. Most repositories are expected to be placed in host formations with permeabilities no greater than the Stripa quartz monzonite. The time it would have taken to resaturate the drift at Stripa is almost 10^9 seconds or about 30 years. If the resaturation period is greater than the time taken to reach peak temperature of the thermal pulse, thermal expansion of the water is not likely to pose any problem. However, if the resaturation period is less than the time taken to reach peak temperature, considerable increases in pore pressure may occur as a result of the relatively great coefficient of volumetric thermal expansion of water, about $0.0006/C^{o}$. To estimate the change in pore pressure it is necessary to balance the thermal increase in the volume of water against the outflow. Outflow will always occur at least as readily as would steady one dimensional flow from the repository to the surface. If the permeability of the strata overlying the repository is k, the depth below surface is H, and the mean thickness of all the water in the excavations averaged over the plan area of the repository is h, and the rate of heating is $\dot{T}$, then the pore pressure increment corresponding to steady flow could be found from

$$h\ \alpha\ \dot{T} = k(\frac{\Delta p}{H}), \tag{28}$$

that is,

$$\Delta p = \frac{H\ h\ \alpha\ \dot{T}}{k} \tag{29}$$

For, say H = 1000 m , h = 1 m, k = 10^{-11} m/s, α = $0.0006/^{o}$C and $\dot{T}$ = 3 x 10^{-8}°C/S (1^{o}/year), Δp = 1800 m or 17.6 MPa. This is not insignificant in relation to the expected values of rock stress.

Stability

Finally, it is necessary to consider the shear stability of fractures subjected to changes in stress, pore pressure, fluid flow and temperature, partly as potential sources orf seismicity but mainly because it has been shown (Barton, *et al.*, 1985) that relative shear displacements between fracture surfaces can enhance the hydraulic conductivity of fractures by a few orders of magnitude.

Jaeger and Cook (1979), and Cook (1981), Rice (1983) and Li and Rice (1983) have used two concepts of a complete stress strain curve, or load displacement curve, and an unloading modulus to analyze the stability of rock fractures.

Essentially, for any rock fracture some relationship must exist between the relative displacement between the two surfaces of the fracture and the shear stresses that arise from the resistance to sliding of these surfaces. This relationship specifies the complete strength of the fracture over all possible values of the relative displacement between its surfaces. (Conventionally, the "strength" is the maximum ordinate of this complete relationship.) We shall refer to this complete displacement-strength relationship as a *reduced Griffith locus*. In general, reduced Griffith loci are non linear and reflect the properties of the material and the changing geometry of the fracture.

Correspondingly, another relationship must exist between the shear stress applied to a fracture by the surrounding rock and the displacements through which the shear stress moves. This relationship specifies the stiffness of the loading system that applies the shear stress. (In conventional engineering "dead weight" loads, the magnitudes of which do not change with displacement, that is, their stiffness is zero, are often used: in this case only the "strength" is needed to determine stability.) The system may be the surrounding rock mass or a testing machine. We shall refer to this relationship as the *unloading modulus*. For loading systems in which the fracture is the only non linearity, unloading moduli are linear. Unloading moduli may be evaluated by applying hypothetical shear displacements to an idealized and frictionless fracture surface and calculating the shear stresses corresponding to each displacement.

An hypothetical reduced Griffith locus for a shear fracture, showing the shear resistance to sliding of the fracture as a function of the shear displacement between the two surfaces is illustrated in Figure 8. This locus represents the complete behavior of the fracture; displacements and stress move along the locus as the fracture grows. Every point on the locus corresponds to some limiting state of equilibrium on the fracture.

A fracture is embedded in rock which essentially behaves elastically. If, as described above, the fracture were replaced by a frictionless system through which the displacements were controlled, the unloading modulus of the rock mass could be determined by calculating the change in shear stress as a function of shear displacement. The slope of this unloading modulus is independent of the magnitudes of the stresses and displacements and of the fracture surfaces; it depends only upon the geometry of the system and the elastic constants of the rock mass.

Consider the stability of a fracture embedded in a rock mass with a given unloading modulus as the fracture evolves along a reduced Griffith locus. Let the shear stress in the rock mass be increased until a limiting state of stress exists at A. The unloading modulus at this point has a flatter slope than the reduced Griffith modulus, so that the fracture growth would be unstable and the applied load would move along the unloading modulus until the shear resistance of the fracture equals the applied shear stress at point B. In fact the energy supplied by the system as it unloads is greater than that absorbed by the fracture as it evolves from A to B in the amount shown by the area ABC, so that the fracture would shoot past the equilibrium position B to some other position such as D. At D the system is again stable and the fracture cannot evolve unless the shear stress increases to point E. Here again, an equilibrium state of stress exists and the fracture remains stable because the unloading modulus lies within the elastic part of the locus. Therefore, the fracture will evolve only if further shear displacement is provided to the system from outside, so as to bring the shear stress and displacements back on to the locus. Although the displacements will increase the stresses will decrease, because the fracture is evolving to a weaker condition. Such stable deformation can continue until the unloading modulus becomes tangent to the reduced Griffith locus at F where the system becomes intrinsically unstable, because the unloading modulus lies completely outside the Griffith locus.

Conceptually, the reduced Griffith locus can be found as follows. A fracture comprising any given geometry of asperities can be deformed elastically until the stress intensity factors at the asperities reach critical values. At this point further deformation would be inelastic. However, this end point of the elastic deformation defines a point on the locus corresponding to asperities of a particular size. As a result of inelastic deformation, or fracture growth, the size of the asperities will diminish. Other points on the locus can be found by determining the end points of elastic loadings for asperities of successively diminished sizes.

The effects of changing temperature on the stability of a fracture can be found, in principle, by using critical stress intensity factors that are functions of temperature. A higher tempeature may lead to lower stress intensity factors and hence a smaller Griffith locus as illustrated by the dashed curve in Figure 8. Similar corrections can be made for the effects of fluid chemistry on the fracture energy or stress intensity factors.

Pressure solution at points of high stress concentration may be a relatively important phenomenon in determining fracture stability. The formation of stylolites has been analyzed in terms of pressure solution at points of high stress concentrations (Fletcher and Pollard, 1981; Merino *et al.*, 1983). The asperities of contact in a fracture constitute points of high stress concentrations at which pressure solution may be expected. This will have the effect of diminishing the size of the asperities in a manner similar to that in which their size is diminished by additional deformation. Therefore, pressure solution would be equivalent to increasing deformation; it may move a fracture from a point such as B to one such as E. At any point on the locus the instantaneous stability would still be determined by the slope of the unloading modulus compared with that of the locus at that point.

CONCLUSION

In this paper I attempted to identify coupled processes in geomechanics, that may be detrimental to repositories, by examining specific changes to the rock around canister holes and storage rooms that could adversely affect the use or the performance of a repository. It appears that the formation of new fractures in zones of the greatest stress concentrations adjacent to excavations, or the mobilization of old fractures, perhaps at quite large distances from the excavations, may generate new conduits or increase the conductivity of old conduits, so that, possibly contaminated, groundwater may reach the accessible environment sooner than is acceptable.

The approach used in this paper led to the analysis of specific potential problems in a repository namely, breakout and spalling in hard rocks and creep in rocksalt around holes and drifts, and fracture closing and opening and stability in the rock mass, rather than the identification of a variety of related phenomena, as was done in the panel report (Tsang and Mangold, 1984). Interestingly, both the approach in this paper and that in the report led to the identification of processes on the basis of relevant past experience rather than on the basis of fundamental scientific prediction. Certainly, well bore breakouts and the spalling of drifts as well as the still incompletley understood, complex mechanical, hydraulic and thermal behavior of fracture are more in the nature of discoveries rather than predictions. The seminal role of the Stripa experiments is obvious. I recognize that the emphasis in this paper has been on processes involving essentially mechanical hydraulic and thermal coupling, and that chemical effects may be more important than is recognized here. To some extent this is because relatively little work has been done on problems involvng mechnanical and chemical effects.

I am forced to conclude that there is no altenative to comprehensive in situ testing, both generic and site specific, to identify and resolve problems relating to waste repository performance in general and coupled processes in particular.

REFERENCES

Bandis, S. C., A. C. Lumsden and N. R. Barton, Fundamentals of rock joint deformation, *Int. J. Rock Mech. Min. Sci.*, 20, 249-268, 1983.

Barton, N., S. Bandis, and K. Bakhtar, Strength, deformation and conductivity coupling of rock joints, *Int. J. Rock Mech. Min. Sci.*, 22, 121-140, 1985.

Chan, C., E. Binnall, P. Nelson, R. Stolzman, O. Wang, C. Werner, K. Ang, J. Braley, and M. McEvoy, Thermal and thermomechanical data from *in situ* experiments at Stripa, Sweden, Lawrence Berkeley Laboratory Report, LBL-11477, SAC 29, 1980.

Chen, G., S. Coen, N. G. W. Cook, and L. R. Myer, Seismic characteristics of an interface in imperfect contact, Annual Report 1984, Lawrence Berkeley Laboratory, 69-73.

Cook, N. G. W., Effect of joints on thermally induced displacmeents and stress, *Proc. 24th U. S. Symp. on Rock Mech.*, Texas A&M University and *Assoc. of Eng. Geology*, 1983.

Cook, N. G. W., Stiff testing machines, stick-slip sliding, and the stability of rock deformation, *Mechanical Behavior of Crustal Rocks*, eds. N. L. Carter, M. Friedman, J. M. Logan and D. W. Stearns, Geophys. Monograph 24, 93-102, Am. Geophysical Union, 1981.

Doe, T. W., R. Ingewald, L. Strindell, B. C. Haimson, and H. Carlsson, Hydraulic fracturing and overcoring stress measurements in a deep borehole at the Stripa test mine, Sweden, *Proc. 22nd U.S. Symp. on Rock Mech.*, M.I.T., 373-378, 1981.

Engelder, T., and C. H. Scholtz, Fluid flow along very smooth joints at effective pressures up to 200 magapascals, *Mechanical Behavior of Crustal Rocks*, eds. Carter, N. L., M. Friedman, J. M. Logan, and D. W. Stearns, Geophys. Monograph 24, 142-152, Am. Geophys. Union, 1981.

Fairhurst, C. and N. G. W. Cook, The phenomenon of rock splitting parallel to the deviation of maximum compression in the neighborhood of a surface, *Proc. First Cong. Int. Soc. Rock Mech.*, 687-693, Lisbon, 1966.

Fletcher, R. C., and D. D. Pollard, Anticrack model for pressure solution surfaces, *Geology*, 9, 419-424, 1981.

Freudenthal, A. M., Stresses around spherical and cylindrical cavities in shear dilatant elastic media, *Proc. 18th U. S. Symp. on Rock Mech.*, Keystone, Colorado, 1977.

Friedman, M., J. Handin, N. G. Higgs, and J. R. Lanz, Strength and ductility of four dry igneous rocks at low pressures and temperatures to partial melting, *Proc. 20th U. S. Symp. on Rock Mech.*, Austin, Texas, 1979.

Gale, J. E., A. Rouleau, P. A. Witherspoon, and C. R. Wilson, Progress in the hydrogeological characterization of the Stripa site, Lawrence Berkeley Laboratory Report, LBL 14878, SAC 49, 1982.

Gangi, A. F., Variation of whole and fractured rock permeability with confining pressure, *Int. J. Rock Mech. Min. Sci.*, 15, 249-257, 1978.

Goodman, R. E., *Introduction to Rock Mechanics*, 478 pp, Wiley, New York 1980.

Goodman, R. E., *Methods of Geological Engineering in Discontinuous Rocks*, West Publishing, New York, 1976.

Gough, D. I. and J. S. Bell, Stress orientations from oil well fractures in Alberta and Texas, *Canad. J. of Earth Sci.*, 18, 638-645, 1981.

Gough, D. I., and J. S. Bell, Stress orientations from borehole wall fractures with examples from Colorado, east Texas and northern Canada, *Canad. J. of Earth Sci.*, 19, 1358-1370, 1982.

Hoek, E. and E. T. Brown, *Underground Excavations in Rock*, 527 pp, The Institution of Mining and Metallurgy, London, 1980.

Horii, H., and S. Nemat-Nasser, Compression-induced microcrack growth in brittle solids: Axial splitting and shear failure, *J. Geophys. Res.*, 90, 3105-3125.

Iwai, K., Fundamental studies of fluiud flow through a single fracture, Ph.D. Thesis, University of California, Berkeley, 1976.

Jaeger, J. C. and N. G. W. Cook, *Fundamentals of Rock Mechanics*, 3rd ed., 593 pp., Chapman and Hall, 1979.

Kim, K., S. A. Dischler, J. R. Aggson and M. P. Hardy, The state of in situ stresses determined by hydraulic fracturing at the Hanford site, Rockwell Hanford Report, Richland, Washington, 1984.

Kranz, R. L., Crack growth and development during creep of Barre granite, *Int. J. Rock Mech. Min. Sci.*, 16, 23-35, 1976.

Li, V. C. and J. R. Rice, Preseismic rupture progression and great earthquake instabilties at plate boundaries, *J. Geophys. Res.*, 88, 4231-4246, 1983, 303-307.

Merino, M., P. Ortoleva, and P. Strickholm, Generation of evenly spaced pressure-solution seams during (late) diagenesis. A kinetic theory, *Contrib. Mineral Petrol.* 82, 360-370, 1983.

Raven, N. G., and J. E. Gale, Water flow in a natural rock fracture as a function of stress and sample size, *Int. J. Rock Mech. Min. Sci.*, 22, 251-262, 1985.

Rice, J. R. Constitutive relations for fault slip and earthquake instabilities, *Pagcopl.* 121, 443-475, 1983.

Springer, J. E., R. K. Thorpe, and H. L. McKague, Borehole elongation and its relation to tectonic stress at the Nevada test site, Lawrence Livermore National Laboratory, Report UCRL-53528, pp. 43, 1984.

Sun, Z., C. Gerrard, and O. Stephansson, Rock joint compliance tests for compression and shear loads, *Int. J. Rock Mech. Min. Sci.*, 22, 197-214, 1985.

Tapponier, P., and W. F. Brace, Development of stress induced microcracks in Westerly granite, *Int. J. Rock Mech. and Min. Sci.*, 13, 103-112, 1976.

Tsang, C. F. and D. C. Mangold, Panel report on coupled thermo-mechanical-hydro-chemical processes assocsiated with a nuclear waste repository, Lawrence Berkeley Laboratory, Report 18250, July 1984.

Tsang, Y. W. and P. A. Witherspoon, Hydromechanical behavior of a deformable rock fracture subjected to normal stress, *J. Geophys. Res.*, 86, 9287-9298, 1981.

Walsh, J. B., Effect of pore pressure and confining pressure on fracture permeability, *Int. J. Rock Mech. Min. Sci.*, 18, 429-435, 1981.

Wang, J. S. Y., C. F. Tsang, N. G. W. Cook, and P. A. Witherspoon, A study of regional temperature and thermohydrological effects of an underground repository for nuclear wastes in hard rock, *J. Geophys. Res.*, 86, 3759-3770, 1981.

Wilson, C. R., P. A. Witherspoon, J. C. S. Long, R. M. Gailbraith, A. O. duBois and M. J. McPherson, Large-scale hydraulic conductivity measurements in fractured granite, *Int. J. Rock Mech. Min. Sci.*, 20, 269-276.

Zoback, M. D., D. Moor, L. Mostin, and R. N. Anderson, Well bore breakouts and in situ stress, *J. Geophys. Res.*, 90, 5523-5530, 1985.

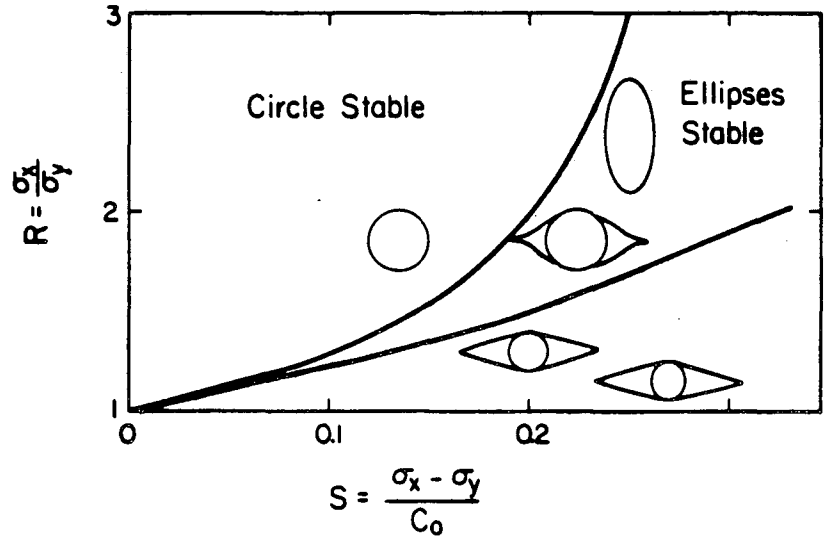

Fig. 1. Regions of stability for excavations with circular, elliptical, and breakout cross sections in terms of the ratio of the principal stresses, R, and the ratio of the difference of the principal stresses to the uniaxial compressive strength, S.

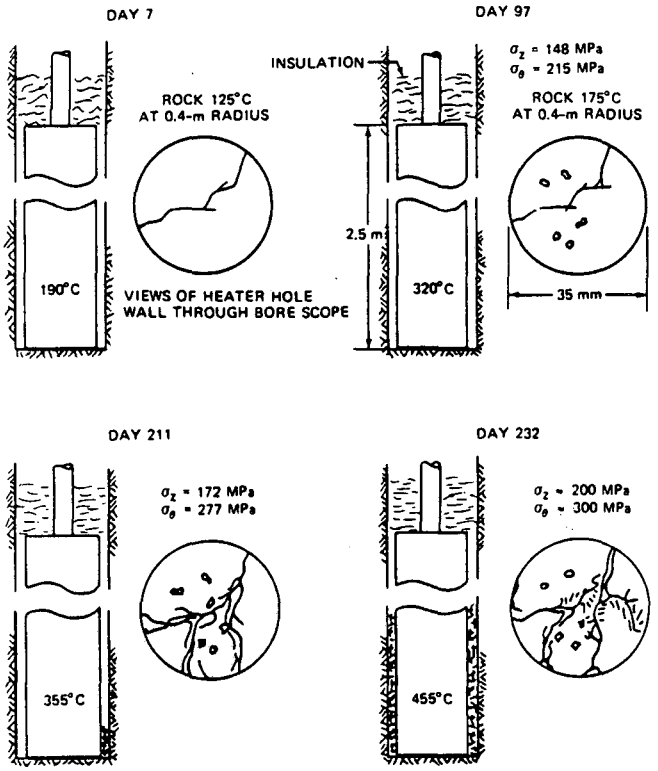

Fig. 2. Axial sections through a canister hole containing a 5 kW heater at different times after emplacement, illustrating the thermal decrepitation of the rock adjacent to the hole. Inserts are sketches of the hole wall made using a borescope.

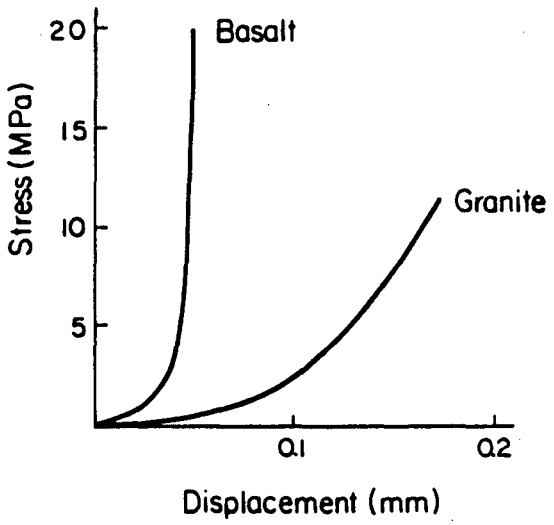

Fig. 4. Experimental relationship between normal stress and fracture aperture in basalt and granite, after Tsang and Witherspoon (1981) and Sun *et al.*, (1985).

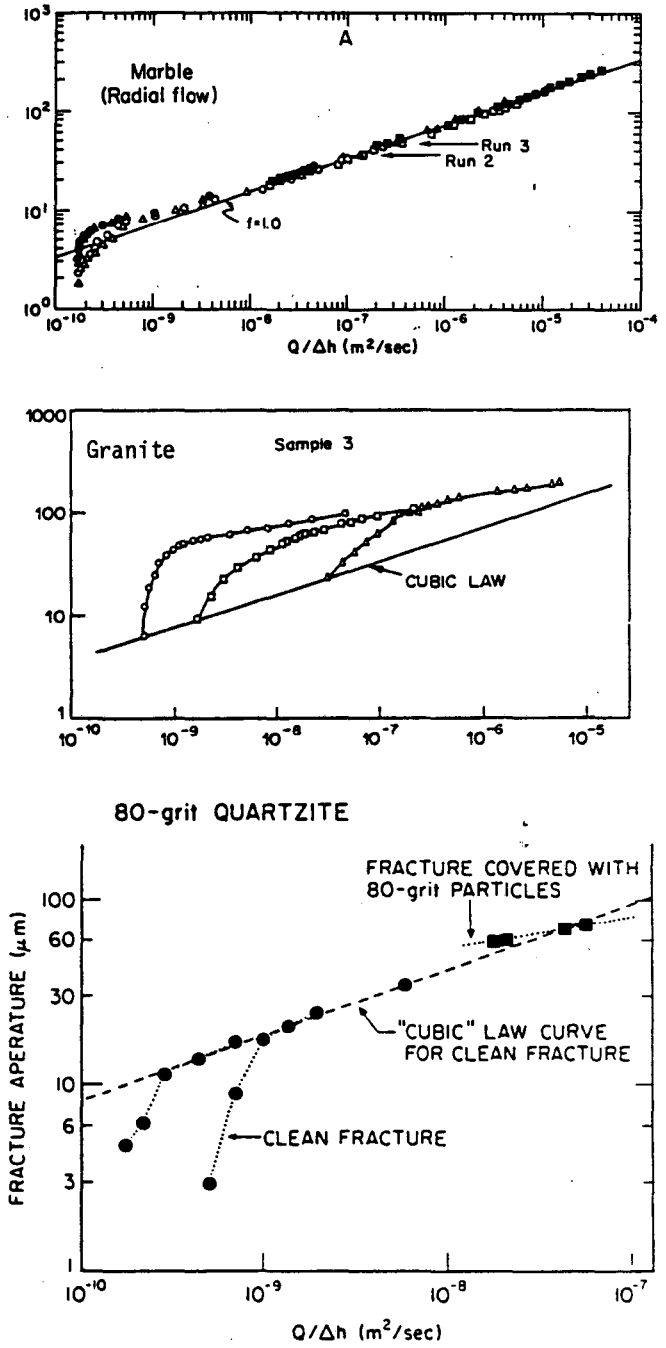

Fig. 3. Relationships between the mean aperture of fractures in rock and specific hydrauic flow through them, after Iwai (1976), Raven and Gale (1985), and Engelder and Scholtz, (1981). Note that the cubic relationship between aperture and flow, a straight line in a semi log plot, breaks down for small apertures.

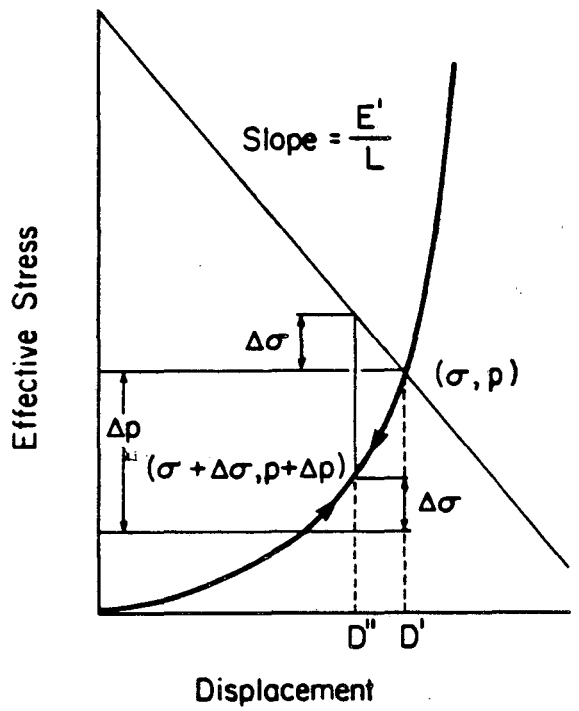

Fig. 5. Changes in fracture aperture brought about by as change in pore pressure, Δp , under constant stress and constant strain conditions.

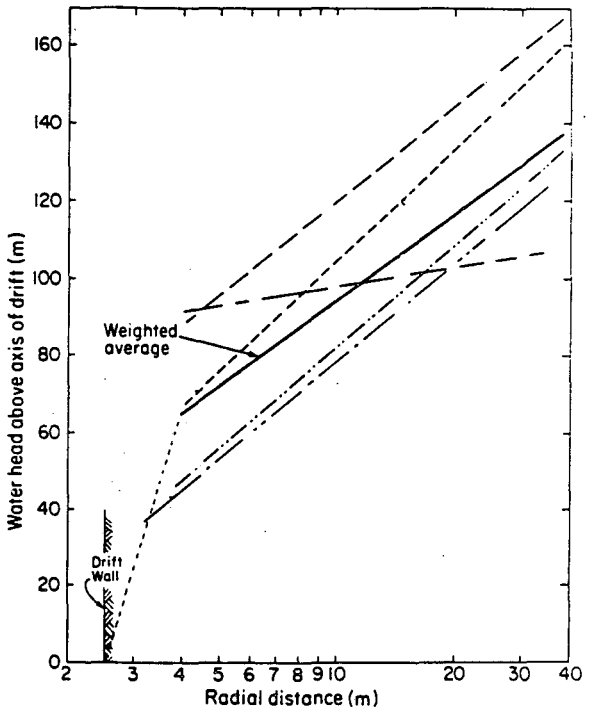

Fig. 6. Regression lines fitted to measurements of pressures at different radial distances for around a drift and the weighted average of these data, showing that the high head loss between the drift well and a radius of about 4 m.

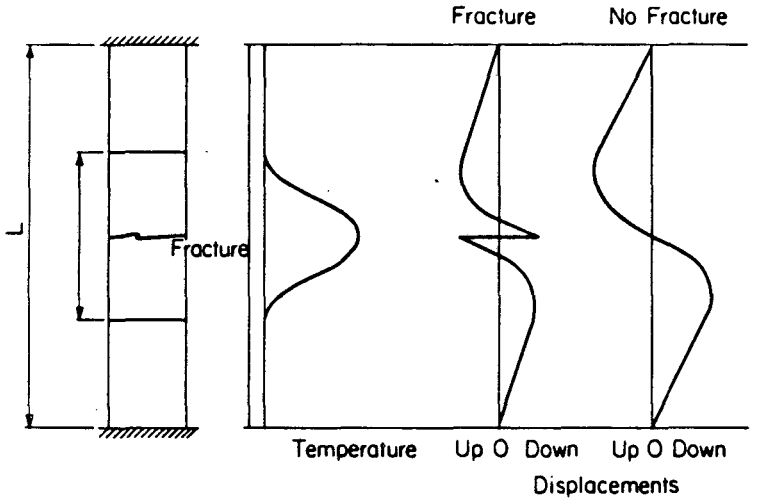

Fig. 7. Sketches illustrating thermally induced displacements in a column of rock with and without a fracture.

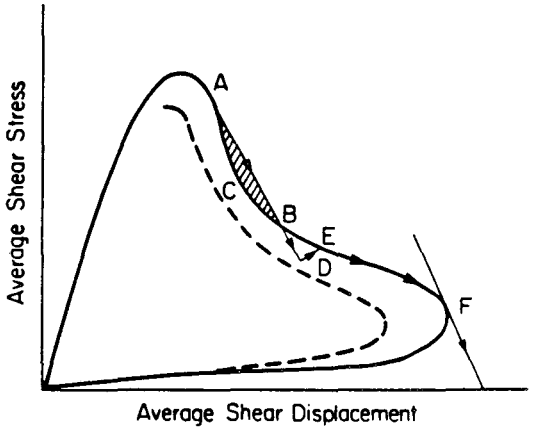

Fig. 8. Sketch showing a reduced Griffith locus and an unloading line, indicating stable (BEF) and unsetable (AB and F) shear displacements. The dashed lows indicate reductions in strength caused by temperature or chemistry.

COUPLING OF FLUID FLOW WITH STEP-WISE ALTERATION OF GLASS WASTE FORMS

M.J. Apted (1), D.L. Lane (2), C.C. Allen (2), R.R. Adee (1) and S.A. Rawson (2)

1- Pacific Northwest Laboratories
Richland, Washington 99352

2- Basalt Waste Isolation Project
Rockwell Hanford Operations
Richland, Washington 99352

ABSTRACT

The effect of flow of a basalt groundwater on the alteration of a borosilicate glass at 150 oC was investigated. The first observable effect is that glass dissolution rates increased appreciably with increasing flow rate. Such effects promote a more rapid alteration of glass to solids that will initially control the release rate of many radionuclides. The second effect is that solution supersaturations are progressively suppressed with increasing flow rate. Under favorable circumstances, this could prevent the formation of some metastable alteration solids and promote the formation of more stable solids. In this way, the progressive step-wise alteration of glass could be studied, and an evaluation made of the long-term controls for radionuclide release from glass waste forms. Failure to demonstrate such step-wise alteration in these preliminary flow tests may be attributable to high initial solution supersaturations developed from non-flow-related factors or to diffusional constraints to continued chemical reaction processes at the glass surface.

INTRODUCTION

The release of radionuclides from glass waste forms emplaced in geologic repositories will be controlled by the forward dissolution ("leach") rate of the waste form (Wicks et al, 1982) or solubility-limits (Wood, 1980; Grambow, 1982). Solubility limits will be imposed by dissolution/precipitation of radionuclide-bearing glass alteration products, and are expected to control the long-term release of most radionuclides under known repository conditions (Apted, 1982; WISP, 1983; Kerrisk, 1985; Zavoshy et al, 1985). Therefore, the performance of glass waste forms depends strongly on what alteration solids form subsequent to initial glass dissolution.

Because of the intrinsically high solubility of glass relative to compositionally related crystalline solids, the dissolution of glass waste forms may lead to supersaturation in groundwater with respect to many possible alteration phases. It is probable, therefore, that alteration solids of intermediate stability (metastable) may form rather than the most stable. This behavior is commonly recognized in the alteration of natural glasses and minerals under both closed and open system conditions as described by the Ostwald step-rule (Fyfe and Verhoogen, 1958; Dibble and Tiller, 1981a; Giggenbach, 1981) or the "rule of stages" based on kinetics of nucleation and crystal growth (van Straten et al, 1984). The empirical Ostwald step-rule states that the transition of a chemical system from an unstable to a stable state typically occurs via a series of irreversible metastable states, with the thermodynamic instability of successively formed metastable states decreasing sequentially with reaction progress (i.e. time).

The initial alteration phases observed in borosilicate glass tests are gels, amorphous oxides, and clays (Grambow and Strachan, 1984; Allen et al, 1985). Although these solids will control the release of many radionuclides, they are metastable (Giggenbach, 1981; Dibble and Tiller, 1981a). A newer assemblage of more stable alteration phases will eventually form, controlling the release of radionuclides at different values. This raises the issue of how to confirm that the metastable alteration phases formed in short-term laboratory tests are representative of the actual alteration phases that will control radionuclide release rates over the 10,000 years or more of regulatory concern. Classical reaction acceleration techniques such as elevating temperature, increasing reactive surficial area, closed-system agitation or periodic solution replenishment simply lead more quickly to the same metastable reaction phases.

The theory of coupling between chemical reaction rates at solid-liquid interfaces and hydrodynamic processes has been developed extensively in electrochemistry and related fields (e.g. Levich, 1962). Dibble and Potter (1982) have demonstrated that fluid flow rate effects can control both reaction rates and alteration pathways for rhyolite glass. These processes are distinct from previous flow tests (e.g. Moore et al, 1983) that have demonstrated chemical effects on fluid flow (i.e. permeability reduction of host rock due to alteration). It is also distinct from, although related to, previous flow tests on glass waste forms that have studied the effect of flow solely on forward dissolution rate (e.g. Apted and Adiga, 1985). This present study conducted by the waste form testing program at the Basalt Waste Isolation Project (BWIP) reviews data from several flow tests conducted on natural alumino-silicate glasses and reports on new data obtained on a borosilicate nuclear waste glass. The effects of fluid flow rate on alteration pathways for glass and the formation of

metastable alteration solids are also discussed.

PREVIOUS STUDIES

Several studies on alteration in geothermal systems have emphasized the evident control of host rock permeability on alteration mineralogy (Browne, 1978; Keith et al, 1978). Permeability and fluid composition are cited to be at least as important as temperature, and more important than rock type or pressure, in determining the alteration assemblage for a broad range of rock types. Flow effects on alteration are particularly pronounced for volcanic glasses; obsidian has been reported as completely altered at temperatures of 85 oC while persisting to 170 oC in an adjacent area of lower permeability (Browne, 1978).

Experiments to evaluate the effect of fluid flow on alteration of natural glasses have also been conducted (Dibble and Potter, 1982; Pohl and Liou, 1983). Dibble and Potter (1982) studied alteration of a rhyolite glass at 300 oC using a 2% NaCl solution using a flow system of standardized dimensions. They found that more stable and well-crystallized alteration minerals were formed with increasing flow rate. Specifically, they showed a progressive change in alteration from poorly crystallized tabular mordenite + cristobalite formed at low flow rate (no flow and 1 ml/day) to well-crystallized albite + analcime formed at high flow rate (100 ml/day). Pohl and Liou (1983) also report that more rapid reaction and the formation of a more stable alteration assemblage were obtained in flow tests compared to a static test conducted on basalt glass/sea water at 300 oC. Lane et al (1985) investigated the alteration of basalt containing a glassy mesostasis phase at 300 oC under closed and open (flow) conditions, and also demonstrated the formation of more stable alteration phases under flow conditions compared to closed (no flow) system tests.

EXPERIMENTAL PROCEDURES

A series of experiments were conducted by the BWIP waste form testing program to determine the effect of fluid flow rate on the reaction of borosilicate glass and basalt in a hydrothermal environment. Tests were conducted in gold-cell, sampling (no flow or "static") pressure vessels (Seyfried et al, 1979) and a flow-through pressure vessel (Dibble and Potter, 1982) at 150 oC and 10 MPa, utilizing crushed (-120 to +230 mesh) Umtanum basalt (Palmer et al, 1984), a similarly crushed borosilicate nuclear waste glass (SRL-131/TDS-3A, Wicks et al, 1982), and a synthetic basalt groundwater (Jones, 1982). The static, no flow tests have been described previously (Allen et al, 1985). A 0.6 cm diameter by 18 cm length titanium tube was packed with approximately equal amounts of basalt and waste glass, with basalt located at the inlet. The inlet was connected to a reservoir with a pressurizing pump and the tube placed in a furnace. Volumetric flow rate was kept constant (± 10%) throughout the flow tests by means of an outlet flow controller (Dibble and Potter,

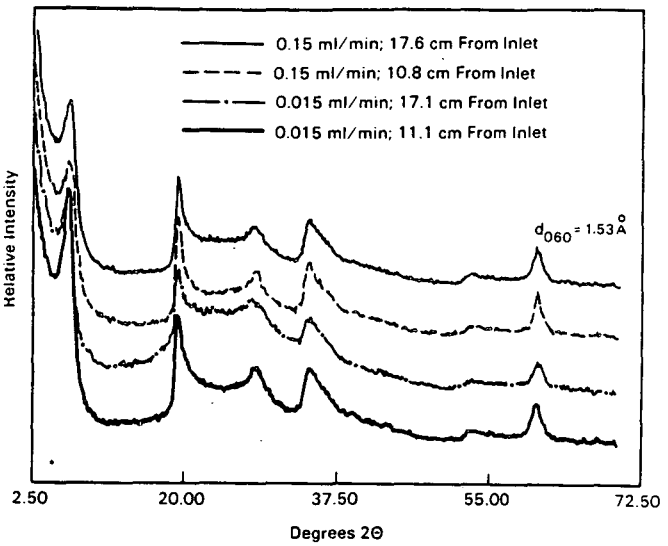

Figure 1. X-ray diffraction (XRD) pattern for glass alteration products, dominately smectite, from various locations within reaction columns for high and low flow rates.

1982). Flow tests at 0.015 ml/min (FT-122) and 0.15 ml/min (FTV2-1) were conducted for 1221 and 1055 hours, respectively. The duration of the static test (D8-1) was 6100 hours. The temperature was 150 ± 5 oC and the pressure was 10.0 ± 1.0 MPa for all tests.

The composition of the reacting fluid was analyzed periodically during each test by inductively-coupled plasma-atomic emission spectroscopy and ion chromatography. The pH was measured at room temperature with a combination electrode. The mineralogy and compositions of reaction products were analyzed by X-ray diffraction (XRD), optical microscopy, and scanning/transmission electron microscopy (SEM/TEM), utilizing energy-dispersive spectrometry (EDS).

RESULTS

The primary glass alteration product for all test conditions was a tri-octahedral smectite (saponite; basal reflection of 12.5 to 13.0 Angstroms expanding to 17 Angstroms with ethylene glycol saturation, d-spacing associated with 060 peak of 1.53 Angstroms) that was Fe-Mn-Ni-rich and Al-poor. Minor amounts of analcime were also found in tests D8-1 and FT-122. The XRD and EDS analyses (Figures 1 and 2) indicate a consistency in composition of the clay, both between different flow tests and from different axial locations within the same test. Figure 2 also compares the composition of the initial borosilicate glass with its subsequent clay alteration product, qualitatively showing the loss of Na (and assumedly B and Li) and enrichment in Fe, Mn, Ni, and Ti, all relative to Si. SEM photographs of reacted glass grains are presented in Figures 3 to 5. Note the severe loss of B from the clay layer (Figure 4) surrounding the unreacted glass cores for the flow tests. Solution concentration as a function of time are plotted

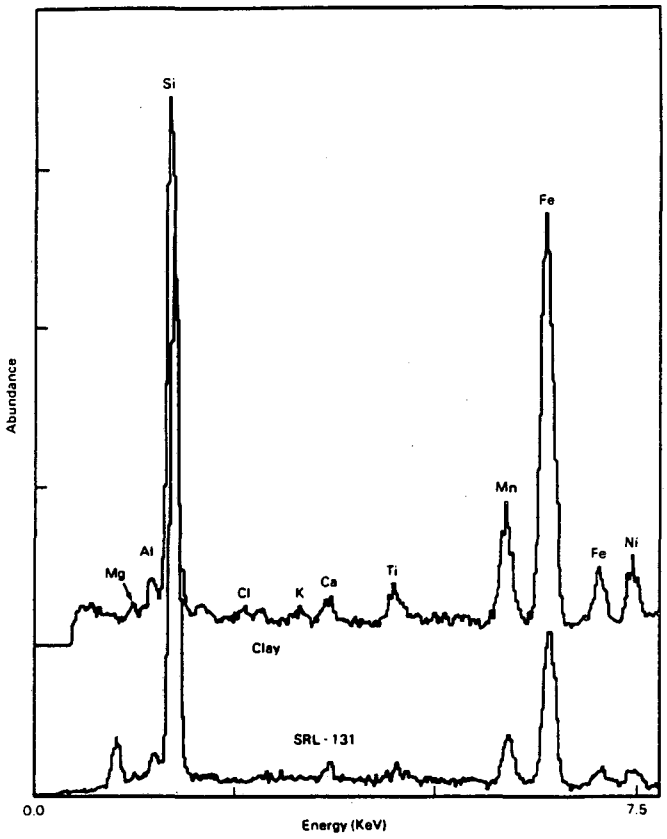

Figure 2. Energy-dispersive spectra (EDS) for primary SRL-131 glass and smectite alteration product from test D8-1. Amounts of elements are scaled versus equal intensity peaks for Si, with "Abundance" representing total counts.

in Figure 6 for Li, B, Na, and Si for all three tests.

DISCUSSION

The first effect of flow on glass alteration is to increase the dissolution rate. This is evident from the alteration of grains that show a greater degree of reaction (i.e. thicker clay layers) with increasing flow rate (Figures 4 and 5). This result is expected from the progressively higher time-integrated fluid flux with increasing flow rate. Confirmation of this can be obtained by calculating the normalized mass removed of a dissolution-index component of glass, such as B or Li, as a function of flow. For example, after 1000 hours of reaction, the total milligrams of B removed per gram of glass, assuming congruent dissolution (Figure 6), was approximately 8 in the static test, 11 in the low flow test, and 26 in the high flow test (a value of about 31 would represent total B removal from the glass). The theoretical basis for this dependence of heterogeneous reaction rates with flow, or stirring, rate has been presented previously (Levich, 1962; Dibble and Tiller, 1981b; Aagaard and Helgeson, 1982). The mass transport rate from a solid/fluid interface to the bulk fluid is inversely proportional to the diffusion boundary layer thickness. As flow rates in-

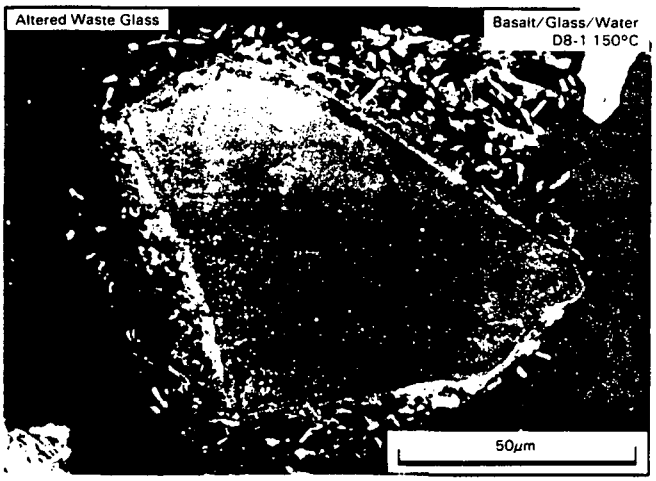

Figure 3. Scanning electron microscopy (SEM) photo of SRL-131 glass with surfical alteration product (smectite) reacted under static (no flow) conditions.

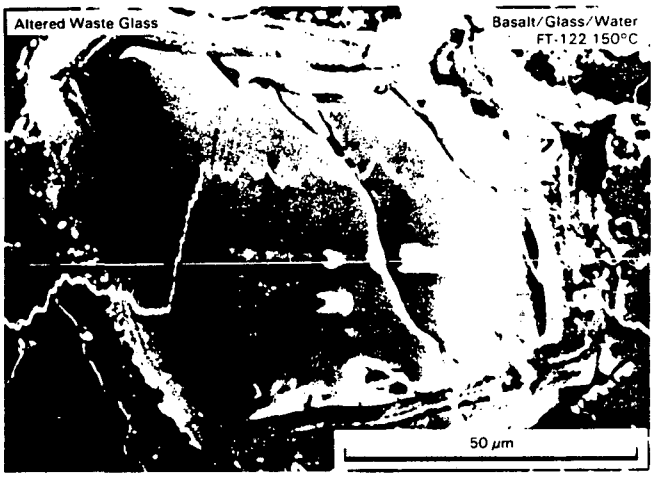

Figure 4. SEM photo of SRL-131 glass with surficial alteration product (smectite) reacted under low flow (0.015 ml/min) conditions. Note the superimposed scan line for boron abundance.

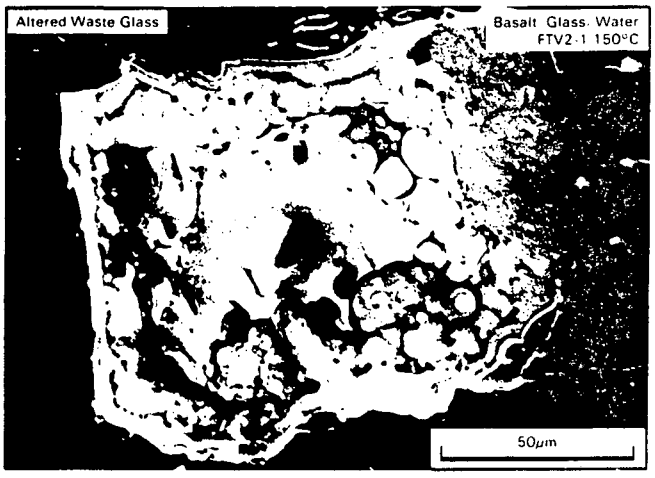

Figure 5. SEM photo of SRL-131 glass with surficial alteration product (smectite) reacted under high flow (0.15 ml/min) conditions.

crease, the boundary layer thicknesses decrease, and the rate of mass transport increases. It has also been proposed that stirring (flow) rates may appreciably increase the rate of precipitation and growth of alteration products in silicate systems (Aagaard and Helgeson, 1982).

A second important effect of flow is the suppression of high degrees of supersaturation with increasing flow rates (Figure 6). The production of metastable alteration products is favored when glass dissolution rates are high relative to growth rates of the most stable products (Dibble and Tiller, 1981a). That is, if high degrees of supersaturation with respect to the most stable phase(s) are maintained, many metastable phases may form. The effect of higher flow rate is to lower the degree of supersaturation that can be maintained by glass dissolution, preventing the formation of metastable solids, thus enhancing the formation of more stable alteration phases. This conclusion is supported by both field evidence (Browne, 1978; Keith et al, 1978) and laboratory tests (Dibble and Potter, 1982; Pohl and Liou, 1983; Lane et al, 1985) cited earlier.

Although flow rate did have an appreciable inverse effect on steady-state concentrations, or degree of solution supersaturation (Figure 6), there was no apparent effect of flow rate on the actual alteration phases of the glass that formed. All three tests showed the pseudomorphic replacement of glass by the same Al-poor smectite as the dominant alteration phase. This may be attributable to the high solution concentrations that developed in the initial period of reaction of the flow tests (Figure 6). These relatively high concentrations, in turn, are probably attributable to the rapid dissolution of fine particles on the unwashed grains of glass and/or to enhanced surficial reactivity of the glass due to preparation by crushing (Holdren and Berner, 1979; Harker et al, 1984). A systematic study of

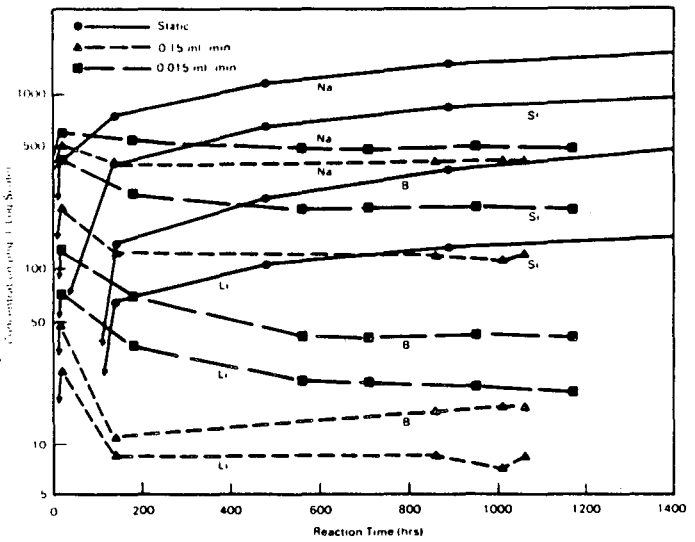

Figure 6. Solution concentrations for Li, B, Na, and Si from static and flow tests plotted as a function of test duration.

glass alteration as a function of surface defect concentration and structure may, therefore, be desirable. A second, contributing cause for the observed persistence of the clay may be its pseudo-morphic replacement of glass, limiting fluid access to the glass surface by liquid diffusion rather than convective flow.

A third potential effect of flow rate on glass alteration, not investigated in our tests, is the effect of solution composition. At high flow rates, the composition of the solution will more strongly affect the composition of the alteration phases (Dibble and Potter, 1982). Under low or diffusion controlled flow conditions, as expected for nuclear waste repositories in basalt and other host rocks (WISP, 1983), alteration will be "solids dominated" (Seyfried and Mottl, 1982; Giggenbach, 1984). With increasing flow rate, the reactions in the system will gradually become "solutiondominated", which can result in a completely different alteration pathway and formation of a different set of alteration minerals (Seyfried and Mottl, 1982). The cross-over from "solids-" to "solution-dominated" conditions will depend on solution and solids compositions, as well as flow and reaction rates.

SUMMARY

Studies by the Basalt Waste Isolation Project have shown two observable effects of increasing fluid flow rate on the alteration of borosilicate glass at 150 oC. The first is that glass dissolution rates increased appreciably with increasing flow rate. After 1000 hours of reaction, over three times as much boron was released from the glass at a flow rate of 0.15 ml/min compared to a static test. It has also been proposed by others (Aagaard and Helgeson, 1982) that precipitation rates also increase with increasing flow rates. Such effects promote a more rapid alteration of glass to solids that will initially control the release rate of many radionuclides.

The second effect is that solution concentrations (i.e. degree of supersaturation) are progressively suppressed with increasing flow rate. Under high, yet readily achievable laboratory flow rates, this effect could be utilized to prevent the formation of some metastable alteration solids and promote the formation of more stable solids. Although such flow rates would be many orders of magnitude greater than expected repository flow rates, the progressive step-wise alteration of glass could be studied, and an evaluation made of the long-term controls for radionuclide release from glass waste forms. Failure to demonstrate such step-wise alteration in these preliminary flow tests may be attributable to high initial solution supersaturations developed from nonflow-related factors or to diffusional constraints to continued chemical reaction processes at the surface of the glass

REFERENCES

Aagaard, P and Helgeson, H.C. (1982). "Thermodynamic and Kinetic Constraints on Reaction Rates among Minerals and Aqueous Solutions. I. Theorectical Considerations," Am. J. Sci., 282, 237-285.

Allen, C.C., Lane, D.L., Johnston, R.G., Marcy, A.D., and Adee, R.R. (1985). "Hydrothermal Studies of Simulated Defense Waste Glass Plus Basalt," Materials Research Society Symposia Proceedings, 44, 451-458, MRS, Pittsburgh, Pa.

Apted, M.J. (1982). "Overview of Hydrothermal Testing of Waste Package Barrier Materials at the Basalt Waste Isolation Project," pp.161-181, PNL-4382, Pacific Northwest Labortory, Richland, Wa.

Apted, M.J. and Adiga, R.B. (1985). "The Effect of Groundwater Flow on Release Rate Behavior of Borosilicate Glass," Materials Research Society Symposia Proceedings, 44, 163-170, MRS, Pittsburgh, Pa.

Browne, P.R.L. (1978). "Hydrothermal Alteration in Active Geothermal Fields," Ann. Rev. Earth Planet. Sci., 6, 229-250.

Dibble, W.E. Jr. and Potter, J.A. (1982). "Effect of Fluid Flow Rates on Geochemical Processes," Society of Petrol. Eng., SPE-10994, 1-8.

Dibble, W.E. Jr. and Tiller, W.A. (1981a). "Kinetic Model of Zeolite Paragenesis in Tuffaceous Sediments," Clays and Clay Minerals, 29, 323-330.

Dibble, W.E. Jr. and Tiller, W.A. (1981b). "Non equilibrium Rock/Water Interactions. I. Model for Interface-controlled Reactions," Geochim. Cosmochim. Acta, 45, 79-92.

Fyfe, W.S. and Verhoogen, J. (1958). "Kinetics of Metamorphic Reactions," in Metamorphic Recations and Metmorphic Facies, W. Fyfe, F. Turner, and J. Verhoogen, eds., Geol. Soc. Amer. Mem. 73, 53-104.

Giggenbach, W.F. (1981). "Geothermal Mineral Equilibria," Geochim. Cosmochim. Acta, 45, 393-410.

Giggenbach, W.F. (1984). "Mass Transfer in Hydrothermal Alteration Systems - A Conceptual Approach," Geochim Cosmochim. Acta, 48, 2693-2711.

Grambow, B. (1982). "The Role of Metal Ion Solubility in Leaching of Nuclear Waste Glasses," Materials Research Society Symposia Procceding, 11, 93-102, North-Holland, New York.

Grambow, B. and Strachan, D.M. (1984). "Leach Testing of Waste Glasses under Near-saturated Conditions," Material Research Society Symposia Proceedings, 26, 623-634, North-Holland, New York.

Harker, A.B., Flintoff, J.F. and Clarke, D.R. (1984). "Surface Layers in Leached Borosilicate Glass High-Level Defense Nuclear Waste Forms," pp. 2.1-2.37, PNL-5157, Pacific Northwest Laboratory, Richland, Wa.

Holdren, G.R. Jr. and Berner, R.A. (1979). "Mechanism of Feldspar Weathering. I. Experimental Studies," Geochim Cosmochim. Acta, 43, 1161-1171.

Jones, T.E. (1982). "Reference Materials Chemistry, Synthetic Groundwater Formulation," RHO-BW-ST-37, Rockwell Hanford Operations, Richland, Wa.

Keith, T.E.C., White, D.E., and Beeson, M.H. (1978). "Hydrothermal Alteration and Self-sealing in Y-7 and Y-8 Drill Holes in Northern Part of Upper Geyser Basin, Yellowstone National Park, Wyoming," U.S. Geol. Survey Prof. Paper 1054A.

Kerrisk, J.F. (1985). "Solubility Limits on Radionuclide Dissolution," Materials Research Society Symposia Proceedings, 44, 237-244, MRS, Pittsburgh, Pa.

Lane, D.L., Allen, C.C., Johnston, R.G. and Rawson, S.A. (1985). "Basalt-water Hydrothermal Reactions: Preliminary Results on the Effect of Fluid Flow," Program and Abstracts of 2nd Intl. Symp. on Hydrothermal Reactions, Penn State Univ., Aug. 12-14.

Levich, V.G. (1962). "Physicochemical Hydrodynamics," Prentice-Hall Inc., Englewood Cliffs, N.J.

Moore, D.E., Morrow, C.A. and Byerlee, J.D. (1983). "Chemical Reactions Accompanying Fluid Flow through Granite Held in a Temperature Gradient," Geochim. Cosmochim. Acta, 47, 445-453.

Palmer, R.A., Aden, G.D., Johnston, R.G., Jones, T.E., Lane, D.L. and Noonan, A.F. (1984). "Characterization of Reference Materials for the Barrier Materials Test Program," RHO-BW-ST-27 P, Rockwell Hanford Operations, Richland, Wa.

Pohl, D.C. and Liou, J.G. (1983). "Flow-through Reaction of Basalt Glass and Seawater at 300 oC and 200 oC, 250 Bars Pressure," Fourth International Symposium on Water-Rock Interaction, Institute for Thermal Springs Research, Okayama University, Japan, pp. 389-392.

Seyfried, W.E. Jr., Gordon, P.C. and Dickson, F.W. (1979). "A New Reaction Cell for Hydrothermal Solution Equipment," Am. Mineral., 64, 646-649.

Seyfried, W.E. Jr. and Mottl, M.J. (1982). "Hydrothermal Alteration of Basalt by Seawater under Seawater-dominated Conditions," Geochim. Cosmochim. Acta, 46, 985-1002.

van Straten, H.A., Holtkamp, B.T.W., and de Bruyn, P.L. (1984). " Precipitation from Supersaturated Aluminate Solutions. I. Nucleation and Growth of Solid Phases at Room Temperature," J. Coll. Interface Sci., 98, 342-362.

WISP (1983). "A Study of the Isolation System for Geologic Disposal of Radioactive Wastes," Waste Isolation Systems Panel, National Research Council, National Academy Press, Washington, D.C.

Wicks, G.G., Robnett, B.M. and Rankin, W.D. (1982). "Chemical Durability of Glass Containing SRP Waste- Leachability Characteristics, Protec-

tive Layer Formation, and Repository System Interactions," Materials Research Society Symposia Proceedings, 11, 15-24, North-Holland, New York.

Wood, B.J. (1980). "Estimation of Waste Package Performance Requirements for Nuclear Waste Repository in Basalt," RHO-BWI-ST-10, Rockwell Hanford Operations, Richland, Wa.

Zavoshy, S.J., Chambre, P.L. and Pigford, T.H. (1985). "Mass Transfer in a Geologic Environment," Materials Research Society Symposia Proceedings, 44, 311-322, MRS, Pittsburgh, Pa.

ASSESSMENT OF THE COMBINED EFFECTS OF TEMPERATURE INCREASE, WATER CONVECTION, MIGRATION OF RADIONUCLIDES AND RADIOLYSIS ON THE SAFETY OF A NUCLEAR WASTE REPOSITORY IN THE BOOM CLAY

L.H. BAETSLÉ, A. BONNE, P. HENRION, M. PUT AND J.PATYN
SCK/CEN, B-2400 MOL, BELGIUM

FOR A POTENTIAL REPOSITORY IN THE BOOM CLAY FORMATION 220 M BENEATH THE NUCLEAR RESEARCH CENTER AT MOL BELGIUM, EXTENSIVE TEMPERATURE CALCULATIONS HAVE BEEN DONE FOR SEVERAL REPOSITORY CONFIGURATIONS. TAKING INTO ACCOUNT, NEAR FIELD AND FAR FIELD TEMPERATURE LIMITATIONS, AN ACCEPTABLE HEAT LOAD OF 2.5 W/M2. AND A COOLING TIME OF 50 YEARS HAVE BEEN DERIVED. A QUALITATIVE DISCUSSION IS GIVEN OF THE IMPACT OF A TEMPERATURE INCREASE ON THE MIGRATION PATTERN AND ON THE GLOBAL EFFECT AS A FUNCTION OF DISPOSAL PERIODS.

HYDROLOGICAL PHENOMENA IN THE WATER TABLES SURROUNDING THE BOOM CLAY LAYER HAVE BEEN STUDIED BY INSTALLING A PIEZOMETRIC OBSERVATION NETWORK OVER A SURFACE OF 2500 KM2. A MATHEMATICAL MODEL HAS BEEN DEVELOPED TO INTERPRET THE PIEZOMETRIC OBSERVATIONS AND TO DERIVE THE REGIONAL FLOW PATTERN AND THE WATER TRANSFER THROUGH THE LOW IMPERMEABILITY CLAY LAYER. IT HAS BEEN ATTEMPTED TO VERIFY THESE RESULTS BY DATING OF THE GROUNDWATERS AND THE INTERSTITIAL CLAY WATER.

A UNIDERICTIONAL ANALYTICAL MODEL HAS BEEN DEVELOPED, TAKING INTO ACCOUNT RADIOACTIVE DECAY AND WATER CONVECTION BY A PRESSURE GRADIENT, AND WHICH SUPPOSES CONCENTRATION EQUILIBRIUM BETWEEN THE MOBILE AND THE STAGNANT FRACTION OF THE LIQUID PHASE. ANALYTICAL SOLUTIONS HAVE BEEN OBTAINED FOR THE ENTIRE RANGE OF PARAMETERS. THE RESULTS OF THE CALCULATIONS, DONE WITH THE EXPERIMENTALLY DETERMINED PARAMETER VALUES, SHOW THAT FOR THE MOST CRITICAL RADIONUCLIDES AS FOR EXAMPLE NP 237, THE MIGRATION DISTANCE IS LESS THAN 1 M AFTER 1000 YEARS.

THEORETICAL AND EXPERIMENTAL WORK IS UNDER WAY TO MODEL THE CONSEQUENCES OF A DIFFERENCE IN THE APPARENT DIFFUSION CONSTANT FOR THE MOBILE AND THE STAGNANT FRACTION OF THE LIQUID PHASE.

EXPERIMENTAL AND THEORETICAL WORK IS UNDER WAY TO DETERMINE THE IMPORTANCE OF THE MIGRATION OF THE ALPHA EMITTERS AND THE PRODUCTION OF RADIOLYSIS GASES, AND THE MIGRATION OF THESE GASIS. THE EXPERIMENTAL WORK CONSISTS OF THE DETERMINATION OF GAS PRODUCTION AND THE MEASUREMENT OF THE DISPERSION CONSTANT. THE THEORETICAL WORK CONCERNS THE MODELING OF THE COMBINED PRODUCTION AND MIGRATION OF THE RADIOLYSIS GASES.

COUPLED PROCESSES AT THE OKLO NATURAL REACTOR

Douglas G. Brookins

Dept. Geology
University of New Mexico
Albuquerque, NM 87131

ABSTRACT

The Oklo Natural Reactor, Gabon, is an excellent site in which to study, assess and evaluate coupled processes of interest to radionuclide migration in natural media. The uranium accumulations in which the fission reactions occurred are dated at about two Gy (billions of years), and the nuclear reactions lasted for some 500,000 y (±). Temperatures in the reactor zones were on the order of 300 - 450°C, although local, higher temperatures may have been reached. This thermal regime aided in the diffusion of some fission products, and possibly actinides, from host pitchblende. Post-reactor diagenesis events have masked some of the radionuclide migration paths, but most can still be studied.

Elements incompatible in the pitchblende structure, such as Cs, Ba, Rb, and Sr were lost by diffusion into the surrounding assemblage of quartz-chlorite-illite-carbonates-oxyhydroxides-sulfides. Mass spectrometric studies show that fissiogenic Rb and Sr were fixed on clay minerals in and near the reactor zones, and indirect evidence suggests the same fate for Cs. Fissiogenic Ba was in part fixed in clay minerals but also fixed on/in sulfate and carbonate minerals in and very near the reactor zones.

Conditions during the reactor's operative lifetime were probably very locally oxidizing in an overall reducing environment. This resulted in loss from reactor zones of fission products which form soluble oxyions under such oxidizing conditions, including Tc, Ru, and Mo. In addition, some loss of Ag, Sn, and Cd is predicted and observed based on theoretical considerations and detailed isotopic measurements. The Tc, Ru, and Mo migration paths, and sites of fixation fairly near the reactor zones have been demonstrated by Curtis and others (LANL). The Ag, Sn, and Cd migration has been documented by DeLaeter and coworkers. While the high temperature, oxidizing conditions promoted the loss of these elements, the nearby low temperature, reducing conditions resulted in their precipitation in sulfides. Interestingly, elements which have large stability fields of solid species in Eh-pH space for 25°C to 200°C such as Rh, Te, Pd, Sb, Nb, and In, apparently did not migrate from the reactor ore.

The actinides, Th, U, Np, Pu, and Am are similar in crystal chemical properties, and UO_2 is structurally compatible with NpO_2, PuO_2 and AmO_2. Hence a strong case is made for Np, Pu, and Am retention even when some U was mobilized. This results from the fact that U forms soluble oxyions in the Eh-pH range of interest while the other species do not. Further evidence for the transuranic elements being retained is shown by presence of Bi formed from Np-decay and excess Th-232 from U-236.

The rare earth elements are compatible in the pitchblende with U, and little migration of these elements has occurred. Curtis and his coworkers suggest some Nd loss, possibly due to radiolytic effects, but, based on solubility and other geochemical arguments, fixation must have occurred almost immediately. Once removed from host pitchblende, the REE (rare earth elements) are likely to be fixed in oxyhydroxide or carbonate phases.

The fate of fissiogenic I is uncertain, in part due to lack of measurements. Not only is I incompatible with U in pitchblende, but it also will not be fixed with the alkali and alkaline earth elements in the clay mineral gangue. It is possible, however, that the I may be removed in sulfides nearby as M(S,I) surface species.

The combined thermal and geochemical aspects of Oklo allow estimates of degree of radionuclide migration to be estimated, and aspects of both near-field and far-field behavior can be evaluated from combined theoretical and experimental studies. After some twelve years research, it appears that most of the Oklo fission products and actinides did not migrate any appreciable distance from the host pitchblende, and that the rocks at the Oklo site are adequate to fix migrating radionuclides in them.

INTRODUCTION

Natural fission reactions occurred in the uranium ores at the site of the Oklo Mine, Republic of Gabon, some 2 Gy, as documented by Naudet (1978), IAEA (1976), and IAEA (1978). The occurrence of such natural fission reactions had been proposed by P. K. Kuroda and others (See Kuroda, 1976) some twenty or so years before discovery of Oklo. The conditions for criticality to be attained in nature include: (a) high grade uranium, (b) ^{235}U content of greater than 2 - 3%, (c) absence of neutron poisons, (d) water content of roughly 12 to 16 percent. The high grade ore at Oklo formed by remobilization of low grade ore (Brookins, 1980). In the low grade ore, uranium is mixed with fairly large amounts of selenium, molybdenum, vanadium, manganese, some boron, and other elements which can act as neutron poisons. When the ore was remobilized, however, uranium only was remobilized and deposited in fractured and faulted zones in sandstone as a mixture of uranium ore-shale infilling material. The ore grade reaches 70 percent U_3O_8 in places, and, at 2 Gy, the ^{235}U content was 3.25 percent, roughly

what uranium today is enriched to for man-made power reactors. The water content can be estimated only indirectly. Naudet (1978) has argued for 14 - 15 percent water based on abundance of hydroxyl-bearing clay minerals present in the zone of the fission reactions; and he reasons that for water content much less than 12 percent too little would be present to serve as an efficient moderator. Similarly, at water content much above 16 percent, the neutron flux would be too diffuse, and criticality might not be achieved. All of the above criteria, thus, were met at Oklo. The nuclear reactions occurred in some dozen or so zones of high uranium concentrations at Oklo and were operative for about 500,000 years, during which some 14,000 MWe-years of energy were produced. Most of the nuclear reactions at Oklo involved ^{235}U, but, locally the neutron flux was sufficient to induce fission of ^{238}U and to produce ^{239}Pu from ^{238}U. The ^{239}Pu then partially fissioned as well. Naudet (1978) has proposed that the average Oklo reactor ore involved 93 percent ^{235}U, 3 percent ^{238}U, and 4 percent ^{239}Pu. Roughly 6,000 kg of ^{235}U fissioned and, with fission of some ^{238}U and ^{239}Pu, fission products of some 30 elements were produced. The early documentation of the fission process, temperature and pressure constraints on the reactor host rocks, and studies of some of the fission yield elements are given in IAEA (1976;1978).

The approach to be used here is to comment on the various trace elements produced by fission at Oklo. Coupled thermal-geochemical and geochemical-hydrologic processes played an important role in distribution of the fission products and actinides at the Oklo site. Further, if all the elements produced by fission processes still reside as stable elements (i.e., either formed directly by fission or as stable daughter products of radioactive fissiogenic parents) in the rocks, then this is a definite "plus" for the ability of rocks to retain radioactive wastes. Alternately, if the rocks at Oklo were not adequate for retention of the fissiogenic elements, then one can argue that these particular rocks are not well suited for radioactive waste disposal.

The identification of fissiogenic elements from their natural counterparts is, in most instances, easy. This results from the fact that the isotopic composition of the naturally occurring element is usually quite different from that resulting from fission, hence 100 percent naturally occurring element, 100 percent fissiogenic element, and any mixture of the two can be determined with today's sophisticated mass spectrometric and other techniques. The documentation of different elements is given in IAEA (1976;1978).

DISCUSSION OF CERTAIN TRACE ELEMENTS AT OKLO

In this section the various elements produced by fission at Oklo are discussed. Data have been gathered for many of the 30 or so elements produced by fission, and estimates of behavior of all elements can be discussed even in the absence of measured data. In the following discussion, the amount of normal element will be designated M_n, the amount of fissiogenic element M_f, and a mixture of the two as M_m.

The alkali and alkaline earth elements, Rb, Sr, Cs, and Ba have been studied by Brookins (1981), Brookins and others (1976), and others (See IAEA, 1976). Early studies (in IAEA, 1976) suggested widespread migration of Rb_f, Sr_f, and Cs_f with possible retention of Ba_f. These studies, however, focussed on only high grade uranium ore samples, in which the alkali and alkaline earth elements are metastable, and loss of these elements from the UO_2 structure is to be expected. Brookins (1981) showed that the clay mineral-rich gangue surrounding the reactor ore contained small percentages of Rb_f and Sr_f, as well as significantly high ^{135}Ba / ^{137}Ba ratios. The barium data are of interest because this ratio will only vary if fissiogenic cesium is produced (i.e., ^{135}Cs and ^{137}Cs decay to ^{135}Ba and ^{137}Ba respectively). When the 135/137 ratio increases markedly from the natural ratio of 0.5835, then some Cs_f has affected this ratio. Further, even though natural cesium contains only one isotope (^{133}Cs), its behavior can indirectly be determined by study of the ^{135}Ba / ^{137}Ba ratio. At Oklo, the clay minerals in the reactor zone gangue contain Ba_f(135, 137,138), and Rb_f and Sr_f. The combined data for the gangue samples show correlation of the amount of Rb_f with Ba $(135/137)_f$ and Sr_f with both Rb_f and Ba_f, indicating that the alkali and alkaline earth elements behaved similarly in transport and fixation after loss from host pitchblende. Of significance is the fact that when the entire mass of near-ore clay mineral gangue is considered, then possibly 100 percent of the alkali and alkaline earths may be present adjacent to the uranium ore sites where first formed. This indicates only local redistribution of these elements as opposed to widespread migration. Since ^{90}Sr and ^{137}Cs are the two most potentially hazardous radionuclides in high level radioactive waste, then the Oklo data are very important as they argue for retentivity of these elements under some natural rock conditions. The Ba_f produced is retained in part in host pitchblende and in part in gangue barite and clay minerals. Rb^+, Sr^{2+}, Cs^+, and Ba^{2+} are large ions not readily compatible with the pitchblende structure, hence it is not surprising that Rb_f, Sr_f, Ba_f, and Cs_f are, for the most part, lost from pitchblende. However, these elements are easily identified in the illitic clay minerals (Brookins, 1981).

The halides at Oklo are not well understood. A deficiency of I_f has been noted (IAEA, 1976), however, and it is not known if the loss was widespread or local. This element is difficult to assess because naturally occurring iodine contains only ^{127}I. This amount of iodine measured at Oklo may be all I_f, all I_n, or some mixture of the two. In the case of Br, no measurements have been made. This is unfortunate, as Br_f is, in theory, easy to distinguish from Br_n as masses 79 and 81 are produced in very different proportions (i.e., roughly 1:3) during fission whereas Br_n contains roughly 1:1 of masses 79:81. If Br_f were to be identified

in some Oklo samples, then, since halides exhibit similar behavior in natural systems, any iodine present would include I_f. These Br measurements are badly needed to help to assess the fate of halides at Oklo.

Yttrium retention has been proposed from theoretical grounds (Brookins, 1978a) and by measurement (IAEA, 1976). This is consistent with its crystal chemical behavior in nature. Y^{3+} is the only species of major importance in the pH range 5-10, and this ion substitutes easily for U^{4+} in pitchblende. It does not complex with sulfur species. Were any Y^{3+} released from pitchblende, it would be readily incorporated into $Y(OH)_3$-bearing phases or in carbonates (i.e., $Y_2(CO_3)_3$ may be stable phase at pH near 6).

Zirconium should also be retained in host pitchblende,as Zr^{4+} is compatible in the pitchblende structure where it substitutes for U^{4+}. The theoretical considerations argue for retention (Brookins, 1978a) and are consistent with measurement (Frejacques, et al., 1976). Any Zr^{4+} loss would be extremely local as $Zr(OH)_4$ or some other insoluble phase would severely restrict transport.

Niobium occurs primarily in nature as Nb^{5+} and is present in a number of extremely stable niobates and tantalates. In fact, the entire Eh-pH stability field of water is very nearly covered by the field of Nb_2O_5 (Brookins, 1978a). The few measurements made for Nb in Oklo ores (See IAEA, 1976) argue for retention.

Molybdenum presents an opportunity to investigate migration of Mo_f. In nature, MoS_2 is an extremely stable mineral under chemically reducing environments, but it will oxide to $HMoO_4^-$ or MoO_4^{2-} ions under conditions when S^{2-} is oxidized to SO_4^{2-} (See Brookins, 1978a). It has been demonstrated (IAEA, 1976) that Mo_f is somewhat depleted in the Oklo ores. Recently Curtis and co-workers at the Los Alamos National Laboratory have identified Mo_f in zones some 5-10 meters from reactor ore in which Ru_f (including $^{99}Ru_f$ formed from Tc_f) are found, suggesting that migration of Mo_f has been local.

No data are available for Kr_f from Oklo (See discussion below on Xe_f).

Some migration of $Tc_f$and Ru_f has been indicated at Oklo, but the site of the remobilized Tc_f and Ru_f is only some 10 meters from reactor ore (Gancarz and others, 1980). In particular, $^{99}Ru_f$, which forms in part from $^{99}Tc_f$, is present in amounts to indicate migration of Tc_f with Ru_f. Theoretical considerations (Brookins, 1978a) argue that under slightly oxidizing conditions, both elements may be soluble as oxyions; e.g., RuO_4^{2-} and TcO_4^-, and this no doubt accounts for their initial loss from reactor ore. When more reducing environments are found, however, then these elements are quickly removed as MO_2 or MS_2 phases or in solid solution in gangue oxides or sulfides. At Oklo, the host for Ru_f and Tc_f (and probably Mo_f) is probably pyrite. Brookins (1978a) has also argued that Tc_f should be retained in the composite Oklo environment based on the Eh-pH diagram for Re species. Re and Tc behave in natural systems in identical fashion, and a wide stability field for ReS_2 is noted which, in theory, should also hold for TcS_2 except that thermodynamic data for this species is lacking.

No evidence for migration of Rh is noted at Oklo. Since Rh^{3+} is compatible with U^{4+} in Oklo pitchblende, this is not surprising; and it has been shown (Brookins, 1978a) that Rh should be immobile in the greater part of the Eh-pH water stability field. Palladium also has not migrated at Oklo. Recently, DeLaeter and others (1980) have shown that Pd_f has been retained even in zones where other elements may have migrated locally. Since Pd is a common chalcophile element, its retention argues that oxyions of Ru, Tc, Mo instead of polysulfides are probably the important transporting ligands; else Pd, too, would have been subject to remobilization, which is not the case.

Migration of Ag_f on a local scale has been noted by DeLaeter and others (1980). This is problematic, as the Eh-pH diagram for Ag species (Brookins, 1978a) shows a wide stability field for native Ag and Ag_2S. The large ionic radius of Ag^+, however, makes it especially susceptible for migration as it is incompatible in the U^{4+} site. Based on very different equilibrium times of formation as a function of temperature (Barton and Skinner, 1979) for Mo and Ag, these two elements should behave differently in simple S-O-H systems; hence, different migration transport is to be expected, while oxyion transport for Mo_f is probable, the transport mechanism for Ag_f is unknown. It should be emphasized, however, that most Ag_f is still in host pitchblende, and the amount of migrated Ag_f may be local.

Migration of Cd_f is well known (IAEA, 1976) and consistent with theoretical considerations (Brookins, 1978a). CdS is stable under reducing conditions, but there exists only a very narrow field of $Cd(OH)_2$ in the sulfate-stable part of Eh-pH space (Brookins, 1983). Thus, Cd_f should migrate, probably as Cd^{2+} or possibly as CdO_2^{2-} (or some hydrolysis product of either) depending on pH. However, under conditions where sulfides are stable, the Cd_f should be removed as CdS (either as greenockite or in pyrite). The Ru_f-Tc_f-Mo_f-bearing pyrite (Gancarz and others, 1980) may also contain Cd_f, but these measurements have not been made.

Retention of In_f has been documented at the Oklo site. Brookins (1978a) has argued for retention at both 25°C and 200°C (See also Brookins, 1979) due to the large Eh-pH stability field for In_2S_3 and In_2O_3, and spark source mass spectometric measurements support the theoretical interpretation (IAEA, 1976). In^{3+} is compatible with U^{4+} in host pitchblende.

Theoretical considerations argue for retention of Sn_f (See Brookins, 1978a; 1979), yet DeLaeter and others (1980) have shown local migration of some Sn_f. The transport mechanism and newly formed site of Sn_f are unknown, but it is

possible if not probable that Sn_f that has migrated may be found in the zone of remobilized Ru_f and Tc_f (and Mo_f). Sn^{4+} is a much smaller ion than U^{4+}, hence loss from the pitchblende structure is probable. Whether the Sn_f lost is located as $Sn(OH)_4$ immediately adjacent to the pitchblende or further away is unknown.

Brookins (1978a) has suggested possible migration of Sb_f, as only a very small field of Sb_2O_3 occurs above the field for Sb_2S_3 in Eh-pH space at 200°C. Transport as $HSbO_2$ or SbO_2^- may be likely, and any Sb_f so remobilized may be found where other chalcophile elements (Ru_f,Tc_f) migrated; yet there are no experimental data to back up the theoretical arguments. This is unfortunate, as $^{123}Sb_f$ is an important product of man-made power reactors, and behavior of Sb_f is important for radioactive waste storage problems.

Retention of Te_f in host pitchblende has been proposed by Brookins (1978a) and supported by the experimental studies of DeLaeter and others (1980).

Large loss of Xe_f has been shown by Drozd and others (1974). This is to be expected, as Xe_f has no way to be structurally bonded in host pitchblende. It is possible, but yet to be demonstrated , that some Xe_f may be trapped in secondary sulfide minerals (See Christensen and others, 1981); and this may also hold for Kr_f for which no measurements on Oklo material have been made.

The REE have been nearly 100 percent retained at Oklo (IAEA,1976;1978). The REE exist as simple M^{3+} ions (in part M^{4+} for Ce and M^{2+} for Eu) which are compatible with U^{4+} sites in host pitchblende. Brookins (1983) has prepared Eh-pH diagrams which show fields of $M(OH)_3$ and $M_2(CO_3)_3$ to cover the Eh-pH range expected at Oklo; hence their retention is to be expected. Transport as a carbonate complex (cf. McLennan and Taylor, 1979) is not considered likely based on new data (Brookin, 1983).

Study of heavy metal behavior at Oklo is also of importance for radioactive waste disposal considerations. Local migration of radiogenic lead (Pb^*) up to three meters from reactor ore at Oklo has been noted (Gancarz and others, 1980). A different path for migration of Pb^* than Ru_f is noted, but this is not surprising as Pb^* accumulates only in a very slow manner due to decay from parent U whereas Ru_f was produced relatively rapidly during the period of fission reactions. Volume diffusion for Pb^* loss is probable, as Pb^{2+} is not compatible with U^{4+} in host pitchblende. Only very limited migration of Pb^* is noted, however.

Retention of Bi^* is well documented at Oklo (IAEA,1976). Formation of ^{207}Bi is due to decay from ^{237}Np (and small amounts from ^{241}Pu and ^{241}Am) formed by neutron capture on U in the high flux parts of reactor zones. Retention of Bi^* has been predicted by Brookins (1978b;1979) based on crystal chemical reasoning and Eh-pH considerations and documented by measurement (i.e., in the interiors of highest grade U ore the neutron flux was sufficient for ^{237}Np and other transuranics to form, and it is in these interiors of ore zones where excesses of Bi^* are found).

Both Th and Th^* are compatible with U^{4+} sites in pitchblende. Th^* forms from ^{236}U, formed by neutron capture on ^{235}U, which then undergoes alpha decay (to ^{232}Th). Slight ^{232}Th excesses are found where Bi^* is found, and both are present in the expected proportions (See IAEA, 1976).

Migration of U on a somewhat local scale is to be expected. Of the actinides and transuranics, only U is readily mobile under sulfate-stable Eh-pH conditions , usually as some U^{6+} oxyion or carbonate complex (See Brookins, 1978b). The locally high temperature (250 - 450°C) would be sufficient to mobilize U, and it would be transported to a site where reducing conditions would favor precipitation of U(IV) phases. Some U movement is post 1 Gy (IAEA,1978) as concentrations of U are found on the up-dip side of a 1 Gy dolerite dike which cuts the Oklo pit. How much reactor ore was involved in this remobilization is unknown.

The transuranics Np, Pu, and Am were produced in various proportions at Oklo. Documentation of the amounts of Np and Pu produced and retained at Oklo has been established (IAEA, 1976;1978) both by theoretical considerations and amounts of ^{207}Bi (from ^{237}Np) and excess ^{235}U (from ^{239}Pu) in highest grade reactor ore. The amounts of ^{241}Am can be calculated, but the amount of ^{207}Bi formed by subsequent alpha-decay is too small to resolve from that produced from ^{237}Np. Theoretical considerations argue for retention of Np, Pu, and Am at Oklo (Brookins, 1978b;1979), as all show large fields of MO_2 which cover not only Eh-pH reducing conditions but much of the sulfate-stable part of the field as well. Their behavior is somewhat different from that of U in that whereas U may be somewhat mobile, the Np, Pu, and Am are not. For these three elements, large fields of NpO_2, PuO_2, and AmO_2 cover most of the Eh-pH water stability field (Brookins, 1978b,c). Further, Np^{4+}, Pu^{4+}, and Am^{4+} (and, to a lesser degree, Am^{3+}) are all diadochic with U^{4+} and easily contained in the structure of host pitchblende. Even if pitchblende were to be completely destroyed by hydrothermal activity, if the Eh-pH conditions are roughly along the sulfide stable:sulfate stable boundary (note: probably slightly above), then released Np, Pu, and Am would be fixed as oxides or hydroxides while U was being remobilized. Although the amount of Cm produced at Oklo may have been very slight, theoretical and crystal chemical arguments (Brookins, 1983) suggest that its behavior is very much like that of Pu and Am, and had it been produced at Oklo, it would have been retained in host pitchblende or in the overall reactor zones. This is important to note, for in man-made power reactor waste both Am and Cm are produced in some abundance, and how these elements will behave in rock repositories is of concern.

DISCUSSION AND CONCLUSIONS

Thirty or so elements were produced by fission at Oklo, plus radiogenic Pb, Bi, and the transuranics Np, Pu, and Am.

Fission reactions at Oklo produced some 30 fission products, and heavy metals were produced by radioactive decay and by nuclear reactions. The suite of the fission products, the radiogenic elements, and the transuranics provides a unique opportunity to investigate radioactive waste product behavior in rocks. Nature kindly conducted the experiment in the distant past, and man has only to synthesize the data and attempt an interpretation. The Oklo reactor was operative for a very lengthy time (about 500,000 years), and temperatures during the fission reactions were on the order of 200°C to 450°C at a pressure of about one Kb. Since man-made radioactive wastes are often discussed in terms of rock repositories at depths less than one Kb and at temperatures lower than those at Oklo (i.e., current estimates are close to 120°C maximum), the Oklo reactor sites actually represent analogues for repositories under higher temperature conditions. The empirical argument is offered that, if radioactive wastes are retained under Oklo conditions, they may be even better retained under lower T,P conditions. Further, the Oklo rocks represent a very common natural assemblage of alternating layers of sandstone, shale and conglomerate rocks. Their porosity and original permeability were both fairly high, certainly well outside the low porosity, low permeability demands placed on rocks being considered for repositories. As such, retention of wastes in the Oklo rocks is less likely than in candidates for repositories built by man.

Yet, without benefit of canisters, overpack, and engineered backfill, most of the elements produced at Oklo have been retained in the rocks in which they were formed or, at worst, migrated from host pitchblende to some ten meters or so (maximum?) from their original site. Only Xe, and probably Kr, are very nearly absent from reactor ore, and it is not known if even these noble gases were totally removed from the Oklo system or else fixed in rocks adjacent or close to the reactor sites. The alkali and alkaline earth elements, of critical interest for man-made radioactive wastes because of ^{90}Sr and ^{137}Cs, were locally redistributed. The studies of $^{135}Ba/^{137}Ba$ ratios (Brookins and others, 1976; Brookins, 1981) indicate, further, that Cs_f and Ba_f did not migrate from reactor ores for at least 25 million years; this time based on other isotopic systematics.

Halides at Oklo are not well studied. A deficiency of ^{127}I may eventually be explained by fixation in gangue minerals. While this has not yet been demonstrated, study of Br_f isotopic systematics would allow this question to be answered.

Many of the fission products remain in or with host pitchblende, including Y, Zr, Nb, Rh, Pd, In, Te, and the REE; and radiogenic Bi and transuranic Np, Pu, and Am were also not mobilized from their original sites. Local migration of Mo, Ag, Cd, Sb, Sn, Tc, and Ru during or just after shutdown of the reactors has been shown, or, based on theoretical grounds, proposed. Yet widespread migration of any of these elements is unlikely. This results from the facts that the overall Oklo environment was chemically reducing, and the conditions in the reactor zone proper were just slightly oxidizing. This is very important, as the data from Oklo suggest that even if locally oxidizing, near-field reactions were to occur near a buried radioactive waste canister, these reactions would be extremely local, and any waste which escaped from the waste package would be quickly removed by the surrounding rocks after reducing conditions. Further, the clay minerals around the Oklo ores very efficiently scavenged fissiogenic alkali and alkaline earth elements (and perhaps others), thus demonstrating that such minerals in engineered overpack indeed work very well.

The exact coupled processes operative at the Oklo natural reactor are difficult to identify, but involve geochemical, thermal, hydrologic and probably mechanical processes. Diffusion of elements incompatible in the host pitchblende (Rb, Sr, Cs, Ba, Mo, Ag, Cd, Sb, I, and Br) was promoted by the moderately high temperatures and a locally oxidizing environment. Hydrologic conditions during the reactor's operative lifetime are not known, but rather restricted flow is likely based on the fact that readily soluble species such as Rb, Sr, and Cs appear to have been adsorbed onto clay minerals in areas immediately adjacent to the host pitchblende as opposed to being carried far distances. However, when the paleohydrologic conditions at Oklo are determined, it should be possible to attempt a quantitative material balance for migration of certain of the fission products and actinides in the rocks, providing a precise determination of the thermal regime of the reactor ores has been well established.

The Oklo experiments convincingly show that rocks are able to retain radioactive wastes under conditions of elevated temperatures with accompanying hydrothermal solutions, presence of water, high porosity and permeability, and without benefit of barriers such as canister, overpack, or engineered backfill. The Oklo data also strongly show that a chemically reducing environment is adequate for storage of radioactive wastes and that clay minerals do indeed act as effective getters for fissiogenic and other elements and, as such, are ideal for engineered backfill. Finally, data for Oklo are incomplete. Analyses of gangue, especially post-uranium ore formation of pyrite near reactor ore, should be carried out to check for Sb_f, Cd_f, Br_f, I_f, and even Kr_f and Xe_f. Oklo offers the scientific community the opportunity to address directly problems of long term storage of radioactive wastes, and its full importance and relevance to this issue has not yet been determined.

References

Barton, P. D., and Skinner, B. J. (1979). "Sulfide mineral stabilities:" in Geochemistry of Hydrothermal Ore Deposits, 2d. Ed.: Barnes, H. L., ed., Wiley-Interscience, New York, p. 278-403.

Brookins, D. G. (1978a). "Eh-pH diagrams for elements from Z=40 to Z=52: application to the Oklo

natural reactor," Chem. Geol., v. 23, p. 324-342.

Brookins, D. G. (1978b). "Retention of transuranic and actinide elements and bismuth at the Oklo natural reactor, Gabon," Chem. Geol, v. 23, p. 309-323.

Brookins, D. G. (1978c). "Application of Eh-pH diagrams to problems of retention and/or migration of fissiogenic elements at Oklo," in IAEA (1978), p. 243-265.

Brookins, D. G. (1979). "Uranium deposits of the Grants, New Mexico Mineral Belt II," U.S. Dept. Energy Rpt. BFEC-GJO-76-029E, 411 p.

Brookins, D. G. (1980). "Syngenetic model for some early Proterozoic uranium deposits: evidence from Oklo," Int. Atomic Energy Agency Sym. on the Pine Creek Geosyncline, p. 709-719.

Brookins, D. G. (1981). "Alkali and alkaline earth studies at Oklo," in Sci. Basis Nuc. Wste. Mngmt. III: Moore, J. G., ed., Plenum Press, New York, p. 275-282.

Brookins, D. G. (1983). "Eh-pH diagrams for the Rare Earth Elements (REE) at 25°C, one bar pressure," Geochem. Jour., v. 17, p. 223-229.

Brookins, D. G., Lee, M. J., Mukhopadhyay, B., and Bolivar, S. L. (1976). "Search for fission-produced Rb, Sr, Cs, and Ba at Oklo," in IAEA (1976), p. 401-414.

Christensen, A. G., Del Debbio, J. A., Knecht, J. D., and Tanner, J. E. (1981). "Loading and leachage of krypton immobilized in zeolites and glass," in Sci. Basis Nuclear Wste. Mngmt. III: Moore, J. G., ed., Plenum Press, New York, p. 267-274.

DeLaeter, J. R., Rosman, J. K. R., and Smith, C.L. (1980). "The Oklo natural reactor: cumulative fission yields and retentivity of the symmetric mass region fission products," Earth Plan. Sci. Lttrs., v. 50, p. 238-246.

Drozd, R. J., Hohenberg, C. M., and Morgan, C. J. (1974). "Heavy rare gases from Rabbit Lake (Canada) and the Oklo mine (Gabon): natural spontaneous chain reactions in old uranium deposits," Earth Plan. Sci. Lttrs., v. 23, p. 28-37.

Frejacques, C., Blain, C., Devilliers, C., Hagemann, R., and Ruffenbach, J. C. (1976). Conclusions tirees de l'etude de la migration des produits de fission," in IAEA(1976), p. 509-526.

Gancarz, A. J., Cowan, G. A., Curtis, D. H., and Maeck, W. L. (1980). Tc-99, Ru and Pb migration around the Oklo natural fission reactors," in Sci. Basis Nuc. Wste. Mngmt. II: Northrup, C. J., ed, Plenum Press, New York, p. 601-608.

IAEA, 1976. "The Oklo phenomenon," Inter. Atomic Energy Agency Sym.204, 646 p.

IAEA, 1978. "Natural fission reactors," Inter. Atomic Energy Agency Tech. Pub. 119, 754 p.

Kuroda, P. K. (1976). "Fossil Nuclear Reactor and Plutonium-244 in the early history of the solar system, " in IAEA (1976), p. 479-487.

McLennan, S. M., and Taylor, S. R. (1979). "Rare earth elements mobility associated with uranium mineralization," Nature, v. 282, p. 247-249.

Naudet, R. (1978). "Les reacteurs d'Oklo: cinq ans d'exploration du site," in IAEA (1978), p. 3-18.

THE EFFECTS OF GEOCHEMICAL PROCESSES ON THE TRANSPORT OF CONTAMINANTS IN MULTICOMPONENT SYSTEMS: A MODELING PERSPECTIVE

Gail A. Cederberg

Los Alamos National Laboratory
MS F665
Los Alamos, NM 87545

ABSTRACT

An equilibrium geochemical transport model for multicomponent systems, TRANQL, was used to investigate the effects of geochemical processes on the transport of contaminants. TRANQL was used to investigate the sensitivity of cadmium transport to a range of initial conditions, pH, complexing ligand concentrations, and concentrations of a simultaneously sorbing solute. Aqueous-phase complexation, dissociation of water, and sorption were the processes considered. First, the transport of an initial pulse of cadmium with a constant concentration of EDTA was examined. Second, the transport of an initial pulse of cadmium and EDTA was simulated. The effects of variations in EDTA concentrations and pH were investigated. Finally, the transport of an initial pulse of cadmium and cobalt was examined. Results show a significant coupling between the geochemical processes of complexation and sorption and mass-transport. In cases where sorption is considered to be an important controlling reaction the transport of a solute in multicomponent systems is a strong function of the initial concentration and distribution of complexing ligands, pH, equilibrium formation constants, and the concentration of a simultaneously sorbing solute.

INTRODUCTION

Geochemical transport modeling plays a significant role in characterizing the macroscopic far-field environment and performance assessment of potential nuclear waste storage sites. The specific geochemical processes and the parameter values considered in the modeling affect the results of these transport simulations and thus the predicted performance of a repository. In particular most transport models currently used in nuclear waste storage programs rely solely on the use of a distribution coefficient to describe the equilibrium interaction and retardation of a radionuclide. However, distribution coefficient models do not take into account complex geochemical or multisolute reactions and have often been inadequate in simulating observed transport. Implicit in these models is also the assumption that the solutes being modeled act independently of the bulk solution composition, i.e., the transport of one particular contaminant does not depend upon the presence of any other constituent in the system. Therefore, more sophisticated multicomponent equilibrium geochemical transport models have recently been developed (Valocchi et al., 1981; Charbeneau, 1981; Cederberg et al., 1985). Multicomponent models have the potential to incorporate the equilibrium chemical reactions which may be significant in describing and predicting transport such as aqueous-phase complexation, ion-exchange, simultaneous adsorption, dissociation of water, and precipitation/dissolution. Because contamination sources and environments at potential nuclear waste repository sites are in reality multicomponent solutions, the application of multicomponent models to such sites should be investigated. As an initial step, one such model, TRANQL (Cederberg et al., 1985), was used to investigate the effects of geochemical processes on the transport of a sorbing solute, cadmium, in a multicomponent system.

The principal objective of this paper is to attempt to answer the question, "does including complex chemistry in transport models make a difference?", i.e., what is the impact of various geochemical processes and parameter values on the transport of a solute in a multicomponent system. In the sections that follow, first, the geochemistry considered in the simulations is described. Second, a general outline of the model, TRANQL, is given. Finally, the effects of changes in initial conditions, complexing ligand concentration, pH, and simultaneously sorbing solute concentrations are detailed. Aqueous-phase complexation, dissociation of water, and sorption were the geochemical processes considered. From these examples it can be concluded that a significant coupling between the geochemical processes of complexation and sorption and mass-transport exists. Further investigations should continue in applying this model to radionuclide transport at potential nuclear waste repository sites in order to validate or invalidate the use of distribution coefficient transport models.

MODEL DESCRIPTION

TRANQL is the model used for the simulations in this paper (Cederberg et al., 1985). In TRANQL the equilibrium interaction chemistry is posed independently of the mass transport equations, which leads to a set of algebraic equations for the chemistry coupled to a set of differential equations for the mass transport. A solution is found by iterating between the two equation sets. The mass transport equations are solved using the Galerkin-Finite Element Method with an implicit time-stepping scheme and the algebraic chemical equation set is solved using the Newton-Raphson Method.

The equilibrium interaction chemistry considered here as a model system and shown in Table 1 includes sorption, complexation, and dissociation of water. The partitioning of species based on these chemical reactions depends

upon a variety of physical and chemical conditions such as temperature, pH, the bulk solution composition, the type and number of sorption sites, and the respective concentration of each species in the system. The set of components which combine to form all species is defined as (Cd^{2+}, Ca^{2+}, HCO_3^-, $EDTA^{4-}$, SOH, H^+) where SOH is the total number of sorption sites in moles/liter.

The value of the binding coefficient, K_{18}, for the sorption reaction of cadmium is a function of pH. Thus, two values of $\log_{10}K_{18}$ are given in Table 1. The values of K_{18} were calculated from data taken from laboratory batch experiments (Leckie et al., 1983). The aquifer material used in the experiments came from a calcareous, sandy, unconfined aquifer near Borden, Ontario, Canada.

To solve the set of chemical equilibrium equations for the eighteen species a computer code, MICROQL (Westall, 1979), is used. The information required from MICROQL for input into the transport equations after the concentrations of all species are calculated is the total aqueous concentrations of all components. For example, Cd_{AQ} (the total amount of cadmium in the aqueous phase) = $[Cd^{2+}]+[CdEDTA^{2-}]+[CdHEDTA^-]+[CdHCO_3^+]+[CdOH^+]$.

For one-dimensional flow in a homogeneous, isotropic porous medium the fundamental transport equations in TRANQL are the following:

$$\frac{\partial (C_T)_i}{\partial t} = D_L \frac{\partial^2 (C_{AQ})_i}{\partial x^2} - v \frac{\partial (C_{AQ})_i}{\partial x} \qquad i=1...N_c \quad (1)$$

where N_c = number of components (=6), $(C_T)_i$ = total (aqueous + sorbed phase) concentration of component i, $(C_{AQ})_i$ = aqueous phase concentration of component i, D_L = coefficient of hydrodynamic dispersion, and v = average groundwater velocity. Instead of formulating the transport equations around the mass balance for each species in the aqueous phase, the transport equations have been written around the mass balance for the total concentration of each component. This formulation allows the interaction chemistry to be posed independently of the mass transport equations and coupling of the two sets in a precise manner. The time derivative of the total component concentration is a function only of the transport by advection and dispersion of the total aqueous component concentration. The $(C_{AQ})_i$'s are determined from the solution of MICROQL, the equilibrium chemistry equation set.

The final set of mass-transport equations is a system of differential equations (in this example two equations). The final set of equilibrium chemistry equations is a system of algebraic equations (here eighteen equations). After initializing the system to equilibrium, Eq. 1 can be solved directly for $(EDTA_T)$ because $(EDTA_T)=(EDTA_{AQ})$. Solution to Eq. 1 for the nonconservative component, (Cd_T), is found by iterating between the two equation sets until some prescribed convergence tolerance is met for the nonconservative component. It is assumed that that concentration of the other components, Ca^{2+}, HCO_3^-, SOH, and H^+, remain constant.

	Reactions		Species	$\log_{10}K$
1	Cd^{2+}	=	Cd^{2+}	0
2	Ca^{2+}	=	Ca^{2+}	0
3	HCO_3^-	=	HCO_3^-	0
4	$EDTA^{4-}$	=	$EDTA^{4-}$	0
5	SOH	=	SOH	0
6	H^+	=	H^+	0
Complexation				
7	$3H^+ + EDTA^{4-}$	=	H_3EDTA^-	6.16
8	$4H^+ + EDTA^{4-}$	=	H_4EDTA	10.26
9	$Cd^{2+} + EDTA^{4-}$	=	$CdEDTA^{2-}$	15.78
10	$Cd^{2+} + H^+ + EDTA^{4-}$	=	$CdHEDTA^-$	18.50
11	$Cd^{2+} + HCO_3^-$	=	$CdHCO_3^+$	1.92
12	$Ca^{2+} + EDTA^{4-}$	=	$CaEDTA^{2-}$	10.52
13	$Ca^{2+} + H^+ + EDTA^{4-}$	=	$CaHEDTA^-$	13.00
14	$Ca^{2+} + HCO_3^-$	=	$CaHCO_3^+$	0.92
15	$Cd^{2+} - H^+ + H_2O$	=	$CdOH^+$	-10.28
16	$Ca^{2+} - H^+ + H_2O$	=	$CaOH^+$	-12.78
Dissociation of Water				
17	$-H^+ + H_2O$	=	OH^-	-13.91
Sorption				
18	$Cd^{2+} + SOH$	=	CdSOH	5.01 pH = 7.46 5.35 pH = 7.97

Table 1. Chemical Reactions for the cadmium/EDTA system.

EFFECTS OF GEOCHEMICAL PROCESSES

TRANQL was used to investigate the sensitivity of cadmium transport to a range of initial conditions, complexing ligand concentrations, pH, and concentrations of a simultaneously sorbing solute. For all the simulations in this paper the multicomponent geochemical parameter values and the physical parameter values are the same and held constant. The geochemical system considered is described in Table 1. Flow was in one dimension with v = 0.10 m/day and D_L = 0.006 m^2/day.

Effect of a Constant Initial EDTA Concentration

The effect of three different constant EDTA concentrations on the transport of an initial pulse of cadmium was investigated. The total concentrations of Ca^{2+}, HCO_3^-, SOH, and pH are held constant throughout the simulations in order to isolate the effect of the constant EDTA concentration on the transport of cadmium. At time t = 0, a pulse of Cd_T is placed in the system which is then assumed to be at chemical equilibrium. Three different constant concentrations of EDTA (10^{-4}, 10^{-6}, and 2.51×10^{-8} M) were used in the simulations. The three respective initial Cd_{AQ} distributions are given in Figure 1. The boundary values are taken to be those at the extremes of the initial distributions. For numerical purposes the background level of Cd was assumed to be two orders of magnitude smaller

than the peak concentration value of the input pulse. Constant aqueous background concentrations for all components were used as the boundary conditions at x = -1.375 m. The center of the pulse was assigned x = 0 at t = 0.

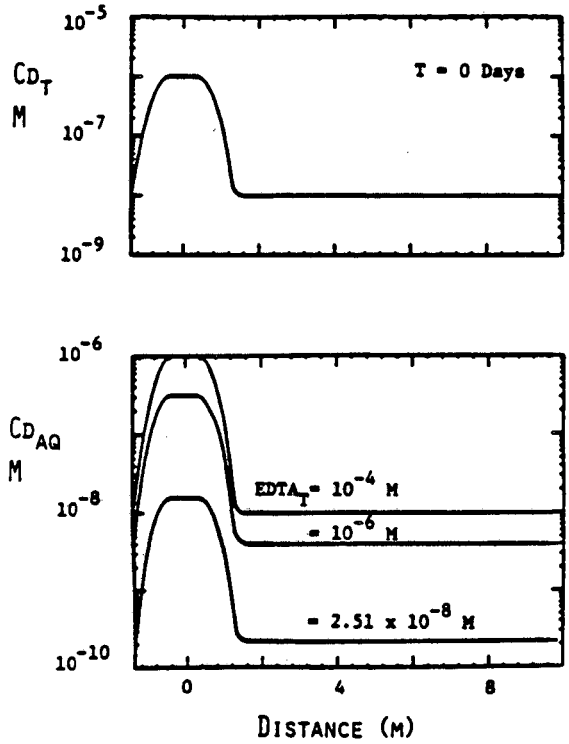

Figure 1. Initial Cd/constant EDTA system.

For each initial concentration of EDTA a different Cd_{AQ} concentration exists. In Figure 1 it shows the more EDTA in the system the more cadmium complexes with the EDTA and remains in the aqueous phase. A two-order-of-magnitude decrease in EDTA concentration results in a two-order-of-magnitude decrease in Cd_{AQ}. So while the initial concentration distribution of total cadmium, Cd_T, is the same in all three cases, the Cd_{AQ} distribution is quite different. The difference is due to the amount of aqueous cadmium complexation which in turn is based on the chemical reactions and formation constants listed in Table 1.

TRANQL was run to simulate a real time of 40 days. A time step of 2 hr and nodal spacing of 0.25 m were used in the simulations. Figure 2 shows the results of the three TRANQL simulations, each with a different initial concentration of EDTA. The total concentration of aqueous cadmium, Cd_{AQ}, is plotted as a function of distance for each EDTA concentration. The differences in the initial distributions of Cd_{AQ} resulted in marked differences in the results of the transport simulations. When EDTA is at its maximum value more cadmium complexes with the EDTA, remains in the aqueous phase, and therefore is transported further in the x-direction. When EDTA is at its minimum value, only 2% of the cadmium remains in the aqueous phase, 98% of the cadmium is immediately sorbed and virtually no cadmium is transported in the x-direction.

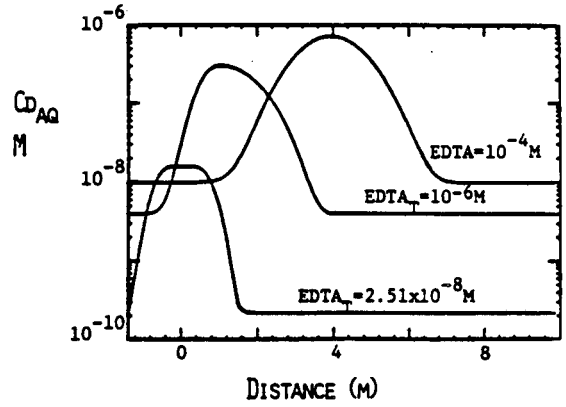

Figure 2. The effect of constant EDTA on Cd_{AQ}.

Effect of an Initial Pulse of EDTA

Instead of a constant concentration of EDTA a pulse of Cd_T and $EDTA_T$ is placed in the system at time t = 0. Four different concentrations of EDTA in the input pulse were used. To reference the simulations back to the varying initial concentrations of EDTA a notation which specifies each case is listed in Table 2. Cases EDTA(1a)-EDTA(4a) were used in this section to simulate the transport of a pulse containing EDTA and Cd. Cases EDTA(1b)-EDTA(4b) were used in the next section to investigate the effect of pH on the transport of Cd. The initial distribution of Cd_{AQ} for Cases EDTA(1a)-(4a) is shown in Figure 3. Initially, with more EDTA in the system more Cd_{AQ} also exits. A two-order-of-magnitude difference in peak concentration of EDTA results in a 50% decrease in the initial peak Cd_{AQ} concentration.

Case	Peak(M) / Background(M)	pH
EDTA(1a)	2.51×10^{-6} / 2.51×10^{-8}	7.97
EDTA(2a)	5.01×10^{-6} / 5.01×10^{-8}	7.97
EDTA(3a)	1.0×10^{-5} / 1.0×10^{-7}	7.97
EDTA(4a)	1.0×10^{-4} / 1.0×10^{-6}	7.97
EDTA(1b)	2.51×10^{-6} / 2.51×10^{-8}	7.46
EDTA(2b)	5.01×10^{-6} / 5.01×10^{-8}	7.46
EDTA(3b)	1.0×10^{-5} / 1.0×10^{-7}	7.46
EDTA(4b)	1.0×10^{-4} / 1.0×10^{-6}	7.46

Table 2. EDTA Concentrations used in cadmium/EDTA simulations

Figure 4 shows the results of four TRANQL simulations, each with a different initial pulse concentration of EDTA. When the peak concentration of EDTA is a maximum [Case EDTA(4a)], most of the cadmium is complexed with the EDTA and therefore remains in the aqueous phase. In this case cadmium behaves in a manner similar to that of EDTA, the conservative component. As the initial peak EDTA concentration decreases, more and more cadmium adsorbs to the porous medium due to the decrease in cadmium complexation. A two-order-of-magnitude decrease in peak EDTA

concentration [Case EDTA(4a) to EDTA(1a)] results in more than an order-of-magnitude decrease in the maximum observed concentration of cadmium. As the peak EDTA concentration decreases, cadmium becomes more and more immobile and the concentration distribution becomes asymmetric.

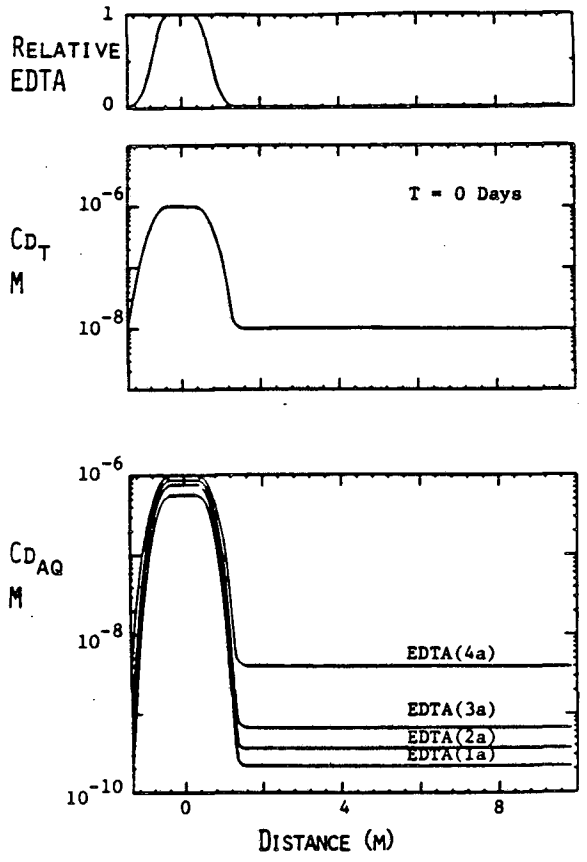

Figure 3. Initial Cd/pulse EDTA system.

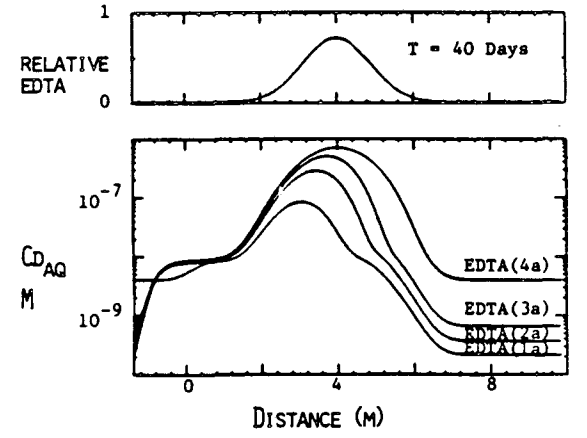

Figure 4. The effect of pulse EDTA on Cd_{AQ}.

The asymmetry in the cadmium distribution can be attributed to the changing speciation everywhere in the system over time and the initial pulse distribution of EDTA. The relative broadening and asymmetry of the Cd_{AQ} curves was not seen in the simulations where EDTA was constant. The asymmetry has been shown to result from the initial pulse distribution of EDTA and Cd and the ever-changing degree of geochemical complexation, speciation, and sorption occurring everywhere in the system (Cederberg, 1985).

The Effect of pH

For the cadmium/EDTA system (see Table 1) the formation or binding coefficient, K_{18}, for the sorption reaction is an implicit function of pH. As the pH increases, so does the value of the binding coefficient. Therefore, cases EDTA(1b)-EDTA(4b) were simulated to investigate the effect of pH on cadmium transport. For direct comparison the concentration of Cd_{AQ} for Cases EDTA(1b) and (1a) and EDTA(4b) and (4a) are shown in Figure 5 for t = 40 days. When the pH is lower the cadmium is more mobile and transported further. The effect is most noticeable when the peak EDTA concentration is lowest [Cases EDTA(1b) and (1a)]. In this case the decrease in pH results in a 75% increase in the observed maximum cadmium concentration. The complexation of the cadmium with the EDTA overwhelms any change in cadmium concentration due to a change in pH. There is little noticeable change between the cadmium concentrations when the EDTA peak concentration is a maximum [Cases EDTA(4a)-(4b)]. Because the binding coefficient has a lower value at a lower pH, the cadmium will bind less strongly with the porous medium and the EDTA will compete for the cadmium more strongly.

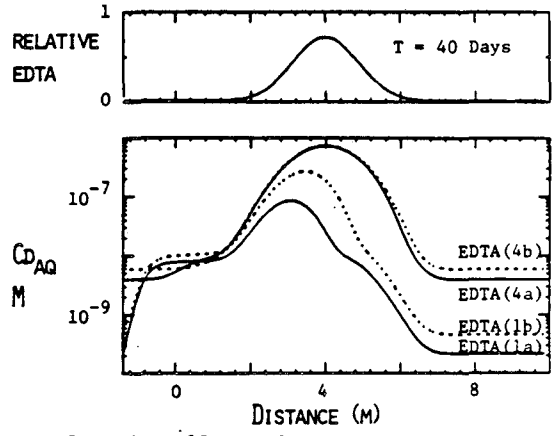

Figure 5. The effect of pH on Cd_{AQ}.

The Effect of Cobalt

More than one reactive component is often found in contaminant systems. A second component may or may not compete with the first component for specific complexing ligands or sorption sites. To investigate the effects of the presence of a second sorbing component TRANQL was used to simulate the transport of cadmium and cobalt. The additional chemical reactions to the cadmium/cobalt/EDTA system are listed in Table 3. The complete system of reactions includes all those reactions from Table 1 plus those reactions specific to cobalt. In this set of reactions cobalt forms complexes similar to those of cadmium. The values of the binding coefficients for cadmium and cobalt in a system together were found by batch experiments.

The transport equation set for the cadmium/cobalt/EDTA system contains one conservative transport equation for EDTA and two

nonconservative transport equations, one each for the components, cadmium and cobalt. The physical parameter values used in the simulations are the same as those of the previous section. The initial and boundary conditions are also similar in value; however, here pH = 7.46 and SOH_T = 0.204 M. For this investigation a pulse of cadmium, cobalt, and EDTA is input while the concentrations of the other components are held constant and remain at the values described in the previous sections.

	Reactions	Species	$\log_{10}K$
19	$Co^{2+} = Co^{2+}$		0
20	$Co^{2+} + EDTA^{4-} = CoEDTA^{2-}$		15.58
21	$Co^{2+} + H^{+} + EDTA^{4-} = CoHEDTA^{-}$		18.40
22	$Co^{2+} + HCO_3^{-} = CoHCO_3^{+}$		2.72
23	$Co^{2+} - H^{+} + H_2O = CoOH^{+}$		-9.88
Sorption			
24	$Co^{2+} + SOH = CoSOH$	pH=7.46	3.0
(18)	$Cd^{2+} + SOH = CdSOH$		3.6

Table 3. Additional chemical reactions for the cadmium/cobalt/EDTA system.

Simulations were run with two different peak concentrations of total cobalt ($Co_T = 10^{-5}$ M and $= 10^{-7}$ M) present. Figure 6 shows the initial distributions of $EDTA_T$, Cd_T, and Co_T. Case Co1 (represented by the dotted line) represents the simulation where $Co_T = 10^{-7}$ M. Case Co2 (represented by the solid line) represents the simulations where $Co_T = 10^{-5}$ M. Figure 7 shows the initial distributions of Cd_{AQ} and Co_{AQ} after chemical equilibrium have been attained. Because the Cd and Co compete for EDTA and sorption sites, the presence of a lower initial concentration of Co_T (Case Co1) results in a higher concentration of Cd_{AQ} after the system comes to equilibrium. As the cobalt concentration decreases, less cobalt complexes with EDTA and more cadmium complexes with the EDTA. Thus, less cadmium is available to sorb and the Cd_{AQ} increases. From these initial conditions one would expect Cd to be transported further and at a higher concentration for the case where $Co_T = 10^{-7}$ M.

Figure 8 shows the results of two TRANQL simulations where the initial peak values of $EDTA_T$ is 10^{-5} M and Cd_T is 10^{-6} M. As the concentration of cobalt increases, the concentration of Cd_{AQ} decreases. The difference in Co concentration has a significant effect on the transport of cadmium. Although Cd_{AQ} initially is higher when Co_T is lower, the difference in the two Cd_{AQ} distributions increases with time. Initially there was approximately a 40% difference in the Cd_{AQ} peak value. At the end of 40 days an order-of-magnitude difference in the peak concentration of Cd_{AQ} exists.

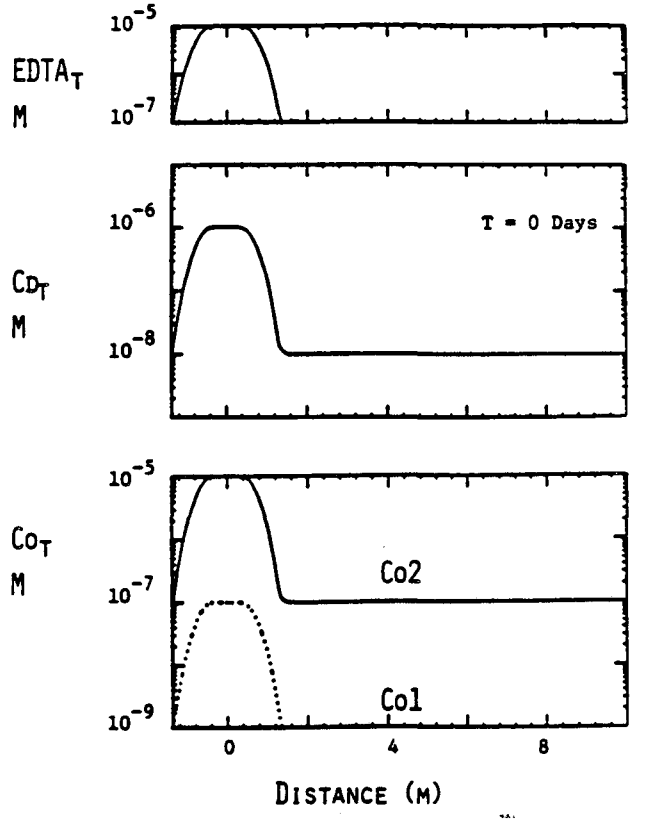

Figure 6. Initial Cd_T/Co_T $EDTA_T$ system.

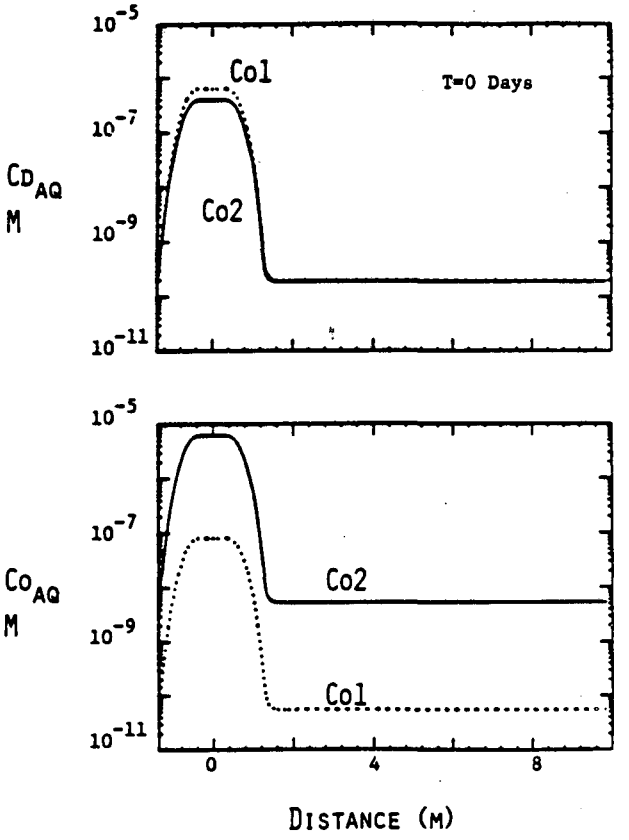

Figure 7. Initial Cd_{AQ}/Co_{AQ}/EDTA system.

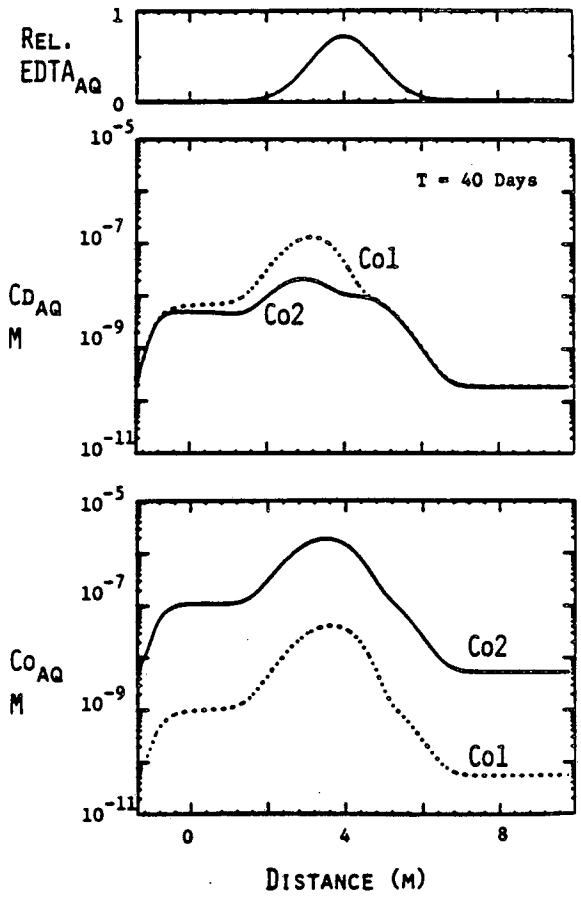

Figure 8. The effect of Co_{AQ} on Cd_{AQ}.

SUMMARY

Results show a significant coupling between the geochemical processes of complexation and sorption and mass-transport. In cases where sorption is considered to be an important controlling reaction the transport of a solute in multicomponent systems is a strong function of the initial concentration and distribution of complexing ligands (here EDTA), equilibrium formation constants, pH, and the concentration of a simultaneously sorbing solute. In the presence of a conservative complexing component such as EDTA the mobility or transport of cadmium increased significantly as the concentration of EDTA increased. A two-order-of-magnitude increase in EDTA resulted in an order-of-magnitude increase in the predicted maximum concentration of aqueous cadmium. When EDTA was constant, the Cd_{AQ} curves retained their symmetry. However, in cases where a pulse of EDTA was input the Cd_{AQ} distributions became asymmetric and significantly broadened. Thus, the initial distributions and concentrations of all components in the system may effect the transport of a sorbing solute. As the pH decreased and the corresponding binding coefficient decreased, the transport of cadmium increased. When the EDTA peak concentration was a minimum, the decrease in pH resulted in a 75% increase in the predicted maximum Cd_{AQ} concentration. However, when the peak concentration of EDTA was a maximum, the change in pH had little effect on cadmium transport. Finally, as the concentration of a second sorbing component ,cobalt, was increased, the transport of cadmium respectively decreased. A two-order-of-magnitude increase in cobalt resulted in a 50% decrease in the Cd_{AQ} concentration.

The specific results from these simulations are a function of the set of reactions considered, the components present, and the equilibrium formation coefficients. However, the results do represent trends one might observe in ground-water contamination systems which concern the transport of inorganics in a multicomponent system. From the viewpoint of nuclear waste disposal programs the results of these calculations raise several important questions. First, what is the effect of multicomponent complexation and sorption on mass-transport and thus performance assessment at potential nuclear waste repository sites? Second, if models such as TRANQL are needed are the necessary data being gathered in order to use these models? Finally, how valid is the application of distribution coefficient models to predict transport at repository sites? Further investigations are continuing in order to answer these questions.

REFERENCES

Cederberg, G. A. (1985). "TRANQL: A Ground-Water Mass-Transport and Equilibrium Chemistry Model for Multicomponent Systems", Ph.D. Dissertation, Stanford University, Stanford, CA.

Cederberg, G. A., R. L. Street, and J. O. Leckie (1985). "A groundwater mass transport and equilibrium chemistry model for multicomponent systems," Water Resources Research, in press.

Charbeneau, R. J. (1981). "Groundwater contaminant transport with adsorption and ion exchange chemistry, method of characteristics for the case without dispersion," Water Res. Res., 17(3), 705-713.

Leckie, J. O., N. B. Ball, G. A. Cederberg, J. A. Davis, and C. Fuller (1983). "Adsorptive control of cadmium mobility in a groundwater aquifer: experimental and mathematical modeling," 6th International Symposium on Environmental Biogeochemistry," Santa Fe, NM, October 10-14.

Valocchi, A. J., R. L. Street, and P. V. Roberts (1981). "Transport of ion-exchanging solutes in groundwater: chromatographic theory and field simulation," Water Res. Res., 17(5), 1517-1527.

ACKNOWLEDGEMENTS

Prepared by Nevada Nuclear Waste Storage Investigations (NNWSI) Project participants as part of the Civilian Radioactive Waste Management Program (CRWM). The NNWSI Project is managed by the Waste Management Project Office (WMPO) of the U.S. Department of Energy, Nevada Operations Office (DOE/NV). NNWSI Project work is sponsored by the Office of Geologic Repositories (OGR) of the DOE Office of Civilian Radioactive Waste Management (OCRWM).

ON NUCLIDE TRANSPORT, PRECIPITATION, DISSOLUTION AND SHARED SOLUBILITY LIMITS

Robert J. Hopkirk and David J. Gilby

Polydynamics Limited
Zeltweg 29
8032 Zurich, Switzerland

ABSTRACT

Most of the actinides and many of the fission and activation products in high level nuclear waste are soluble in some groundwaters only to a very limited extent. In addition, the solubility capacity for certain elements is shared amongst several isotopes. This becomes critical when dealing with the members of the actinide decay chains. Solubility limitations and transport rates are strongly coupled for all the important isotopes.

An iterative dynamic relaxation method has been developed in order to allow the simultaneous treatment of this coupled problem for the members of the actinide decay chains within the framework of an implicit finite difference code (TROUGH).

The code has been used to study the diffusive release of radionuclides from the near field of a repository for reprocessed high level waste where a reducing groundwater is expected. A simple relationship for establishing the instantaneous, local level of solubility for each isotope has been employed.

Solubility limitation in conjunction with the sorption capacity of the clay backfill in the repository storage tunnels results in many nuclides decaying to insignificant activity levels before release to the geosphere.

BACKGROUND

Most of the nuclides which require treatment in the safety analysis of a radionuclide waste repository are subject to solubility limitation in groundwater. The nature of the resulting concentration field and of the precipitation or dissolution rate places a special requirement on nuclide migration calculations.

A further complication arises when the solute and precipitate contain several isotopes of the same element, which have to then share the total elemental solubility capacity. The demands on the migration code are extended yet again when the actinide decay chains are treated, since now the total amount of an element present at any point of a migration path can depend to some extent on ingrowth of its individual isotopes from their precursors in the different decay chains. Table 1 lists the four principal actinide chains in simplified form.

Inspection of Table 1 reveals the extent to which all of the actinides are interrelated and indicates that their migration processes, while solubility limits are varying due to the sharing amongst isotopes, must be strongly coupled.

Table 1. Simplified actinide decay chains

Chain 1 -	$^{245}Cm \rightarrow {}^{241}Am \rightarrow {}^{237}Np \rightarrow {}^{233}U \rightarrow {}^{229}Th$
Chain 2 -	$^{246}Cm \rightarrow {}^{242}Pu \rightarrow {}^{238}U \rightarrow {}^{234}U \rightarrow {}^{230}Th \rightarrow {}^{226}Ra$
Chain 3 -	$^{243}Am \rightarrow {}^{239}Pu \rightarrow {}^{235}U \rightarrow {}^{231}Pa$
Chain 4 -	$^{240}Pu \rightarrow {}^{236}U \rightarrow {}^{232}Th$

It is the purpose of this paper to present briefly the manner in which the shared saturation limits and the precipitation/dissolution processes have been integrated into the one-dimensional version of the TROUGH finite difference code and an example of its application (see also Hopkirk, Gilby and Wagner (1985)).

SATURATION AND DISSOLUTION

If a chemical species is injected into a body of water it will continue to pass into solution until the concentration exceeds the saturation limit. Precipitate will then start to form locally. Solute will diffuse away from the injection point and may also be advected away with a moving stream. The solute concentration will, in a homogeneous system, slowly decrease as the distance from the injection point increases so that precipitation can only occur again if there is a further local production of the species. If the system is not homogeneous and the solubility, due for example to a change in concentrations of other species or to a change of temperature, is locally lower at some point on the transport path, further precipitation may also occur. Conversely, if there is a sufficient decrease in injection or production rate where precipitation has occurred, or if the solubility limit increases at that point, an unstable precipitate may redissolve.

These processes are easier to visualise in a one-dimensional situation, so the equation for advective/diffusive transport with allowance for radioactive decay, ingrowth, sorption and precipitation may be written:

$$\frac{\partial}{\partial t}(\varepsilon\rho RC) = \frac{\partial}{\partial x}\left\{\rho(\varepsilon D_p + D_h)\frac{\partial C}{\partial r}\right\} - \frac{\partial}{\partial x}(\varepsilon\rho uC) - \varepsilon\rho\lambda RC + \lambda^*(\varepsilon\rho R^*C^* + N_P^*) - \dot{N}_P + N_I \quad (1)$$

where:

C	solute concentration	[mol kg^{-1}]
D_p	coefficient of diffusion in pore water	[m^2 s^{-1}]
D_h	hydrodynamic dispersion coefficient	[m^2 s^{-1}]
N_P	spatial concentration of precipitate	[mol m^{-3}]
$\dot{N}_P$	precipitation(+ve) or dissolution (-ve) rate	[mol m^{-3} s^{-1}]
$\dot{N}_I$	injection rate	[mol m^{-3} s^{-1}]
R	retention factor for equilibrium sorption = $(1 + \frac{1-\varepsilon}{\varepsilon} \rho_s K_d)$	[-]
K_d	equilibrium distribution coefficient	[m^3 kg^{-1}]
t	time	[s]
u	hydraulic water flow velocity	[m s^{-1}]
x	distance	[m]
ε	connected porosity	[-]
λ	decay coefficient	[s^{-1}]
ρ	water density	[kg m^{-3}]
ρ_s	density of the pore-free solid component	[kg m^{-3}]

* refers to the parent nuclide

This equation is solved in the TROUGH-1D code by an implicit finite difference scheme (see Gilby and Hopkirk (1985)). Figure 1 below contains a conceptual diagram of a segment from a one-dimensional migration path using finite difference terminology. It shows a cell P, the i'th cell of the discretised path, together with its neighbours W (West) and E (East). Precipitation is taking place so $C_i = C_{sat}$. The conservation equation (1) for the finite difference cell i will be reduced to the canonical form:

$$\sum_j A_j C_i = \sum_j A_j C_j + S_R + S_I + S_P \qquad (2)$$

where:

j	= i-1, i+1 and o (= "old" value in cell i from the previous timestep)
A_j	coefficients in the finite difference formulation of (1)
S_R	balance of the radioactive decay (sink) and ingrowth (source) in both solute and precipitate
S_I	injection source term, where applicable
S_P	precipitation source/sink, where applicable

so that for instance

$$S_P = 0 \text{ for } C_i < C_{sat}$$

but when saturation is reached $C_i = C_{sat}$ by definition and:

$$S_P = \sum_j A_j (C_i - C_j) - S_R - S_I \qquad (3)$$

providing that the precipitation/dissolution processes are rapid with respect to the advection and diffusion.

Figure 1. Segment of a discretised one-dimensional migration path with precipitation taking place.

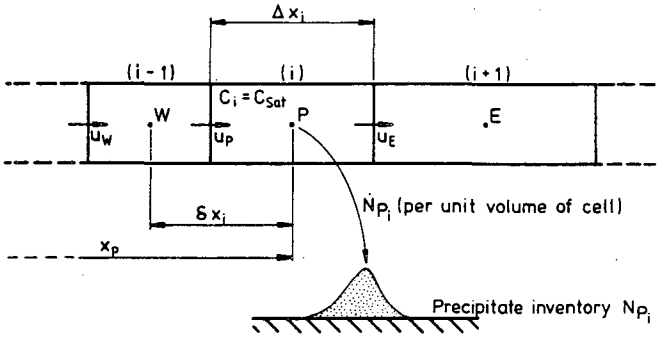

It should be noted that the ingrowth due to decay of a parent nuclide in precipitate is included in the S_R term. For the precipitate, the concentration present in the cell i is (see Figure 1) N_{Pi}, so that:

$$N_{Pi} = \int S_P dt - \int \lambda N_{Pi} dt$$

Thus the integral change in precipitate content per unit volume in cell i during a discrete timestep Δt may be written in simple difference form:

$$N_{Pi} - N^o_{Pi} = (S_P \frac{\Delta t}{\lambda} + N^o_{Pi})(1 - e^{-\lambda \Delta t}) \qquad (4)$$

where o = "old" as before.

Careful bookkeeping of the precipitate inventory is necessary in particular to determine when the end of the saturation condition in cell i occurs. During the saturation period C_i may be set at C_{sat}, in (3), but when re-dissolution is complete, there will be a timestep giving a solution:

$$N_{Pi} < 0$$

In this case C_i must be permitted to fall below C_{sat} during the timestep and the value of S_P calculated from (4) with N_{Pi} set to zero at the end of the step.

Since it is not known a priori when or where precipitation will start or stop, an iterative solution method has been selected. A preliminary solution sweep over the migration path reveals where precipitation is either starting or stopping according as:

$$C_i > C_{sat}$$
or $$N_{Pi} < 0$$

Subsequent iterations of the solution will only change the concentrations now at points downstream of a newly revealed precipitation/redissolution process discontinuity.

ISOTOPE SOLUBILITY LIMITS

In those cases where several isotopes of an element exist simultaneously there can be expected to be competition for solubility amongst them. If species adaptation of newly formed isotopes to the chemical environment is rapid, an expression giving the solubility limit of isotope k of a total of m of an element e as proportional to the total amount of that isotope present locally may be written for cell i:

$$C_{sat_{k,i}} = \frac{(\varepsilon\rho\Delta V)_i \, C_{k,i} + N_{Pk,i}}{\sum_{n=1}^{m} \left((\varepsilon\rho\Delta V)_i \, C_{n,i} + N_{P_{n,i}} \right)} C_{sat\ e} \qquad (5)$$

or

$$C_{sat_{k,i}} = r \, C_{sat_e}$$

Other schemes may be equally well employed, for instance as suggested by Hartley (1985). However, equation (5) has been used in the present work. No problems have been experienced with convergence of the numerical solution, even for the simultaneous treatment of the 18 actinides shown in Table 1 provided that an appropriate sequence of solution of the nuclides is followed. This is detailed in Table 2 below and shows how the isotopes have to be grouped under their element headings and solved in such an order that all precursor information is available before the members of each group can be handled.

Table 2. Solution sequence for isotopes of the actinides interrelated by membership of decay chains and by solubility limits.

Element	Isotopes				Solution Group
	Chain 1	Chain 2	Chain 3	Chain 4	
Curium	Cm-245	Cm-246			1
Americium	Am-241		Am-243		2
Neptunium	Np-237				3
Plutonium		Pu-242	Pu-239	Pu-240	4
Uranium	U -233	U-238/234	U- 235	U -236	5
Thorium	Th-229	Th-230		Th-232	6
Radium		Ra-226			7
Protactinium			Pa-231		8

APPLICATION TO NEAR FIELD RELEASE

The approach outlined above has been applied on behalf of NAGRA (Swiss cooperative for radioactive waste storage) to examining the effects of a bentonite backfill in the relatively large diameter storage tunnels (3.7 m) of a deep repository for reprocessed high level waste upon the radionuclide releases to the geosphere.

Dissolution of the vitrified glass matrix is assumed to commence for this study 10^3 years after disposal due to breakdown of an iron overpack of 0.47 m outside diameter. The bentonite is assumed water-saturated and the near-field chemistry, buffered by the clay and by strong presence of iron, results in a uniform reducing environment (Mc Kinley (1985)). Undisturbed host rock temperature at the repository depth is 55°C and from 1000 years after storage the temperature gradients are assumed insignificant across the near field region. Temperature distributions have been presented by Hopkirk, Gilby and Schwanner (1983).

Figure 2 gives an overview of this situation. The remaining diagrams show some aspects of the migration process of the actinides during the first million years after storage. For these calculations the waste matrix dissolution has been assumed to proceed at a uniform rate decoupled from all changes to the local water chemistry over 155'000 years. The migration was computed using TROUGH-1D in cylindrical radial mode (i.e. assuming perfect axial symmetry, described in more detail by Hopkirk, Gilby and Wagner (1985)) and considering an effective diffusion as the only transport mechanism. The advective term in equation (1) thus becomes zero.

Figure 2. Schematic overview of the near field storage tunnel for which results are presented. Geosphere starts at the tunnel wall.

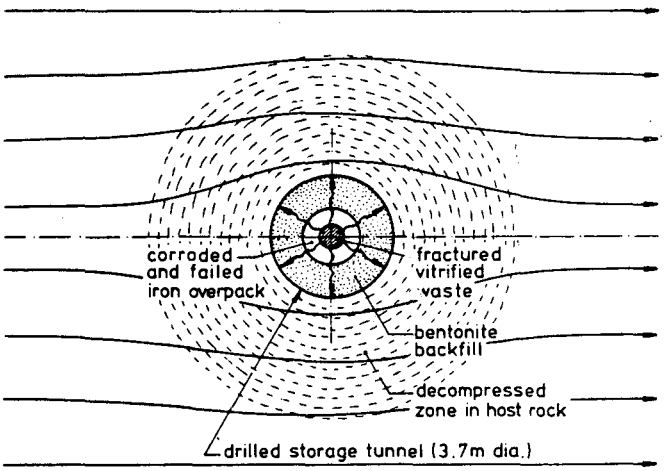

The outer boundary was a "mixing tank", whereby the nuclide flux crossing the boundary represented by the tunnel wall into the relatively permeable host rock was assumed to mix immediately with the passing groundwater.

Figures 3, 4 5 and 6 respectively show the release flux time histories across the tunnel wall for the chains 1, 2, 3 and 4 shown in Tables 1 and 2. Figure 7 shows a time history for Chain 1 alone to the same scale, but for the situation with no backfill. The effect of the backfill is quite clear:

Figure 3. Radionuclide fluxes into geosphere from backfill buffer - actinide chain 1.

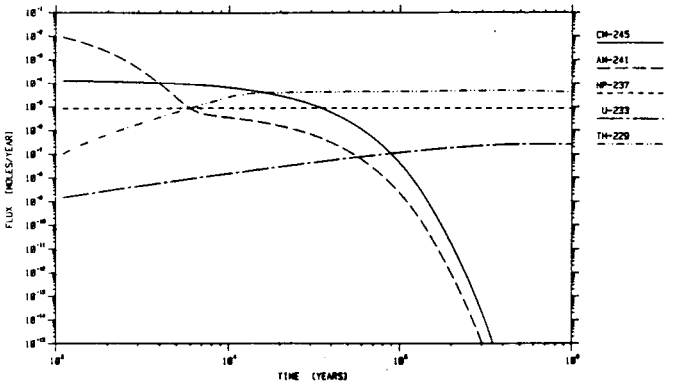

Figure 4. Radionuclide fluxes into geosphere from backfill buffer - actinide chain 2.

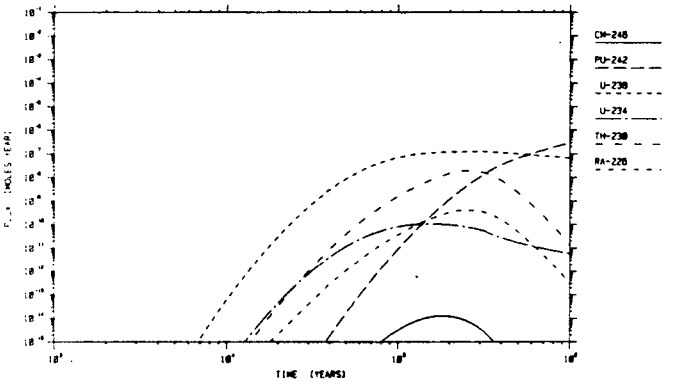

Figure 5. Radionuclide fluxes into geosphere from backfill buffer - actinide chain 3.

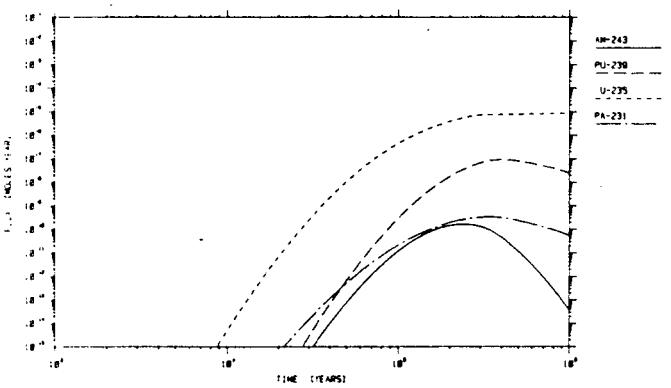

Figure 6. Radionuclide fluxes into geosphere from backfill buffer - actinide chain 4.

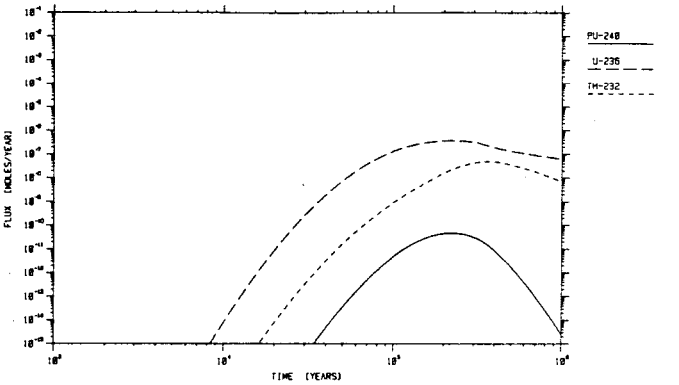

Figure 7. Radionuclide fluxes from waste matrix directly into geosphere (no backfill) - actinide chain 1.

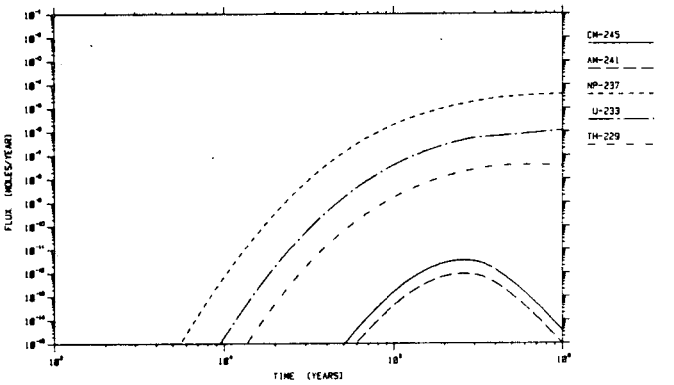

Retardation by sorption and diffusion delay release to such an extent that the short lived ^{245}Cm and ^{241}Am only emerge in rather insignificant quantities. The other nuclides are severely retarded, although by 10^6 years the ^{237}Np release is approaching its peak with ^{233}U and ^{229}Th in transient equilibrium with it.

Figures 8 and 9 show the releases of the five uranium isotopes respectively with and without backfill between waste and rock. Again the delay time rather than the absolute reduction of the maximum release rate is significant. It should be noted that slight differences in the water chemistry assumptions for the situations with and without backfill result in variations in solubility limits (see Schweingruber (1983, 1984a, 1984b) and Mc Kinley (1985)). For instance ^{237}Np is limited to 10^{-8} mol/l with backfill and 2×10^{-9} mol/l without backfill. Thus, fine comparisons of the peak release rates are not possible. However, Table 3 shows for the nuclides of Chain 1 and the remaining uranium isotopes the maximum release rates from the waste package to be expected due to matrix dissolution at 10^3 years the time of waste package failure.

Figure 8. Fluxes of the uranium isotopes to the geosphere from the backfill buffer.

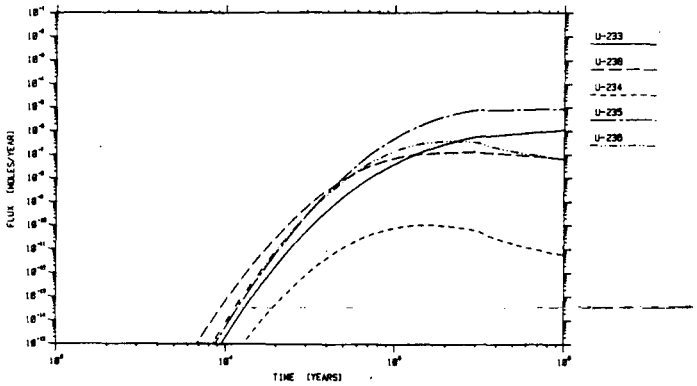

Figure 9. Fluxes of the uranium isotopes when released directly to the geosphere.

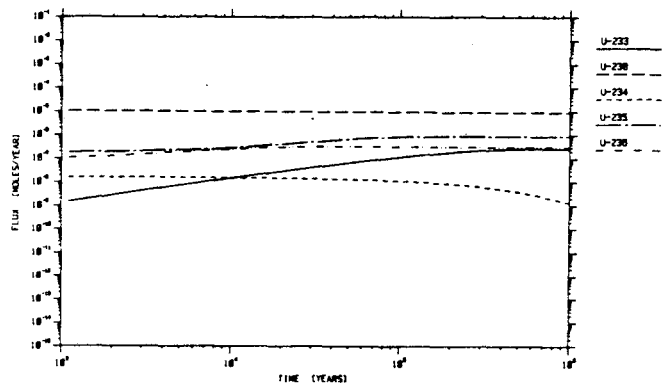

Table 3. Maximum release rates from the waste matrix due to waste dissolution

Nuclide	Max. release by congruent dissolution [mol/yr]
Cm-245	3.9×10^{-4}
Am-241	3.1×10^{-2}
Np-237	4.1×10^{-1}
U -233	1.2×10^{-4}
Th-229	2.4×10^{-7}
U -238	9.4×10^{-1}
U -234	1.5×10^{-3}
U -235	1.7×10^{-2}
U -236	9.4×10^{-3}

In particular, Figure 8 reflects a combination of the effects of the precursors of the uranium isotopes and the progress of the precipitation front radially outwards towards the near field/geosphere interface defined at the tunnel wall. It is indeed the five uranium isotopes which exhibit the most complex precipitation behaviour. An uranium precipitation front moves slowly radially outwards so that by the end of the one million years period examined here it has (see Figure 10) only reached a radius of 1.55 m.

Figure 10. Progress of the uranium precipitation front radially outwards through the backfill.

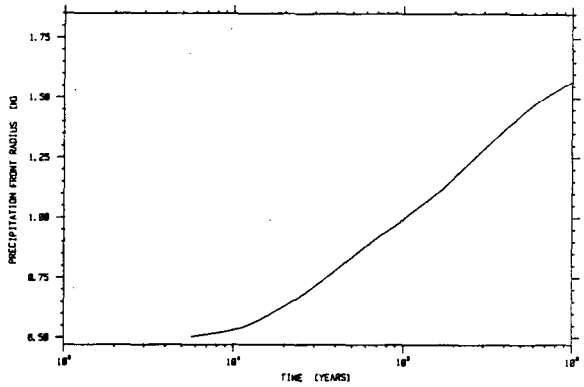

Figures 11 and 12 show the relative proportions of each of the five uranium isotopes in the remains of the waste package (at a fixed point) and at the moving precipitation front respectively. It is seen that in the waste region ^{238}U dominates, whereas with increasing radial progression of the saturation front ^{235}U rapidly takes over the dominant role. The reason is that in the model waste inventory the availability of ^{238}U is almost two orders of magnitude greater than ^{235}U which is the next most abundant uranium isotope. During the transport process, however, the ^{235}U is produced by a shorter lived plutonium parent. A similar contrast can be seen in the release rates to the geosphere with and without the backfill buffer.

Figure 11. Isotopic mix of uranium precipitate within the waste package volume.

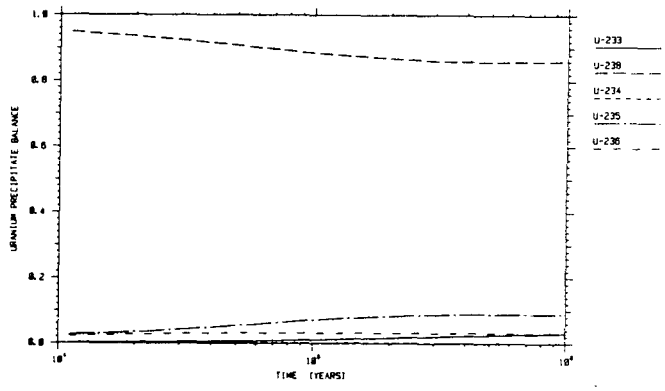

Figure 12. Isotopic mix of uranium precipitate at the moving precipitate front.

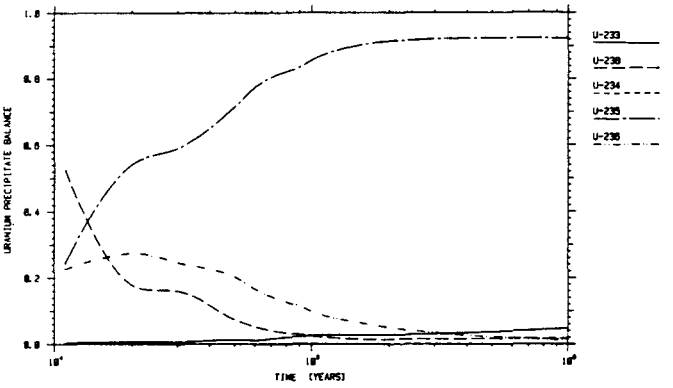

SUMMARY

The results presented above demonstrate the importance of considering solubility limitations in migration modelling. Equally important however is the further coupling of these effects with other aspects of the near field chemistry in order to arrive at an undistorted image of the release and migration processes.

ACKNOWLEDGEMENTS

The authors would like to thank all their colleagues at NAGRA for enabling them to engage on this work, but in particular to Charles Mc Combie, Urs Frick, Bernard Knecht and Piet Zuidema for the stimulating discussions. They are also grateful for the constructive interaction with Ivars Neretnieks, KTH Stockholm and with Jörg Hadermann and Ian Mc Kinley of the EIR, Würenlingen. Thanks are also due to Christina Künzle at Polydynamics for all her help in organising and presenting our work.

REFERENCES

Gilby D.J. and Hopkirk R.J. (1985). "TROUGH-1D. A one-dimensional computer code for calculation of radionuclide transport in groundwater." NAGRA NTB 85-38, NAGRA, Baden, Switzerland, Feb. 1985.

Hartley R.W. (1985). "Release of radionuclides to the geosphere from a repository for high level waste -mathematical model, results." NAGRA NTB 85-41, NAGRA, Baden, Switzerland, Feb. 1985.

Hopkirk R.J., Gilby D.J., Schwanner I. (1983). "Preliminary calculations of the temperature distributions around a Type C (highly active) nuclear waste repository." NAGRA NTB 83-20, NAGRA, Baden, Switzerland, Oct. 1983.

Hopkirk R.J., Gilby D.J., Wagner W.H., (1985). "Modelling of solute transport in the near field of a high level waste repository." NAGRA NTB 85-26, NAGRA, Baden, Switzerland (in press).

Mc Kinley I. (1985). "The geochemistry of the near field." NAGRA NTB 84-48, NAGRA, Baden, Switzerland (in press).

Schweingruber M.R. (1983). "Actinide solubility in deep groundwaters. Estimates for upper limits based on chemical equilibrium calculations." NAGRA NTB 83-24, NAGRA, Baden, Switzerland, 1983.

Schweingruber, M.R. (1984a). "Actinide and Tc solubilities in deep crystalline reference water defined for NAGRA project Gewähr." EIR TM-45-84-30, EIR Würenlingen, Switzerland, 1984.

Schweingruber M.R. (1984b). "Technetium solubility in deep groundwaters - estimates for upper limits based on chemical equilibrium calculations." EIR TM-45-84-14, EIR Würenlingen, Switzerland, 1984.

THE ROLE OF URANIUM SERIES DISEQUILIBRIUM STUDIES OF FLUIDS AND SOLIDS IN GEOLOGICAL SYSTEMS WITH POTENTIAL FOR RADIOACTIVE WASTE DISPOSAL (H-C)

M. Ivanovich

Nuclear Physics Division, AERE, Harwell, Oxon., OX11 ORA, UK.

ABSTRACT

Uranium series radionuclides provide one of the most sensitive natural isotopic signatures in groundwater studies and as such have been used successfully to identify water masses and to evaluate quantitatively the mixing of waters on a regional scale. An example of such an application is a recently completed study of a multi-lithological system in the Harwell region. The principal aim of the programme was to establish the groundwater flow patterns using hydro-geological and geochemical methods in association with isotope contents and uranium series disequilibrium and thus provide an independent approach to the study of effective permeabilities of clay lithologies in a sedimentary sequence. The uranium isotopic signatures in groundwater samples collected from the region have been interpreted in terms of the regional groundwater circulation and mixing, and the most significant zones of groundwater movement through clay lithologies have been identified.

A complementary approach is to measure isotopic signatures in various phases of the solid matrix. The presence of radioactive equilibrium amongst various daughter/parent radionuclide pairs of the naturally occurring decay series in various solid phases will indicate lack of geochemical disturbance for hundreds of thousands of years. Alternatively, the existence of radioactive disequilibrium will indicate not only the disturbance to the system but, in some instances, the magnitude of the departure from the radioactive equilibrium for a given daughter/parent pair may give an estimate of the time since the disturbance occurred and its nature. This latter approach is illustrated by a recent study of the distribution of the longer-lived radionuclides ^{238}U, ^{234}U, ^{230}Th, ^{232}Th and ^{228}Th between the pore water, iron oxyhydroxides and clay mineral phases in a thick surface deposit at Elstow, England. Such data are useful in studying the nature of retention mechanisms of uranium series radionuclides in a given geological formation and by inference their geochemical analogues such as plutonium and neptunium.

INTRODUCTION

The disposal of radioactive wastes in geological formations relies on what is known as the multi-barrier concept. The main processes involved are (1) migration of waste radionuclides by diffusion from the near-field barriers to the repository host rock and hence its groundwater, (2) leaching of waste forms by groundwater once exposed by canister corrosion, (3) migration by groundwater transport, and (4) retardation by interaction with the host rock. The principal mechanism by which radioactive waste components can be returned to man's environment is by circulating groundwaters. Thus, it is useful to develop techniques capable of delineating water bodies on a regional scale by their geochemical and isotopic signatures in order to establish their flow rates and mixing patterns. An example of this approach is a study of uranium series radionuclides in the Harwell regional groundwater system given in this paper.

Furthermore, the suitability of a given site for radioactive waste disposal cannot be established reliably in the absence of realistic data relevant to the predictive models designed for a safety assessment. Many parameters characteristic of a given geological formation such as permeability, porosity etc. can be measured directly in the field or from field specimens. However, many others such as sorption parameters for a given geological formation and for different nuclides have not been measured hitherto directly, and there is a need to design methods for direct measurement of sorption parameters such as retardation factors etc. The second case study described here concerns a study of the distribution of the longer-lived radionuclides from the uranium and thorium radioactive decay series, ^{238}U, ^{234}U, ^{230}Th, ^{232}Th and ^{228}Th between the pore water and different mineralogical phases in a thick near surface clay deposit at Elstow, England. It is shown that the uranium series disequilibrium data presented here could be useful in evaluating the nature of uranium and thorium radionuclide retention mechanisms in clay and by inference their geochemical analogues such as plutonium, neptunium etc.

CASE STUDY 1: STUDY OF THE GROUNDWATER REGIME IN THE HARWELL REGION

The existence of one or more groundwater flow cells and the interaction between both local and regional groundwater flow systems will determine the overall groundwater circulation pattern in a given region. A combination of hydraulic, geochemical and isotopic data may provide sufficient information about the geochemical history and flow rates of regional groundwaters. Therefore, the knowledge of these parameters is crucial to any safety assessment of potential

sites for radioactive waste disposal.

The regional groundwater system incorporating argillaceous formations beneath the Harwell site has been studied as part of a national research programme of investigation into the feasibility of disposal of low and intermediate radioactive wastes into argillaceous rocks. The principal aim of the programme is to establish the groundwater flow and mixing patterns using hydrogeological and geochemical methods (Alexander, 1984) in association with isotopic contents and uranium series disequilibrium and thus provide an independent approach to the study of effective permeabilities of clay lithologies in a sedimentary sequence. The principle behind this approach is based on the interpretation of the expected differences in hydrochemistry, isotopic content and uranium series disequilibrium at different depths and locations between the deep groundwaters which entered the system many thousands of years before at considerable distances from the Harwell site, and the shallow more recent waters. Any significant differences can then be assessed in terms of subsequent circulation and mixing patterns.

The local hydrogeology of the Harwell site, the regional groundwater flow system and the interpretation of uranium series disequilibrium signatures in terms of the regional groundwater circulation and mixing patterns have been considered in separate reports (Alexander and Holmes (1983), Alexander (1983), and Ivanovich and Alexander (1985), respectively). The studied area is shown in Figure 1. It consists of the north-western parts of the river Thames basin and comprises predominantly Cretaceous and Jurassic strata.

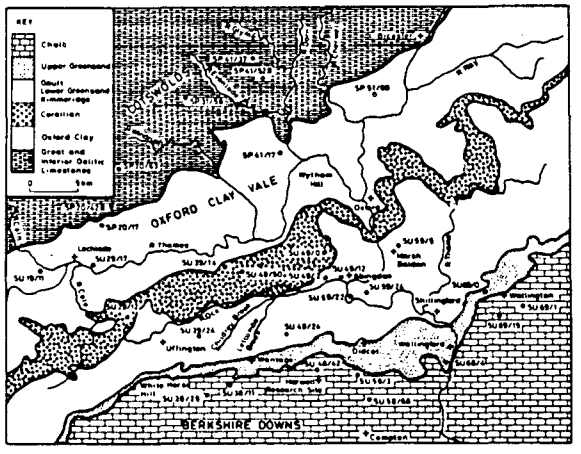

Figure 1. Geology of the Harwell Region and hydrochemical, isotope and uranium series sampling sites.

A synthesis of currently available hydraulic information for the Harwell region (Alexander, 1983), demonstrates that the groundwater movement in the Chalk, Greensands, Corallian and Great Oolite group formations takes place predominantly in the horizontal direction. A smaller proportion of vertical flow takes place between adjacent formations in the region. However, vertical groundwater movement through the intervening clay lithologies is the predominant direction of movement in the low permeability formations.

Hydrochemical results show that salinity increases in the down-dip direction in both the Corallian and Great Oolite formations. This trend suggests groundwater components of progressively greater 'age' at down-dip locations (Schwartz et al, 1981) and is also reflected in both environmental isotopes and inert gas data from both the Corallian and Great Oolite formations in the area (Alexander and Andrews, 1985).

Thirty four groundwater samples derived from the high permeability formations in the Harwell region have been analysed for uranium and thorium content and $^{234}U/^{238}U$, $^{230}Th/^{232}Th$ activity ratios. The locations of all sampling points are shown in Figure 1. Radiometric data are summarized in Table 1; ranges of measured values are given for confined and unconfined groundwater in each formation.

Table 1: Summary of the radiometric data

Type of water	Content ($\mu g\ kg^{-1}$) U	Th	Activity Ratios $^{234}U/^{238}U$	$^{230}Th/^{234}U$	$^{230}Th/^{232}Th$
G.Oolite (Unconfined)	0.41-0.47	0.002-0.02	1.04-1.22	0.19-0.23	4.4-1000
G.Oolite (Confined)	0.002-0.38	0.002-0.02	1.19-18.0	0.01-1.54	3.7-22.5
L.Oolite	0.04	0.1	8.51	0.33	18.3
Corallian (Unconfined)	0.12-0.34	0.0-0.02	1.35-2.75	0.05-0.18	1.3-1000
Corallian (Confined)	0.01-0.10	0.003-0.02	1.50-10.46	0.02-1.73	1.0-10.0
Chalk (Unconfined)	0.16-0.41	0.0-0.001	1.75-2.70	0.01-0.05	5.7-1000
U.Greensand (Unconfined)	0.81	0.02	1.40	0.07	5.2
U.Greensand (Confined)	0.01-0.48	0.002-0.08	1.69-3.26	0.02-0.54	2.3-9.5
L.Greensand	0.29	0.02	1.64	0.21	5.3

Characteristic uranium isotopic signatures delineate these groundwaters not only according to formation but also within each lithology; unconfined groundwaters are clearly differentiated from the confined groundwaters particularly in the Corallian and Great Oolite formations by having higher uranium content. However, the pattern is not so clear for the Chalk and Greensand lithologies. These formations are in hydraulic continuity with each other and in the Harwell region the Chalk is unconfined. Uranium contents in the unconfined waters are generally an order of magnitude higher than in the confined groundwaters in each of three high permeability formations. Similarly, the $^{234}U/^{238}U$ activity ratios in the unconfined groundwaters are in the range 1 to 3 whereas the confined groundwaters' activity ratios

Table 2: Definition and identification of old and young end-members in each of the high permeability formations.

High permeability formation	Sample	[U] content (dpm kg^{-1})	[^{234}U excess] (dpm kg^{-1})	$^{234}U/^{238}U$ Activity ratio	^{14}C (pmc)	^{3}H (T.R.)***	Cl^- (mg l^{-1})	End-member type
Great Oolite	SU19/11	0.05	0.42	9.31	0.8	2.4	380	old
	SP20/63	0.38	0.07	1.19	91.0	59.2	15	young
Corallian	HW5/20 or SU49/24	0.02	0.19	10.46	3.2	1.5	7,500	old
		0.04	0.14	4.60	1.3	4.2	770	old*
	SU49/0 or SU39/14 or SU49/50	0.34	0.12	1.35	85.0	7.2	22	young
		0.12	0.21	2.75	—	34.4	38	young**
		0.16	0.06	1.37	—	38.7	26	young
U.Greensand	SU68/4	0.01	0.02	3.26	—	4.0	16	old
	SU69/0	0.81	0.32	1.40	—	42.0	26	young

* SU49/24 sample is itself most likely a mixture of an old end-member represented by HW5/20 and a younger member such as SU49/0 or SU49/50.

** SU39/14 sample has an uncharacteristically high $^{234}U/^{238}U$ activity ratio for a young end-member and is most likely a mixture of an older water possibly from the Great Oolite below and the true young end-member for the sequence such as SU49/0 and SU49/50.

*** T.R. = Tritium Ratio: one ^{3}H atom to 10^{18} ^{1}H atoms (previously denoted T.U. = Tritium Unit).

are higher and increase in the down-dip direction in the Great Oolite and Corallian. The observed delineation of the groundwaters in terms of their uranium isotopic signatures within individual strata suggest different geochemical histories in different lithologies of the Harwell regional system. This, in turn, suggests a combination of longer residence times necessary to develop such rock controlled characteristics and different mixing patterns of end-member groundwaters in each formation.

Considerations of mixing groundwaters in each formation have led to identification of young and old end-members in each formation. These are listed in Table 2 and were identified by considering uranium content, $^{234}U/^{238}U$ activity ratios, and hydraulic, hydrochemical and isotope data available. Mixing equations of the following form were used (Osmond and Cowart, 1976)

$$[U]_M = [U]_o f_1 + [U]_y f_2 \quad (1)$$

$$[X]_M = [X]_o f_1 + [X]_y f_2 \quad (2)$$

where $[U]_M$, $[U]_o$ and $[U]_y$ are uranium concentrations in the mixed, old and young end-member waters, respectively; $[X]_M$, $[X]_o$ and $[X]_y$ are ^{234}U excess relative to its parent ^{238}U defined as $(^{234}U/^{238}U - 1)$ [U] in the three waters, respectively; and f_1 and f_2 are volume fractions ($f_1 + f_2 = 1$), old end-member to mixed water and young end-member to mixed water, respectively.

Mixing considerations in the case of groundwaters from the Great Oolite and the Upper Greensand have led to the conclusion that most of the intermediate groundwaters' isotopic signatures can be explained in terms of mixing between the young and old end-member waters within and across each formation. In the case of the Corallian groundwaters the uranium isotopic data indicate mixing with groundwaters deriving from sources outside the formation through clay lithologies above and below. Due to the nature of the multi-component mixing system relative mixing proportions derived from the uranium model (in conjunction with values calculated using chloride concentrations) are at best indicative of the scale of cross-formational flow in the region.

The uranium data have been useful in highlighting groundwater samples which yielded anomalous signature explicable in terms of contamination and local geological variations. Some anomalies in the regional system have been more difficult to explain mainly due to the lack of understanding of the geochemical controls and their influence on the uranium series disequilibrium.

In summary, the most significant zones of groundwater mixing determined from uranium isotopic data, and in agreement with hydrochemical considerations, are situated just beneath the edge of the confining strata (see Fig. 2). This is

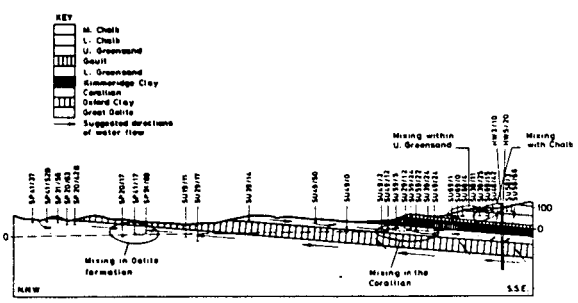

Figure 2. Groundwater movement in the Harwell Region and mixing patterns.

particularly true for the Great Oolite and the Corallian formations and coincides with the locations of hydraulic lows in both of these formations towards which the regional groundwaters move. Thus, mixing patterns established by uranium isotopic measurements are in general consistent with the conclusions derived independently from hydraulic, hydrochemical and other isotopic studies. From the work reported here it is concluded that the uranium isotopic signatures can be used to identify water masses and evaluate the mixing of waters in a sedimentary sequence of lithologies on a regional scale thus effectively supplementing hydrogeological, hydrochemical and isotope methods.

CASE STUDY 2: STUDY OF URANIUM SERIES RADIONUCLIDES IN ELSTOW CLAY

The aim of this pilot project was to study the distribution of the longer-lived radionuclides from the uranium and thorium decay series between different phases in Elstow Clay. Thus, partition of uranium and thorium isotopes between the pore water, amorphous and crystalline iron oxy-hydroxides and clay minerals was studied by direct isotopic measurements carried out on each of the four separated phases. Such data should be useful in evaluating the nature of retention mechanisms in Clay.

The clay samples have been analysed for ^{238}U, ^{234}U, ^{230}Th, ^{232}Th and ^{228}Th. The results are distinguished by their uniformity. Thus, the average uranium content is 1.8 ppm, the average $^{234}U/^{238}U$ activity ratio is within 2σ of unity, and the ^{230}Th radionuclide is deficient relative to its parent ^{234}U by approximately 15% indicating slight uranium accumulation is taking place. Similarly, one of the striking features of the results obtained from the separated phases is their general uniformity both with depth in each core and from core to core. Thus, the clay content of each sample is about 70%, the pore water content between 20 and 30% and the iron oxyhydroxide component 1 to 10%. Radionuclide distribution in different phases of each sample analysed show similar trends. Generally, pore water contains only fractions of one percent of most radionuclides measured. The amorphous and crystalline iron oxyhydroxide phases contain collectively between 25 and 35% of total ^{238}U in each sample; about 35% of total ^{234}U; between 25 and 35% of ^{230}Th; about 35% of total ^{232}Th; and between 15 and 30% of total ^{228}Th. Uniformity in the $^{234}U/^{238}U$, $^{230}Th/^{234}U$ and $^{228}Th/^{232}Th$ activity ratios is also found in different phases and their weighted means and associated errors together with those for uranium and thorium content are given in Table 3.

The amorphous iron oxyhydroxide phase contains an excess of ^{234}U daughter relative to ^{238}U parent (see Table 3); the observed deficiency of ^{230}Th in the amorphous phase has been interpreted to reflect its much lower solubility than that of ^{234}U particularly because the isotopic inventory of that phase is thought to be derived on a shorter time-scale predominantly from the fluid phase with which it is in chemical equilibrium. The magnitude of $^{230}Th/^{234}U$ activity

Table 3: Weighted means of U and Th content and their isotopic activity ratios in total samples and the four seperated phases of Elstow Clay

Phase	U content (dpmg^{-1})	Th content (dpmg^{-1})	$^{234}U/^{238}U$	$^{230}Th/^{234}U$	$^{228}Th/^{232}Th$
Total sample	1.32 ±0.02*	1.68 ±0.02	1.03 ±0.02	0.85 ±0.02	1.72 ±0.04
Amorphous Fe oxyhydroxide	3.73 ±0.45	6.86 ±0.11	1.48 ±0.11	0.66 ±0.05	1.12 ±0.06
Crystalline Fe oxyhydroxide	2.43 ±0.44	9.33	1.01 ±0.13	0.88 ±0.12	0.65 ±0.05
Clay minerals	1.24 ±0.02	1.12 ±0.11	0.91 ±0.03	0.87 ±0.06	1.87 ±0.24
Pore water	(1.8 ±0.8)$\times 10^{-3}$	(0.010 ±0.001)$\times 10^{-3}$	2.6 ±1.1	1.7 ±0.3	1.00** ±0.14

* All errors based on 1σ uncertainties due to nuclear counting statistics only

** Based on only one measurement.

ratio in the amorphous phase is interpreted as the result of recoil flux from the other two solid phases. Similarly, the slight excess of ^{228}Th relative to its grandparent ^{232}Th in the amorphous phase is ascribed to the same cause.

In the crystalline iron oxyhydroxide phase the longer-lived daughter nuclides ^{234}U and ^{230}Th are both in radioactive equilibrium with their respective parents (see Table 3). This feature is consistent with the suggestion that the crystalline iron hydroxide phase is effectively buffered from direct contact with pore water by the amorphous phase, and as it enjoys stable geochemical conditions, the radionuclides resident in this phase grow into radioactive equilibrium in the presence of balanced fluxes of recoil losses and gains to and from the neighbouring solid phases.

In contrast, the deficiency of ^{234}U relative to ^{238}U and that of ^{230}Th relative to ^{234}U in the clay mineral phase are interpreted to be a result of the clay phase being a net supplier of ^{234}U and ^{230}Th recoils to the other phases present in the system.

The apparent radionuclide distribution in the four phases of the Elstow Clay geochemical system provides evidence that amorphous iron oxyhydroxide is the phase primarily involved in the sorption of metal ions from groundwater solution. The data also provide evidence that a substantial proportion of uranium and thorium is associated with secondary crystalline iron phase. Since it appears that the amorphous and crystalline iron oxyhydroxides do exchange, and that the former acts as a buffer for the latter from direct interaction with groundwater, at least over time-scales commensurate with the ^{230}Th half-life, a mechanism exists for the long-term retardation of radio-nuclide transport in clay systems. These findings are in excellent agreement with the observations made in the weathered shists containing uranium deposits of the Alligator Rivers region of Australia (Airey et al, 1983). A model proposed to describe the above findings

should be validated with an extended data set including the existing sets.

SUMMARY AND CONCLUSIONS

The purpose of this paper was to illustrate the application of the uranium series disequilibrium concept to two aspects of radionuclide migration studies. This has been achieved by describing two case studies. The first of these concerns the regional groundwater system incorporating argillaceous formations beneath the Harwell site investigated as part of a national research programme of investigation into the feasibility of disposal of low and intermediate radioactive wastes into argillaceous rocks. The principal aim of the programme is to establish the groundwater flow patterns using hydrogeological and geochemical methods in association with isotope contents and uranium series disequilibrium and thus provide an independent approach to the study of effective permeabilities of clay lithologies in a sedimentary sequence. Thirty four groundwater samples derived from the high permeability formations in the Harwell region have been analysed for uranium and thorium content and $^{234}U/^{238}U$, $^{230}Th/^{234}U$ and $^{230}Th/^{232}Th$ activity ratios. The uranium isotopic signatures have been interpreted in terms of the regional groundwater circulation and mixing patterns. The most significant zones of groundwater mixing determined from uranium isotopic data are situated just beneath the edge of the confined strata. These zones coincide with the locations of hydraulic lows in the Great Oolite and the Corallian formations towards which the regional groundwaters move. The work reported here concludes that the uranium isotopic signatures can be used to identify water masses and to evaluate mixing of groundwaters in a sedimentary sequence on a regional scale thus effectively supplementing hydrogeological, hydrochemical and isotopic methods.

The second case study concerns a study of the distribution of ^{238}U, ^{234}U, ^{230}Th, ^{232}Th and ^{228}Th between the pore water and the three solid phases of Elstow Clay, amorphous and crystalline iron oxyhydroxides and clay minerals. It has been demonstrated that direct measurement of uranium and thorium isotopic concentrations in small (10 cm^3) volume samples of squeezed pore water is feasible yielding uranium concentrations of the order of 2 ppb. The observed isotopic signatures lead to the conclusion that the amorphous iron oxyhydroxide phase is in chemical equilibrium with pore water from which it derives most of its uranium and thorium. Quite different signatures observed in the crystalline iron phase (both $^{234}U/^{238}U$ and $^{230}Th/^{234}U$ activity ratios are statistically indistinguishable from unity) suggest that this iron phase is effectively buffered by the amorphous phase from direct interaction with the fluid. Isotopic deficiencies and excesses relative to their respective parent radionuclides observed in the three solid phases in Elstow Clay indicate that the alpha recoil mechanism is one of the significant processes controlling the distribution of the daughter radionuclides in this geochemical system. By inference, the observed disequilibrium pattern confirms that the mineralogical assemblage in Elstow Clay must have remained stable for a period of time commensurate with the ^{230}Th half-life ($t_{\frac{1}{2}}$ = 75,200 years) at least. Thus, it is inferred that a mechanism exists for the long-term retardation of radionuclide transport in clay systems.

ACKNOWLEDGEMENTS

The author wishes to thank Mr. M. A. Wilkins, AERE, Harwell who carried out all the analytical work referred to in this paper. He also wishes to acknowledge the collaboration with Dr. Jean Alexander of FPRG of the British Geological Survey who directed the field work in the Harwell region and who collaborated in preparing the AERE Report R-11688 which forms the basis for the summary given in the case study 1. Thanks are also due to Mr. Mark Brightman, BGS for his assistance with the high pressure rig for squeezing pore water from clay samples and for supplying the hydrochemical data for some of the extracted pore water samples. The author is also indebted to Drs. E. W. Lees, AERE, Harwell and A. H. Bath, BGS for fruitful discussions of various aspects of the work presented in this paper. The work described in Case Study 2 was funded by NIREX. Finally, the author is indebted to Mrs. Pam Pullen for producing this excellent copy.

REFERENCES

Airey, P. L. et al. (1983). "Radionuclide migration around uranium ore bodies - analogue of radioactive waste repositories", Quarterly Report No. 9 to USNRC (contract NRC-04-81-172). Oct. to Dec. 1983.

Alexander, J. (1983). "Groundwater regime of the Harwell region", Rep. Inst. Geol. Sci., FLPU 83-10.

Alexander, J. (1984). "Hydrochemistry of the groundwater flow systems in the Harwell region", Rep. Brit. Geol. Surv. FLPU 84-6.

Alexander, J. and Andrews, J. N. (1985). "Hydrological investigations in the Harwell Region: The use of environmental isotopes, inert gas contents, and the uranium decay series", Rep. Brit. Geol. Surv. FLPU 84-7. (In preparation)

Alexander, J. and Holmes, D. C. (1983). "The local groundwater regime at the Harwell research site", Rep. Inst. Geol. Sci. FLPU 83-1.

Ivanovich, M. and Alexander, J. (1985). "Uranium series disequilibrium: application to studies of the groundwater regime of the Harwell region", AERE Harwell Report R-11688.

Osmond, J. K. and Cowart, J. B. (1976). "The theory and uses of natural uranium isotopic variations in hydrology", Atomic Energy Rev., 144, 621-679.

Schwartz, F. W., Muehlenbachs, K., Chorley, D. W. (1980). "Flow system control of the chemical evolution of groundwaters", J. Hydrology, 54, 225-243.

Electrolyte Diffusion in Compacted Montmorillonite Engineered Barriers.

F. M. Jahnke and C. J. Radke

Chemical Engineering Department
University of California
Berkeley, CA 94720

Abstract

The bentonite-based engineered barrier or packing is a proposed component of several designs conceived to dispose of high-level nuclear waste in geologic repositories. Once radionulcides escape the waste package, they must first diffuse through the highly impermeable clay-rich barrier before they reach the host repository. To determine the effectiveness of the packing as a sorption barrier in the transient release period and as a mass-transfer barrier in the steady release period over the geologic time scales involved in nuclear waste disposal, a fundamental understanding of the diffusion of electrolytes in compacted clays is required. We present, and compare with laboratory data, a model quantifying the diffusion rates of cationic cesium and uncharged tritium in compacted montmorillonite clay. Neutral tritium characterizes the geometry (i.e., tortuosity) of the particulate gel. After accounting for cation exchange, we find that surface diffusion is the dominant mechanism of cation transport, with an approximate surface diffusion coefficient of 2×10^{-6} cm^2/s for cesium. This value increases slightly with increasing background ionic strength.

The implications of this work for the packing as a migration barrier are twofold. During the transient release period, K_d values are of little importance in retarding ion migration. This is because sorption also gives rise to a surface diffusion path, and it is surface diffusion which controls the diffusion rate of highly sorbing cations in compacted montmorillonite. During the steady release period, the presence of surface diffusion leads to a flux through the packing which is greatly enhanced. In either case, if surface diffusion is neglected, the appropriate diffusion coefficient of ions in compacted packing will be in considerable error relative to current design recommendations.

Introduction

High-level nuclear wastes will be stored in underground repositories. To aid the host formation in protecting the biosphere from the harmful, long-lived radioisotopes contained in the waste package, use of an engineered barrier or packing is being considered [6]. This barrier, based upon the clay mineral montmorillonite, is envisaged as an impermeable barrier surrounding the waste canisters which retards the migration of ions in the transient release period due to its high cation exchange capacity [3] and low hydraulic permeability [7]. As time passes and steady-state diffusion through the packing is established, it further serves as a mass-transfer resistance retarding the escape of ions from the canister to the fluid percolating around the waste package. To determine the steady-state plume of radionuclides eminating from the waste repository in the steady-state period and the protection an engineered barrier affords the waste disposal scheme in the transient release period, the diffusion rate of ions in compacted montmorillonite clay must be determined.

In this paper we summarize our findings on the diffusion of cesium chloride and tritium in compacted sodium-montmorillonite clays. Cesium is a representative radioisotope present in the waste form which is particularly toxic for the first few thousand years after the waste is stored. Tritium is used to characterize the geometric structure or tortousity of the swollen clay gel. Our approach is to determine independently the physico-chemical properties which parameterize the diffusion process within compacted packing, and then to compare experimental data with physically-based diffusion models. Only then is it possible to extrapolate with confidence laboratory data to the geologic time scales of nuclear waste disposal.

Theoretical

We visualize the diffusion process as follows. The local ion flux, N_x, is comprised of two parts, one due to pore diffusion and the other due to surface diffusion. These fluxes are additive, so

$$N_x = N_x^{\infty} + N_x^{\sigma} . \qquad (1)$$

If the concentration of the diffusing ion is small relative to the background electrolyte concentration, the pore fluid and clay surface are in local equilibrium, and all ions are sorbed in the Stern layer, then each flux is described by Fick's first law. Thus,

$$N_x^{\infty} = -\frac{D_{\infty}}{\tau^2}\frac{\partial c}{\partial x} \qquad (2)$$

and

$$N_x^{\sigma} = -\frac{1-\epsilon}{\epsilon}\frac{D_s}{\tau_s^2}\frac{\partial n}{\partial x} . \qquad (3)$$

Here, ϵ is the porosity of the clay gel, D_{∞} and D_s are the molecular and surface diffusion coefficients, respectively, and n is the adsorption on the clay surface. τ^2 and τ_s^2 are the tortuosity of the pore and the surface paths. D_s has units identical to a bulk diffusion coefficient (cm^2/s), and n has units of a concentration (moles/solution volume). Invoking local equilibrium, we have

$$\frac{\partial n}{\partial x} = \frac{dn}{dc}\frac{\partial c}{\partial x} ,$$

where $\frac{dn}{dc}$ is the slope of the equilibrium ion-exchange isotherm. If we further assume that the pore and surface paths are identical, $\tau^2 = \tau_s^2$. Hence, by inserting the flux expressions (2) and (3) into Equation (1), we find

$$N_x = -D\frac{\partial c}{\partial x} , \qquad (4)$$

where

$$D = \frac{D_{\infty}}{\tau^2}\left[1+\frac{1-\epsilon}{\epsilon}\frac{dn}{dc}\frac{D_s}{D_{\infty}}\right] . \qquad (5)$$

For surface diffusion to be significant, we must have the far right term in the brackets of Equation (5) be of order unity, or

$$\frac{1-\epsilon}{\epsilon}\frac{dn}{dc}\frac{D_s}{D_{\infty}} = O(1) .$$

In the Henry's law region of the isotherm, the slope $\frac{dn}{dc}$ is typically large for cations contained in the waste package [10]. The validity of the assumptions listed above for ions and conditions expected in a nuclear waste repository is good. For details refer to Jahnke [4].

To relate the local flux to macroscopically measurable quantities, we write the mass balance as

$$\frac{\partial c}{\partial t}+\frac{1-\epsilon}{\epsilon}\frac{\partial n}{\partial t} =$$

$$\left[1+\frac{1-\epsilon}{\epsilon}\frac{dn}{dc}\right]\frac{\partial c}{\partial t} = -\frac{\partial N_x}{\partial x} . \qquad (6)$$

Here we have made the additional assumption that the gel is homogeneous and hence that diffusion is one-dimensional. That is, all structural information relevent to axial ion diffusion is contained in the tortuosity, which does not vary spacially in a macroscopic sense. Thus, inserting Equation (4) into Equation (6), we obtain Fick's second law of diffusion,

$$\frac{\partial c}{\partial t} = D_e\frac{\partial^2 c}{\partial x^2} . \qquad (7)$$

This defines the effective diffusion coefficient D_e of ions in the swollen clay gel as

$$D_e = \frac{D_{\infty}}{\tau^2}\left[\frac{1+\frac{1-\epsilon}{\epsilon}K_d\rho_s\frac{D_s}{D_{\infty}}}{1+\frac{1-\epsilon}{\epsilon}K_d\rho_s}\right] \equiv \frac{D}{\alpha} \qquad (8)$$

where we have replaced $\frac{dn}{dc}$ by the Henry's law slope, $K_d\rho_s$. K_d is the distribution coefficient used commonly in the nuclear waste disposal field [6], and ρ_s is the density of the clay. We further separate D_e into its components: D, from Equation (5) and α ($= 1+\frac{1-\epsilon}{\epsilon}K_d\rho_s$), the retardation coefficient [6] from the Equation (6). We see that ion adsorption on the clay surface, in the absence of surface diffusion, reduces the effective diffusion coefficient from its molecular value. Indeed, this is a primary motivation for the bentonite-based, engineered-barrier concept. If the surface diffusion coefficient is nonzero, the effective diffusion coefficient increases. We will return to this point below.

To determine if Equation (3) describes correctly the diffusion of ions in compacted clays, we must determine:

1. the ion-exchange isotherm,
2. the molecular diffusion coefficient,
3. the tortuosity of the medium, and
4. the surface diffusion coefficient.

The experimental determination of these parameters is described in the following section.

Experimental

Soudek [11] has measured the adsorption isotherm of uni- and divalent cations on disaggregated sodium montmorillonite clay in batch experiments. K_d values for cesium and strontium as a function of ionic strength are shown in Table 1 below. Observe that K_d varies by about one order of magnitude for each order of magnitude change in the background ionic strength.

Table 1: Measured K_d values for cesium and strontium on sodium montmorillonite at 22° C [11]. K_d in cm^3/g.

Ion	Background NaCl (M)		
	10^{-3}	10^{-2}	10^{-1}
Cs	6700	850	150
Sr	1.8×10^5	1.9×10^4	380

The ion-exchange equilibria were interpreted using an extension of the site-binding model of Davies, James and Leckie [1]. This model predicted correctly the effect of ionic strength on ion sorption, as well as multi-ion sorption. It shows further that the majority of the adsorbed cations are found in the Stern layer, as we assumed above.

The molecular diffusion coefficient was obtained by converting the limiting ionic mobility of cesium to a diffusion coefficient, using values from Robinson and Stokes [9]. We find $D_\infty=2\times10^{-5}$ cm^2/s. The tortuosity and dynamic concentration determinations were measured using a radially perfused diffusion cell developed in this laboratory. It is described here briefly; the interested reader is referred to Jahnke and Radke [5] for details.

The configuration of the diffusion cell is shown in Figure 1 (all figures are at the end of the paper). The clay gel G, initially devoid of solute, is confined below by a piston P and above by N, a Nuclepore membrane with pore size sufficiently small to confine the individual clay particles. The fragile Nuclepore membrane is supported by a sintered metal disk SD, which is in turn confined by the top of the apparatus. The ion whose diffusion behavior is being studied is initially contained in a well-stirred solute chamber, which is not shown in the figure. At $t=0$ the fluid is pumped from the solute chamber through the sintered metal disk and returned. As liquid flows through the sintered disk, ions diffuse from the convecting liquid through the Nuclepore membrane and into the clay gel. Special care is taken to assure that the mass transfer coefficient of the cell is sufficiently high that the diffusion data measured are not obfuscated by artifacts of the experimental design [5].

As the experiment proceeds, ions deplete from the solute chamber and a concentration profile develops in the gel. The solute chamber is sampled intermittantly to determine its concentration history. At the conclusion of an experiment, the diffusion cell is disassembled, and the gel is incrementally extruded, sectioned, and analyzed to determine the final concentration profile in the gel. It can be shown [4] that the effects of diffusion and sorption within the clay gel are decoupled by this experimental

procedure. This allows us to determine D and α uniquely, since we have equations describing the tank depletion and the gel profile, and two unknowns, D and α.

Since the tortuosity is governed by the geometry of the clay particles at a given compaction, we choose to measure τ^2 in the diffusion cell. To eliminate the effects of sorption (and hence surface diffusion), we measure the diffusion of neutral tritium [8]. Any deviation from its molecular diffusion coefficient is then due to the tortuosity of the clay gel. For a 16 w/o gel, we find the tortuosity to be about 4.

The surface diffusion coefficient can not be predicted *a priori*. It must be determined as a parameter fit to "anomolous" or enhanced diffusion or electrical conductivity data [2].

Results and Discussion

Typical experimental results are shown in Figures 2 and 3. Here, cesium is diffusing into a 16 w/o sodium-montmorillonite clay gel with a 10^{-2} M sodium chloride background electrolyte. Figure 2 plots the concentration in the solute chamber as a function of time. Data are indicated by the solid circles. Figure 3 shows the total concentration in the clay gel at the completion of the experiment against nondimensional distance. Data are denoted by the solid steps. Dashed lines in Figures 2 and 3 indicate the *a priori* prediction using the parameters determined above, neglecting surface diffusion. Notice that the uptake and the penetration of ions into the gel is severely underpredicted if surface diffusion is neglected. Solid lines are the best fit to the data. The value of α is predetermined from the measured isotherm and porosity. The best fit of the data gives $D = 2.8\times10^{-4}$ cm^2/s. Using Equation (5), we recover $D_s = 2\times10^{-6}$ cm^2/sec, or $D_s/D_\infty = 0.1$. Also observe that α scales the ordinate of Figure 3. That the data fit well with α predetermined is strong evidence that our physical picture of the diffusion process is correct.

As mentioned above, K_d depends strongly on the background ionic strength. Thus, varying the background ionic strength is a severe test of the surface diffusion model, since both the retardation coefficient α and the diffusion coefficient D change drastically. Figure 4 below shows the ionic strength dependence of the surface diffusion coefficient. Observe that D_s is nearly constant with ionic strength; the slight increase of D_s with ionic strength has been observed by others [2]. This evidence is conclusive: the existence of surface diffusion is real, and for cesium, is the major mode of ion migration in montmorillonite.

We note that in our experiments, the porosity of the clay gels studied is low ($\approx$0.92), and that waste repositories are expected to have much more highly compacted clays [7]. The impact of surface diffusion on the expected performance of a clay-based engineered barrier is discussed in the following section.

Ramifications

In the unsteady release period, the effective diffusion coefficient is given by Equation (7). If we note from Table 1 that at repository conditions, $K_d\rho_s$ values are large (>2000), that the porosity expected in the engineered barrier is about 0.50 [7], and that $\frac{D_s}{D_\infty}$ is typically 0.1 for cations [2], the effective diffusion coefficient takes the form

$$D_e = \frac{D_s}{\tau^2}.$$

No retardation coefficient appears in this expression. By providing a parallel path for cation migration, sorption does not reduce the effective diffusion coefficient within compacted packing much at all. This implies that K_d values are irrelevant during the transient release period. That is, we do not anticipate large reductions in transient ion migration rates due to sorption retardation on montmorillonite. Rather, as an approximation for the diffusion coefficient of ions in compacted packing, we use $\tau^2 = 10$ [8] and we calculate that

$$\frac{D_e}{D_\infty} \approx 10^{-2};$$

a fixed two order of magnitude reduction from the molecular diffusion coefficient.

In the steady release period, the effective cation diffusion D_e in Equation (8) coefficient no longer applies. The effect of packing as a mass-transfer barrier is now governed by the flux depicted in Equation (4). Hence, the packing resistance to migrating cations is proportional to D and not to D_e. Given a gel porosity of 0.5 and a tortuosity of 10, as above, and for highly sorbing cations, we find that

$$D \approx 0.1 K_d \rho_s D_s \,. \qquad (9)$$

Thus, K_d values are of extreme importance during the steady release period. Counter to what may have been anticipated, larger K_d values lead to higher release rates.

In both the unsteady and steady release periods, the deviation in currently predicted repository performance due to cation surface diffusion is identical and towards a diffusion coefficient that is dramatically in excess of accepted estimates. Surface diffusion of cations in a bentonite-based packing reduces its effectiveness. This does not imply that packing is ineffective in the waste disposal scheme. Montmorillonite clay is known to influence the oxidation potential, or Eh, near the canister and aid in radionuclide precipitation. Transport rates of precipitated colloidal material through bentonite should be nil. Smectite clay also can impede ground water imbibition up to the canister. Finally, and most importantly, the hydraulic impermeability of montmorillonite to bulk water flow can extend the integrity of the waste package.

If the surface mobility of cesium and other radionuclides found in the waste package is comparable, we caution that neglect of cation surface diffusion will result in a predicted packing performance which overestimates the actual protection such a barrier affords. As a corollary, we recommend that careful measurements of cation diffusion rates be made under realistic repository environments to assess the quantitative role of surface diffusion.

Acknowledgments: This work was supported by the United States Nuclear Regulatory Commission under interagency agreement DOE-50-80-97 through contract DE-AC03-76-SF00098 to the Lawrence Berkeley Laboratory.

References

1. Davies, J. A., James, R. O., and Leckie, J. O., "Surface Ionization at the Oxide/Water Interface," *J. Coll. Int. Sci.*, vol. 63, no. 3, p. 480, 1978.
2. Gast, R. G., "Applicablilty of Models to Predict Rates of Cation Movement in Clays," *Soil Sci. Soc. Amer. Proc.*, vol. 30, p. 48, 1966.
3. Grim, R. E., *Clay Mineralogy, Second Edition*, McGraw-Hill, New York, 1968.
4. Jahnke, F. M., "The Diffusion of Ion-Exchanging Electrolytes in Compacted Montmorillonite Clays," *Ph.D. Thesis*, University of California, Berkeley, 1986.
5. Jahnke, F. M. and Radke, C. J., "A Radially Perfused Cell for Diffusion in Compacted, Sorbing Systems," *submitted to Chem. Eng. Sci*, 1986.
6. Panel, Waste Isolation Systems, *A Study of the Isolation of Geologic Disposal of Radioactive Wastes*, Nat. Acad. Press, Washington, DC, 1983.
7. Pusch, R., "Highly Compacted Sodium Bentonite for Isolating Rock-Deposited Radioactive Waste," *Nuclear Tech.*, vol. 45, p. 153, 1979.
8. Relyea, J. F., Trott, D. P., McIntyre, C. V., and Rieger, C. G., "Diffusion of Tritium and Chloride in Basalt-Bentonite Mixtures.," RHO-BW-SA-431 P, Rockwell Hanford Operations, Richland, WA, 1985.
9. Robinson, R. A. and Stokes, R. H., *Electrolyte Solutions, Second Edition*, Academic Press, New York, 1959.
10. Serne, R. J., Rai, D., and Relyea, J. F., "Preliminary Results on Comparison of Adsorption-Desorption Methods and Statistical Techniques to Generate K_d Predictor Equations," U.S. DOE Report PNL-SA-7352, 1979.
11. Soudek, A., "Binary and Ternary Ion Exchange on Sodium Montmorillonite for Application to Backfill in Nuclear Waste Disposal," *M.S. Thesis*, University of California, Berkeley, 1984.

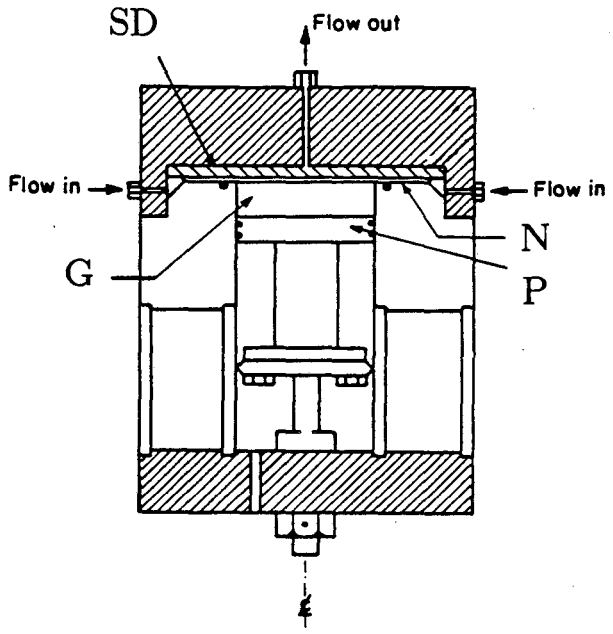

Figure 1: The Diffusion Cell. Captions explained in the text.

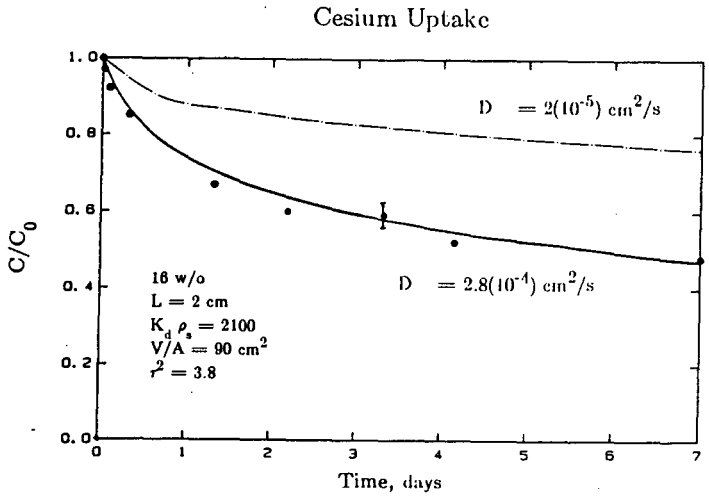

Figure 2: Concentration History of External Tank.

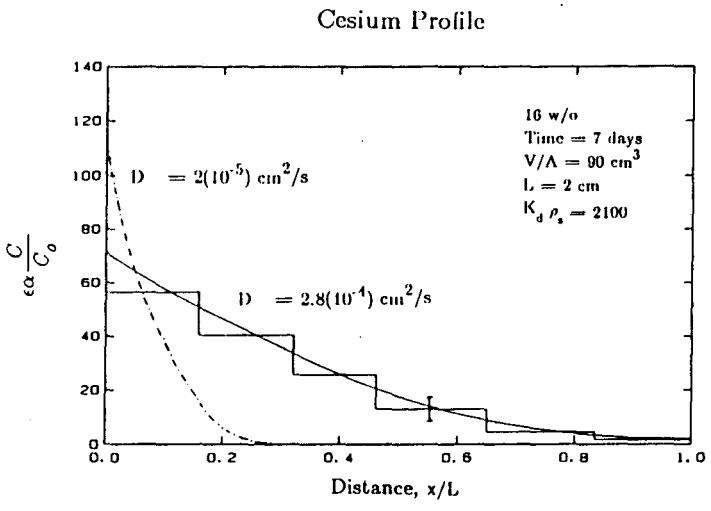

Figure 3: Concentration Profile in Gel at Completion of Experiment.

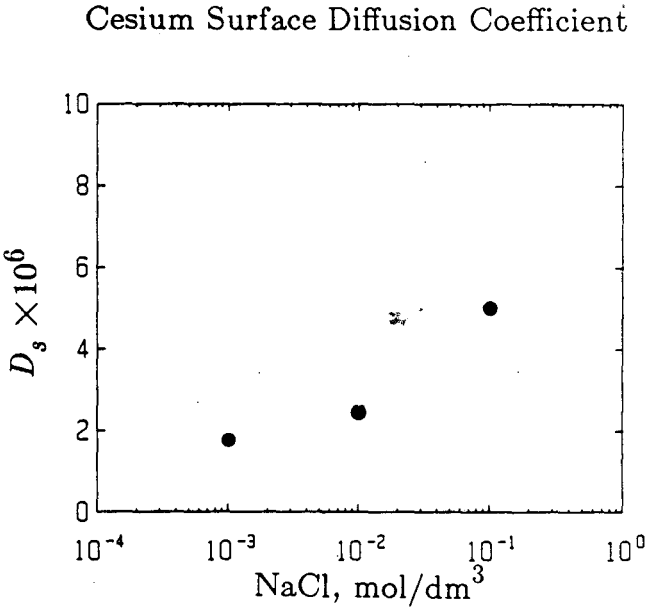

Figure 4: Dependence of Cesium surface Diffusion Coefficient with background electrolyte concentration.

STEADY RADIONUCLIDE RELEASE RATES FROM A BENTONITE-PROTECTED WASTE CANISTER

D.J. Jensen and C.J. Radke

Department of Chemical Engineering
University of California
Berkeley, California 94720

ABSTRACT

A bentonite-based packing or engineered barrier is one ingredient of the multibarrier concept for underground storage of high-level nuclear waste. This paper investigates the possible effectiveness that such a smectite-laden barrier might have in controlling steady, solubility-limited release rates from a cylindrical waste canister.

Darcy's law and the convective-diffusion equation in two dimensions are solved numerically with and without an annulus of packing material. Reduced fractional release rates quantifying the role of the packing are studied over wide ranges of ground water velocities, packing amounts, and packing permeability and effective diffusivity. Release rates are shown to be strongly dependent on the physical properties of the packing, particularly the effective diffusivity.

Although the low permeability of a bentonite-rich packing negates convection next to the canister, calculated release rates of the packing-protected waste canister do not differ dramatically from the those for the unprotected canister, except at high ground water velocities. To afford more protection, consideration must be given to reducing the porosity of the packing material.

INTRODUCTION

Design of high-level nuclear waste repositories in geologic media relies on minimizing the rate at which hazardous radionuclides might be released into the accessible environment. To aid in reducing release rates, it is proposed that a bentonite-based packing or engineered barrier surround each waster canister.

At early times, during the transient regime, the smectite-rich packing inhibits water imbibition thereby delaying the onset of canister corrosion [1]. Also, once the canister is breached, the favorable ion-exchange properties of montmorillonite retard the migration of cations into the host rock [6]. Further discussion of transient cation diffusion in compacted montmorillonite is found in our companion paper [4].

In a mature repository approaching steady conditions, the low hydraulic permeability of montmorillonite prevents convective transport near the canister surface and provides an additional mass-transfer resistance influencing radionuclide release rates. This paper addresses the quantitative calculation of steady, solubility-limited radionuclide release from a bentonite-protected waste package into an isotropic host porous medium. Such a calculation applies only after transient release has subsided. The time necessary to reach steady repository behavior under purely diffusive conditions can be estimated as

$$\varepsilon_m D_m t/\alpha R_o^2 = O(1),$$

where ε_m is the geologic-medium porosity, D_m is the solute diffusion coefficient in the medium, t denotes time, α is the sorption retardation factor [12] (see Equation (8) of reference [4]), and R_o is the canister radius. With $\varepsilon_m = 0.01$, $D_m = 10^{-5}$ cm^2/s, $\alpha = 100$, and $R_o = 15$ cm, this results in a steady state after about 10^4 years. With additional convective transport this time will be considerably shortened [2]. Since repository life times must be orders of magnitude longer, a steady analysis of radionuclide release is useful [3,12].

Relyea and Wood [8] have performed an analysis of packing effectiveness with similar intent to ours. However, because they impose a one-dimensional flow field, steady state is not attained. More importantly, their one-dimensional hydrodynamics requires convective flow in the bentonite packing to be independent of absolute permeability. To relieve these restrictions, we analyze a two-dimensional geometry.

THEORY

Consider a unit length of an infinitely long, cylindrical fuel canister of radius R_o surrounded by packing out to radius R_p. The porosity and permeability of the packing are ε_p and K_p, respectively, while those of the geologic medium are ε_m and K_m. Ground water flows transverse to the isolated canister with a uniform approach superficial velocity designated by U. Fluid continuity, $\nabla \cdot v = 0$, and Darcy's law combine to specify the pressure and velocity fields in the two concentric porous media encompassing the waste rod.

Let r be the radial coordinate measured from the center of the waste cylinder, and let θ be the angular coordinate gauged from the

forward stagnation point. The velocity components in the host rock are then

$$v_{r,m} = -U\left[1 - \frac{(1-\beta)}{(1+\beta)}\left(\frac{r^{-2}}{R_p}\right)\right]\cos\theta, \quad (1)$$

and

$$v_{\theta,m} = U\left[1 + \frac{(1-\beta)}{(1+\beta)}\left(\frac{r^{-2}}{R_p}\right)\right]\sin\theta, \quad (2)$$

where the parameter β is defined by

$$\beta \equiv \left(\frac{K_p}{K_m}\right)\frac{\left[1 - (R_p/R_o)^{-2}\right]}{\left[1 + (R_p/R_o)^{-2}\right]} . \quad (3)$$

Likewise, for the packing we find that

$$v_{r,p} = -U\left(\frac{K_p}{K_m}\right)\left[1 + \frac{(1-\beta)}{(1+\beta)}\right]\frac{\left[1 - (r/R_o)^{-2}\right]}{\left[1 + (R_p/R_o)^{-2}\right]}\cos\theta, \quad (4)$$

and

$$v_{\theta,p} = U\left(\frac{K_p}{K_m}\right)\left[1 + \frac{(1-\beta)}{(1+\beta)}\right]\frac{\left[1 + (r/R_o)^{-2}\right]}{\left[1 + (R_p/R_o)^{-2}\right]}\sin\theta . \quad (5)$$

Note the explicit dependence on the permeability of the packing material. To recover the case of no engineered barrier, one simply replaces R_p in Equations (1) - (3) with R_o.

The absolute permeability the packing is reported to vary from 10^{-8} μm^2 for pure bentonite [9] to 10^{-4} μm^2 for a mixture of bentonite and quartz [10]. A granite permeability of 1 μm^2 [11] then yields a range for the permeability ratio, K_p/K_m, from 10^{-8} to 10^{-4}. Hence, Equations (4) and (5) demand velocities in the packing which are at most four orders of magnitude smaller than the ground water flow. A bentonite-impregnated packing material is very effective in preventing convection immediately adjacent to the canister. This contradicts the one-dimensional treatment where the superficial velocity in the packing is determined erroneously from mass balance to be U [8].

A dilute radionuclide in a supporting background electrolyte solution obeys, at steady state, the convective-diffusion equation:

$$\underset{\sim}{v}_n \cdot \nabla C_n = \varepsilon_n D_n \nabla^2 C_n, \qquad \begin{matrix} n = p \text{ for } & R_o < r < R_p, \\ n = m \text{ for } & r > R_p, \end{matrix} \quad (6)$$

where $\underset{\sim}{v}_n = v_{r,n}\,\underset{\sim}{i}_r + v_{\theta,n}\,\underset{\sim}{i}_\theta$.

Also, $D_n = D_\infty/\tau_n^2$ where D_∞ is the species molecular diffusion coefficient in water and τ_n^2 is the tortuosity of medium n. With this definition of D_n, we have neglected parallel and transverse dispersion. Equations (6) are combined with Equations (1) - (5) and solved subject to the following boundary conditions:

$$C_p(R_o,\theta) = C_s , \quad (7a)$$

$$C_m(R_p,\theta) = C_p(R_p,\theta) , \quad (7b)$$

$$\varepsilon_m D_m \frac{\partial C_m}{\partial r}(R_p,\theta) = \varepsilon_p D_p \frac{\partial C_p}{\partial r}(R_p,\theta) , \quad (7c)$$

$$\frac{\partial C_m}{\partial \theta}(r,0\ \&\ \pi) = \frac{\partial C_p}{\partial \theta}(r,0\ \&\ \pi) = 0 , \quad (7d)$$

$$C_m(\infty,\theta) = 0 . \quad (7e)$$

Restriction to solubility-limited canister dissolution is invoked with Equation (7a). Numerical solution of the linear Equations (6) is by Galerkin finite elements with bilinear basis functions. A critical test applied to assess the accuracy of the numerical procedure was matching of the integrated net radial flux at two arbitrary radial positions.

Following others [3,12] we ascertain the fractional release rate of a radionuclide, f. f is the angular-integrated species flux from the waste-canister surface divided by the amount of that nuclide originally in the canister [3,12]. To evaluate the role of packing, it proves convenient to report the reduced fractional release rate, f_p/f_o, or the ratio of the fractional release rates with and without packing:

$$f_p/f_o = \left(\frac{\varepsilon_p D_p}{\varepsilon_m D_m}\right)\frac{\int_0^\pi \left[\frac{\partial C_p}{\partial r}(R_o,\theta)\right] d\theta}{\int_0^\pi \left[\frac{\partial C_m}{\partial r}(R_o,\theta)\right] d\theta} , \quad (8)$$

where the integral in the denominator is evaluated with no packing present. In this manner we probe the effects of packing independent of any particular dissolving chemical species.

The reduced fractional release rate depends on the Peclet number

$$Pe \equiv UR_o/\varepsilon_m D_m ,$$

and on the effective diffusivity ratio $\varepsilon_p D_p/\varepsilon_m D_m$, the permeability ratio K_p/K_m, and the amount of packing or R_p/R_o. Superficial ground water velocities for candidate geologic media range from 10^{-6} to 0.1 m/yr [5,7]. For R_o = 15 cm, $\varepsilon_m = 0.01$ (i.e., granite [9]), and $D_m = D_\infty/\tau_m^2 = 10^{-5}$ cm^2/s, the Peclet numbers extend from $5(10^{-4})$ to 50. In this work Pe is varied from 10^{-4} to 10^3.

The effect diffusivity in the packing, $\varepsilon_p D_p$, is an important parameter. With compacted bentonite, $\varepsilon_p \sim 0.5$ to 0.75. Knowledge of $D_p = D_\infty/\tau_p^2$ is sparse. Estimates might be from 10^{-7} to 10^{-5} cm^2/s. The latter high value of 10^{-5} cm^2/s appears likely for cations and arises from surface migration [4]. We study the ratio $\varepsilon_p D_p/\varepsilon_m D_m$ from 0.1 to 10. Expected amounts of packing might be from one canister radius, $R_p/R_o = 1$, out to 5 or 6 canister radii.

As indicated earlier, permeabilities in bentonite and bentonite-sand mixtures are extremely small: $10^{-4} > K_p/K_m > 10^{-8}$. For K_p/K_m less than about 10^{-3} we find no influence whatsoever on f_p, independent of the Peclet number. This means that transport through bentonite packing is purely by diffusion [4]. For the calculations presented below, K_p/K_m is set at 10^{-5}.

RESULTS AND DISCUSSION

Figure 1 (all figures are at the end of the paper) gives reduced fractional release rates as a function of Pe for two different amounts of packing. If the packing were to have no influence, f_p/f_o would be unity for all Peclet numbers.

At low Pe ($< 5(10^{-2})$), release from the canister-packing system is by diffusion. Here, f_p/f_o is greater than unity because the diffusive resistance in the packing with $\varepsilon_p = 0.75$ is less than that in the host medium with $\varepsilon_m = 0.01$. At high Pe (> 50), nuclide transport is by diffusion in the packing and convection in the medium. In this large Pe regime, f_p approaches a constant asymptote characteristic of diffusion in the packing while f_o increases as $\sqrt{Pe}$ [2]. Accordingly, in Figure 1, f_p/f_o decreases as $1/\sqrt{Pe}$ in the high Pe range.

At intermediate Peclet numbers, a slight maximum appears. This is because the more porous packing, which in Figure 1 has a lower diffusive resistance than in the geologic medium, feels the onset of convection before the medium does. Hence, f_p rises more quickly with Pe than does f_o.

Figure 1 shows that unless high ground water flows exist in the respository, a packing with $\varepsilon_p D_p / \varepsilon_m D_m = 7.5$ has little benefit in the steady state. Additional packing does not mitigate this conclusion.

Figure 2 investigates the role of the effective diffusivity in the packing on the reduced fractional release rates for $R_p/R_o = 6$. As the effective diffusivity ratio is reduced, fractional release rates from the canister-packing assemblage are diminished significantly. Especially noteworthy is the lowering of the transition Peclet number between convective and diffusive transport. Figure 2 indicates that effort should be directed towards designing packing with $\varepsilon_p D_p$ small. Also, quantitative information on D_p is needed [4].

RAMIFICATIONS

Figures 1 and 2 ascertain that reduction in steady release rates with a bentonite-based packing is not dramatic except at very high Peclet numbers. The reasons are two-fold.

First, the porosity of host medium used in this work is very small: $\varepsilon_m = 0.01$. To design a packing that exhibits a higher diffusive resistance than the host medium requires that ε_p be reduced. This can be accomplished by using large weight fractions of clay in conjunction with a finely divided matrix solid, such as crushed host rock. As long as all voids between the matrix solids are filled with the smectite clay, low permeability can be maintained while also reducing overall porosity [13]. Large grained or porous matrix particles would not be desirable.

Second, comparison of fractional release rates of the canister-packing-medium system to those of the canister-ideal medium system is unrealistic. After drilling, there will be a damaged zone of higher fracture density and porosity around the canister sites and a gap between the fuel canister and the damaged host rock. This gap requires backfilling with some material. Thus, comparison of bentonite-based packing should be made against other types of backfill and not against a uniform host medium that extends directly up to the canister surface.

We note that in our model calculations no account has been made for solute dispersion, for a fractured host medium, or for nonisothermal excursions. Our results hold only for isothermal, homogeneous porous media.

ACKNOWLEDGEMENTS

This work was supported by the United States Nuclear Regulatory Commmission under interagency agreement DOE-50-80-97 through contract DE-AC03-76-SF-00098 to the Lawrence Berkeley Laboratory.

REFERENCES

1. Andersson, G., Rasmuson, A., and Neretnieks, I., "Model for Near Field Migration," Scientific Radioactive Waste Management, Elsevier Science Publishing Co., ed. Werner Lutze, vol. 5, p. 539, 1982.

2. Chambre, P.L., Pigford, T.H., Fujita, A., Kanki, T., Kogayashi, A., Lung, H., Ting, D., Sato, Y., and Zavoshy, S.J., "Analytical Performance Models for Geologic Repositories", Lawrence Berkeley Laboratory, Berkeley, Ca, LBL-14842, vol. 2, 1982.

3. Chambre, P.L., Pigford, T.H., and Zavoshy, S., "High Level Waste Form Characteristics," American Nuclear Society Transactions, vol. 40, no. 67, p. 153, 1982.

4. Jahnke, F.M., Radke, C.J., "Electrolyte Diffusion in Compacted Montmorillonite Engineered Barriers," presented at the International Symposium on Coupled Processes Affecting the Performance of a Nuclear Waste Repository, Lawrence Berkeley Laboratory, University of California, Berkeley, CA, Sept. 18-20, 1985.

5. Neretnieks, I., "Leach Rates of High Level Waste and Spent Fuel-Limiting Rates as Determined by Backfill and Bedrock Conditions," Scientific Basis for Radioactive Waste Management, Elsevier Science Publishing Co., ed. Werner Lutze, vol. 5, p. 559, 1982.

6. Nowak, E.J., "The Backfill as an Engineered Barrier for Nuclear Waste Management," Scientific Basis for Radioactive Waste Management, Elsevier Science Publishing Co., vol. 2, p. 403, 1980.

7. Rasmuson, A., and Neretnieks, I., "Model for Far Field Migration," Scientific Basis for Radioactive Waste Management," Elsevier Science Publishing Co., ed. Werner Lutze, vol. 5, p. 549, 1982.

8. Relyea, J.F., and Wood, M.I., "An Analytical One-Dimensional Model for Predicting Waste Package Performance," BWIP Project, Hanford, WA, SD-BWI-TI-232, 1984.

9. Rolfe, P.F., and Alymore, L.A.G., "Water and Salt Flow Through Compacted Clays: 1. Permeability of Compacted Illite and Montmorillonite," Soil Sci. Soc. Am. J., vol. 41, p. 489, 1977.

10. Seitz, M.G., and Couture, R.A., "Physical Response of Backfill Materials to Mineralogical Changes in a Basalt Environment," NRC, Nuclear Waste Geochemistry, Washington, D.C., NUREG/CP-0052, p. 204, 1983.

11. Vutukuri, U.S., and Lama, R.D., "Handbook on Mechanical Properties of Rocks," Trans. Tech. Publications, vol. 4, 1978.

12. Waste Isolation System Panel, "A Study of the Isolation System for Geologic Disposal of Radioactive Wastes," Nat. Acad. Press, Washington, D.C., 1983.

13. Wheelwright, F.J., "Development of Backfill Material as an Engineered Barrier in the Waste Package System," interim topical report, Pacific Northwest Laboratory, Hanford, WA, PNL-3873, 1981.

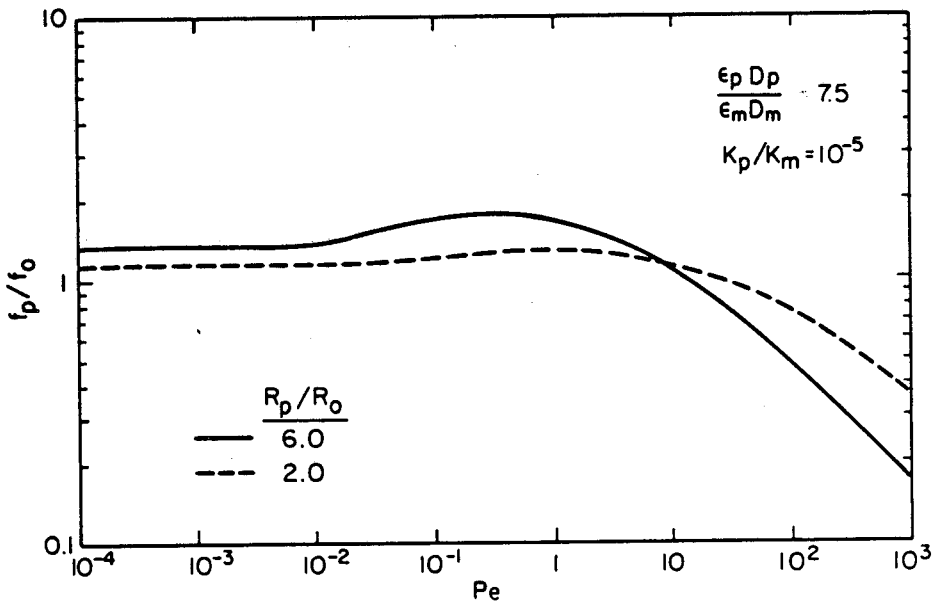

Figure 1. Reduced fractional release rates: effect of packing amount.

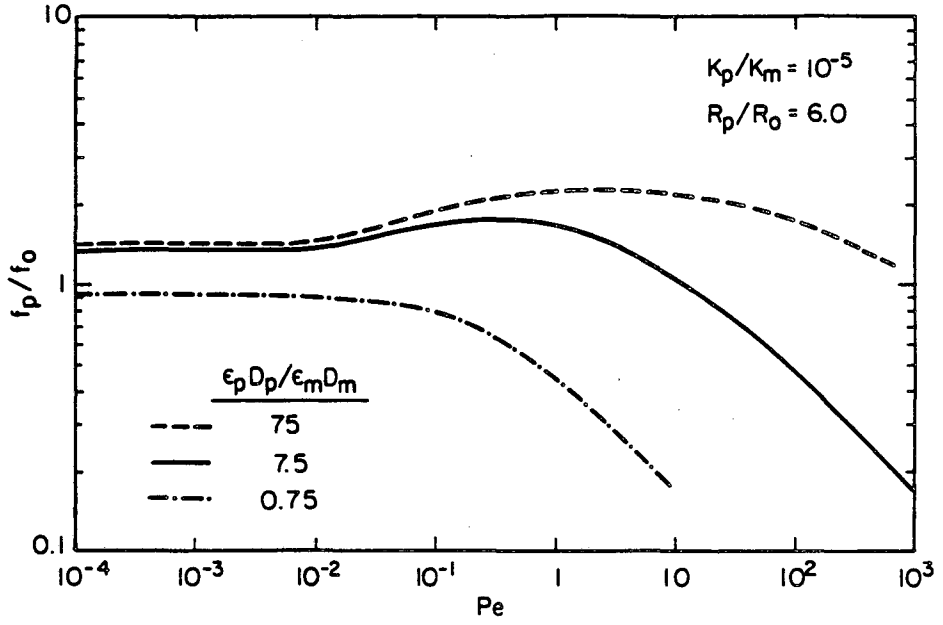

Figure 2. Reduced fractional release rates: effect of packing diffusivity.

PRINCIPLE OF A CODE COMPUTING THE MIGRATION OF IONS WITH PRECIPITATE

J.P. MANGIN
Centre d'Etudes Nucléaires
BP n° 6
92265 FONTENAY-AUX-ROSES Cedex
FRANCE

NGUYEN NGOC HOAN
C.I.S.I.
91191 GIF-SUR-YVETTE Cedex
FRANCE

ABSTRACT

We present a computationnal method to describe the migration of the ions in porous rocks. For the description of the migration, due to convection and Fick diffusion we take account of creation and annihilation of precipitate. The separation between regions with and without precipitate is evolving in time, but the meshes are fixed.

INTRODUCTION

In geochemistry, one usually study ions migrations when the ions concentration, by example Ca^{++}, is important. The mass action law leads to a non linear equation governing the evolution of different ions concentrations. This case is studied in the references [1] [2] [3] [4] [5] .

The problem of migrations of ions might be reduced to 2 more simple problems :

1) a computationnal problem of the linear Fick equation
2) a pure problem of chemistry.

We have to study the transfer of ions implanted by man in a waste storage. Dissolution and reprecipitation then take place according to the regions, the mass action law is written under different forms.

In this work, we give an algorithm of computation taking in account this change of form of the mass action law, in the simple case where we have only 2 ions.

POSITION OF THE PROBLEM

We consider a rock, of porosity ε, crossed by a stream of water with a DARCY speed $\vec{U}$. In this rock, N ions I_i, diffuse with the same coefficient D, their concentration in water are called i. We assume, in a first time, no interaction between ions and rock, and, consequently, their delay factor is equal to 1. The case : $\tau \neq 1$, will be studied later on. In these conditions, if we neglect the interaction between ions, C_i is governed by :

$$(1)\quad \varepsilon \frac{\partial c_i}{\partial t} = D\Delta C_i - \vec{U}.\vec{\text{grad}}\, c_i$$

In fact, we cannot neglect the interaction, we have to write :

$$(2)\quad I_i + I_j \rightarrow P_k$$

The compound P_k has a very low solubility. We design by p_k the ratio of the quantité of compound P_k present in the volume dU by the volume of water corresding εdU. If we call $p_{o,k}$ the limit of solubility of the compound P_k, we have, by virtue of the mass action law :

$$(3)\quad c_i c_j = Kp_k$$

where K is a constant, determined experimentally, when the concentration is low ($p_k < p_{o,k}$). When this concentration is important, we have :

$$(4)\quad c_i c_j = Kp_{o,k} = PS_k$$

By following, we call :

$$p_k = p_k^* \qquad (p_k < p_{o,k})$$

$$p_k = p_k^* + (p_k - p_o) \qquad (p_k > p_{o,k})$$

where, p_k^* is the solubilized fraction of the compound P_k and $(p_k - p_o)$ the nonsoluble fraction, in precipitate.

If, $p_k > p_o$, everywhere for all values of k, the problem is reduced to the problem of linear convection diffusion and to a pure problem of chemistry.

Case of decay of the problem

The equation (1) becomes, due to the existence of the P_k, the equation (5) :

$$(5)\quad \varepsilon \frac{\partial c_i}{\partial t} + \Sigma \frac{\partial p_k}{\partial t} = \Delta C_i + \Sigma \Delta p_k^* - \vec{U}\ \vec{\text{grad}}\, c_i + \Sigma\, \vec{\text{grad}}\, p_k^*$$

The sign Σ showing the manifold of the k when the compound P_k includes the ion I_i.

If the number m of compounds P_k is lower than N, we can reduce, by linear combinations, the manifold of the equations (5) to (N-m) equation (6), formally similar to the equations (1) :

$$(6)\quad \varepsilon \frac{\partial u_i}{\partial t} = D\Delta u_i - \vec{U}.\vec{\text{grad}}\, u_i$$

where the u_i are the (N-m) linear combinations of the c_i, and where the p_k and p_k^* were eliminated. Now, if we have everywhere compounds P_k in an insoluble form, we have, between the c_i, m equations (4) independants of p_k. So, the problem is reduced to two problems :

a) a problem of pure convection-diffusion, with the equations (6)

b) this problem resolved, the individual values of c_i were determined by a problem of pure chemistry, involving m non linear equations (4) and (N-m) linear equations defining the u_i. This probleme is usually solved by the method of NEWTON-RAPHSON we remark that we don't have to compute the values of p_i.

GENERAL CASE

In fact, we have regions where we have precipitate, and other regions where we have not preci-

pitate. To simplify, in the following of the paper, we shall only consider N=2, m=1 (2 ions, 1 précipitate). This case shows clearly the problems by elimination of many problems of software (multiple indexations) that we will solve later on.
To simplify, we will call : $c_2 = a$ and we will omit the index in c, p and u, as they become useless.

We combine the equations (3) and (4) in a formal equation

$$ac = f(p) \tag{7}$$

which comes from the mass action law where f(p) is defined by the figure 1 (continuous line)

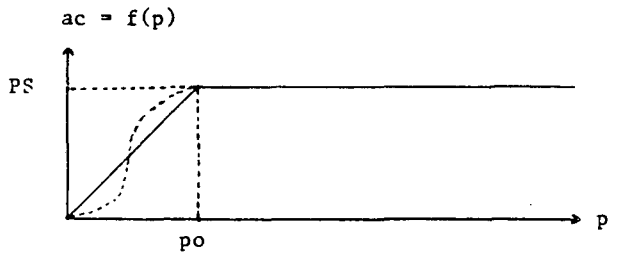

The manifold of the equation takes the form :

$$\varepsilon \frac{\partial p}{\partial t} + \frac{\partial a}{\partial t} = D\Delta a - \vec{U}.\vec{\text{grad}}\, a \tag{5}$$

$$\varepsilon \frac{\partial p}{\partial} + \frac{\partial c}{\partial} = D\Delta c - \vec{U}.\vec{\text{grad}}\, c \tag{6}$$

I

$ac = f(p)$

with the definition $u = \frac{c-a}{2}$, the system (I) is equivalent to the system (II)

$$\varepsilon \frac{\partial u}{\partial t} = D\Delta u - \vec{U}.\vec{\text{grad}}\, u$$

$$\varepsilon \frac{\partial p}{\partial t} + \frac{\partial}{\partial t}\left[u + \sqrt{u^2 + f(p)}\right] =$$

$$D\Delta\left[u+\sqrt{u^2+f(p)}\right] - \vec{U}.\vec{\text{grad}}\left[u+\sqrt{u^2+f(p)}\right]$$

In this form, the problem decays in :

a) a problem of pure diffusion, like previously
b) a non linear problem concerning the p.

This problem is solved by discretization, this gives 2 questions :

a) under what conditions the scheme of discretization is it stable ?

b) can we use the method of NEWTON RAPHSON ? If yes, in which conditions ?

STABILITY [6]

To study it, we write the variables under the form :

$$a = a_o + \delta a$$

$$c = c_o + \delta c$$

$$p = p_o + \delta p$$

a_o, c_o, p_o being the accurate solution, δa, δc, δp the discardes, assumed little. We get so a linear system (III), the 2 first equations are these of (I) and the third

$$a_o \delta c + c_o \delta a = f'(p)\delta p$$

with :

$$f'(p) = \frac{df}{dp}$$

We decompose δa, δc, δp in serie of FOURIER [6]

$$\delta a = \Sigma \delta a_k e^{ikx} e^{nt}$$

The solution is stable if, always, n<0. We verify that, if the stability conditions are satisfied for the equation (6) and if f' > 0, they are satisfied for the system III, and, consecutively, for the equivalent systems (I) and (II).

METHOD OF NEWTON RAPHSON [7] [8] [9]

Let us take, the explicit discretization of the second equation of (II), in the case U = 0. Like in [6], the upper index corresponds to the time, the lower index corresponds to the space :

$$8)\ c\left[p_i^{n+1} - p_i^n + u_i^{n+1} - u_i^n + \sqrt{u_i^{n+1}\cdot u_i^{n+1} + f(p_i^{n+1})} - \sqrt{u_i^n \cdot u_i^n + f(p_i^n)}\right] - \frac{D\Delta t}{\Delta x^2}\left[u_{i+1}^n + u_{i-1}^n - 2u_i^n + \sqrt{u_{i+1}^n \cdot u_{i+1}^n + f(p_{i+1}^n)} + \sqrt{u_{i-1}^n \cdot u_{i-1}^n + f(p_{i-1}^n)} - \sqrt{2\, u_i^n \cdot u_i^n + f(p_i^n)}\right] = 0$$

1st order terms cancelled themselves, from (6), we have a non linear equation on the system of unknown variables p_i^{n+1}. The Jacobian J is a diagonale matrix, these elements are :

$$J_{ii} = \varepsilon\left(1 + \frac{f'(p_i^{n+1})}{2\, u_i^{n+1} \cdot u_i^{n+1} + f(p_i^{n+1})}\right) \tag{9}$$

For the method of NEWTON-RAPHSON may converge, we must the following conditions :

a) we must begin "enough near" of the solution
b) the matrix J must be regular
c) the matrix J must be continuous

The condition a) introduces a limitation of the time path, difficult to estimate, that we must take in account in the case of the implicit discretization.
The condition b) is satisfied if f'(p) > 0, following (9). But the condition c) be satisfied if f(p) has the form given figure 1. We must choose between

1) change the natural law f(p)
2) use an other method than NEWTON RAPHSON.

We have choosed 1), that obliged us to verify, at least on an example, that we don't modify the results.

We will, however, give a solution of type 2), the method of WEGSTEIN, to justify our choice. In fact we will see, that this method is very low performant and needs a lot of computation time.

Method of WEGSTEIN

We use the property of the sequence

$$v_{n+1} = F(v_n)$$

to converge, under some conditions, to

$$v_\infty = F(v_\infty)$$

we write the equation (8) on the form :

$$(10) \quad p_i^{n+1} = F_i(p_i^{n+1}, \ldots)$$

The sequence :

$$v^k = F(v^{k-1})$$

converges to p_i^{n+1} if the matrix :

$$M_{ij} = \frac{\partial F_i}{\partial p_j}$$

has all its eigenvalue less than 1.

The discard between the accurate solution and the successive values decreases in geometric progression, its reason is the greater eigenvalue : we need very much iterations.

In the case of the implicit discretisation, we may have a strong limitation on the path time. For these reasons :

- slow convergence
- limitation of the path time

we don't use the method of WEGSTEIN, in spite of it allow to use the natural law and be easy to program. Indead, for a given time of computation, the method of WEGSTEIN required a coarser grid, hence a loss of precision, greater than this resulting of the discard to the natural law.

Modification of the natural law

We replace hence the natural law by a law with continuous derivative (figure 1, dot line).

We tried the method of NEWTON RAPHSON for 2 cases for which we know accurate solution. The agreement is very good.

1st test case

It's the simulation of the agression of a container of ion by sulphurous water

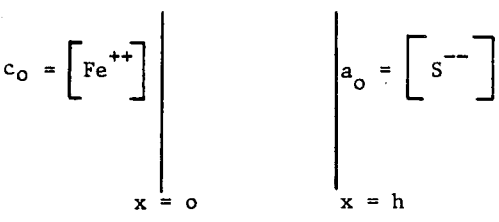

Figure 2

We consider a plane plate of thickness h ($o < x < h$) (figure 2) we have :

Boundary conditions

$$x = o \begin{cases} a = o \\ c = c_o \\ p = o \end{cases} \qquad x = h \begin{cases} a = a_o \\ c = o \\ p = o \end{cases}$$

Initial conditions

c = a = p = o, except on the bounds

Steady state

$$(11) \quad u = \frac{1}{2}\left[c_o - (c_o + a_o)\frac{x}{h}\right]$$

$$(12) \quad c = u + \sqrt{u^2 + PS}$$

$$(13) \quad a = -u + \sqrt{u^2 + PS}$$

$$(14) \quad \frac{\partial p}{\partial t} = \frac{D(c_o+a_o)^2}{4h^2\varepsilon} \cdot \frac{PS}{(u^2 + PS)^{3/2}}$$

The production of précipitate is almost entirely concentrated in a band of half width :

$$\frac{2h\sqrt{PS}}{c_o + a_o}$$

centered on u = o

obviously, such a situation cannot exist a long time, the précipitate would fill the pores and modify D and ε.

The agreement of numérical computation and of steady state is very good, even for values of PS like 10^{-50}.

The path time begins with the value of the explicit iteration Δt_o, and it will be doubled when $t = 4^n \Delta t_o$, n integer.

2nd Test case (figure 3)

It's the simulation of the release of the lime in a cement attacked by pure water (in particular without ions Cl^-, So_4^{--}, CO_3^{--}, CO_3H^-)

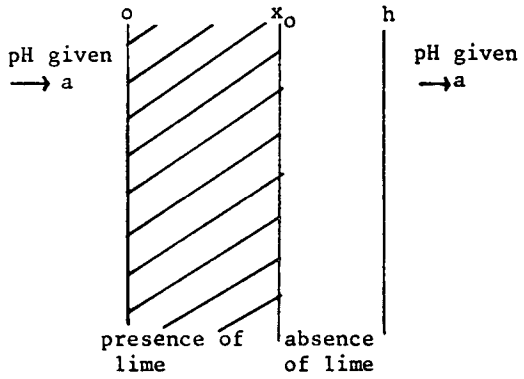

Figure 3

For $x \leq x_o$, we have an insoluble hydroxyd ($p = p_1$ given) for $x_o < x < h$, no precipitate

Boundary conditions

$$x = o \begin{cases} a = 1 \\ c = c_o = PS \\ p = p_1 \text{ given} \end{cases} \qquad x = h \begin{cases} a = 1 \\ c = o \\ p = o \end{cases}$$

Initial conditions

$a = 1$ everywhere

$c = c_o \quad p = p_1 \quad (x \leq x_o)$

$c = 0 \quad p = 0 \quad (x > x_o)$

a remains always near 1, the region where p is near of p_1 decreases, the transition from $p = p_1$ to $p < PS$ (PS is the limit of solubility) is on 2 meshes.

We can solve the problem by the following way : p_1 is an hydroxyd, in equilibrium with a solution at the concentration PS. For $x > x_o$, c follows strictly the FICK law.

In $x = x_o$, we have a flow of ions, $-D \frac{\partial c}{\partial x}$, compensated by the recession of the bound x_o :

$$\frac{dx_o}{dt} = \frac{D}{\epsilon p_1} \frac{\partial c}{\partial x}$$

and $c = c_o$

We solve the equation of FICK in the compact $x_o < x < h$, with boundary conditions of DIRICHLET.

The agreement between the two methods is very good ; this justifies our discard to the natural law.

Future program

1) extension of the method of computation to the case of more than 2 ions.
2) we will take in account the adsorption, by introducing a delay factor.
3) case of the complexes, where we cannot neglect the diffusion of the compound P dissolved.
4) case where the number of compounds is greater or equal to the number of ions, that askes the insertion of a complex program of chemical équilibrium. We must then seek a compromise between the sevetery of the treatment of chemical equations and the computation time.

REFERENCES BIBLIOGRAPHIQUES

(1) CHAPMAN B.M. (1982) - Numerical simulation of the transport and speciation of nonconservative chemical reactants in rivers, Water Resources Research, vol.18 (1), p. 155-167

(2) CARNAHAN C.L., MILER C.W., REMER J.S. (1984) Experience in coupling chemistry to fluid flow in CHEMTRN code. Communication at workshop on the coupling of Hydrologic and Geochemical models. OCDE, NEA, Paris 12-13 Juin 84, 13 p.

(3) TORO D.M. (1976) - Combining Chemical equilibrium and phytoplankton models a general methodology, in Modelling biochemical processes in aquatic ecosystems, Canale (ed), An Arbor Science Pub., Inc., Michigan, p. 233-235

(4) RUBIN J. (1983) - Transport of reacting solutes in porous media : relation between mathematical nature of problem formulation and chemical nature of reactions. Water Resources Research, vol. 19(15), p. 1231-1252

(5) SCHWEICH D., SARDIN M. (1985) - Transient ion-exchange and solubilization of limestone in oil-field sandstone : experimental and theoretical wave fourier analysis, à paraître dans A.I.Ch.E.

(6) RICHTMYER and MORTON - Difference Methods for initial value problems - Interscience Publisher (New-York - NY)

(7) B. CARNAHAN - Applied numérical methods (p.308) J. WILEY and SONS

(8) STOER and BULIRSCH - Introduction to numérical analysis (p. 244) SPRINGER VERLAG

(9) KANTOROVICH L.V. and AKILOV G.P. - Functional analysis in normed Spaces (p. 694) PERGAMON PRESS.

EXPERIMENTAL STUDY OF LOW TEMPERATURE (50-100°C) WATER FLOW IN GRANITE FISSURES : NEOFORMATIONS, MOBILITY OF ELEMENTS

OUSTRIERE Pascal, FABRIOL Robert, BOURG Alain, SUREAU Jean-François

BRGM - Département Gîtes Minéraux
Division Processus Géochimiques
BP 6009 - 45060 ORLEANS, FRANCE

The introduction of a nuclear waste repository in a granitic massif can induce a thermal desequilibrium and give rise to a convective water flow through the granite fissures. This circulation can have different consequences with respect to the rock permeability and the possible migration of radionuclides, through chemical reactions (precipitation-dissolution, adsorption-desorption). The aim of the present study is to evaluate experimentally qualitative and quantitative aspects of these chemical exchanges.

The experiments were performed two ways :

- batch experiments : crushed granite is maintained in contact with water at different temperatures (50 and 100°C) from one to thirty five days ;
- percolating experiments : water flows through an artificial crack in a granite core, at a temperature of 50°C, after equilibration at 80°C in a precolumn filled with alumina or dolomite (fig. 1), or without any precolumn.

The percolating solution is synthetised according to the chemical composition obtained from the long duration batch experiments, in which water is considered to be in equilibrium with granite. Then three elements (Co, I, Cs) are added to solution, which is percolated through the core.

These experiments show that the various elements have a very different behaviour. Iodine passes through the precolumn (alumina or dolomite) and the core without any significant change in its concentration. Cobalt is always very strongly depleted in the solution, either in the precolumn or in the core. Cesium has an intermediate behaviour. Its concentration is only slightly lowered in the core, in all the experiments. (fig. 2).

SEM observations of the granite fissures after percolation show neoformation of pure silica and unknown Si-Al-Fe-Ca-Mg and Co-Si-Al-Fe-Ca-Mg minerals.

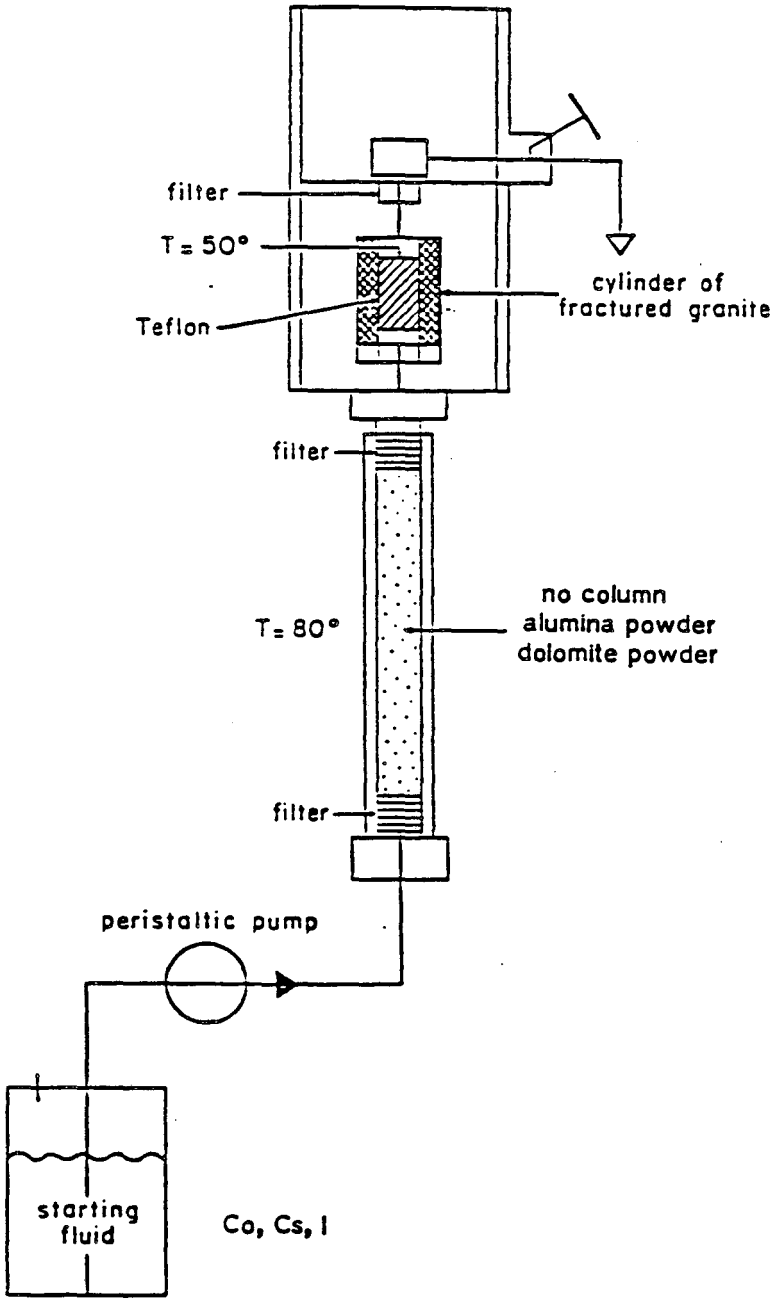

Fig. 1 - Experimental assembly

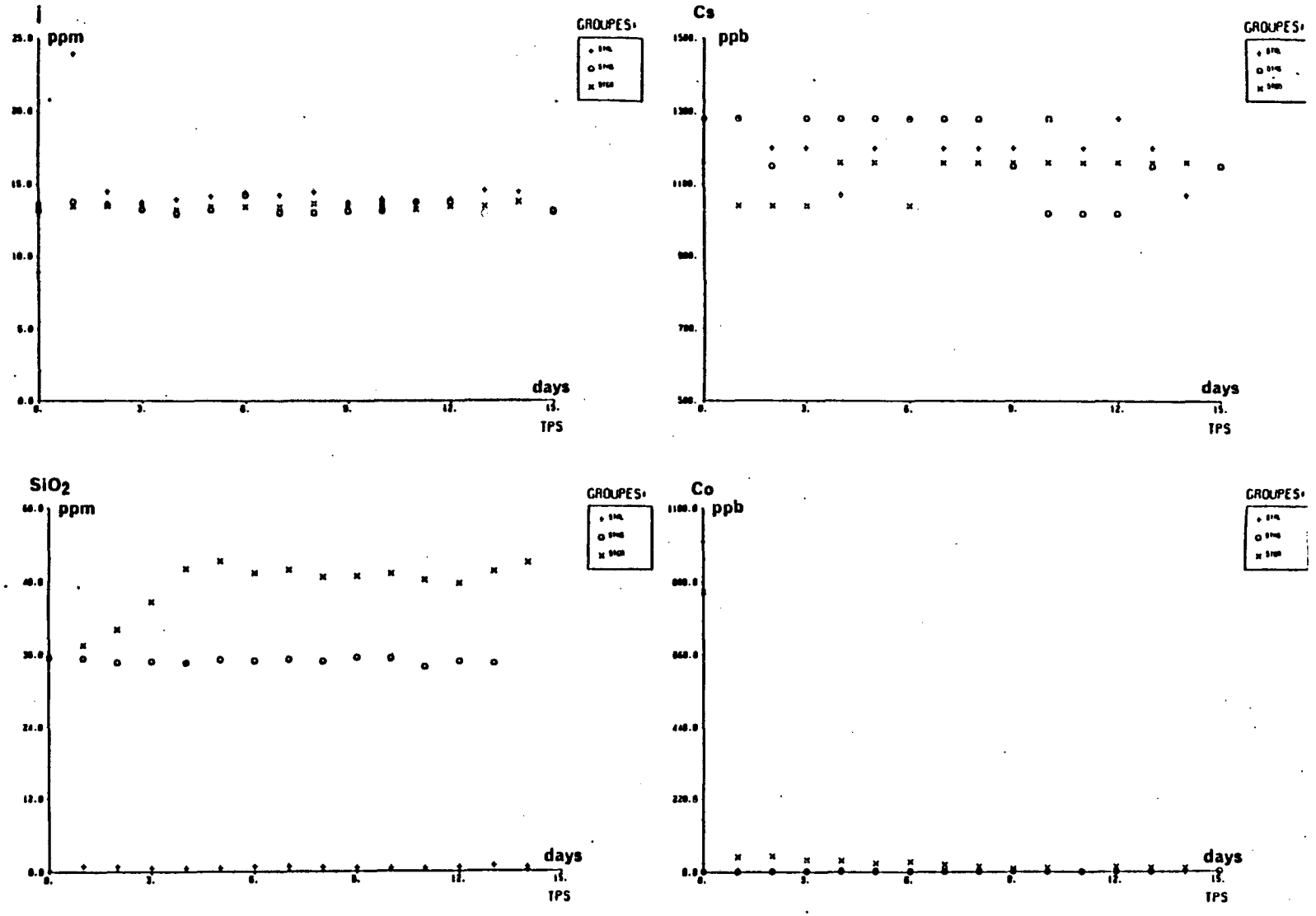

Fig. 2 - Evolution of Cs, I, Co and SiO_2 in the solution after the granite fissure as a function of time. Experiments with a column of alumina (STAL), of dolomite (STMG) or without any column.

A COUPLED APPROACH TO RADIOELEMENT MIGRATION MODELLING IN THE UNITED KINGDOM

D.Read*, D.R.Williams* and S.K.Liew+
*Department of Applied Chemistry, UWIST, Cardiff CF1 3XF, U.K.
+Atkins Research & Development, Epsom, U.K.

Abstract

At present, the United Kingdom Department of the Environment is applying a series of computer models based on the AECL SYVAC code to assess the radiological impact of low to intermediate - level waste disposal under conditions appropriate to the UK. As detailed representation of chemistry is not an integral part of these models, output needs to be cross-verified by comparison to coupled geochemical-hydrologic codes. This paper describes a coupled approach involving the chemical transport simulator, CHEMTRN, in conjunction with the mass transfer program, PHREEQE. In the sense that CHEMTRN is itself a stand-alone direct approach to coupling, the procedure is a combination of direct and iteratively coupled geochemical-hydrologic modelling but one in which the chemistry of the system is monitored throughout. The results of independent verification studies are summarised and recommendations are made regarding the potential rôle of CHEMTRN in radiological assessment. Case studies on a prospective UK site are described. They emphasise the importance of including the effects of aqueous complexation on sorption processes when modelling the migration of radioelements from a disposal vault to the surface.

Introduction

In the UK, regulatory bodies are not, themselves, directly involved in the management of radioactive waste disposal but rather establish the principles by which the acceptibility of any waste management proposal is judged. In the first instance, the provision of disposal facilities rests with the nuclear industry, represented by NIREX, an executive comprising members of British Nuclear Fuels plc (BNF), the Electricity Boards and the UK Atomic Energy Authority. The Government departments with prime responsibility for authorising disposal are the Department of the Environment (DoE), the Ministry of Agriculture, Fisheries and Food (MAFF), and the regional government offices of Scotland and Wales.

In order to evaluate the potential of sites proposed by NIREX, the DoE are involved in preparing an independent safety assessment. This research programme includes development of computer-based methods and, as a first stage, a procedure based on the Atomic Energy of Canada Ltd. (AECL) SYVAC variability analysis approach has been adopted. The SYVAC simulation is probabilistic, using Monte Carlo sampling methods to represent mathematically the sequence of barriers to radionuclide migration from waste to man. Although new software has been developed by the DoE and its contractors for comparative radiological assessment, detailed modelling of chemistry is not, at present, included in SYVAC. For this reason, the rôle of UWIST is to supplement the above work by recourse to more sophisticated, deterministic models describing the chemical speciation of radioelements within a disposal vault and along migration pathways from the vault to the biosphere.

This paper outlines recent modelling studies of chemical speciation and coupled chemical-hydrologic processes in low and intermediate-level waste disposal systems. The rationale behind the choice of programs used is discussed in terms of their applicability, compatibility, computing requirements and ease of use. The results of verification studies are described and the application of the adopted coupling approach is illustrated by reference to pilot studies on a potential disposal site for radioactive waste in the UK.

Coupling chemistry to transport

Approaches to coupling may be conveniently categorised as direct or iterative methods. An iterative model [1,9,20] used a hydrologic flow code to simulate the transport of non-reacting solutes through a geological system. After a prespecified time interval, a geochemical package is called, reactions are modelled to equilibrium and the flow code recalled to transport the solution to the next time step. Such models have the advantage of including detailed, powerful codes to represent both transport in complex flow systems and chemical processes in the vault and far-field. A major disadvantage is the lack of interaction between the two-component parts of the model, for example, no account is taken of the effect of precipitating solids on porosity and permeability. The feasibility of coupling a three-dimensional finite-element hydrologic model to advanced mass transfer and reaction-path chemical programs, such as PHREEQE [17] and EQ3/6 [25], has been investigated [16] but the lengthy operating procedure, together with the substantial computing resources needed suggest the approach to be unrealistic at present. It could be justified in the future as a final step in an overall assessment following detailed modelling of the component parts of the system; principally, speciation in the aqueous phase, sorption/co-precipitation processes at the solid-liquid interface, mass transport and flow-field calculations.

In a directly coupled approach, transport equations are written for each chemical species, resulting in a single set of compound, partial differential equations which are solved simultaneously. A fully coupled model of this type would represent the ideal situation but, unfortunately, the compound equations tend to be highly non-linear and require sophisticated solution techniques. In view of this, several more limited models have been proposed, e.g. [11,21,23], of which the most developed and well-documented is CHEMTRN [5,13,14]. This program simulates the transport of chemical species according to a simple one-dimensional linear or radial flow model and assumes constant fluid velocity, diffusion and dispersion. The chemical model includes aqueous complexation, sorption of charged species and reversible precipita-

tation - dissolution of solids. As no external database is used by the program and preliminary work suggested it to be an expensive package to run [12], it was realised that judicial selection of only the most significant species by prior use of a chemical speciation code was essential. Consequently, studies to date have concentrated on the use of CHEMTRN in conjunction with PHREEQE [17].

The mass transfer program, PHREEQE, is used to "prime" CHEMTRN by predicting the chemical speciation and maximum solubility of radioelements as determined by the waste form and ambient environment. PHREEQE was chosen for its flexibility and ability to simulate both the mixing or titration of solutions and the addition of reactants to a system in equilibrium. The dominant aqueous species and solubility-limiting phases are input to the chemical transport model, together with coefficients expressing the selectivity of the sorbing medium for the species of interest. CHEMTRN then simulates movement of the groundwater, according to the 1-D flow model, giving the concentration distribution of sorbed and aqueous species as a function of distance and time. Further sophistication is possible by operating the model in tandem with a detailed hydrologic code, such as NAMMU [18]. The latter is used to characterise the flow field, after which CHEMTRN may be employed to predict concentration distributions along the principal streamlines.

The net result of the above is a combination of direct and iterative geochemical-hydrologic coupling but one in which the chemistry of the system is represented throughout. Before discussing the results of preliminary modelling studies on an actual UK site, the means by which the above programs have been independently verified is described.

Verification

Verification of the programs used in simulation studies is essential for ensuring that all calculations are performed correctly and to identify any coding discrepancies or "bugs". The most convenient method involves inter-code comparison exercises whereby the solutions to a common problem are compared. Three such exercises have now been undertaken for geochemical codes [4,10,15] and as the results obtained were generally in good accord, the treatment of chemical speciation used by CHEMTRN was verified by reproducing the base case of the most recent intercode comparison programme [4]. The problem entailed computing the distribution of species in a hypothetical groundwater solution at near neutral pH under mildly oxidising conditions. Thermodynamic data for all aqueous and solid species were taken from an "in house" database compilation [7]. The results obtained showed excellent agreement with those derived from eight geochemical codes used at a number of institutions in the UK and overseas. Those for carbonate speciation are summarised in Figure 1.

The transport solver in CHEMTRN was verified by comparison with the SYVAC GEO1 code and several other migration programs investigated during the course of a CEC MIRAGE exercise [12]. GEO1 is an analytical solution for transport of radionuclides through up to five layers of saturated porous media, including provision for six-member decay chains. Following minor code modifications within CHEMTRN to allow for a fixed duration of source

Figure 1. Comparison of CHEMTRN with chemical speciation codes: carbonate system

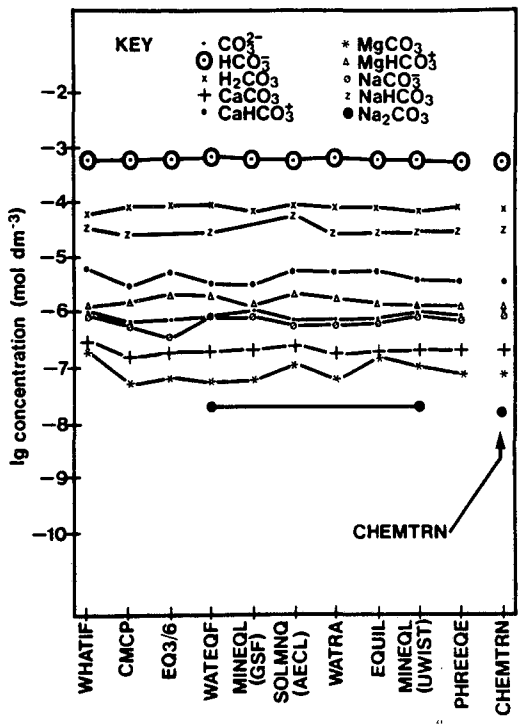

release and choosing time steps to minimise numerical dispersion, both codes were used to simulate the movement of an unretarded species. Agreement between CHEMTRN and GEO1 was found to be excellent (Figure 2). Similar good agreement was obtained for the six other transport simulators studied.

Figure 2 Comparison of CHEMTRN and GEO1

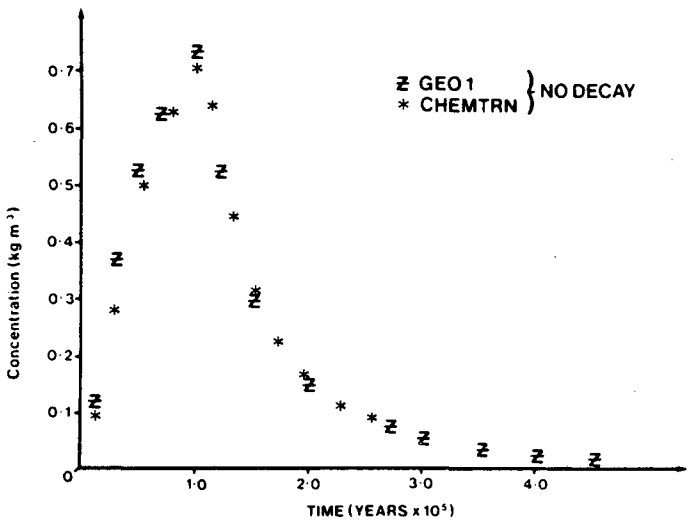

Case Studies

In order to construct a detailed chemical-hydrologic model of any system, accurate site-specific data are essential. These were largely unavailable for the site examined, as is typical during the early stages of an assessment, and so the present studies remain unvalidated. Nevertheless, they serve to illustrate the type and extent of information which even elementary numerical modelling can provide.

The example involves modelling the chemical speciation of americium in, and its migration from, a proposed shallow repository sited within clay deposits in Bedfordshire, England. The geology of the area is simple, consisting of very gently dipping Jurassic sedimentary rocks overlain by glacial and periglacial drift (Figure 3). For modelling purposes, the repository is assumed to be located at a depth of 10 metres below the surface, within the Oxford Clay, a compacted shale-mudstone. The principal formations with significant permeability, excluding surface deposits, are the Kellaways Sand and, where fractured, the Cornbrash and Blisworth Limestones [24].

Piezometric data are available for both the Oxford Clay and the aquifers. Information on the regional hydrogeology derived from borehole data and consideration of discharge and recharge areas suggests that groundwater movement in the Oxford Clay is vertically downwards and, as a first approximation, the Kellaways Sand may be regarded as a confined aquifer [24]. A decrease in head northwards within the Kellaways Sand suggests discharge northwards along the aquifer to the River Ouse. The flow model used thus considers leaching of waste from the repository into the Oxford Clay where equilibrium with the interstitial groundwater is established. The contaminated water then percolates downwards into the Kellaways Sand and migrates laterally to the River Ouse. The possible effects of aquifer inhomogeneity, faulting and recharge from the river are ignored.

Figure 3 Simplified geological cross-section of the study site

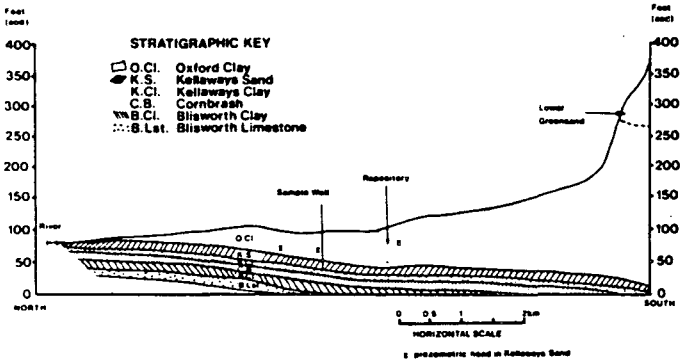

Current vault designs for low and intermediate level radioactive wastes in the UK envisage extensive use of concrete in their construction. Hence, the source term aqueous phase is assumed to be a solution in equilibrium with a concrete/cement matrix. The composition of the "concrete water" used (Table 1) is a representative compilation derived from a number of sources [6,8]. Groundwater analyses were obtained from borehole data [2,24] and surface water analyses from a tributary of the River Ouse which drains the study catchment [19,24].

Three different calculations were performed for each water analysis using PHREEQE. The first show the speciation and solubility of americium in equilibrium with a solubility limiting phase. The second set simulate addition of calcium sulphate until equilibrium with gypsum is attained, in order to investigate the relative importance of sulphate and carbonate complexing on americium solubility. Equilibria with calcite and another solid controlling americium solubility is maintained throughout this "reaction". Finally, PHREEQE is used to simulate the mixing of concrete and groundwaters allowing americium behaviour to be traced along possible flow paths from the vault to the surface.

TABLE 1 Surface and groundwater compositions used in the case study. Concentration in mol dm^{-3}

	Surface Water	Kellaways Sand	Blisworth Lst	Oxford Clay	Concrete
Ca^{2+}	4.0×10^{-3}	2.4×10^{-3}	2.7×10^{-3}	8.7×10^{-4}	1.1×10^{-2}
Mg^{2+}	8.2×10^{-5}	1.1×10^{-3}	1.7×10^{-3}	1.3×10^{-4}	2.0×10^{-6}
K^{+}	1.8×10^{-4}	3.6×10^{-4}	3.0×10^{-4}	8.9×10^{-5}	1.0×10^{-4}
Na^{+}	1.1×10^{-3}	0.01	9.0×10^{-3}	7.8×10^{-4}	5.0×10^{-5}
$\sum Si$					3.0×10^{-5}
CO_3^{2-}	1.0×10^{-3}	5.2×10^{-3}	1.1×10^{-3}	5.1×10^{-3}	2.0×10^{-5}
SO_4^{2-}	3.1×10^{-3}	3.8×10^{-3}	6.1×10^{-3}	6.4×10^{-4}	2.0×10^{-3}
Cl^{-}	1.6×10^{-3}	1.4×10^{-3}	1.3×10^{-3}	8.5×10^{-4}	2.0×10^{-3}
pH	8.0	7.6	7.7	8.7	12.7

Americium does not display the complex redox chemistry of the neighbouring actinides under environmental conditions, making it a relatively simple element to model. At the high pH of concrete water, the hydroxy species, $Am(OH)_3$ and $Am(OH)_4^-$, dominate in solution (Table 2). The predicted maximum solubility is low (5×10^{-10} mol dm^{-3}) and controlled by the hydroxide $Am(OH)_3$. In the more neutral environment of ground and surface water, carbonate, hydroxy-carbonate and sulphate complexes form at the expense of hydroxy species and are responsible for an increase in the solubility of americium by about two orders of magnitude (Table 2). The stable solubility limiting phase changes to $AmOHCO_3$ between pH 9 and 10. Recent experimental solubility measurements [6] corroborate these findings, providing useful validation of both the code and the thermodynamic data available for americium.

TABLE 2 Americium solubility and speciation

Water	Solubility (mol dm^{-3})	Limiting Phase	Dominant Species
Surface Water	1.8×10^{-8}	$AmOHCO_3$	$AmOH(CO_3)_2^{2-}$, $AmSO_4^+$ $AmOHCO_3$, $AmCO_3^+$
Blisworth Lst.	3.1×10^{-8}	$AmOHCO_3$	$AmSO_4^+$, $AmOH(CO_3)_2^{2-}$, $AmCO_3^+$, $AmOHCO_3$
Kellaways Sand	3.7×10^{-8}	$AmOHCO_3$	$AmOH(CO_3)_2^{2-}$, $AmCO_3^+$ $AmSO_4^+$, $Am(CO_3)_2^-$ $AmOHCO_3$
Oxford Clay	2.9×10^{-8}	$AmOHCO_3$	$AmOH(CO_3)_2^{2-}$, $AmOHCO_3$
Concrete Water	5.1×10^{-10}	$Am(OH)_3$	$Am(OH)_3$, $Am(OH)_4^-$

Predicted solubilities are not significantly different for the three groundwaters and are up to a factor of two higher than in surface water

possibly due to increased competition from calcium for the anionic ligands. Figure 4 shows the variation in americium solubility expected along a hypothetical pathway from the concrete vault via the Oxford Clay and Kellaways Sand to the surface, based solely on the PHREEQE simulations. The Blisworth Limestone data is included for completeness. A sudden change in solubility accompanies a change in the solid limiting phase from $Am(OH)_3$ to $AmOHCO_3$. The concrete water acts as a buffer and even at a concrete:clay water ratio of 1:9 americium solubility is still close to that in the concrete solution.

Figure 4 Solubility of americium along a hypothetical flow path from vault to surface.

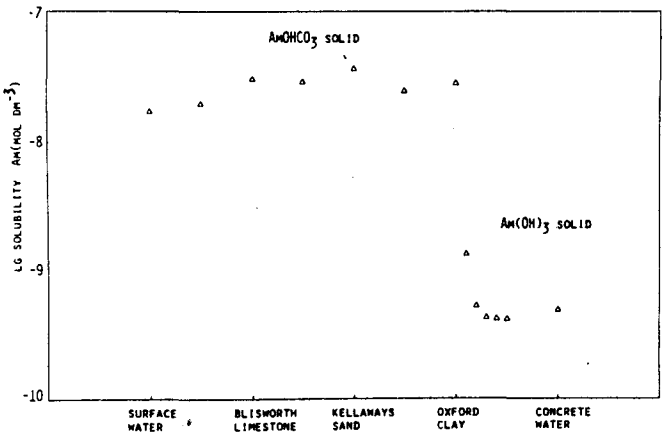

In assessing the migration behaviour of americium, a knowledge of its chemical speciation is essential as this controls the sorption characteristics of the transported species. The aqueous species calculated to be dominant for any system will change in response to environmental controls, such as pH, Eh and the concentration of major ions. In the case of americium, Eh has been found to have relatively little effect in comparison to pH variation and complexation, principally by sulphate and carbonate.

The effect of sulphate complexing is quantified in Table 3.

TABLE 3 Effect of sulphate complexation (Solutions at equilibrium with calcite and an Am solid phase. All concentrations in mol dm^{-3})

Water	Am solubility at gypsum boundary	Am carbonate + hydroxy-carbonate : sulphate	
		Raw data	At equilibrium with gypsum
Surface Water	2.4×10^{-7}	9.7	7×10^{-2}
Blisworth Lst	2.4×10^{-7}	0.81	8×10^{-2}
Kellaways Sand	8.5×10^{-7}	13.9	6×10^{-2}
Oxford Clay	1.2×10^{-7}	1030	9×10^{-2}
Concrete Water	4.9×10^{-10}	3.2×10^{7}	7.4×10^{5}

The two right-hand columns show the relative importance of sulphate and carbonate/hydroxycarbonate species for the raw data and in solutions saturated with respect to gypsum. It is evident that a sudden influx of SO_4^{2-} ions would markedly alter the speciation of americium in the groundwater and surface water systems. Furthermore, as the dominant americium sulphate species, $AmSO_4^+$ is cationic, whereas the hydroxy-carbonate species tend to be neutral or anionic, the potential for retention of americium in the geosphere would be expected to change substantially.

CHEMTRN was used to study groundwater flow through the Kellaways Sand from its junction with the Oxford Clay to an outer boundary at the River Ouse. Breakthrough curves were then calculated for a well situated 1 km north of the repository as shown (Figure 3). It is assumed that americium-contaminated inflow water has reached equilibrium in the Oxford Clay, given the low flow rates likely in this formation [24]. Transport through the Kellaways Sand was simulated for the aqueous americium species identified from the earlier chemical modelling (Table 2). Complexation of the major groundwater components and water dissociation were included. Sorption of the cationic species, $AmSO_4^+$ and $AmCO_3^+$, was assumed to take place by ion-exchange for Ca^{2+}, Mg^{2+} and Na^+, with neutral and anionic species unretarded. All thermodynamic data were taken from the UWIST database [7] except for ion-exchange constants [3]. As the equilibrium constants for exchange of $AmSO_4^+$ and $AmCO_3^+$ are not known a selectivity coefficient was assigned to the cations by comparison with monovalent ions, such as Na^+. Estimates of exchange constants may also be obtained from whole-element sorption coefficients by allowing for the proportion of americium not in cationic form. Reported measurements of K_d values show extreme variation however, and in the absence of better experimental data a more rigorous approach than the method adopted was not thought justified. It must be noted that not only are thermodynamic constants lacking but the actual processes by which americium abstraction occurs are poorly understood. In addition to ion-exchange surface complexation, non-specific adsorption, co-precipitation and colloid coagulation are all possible mechanisms for removal of americium from solution.

The average porewater velocity, (V) within the sandstone may be calculated from its hydraulic conductivity (K), porosity (P), and the hydraulic gradient (i) from Darcy's Law: $V = Ki/P$. Measured conductivities vary between 1.3×10^{-6} and 1.5×10^{-9} m s^{-1}, from which a value of 10^{-7} m s^{-1} was taken, and porosity is reported as 6% [24]. If pumping the sample well produces a head difference of 10 metres, the average water velocity through the aquifer would be 0.53 m yr^{-1}. A value of 0.5 m yr^{-1} was, therefore, used in the simulations. Clay minerals in the sequence are predominantly illite and mixed layer illite-smectite for which typical cation exchange capacities would be 0.2 meq g^{-1} and 0.5 meq g^{-1}, respectively. To allow for the proportion of quartz grains in the aquifer, an average CEC of 0.02 meq g^{-1} was used. The solid matrix density was taken as 2.5 kg dm^{-3} and a dispersion coefficient assumed as 0.1 m^2 yr^{-1}. A constant flux condition at the inner boundary was employed for the two simulations shown. Both outer boundary options (zero flux and constant concentration equal to the initial concentration) were investigated but found to have little effect on levels at inner nodes.

Figure 5 shows breakthrough curves at the sample well 1 km from the repository. As anionic and neutral americium species are unretarded and have identical travel times, their concentrations have been summed and are represented by Am_{An}. Similarly, as there are no grounds in this simple model for differentiating between the sorption characteristics of $AmSO_4^+$ and $AmCO_3^+$, their concentrations have also been summed to produce Am_{Cat}. Equilibrium constants for ion-exchange were taken to equal those of Na^+. Initial concentrations of Am_{Cat} and Am_{An} for the inflow water, obtained from PHREEQE calculations, were 4.7×10^{-10} mol dm^{-3} and 2.9×10^{-8} mol dm^{-3}, respectively. The cut-off concentration for the simulation was taken as 1×10^{-10} mol dm^{-3}.

It can be seen from Figure 5 that Am_{Cat} levels do not exceed 10^{-10} mol dm^{-3} and thus at an inflow concentration of 4.7×10^{-10} mol dm^{-3}, cationic americium is quantitatively retained within 1 km of the source. In contrast, the anionic and neutral species, principally hydroxy-carbonates and carbonates, which travel at the same rate as the flowing groundwater display a sharply increasing concentration profile reaching a level of 2.9×10^{-8} mol dm^{-3} after 3000 years. This is the saturation limit computed for the Kellaways Sand (Table 2) and, therefore, all americium species encountered at the well will be in labile form.

Figure 5 Breakthrough curves for sorbing (Am_{Cat}) and non-sorbing (Am_{An}) americium species at sample well.

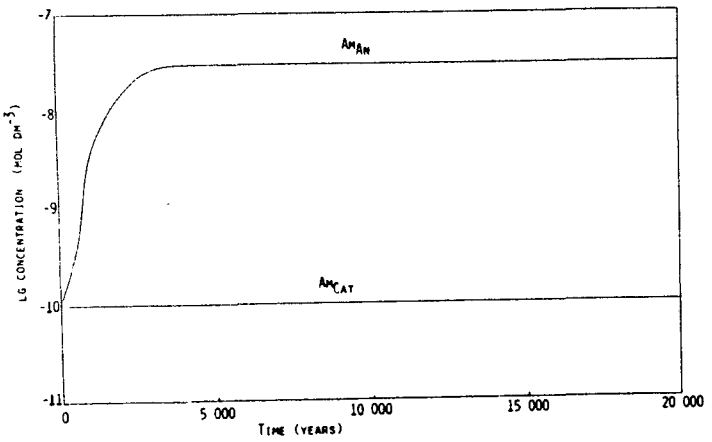

As sulphate has been shown to be an important complexant for americium and the mineral selenite ($CaSO_4.2H_2O$) is common within the Oxford Clay, further calculations were performed to assess the impact of SO_4^{2-} on americium mobility. In Figure 6 breakthrough curves are plotted for the well assuming that inflow water from the Oxford Clay is first saturated with respect to gypsum.

The profile of anionic and neutral species is similar to that in the previous example as they move at the velocity of the water. The profile for Am_{Cat}, however, is quite different and may be divided into two distinct regions. The cations, predominantly $AmSO_4^+$, are retarded for 4000 years but aqueous concentrations then increase steadily with time until at 20,000 years levels of cationic and anionic plus neutral species are approximately equal. It would seem that whereas the solid matrix is able to retain Am_{Cat} concentrations of $\approx 5 \times 10^{-10}$ mol dm^{-3}, at higher levels, the sorbing medium becomes saturated resulting in $AmSO_4^+$ and $AmCO_3^+$ ions being displaced "downstream" by the more strongly bound Ca^{2+} and Mg^{2+}.

Figure 6 Breakthrough curves for americium species at gypsum saturation

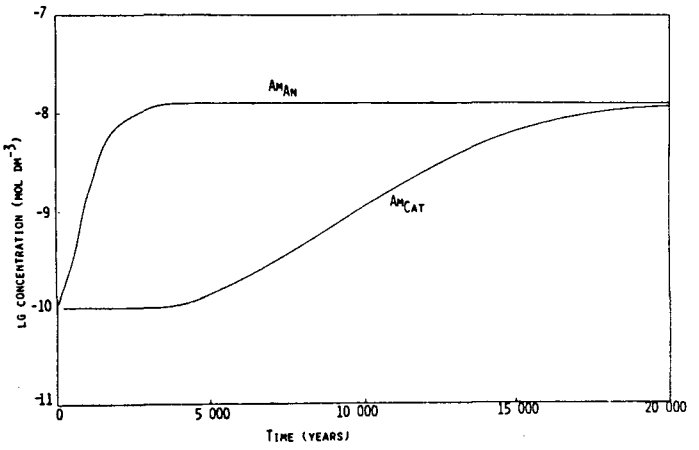

An interesting point to note from Figure 6 is that although americium cations are eventually mobilised, retardation is sufficient to maintain total americium concentrations below the saturation limit for 20,000 years (compare Figure 5). Despite inflow values an order of magnitude greater than in the previous example aqueous americium levels are significantly lower in the presence of sulphate. This clearly demonstrates the need to consider speciation in all groundwater migration studies where there is a capacity for differential sorption of a given radioelement.

Discussion

Recent modelling studies carried out in the UK indicate that the transport simulator, CHEMTRN, when used in conjunction with a flexible mass transfer program such as PHREEQE, is an extremely useful tool for describing coupled chemical-hydrologic processes in groundwater systems. CHEMTRN, developed at Lawrence Berkeley Laboratory, is probably the best documented coupled chemical transport model currently available. Its modular structure suggests advances in the calculation of chemistry, or migration, may be incorporated without undue difficulty and it is certainly desirable for radiological assessment purposes that CHEMTRN be extended to account for nuclide decay and chain decay. In terms of the flow model, the rather restricted boundary conditions could be generalised so that time-dependent values of concentration or flux may be read from a pre-specified data file. Further, the chemical model would be greatly improved by the incorporation of redox capabilities as for elements such as uranium and plutonium the oxidation state will be a critical control on migration behaviour. It is realised, however, that whilst the computing resources needed for uncoupled flow and chemistry modelling are manageable, the requirements of coupling may be very large. As a result of this, studies to date suggest that CHEMTRN may never be used within the

context of a probabilistic code such as SYVAC. A more suitable rôle would be to verify that results obtained from SYVAC conform to those expected on chemical and hydrological grounds.

The calculations described in this paper have served to highlight only a few of the possibilities offered by coupling PHREEQE with CHEMTRN and more exhaustive validation studies are underway. Together with related studies, they have shown that models which incorporate aqueous speciation and competitive sorption within the flow model provide far more insight into the behaviour of geochemical systems than can be obtained from iterating pure hydrologic and chemical codes. CHEMTRN already has the capability to simulate phenomena such as the remobilisation of sorbed species along a flow path and, with development, could possess the potential to reproduce the propagation of redox fronts. Thus, although there is undoubtedly room for further code development, the programs available have, to a large extent, reached a stage where the acquisition of high quality thermodynamic data is a more critical source of concern. Greater emphasis on measuring the fundamental constants is essential if recent progress in geochemical modelling is to be maintained.

Acknowledgements

We are indebted to Drs. Chalon Carnahan and Janet Remer of Lawrence Berkeley Laboratory for providing us with the CHEMTRN program and for their helpful advice. Thanks are also due to Drs.T.Broyd and G.Williams for commenting on aspects of this work. We would like to acknowledge the financial support of the UK Department of the Environment.

References

1. Ahlstrom,S.W., Foote,H.P., Arrett,R.C., Cole,C.R. and Serne,R.J. (1977). Multicomponent mass transport model, Rep. BNWL-2127, Battelle Northwest Lab., Richland, Washington.
2. Alexander,J. (1984). British Geological Survey, Keyworth. Personal communication.
3. Benson,L.W.(1980). A tabulation and evaluation of ion exchange data on smectites, certain zeolites and basalt, Lawrence Berkeley Lab. Rep. LBL1054, Natl.Tech.Inform.Serv., Springfield, Virginia.
4. Broyd,T.W., Grant,M.McD. and Cross,J.E. (1985). A comparison of computer programs which model the equilibrium chemistry of aqueous systems, CEC/Mirage project, Progress Rep. Contract No.219/1B.81.7 WAS. UK(H).
5. Carnahan,C.L., Miller,C.W. and Remer,J.S. (1984). Experience in coupling chemistry to fluid flow in the CHEMTRN code, Proc. OECD/NEA Workshop on the Coupling of Hydrologic and Geochemical Models, Paris, France.
6. Cross,J.E. (1985). AERE Harwell. Personal communication.
7. Cross,J.E., Read,D., Smith,G.L. and Williams,D.R. (1985). Progress Report on SYVAC chemical modelling studies during 1984/85, DoE SYVAC Technical Note, TN-UWIST-3.
8. Glasser,F.P. (1984). University of Aberdeen. Personal communication.
9. Grove,D.B. and Wood,W.W. (1979). Prediction and field verification of subsurface-water quality changes during artificial recharge, Lubbock, Texas, Ground Water, 17: 250-257.
10. INTERA Environmental Consultants Inc. (1982). PHREEQE: A geochemical speciation and mass transfer code suitable for nuclear waste performance assessment, Rep. ONWI/E512-02900/CD-15 420-01G-01A, Houston, Texas.
11. Jennings,A.A., Kirkner,D.J. and Theis,T.L. (1982). Multicomponent equilibrium chemistry in groundwater quality models, Water Resour. Res., 18: 1089-1096.
12. Liew,S.K., Read,D. and Broyd,T.W. (1985). Report on a study of the feasibility of use of the CHEMTRN computer program for radiological assessment purposes, DoE SYVAC Technical Report, TR-WSA-14.
13. Miller,C.W. (1983). CHEMTRN user's manual, Lawrence Berkeley Lab. Rep.LBL-16152, Natl. Tech.Inform.Serv., Springfield, Virginia.
14. Miller,C.W. and Benson,L.V. (1983). Simulation of solute transport in a chemically reactive heterogeneous system: model development and application, Water Resour.Res., 19: 381-391.
15. Nordstrom,D.K. and others (1979). A comparison of computerised chemical models for equilibrium calculations in aqueous systems, in E.A.Jenne (ed.), Chemical Modelling in Aqueous Systems, ACS Symp.Series, 93: 857-892.
16. Noy,D.J. (1983). Coupling of transport and geochemical models, Final Rep. CEC Contract No. 413-83-7 WAS. UK.
17. Parkhurst,D.L., Thorstenson,D.C. and Plummer,L.N. (1980). PHREEQE - A computer program for geochemical calculations, U.S. Geol.Surv., Water Resour.Invest. 80-96, NTIS Tech.Rep. PB81-167801. Revised 1985.
18. Rae,J., Robinson,P.C. and Wickens,L.M. (1981). A user's guide for the program NAMMU. 1. General Information, Harwell Rep. AERE-R-10120.
19. Read,D. and Williams,D.R. (1985). Preliminary chemical modelling studies in support of the radiological assessment of a LAND-1/LAND-2 type repository at Elstow, Bedfordshire, DoE SYVAC Technical Note, TN-UWIST-4.
20. Routson,R.C. and Serne,R.J. (1972). One-dimensional model of the movement of trace radioactive solute through soil columns: The Percol model, Rep. BNWL-1918, Battelle Northwest Lab., Richland, Washington.
21. Rubin,J. and James,R.V. (1973). Dispersion-affected transport of reacting solutes in saturated porous media: Galerkin method applied to equilibrium-controlled exchange in unidirectional steady water flow, Water Resour.Res., 9: 1332-1356.
22. Thompson,B.G.J., Duncan,A.G. and Hall,P. (1985). The development of post-closure radiological assessment methods by the Department of the Environment, Proc. BNES Conf., London.
23. Valocchi,E.J., Street,R.L. and Roberts,P.V. (1981), Transport of ion-exchanging solutes in ground water: chromatographic theory and field simulation, Water Resour.Res., 17: 1517-1527.
24. Williams,G.M. (1985). Preliminary assessment of the hydrogeology of the Elstow storage depot, Bedfordshire, NIREX Rep.No.16.
25. Wolery,T.J. (1979). Calculation of chemical equilibrium between aqueous solution and minerals: the EQ3/EQ6 software package. Lawrence Livermore Lab. Rep. UCRL-52658, Livermore, California.

EFFECT OF IONIZING RADIATION ON WASTE PACKAGE PERFORMANCE IN A BASALT HIGH LEVEL WASTE REPOSITORY

ABSTRACT

D.T. Reed

This paper presents and discusses current data on the effect of ionizing radiation on the performance of the waste package in the proposed high level waste repository in the Columbia River basalts.

The potential of ionizing radiation to alter chemical and geochemical processes has been well established. The primary mechanism is the formation of radiolytic species which will affect the transport of radionuclides, their speciation, the stability of the packing and container corrosion. These effects are not additive and must be integrated into the performance models developed for the waste package.

Ionizing radiation will have the most impact on the performance of the waste package since radiation levels are highest there. The coupling of radiolytic processes with geochemical/chemical processes in basalt groundwater/packing/waste form systems is being investigated as part of an ongoing effort in the Basalt Waste Isolation Project (BWIP). Of primary concern are the effect of radiation on the composition of the groundwater, redox environment, packing alteration, pH and formation of organic polymers.

Experimental Results

The results of investigations in three areas will be presented. These are: Recent calculations on the radiation environment of the waste package, the effect of gamma radiation on processes in the containment period, and the effect of high LET (alpha) radiation on radionuclide speciation in the isolation period.

The radiation environment of the waste package during the containment period is currently being characterized in terms of the gamma dose outside the container as a function of time, fuel burnup and thickness of the container. In the isolation period (anticipated to be ≥1000 years after waste emplacement) the alpha dose will be calculated as a function of the surface area of the spent fuel. This will be extrapolated to conditions expected in the repository to predict the range of dose rates expected.

The gamma radiation testing has been performed by subjecting samples consisting of various waste package constituents to radiation dose levels expected in the repository. Two major effects identified are the formation of polymers from methane found in the groundwater and the possible enhancement of corrosion rates. Preliminary data obtained on the mechanism of these processes will be presented. Additionally data on the formation of radiolytic products, such as hydrogen and hydrogen peroxide, under repository conditions has been obtained.

The ability of alpha radiation (self radiolysis) to reduce and oxidize radionuclides has been well established in simple aqueous systems under standard temperature and pressure conditions. Current testing qualitatively establishes the effect of hydrothermal conditions on this mechanism and quantitatively determines the effect of dose rate and concentration on radionuclide speciation (oxidation state).

Significance of Radiolytic Effects on Waste Package Performance

The effect of ionizing radiation on the geochemistry and chemistry of the waste package depends significantly on the radiation dose rate and temperature. The time profiles of these two parameters, combined with the experimental data on radiolytic effects obtained, are used to qualitatively predict long term effects. This will identify key radiolytic processes and help determine the importance of radiolytic effects. Key parameters estimated:

1. Yield of oxidants; impact on redox environment
2. Yield of reductants; impact on redox environment
3. Impact of early container failure from a radiolytic standpoint

DEVELOPMENT OF AN ALGORITHM FOR THE BIOGEOCHEMICAL EVOLUTION OF URANIUM MILL TAILINGS

W.J. Snodgrass*, R.V. Nicholson*, and N.C. Garisto**

* Beak Consultants Limited, 6870 Goreway Drive, Mississauga, Ontario, L4V 1P1

** Whiteshell Nuclear Research Establishment, Atomic Energy of Canada Ltd., Pinawa, Manitoba, R0E 1L0

ABSTRACT

This paper presents an analysis of relevant time scales for modelling the geochemical evolution of uranium mill tailings (seconds to millions of years). It is suggested that the chemical retention time of pore water is an appropriate parameter for assessing the interaction of transport and kinetics in formulating an algorithm for the evolution of uranium mill tailings.

Two special sub-studies are presented. In one, a reaction-transport model is used to examine the sensitivity of pyrite oxidation to kinetics and transport in the unsaturated zone. The results suggest that the oxygen flux (acid production flux) from a column of tailings is most sensitive to the diffusion coefficient and relatively insensitive to the pyrite oxidation rate constant. This suggests priorities for research (measurement of diffusion coefficient) and management strategies (low diffusion cover).

In a second study, reaction code pathway calculations of an equilibrium mineral assemblage for Fe-Ca-Al-S-CO_2-H_2O are made. The evolution of minerals along an "oxygen-added" reaction pathway is quite sensitive to the initial ratio of goethite and pyrite present. A comparison with available field data suggests that the model simulates the expected trend of pH, but that the simulated trend of pe is in error. This uncertainty may result from the presence of pseudo-stable phases or the lack of equilibrium with pyrite. An approach for coupling these processes is to titrate an equilibrium mineral assemblage with pyrite oxidation products and use results from the reaction-diffusion model to ascribe a time dimension to the reaction pathway.

1.0 INTRODUCTION

Tailings may be defined as the waste mineralogical assemblages that result from U-milling processes. They are deposited within a suitable containment system either natural or man made. Uranium mill tailings are of environmental concern both from the perspective of long-term exposure to low level radiation and the ongoing discharge of non-radioactive contaminants from these tailings.

The objective of this paper is to evaluate the coupled nature of a few of the physical, chemical, and biological processes influencing the long-term biogeochemical evolution of uranium mill tailings in wet Canadian-Shield environments. The following aspects are presented:

(a) the typical mineral assemblages present;
(b) time scales of concern;
(c) the calculated evolution of an equilibrium mineral assemblage;
(d) an evaluation of geochemical controls upon fluxes of acidity.

2.0 MINERAL ASSEMBLAGES

There are two major uranium producing areas in Canada. The Elliot Lake region is located on the Canadian Shield on the North Shore of Lake Huron and has historically been the main source of uranium in Canada. The ore bodies are a pebble conglomerate formed in Precambrian times and typically contain 0.1% uranium as UO_2. The main minerals in the tailings are quartz, calcite, pyrite, barite, gypsum, jarostie, chlorapatite, iron oxides, manazite, sericite and other trace minerals. The Northern Saskatchewan ore bodies, found in sandstone deposits on the edge of the Canadian Shield, are currently being developed. They typically contain low percentages of uranium. The main minerals in Sask. tailings are quartz, feldspars, micas, clays, arsenides, metal oxides, gypsum, arsenates and selenates.

The tailings reflect the original properties of the ore but contain substantial amounts of gypsum and other secondary mineral precipitates formed during the milling process. These secondary precipitates form from both addition of mill chemicals (e.g., gypsum from sulphuric acid leaching and lime/limestone neutralization) and leaching of the ore (e.g., calcium arsenate from leaching of arsenides and lime addition). This results in a heterogeneous tailings mass composed of large sand-sized solids (mean diameter 70-150 um) on which the secondary precipitates form and slimes containing clay-sized solids formed from and/or cemented together by the secondary precipitates.

Weathering of tailings results in the potential export of several contaminants. The basic radionuclides common to all tailings are U-238 decay series. In Elliot Lake tailings, pyrite oxidation in the unsaturated zone and the resultant production of acidity are major processes which may affect the geochemical evolution of tailings over the short term. In the Northern Saskatchewan tailings, the major geochemical processes are less well known, but the potential export of such contaminants as arsenic, nickel and selenium are of major regulatory concern.

The chemical elements for which predictive tools are required to describe their solid-solution distribution over time are: Si, Al, Ca, Mg, K, Na, Fe,

S, C, H^+, Cu, Ni, As, Ba, Co, Mn, Pb, Ti, Se, Sr, and Mo. Radionuclides requiring predictive tools are: U-238, U-234, Th-230, Ra-226, Pb-210, Po-210, Th-232, Ra-228, and Th-228. The major elements are controllers on the geochemical evolution of the tailings whereas the "trace elements" and "radionuclides" influence the "health" of the ecosystem or humans.

3.0 TIME SCALES

Three time scales are of concern for developing a source term model:

(i) the computational time step;
(ii) the time scale for monitoring and regulation; and
(iii) the contaminant release period of the tailings.

The computation time step influences whether mineral dissolution will be modelled as an equilibrium or kinetically controlled process. The contaminant release period of the tailings is influenced by the dissolution rates of minerals and the flux of radionuclides from the tailings. Given present data, it is estimated that a time scale in excess of a century will be required before the flux of radionuclides and trace elements of potential environmental concern will cease.

From a regulatory point of view, two time scales exist in current thinking: the short-term and the long-term. Models to describe the geochemical evolution of tailings are required for both time scales. A time frame of 100 years is often used to define short-term because it is felt by regulatory authorities that institutional controls cannot be guaranteed by our present society for a longer period of time. The long-term can be defined as 100-10,000 years because

(i) previous studies have suggested that most of the export of radionuclides and trace elements of environmental concern occurs within 10,000 years, and

(ii) after 10,000 yr, major climatological changes will likely be more significant factor than the tailings management techniques originally employed.

These time scales are summarized in Figure 1. The figure is composed from kinetic data for dissolution of far-from-equilibrium minerals, mill leaching data, radionuclide decay constants, seasonal considerations, and the hydraulic detention time of groundwater. Analysis of these time scales lead us to suggest the use of a parameter, the chemical retention time in pore water, for relating these time scales to the computational time step. Consider a volume of pore water (V; m^3) influenced by dissolution (r_d; $mol/m^3/yr$), recrystallization (k; yr^{-1}) and hydrological outflow (Q; m^3/yr). The mass balance equation gives the pore water concentration (C) as:

$$V \frac{dC}{dt} = Vr_d - kCV - QC \qquad (1)$$

These kinetics are analogous to those of Rimsted and Barnes (1980) for silica. Defining the chemical residence time (t_c) as the time to displace the mass of C present in V results in

$$t_c = \frac{CV}{r_d} = \frac{1}{k + 1/t_w} \qquad (2)$$

where t_w is the hydraulic detention time of the box (cell) under consideration ($t_w = V/Q$).

Equation (2) shows that the chemical residence time is a function of the hydraulic detention time of the groundwater and the recrystallization rate. Some care must be taken in using this expression because it is specific to the terms considered in the mass balance equation (1) and the kinetic expressions used. But it illustrates the point of concern. It shows that at short hydraulic detention times (e.g., 2 yrs), the chemical retention time (2.1 yrs) is essentially determined by the hydrological character of the tailings when the recrystallization rate is 0.012 yr^{-1}. At long detention times (t = 10,000 yr; t = ∞), the chemical retention time (85 yr) is essentially determined by the chemical processes and is independent of groundwater hydrology.

These calculations also point out that the kinetics of recrystallization of minerals are a key component for estimating pore-water time scales and coupling physical, biological and geochemical processes in models. The paucity of kinetic data in the literature is currently one of the limits for analyzing such processes within a mathematical framework.

4.0 SIMULATION OF AN EQUILIBRIUM MINERAL ASSEMBLAGE

A mineral assemblage containing iron, calcium, aluminum, sulphur, carbon, oxygen and water was selected for reaction-path-code simulation. The following solids occurred in the simulation: Pyrite (FeS_2; .417 mol/kg); Goethite (alpha - FeOOH)*; Amorphorus iron hydroxide ($Fe(OH)_3$(am); 0.305 mol/kg); Gibbsite ($Al(OH)_3$(s); 0.204 mol/kg); Gypsum ($CaSO_4.2H_20$; 0.555 mol/kg); Calcite ($CaCO_3$; 0.02 mol/kg); Mallamerite ($FeSO_4.7H_20$)*; Siderite ($FeCO_3$)*; and Jarosite ($KFe_3(SO_4)_2(OH)_6$)*. The minerals initially present are indicated with their composition per kilogram. The initial quantities reflect fresh tailings in the Elliot Lake area. Those marked by an (*) precipitated during one or more of the simulations. Pyrite and calcite are primary minerals while amorphorus iron hydroxide, gibbsite and gypsum are secondary minerals formed in the mill on the surface of host solids.

The objectives of the simulation are to examine the acidification of the tailings resulting from pyrite oxidation, to obtain insights concerning possible simplifications for coupled systems modelling, and to evaluate the equilibrium hypothesis. The simulation is incomplete because far-from-equilibrium micas, feldspars and other aluminosilicates are not evaluated; however the minerals chosen represent pertinent geochemical features in the tailings.

The calculations were made using CHEMP, a chemical reaction pathway computer program (Garisto and Garisto, 1984). Free energy data were selected from the literature with preliminary critical analysis attempting to ensure that all data are internally consistent. This data base is documented elsewhere (Garisto et al, 1984, 1985; Snodgrass et al, 1985).

Simulation of a Complete Suite of Solids Using Different Oxidants

Two simulations were performed using all solid phases but different oxidants. In the first example (Figure 2a), oxygen was used to titrate the system. In the second example (not shown) the acid-sulphate solution containing Fe^{3+} + Fe^{2+} was used (Fe_T + 2 SO_4^{2-} + H^+ where Fe_T is total iron with $(Fe^{3+})/(Fe^{2+})$ = 10^{-4}). This simulates the addition of pyrite oxidation products to the upper levels of the saturated groundwater zone. The overall effects with regard to solid-phase and pH behaviour are similar.

Calcite ($CaCO_3$) dissolves early in the titration resulting in formation of siderite ($FeCO_3$). Siderite dissolves later in the titration in both cases (see Figure 2a). Gibbsite ($Al(OH)_3$) and pyrite, both initially present, are also depleted in both cases. In the first case, however, $FeSO_4.7H_2O$ is formed and then dissolved in response to oxidation by oxygen; its dissolution results in formation of goethite. In contrast, $FeSO_4.7H_2O$ is formed and remains in the second case, whereas the secondary goethite forms and redissolves; this stability of $FeSO_4.7H_2O$ is maintained by the addition of Fe^{2+} while the dissolution of goethite results from the low pH.

The pH responses to the titration are almost identical (Figures 2b). First, calcite dissolves and buffers the pH at a value of about 6.3. The pH buffer in this case results from an overall reaction between two solid phases:

$$FeS_2(s) + 14FeOOH(s) + 26H^+ = 15Fe^{2+} + 2SO_4^{2-} + 20H_2O \quad (3)$$

Because concentrations of Fe^{2+}, SO_4^{2-} and their complexes are controlled by these solid phases at relatively stable levels, the pH (or H^+ concentration) is also relatively stable. The pH can be calculated from equation (3) as follows:

$$pH = 1/26 (\log K_{so} - 15 \log Fe^{2+} - 2 \log SO_4^{2-}) \quad (4)$$

in which the equilibrium constant (K_{so}) has a value of 98.46. In this case, when the $\log Fe^{2+}$ = -2 and $\log SO_4^{2-}$=1 the resulting pH is about 5. The former values for Fe^{2+} and SO_4^{2-} are close to those predicted and also are reasonable in terms of observations in pyrite oxidation systems. After calcite is depleted, the pH decreases in response to H^+ addition until the FeS_2 - FeOOH buffer is initiated at a pH value of about 5. The pH again decreases after FeOOH is depleted and a slight buffering effect is observed at a pH of about 3.4. This buffering is due to the dissolution of gibbsite.

Further reduction in pH occurs in the oxygen titration until pyrite is depleted, at which point the pH remains stable. In the case of titration by the acid-sulphate solution, further buffering occurs at a pH of about 1 by dissolution of goethite. After the goethite is depleted, the pH again decreases in response to further addition of H^+ in the titrating solution.

The redox responses for the two different oxidants exhibit the most significant differences, but only after the pyrite is depleted in the oxygen titration (Figure 2c). In the oxygen titration the redox potential increases abruptly in response to addition of excess oxygen and subsequent oxidation of Fe^{2+}. In contrast, the addition of Fe^{3+} as the sole oxidant for the acid-sulphate titration does not result in as significant a change in the Fe^{2+}/Fe^{3+} ratios.

Simulation of Pyrite-Free System With a Acid-Sulphate Titration

One simulation was performed to examine chemical evolution in an acid-generating system in which pyrite does not attain equilibrium with the other components in the system. The non-equilibrium condition was simulated by titrating oxidation products into a set of solids devoid of pyrite. A number of notable differences exist.

Although calcite, gibbsite and goethite all dissolve, and jarosite forms and redissolves along the reaction pathway as in the previous two simulations, the absence of siderite formation and the reappearance of goethite is evident. The pH response is also different in that no buffer exists at pH=5; instead the pH is buffered at pH=3.4 by gibbsite. In this case, the FeS_2 - FeOOH buffer has not masked the effect of the aluminum buffer, allowing the latter to become significant. Also, because no significant redox reactions occur in the system, the redox potential remains relatively constant, as exhibited by the relatively stable Fe^{2+}/Fe^{3+} ratios. The changes in the ratio that do occur are due to solubility constraints on Fe^{3+} as well as the stability of Fe(III) and Fe(II) complexes.

Comparison of Simulation Results with Field Observations

Many of the general trends noted in the simulations agree with field studies. Field observations suggest that pH buffering occurs at values of about 6 and also at about 3.5 (Dubrovsky et al, 1985). These pH values agree fairly well with those of calcite and gibbsite shown previously. In addition, the formation of siderite in zones containing residual calcite and the formation of jarosite in active oxidation zones have been postulated from field evidence. This agrees with the model predictions.

Some uncertainty exists in other predictions (field pH and field redox conditions). There does not appear to be a buffering mechanism at pH=5 in the field as is calculated in the simulations. This apparent disagreement may be due to two reasons. Firstly, equilibrium may not actually exist between the pyrite and the goethite phases. Secondly, equilibrium may exist but the thermodynamic characteristics of the ferric hydroxide phase may be different than those specified by the solubility product used in the simulations. If the active ferric solid is less stable than goethite, the buffered pH would be higher than predicted by the simulation model. Reaction of pyrite with an amorphous ferric hyroxide rather than goethite could result in such a condition.

With respect to redox conditions, field data describing concentrations of Fe^{2+} and Fe^{3+} and the trend of pE suggest that the Fe^{3+} concentration is controlled by its solubility relationship with amorphous $Fe(OH)_3$, and that there is no apparent control on Fe^{2+} concentrations. In contrast, the model calculations indicate that an equilibrium exists between pyrite and goethite. Existence of equilibrium between an

"oxidized" phase (FeOOH) and a "reduced" phase (FeS_2) may not intuitively make sense. But it is explained by an equilibrium between

(i) solution (Fe^{2+}) and pyrite,
(ii) solution (Fe^{3+}) and goethite, and
(iii) solution (Fe^{2+}) and solution (Fe^{3+}) via the redox reaction.

At neutral and near-neutral pH, the solution concentration of Fe^{3+} is so low that Fe^{2+} and Fe^{3+} equilibria are maintained, hence allowing goethite and pyrite to coexist at equilibrium. Goethite and pyrite can coexist at equlibrium as long as the amount of oxidant is limited. All of the oxidized phases would be reduced at the start of the simulation only if lower redox conditions were initially imposed upon the system (i.e., more electrons donated to the system).

The disagreement between the field evidence and the simulations suggests that an overall equilibrium does not occur between pyrite and goethite because observed Fe^{2+} concentrations and measured values of pE are not at equilibrium with pyrite (Dubrovsky et al., 1985). The actual control on Fe^{2+} concentrations is not clear, precluding a definitive statement concerning whether equilibrium with pseudo-stable phases or kinetics controls the Fe^{2+} concentrations. It does, however, represent one limitation of using reaction path calculations when pyrite is present.

Geochemical Control on Pyrite Oxidation

For conditions where pyrite oxidation, catalyzed by bacteria, causes pyrite to be out of equilibrium with its environment, one can attempt to include the effects of kinetics in the simulation of an equilibrium mineral assemblage by introducing the reaction products as an oxidant. This has been illustrated above. To determine the rate of production of reaction products, either reaction kinetics or gaseous transport of oxygen or both will be rate controlling.

The interaction of transport and reaction can be examined by solving the diffusion-reaction equation

$$\frac{\partial C}{\partial t} = D \frac{\partial^2 C}{\partial z^2} - KC \qquad (5)$$

in which C is the partial pressure of oxygen in the void spaces of the unsaturated zone, D is the effective diffusion coefficient of gaseous oxygen, and K is the composite first-order rate constant. This equation was solved by assuming steady-state conditions because steady-state is rapidly approached for the time scales considered. The loss of pyrite mass was calculated for finite sized boxes whose thickness is sufficiently small to maintain definition of concentration gradients. This allows us to incorporate the steady-state solution into a box model framework that simulates the time step progression of pyrite oxidation.

The first-order rate constant is a function of several parameters including pH and surface area of pyrite particles. The shrinkage of pyrite was calculated by assuming that spherical particles of a uniform radius are present throughout the media. The effects of pH and microbial activity are simulated by using two extreme values for Kp: 5×10^{-6} m/h reflecting near-neutral pH, abiotic conditions (Nicholson, 1984) and 5×10^{-2} m/hr, reflecting low pH conditions where bacteria are quite active. "Kp", a mass transfer coefficient, is derived from the decay rate "K" by multiplying by the volume of void spaces and dividing by the surface area of the pyrite particles. These data are derived from the tailings characteristics of bulk density = 1.6 g/cc; moisture content = 20%, pyrite content = 0.05 g/g, and pyrite particle diameter = 70 um.

Simulation results are presented in Figure 3 in the form of a sensitivity analysis for two different values of the gaseous diffusion coefficient. The upper value, 5×10^{-4} m^2/h, is characteristic of diffusion through air-filled void spaces while the lower value 5×10^{-6} m^2/h describes molecular diffusion of oxygen in water (completely filled void spaces). The results indicate:

(i) that the oxygen flux into the tailings, and hence, the pyrite oxidation rate and the rate of production of acidity decrease over time; and

(ii) that the oxygen flux (acid production rate) is substantially more sensitive to transport processes than to reaction control.

These results suggest priorities for further research into modelling and management of tailings. These include the following.

(i) More research is required into methods for measuring diffusivity of oxygen in the unsaturated zone of tailings rather than into methods for quantifying reaction rate kinetics. At present, most efforts centre upon characterizing reaction kinetics and temperature relationships.

(ii) More research is required into characterizing the rate at which acid production decreases with time. This would allow estimates of when institutional controls and monitoring could be reduced in scope and/or phased out.

(iii) An effective method to decrease immediately the rate of acid production is to engineer a cover composed of depyritized tailings and devoid of organic carbon. The lower the effective diffusivity of this cover, the lower will be the acid production rate.

SUMMARY

In this paper, an overview of the minerals of concern in uranium mill tailings and an analysis of relevant time scales for modelling their geochemical evolution are presented. For one major uranium-producing area, pyrite oxidation is a major geochemical driving force over the short-term. A simulation of an equilibrium mineral assemblage predicts pH trends which are similar to field observations but predicts absolute pH values and redox conditions which seemingly differ from field observations. The model predictions are dominanted by equilibrium between goethite (Fe00H) and pyrite (FeS_2). Field observations of pH would be predicted by the model if a different oxyhydroxide of Fe(III) occurred. Observations for pe would be simulated if

other phases are present or if the system is not in equilibrium with pyrite. These results suggest that modelling coupled processes in this system requires consideration of pyrite dissolution as kinetically controlled.

Analysis of the geochemical control on pyrite oxidation and resultant acid production suggests that transport processes (diffusion of oxygen) are substantially more important than the pyrite oxidation rate. This suggests that more research efforts are needed to obtain better estimates of the diffusion coefficient of oxygen rather than to estimate the pyrite oxidation rate. A steady-state solution of the diffusion-reaction equation, appropriate time steps and the mass of pyrite remaining in a cell after oxidation can be used for coupling transport and reaction. Simplification of these results to a box format (e.g., the unsaturated zone) allows one to estimate the time dimension of a reaction pathway in the simulation of an equilibrium mineral assemblage in which pyrite oxidation products are the oxidant.

ACKNOWLEDGEMENTS

The authors were stimulated to write this paper by topics proposed for the "International Symposium on Coupled Processes Affecting the Performance of a Nuclear Waste Repository". This work was funded by a research contract from the National Uranium Tailings Program, Department of Energy, Mines and Resources, Government of Canada to Beak Consultants Limited and via a subcontract to Atomic Energy of Canada Ltd. The interaction with the scientific authority (Mr. Walter Harrison) and his colleagues at the National Uranium Tailings Program (CANMET) on this contract, and with fellow workers at BEAK (D. Lush, M. Holloran, P. Groeneweg), at AECL (R. Lemire, F. Garisto) and other institutions (J. Cherry, N. Dubrovsky at the University of Waterloo; O.E. Hileman at McMaster University) are gratefully acknowledged.

REFERENCES

Dubrovsky, N.M., J.A. Cherry, E.J. Reardon and A.J. Vivyurka (1985). "Geochemical evolution of inactive pyrite tailings in the Elliot Lake uranium district: I The groundwater zone". Can. Geotech. J., 22, 110-128.

Garisto, N.C., R.J. Lemire, V.N. Fleer, and F. Garisto (1984). "Chemical modelling of mineral dissolution in the uranium tailings system". Unpublished report. Atomic Energy Canada Ltd., C-8206. 195.3. October 1984.

Garisto, N.C. and F. Garisto (1984). "Reaction path calculations of mineral alteration products: application to nuclear full waste management". Nucl. Chem. Waste Management, 5,17.

Garisto, N.C. R.J. Lemire and F. Garisto (1985). "Chemical modelling in the Uranium Tailings System: Pyrite Dissolution". Unpublished report. Atomic Energy Canada Ltd., C-8206.195.4. March 1985.

Nicholson, R.V. (1984). "Pyrite-oxidation in Carbonate-Buffered Systems: Experimental Kinetics and Control by Oxygen Diffusion in a Porous Media". Ph.D. Thesis, University of Waterloo. pp 176.

Rimsted, J.D. and H.L. Barnes (1980). "The kinetics of silica-water reactions". Geochimica Cosmochimica Acta, 44, 1683-1699.

Snodgrass, W.J. R.V. Nicholson and N.C. Garisto (1985). Descriptive Algorithm Development for Physical, Chemical, and Biological Processes Operational in Uranium Mill Tailings". Report for National Uranium Tailings Program, Government of Canada.

Figure 1: SUMMARY OF TIME SCALES OF CONCERN

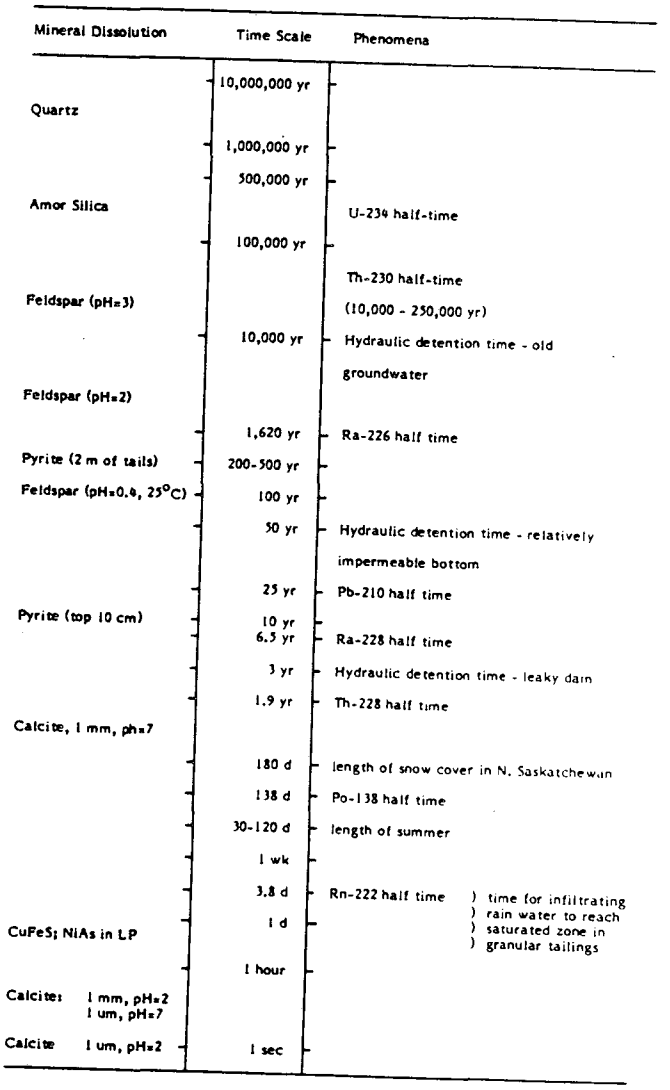

Figure 2a: The abundances of solids as a function of the reaction coordinate oxygen, for the full mineral assemblage

0 - $CaSO_4 \cdot 2H_2$), - FeS_2 (pyrite),
x - FeOOH ( ), - $Al(OH)_3$, (gibbsite),
Δ - $FeSO_4 \cdot 7H_2O$, - $FeCO_3$ (s),
* - $CaCO_3$ (s).

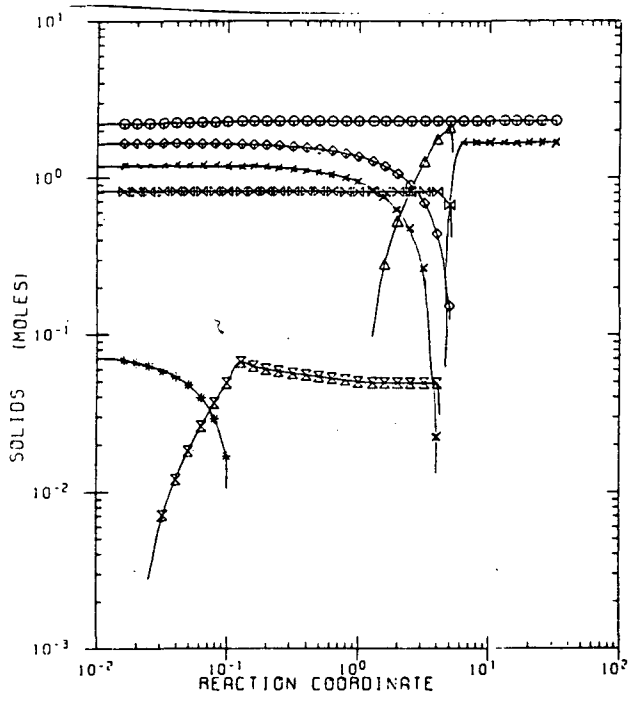

Figure 2b: H^+ concentration as a function of the reaction coordinate oxygen, for the full mineral assemblage

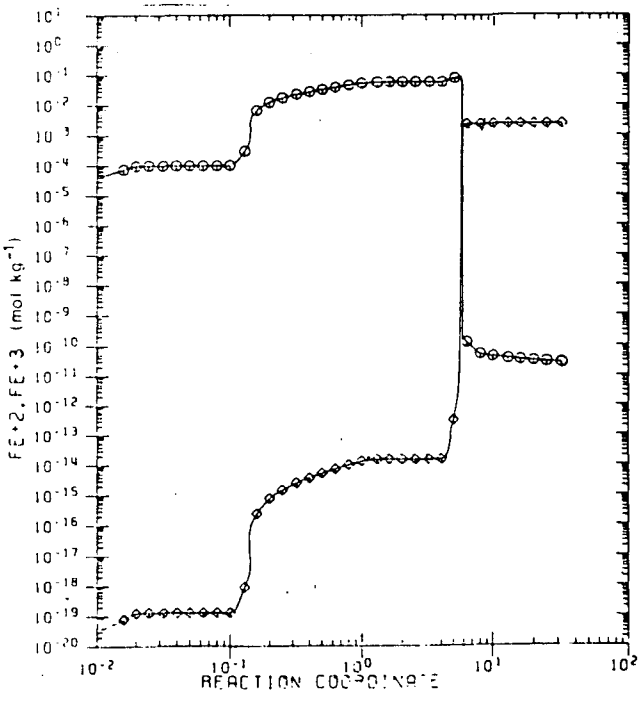

Figure 2c: The concentration of Fe^{2+} (0-) and Fe^{3+} (◇ -) as a function of the reaction coordinate, oxygen for the full minral assemblage.

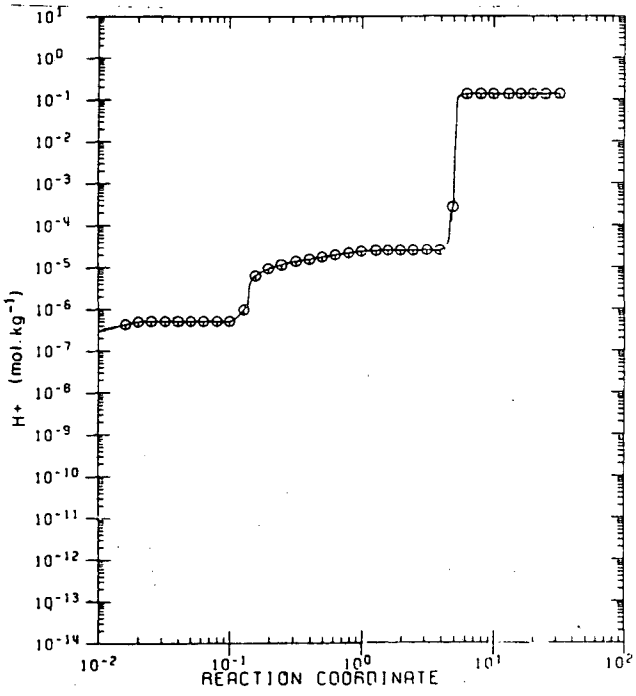

Figure 3: Total Flux of Oxygen with Time

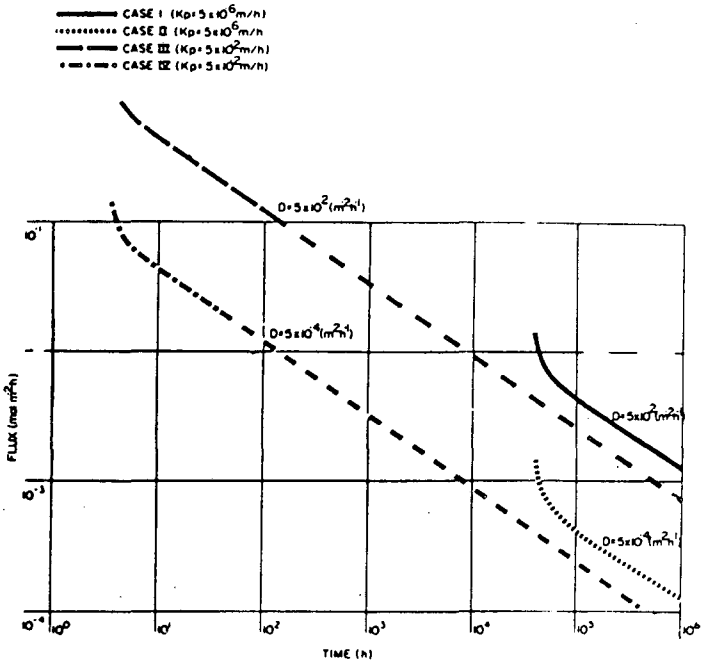

CHEMICAL AND DIFFUSIONAL EFFECTS IN A THERMAL GRADIENT: RESULTS OF RECENT EXPERIMENTAL STUDIES AND IMPLICATIONS FOR SUBSEABED DISPOSAL OF NUCLEAR WASTE

Edward C. Thornton and William E. Seyfried, Jr.

Department of Geology and Geophysics
University of Minnesota
Minneapolis, MN 55455

ABSTRACT

Solute transport in response to a thermal gradient (thermal diffusion or the Soret effect) is likely to be an important consideration in the disposal of nuclear waste in low-permeability, fluid-saturated media. Thus, thermal gradient experiments and a large-scale heat transfer experiment were conducted with marine clay and inert matrices to assess Soret diffusion and rock alteration effects. These data are particularly applicable to the subseabed disposal concept, but provide a basis as well for assessing mass transport phenomena for clay backfill materials.

INTRODUCTION

Subseabed disposal of high-level nuclear waste is currently being considered as an alternative to onland disposal options (Hollister, 1977). Desirable features of marine, clay-rich sediments include high plasticity, low permeability, and high adsorptive capacity. Feasibility assessment of subseabed disposal requires, however, detailed knowledge of the effect of temperature on solution-mineral equilibria and adsorption processes; information has been obtained for this purpose through sediment-seawater experiments conducted at constant temperature (Seyfried et al., 1980; Thornton, 1983). The chemical environment in the immediate vicinity (near-field region) of a buried waste canister will in addition be characterized by thermal gradients wich will promote chemical and thermal diffusional transport. This aspect has been recently studied by conducting a number of thermal gradient experiments and, on a larger scale, through a heat transfer experiment conducted with marine clay. Results of these experiments are summarized here to illustrate the nature of coupling of chemical and thermal effects in the near-field subseabed environment and possible changes in the geomechanical properties of marine clay resulting from these effects.

THERMAL GRADIENT EXPERIMENTS

Marine pelagic clay from the North Pacific and North Atlantic was used for thermal gradient experiments at the University of Minnesota. A titanium-lined pressure vessel specifically designed for this purpose provided a stable temperature gradient of 200°C between a "hot" zone (300°C) and a "cool" zone (100°C) over a distance of approximately 30 cm at seafloor pressures of 500 bars (Thornton, 1983; Thornton and Seyfried, 1983). Thermodiffusional transport was observed to produce significant separation of aqueous components between the "hot" and "cool" zones in less than 1000 hours, with the solute migrating towards the "cool" zone (Fig. 1). Soret coefficients were obtained by monitoring the steady

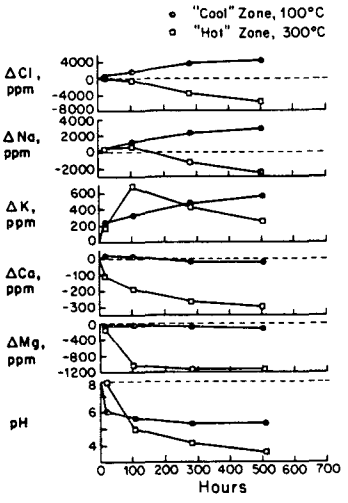

Figure 1. Relative change in fluid composition of "hot" and "cool" zones with time in a typical thermal gradient experiment conducted with a mixture of marine pelagic clay and seawater.

state distribution of Na^+ and Cl^- in "hot" and "cool" zone pore fluids. The distribution of these species was totally a function of the thermal gradient in that they were unaffected by water-rock interaction. K^+ was initially enriched in the "hot" zone owing to rock-water interaction but was subsequently mobilized towards the "cool" zone in response to Soret diffusion. Other components, notably Mg^{2+} and Ca^{2+}, were retained in varying degrees in the "hot" zone due to formation of stable alteration phases such as smectite and anhydrite. Mg mobility, in particular, is important in this regard as it has an important role in regulating pH of the "hot" zone fluids. Silica depletion in the "hot" zone was also observed owing to significant mass transport by diffusion down the thermal gradient.

To complement the sediment experiments, thermal gradient experiments were performed with seawater and alumina as an inert matrix in order to obtain diffusional data in the absence of rock-water interaction effects. These experiments permitted accurate measurement of Soret coefficients of various solute components for the temperature gradient of 300°C to 100°C and for lower temperatures, down to 50°C, where data has been obtained in previous investigations. Thus, we are now able to assess diffusional transport

in a thermal gradient over the entire range of temperatures that would exist during the lifetime of a nuclear waste repository (Seyfried and Thornton, in press).

IN SITU HEAT TRANSFER SIMULATION EXPERIMENT

To model the entire three dimensional zone around a buried waste canister, a heat transfer experiment was conducted by Sandia National Laboratories at the Naval Ship Research and Development Center, Annapolis, Md (Crisenzo and Silva, 1981; Percival, 1982). This experiment utilized an autoclave sufficiently large to contain one cubic meter of pelagic clay overlain by two cubic meters of artificial seawater; the design employed effectively permitted modelling of both the far-field and the near-field/far-field transition zone. The autoclave was maintained at approximately 500 bars and 5°C and contained an electrical heat source emplanted in the sediment (Fig. 2). The thermal gradient

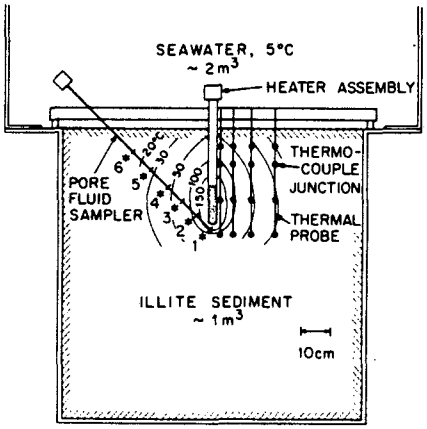

Figure 2. Schematic illustration of heater, pore fluid sampler, and thermocouple and pore fluid sample locations (*) utilized during in situ heat transfer experiment.

ranged from approximately 270°C adjacent to the heater to 150°C within a distance of about 3 cm; a pore fluid sampler collected pore fluids from the sediment over the temperature range from about 150°C to 5°C after 20 days of operation.

Analysis of the pure fluids and chemical/mineralogical characterization of the sediments indicate that two decoupled systems existed, one near the heater at temperatures > 170°C and the other at < 170°C (Seyfried et al., 1985). Anomalous concentrations of sodium and significant amounts of analcime, a sodium silicate, were found adjacent to the heater. Mass balance considerations indicate that the sodium was introduced by the convective circulation of salt water from the tank above the sediment through a disrupted zone adjacent to the heater. McTigue et al. (1985) have also suggested that pore pressure measurements obtained near the heater during the experiment indicate fluid penetration. The hotter zone, furthermore, exhibited substantial sediment alteration owing to mass transfer of silica away from the heat probe via a combination of chemical and thermal diffusion; this process may have further promoted convective circulation near the heater owing to enhanced permeability of the sediment. Permeability decreased markedly at the edge of the hotter zone due to silica (quartz) precipitation, however, effectively eliminating mass transport between the hot and cool zones. The cooler zone was thus characterized by a normal diffusional regime unaffected by physical and chemical effects in the hot zone (Fig. 3). Soret coefficients calculated from the chemistry of the pore fluids in

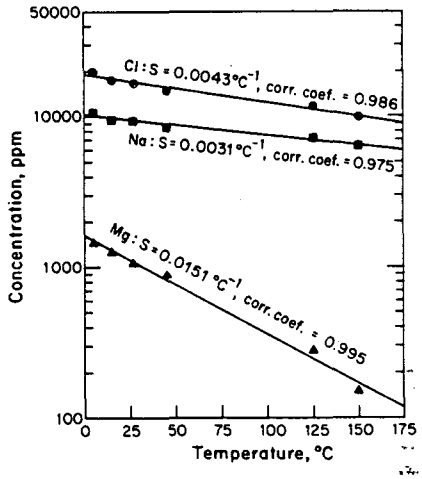

Figure 3. Semilogarithmic plot of aqueous concentrations of Cl, Na, and Mg versus temperature for the in situ heat transfer experiment. Values are presented for Soret coefficients with correlation coefficients based upon a linear regression analysis of the data.

this zone were found to be consistent with those obtained in thermal gradient experiments conducted at the University of Minnesota (Thornton, 1983; Seyfried et al., 1985).

SUMMARY

Results of thermal gradient experiments have provided much useful data for evaluation of the Soret effect in the immediate vicinity of a radioactive heat source and have provided insight on geomechanical effects resulting from mass transfer of silica and rock alteration effects. This information is directly applicable to subseabed disposal but the implications of these data should also be considered for nuclear waste disposal in crystalline rock employing clay backfill materials.

ACKNOWLEDGMENTS

We gratefully acknowledge research support by Sandia National Laboratories under contracts 74-1158, 16-3105, and 25-5645.

REFERENCES

Crisenzo, S. and Silva, A.J. (1981). "Simulation Experiment," Subseabed Disposal Annual Report, January-December 1980, Sandia National Laboratories, Albuquerque, N.M.

Hollister, C.D. (1977). "The Seabed Option," Oceanus, v. 20, p. 18-25.

McTigue, D.F., Lipkin, J., and Bennet, R.H. (1985). "Isothermal Mechanical Response of Sediments During the ISHTE Simulation Experiment," SAND83-1847, Sandia National Laboratories, Albuquerque, N.M.

Percival, C.M. (1982). "Laboratory Simulation of Deep Ocean In Situ Heat Transfer Experiment," Marine Tech '82, Proc. Annual Conference of Marine Technology Society, September, 1982.

Seyfried, W.E. and Thornton, E.C. (in press). "Experimental Studies of Water-rock Interaction Processes in a Thermal Gradient," Subseabed Disposal Annual Report, April 1984 through April 1985, Sandia National Laboratories, Albuquerque, N.M.

Seyfried, W.E., Thornton, E.C., and Janecky, D.R. (1980). "Seawater-sediment Interaction at 300°C, 500 Bars: Implications for Seabed Disposal of Nuclear Wastes," Proc. 3rd International Symposium on Water-Rock Interaction, Edmonton, Canada, p. 135-137.

Seyfried, W.E., Jr., Thornton, E.C., and Sayles, F.L. (1985). "Heat-transfer Experiment in Marine Pelagic Clay: Implications for Subseabed Disposal of High-level Radioactive Waste and Contact Metamorphism in the Guaymas Basin, Gulf of California," Chemical Geology, in press.

Thornton, E.C. (1983). "Experimental and Theoretical Modeling of Sediment-seawater Hydrothermal Interaction at Constant Temperature and in a Thermal Gradient: Implications for the Diagenesis and Metamorphism of Marine Clay and the Subseabed Disposal of Nuclear Waste," Ph.D. Thesis, University of Minnesota, Minneapolis, MN, 193 pp.

Thornton, E.C. and Seyfried, W.E., Jr. (1983). "Thermodiffusional Transport in Pelagic Clay: Implications for Nuclear Waste Disposal in Geological Media," Science, v. 220, p. 1156-1158.

FLOW AND TRACER EXPERIMENTS IN CRYSTALLINE ROCKS. RESULTS FROM SEVERAL SWEDISH IN SITU EXPERIMENTS

H. ABELIN, L. BIRGERSSON, J. GIDLUND, L. MORENO, I. NERETNIEKS, S. TUNBRANT
Department of Chemical Engineering, Royal Institute of Technology, S-100 44 Stockholm, Sweden

BACKGROUND

In a final repository for radioactive waste in crystalline rock, water flowing in the fractures may transport the radionuclides eventually leached from the waste. To be able to predict the migration of the radionuclides the processes involved must be understood. To quantify the processes, data from flow and transport in real fractures under realistic conditions are needed. Models used for prediction must include descriptions of the important processes and mechanisms.

Most previous studies concerning water flow in rocks are based on the assumption that the water flow can be described as porous media flow. This might be true for very large distances where the flow would encounter a multitude of fractures, and some averaging may be conceivable at the scale considered.

Transport over short distances, i.e. in the vicinity of the canister, most probably occurs in individual fractures. On an intermediate scale where more than a few fractures conduct the flow, well-type tracer tests alone cannot give the detailed information needed to understand dispersion and sorption phenomena in fissured rock. Actual tracer tests are needed to obtain data on pathways and flow porosities. Tests with sorbing tracers are needed to compare predictions based on models and laboratory data, i.e. to validate the transport models.

The migration modelling in the safety analysis for a repository in granitic rock is based on the assumption that if and when any radionuclides are leached from the waste, practically all of the important radionuclides will interact chemically or physically with the bedrock and will thereby be considerably retarded. The magnitude of this retardation depends upon the flow rate of the water, the uptake rates and equilibria of the reactions as well as the surface area in contact with the flowing water.

PURPOSE

The main purpose of the two investigations performed in the Stripa mine is to understand and describe water movement in sparesly fractured crystalline rock. The first experiment, now finished, concerned water flow within a single fracture and also dealt with sorbing tracers interaction with the rock matrix, such as sorption and diffusion into the matrix. The second experiment, now underway, concerns water flow paths within a larger block of rock.

Flow and migration within a single fracture (2-D)

The main purposes of this experiment were to investigate if it is possible to extend results on sorption and retardation of radionuclides in granitic rock, obtained from laboratory experiments, to a real environment with migration distances up to 5 m and to try to determine the extent of channelling within single fractures.

Flow and migration within a large rock volume (3-D)

The main purpose of this experiment is to investigate the spatial distribution of water flow paths in a larger block of rock. Migration distances of up to 50 m are utilized. Flow parameters like mean residence time, dispersion, longitudinal as well as transverse, will also be studied.

EXPERIMENTAL DESIGN

The experiments are performed at the 360 m level. Water flows constantly into drifts at this level since it is located well below the water table.

The 2-D experiment

The design of the experiment was based on the idea that reasonably well defined individual fractures can be located and that tracers, non-sorbing and sorbing, can be introduced into the natural water flow within a single fracture without a large disturbance of the flow field.

Almost all water coming out from the fracture at the face of the drift was collected. Figure 1 shows the layout of the test site with two fractures and five injection holes intersecting the fracture planes. Each of the fractures had about 15 sampling holes at the face of the drift. Tracers, sorbing and non-sorbing, were only injected into fracture number 2.

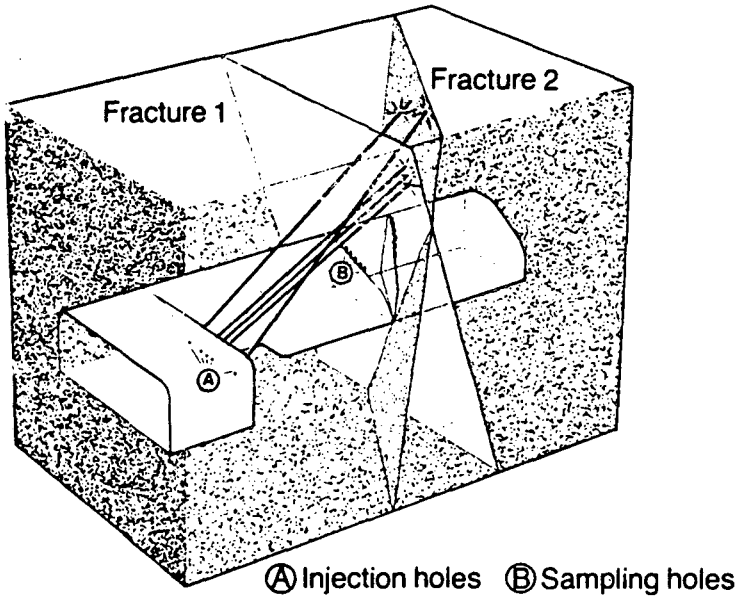

Figure 1. Schematic view of the 2-D test site.

Migration distances of 5 and 10 m have been used, which is more than one order of magnitude larger than distances that have been used in the laboratory experiments, Moreno et al. 1984 [1]. Conservative (non-sorbing) tracers were used to characterize the flow within the fracture.

The following sorbing tracers, analogs for radionuclides, were used: Cs (I), Sr (II), Eu (III), Nd (III), Th (IV), U (IV and VI). The sorbing tracers were continuously injected at one injection point during seven months (Sr 5 1/2 months, U 3 months).

The results from the runs with the non-sorbing tracers and laboratory data on sorption and porosity have been used to predict the breakthrough curve for a sorbing tracer. The predicted curve would later be compared with the experimentally obtained breakthrough curve.

Of the sorbing tracers only Sr was predicted to reach the sampling holes within the time of the experiment, the rest of the tracers would be sorbed in the rock surrounding the injection point. To make it possible to analyse surface concentration and penetration depth of the sorbing tracers, part of the fracture around the injection point was excavated.

The 3-D experiment

From the test site, which has a total length of 100 m, three vertical holes (length 70 m) have been drilled.

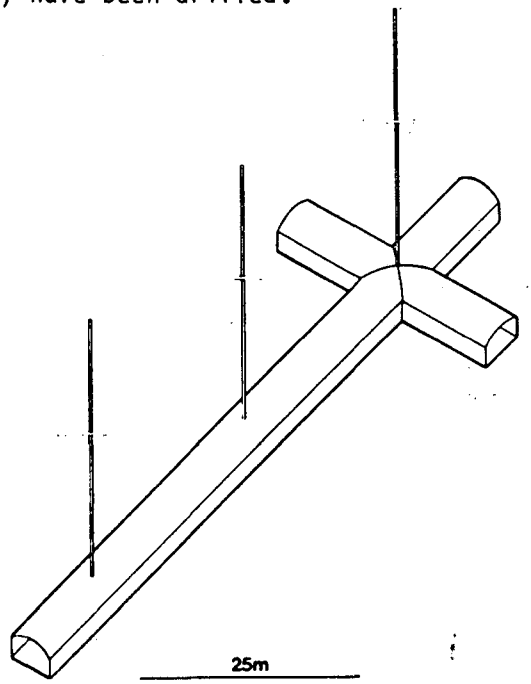

Figure 2. Layout of the 3-D test site with 3 vertical injection holes.

Injection of conservative (non-sorbing) tracers are carried out from a total number of 9 separate high permeability zones within the three vertical holes, each zone about 2.5 m in length. The injection zones are located between 10 and 55 m above the test site. The tracers will be injected continuously for 1 year. The injections are carried out with a "constant" over pressure, approximately 10-15% above the natural pressure. The concentrations of the injected tracers are between 1000 and 2000 ppm, and the different flow rates vary from 1 to 20 ml/h. The following tracers are injected: Uranine, Eosin blueish, Eosin yellowish, Phloxine B, Rose Bengal, Elbenyl Brilliant Flavine, Duasyn Acid Green, Bromide and Iodide.

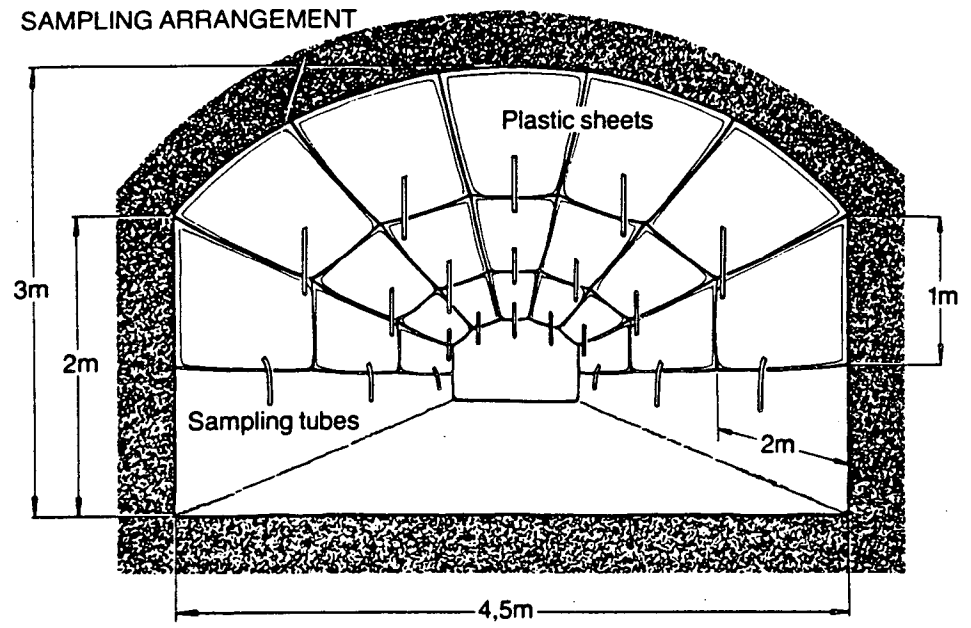

Figure 3. Sampling arrangement at the 3-D test site.

The upper part of the test site has been covered with plastic sheets, each sheet with an area of about 2 m^2. A total number of about 350 sheets serves as sampling areas (points) for water emerging into the upper part of the test site. The sampling arrangement completely covers a surface area of 700 m^2. When sampling over an area the spatial distribution of water flow path ways can be obtained. The presence of the cross increases the resolution of the 3-dimensional distribution of tracers in that part of the test site.

MODELLING OF TRACER TESTS

Tracer tests are analysed using different models. Hydraulic data such as permeabilities, fissure widths and flow porosities are evaluated by means of tracer test with the non-sorbing species. Tracer interaction mechanisms with the matrix for sorbing species are evaluated and compared with laboratory data when available.

The following models have been considered:

- Advection-dispersion-surface sorption model (A-D). This model includes hydrodynamic dispersion in the fissures and sorption onto the surface of the fissures, but no diffusion into the matrix. Flow through several individual fissures may be considered.

- Advection-dispersion-matrix diffusion model (A-D-D). The model describes flow through an individual fissure including, moreover, diffusion into the rock matrix and sorption onto the surface of the microfissures within the rock matrix.

- Advection-channeling-matrix diffusion model. In this case the dispersion is taken in account by channeling. Channeling occurs when water flows through non-interconnected or seldom connected channels with different water velocities. Dissolved species will be transported different distances over a given time.

The concentration at the outlet, for the advection-dispersion model (A-D), can be written in a condensed form as:

$$C(t) = C_o\ P_f\ f(Pe,t_w,R_a,t)$$

C_o is the injection concentration, P_f accounts for dilution effects, Pe is the Peclet number, t_w the water residence time, R_a is the surface retardation factor. When fitting the data from the runs with the conservative tracers (R_a=1), values for the parameters P_f, t_w and Pe will be obtained.

The corresponding outlet concentration for the advection-dispersion-matrix diffusion model (A-D-D) is:

$$C(t) = C_o\ P_f\ f(Pe,t_w,A,t)$$

The A parameter accounts for the interaction with the solid matrix and includes data on diffusion into the matrix and sorption within the matrix. The fitting of experimental data to this model was done in two ways. It was either a three parameter fit giving values of Pe, t_w and P_f where A is calculated from laboratory data or a four parameter fit where also the value of A was determined by the fitting procedure.

The corresponding outlet concentration for the advection-channeling-matrix diffusion model is:

$$C(t) = C_o\ P_f\ f(\sigma_1,t_w,D_D,t)$$

The D_D parameter accounts for the interaction with the solid matrix and includes data on diffusion into the matrix and sorption within the matrix. σ_1 is the standard deviation in the log-normal distribution of channel widths. The fitting of experimental data to this model was done in two ways. It was either a three parameter fit giving values of σ_1, t_w and P_f where D_D is calculated from laboratory data or a four parameter fit where also the value of D_D was determined by the fitting procedure.

In general, the models were solved for a constant concentration in the injection hole. This boundary condition gives large errors when the concentration in the matrix near the injection point is calculated using A-D-D model. In this case a constant flux is used as boundary condition at the injection point.

RESULTS

Water flow monitoring (2-D)

Figure 4 shows the results from the water flow monitoring in the sampling holes of the two fractures. Also the tracer flux from the different sampling holes is presented.

As can be seen in Figure 4, the water flow is unevenly distributed within single fractures. This type of flow pattern was also seen in the fracture used in a preparatory investigation, Abelin et al. (1982) [2].

Water flow monitoring (3-D)

The results from the water flow monitoring in the 3-D site shows that water does not flow uniformly in the rock over the scale considered (700 m^2), but seems to be localized to wet areas with large dry areas in between.

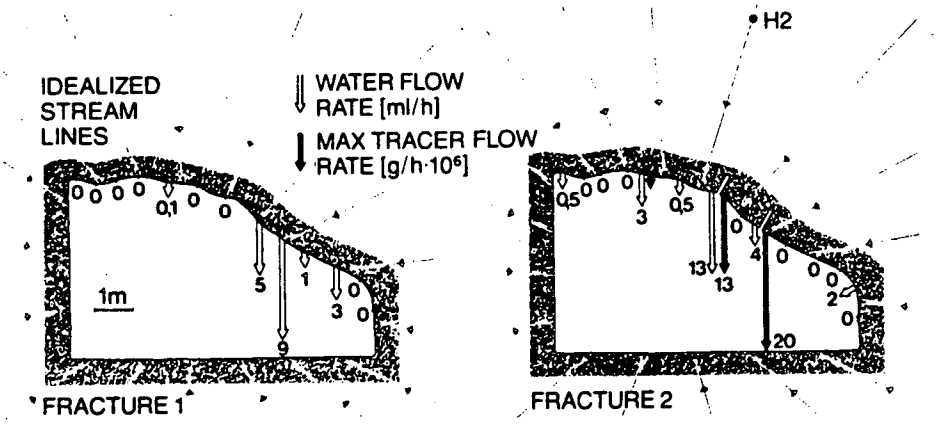

Figure 4. Water flow rates in fractures 1 and 2 (2-D).

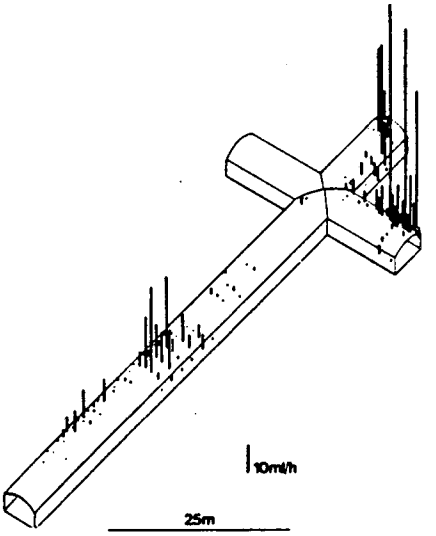

Figure 5. 3-D site. Water inflow rates into the sampling areas (before drilling the injection holes).

Measurable amounts of water emerge into just 1/3 of the 350 sampling areas. 10% of these "wet" sampling areas give more than 50% of the total water inflow.

Non-sorbing tracer injection and modelling (2-D)

Figure 6 shows the breakthrough curve for Uranine at one of the sampling holes in fracture 2. It also shows the fit between different models and experimental data.

As can be seen in Figure 6 it is possible to obtain a good fit with any of the choosen model concepts. It is not possible to select between the models with the results from this experiment only. Some of the mechanisms and their parameters have to be determined independently.

Table I and II shows the flow parameters obtained when fitting the models to experimental data, obtained from two different sampling holes.

The A-parameter in the three and four parameter fits of the A-D-D' model for sampling hole 2-6, Table I, only differs with a factor 1.4. On

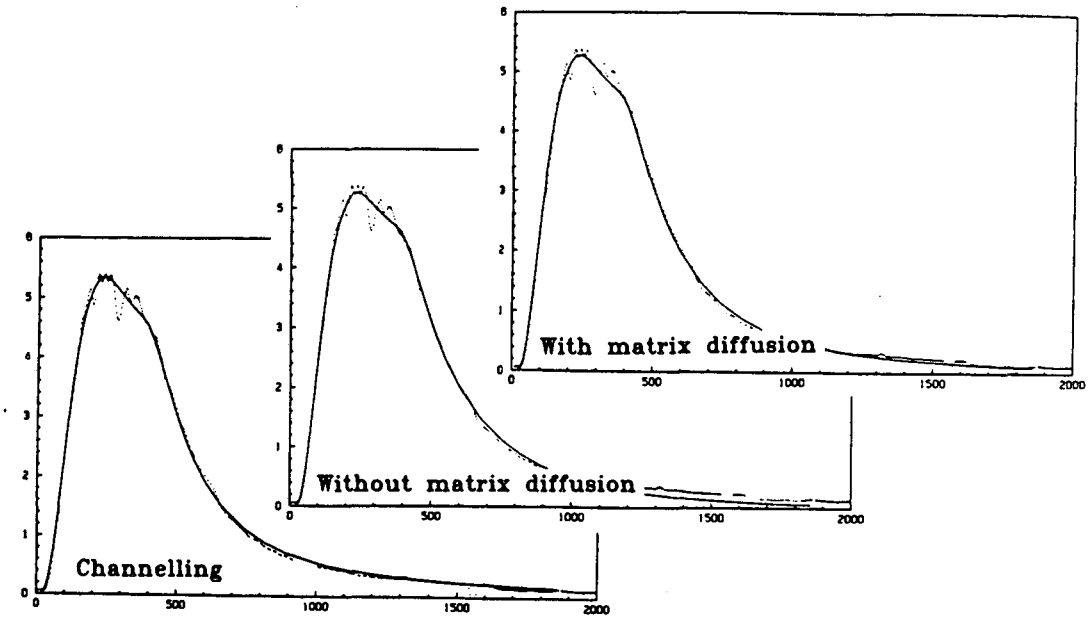

Figure 6. Breakthrough curve for fracture 2 and the fit of different models (2-D).

the other hand the A-parameter for sampling hole 2-8, Table II, in the four parameter fit, was found to be 133 compared with a value of 30 000 when independent laboratory data were used to determine A. This indicates a high interaction with the rock matrix. This seemingly large interaction may be due to presence of stagnant water zones into which the tracer can diffuse, Moreno et al. (1983) [3].

Calculation of fracture "widths" (2-D)

Any calculations of the fracture openings will include some assumptions on the properties within the fracture.

The average volume of the fracture could be determined from measuring the flow rate (Q) over a breadth (B) of the fracture and the residence time (t_w) of the water. We call this the mass balance fracture width.

$$d_f = f(Q, t_w, L, B)$$

L is the path length. When calculating d_f one assumes that all water collected over the breadth B passes the injection point and that the injected tracer directly enters this flow.

Another property of interest is that equivalent fracture width which would permit a certain flowrate at a given pressure drop (Δh). This we call the cubic law fracture width.

$$d_c = f(Q, \Delta h, L, B)$$

A third equivalent fracture width is that which would give a certain water velocity for a given pressure drop. This we call the frictional loss fracture width.

$$d_l = f(\Delta h, t_w, L)$$

Table I. Flow parameters from model fitting, sampling hole 2-6 (2-D).

Flow par.	A-D	A-D-D		Channelling	
		3 par.	4 par.	3 par.	4 par.
P_f	3.0	2.8	2.7	2.8	2.5
t_w, h	366	293	279	348	291
Pe	1.96	2.33	2.46	-	-
A	-	4926	3548	-	-
σ_1	-	-	-	.40	.36
$D_D \cdot 10^7$	-	-	-	2.65	7.88

Table II. Flow parameters from model fitting, sampling hole 2-8 (2-D).

Flow par.	A-D	A-D-D		Channelling	
		3 par.	4 par.	3 par.	4 par.
P_f	10.5	10.5	8.5	11.5	8.4
t_w, h	710	548	44.5	530	90
Pe	0.86	1.16	36.9	-	-
A	-	30000	133	-	-
σ_1	-	-	-	.47	.17
$D_D \cdot 10^7$	-	-	-	2.65	48.49

Table III. Calculated equivalent fracture widths (2-D).

Sampling hole	$K_{pf} \cdot 10^6$ [m/s]	linear			radial		
		d_f	d_1	d_c [μm]	d_f	d_1	d_c
2-6	1.1	240	1.1	6.7	130	1.2	5.5
2-8	3.4	280	2.0	10	150	2.0	8.5
4*	1.5	2200	1.3	16	1200	1.4	13
5*	0.75	1500	0.9	11	820	0.96	9.1

* Fracture in preliminary investigation. Abelin et al. (1982) [2].

There is a large difference between the different calculated equivalent fracture widths, Table III. It should be noted that d_c underestimates the mean residence time for the water and d_1 corresponds to a fracture that can not carry all the water actually measured, there would have to be several of these fracture within the fracture "plane".

Comparison with other field data

The results from the 2-D experiment, Table I, II and III, are compared with results from another tracer test in crystalline rock over a larger distance (30 m), carried at Finnsjön area. Iodide and strontium were here simultaneously injected, during 350 h, at a depth of about 100 m. The detection hole was located at 30 m distance where water was continuously pumped up to get a drawdown zone. The results (Moreno et al., 1983) [3] are shown in Table IV.

Table IV. Flow parameters from model fitting for experiments at the Finnsjön area.

	A-D-D		Channelling	
Flow par.	3 par.	4 par.	3 par.	4 par.
P_f	370	334	383	336
t_w, h	38.5	18.3	41.4	18.8
Pe	5.24	86.9	-	-
A	30000	320	-	-
σ_1	-	-	0.285	0.072
$D_D \cdot 10^7$	-	-	0.155	7.24
Fracture width				
d_f, µm	981	466	1060	479
d_1, µm	61	89	59	88
d_c, µm	155	155	155	155

In the Finnsjön tracer test the water residence time was shorter (about 20-40 hrs) than in the Stripa 2-D runs.

A dispersion length of about 1.9 m was obtained for sampling hole 2-6. For sampling hole 2-8 these lengths were 0.12 and 3.9 m when 3 or 4 parameters are included in the fitting process. In tracer test at Finnsjön these values were 0.34 and 5.7 m respectively. The low dispersion obtained when 4 parameters are fitted may be explained by the low value of A. Part of the spreading is accounted by the model as diffusion into the matrix and thus not included in the dispersion.

These comparisons show that the Stripa test 2-8 has a shorter dispersion length than the test in Finnsjön. On the other hand σ_1 is higher in the Stripa run. The principal difference between the two tests is the different travel lengths used (4.5 m in Stripa and 30 m at Finnsjön). A compilation of dispersion lengths from experiments in crystalline rocks, Neretnieks 1985 [4], seems to indicate that the dispersion length increases with distance.

Non-sorbing tracer injection (3-D)

After 6 months of injection (April-85), tracers from at least 5 injection zones are seen in about 35 sampling areas (see Figure 7 and 8).

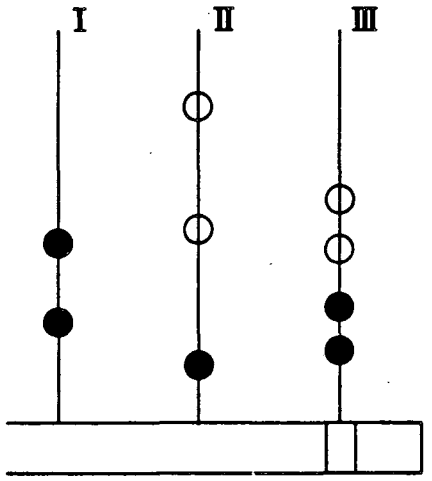

●-Injection points from which tracers have emerged into the 3-D test site.

Figure 7. Tracers emerged into the test site (3-D).

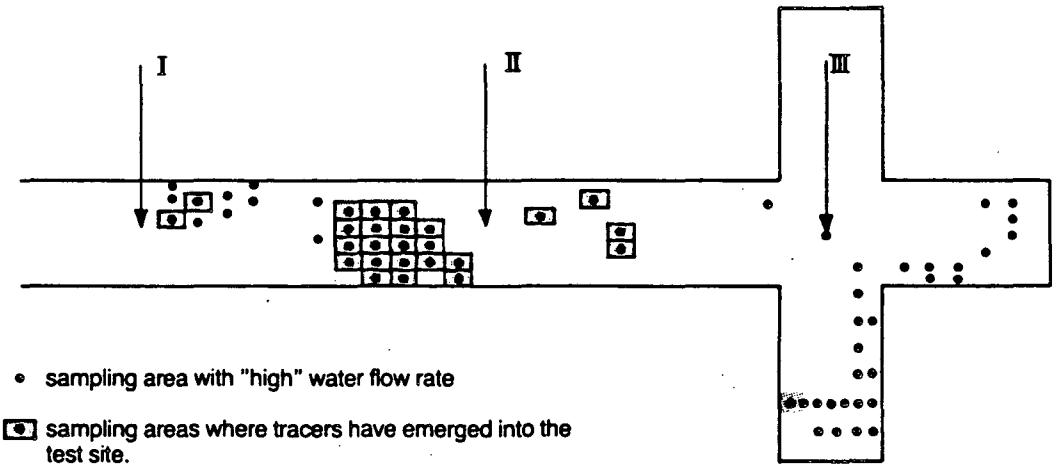

Figure 8. Tracer distribution (3-D).

Looking at Figures 7 and 8 it is remarkable that the tracer injected closest to the drift in hole III (Br^-), has not been found in any of the sampling areas close to hole III, but in many of the sampling areas around hole II.

Figure 8 shows those sampling areas that have "high" water flow rates and in which of these tracers have been found.

Results from the injection of sorbing tracers

The flow parameters obtained in the runs with the conservative tracers and independent laboratory data on sorption and porosity have been used to predict the breakthrough curve for Sr. Sr was predicted to reach the sampling holes well within the time of the experiment. However, Sr did not arrive in detectable concentrations at the sampling holes. As mentioned earlier, part of the fracture has been excavated. Figure 9 shows the concentration of Cs on some points of the fracture surface. It also shows the concentrations in the matrix.

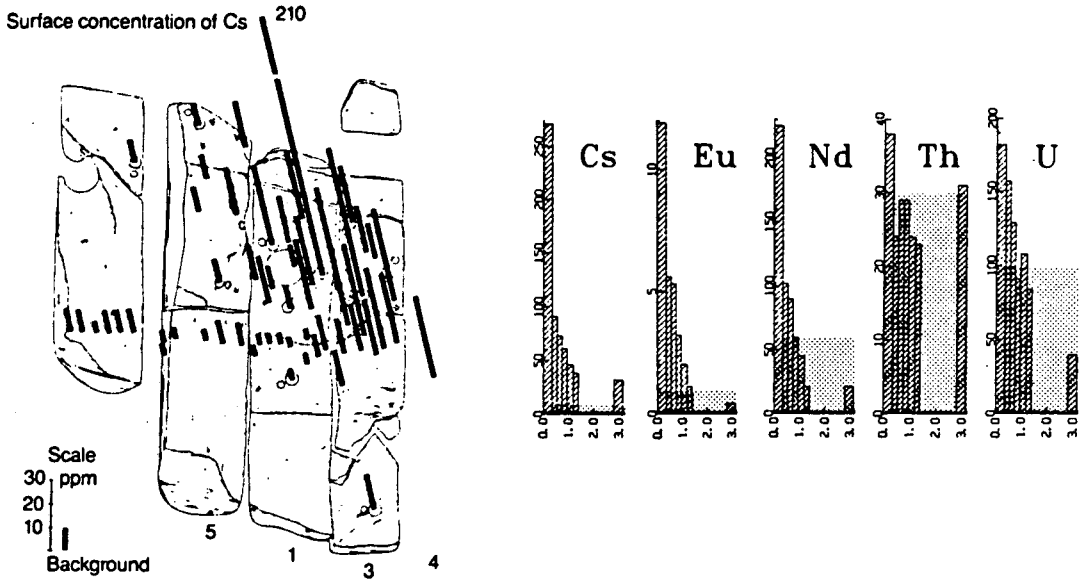

Figure 9. Excavated fracture with surface and matrix concentrations of Cs (2-D).

It can be seen in Figure 9a that there are elevated concentrations of Cs around the injection point, but there seems to be an area to the right of the injection hole which has the highest concentrations. This could indicate that the injected water was not evenly distributed around the injection point but had a prefered direction of flow.

Figure 9b shows concentration profiles into the rock obtained in one of the samples taken close to the injection hole.

It can be seen in Figure 9b that elevated concentrations of Cs, Eu and Nd, at this sampling point, can be found to a depth of 1.4 mm into the matrix.

In the Finnsjön test, a very high concentration solution of Sr was injected. This high concentration of Sr gives a low volume sorption coefficient, Sr behaved almost as a non-sorbing tracer. Probably precipitation of Sr also occurred within the fracture due to the high concentration.

DISCUSSION AND CONCLUSIONS

There are some inherent difficulties to interpret tests with sorbing tracers. Among these one could mention the variation in the natural content of the tracer over the fracture surface, variation in mineral composition giving different K_d values at different sites in the fracture and variations of the thickness of the fracture filling and coating materials.

As can be seen in Figure 6 it is possible to obtain a good fit with all of the models. The fitting thus cannot differentiate between the mechanisms. The correct mechanism(s) must be selected by some other independent process.

The calculated surface concentrations and the concentration profiles within the rock matrix could partly be confirmed by experimental data. They show sorbing tracers concentration profiles into the rock matrix, which can be explained by matrix diffusion.

Supporting in-situ experiments with the aim to ascertain a connected pore system in "undisturbed" granitic rock have been performed in the Stripa mine at the 360 m level (Birgersson et al., 1984) [5]. A mixture of conservative tracers (Uranine, Cr-EDTA and I^-) were injected for a time period of months. The subsequent analysis of tracer content close to the injection hole showed that all three tracers had migrated cm's to tens of cm's into the rock matrix. The penetration depths were in all cases beyond the zone disturbed by the presence of the injection hole. Therefore, these experiments indicate the existence of a connected pore system in "undisturbed" granitic rock at levels relevant for a nuclear waste repository.

Available observations show that it is not realistic to treat a fracture as two planar parallel surfaces with a constant width. Blocks of rock can not hover over each other but have to have points where they are in contact. If this is the only effect that causes channelling the direction and magnitude of the channels would be randomly distributed and there would not be any preferred direction for the water flow. The flowing water in the channels might, however, in some way affect the channels, so that preferred flow directions might develop with time. If there is a preferred direction of the channels, the results of a tracer test must be different depending on if the induced pressure drop is perpendicular to or parallel with the direction of the channels. The present experiment has given no information which could be used to determine preferential flow directions.

Our present concept of flow in a fracture is that there are different channels which may mix their waters at irregular distances. The channels may have zones of stagnant or near stagnant water which may be reached mainly by diffusion. This is illustrated in Figure 10.

With this concept of the fracture it is easy to see the difficulties to model the response of tracer tests in natural fractures in detail.

In the 2-D experiment, diffusion into the matrix was observed by direct observation of penetration depths, channeling was observed by using a large amount of collecting points. The presence of stagnant "lakes" was

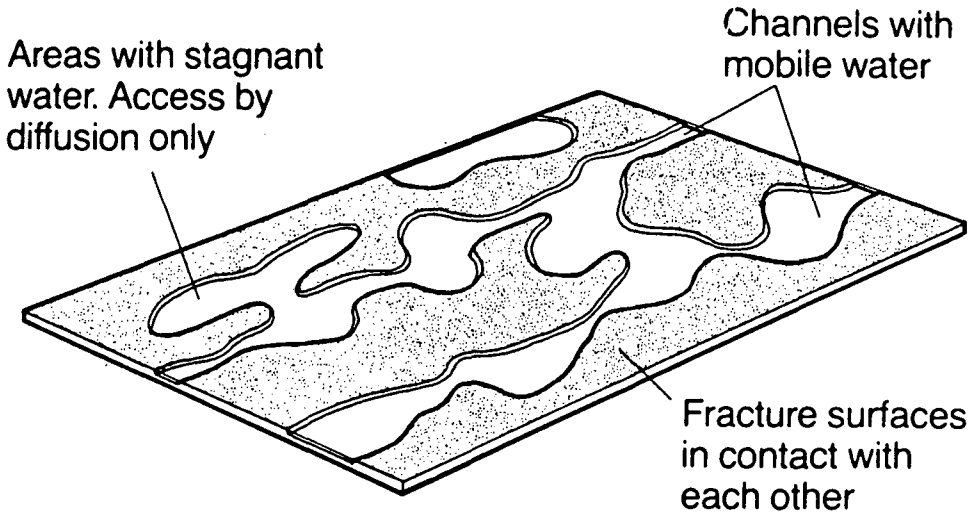

Figure 10. Concept of water flow within a fracture.

not observed directly but inferred from general observations on the necessity of points of contact between rock blocks. The water monitoring in the 3-D test site shows that water does not flow uniformly in the rock but seems to be localized to wet areas with large dry areas in between.

The observed fracture openings determined from the water volume that resides in the fractures is considerably larger than what is needed to induce the observed pressure drop. This means that hydraulic testing may not be used to obtain the actual flow porosity of a fissured natural rock using the presently available interpretation methods.

REFERENCES

1. Moreno, L., Neretnieks, I., Eriksen, T.: "Analysis of some laboratory tracer runs in natural fissures". KBS TR 84-04, Nuclear Fuel Safety Project, Stockholm (1984). To be published in Water Resources Res. 1985.

2. Abelin, H., Gidlund, J., and Neretnieks, I.: "Migration in a single fissure". Scientific Basis for Nuclear Waste Management V, p 529-538, North-Holland 1982.

3. Moreno, L., Neretnieks, I. and Klockars, K.E.: "Evaluation of some tracer tests in the granitic rock at Finnsjön", KBS TR 83-38, Nuclear Fuel Safety Project, Stockholm (1983).

4. Neretnieks, I.: "Transport in fractured rocks". Paper at the IAH 17th International Congress on the Hydrology of Rocks of Low Permeability. Tucson, Arizona, Jan 1985. Proceedings in print.

5. Birgersson, L., Neretnieks, I.: "Diffusion in the matrix of granitic rock. Field test in the Stripa mine". Scientific Basis for Nuclear Waste Management VII, p 247-254, North-Holland 1984.

HYDROLOGY AND CHEMISTRY OF HOSOKURA TUFF IN JAPAN

S.Araya, T.Mishima, and K.Maekawa
Power Reactor and Nuclear Fuel Development Corporation
Akasaka, Minato-ku, Tokyo, Japan

T.Asano, S.Saito, and S.Ueta
Mitsubishi Metal Corporation
Ohte-machi, Chiyoda-ku, Tokyo, Japan

ABSTRUCT

Various kinds of in-situ tests have been conducted on the Hosokura Tuff in Japan. Several results on hydrological and chemical tests are presented in this paper. The permeability tests were carried out by the rock mass, 3 m diameter and 4 m long, and the value of 1.2×10^{-12} m/s was determined. In the in-situ migration test, the water contained four stable elements (Co, Sr, Cs, and I) was pumped down into a injection hole, and the test results implied the retardation factors of Co, Sr, and Cs being about 70, 70, and 110, respectively.

INTRODUCTION

It was in 1976 that the research and development of high level waste management started under the jurisdiction of Power Reactor and Nuclear Fuel Development Corporation in Japan regularly. It is planned to operate the high level waste disposal facility after the four phases of investigations as follows.

(1) Survey on potentially suitable geologic formations for disposal.
(2) Selection of the candidate site.
(3) Demonstration of disposal technilogy.
(4) Disposal of actual waste.

The first phase was finished in FY 1984. The in-situ test of Hosokura Tuff described here was started in FY 1981 and brought to FY 1984. It was one of the first phase researches for the purpose of the studies on the isolation capacity of geologic formation. Another in-situ test had been performed in the Diabase media of Shimokawa mine from FY 1980 to FY 1982 in order to review the in-situ test methods conducted in Stripa mine, Swd, to fractured diabase media. The permeability of Hosokura Tuff is very low and there are a few fractures in it. Therefore the in-situ tests here were carried out with somewhat different purposes as follows.

- Development of in-situ test methods for low permeability media.
- Study on evaluation models for in-situ test results.
- Development of complementary laboratory test

SITE CHARACTERISATION

The Hosokura mine is located in the northeast part of Japan, about 300 km north of Tokyo as shown in Fig.1, Which is now being operated and mainly produces the minerals of lead and zinc.

An in-situ test room, about 5 m wide, 7 m long, and 3 m high, was excavated at the depth of 340 m below the surface. Figure 2 shows the layout of the test room and the holes for permeability tests and migration tests. The design of the borehole layout in Stripa mine was fundamentary applied here. N-1 to N-12 holes were additionally drilled after finishing some of permeability tests with B-2 to B-9 holes.

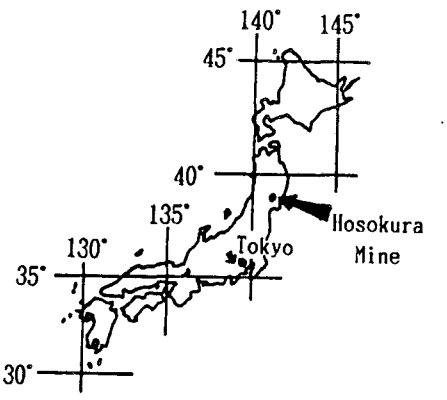

Figure 1. Location of Hosokura mine.

The lithology of the Hosokura mine area consists of mainly altered pyroclastics, propylite, and rhyolite of Tertiary age. The Pre-Tertiary rock presumed as the basement here is granodiorite. The test room was excavated in the layer of pale green dacitic tuff breccia. Table 1 shows the physical properties of Hosokura Tuff.

Mineral composition was identified by means of X-ray diffraction method. Calcite, quartz, feldspar, and some clay minerals such as chlorite, illite, montmorillonite, and kaoline were mainly detected. The chemical analysis results of Hosokura Tuff and in-situ test water were listed in Table 2 and Table 3, respectively.

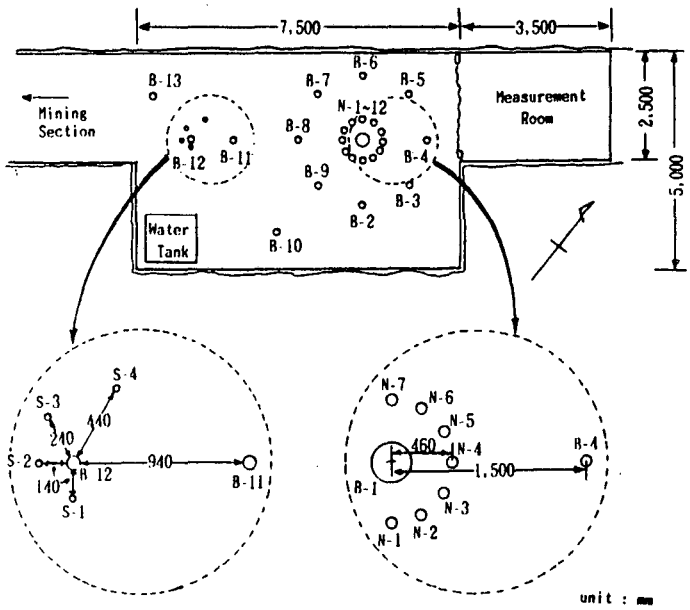

Figure 2. Layout of test holes.

Diameter of each hole
B-1 : 322 mm
B-2-13 : 76 mm
N-1-12 : 76 mm
S-1-4 : 37 mm

Table 1. Physical properties of Hosokura Tuff.

Parameters	Measured Value
Primary stress	max 7.5 MPa, min 4.3 MPa
Specific gravity	2.65±0.01
Apparent density	2.47±0.01 g/cm³
Water content	3.56±0.08 %
Effective porosity	8.28±0.45 %
Compression strength	59.3±15.4 MPa
Elastic modulus	21.0± 6.9 ×10³Pa
Poisson ratio	0.168 ±0.036
Specific heat	8.55±0.42 J/kg·K
Thermal conductivity	2.98±0.37 kW/m·K
Thermal expansion coefficient	9.03±0.80 ×10⁻⁶
Shear strength	16.3± 8.4 MPa

Table 2. Chemical analysis of Hosokura Tuff.

Elements	Value	Elements	Value
SiO_2	64.78 ± 3.58 %	P_2O_5	0.19 ± 0.09 %
TiO_2	0.68 ± 0.17 %	CO_2	1.80 ± 1.02 %
Al_2O_3	15.18 ± 3.03 %	S	0.11 ± 0.07 %
Fe_2O_3	1.11 ± 0.16 %	SO_3	0.00 ± -- %
FeO	3.53 ± 0.17 %	Cu	6 ± 2 ppm
MnO	0.16 ± 0.04 %	Pb	17 ± 1 ppm
MgO	1.05 ± 0.10 %	Zn	79 ± 7 ppm
CaO	2.57 ± 1.22 %	Co	24 ± 2 ppm
Na_2O	3.33 ± 0.98 %	Sr	133 ±14 ppm
K_2O	2.31 ± 0.26 %	Cs	3.1 ± 1 ppm
H_2O^+	1.84 ± 0.18 %	Ce	41 ± 8 ppm
H_2O^-	0.65 ± 0.05 %	Eu	1.69 ± 0.19ppm

Table 3. Chemical analysis of in-situ test water.

Elements	Value	Elements	Value
Ca (mg/ℓ)	5.4	SiO_2 (mg/ℓ)	12.9
Mg (mg/ℓ)	1.2	Br (mg/ℓ)	<0.1
Na (mg/ℓ)	5.9	I (mg/ℓ)	<0.1
K (mg/ℓ)	1.1	Co (mg/ℓ)	<0.1
Fe^{2+} (mg/ℓ)	<0.1	Sr (mg/ℓ)	<0.1
Fe^{3+} (mg/ℓ)	0.2	Cs (mg/ℓ)	<0.1
Cu (mg/ℓ)	<0.1	$T\text{-}CO_3$ (mg/ℓ)	7.5
Al (mg/ℓ)	0.2	pH	6.9
Cl (mg/ℓ)	7.1	E.C. (μS/cm)	74.8
SO_4 (mg/ℓ)	8.5	1000	1520

E.C.:Electric Conductivity

MEASUREMENT OF PERMEABILITY

The permeability tests have been conducted on the same rock mass assumed the cylindrical shape of 3 m diameter and 4 m deep, centered B-1 hole. The layout of apparatus for permeability tests are shown in Fig.3. Water was injected with the constant pressure of 0.5 to 1.2 MPa and effluent was measured.

For the measurement of the permeability under the condition of high temperature, hot water of 70 °C was injected into B-1 hole. Concerning the measurement of effective porosity, bromine was used as tracer of water and effective porosity was calculated with its breakthrough curve. In these cases the hydraulic conductivity was calculated, assuming that the rock mass was homogeneous and Darcy's law was applicable to it.

The effluent volume of water was larger than that obtained at normal rock mass temperature of 32 °C and the hydraulic conductivity was on the order of 10^{-11} m/s as shown in Table 4. The increase of the measured value cannot explaned by the decrease of water viscosity. As the other reasons, the increase of effective area for water flow caused by the expansion of aperture and/or dissolution of fracture filling material was considered.

The breakthrough curve of bromine for the measurement of effective porosity is shown in Fig.4. This curve was clearly divided two parts of first rising and second one. It could be explaned assuming the high permeability channels and low ones being in the rock mass together. Assuming that the first saturation of the breakthrough is 0.68, the effective porosity of the high permeability part was calculated at 0.10 % and residual part at 0.71 %, then the total effective porosity of test rock was determined at 0.81 %. This value was not in good agreement with the value obtained by the room tests as shown in Table 1.

Table 4. Hydraulic conductivities determined under condition of high temperature.

Condition	Value
Room temp. (32°C)	1.2×10^{-12}
Inject hot water(70°C)	6.9×10^{-11} m/s

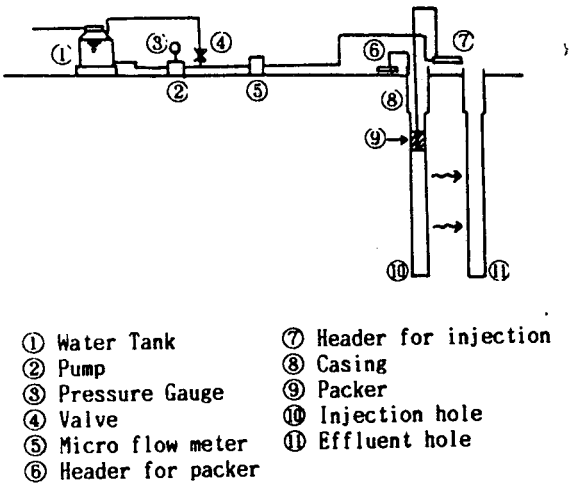

Figure 3. Layout of permeability test apparatus.

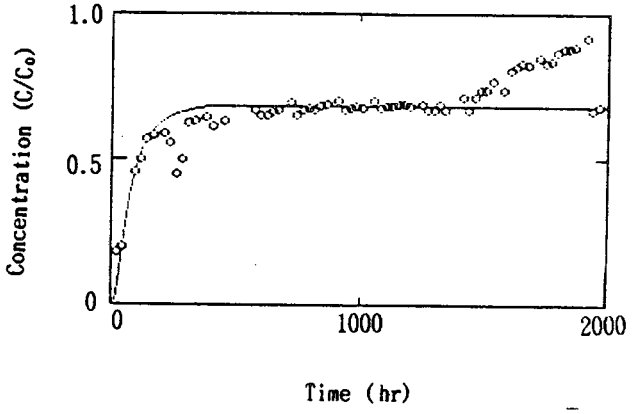

Figure 4. Breakthrough curve of bromine.

IN-SITU MIGRATION TEST

The in-situ migration test was carried out with B-12 hole and S-1 to S-4 holes which were shown in Fig.2. Tracer elements used were Co, Sr, and Cs of 60 mg/l, and iodine, 72 mg/l as tracer of water. Tracer solution have been pumped down into B-12 hole with constant pressure of 1.0 MPa for about four months. After tracers injection, the concentration of tracers absorbed in the rock mass was analized.

A migration test was conducted in a laboratory on a similar setting of in-situ migration test. Water added with same tracers was injected at the constant pressure of 0.4 MPa for four months.

Table 5. Retardation factors determined by in-situ tests.

Element	In-Situ Test	Laboratory Test	Caluculated
Co	70	40	700~10000
Sr	70	20	500~30000
Cs	110	70	700~ 9000

In both of the migration tests, Co and Cs were not detected in effluent. Detected Sr was considered as dissolved material from rock. The breakthrough curve of iodine obtained by in-situ test are shown in Fig.5. The concentration of iodine, represented C/Co, could not reach to 1.0. Assuming that the iodine concentrations in effluent of S-1, S-1, and S-3 holes saturated at 0.74, 0.70, and 0.42, respectively, these breakthrough curves are in good agreement with the calculations using the analytic dispersion model. In the laboratory migration test, the concentration of iodine also did not reach to 1.0. These phenomena could be considered as the same phenomena of the bromine breakthrough that was observed at the measurement of effective porosity mentioned above

The distribution of tracers, Co, Sr, and Cs, in rock mass obtained by the in-situ test are shown in Fig.6. In the in-situ migration test, the retardation factors of Co, Sr, and Cs are determined at 70, 70, and 110, respectively, assuming that these tracers migrated to the distance of 30 mm, 30 mm, and 20 mm, respectively, where their concentrations were negligible compared with the backgroung concentrations. Also retardation fsctors for the laboratory migration test are determined as shown in Table 5.

Retardation factors calculated with distribution coefficient, effective porosity, and specific gravity are listed together. The retardation factors determined by both two of migration tests are very similar but the value calculated are one order larger at least.

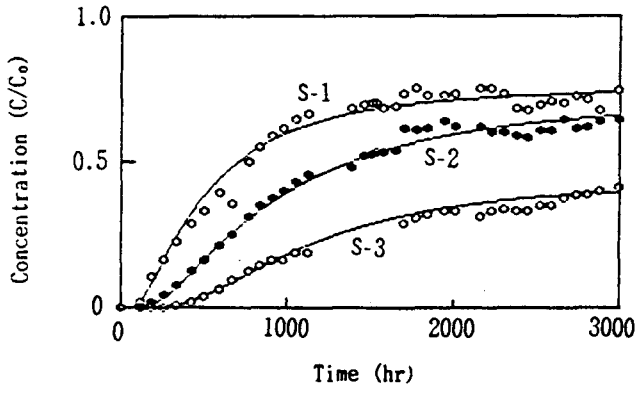

Figure 5. Breakthrough curve of iodine obtained by in-situ migration test.

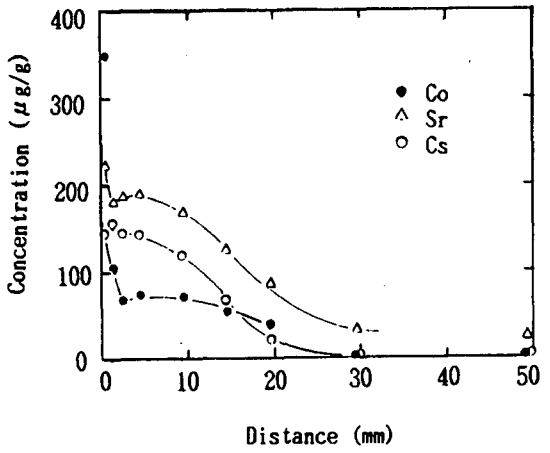

Figure 6. Distribution of Co, Sr, and Cs absorbed obtained by in-situ migration test.

MIGRATION IN ARTIFICIAL SINGLE FRACTURE

Migration tests, using rock columns with an artificial single fracture were carried out in order to estimate the migration behavior of tracer elements in an open fracture. Figure 7 shows the shape of a rock column. The artificial fracture is the rectangular prism, 0.2 mm aperture, 40 mm wide, and 100 mm long. The four tracer elements of Co, Sr, Cs, and Eu were supplied. Tracer solutions were prepared in order to estimate the influence on migration caused the difference of concentration and kinds of tracer contained. The initial concentrations of tracers for each column are 50 mg/l for high concentration condition and 10^{-5} to 10^{-2} mg/l for low concentration condition. To prepare the low concentration solution, radioactive isotopes of ^{60}Co, ^{85}Sr, ^{137}Cs, and ^{152}Eu were used. Tracer solutions were supplied at the same flow rate of 45 ml/d (= 5.6 m/d) for twenty days.

The breakthrough curves of each tracer element were shown in Fig.8. As the result, following interesting facts were found out.

Concerning the condition of high concentration and coexistence, the breakthrough curves of Co, Sr, and Cs showed the similar shapes and the concentrations of these elements in effuluent could reach to 1.0 of C/Co. For high concentration and single element condition, the breakthrough curves of Co, Sr, and Cs indicated the plateau at about 0.65 of C/Co. In these cases, the breakthrough was clearly observed and the retardation factors could be determined as shown in Table 6 . The retardation factors obtained by those migration tests using coexistence and high tracers were very similar to those obtained by the in-situ migration tests.

In the case of low concentration condition, evident breakthrough of each element was not observed. And the detected concentrations under the single element condition were higher than that under the coexistence cindition. The observed migration behaviors are different from our expectation. This shows that migration tests would have to be carried out in very low concentration condition.

Compared with the breakthrough behaviors of Co, Sr, and Cs, that of Eu was completely different. Therefore furture tests with different elements would be necessary.

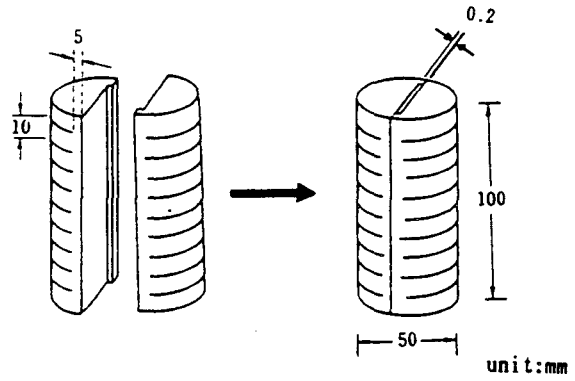

Figure 7. Shape of rock column with artificial single fracture.

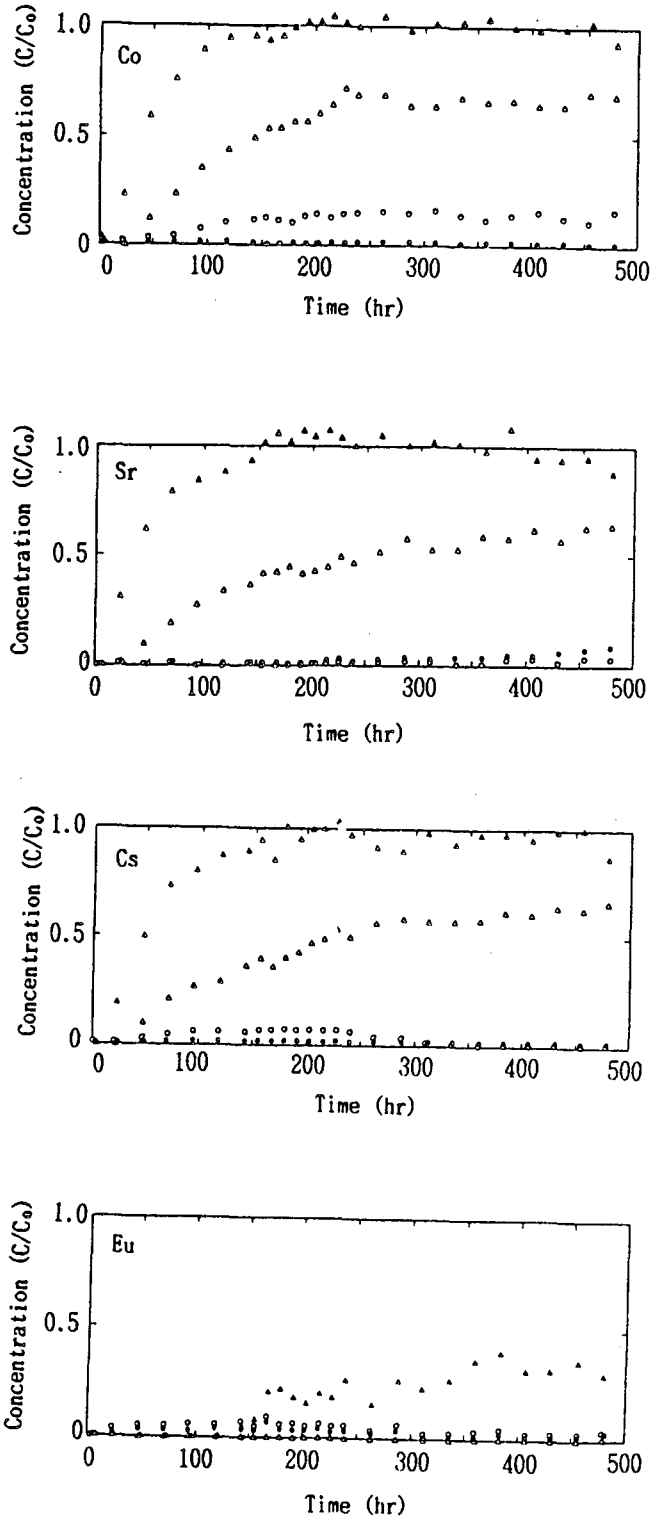

Figure 8. Effluent Co, Sr, Cs, and Eu activity from artificial single fracture in different four initial conditions.

Condition:

- ○ Low concentration and single element
- ● Low concentration and coexistence
- △ High concentration and single element
- ▲ High concentration and coexistence

Table 6. Retardation factors determined by fracture migration test.

Element	Coexistence	Single
Co	90	210
Sr	90	260
Cs	110	310
Eu	>600	>600

CONCLUSIONS

As the results of permeability tests and migration tests, the following facts are drawn.

- Hosokura Tuff has the very low permeability of the order of 10^{-12} m/s.
- In-situ retardation factors of Co, Sr, and Cs were determined as 70, 70, and 110, respectively, when those elements were supplied in the high and coexistence condition.
- Migration tests using the rock column with an artificial single fracture are the effective test method for the study on the migration phenomena in the open fracture.

In-situ test methods that had previously been reported were not always effective to the low permeability rock media such as Hosokura Tuff. Therefore in-situ tests using larger scale and longer term and laboratory tests using low concentration nuclides will be expected as studies in future program at Hosokura mine. And it is planned to constract the underground research laboratory and the hot facility called environmental research laboratory for studies on the geological disposal. Adding the domestic studies which will be conducted in those facilities, the cooperation and the interchange of informations with the other foreign research institute will be desirable.

REFERENCES

Interim Report published by Atomic Energy Commission in Japan (1984).

Gaustafsson,E., Klockers,C.E. (1981). "Studies on Groundwater Transport in Fractured Crystalline Rock under Controlled Conditions using Nonradioactive Tracers," SKBF 81-07

Kojima,T., Shoji,T., Takahashi,H. (1984). "Stress Corrosion Cracking Behavior of Granite in Pressurized High Temperature Water Environment," Proceedings of the 6th Japan Symposium in Rock Mechanics.

Lundstom,L., Stille,H. (1978). "Large Scale Permeability Test of the Granite in the Stripa Mine and Thermal Conductivity Test," LBL-7052,SAC-02,UC-70,TID-4500-R66

Neretnieks,I., Eriksen,T., Tahtinen,P. (1982). "Tracer Movement in a Single Fissure in Granitic Rock: Some Experimental Results and Their Interpretation," Water Resource Research,Vol.18, No.4,849-858

Rundberg,R.S., Thompson,J.L., Maestas,S. (1982). "Radionuclide Migration: Laboratory Experiments with Isolated Fractures," The Scientific Basis for Nuclear Waste Management, 239-248

Sato,K., Sasaki,Y. (1984). "Experimental Determination of Solute Dispersion Coefficients in Rock Seepage," J. of the Japan Society of Eng. Geology, Vol.25,No.3, 103-110

Tsunoda,N., Maekawa,K., Kashiwagi,T. (1982) "In-Situ Permeability and Heater Tests on HLW Disposal Technology Developments in Japan," Proceedings of International Conference on Radioactive Waste Management.

HYDRAULIC AND IONIC DIFFUSION PROPERTIES OF BENTONITE/SAND BUFFER MATERIALS

S.C.H. CHEUNG AND M.N. GRAY
Atomic Energy of Canada Limited, Whiteshell Nuclear Research Establishment, Pinawa, Manitoba ROE 1LO, Canada.

ABSTRACT

The Canadian Nuclear Fuel Waste Management Program is assessing the concept of safe disposal of nuclear fuel waste in a vault mined deep in plutonic rock [1]. Groundwater, which will penetrate to the waste, has the potential to leach out radionuclides and transport them to the surface. A number of protective barriers will minimize the rate at which this will occur: these include a corrosion-resistant container, buffer and backfill materials and the surrounding rock. The buffer material is likely to be a compacted mixture of bentonite and sand [2]. A knowledge of the rate of radionuclide transport through the buffer is required as input for the safety assessment of the disposal concept.

Mass transport in the buffer can occur by diffusion and/or convection; each of these processes will depend on the combined effects of thermo-hydro-chemical-mechanical phenomena associated with the vault. In this paper, an attempt is made to determine which of these phenomena has the greatest significance on the hydraulic conductivity and the diffusion coefficient of a saturated bentonite/sand buffer mixture. The hydraulic conductivity and diffusion coefficient are studied as functions of buffer temperature and dry density; the influence of hydraulic gradient and ionic concentration in the water in contact with the buffer on the transport coefficients is also examined.

Based on diffuse-double-layer theory, a model is developed to study the combined effects of temperature, ionic concentration, hydraulic gradient and dry density on the effective porosity and, hence, the hydraulic conductivity of the buffer, as described by the Kozeny-Carman equation. The analyses show that the hydraulic conductivity of the buffer primarily depends on the effective clay dry density (i.e., the ratio of the dry mass of clay to the combined volume of the clay plus voids in the system). At low effective clay dry density, the hydraulic conductivity increases with increasing temperature, ionic concentration in the pore water and hydraulic gradient across the buffer. At the high effective clay dry density expected in a vault (1.3 to 1.4 Mg/m^3) [3], the hydraulic conductivity is very low in the vault environment. This indicates that the major radionuclide transport will occur via diffusion.

A model based on the relative volumes of surface and interstitial water in bentonite/sand mixtures is developed to describe the diffusion coefficient. The model assumes that the rate of ionic diffusion in surface water is low compared with that in interstitial water and can be neglected.

Data are presented to show that the diffusion coefficient for ionic species that do not interact with the clay is mainly dependent on the effective clay dry density. An increase in the effective clay dry density will decrease the diffusion coefficient, due to a relative increase in the proportion of surface water present in the system. Measurements indicate that the diffusion coefficient for a bentonite/sand buffer is approximately 10^{-11} m^2/s.

REFERENCES

[1] T.E. Rummery and E.L.J. Rosinger, "The Canadian Nuclear Waste Management Program," Proceedings of the Canadian Nuclear Society International Conference on Radioactive Waste Management, Winnipeg, Canada, 1982, p6; also Atomic Energy of Canada Limited Report AECL-7787 (1983).

[2] K. Nuttall and P. Sargent, "Comparison of Used-Fuel and Reprocessing Waste Disposal - Technical Implications," Proceedings of the American Nuclear Society International Topical Meeting on Fuel Reprocessing and Waste Management. Jackson, Wyoming, U.S.A. 1984 (In Press).

[3] D.A. Dixon, M.N. Gray and A.W. Thomas, "A Study of the Compaction Properties of Potential Clay-Sand Buffer Mixtures for Use in Nuclear Fuel Waste Disposal," Symposium on Clay Barriers for Isolation of Toxic Chemical Wastes, Stockholm, Sweden. Elsevier Scientific Publishing Company, Amsterdam, 1984.

COUPLED HYDROTHERMAL FLOWS OF LIQUID AND VAPOR IN WELDED TUFF: NUMERICAL MODELING OF PROPOSED EXPERIMENT

Roger R. Eaton, Nathan E. Bixler, and Daniel C. Reda

Fluid & Thermal Sciences Department
Sandia National Laboratories
Albuquerque, NM 87185

ABSTRACT

Pretest calculations of a proposed small-scale, heat-pipe experiment have been made using a finite element, multiphase flow, computer code. The purpose of the experiment is to characterize the response of partially saturated, welded, volcanic tuff to the two-phase countercurrent flow induced by an applied temperature gradient. The experimental measurements will be used to refine the presumed permeability and capillary pressure functions, which are used in the finite element analysis. The calculations presented in this paper, using the presumed material functions, show that saturation profiles and experimental time scales are sensitive to applied temperature gradients and initial liquid saturations. The results have been used to predict appropriate experimental parameter ranges.

INTRODUCTION

Recent interest by the Nevada Nuclear Waste Storage Investigations (NNWSI) Project[1] in the hydrological performance of a potential nuclear waste repository located in partially saturated, welded, volcanic tuff at Yucca Mountain in Nevada has prompted the development of computational tools to be used for predicting the transport of mass (water vapor, liquid water, air, and solute) and energy in partially saturated porous media. Proper application of these codes in performance analyses and engineering design studies strongly depends on the availability of accurate material properties, particularly for unsaturated regions where relative permeability and capillary pressure are strong functions of liquid saturation. At present, limited material information is available (Peters *et al.*, 1984). If codes are required for repository analysis, these properties should be verified by laboratory and/or field experiments to improve the confidence in computed results.

The results of a series of computions made using a multiphase flow code are presented. These results are being used: 1) to aid in experiment design by defining appropriate experimental ranges for applied temperature gradients and initial liquid saturations and 2) to aid in the material property verification process.

Details of the counterflow laboratory experiment are presented in the Experimental Procedure Section. A brief description of the finite element code NORIA (Bixler, 1985), which was used to make the pretest predictions, and modeling parameters are discussed in the Numerical Simulation Section. A summary of the computed results and predictions of the time-scale requirements for the laboratory experiments are given in the Results Section.

EXPERIMENTAL PROCEDURE

The proposed experimental approach is illustrated in Figure 1. The experiment is referred to as a closed-system heat pipe. All of the relevant fluid physics operative in the near field of a buried waste canister, such as multiphase countercurrent water flow, are encountered in this laboratory simulation. The volcanic tuff sample to be used in the experiment was obtained from the Busted Butte outcrop of the Topopah Spring member of the Paintbrush Tuff on the Nevada Test Site. The material properties of this outcrop are expected to be similar to those of the Topopah Spring member of Yucca Mountain as defined by Peters (1985). To run the experiment, a cylinder of the welded tuff is placed in a core holder and wetting/drying procedures are used

[1] The Nevada Nuclear Waste Storage Investigations (NNWSI) Project, managed by the Nevada Operations Office of the U. S. Department of Energy, is examining the feasibility of a repository for high-level nuclear wastes at Yucca Mountain on, and adjacent to, the Nevada Test Site. The work discussed in this paper, which is intended to be a step in the validation of computer codes that are being used to extend our understanding of the long-term hydrologic and geochemical systems at Yucca Mountain, was funded by the NNWSI project.

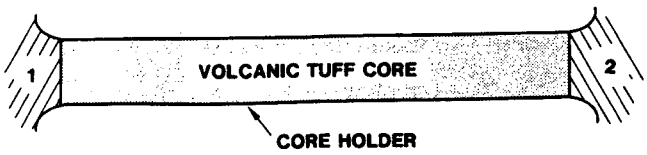

(a) Schematic of volcanic tuff in core holder.

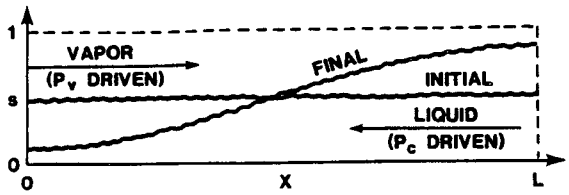

(b) Schematic of closed-system heat pipe.

Figure 1. Proposed approach for countercurrent liquid/vapor laboratory experiment.

to create an initial uniform liquid-saturation distribution $s(x,t = 0)$ where $s < 1$. The experiment is started by increasing the temperature at one end of the rock from T_2, the uniform initial value, to T_1. The temperature differences ($T_1 - T_2 = \Delta T$) used in the calculations were 110, 130, and 150 K. Evaporation occurs at the hot end causing vapor to be driven toward the cold end due to the resulting vapor pressure gradient (ΔP_v). Condensation occurs at the cold end. Liquid water is transported back toward the hot end due to the resulting capillary-pressure gradient (ΔP_c). A heat-pipe effect thus occurs, with the final liquid saturation distribution being measurably different from the initial condition.

Gamma-beam densitometry (Reda *et al.*, 1981), a nonintrusive diagnostic technique, will be used to measure transient saturation distributions. A schematic of this instrumentation system is shown in Figure 2, where I_0 is the initial beam intensity, I is the attenuated beam intensity, and R is the count rate.

NUMERICAL SIMULATION

The heat-pipe experiments were simulated using the multiphase flow code NORIA (Bixler, 1985). Calculations were made by varying the imposed temperature difference along the rock, the initial saturation state, and the rock permeability. The following two subsections briefly describe the numerical and physical aspects of the analysis.

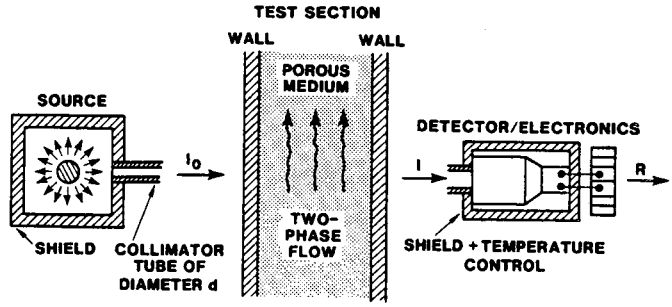

Figure 2. Schematic of gamma-beam densitometry instrumentation.

Numerical Formulation

NORIA is a finite element computer program which simultaneously solves four nonlinear, parabolic, partial differential equations. The four equations describe the transport of water, water vapor, air, and energy through partially saturated porous media. The numerical procedure uses the standard Galerkin finite element method to handle spatial discretization of two-dimensional domains. Time integration is performed by a third-order predictor/corrector scheme that uses error estimates to automatically adjust time-step size. Nearly all material properties can be defined as functions of the dependent and independent variables by user-supplied subroutines. The gas phase is taken to be ideal. Additional information regarding this code is given in the user's manual (Bixler, 1985).

The finite element mesh used in this study consists of 25 eight-node quadrilateral elements, as shown in Figure 3. The elements are compressed near the hot end in order to obtain better resolution in the region of low saturation. All calculations were done on a Cray 1S computer. Typical CP requirements were 400 to 1000 seconds per run. CP time usage increased as the initial saturation decreased. This results from a diminished physical time scale for transport of liquid water when saturation approaches zero.

Physical Model

Figure 3 shows the boundary conditions that were imposed in this analysis. Zero mass flux of liquid water and water vapor were enforced at each boundary. Temperatures were fixed at the two ends of the heat pipe: the temperature at the cold end (T_2) was held at 300 K for each of the cases; the temperature at the hot end (T_1) was held at either 410, 430, or 450 K. In the experiment, air will be evacuated from the system prior to testing; therefore, air pressure was uniformly set to a small value (1.0 Pa) over the entire domain.

The values for matrix porosity, 0.11, and saturated rock permeability, $5 \cdot 10^{-19}$ m^2, used in this study are obtained from laboratory experiments performed by Reda and

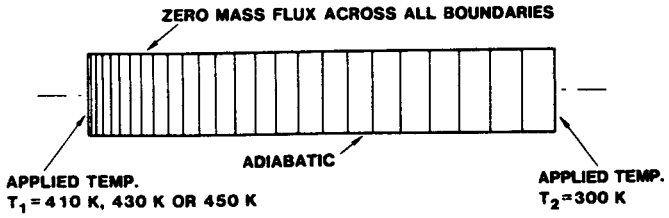

Figure 3. Finite element mesh (25 elements).

Hadley (1985). The rock sample tested to obtain these values was from the Topopah Spring member outcrop at Busted Butte. The dependence of saturation on capillary pressure for similar welded tuff has been experimentally measured by Peters *et al.*, (1984). The data were fit by a van Genuchten (1984) relationship, as shown in Figure 4. Using the theory of Mualem (1976), these data were used to calculate the dependence of liquid permeability on capillary pressure, see Figure 5. The above rock properties have not been designated by the NNWSI project as representative property data but are used here because the above rock properties are expected to be similar to the sample to be investigated. These relationships were recently used by Peters *et al.* (1985) for calculations involving the same type of welded tuff as considered here.

A series of ten cases was analyzed to determine the effects of initial saturation, applied temperature difference, and rock permeability on saturation distributions $s(x,t)$. All nine combinations of the three initial saturations (s_i = 0.25, 0.5, and 0.75) and the three temperature differences

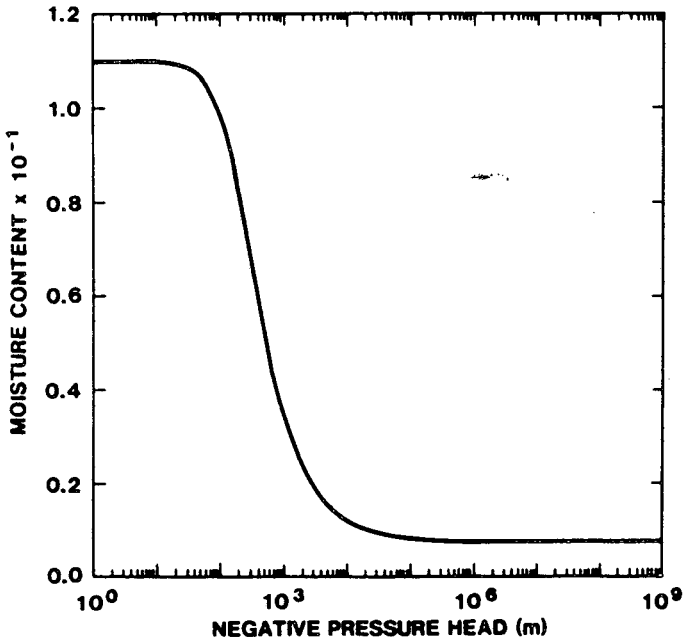

Figure 4. Material characteristic curve relating moisture content to pressure head for a welded volcanic tuff.

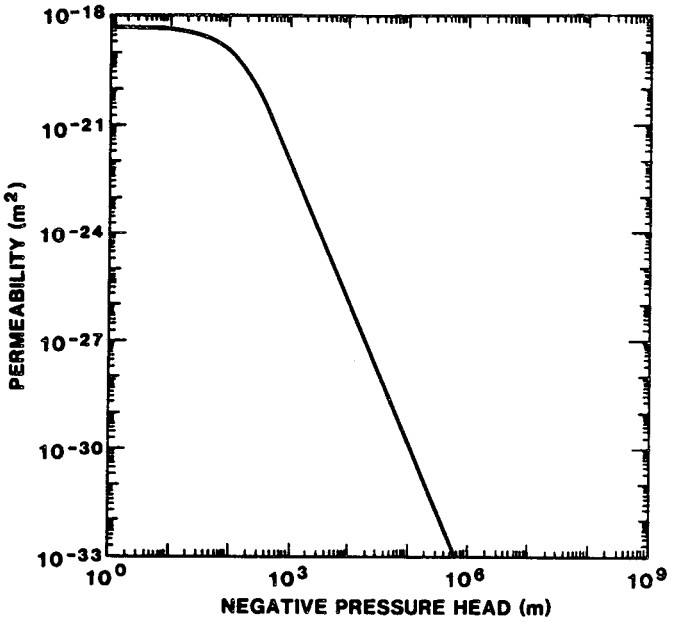

Figure 5. Material characteristic curve relating permeability to pressure head for a welded volcanic tuff.

(ΔT = 110, 130, and 150 K) were investigated. In the tenth case, liquid permeability was decreased by an order of magnitude to $5 \cdot 10^{-20}$ m^2, with s_i = 0.75 and ΔT = 150 K.

RESULTS

The case in which initial saturation is 0.75 and imposed temperature difference is 150 K was computed using meshes consisting of 25 and 50 elements. The 50-element mesh was constructed by subdividing each element in the 25-element mesh into two elements. It was found that the predicted saturations differed by less than 2% for the two meshes. Therefore the 25-element mesh was used for all of the reported results.

Figures 6 and 7 show the computed change in saturation at the hot end of the test rock ($x = 0$) when s_i = 0.75 and 0.5, respectively, for all three temperature differences. Note that the time scale for Figure 6 is months, while days has been used for Figure 7. These figures show that the saturation at the hot end is a strong function of applied temperature difference ΔT. Steady state is attained after about 2 months for ΔT = 110 and 130 K when s_i = 0.75, as shown in Figure 6. The hot end is nearly dry after two months when ΔT = 150 K. When dry out is approached, the computational time-step becomes small (less than 1 second). Figure 7 shows that when s_i = 0.5, dry out occurs near the hot end for ΔT = 150 and 130 K. When s_i = 0.25, dry out occurs for all three temperature differences.

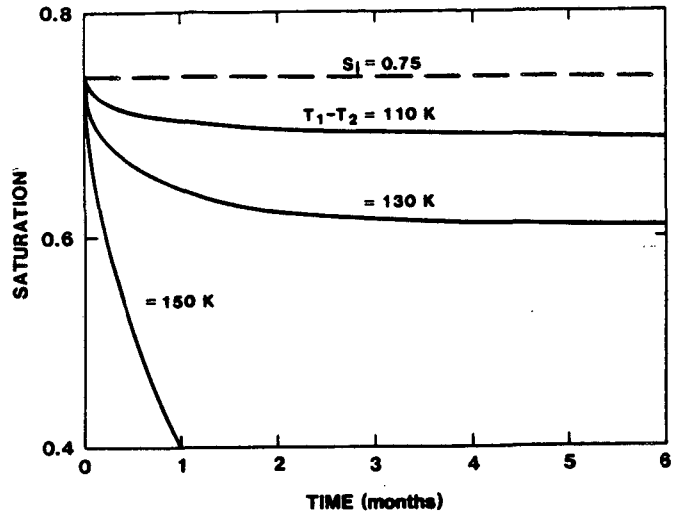

Figure 6. Liquid saturation histories at $x = 0$ for applied temperature differences of 110, 130, and 150 K, $s_i = 0.75$.

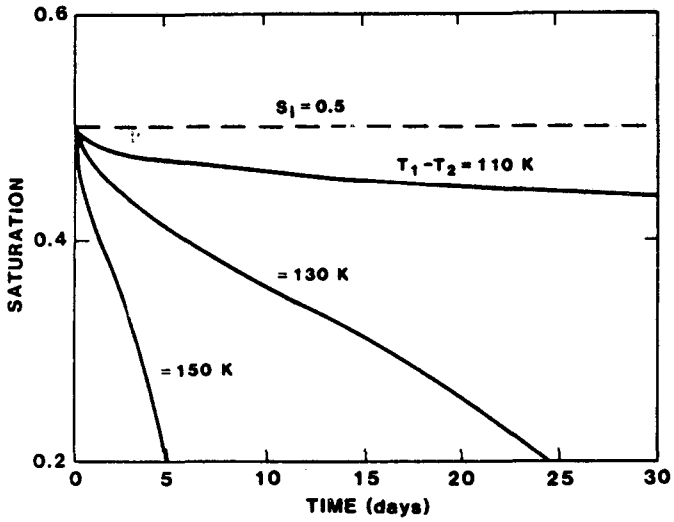

Figure 7. Liquid saturation histories at $x = 0$ for applied temperature differences of 110, 130, and 150 K, $s_i = 0.5$.

Figure 8 shows the predicted axial saturation distribution at 45 days when $s_i = 0.75$ for all three applied temperature differences. When $\Delta T = 130$ and 150 K, the computed saturation distributions are sufficiently different from the initial uniform saturation to be accurately measured using gamma-ray densitometry (see error analysis in Reda *et al.*, 1981). The distribution predicted for $\Delta T = 110$ K is not measurably different from the initial uniform saturation; thus this case is of little experimental interest.

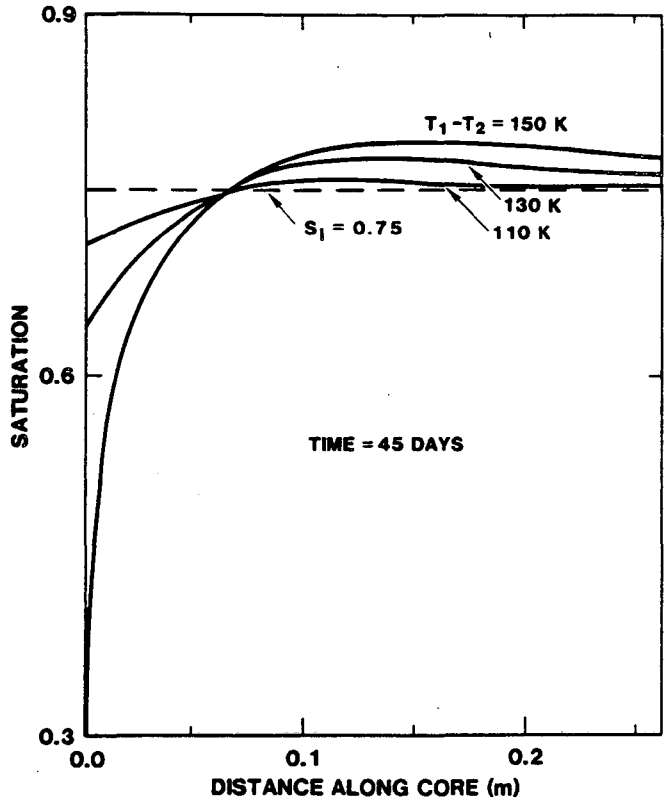

Figure 8. Liquid saturation profiles at 45 days for applied temperature differences of 110, 130, and 150 K, $s_i = 0.75$.

Saturation profiles for the case of $s_i = 0.75$ and $\Delta T = 150$ K are given in Figure 9 for times of 7, 15, 30, and 45 days. At 45 days 80% of the rock is at a saturation that is measurably different from the initial value (*i.e.*, a change in saturation of $\pm$ 5%). Figure 10 shows the saturation profiles when $s_i = 0.5$ and $\Delta T = 130$ K for times up to 30 days. Even though ΔT is smaller for this case than the one shown in Figure 9, dry out occurs between 30 and 45 days because of the lower initial saturation. However, even though dry out occurs when $s_i = 0.5$ and $\Delta T = 130$ K, the saturation over 40% of the core does not change from its initial value so that saturation measurements would be effectively confined to less than 60% of the sample.

To date, experiments have been performed to determine the saturated permeability of welded volcanic tuff from the Topopah Spring member of the Paintbrush Tuff; however no experiments have been performed to establish how permeability depends on saturation, or equivalently, how permeability depends on capillary pressure. The sensitivity of predicted saturation to permeability was investigated by analyzing the heat-pipe experiment when relative permeability for both phases is decreased by an order of magnitude over the whole range of capillary pressures. Figure 11 shows that the saturation at $x = 0$ (at any value of time) decreases appreciably when permeability increases.

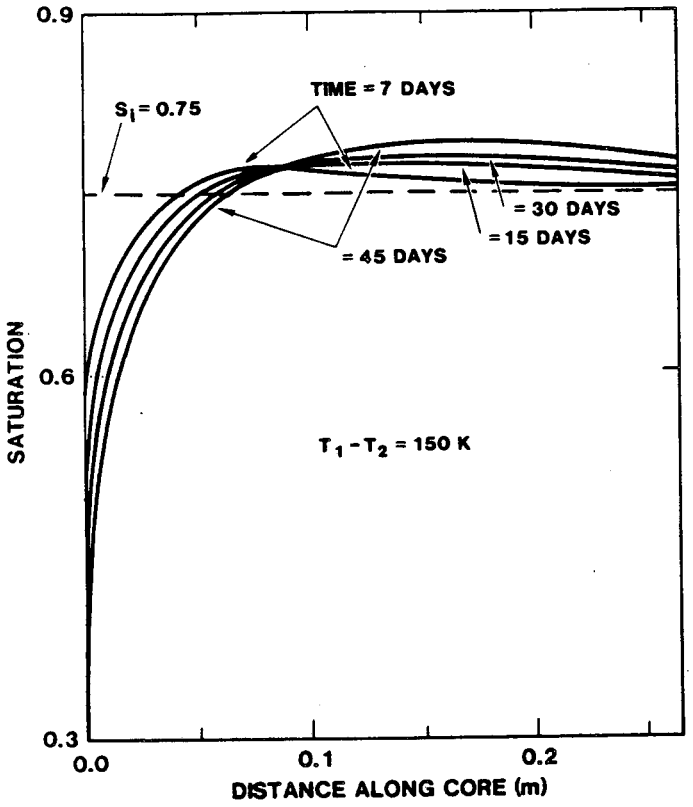

Figure 9. Liquid saturation profiles for applied temperature difference of 150 K at times 7, 15, 30 and 45 days, $s_i = 0.75$.

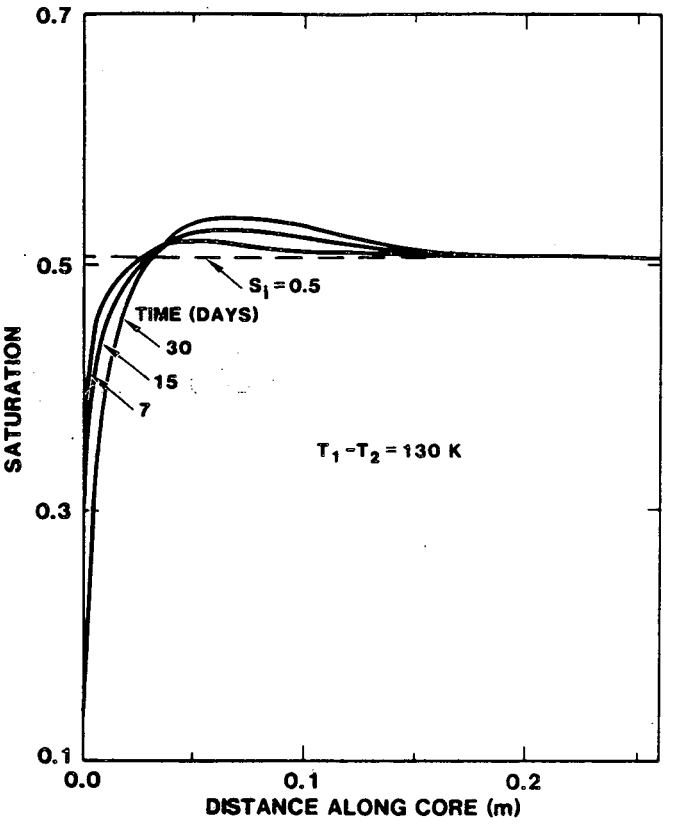

Figure 10. Liquid saturation profiles for applied temperature difference of 130 K at times 7, 15, and 30 days, $s_i = 0.5$.

From another point of view, the amount of time needed to reduce saturation to a specified level at $x = 0$ increases appreciably as permeability decreases. Thus, the time needed to run experiments in the partially saturated regime will strongly depend on the relative liquid permeability.

CONCLUSIONS

Pretest calculations of a proposed heat-pipe laboratory experiment have been made using the multiphase flow code NORIA. The sensitivity of predicted saturations to imposed temperature differences, initial saturations, and liquid permeabilities was analyzed. Variation of calculated saturation from the initial prescribed value (s_i) is shown to be a strong function of applied temperature difference. Measurable changes in the saturation profiles are shown to be obtained when temperatures imposed at the ends of the sample differ by 130 K or more.

A portion of the rock dries out for several combinations of initial saturation and applied temperature difference. This situation is undesirable in experiments because it leads to difficulties in maintaining a zero mass-flux condition at the dry end of the rock sample due to the liquid-vapor interface that exists between the rock and the pressure instrumentation port. The calculations show that an applied

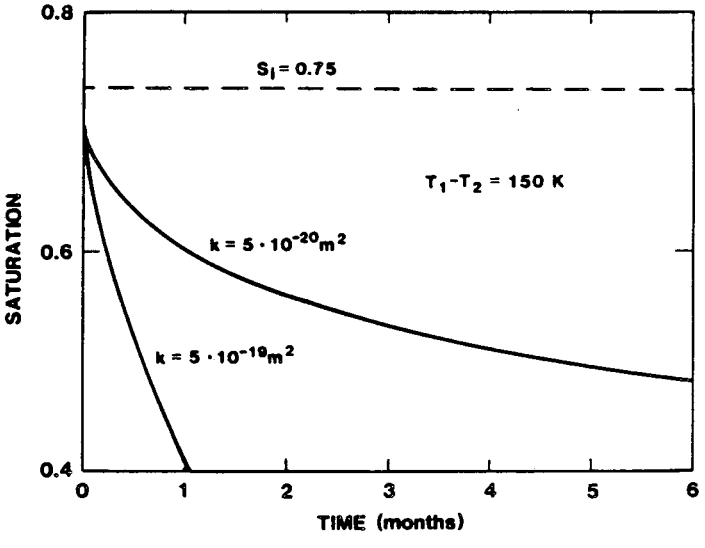

Figure 11. Saturation histories at $x = 0$ for two permeabilities, $5 \cdot 10^{-19}$ and $5 \cdot 10^{-20}$ m^2.

temperature difference ΔT of 150 K results in dry out for all initial saturations investigated here ($s_i = 0.25, 0.50$, and 0.75). However, dry out does not occur until approximately

2 months when $s_i = 0.75$. When $\Delta T = 130$ K, dry out will not occur, within the 6 month time period, for $s_i = 0.75$ but will occur, at about 1 month, for $s_i = 0.5$. When $\Delta T = 110$ K, dry out occurs only for the smallest value of initial saturation, $s_i = 0.25$. Based on the material properties used to perform these numerical calculations, the optimum laboratory testing conditions investigated here are $s_i = 0.75$ and $\Delta T = 130$ K. Initial laboratory tests will be made using these conditions.

Estimated experiment time scales and predicted saturation profiles are sensitive to the assumed rock permeability. Additional laboratory testing on the rock core is scheduled. This testing should help confirm whether or not the material properties used in these calculations are indeed representative of the sample taken from the Topopah Spring outcrop at Busted Butte.

REFERENCES

Bixler, N. E. (1985). "NORIA-A Finite Element Computer Program for Analyzing Water, Vapor, Air, Energy Transport in Porous Media," SAND84-2057, Sandia National Laboratories.

Mualem, Y. (1976). "A New Model for Predicting the Hydraulic Conductivity of Unsaturated Porous Media," Water Resources Research 12(3):513-522.

Peters, R. R., E. A. Klavetter, I. J. Hall, S. C. Blair, P. R. Heller, and G. W. Gee (1984). "Fracture and Matrix Hydrologic Characteristics of Tuffaceous Materials from Yucca Mountain, Nye County, Nevada," SAND84-1471, Sandia National Laboratories.

Peters, R. R., J. H. Gauthier, and A. L. Dudley (1985). "The Effect of Infiltration on Water Saturation Time in Deep, Partially Saturated Zones," *Proceedings of the Symposium on Groundwater Flow and Transport Modeling for Performance Assessment of Deep Geologic Disposal of Radioactive Waste: A Critical Evaluation of the State of the Art*, Eds. C. R. Cole and T. Nicholson.

Reda, D. C., G. R. Hadley, and J. R. Turner (1981). "Application of the Gamma-Beam Attenuation Technique to the Measurement of Liquid Saturation for Two-Phase Flows in Porous Media," presented at the 27th International Instrumentation Symposium, Instrument Society of America, Indianapolis, IN.

Reda, D. C. and G. R. Hadley (1985). "Saturated Permeability Measurements on Pumice and Welded-Tuffaceous Materials," presented at the 17th International Congress of the International Association of Hydrogeologists, Tucson, AZ.

van Genuchten, R. (1978). "Calculating the Unsaturated Hydraulic Conductivity with a New Closed Form Analytical Model," *Water Resources Bulletin*, Princeton University Press, Princeton University, Princeton, New Jersey.

RADIONUCLIDE TRANSPORT AS VAPOR IN A NON-ISOTHERMAL DUAL POROSITY SYSTEM

by

Ronald T. Green[1], William Filippone[2], and Daniel D. Evans[1]

[1]Department of Hydrology & Water Resources
[2]Department of Nuclear Engineering
University of Arizona, Tucson, Arizona 85721

ABSTRACT

The importance of forced diffusion relative to ordinary diffusion is investigated as to its potential as a transport mechanism of radionuclides near a HLW repository. Two cases are considered: 1) the canister is located in a rock mass and 2) the canister is located in air. Forced diffusion appears insignificant in the first case but potentially important in the second.

INTRODUCTION

Vapor transport of radionuclides in unsaturated fractured rock at a HLW repository is a potentially important transport mechanism. One aspect of vapor transport is mass flux resulting from forced diffusion. Mass flux of a gas by forced diffusion is, under most conditions, considered insignificant when compared to ordinary diffusion. However, gamma radiation emitted during decay of high-level waste can induce an electric field caused by Compton scattered electrons which in turn can create conditions conducive to forced diffusion. The magnitude of the resulting electric field and the related forced diffusion of an ionized gas through the air space of a partially saturated fracture will depend upon the physical characteristics of the high-level waste and the repository site.

THEORY

The mass flux (ions/cm^2-sec) of gas resulting from forced diffusion caused by an electric field can be expressed as (MacDaniel and Mason, 1973)

$$J = n K E \qquad (1)$$

where

n = number density of ions (ions/cm^3)
E = electric field (V/cm)
K = mobility (cm^2/V-sec)

The mobility term is a constant of proportionality and is a measure of the ease at which an ion can move through a gas. K is related to the diffusion coefficient by the expression

$$K = e D/(k T) \ (cm^2/V\text{-}sec) \qquad (2)$$

where

e = ionic charge (coulombs)
D = diffusion coefficient (cm^2/sec)
k = Boltzmann constant (joules/^{0}K)

The flux resulting from forced diffusion is considered potentially significant when it exceeds the flux by ordinary diffusion. A field energy parameter, E/P, is useful as an indicator of the relative importance of forced diffusion as a mechanism of transport. If a singly charged ion is transported through a gas of similarly sized molecules and the collision cross-section is assumed to be 5×10^{-17} cm^2 then forced diffusion is approximately equal to ordinary diffusion when

$$E/P << 2 \ V/cm\text{-}atm \qquad (3)$$

Thus, at atmospheric pressure, forced diffusion is considered insignificant when the external electric field is less than 2 V/cm.

The first term examined from equation (1) is the electric field. The electric field is related to current density, j (amps/cm^2), and the resistivity of the medium, ρ (ohms-cm), by Ohm's law which can be expressed

$$E = \rho j \qquad (4)$$

Current density is by definition related to the current, I (amps), by the expression

$$j = I/A \qquad (5)$$

where A is area (cm^2). The electric field surrounding a HLW repository can therefore be determined if current and resistivity are known.

Gamma radiation (or photons of elecromagnetic radiation) loses a relatively large amount of energy when it interacts with matter. Interaction of gamma radiation with matter can occur during several different processes. Three of the more important processes are 1) the photoelectric effect, 2) the Compton effect, and 3) pair production. The Compton effect is the phenomenon of interest is this study.

The Compton effect results from an interaction of a photon with either a bound or free electron in the absorbing material. The resulting preferential movement of electrons emitted during the interaction creates the Compton current. An algorithm has been written to record the movement of a photon, which is

initially emitted by high-level waste, to a collision, then tracking each collision-produced photon from collision to collision until the energy of the collision-produced photon is considered insignificant at which time a single history is completed. A Monte Carlo simulation program, COMPMC, computes a sufficient number of histories of photon emissions from a HLW canister to account for the random nature of actual photons.

The waste package is characterized as an infinite line source thus end or edge effects are ignored. A further assumption made in this simulation is that the HLW cannister is located in an homogeneous isotropic medium. This assumption simplifies the procedure employed in tracking individual photons. However, once the Compton current is calculated along with the accompanying electric field, partially drained fractures which intersect the cannister can be superimposed onto the system. Forced diffusion of vapor in the partially drained fracture can then be evaluated.

The effective range of travel of the collision electron is determined by a separate computer routine, SR (Filippone, Dept of Nuclear Engineering, U of Arizona), which calculates the effective range of an electron based upon the properties of the medium through which the electron is travelling and the energy of the electron.

The effective range of electrons through a hypothesised material (with properties resembling the properties of an unsaturated tuff, i.e.: atomic weight of 33 and atomic mass of 68) is calculated at a total of 22 different electron energies. A graph of the effective range of a electron is plotted versus electron energy in Figure (1). Three second order polynomials were used to approximate a smooth curve through the data in a spline-like fashion. Therefore, after each collision, the radial distance travelled by each electron can be calculated.

There is no known analytic solution available to validate the full extent of COMPMC (which is based upon transport theory), that is, to calculate the radial density of collisions between anisotropically scattered photons and particles in the medium. However, an analytic solution (based upon diffusion theory) is available to calculate diffusion of isotropically scattered photons emitted from an infinite line source. In general, photons emitted from a line source will not collide in a manner resembling diffusion because of the preferential outward movement of the subsequent collision produced photons. Therefore, by voiding this aspect of

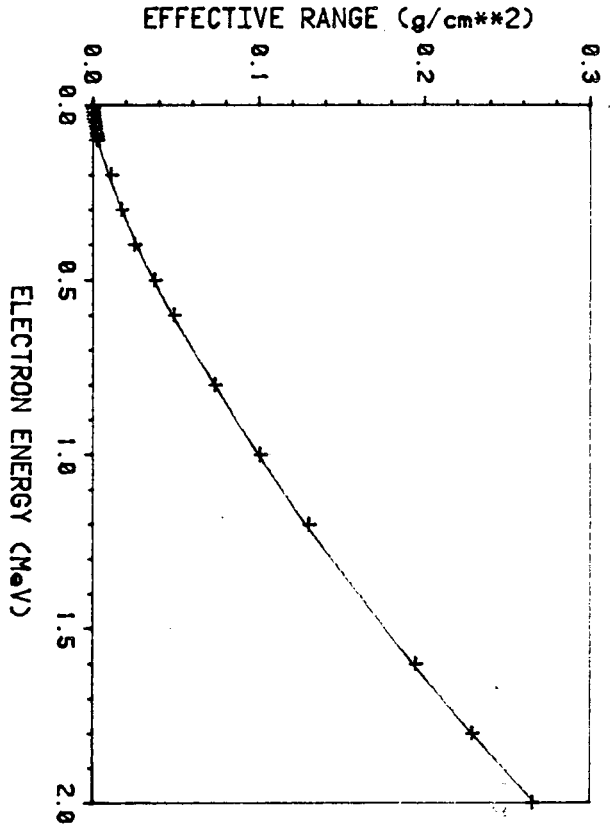

Figure 1. Effective range of electron versus electron energy in rock.

COMPMC (i.e., by making the collisions isotropic and maintaining the photon energy at 1 MeV), the radial collision density of the photons emitted by a line source should asymptotically approach the radial collision pattern predicted by the diffusion equation as the radial distance increases. The analytical solution therefore appears (Lamarsh, 1966)

$$N_c = \mu \Delta r \, K_0(r/L)/(2\pi D) \qquad (7)$$

where N_c is the collisions per unit length, μ is the absorption coefficient, r is the radial distance, K_0 is the zeroth order Bessel function of the second kind, and L is a parameter referred to as the length of diffusion.

The normalized radial collision density determined from the results of COMPMC are compared with the analytical solution to the diffusion equation. As is illustrated in Figure (2), there is a discrepancy between the results near the line source where diffusion theory does not adequately represent the initial preferential outward movement is apparent in the results from COMPMC. However, after the region where the initial collisions occur and beyond where outward preferential movement is observed, the

results from COMPMC and the diffusion equation approach each other asymptotically.

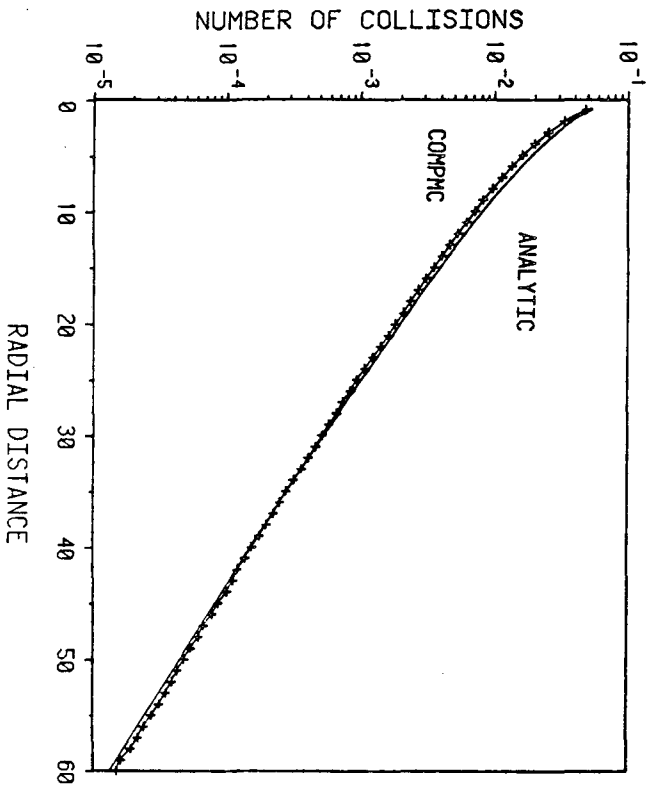

Figure 2. Comparison of COMPMC with analytic solution.

The Compton current density, j (amp/cm^2), is calculated by the following expression (Gross, 1965)

$$j = R_{eff}\, e\, \mu\, \Phi_e \qquad (8)$$

where R_{eff} is the effective range of the collision electron and Φ_e is the flux of radiant energy per unit area at the point of interest. The gamma ray source employed in COMPMC is normalized so that any HLW inventory can be represented and examined in terms of the resulting forced diffusion caused by emitted photons. The particular gamma ray source used in this analysis is based on the radionuclide inventory of a single fuel assembly of defense high-level waste (DHLW) from a light water reactor (LWR) predicted using the SANDIA-ORIGIN code (Sutherland and Bennett, 1979). Spent fuel from a pressurized water reactor (PWR) is assumed to be canistered without being reprocessed. It is assumed that the fuel assembly has been immobilized in a matrix and placed in a canister.

COMPMC determines the Compton electric current density per photon per second at a designated initial photon energy. The number of and energy level of photons are determined from results from a summary of the gamma spectrum (photons/sec) per fuel assembly (as described above) at 100, 300, 1000, 10000, and 100,000 years after emplacement. All photons originating in the structural material, actinides, and fission products of the fuel assembly are included in the summary. Values of the gamma-spectrum at discrete energy levels are listed in Table (1). The electric current density caused by Compton scattered electrons in a dry tuff are calculated using the gamma ray source defined in this table.

Table 1

Summary of gamma spectrum (photons/sec) per fuel assembly (structural materials + actinides + fission products)

MeV	100y	300y	1000y	10000y	100000y
0.30	2.4E13	1.8E13	7.8E12	1.1E12	5.6E10
0.63	1.6E14	1.8E12	2.5E11	1.1E11	1.4E10
1.10	1.4E11	7.6E10	7.2E10	3.7E10	9.8E09
1.55	5.6E06	3.2E06	1.8E07	7.6E08	6.1E09
2.75	1.3E09	1.3E09	1.3E09	1.2E09	6.9E08

An additional routine was incorporated into COMPMC to indicate the degree of accuracy of the values for the current density for different numbers of histories. The standard deviation of the values of the current density for each compartment was determined in order to indicate the accuracy of the resulting normalized values.

The Central Limit Theorem determines the probability that the difference between the Monte Carlo approximation for current density, j, and the true value of the current density, $\langle j \rangle$, is less than a given ε. This theorem is stated as

$$P(|j - \langle j \rangle| < \varepsilon) \underset{n \to \infty}{\to} (2/\pi)^{1/2} \int_0^{(\varepsilon \sqrt{n})/\sigma_d} e^{(-t^2/2)}\, dt \qquad (9)$$

where n is the number of histories and σ_d is the standard deviation. The right hand side of equation (9) is referred to as the confidence level and was assigned a value of 90%. Thus, 90% of the values for the current density determined by COMPMC are therefore assumed to be accurate to + ε of the true value of the current density.

The value of $_d$ is calculated for current density at each radial centimeter to give an indication of the scatter of the results at various history levels. The values of current density and determined for a 90% confidence interval are plotted versus radial distance in Figure (3) for energy 1.55 MeV. The

anomalous behavior in current density near the canister is believed to be a result of edge effects and not important. Figures for the other energy levels are similar to this one.

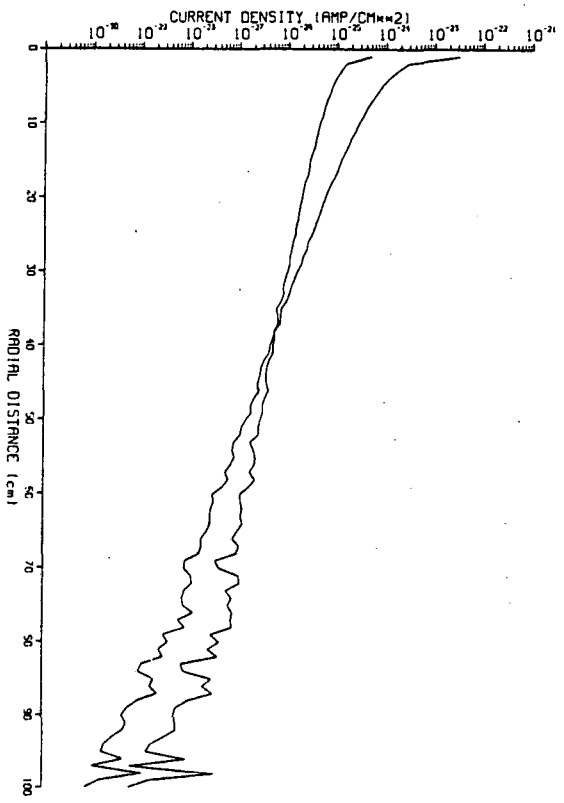

Figure 3. Current density versus radial distance from canister. Lower curve at left is ε.

The Compton current creates a displacement of electrons away from the canister. A return flow of conduction electrons which is equal and opposite to the Compton current results in an electric field as defined by Ohm's law (equation 4). The electric current density is determined at each radial centimeter at discrete gamma ray energies for each of the five time periods. The total electric field encompassing the HLW canister is the summation of the five contributing electric field values which were determined at the five discrete energy levels. The resulting quantities are plotted versus radial distance at 100, 300, 1000, 10000, and 100,000 yrs in Figure (4). A value of 1,000,000 ohm-cm was assigned to the resistivity of dry tuff in this calculation (Telford et al., 1976). As is illustrated in Figure (4), the electric field never exceeds the minimum threshold necessary for forced diffusion to be significant in the rock mass case.

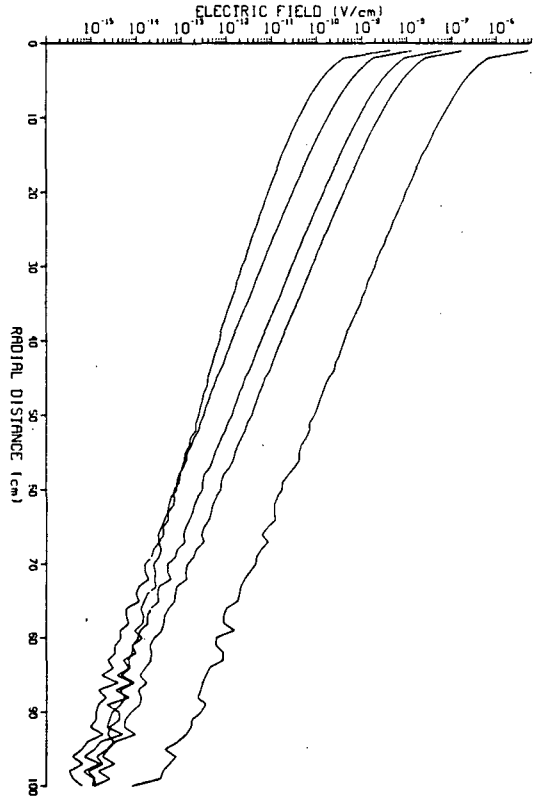

Figure 4. Electric field versus radial distance. Upper curve is at 100 yrs and lower curve is at 100,000 yrs.

A second scenario is investigated for the potential of forced diffusion near a HLW canister. The significance of forced diffusion in a significantly large air space immediately proximal to a canister will differ from the case where the canister is completely enveloped in rock mass. Large air spaces around a canister can result from large fractures possibly induced by the thermal load caused by the canister, by the mechanical loading and unloading of stress in the disturbed zone around the borehole or if the borehole intersects a region of highly fractured rock. Leaving the borehole absent of backfill has been suggested (Fernández and Freshley, 1983) as a means of reducing liquid flow under conditions of negative pressures.

COMPMC and RS are used to predict the current density in air by the same methodology that was used for the previous rock mass model. The effective electron range versus electron energy relationship is dependent upon the medium through which the electron in travelling. RS is again used to calculate this relationship for electrons travelling through air. The atomic mass of air has an assigned value of 28.9 and the atomic number has the

value of 14.2 in these calculations.

As in the case for the rock mass model, the coefficients for three second order polynomials are calculated from 23 data points to approximate the effective electron range/electron energy relationship. Figure (5) illustrates the computed values of effective electron range versus the electron energy and the associated approximating polynomials.

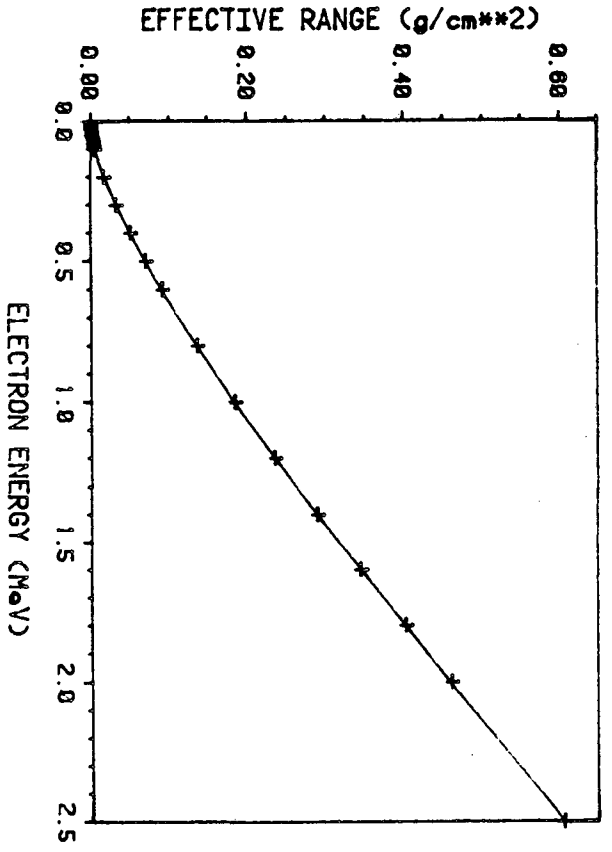

Figure 5. Electron energy versus effective range in air.

COMPMC determines the current density in air for the same five energy levels of the gamma ray source summarized in Table (1). The variable ε was calculated at a 90% confidence interval for each energy level. The values of current density and are plotted versus radial distance and ε illustrated in Figure (6) for energy 1.55 MeV as an example.

The edge effects of current density nearest the cannister are more pronounced than was observed for current density in the rock mass. Additionally, the falloff of the magnitude of current density versus radial distance is substantially less in air than in the rock mass. Although Figure (6) is only for the distance out to 100 cm, the current density was calculated out to 400 cm through air with a continuing gradual decrease in current density observed.

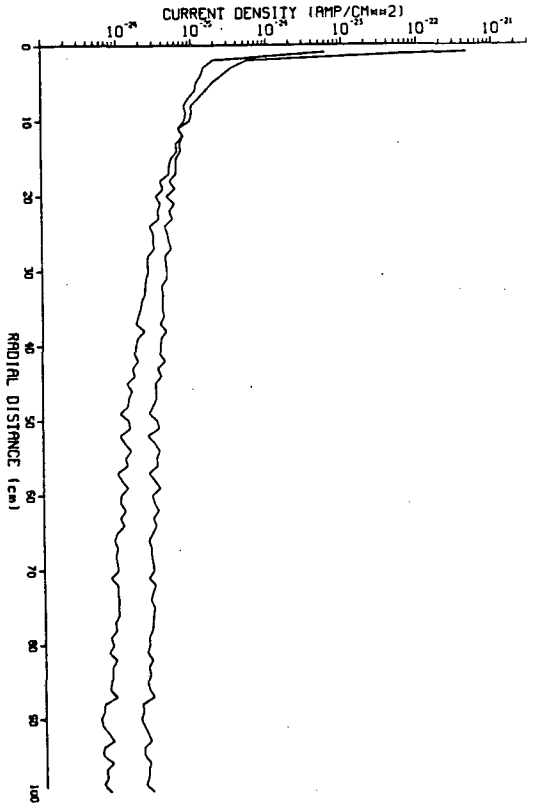

Figure 6. Current density versus radial distance. Lower curve at left is .

The electrical conductivity of a gas, σ_{cond}, (amp/V-cm) can be calculated for a binary gas mixture using the expression (Chapman and Cowling, 1970)

$$\sigma_{cond} = (n_1 n_2 n/(k^2 T) \cdot (e_1 m_2 - e_2 m_1) D_{12} \qquad (11)$$

where gases 1 and 2 are ionized. e_i, m_i and n_i denote the charge, mass and number density of the i^{th} gas molecule. If it is assumed that one of the of gases is neutral and the mass of the ionized gas is negligible when compared to the overall mass of the gas mixture, then n equals n_1. Equation (11) is further simplified by assuming that ions are singly charged, leaving only the ion density as an unknown. The coefficient of diffusion is assigned a value of 0.25 cm^2/sec at a temperature of 373°K for these calculations.

The value of ion density is the most difficult variable in equation (11) to determine. The value of n will depend on

several parameters indirectly (such as temperature, matric potential, degree of fracturing, and geochemical composition of the water and the rock mass) and depend directly upon the vapor pressure of the species of interest and its thermodynamic and kinetic properties. An approximation of n is based upon the gaseous iodine content of marine air, 5 ng/m^3 (Moyers and Duce, 1972), which corresponds to an electrical conductivity of about 1.0E-15 mhos/cm. A critical assumption in this calculation is that all iodine molecules are ionized and that the iodine molecules account for the entire electrical conductivity of the gas. A gas with an electrical conductivity of 10^{-15} mhos/cm therefore has a resistivity of 10^{15} ohms-cm. The electric field in air caused by Compton scattered electrons is determined using this value of electrical resistivity for the gas.

The electric field resulting from the current densities is illustrated in Figure (7) calculated at periods of 100, 300, 1000, 10000 and 100,000 years. If the threshold of importance of forced diffusion as a transport mechanism relative to ordinary diffusion is 2 V/cm, then forced diffusion is potentially significant in an air environment surrounding a HLW canister for the initial 10,000 or so years after emplacement.

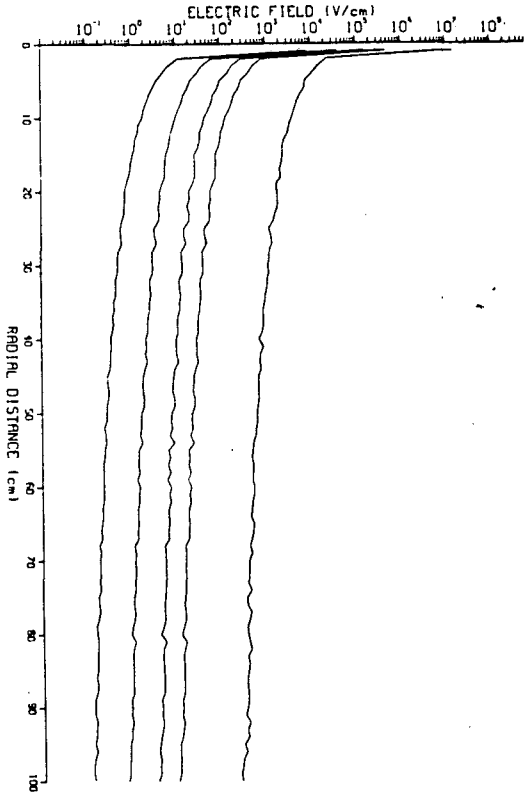

Figure 7. Electric field versus radial distance. Upper curve is at 100 yrs and lower curve is at 100,000 yrs.

Electric fields with an order of magnitude of intensity as indicated in Figure (7) can only be expected in a region totally devoid of material. Any material present in the electric field will tend to short circuit the return flow of electrons resulting in electric fields of lower intensity.

DISCUSSION

Two limiting cases have been presented which illustrate the magnitude of flux which can be theoretically expected by forced diffusion under different conditions. A more probable scenario to be expected at a HLW repository will be a transitional case which incorporates properties from both extremes. Further analysis is necessary to evaluate a transitional case.

REFERENCES

Chapman, S. and T.G. Cowling (1970). The Mathematical Theory of Non-Uniform Gases, Cambridge Press, New York.

Fernandez, J.A. and M.D. Freshley (1984). "Repository Sealing Concepts for the Nevada Nuclear Waste Storage Investigations Project," SAND83-1778.

Filippone, W. (1985). SR--Electron Transport Computer Program, Dept of Nuc Eng, U of AZ.

Gross, B. (1959). "The Compton Current," Zeitschrift fur Physik, 155, p479-487.

Lamarsh, J.R. (1966). Introduction to Nuclear Reactor Theory, Addison-Wesley, Reading, Mass.

McDaniel, E.W. and E.A. Mason (1973). The Mobility and Diffusion of Ions in Gases, John Wiley, New York.

Moyers J.L. and R.A. Duce (1972). "Gaseous and Particulate Iodine in the Marine Atmosphere," J Geoph Res, 77(27), p5229-5238.

Sutherland, S.H. and D.E. Bennett (1979). "Defense High-Level and Spent Fuel Characterization for Geologic Waste Repositories," SAND79-0172.

Telford, W.M., L.P. Geldart, R.E. Sheriff and D.A. Keys (1976). Applied Geophysics, Cambridge Press, New York.

COUPLED PROCESS ANALYSES FOR SALT REPOSITORY PERFORMANCE ASSESSMENT

Sumant K. Gupta, Sanford G. Bloom,
Amy M. Monti, and Gilbert E. Raines

Office of Nuclear Waste Isolation
Battelle Project Management Division
505 King Avenue
Columbus, Ohio 43201

ABSTRACT

Salt sites are being investigated as potential candidates for a deep geologic repository for high-level nuclear waste. To assess the performance of a repository in salt it is necessary to estimate the potential for naturally occurring and/or intrusive fluids to contact the radioactive waste and transport it to the accessible environment. The long-term performance assessment of a salt repository consists of multidisciplinary studies of the coupled physical and chemical interactions in geologic systems involving heat transfer, ground-water hydrology, geomechanics, geochemistry, and radionuclide transport. The coupled process analyses performed or planned to be conducted include coupled thermal, stress, and pressure-induced brine migration; flow, thermal, mechanical, and geomechanical (corrosion and leach rate) analyses for waste package and waste form performance; flow, thermal, and mechanical analyses for shaft seals and near-field performance; flow, thermal, dissolution, and salt creep analyses for borehole scenarios; flow, energy, and solute transport analyses of the groundwater system in the vicinity of site; and coupled analyses of hydrologic, mechanical, geochemical, and radionuclide transport.

INTRODUCTION

The long-term performance assessment of a salt repository consists of multidisciplinary studies of the coupled physical and chemical interactions in geologic systems involving heat transfer, ground-water hydrology, geomechanics, geochemistry, and radionuclide transport. Figure 1 illustrates the interaction among different processes in the repository (near-field) subsystem. Similar interactions for other subsystems, such as site, have been developed (ONWI, 1984). Ideally, simultaneous solution of all the coupled processes is desirable; however, due to the complexity of simultaneous solutions, the only processes solved in this manner are those that are strongly coupled to each other and have highly nonlinear responses. Coupled processes are normally solved sequentially for a given time step, and iterated within each time step until convergence is achieved. Weakly coupled processes (whose results are not significantly affected by other processes) are solved sequentially using the output of one process code as input to the next process code.

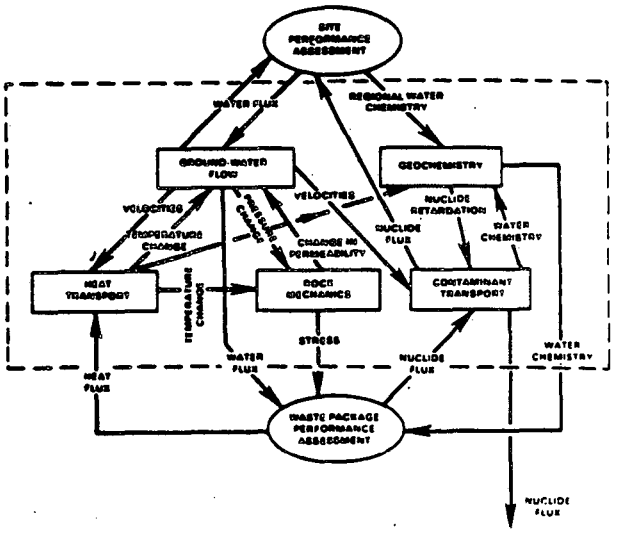

Figure 1. Interaction among different processes in the repository (near-field) subsystem (ONWI, 1984).

Salt has favorable characteristics and properties as a host for long-term storage and isolation of nuclear waste from the accessible environment. These characteristics include structural strength, good radiation-shielding capability, high plasticity, extremely low permeability, and low moisture content. The low moisture content is important because of the corrosive nature of brine and its potential to degrade the waste package. The fluids that normally occur within salt deposits are in the form of intracrystalline inclusions, intergranular moisture, moisture associated with interbed impurities, and chemically bound water. The movement of these fluids under thermal, mechanical, pressure, and other significant driving gradients must be considered to assess the potential degradation of the waste package and the performance of engineered systems. In addition to naturally occurring moisture, there is a possibility for larger amounts of moisture to enter the repository due to natural- or human-induced events or processes. The potential for salt dissolution under such disruptive changes requires coupled analyses of several processes such as flow, temperature, dissolution, precipitation, and salt creep.

The following is a preliminary list of strongly coupled process analyses conducted or planned for performance assessment of a salt repository:

(1) Coupled thermal-, stress-, and pressure-induced brine migration studies in the neighborhood of the waste package.

(2) Coupled flow, thermal, mechanical, and geochemical (corrosion and leach rate) analyses for the waste package and waste form performance.

(3) Coupled flow, thermal, and mechanical analyses for shaft seal and near-field performance.

(4) Coupled flow, temperature, dissolution/precipitation, and salt creep analyses for borehole scenarios.

(5) Coupled flow, thermal, and solute transport to account for density effects in estimating travel paths and travel times from the disturbed zone to the accessible environment.

(6) Coupled hydrologic, mechanical, geochemical, and radionuclide transport analyses.

The above list of coupled processes defines the quantity of fluid migration to the waste package, shaft seal and near-field evaluations, size of cavity caused by salt dissolution in the uncased borehole, variable density effects on ground-water travel time and path, and radionuclide transport. Some of the analyses being currently considered as sequential will be simulated as coupled processes with enhanced computer codes.

Much site-specific information remains to be collected and analyzed. Site-specific engineering designs (such as waste package, repository, and shaft seal designs) are yet to be completed. In situ tests are being planned (Roberds et al, 1985) to provide input data and experimental results for detailed coupled process analyses and validation of computer codes and conceptual models.

This paper briefly describes the status of the six above-mentioned coupled process analyses completed under the Salt Repository Program using available information. This paper also discusses planned coupled process analyses. Simulation examples are included from the draft Environmental Assessment (EA) reports (DOE, 1984) and other works under progress.

COUPLED THERMAL-, STRESS-, AND PRESSURE-INDUCED BRINE MIGRATION IN THE NEIGHBORHOOD OF THE WASTE PACKAGE

Migration of the different forms of naturally occurring moisture may be driven by various mechanisms. It has been postulated that intracrystalline inclusions will tend to migrate under the influence of temperature gradients and that intergranular and interbed moisture will move in response to pressure and stress gradients (Jenks and Claiborne, 1981; Gnirk et al, 1981; Olander, 1982). Another assumption is that moisture can also move under the influence of concentration gradients by a diffusion-like mechanism (DOE, 1984). However, this latter assumption is based only on successful curve-fitting and, as yet, has no theoretical justification. The temperatures in a salt repository are not expected to reach levels high enough to mobilize chemically bound water (Shefelbine, 1982).

Most simulations of fluid migration in salt, in the absence of any intrusion, have thus far been based on coupled flow and temperature using an empirical expression for the velocity of intracrystalline inclusions, the so-called Jenks' equation (Jenks, 1979). Pressure coupling is included in some models (Olander, 1982; Ratigan, 1984) in which inclusions are allowed to move to grain boundaries by this mechanism. The moisture then collects in the intergranular spaces and moves further in response to pressure gradients either as vapor or liquid. However, Jenks and Claiborne (1981) assume the Jenks' equation could apply continuously throughout the salt. Calculations for the draft EA reports (DOE, 1984) are based on coupled temperature and fluid migration analyses using Jenks' equation. There is a strong dependence of velocity on temperature through the Jenks' equation but only a weak dependence of temperature on changes due to fluid migration. Consequently, the model equations were solved sequentially rather than simultaneously.

Figure 2 compares two solutions (finite difference and semianalytical) of the model with data from the Salt Block II experiment (Hohlfelder, 1980). This experiment measured brine accumulation in a heated borehole at the center of a salt cylinder 1 m in diameter and 1 m high. Both solutions show reasonable agreement with the experiment. The BRINEMIG code uses the finite-difference method while the semianalytical solution is based on methods presented by Bloom and Raines (1985). BRINEMIG was also applied to estimate the brine accumulation around a waste package (Figure 3) at the Deaf Smith site (DOE, 1984). The rate of heat generation from a waste package declines with time and results in decreased temperatures in the neighborhood of the package. The decreased temperatures, in turn, result in decreased velocities and decreased brine flow rates. Consequently, the accumulated brine initially increases rapidly with time but levels off to a constant value as the flow rate goes to zero. This behavior is shown in Figure 3 for both commercial, high-level wastes (CHLW) and spent fuel from pressurized water reactors (SFPWR).

Some uncertainty still exists in the details of coupling stress and pressure gradients to brine migration. Although some models include stress and pressure mechanisms, they generally require parameters that cannot presently be measured and must be adjusted to make the model results comparable with experiments. While the calculations summarized here did not include

pressure or stress considerations, future studies will try to resolve these difficulties in order to achieve a fully coupled model.

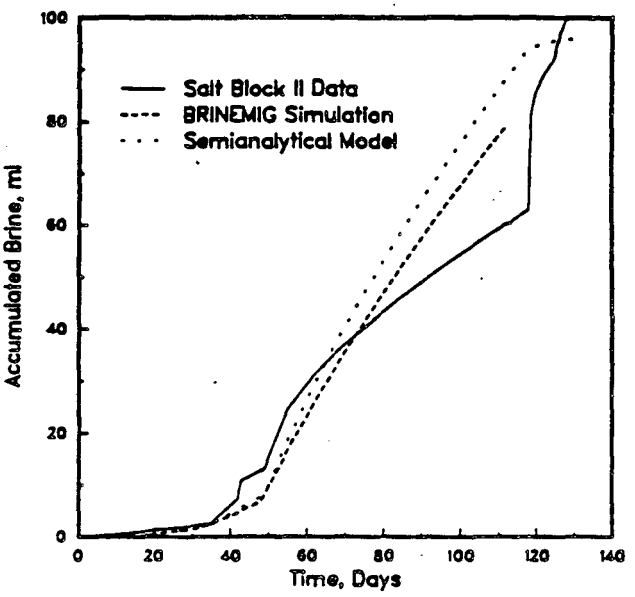

Figure 2. Accumulated moisture vs. time salt block II comparison.

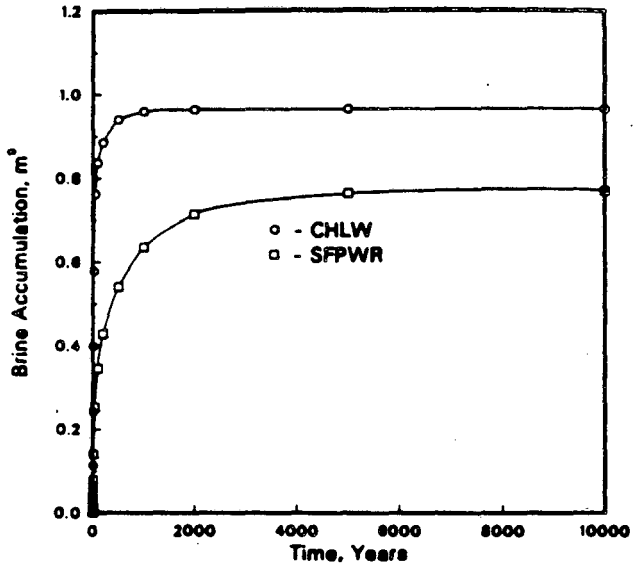

Figure 3. Brine accumulation vs. time at the waste package (DOE, 1984).

COUPLED FLOW, THERMAL, MECHANICAL, AND GEOCHEMICAL ANALYSES FOR THE PACKAGE AND WASTE FORM PERFORMANCE

Analysis of the waste package must include the degradation of the package wall, and if that happens, the release of radionuclides. The present degradation model (Jansen, 1985; INTERA, 1983) includes five distinct degradation submodels (radiation, thermal, mechanical, corrosion, and leaching) that are driven both internally by waste decay and externally by repository stress and fluids. The model, therefore, must include coupling among submodels for radiation, temperature, mechanical effects, fluid migration, and chemical reactions.

If the package fails, radionuclide release rates are determined by radionuclide solubilities and the following mechanisms: (1) the rate of dissolution of the waste form, (2) the rate of mass transfer across any waste form resistance, and (3) rate of fluid flow away from the neighborhood of the waste package. These rates are also functions of radiation, temperature, mechanical effects, fluid migration, and chemical reactions. The present model (Jansen, 1985) estimates radionuclide releases with the assumption that only one of the above rate mechanisms is significant and there are no interactions between these rates.

The waste package degradation process can be expressed in the form of waste package wall thickness as a function of time. The magnesium concentration in brine significantly affects the degradation of the waste package. Figures 4 and 5 show the results for fluids with both high (35,000 ppm) and low (about 150 ppm) magnesium content and for expected (without disruptive events) and unlimited fluid rates. These calculations predict that the package will contain waste for at least 1,000 years under the expected conditions.

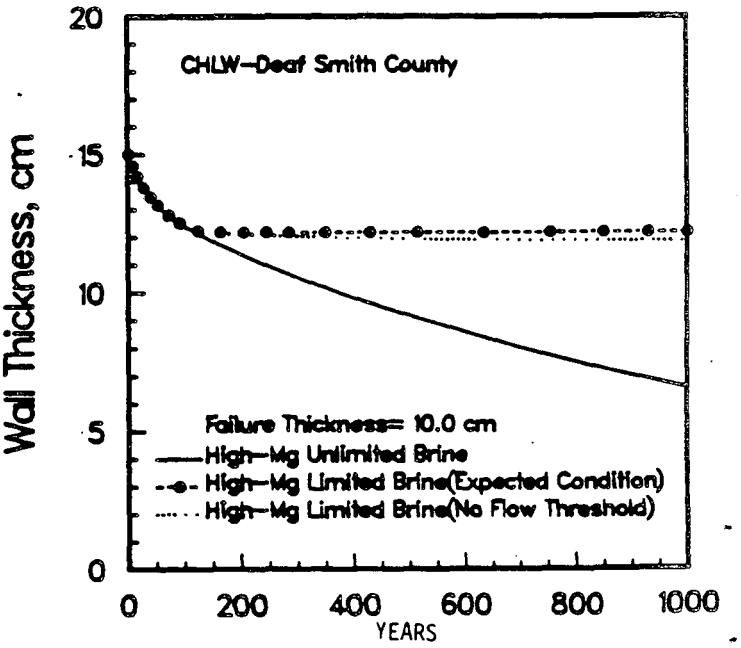

Figure 4. Corrosion and failure of waste package in high-magnesium brine (Jansen, 1985).

Future degradation analyses will include effects of consumption of fluids in geochemical processes on: (1) possible pressure buildup due

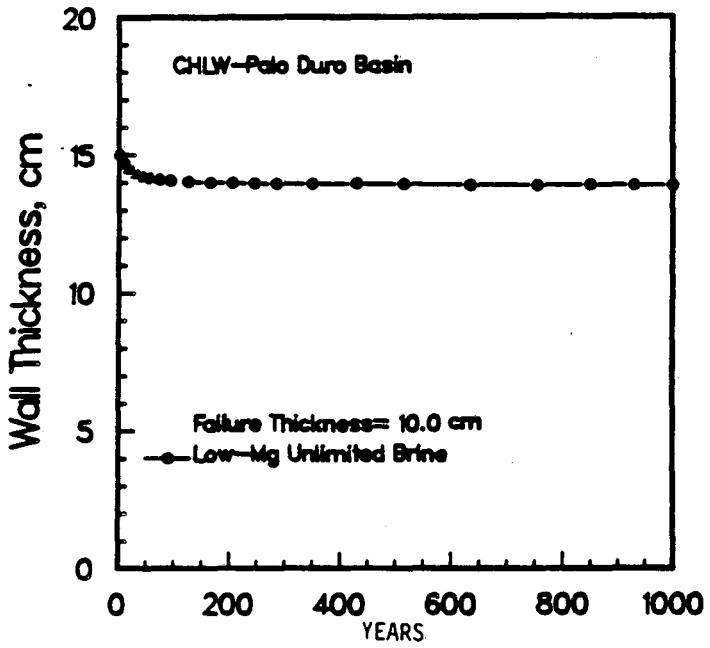

Figure 5. Corrosion and failure of waste package in low-magnesium brine (Jansen, 1985).

to hydrogen released from the corrosion reaction on fluid migration, stresses, and corrosion rates, (2) the effect of corrosion products on solubilities, and (3) the effects of corrosion reactions on the mechanical properties of the waste package wall. Future analyses of radionuclide releases will include combined hydrologic, thermal, mechanical, and geochemical (corrosion and its products) effects on the radionuclide release mechanisms.

COUPLED FLOW, THERMAL, AND MECHANICAL ANALYSES FOR SHAFT SEAL AND NEAR-FIELD PERFORMANCE

Shafts and tunnels used to access the repository will be sealed after waste emplacement in order to minimize the penetration of water and the transport of any radionuclides that may escape from the waste package. The properties of the seal system that affect water flow (including interfaces with the undisturbed salt and other host rock) are strongly coupled with flow, temperature, and mechanical conditions. The STEALTH (Hofmann, 1981) and SNEAKY (Hart, 1981) computer codes are used to solve the highly nonlinear coupled flow, thermal, and mechanical equations for dynamic or quasi-static, porous geologic systems. The mathematical models are based on the continuum theory to describe the multiphase nature of the system, and on the incremental linear constitutive theory to describe the path dependency of nonlinear material behavior. Following are some of the preliminary analyses used either for benchmarking or developing techniques for performance assessment:

(1) Near-Field Flow Analyses. A near-field waste repository setting (Figure 6) is used by Hart (1981) to account for both the thermal buoyancy and stress effects on initiation and development of fluid flow currents in mined and backfilled rooms above the waste canisters (Figure 7). More detailed simulations will be performed using site-specific data and design to provide an understanding of the interaction of the thermal, mechanical, and fluid flow processes, and to quantify the effects which may be missed in a partially coupled or uncoupled analysis.

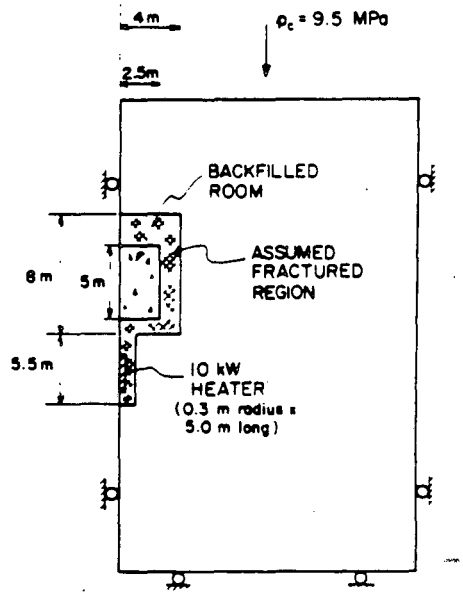

Figure 6. Schematic of near-field waste-repository setting (Hart, 1981).

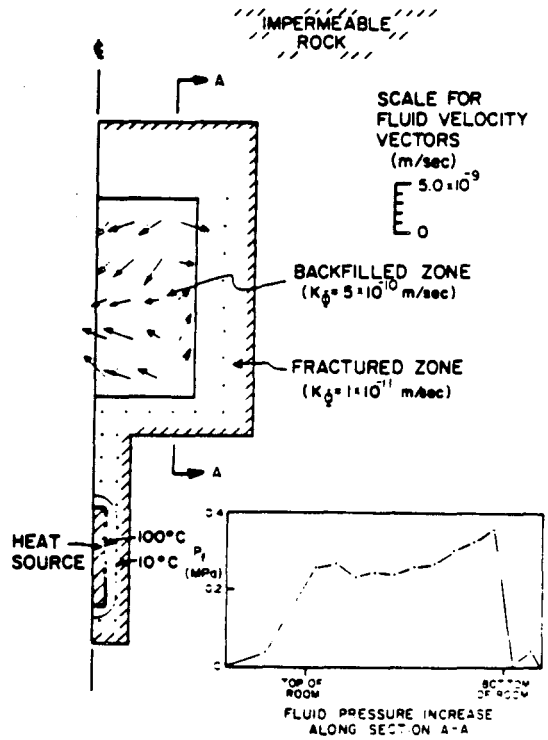

Figure 7. Thermomechanical-induced fluid pressure in backfill (Hart, 1981).

(2) Shaft-Seal Analyses. The CAVS (Crack And Void Strain) material model in submodules of the STEALTH code was used in preliminary studies to analyze (a) the behavior of existing joints, and (b) the initiation of new fractures during the construction and operational lifetime of the shaft and their effect on hydraulic conductivity. Figure 8 is a schematic showing the shaft/repository region and the hydraulic conductivity changes in the geologic media due to shaft construction.

(3) Room Closure Estimates. Figure 9 illustrates a sample of (a) temperature distribution and (b) roof-to-floor closure simulated by coupled temperature and deformation analyses.

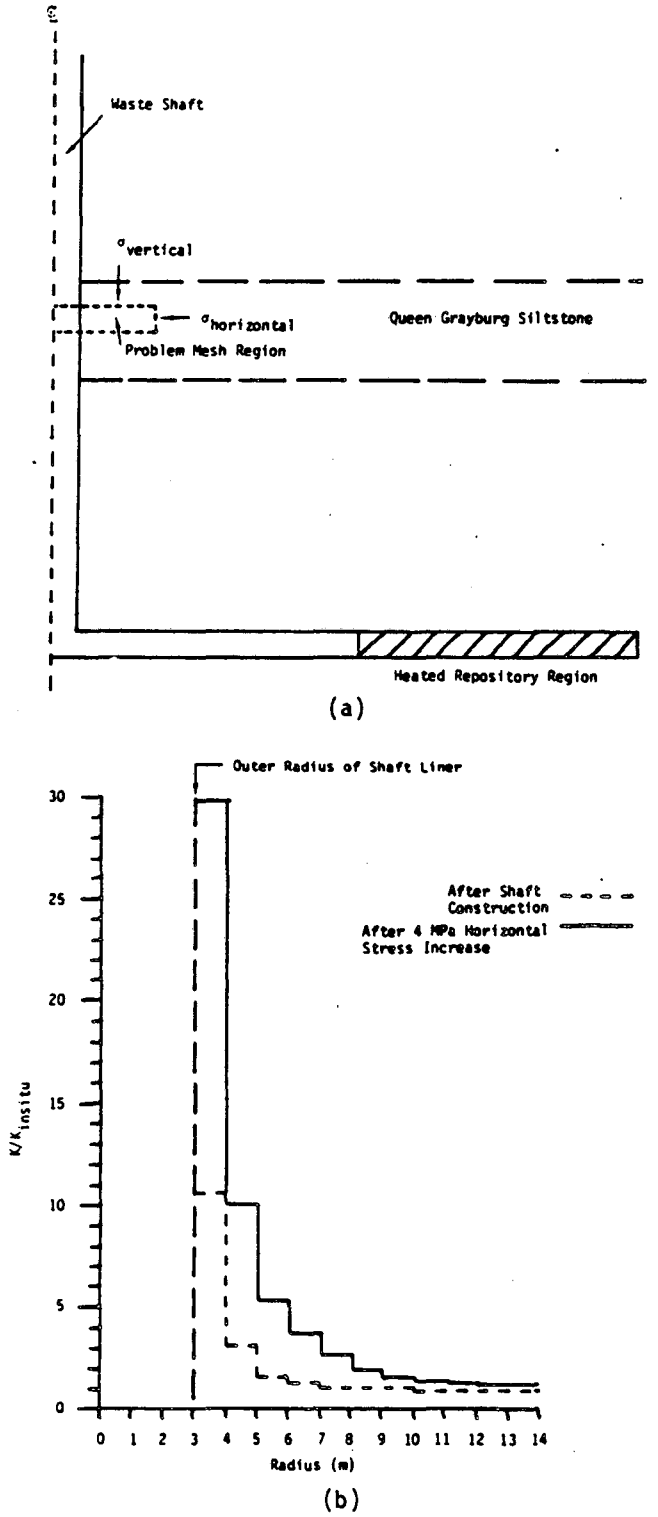

Figure 8. (a) Schematic of shaft/repository region; (b) Hydraulic conductivity changes (Maxwell et al, 1984)

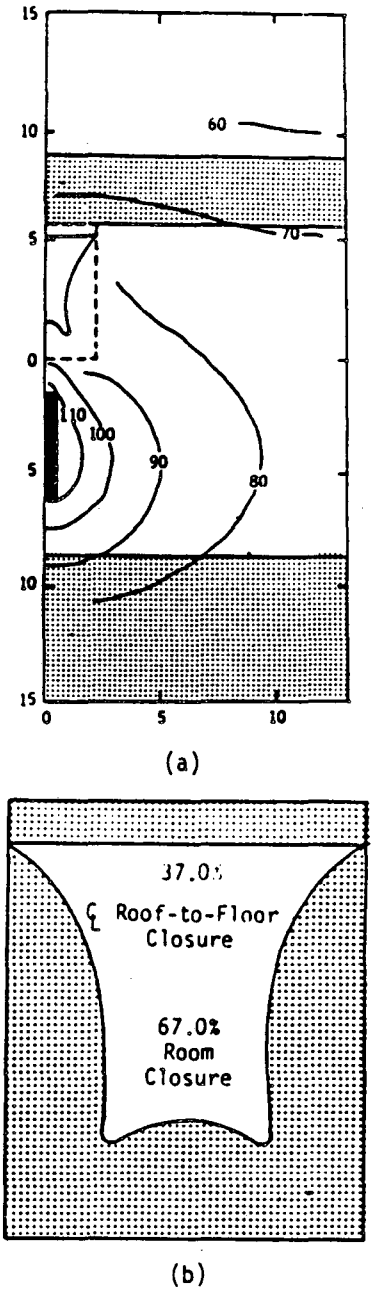

Figure 9. (a) Temperature (C^{o}) contours; (b) Roof-to-floor closure at 5 years (Dial et al, 1985)

COUPLED FLOW, TEMPERATURE, DISSOLUTION/PRECIPITATION AND SALT CREEP ANALYSES FOR BOREHOLE SCENARIO

Coupled analyses of flow, temperature, salt dissolution/precipitation, and salt creep are planned to evaluate the effects of foreseeable human activities, such as exploratory boreholes, on salt repository performance. A computer code, BORHOL (INTERA, 1984), has been developed to evaluate the progressive saturation of fluid flowing in a borehole through salt units. The code evaluates the process of salt dissolution from borehole walls and takes into account its dependence on temperature and salt solubility. Creep deformation of the borehole in the salt units is also evaluated.

The BORHOL code was used to quantify the maximum increase in the diameter of the existing boreholes at the repository horizon at the proposed Cypress Creek Dome site in Mississippi (Monti and Gupta, 1984). The analysis examined the effects of salt dissolution and the opposing effects of salt creep on borehole closure under the conservative assumption that the borehole is uncased. Figure 10 is a schematic of the borehole and Figure 11 illustrates the diameter of the borehole vs. depth for 5, 10, 20 and 30 years. Ground water in the lower aquifer was conservatively assumed to have zero salt concentration. With an upward flow gradient, the maximum size of cavity formed is at the lower salt interface. Creep closure of the borehole is reached at 30 years.

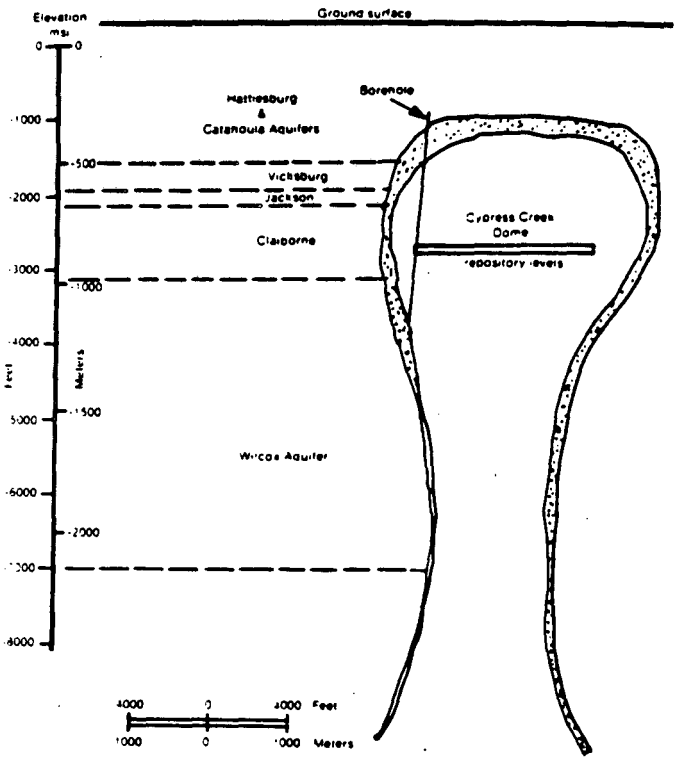

Figure 10. Schematic of a borehole (Monti and Gupta, 1984).

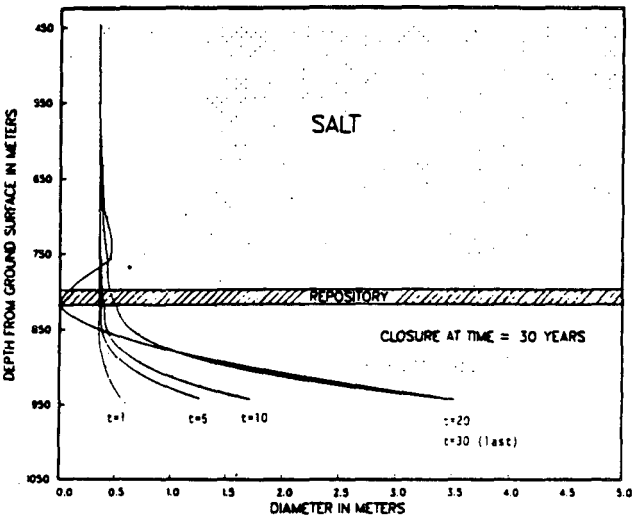

Figure 11. Borehole diameter vs. depth over time (Monti and Gupta, 1984).

A system code is under development for assessing salt repository scenarios using a flow network considering temperature, creep closure, and salt dissolution. The code capabilities will include preprocessor for statistical sampling and a postprocessor for developing Complementary, Cumulative Distribution Functions (CCDF).

COUPLED FLOW, ENERGY, AND SOLUTE TRANSPORT ANALYSES OF GROUND-WATER SYSTEM IN THE SITE VICINITY

Evaluations of ground-water travel times from the repository to the accessible environment must include density variation effects due to pressure, temperature, and solute concentration. The need for coupled analyses obviously increases as temperature increases due to waste emplacement. The geohydrologic codes used in performance assessment include capabilities for coupled flow, energy, and solute transport. The mechanical effects on hydraulic properties will be simulated explicitly by using conservative (towards increasing flow velocity) effects of thermomechanical stresses on hydraulic parameters.

Site-specific data for coupled flow, thermal, and solute transport analyses of local ground-water system are yet to be collected. A series of preliminary simulations have been made using CFEST (Gupta et al, 1982) code to understand system performance. Due to the extremely low permeability of salt, the buoyancy and convection effects are not very significant. Figure 12 illustrates the temperature distribution, estimated with coupled flow and thermal analysis after 3,000 years of waste emplacement. The effects of hydrodynamic dispersion of the thermal plume are not very prominent.

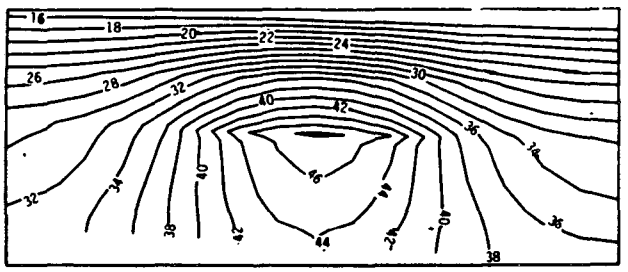

Figure 12. An illustrative temperature (°C) distribution after 3,000 years with coupled flow and energy transport in the site vicinity.

Coupled flow, energy, and solute transport analyses for regional and local ground-water systems in the vicinity of the site are under progress. Regional-scale modeling will define appropriate spatial limits and boundary conditions for local ground-water system analyses. The detailed local ground-water system analyses are planned to be conducted to address uncertainties in the geologic parameters. The Latin Hypercube sampling approach will be used to estimate bounds on alternate travel paths and travel time.

COUPLED HYDROLOGIC, MECHANICAL, GEOCHEMICAL, AND RADIONUCLIDE TRANSPORT ANALYSES

Radionuclides that escape from the waste package may be transported to the accessible environment by fluids that contact the waste package. The mechanisms involved are (1) the release of radionuclides to the fluid from the waste package and waste form, and (2) transport with the fluid. The transport mechanisms depend on temperature, pressure, mechanical effects, and chemical reactions. The radionuclide transport calculations in the EA reports (DOE, 1984) used the diffusion-like mechanism, described earlier, to simulate fluid transport without disruptive events. Figure 13 (McNulty et al, 1985) shows that releases equal to the EPA standards at 5 km (40 CFR 191) travel less than two meters from the package in 10,000 years.

Future analyses will include detailed coupled hydrologic and mechanical interactions. Human intrusion or other disruptive events could result in transporting radionuclides to the aquifer system. The ground-water flow field (direction and magnitude) defined by flow, thermal, and solute concentration gradients will be coupled with the geochemical model for estimating radionuclide transport. The effects of chemical reactions or interactions would be very significant and a detailed geochemical model, such as EQ3/EQ6 (Wolery, 1983, 1985) may be required.

CONCLUSIONS

Analyses of many coupled processes are required to assess the performance of a salt repository. Some analyses have been conducted using existing data and models. More detailed analyses require site-specific information and detailed repository designs, but neither a specific site nor a specific design has been selected for a salt repository.

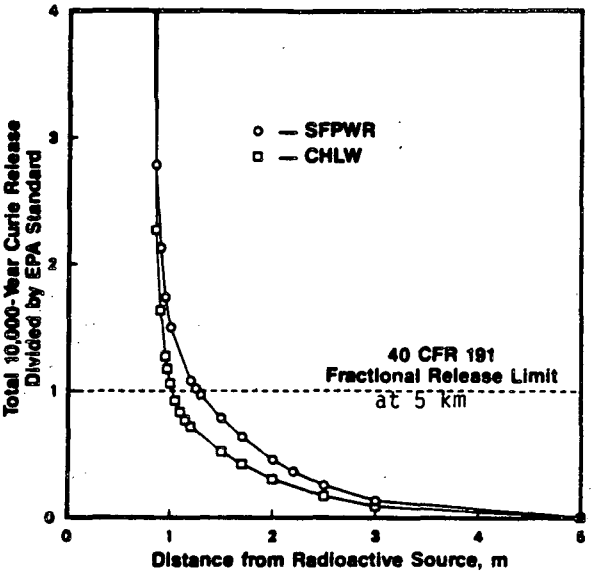

Figure 13. Total 10,000 year Curie release divided by EPA standard for various distances from a radioactive source for bedded salt.

Coupled-process models have been developed to aid in performance assessment and repository design. These models are for simultaneous and sequential solutions. The former type includes models for coupled flow, thermal, and mechanical processes and coupled flow, energy, and solute transport. The latter type includes a number of single-process models in which the output from one is used as the input to the other. As more information becomes available, the need for more coupled process models will be assessed and additional models will be developed. Some analyses which are performed as sequential will be replaced by simultaneous solution.

ACKNOWLEDGMENT

The authors would like to acknowledge the contributions by Dr. T. L. Steinborn for his review comments and helpful suggestions.

REFERENCES

Bloom, S. G., and G. E. Raines. (1985). "Analytical and Semianalytical Models for Estimating Temperature, Brine Migration, and Radionuclide Transport in a Salt Repository." Paper presented at the International Topical Meeting on High-Level Nuclear Waste Disposal, Pasco, WA, September 24-26.

Dial, B. W., D. E. Maxwell, and W. Yeung. (1985). Room and Canister Scale Thermal Mechanical Benchmarks Between STEALTH 2D and SPECTROM-41/SPECTROM-21, SAIC-85/1068, (Draft),

prepared for Office of Nuclear Waste Isolation, Battelle Memorial Institute, Columbus, OH.*

DOE. See U.S. Department of Energy.

Gnirk, P. F., W. B. Krause, and A. F. Fossum. (1981). State-of-the-Art Review of Brine Migration in Salt, SAND81-7054, prepared by RE/SPEC, Inc., Rapid City, SD, RSI-0075, for Sandia National Laboratories, Sandia Corporation, Albuquerque, NM.

Gupta, S. K., C. T. Kincaid, P. Meyer, C. Newbill, and C. R. Cole. (1982). A Multidimensional Finite-Element Code for the Analysis of Coupled Fluid, Energy, and Solute Transport (CFEST), PNL-42670, Battelle's Pacific Northwest Laboratory, Richland, WA.

Hart, R. D. (1981). "A Fully Coupled Thermal-Mechanical-Fluid Flow Model for Nonlinear Geologic Systems," Ph.D. thesis, University of Minnesota, Minneapolis, MN.

Hofmann, R. (1981). STEALTH--A Lagrange Explicit Finite Difference Code for Solids, Structural, and Thermohydraulic Analysis. Introduction and Guide, EPRI NP-2080-CCM-SY, prepared by Science Applications International Corporation for Electric Power Research Institute, Palo Alto, CA.

Hohlfelder, J. J. (1980). Salt Block II: Description and Results, SAND79-2226, Sandia National Laboratories, Albuquerque, NM.

INTERA Environmental Consultants, Inc. (1983). WAPPA: A Waste Package Performance Assessment Code, ONWI-452, prepared for Office of Nuclear Waste Isolation, Battelle Memorial Institute, Columbus, OH.

INTERA Environmental Consultants, Inc. (1984). BORHOL, A Computer Code to Evaluate Dissolution, Precipitation, Creep, and Temperature Effects in Boreholes in Salt, Final Draft, prepared for Office of Nuclear Waste Isolation, Battelle Memorial Institute, Columbus, OH.

Jansen, G., 1985. Expected Waste Package Performance for Nuclear Waste Repositories in Three Salt Formations. (1985). ONWI-Draft*, Office of Nuclear Waste Isolation, Battelle Memorial Institute, Columbus, OH.

Jenks, G. H. (1979). Effects of Temperature, Temperature Gradients, Stress, and Irradiation on Migration of Brine Inclusions in a Salt Repository, ORNL-5526, Oak Ridge National Laboratory, Oak Ridge, TN.

Jenks, G. H., and H. C. Claiborne. (1981). Brine Migration in Salt and Its Implication in the Geologic Disposal of Nuclear Waste, ORNL-5818, Oak Ridge National Laboratory, Oak Ridge, TN.

Maxwell, D. E., B. W. Dial, and M. B. Gross. (1984). Joint Response of Queen Grayburg Siltstone Due to Excavation and Construction of a Repository Shaft, SAI-83/1247, Draft Final Report, prepared for INTERA Environmental Consultants, Inc., Houston, TX.*

McNulty, E. G., S. G. Bloom, and G. E. Raines. (1985). Expected Near-Field Radionuclide Transport for Nuclear Waste Repositories at Potential Salt Sites, ONWI-Draft*, Office of Nuclear Waste Isolation, Battelle Memorial Institute, Columbus, OH.

Monti, Amy M., and S. K. Gupta. (1984). Salt Dissolution Anmalysis in Existing Boreholes at Cypress Creek Dome, (Draft*), Office of Nuclear Waste Isolation, Battelle Memorial Institute, Columbus, OH.

Olander, D. R. (1982). "A Model of Brine Migration and Water Transport in Rock Salt Supporting a Temperature Gradient", Nuclear Technology, Vol. 58, p. 256.

ONWI, 1984. Peformance Assessment Plans and Methods for the Salt Repository Project, BMI/ONWI-545, Office of Nuclear Waste Isolation, Battelle Project Management Division, Columbus, OH.

Ratigan, J. L. (1984). "A Finite Element Formulation for Brine Transport in Rock Salt," Proceedings of the International Journal of Numerical Analytical Methods Geomechanics, Vol. 8, No. 3, p. 225.

Roberds, W. J., R. J. Byrne, and H. Kalia. (1985). "Coupled Processes Addressed by Underground Testing for the Salt Repository Project," Paper presented at the International Symposium on Coupled Processes Affecting Performance of a Nuclear Waste Repository, September 18-23, Lawrence Berkeley Laboratory, Berkeley, CA.

Shefelbine, H. C. (1982). Brine Migration: A Summary Report, SAND82-0152, Sandia National Laboratories, Albuquerque, NM.

U. S. Department of Energy. (1984). Draft Environmental Assessment (Deaf Smith County Site, Texas, DOE/RW-0014, Washington, DC.

Wolery T. J. (1983). EQ3NR, A Computer Program for Geochemical Aqueous Speciation--Solubility Calculations: User's Guide and Documentation, UCRL-53414, Lawrence Livermore National Laboratory, Livermore, CA.

Wolery, T. J. (1985). EQ3/6 Modifications for Geochemical Modeling of Brines, UCRL-report in preparation, Lawrence Livermore National Laboratory, Livermore, CA.

40 CFR Part 191. (1983). Environmental Standards for the Management and Disposal of Spent Nuclear Fuel, High-Level and Transuranic Radioactive Wastes, U.S. Environmental Protection Agency, Proposed Rule, November 1.

* Draft references available upon request from senior author.

COLLOID MIGRATION IN POROUS MEDIA

James R. Hunt, Laura McDowell-Boyer and Nicholas Sitar

Department of Civil Engineering
University of California
Berkeley, CA 94720

ABSTRACT

Retention of radionuclides for long periods near waste repositories depends upon multiple barriers, one of which is adsorption to immobile solid surfaces. Since small particles and colloidal matter have high adsorption capacities per unit mass and can be mobile in subsurface flows, colloidal transport of waste components requires analysis. Theories for predicting colloid migration through porous media have been developed in the filtration literature. In this paper we review the applicablity of filtration theories for predicting particle and colloid transport. Emphasis is on suspended matter much smaller than pore sizes, where physical and chemical forces control migration rather than size dependent physical straining. In general, experimentally verifiable theories exist for particle filtration by clean media, and a sensitivity analysis is possible on particle and media properties and fluid flow rate. When particle aggregates accumulate within pores, media permeability decreases, resulting in flow field alteration and possible radionuclide isolation. An analysis of the limited experimental data available indicates that present theories cannot predict long-term colloid transport when permeability reduction occurs. The coupling of colloid attachment processes and the hydrologic flow processes requires more extensive laboratory and field research than has currently been carried out. An emphasis on fundamental mechanisms is necessary to enhance long-term predictability.

INTRODUCTION

Evaluation of disposal alternatives for nuclear waste requires an understanding of radionuclide transport in altered hydrogeologic systems over time scales far exceeding what can be assessed from laboratory or field experiments. For that reason considerable effort is needed to gain a more fundamental understanding of all the dominant transport processes than is currently available. Only in this way will long-term prediction of radionuclide migration and resulting environmental risk be more feasible.

It has long been recognized that radionuclides present in groundwaters would have limited mobility because of their tendency to adsorb to mineral surfaces. It is often predicted that partitioning between dissolved and adsorbed species will limit radionuclide migration such that effective migration velocities will be orders of magnitude less than groundwater flow velocities. Contaminant retardation predicted by measured distribution coefficients has been criticized because of the simplifications involved in representing adsorption as a linear, equilibrium process (Reardon, 1981; Valocchi, 1984). One aspect of radionuclide migration in subsurface flows that casts further doubt on the distribution coefficient approach is the possibility that colloidal matter and small particles to which radionuclides adsorb are mobile. Particles of sizes less than a few micrometers are much smaller than inter-granular pores or fracture sizes and could migrate considerable distances with flowing fluid. Colloid migration becomes significant in predicting contaminant migration because small particles have high surface areas per unit mass and represent available sites for adsorption. Contaminant transport is thus controlled not solely by adsorption, but also by colloid transport. Colloid transport is controlled by factors that affect accumulation on porous media and subsequent permeability alteration and possible erosion. This paper examines available theories and limited experimental data that quantify colloid migration in porous media.

RADIONUCLIDES AND COLLOID MIGRATION

The literature on colloid transport in subsurface flows is scattered throughout the hydrogeolocial literature with most of the initial work arising from concerns about radionuclide migration following disposal. Champlin and Eichholz (1968) have suggested that fine particle transport may be a significant mode of radionuclide migration in porous media. They reference a number of reports that implicate radionuclide migration in the colloidal state. In laboratory experiments they measured clay particle migration through a fine sand at a flow velocity of 1.2 m/d. Radio-labeled clay and bacteria were found to penetrate only 20 cm after seven days of flow, but a detergent solution was able to remobilize the adsorbed tracers so that tracer migration nearly equaled the fluid flow rate (Champlin and Eichholz, 1976). Sheppard et al. (1980) demonstrated that submicrometer colloidal matter in soil was important in binding radionuclides with the result that many radionuclide adsorption studies now rely on 1.5 nm pore size filters for distinguishing dissolved from colloidal species (e. g., Shade et al., 1984). Nelson et al. (1985) found that colloidal organic carbon competed with lake sediments for binding plutonium, such that measured distribution coefficients decreased with increasing colloidal organic carbon.

The presence of mobile submicrometer colloidal matter may offer an explanation for the observations that batch adsorption studies do not accurately predict radionuclide migration in observed both in continuous flow column studies and in field experiments. Coles and Ramspott (1982) found that ruthenium migrated in the field at a velocity comparable to tritium while laboratory batch sorption measurements predicted migration at less than 1/64 that of the water. However, Reynolds et al. (1982) observed that batch sorption studies for cesium and strontium overestimated migration observed in laboratory columns. Some cases of observed contaminant transport have been attributed to complexation by strong organic ligands like EDTA that tend to prevent adsorption to immobile solids (Cleveland and Reeves, 1981).

Radionuclide sequestering at disposal sites depends upon the limited mobility of the nuclides. Surrounding waste canisters with a bentonite clay backfill is thought to provide a zone of low water permeability and a region of high adsorption capacity. Some concern has arisen over particle release from these barriers and canisters. Le Bell and Stenus (1980) have shown that a bentonite gel would release particles into distilled water because of colloidal dispersion. For natural groundwaters they found the divalent cation concentration was sufficient to coagulate the clay particles and prevent their release into the water, thus limiting radionuclide migration into rock fissures surrounding the clay seal. Shade et al. (1984) showed that colloidal matter was leached from waste canister materials when exposed to hot alkaline water, and this colloidal material adsorbed radionuclides. The released colloidal matter was not observed to coagulate or precipitate and concern was raised on colloidal transport of adsorbed waste components. Avogadro and de Marsily (1984) and Saltelli et al. (1984) have measured the release of submicrometer sized colloids from proposed waste canisters and they have recognized that waste migration has a component associated with colloidal transport through porous media. A combined filtration and adsorption model was fit to their experimental data on americium migration in a sand column.

Similar issues of colloid transport have been addressed by

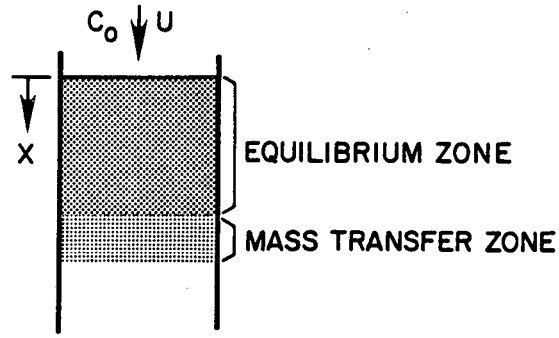

Figure 1. Conceptual representation of colloid deposition within porous media under constant flow conditions.

those interested in soil formation, bacteria and virus migration, artificial groundwater recharge, and petroleum extraction. These fields have adopted various empirical or semi-empirical approaches to characterize colloid migration and porous media permeability alteration as reviewed elsewhere (McDowell-Boyer et al., 1985). The most quantitative work to date has been undertaken in the field of water filtration where deep bed granular media filters are designed for product recovery or waste concentration from liquids. The water filtration literature employs concepts and theories that have direct application to understanding the mechanisms of colloid migration in natural and altered hydrogeologic environments. Within the filtration literature only limited theoretical predictability is recognized and most designs are heavily dependent upon site specific experimental data.

APPLICATIONS OF FILTRATION THEORY

Before embarking on a discussion of pertinent fundamental aspects of filtration theory, a more general picture of the filtration process is in order. In the analysis of colloid retention by porous media, two distinct cases are considered as represented in Figure 1. A fluid with a suspended solids concentration C_o flows into a porous media with a steady approach velocity of U. The porous media then accumulates immobilized colloids up to some steady state level, at which time an "equilibrium zone" exists where no further deposition takes place. Particles exiting the equilibrium zone enter a "mass transfer zone" or clean media zone, where particles are collected by the surface of the porous media. This simplistic one-dimensional picture is used as an outline of what follows: first, colloid collection by clean media is examined to estimate the length of the mass transfer zone, and second, some consideration is given to the particle deposit within the equilibrium zone and the resulting reduction in permeability.

Particle Migration In Clean Media

Particle mobility in clean porous media has been analyzed theoretically and experimentally for some time and quantitative predictions agree with observations under specific limiting conditions. Because of the wide variation in particle and media properties, no single mechanism or empirical relationship should be expected to hold universally true.

One of the simpler mechanism hindering particle migration into porous media is geometric straining. Experimental data collected by Sakthivadivel (1969) and Sherard et al. (1984) have established the criterion that straining will occur if

$$\frac{d_p}{d_m} > \frac{1}{9} \qquad (1)$$

where d_p is the suspended particle diameter and d_m is the media diameter. Herzig et al. (1970) have presented an analysis based on particle and media geometry that predicts very little removal by straining will occur if $d_p < d_m/50$.

Particles much smaller than the porous media size are retained within the pores only if particle-media attachment is favorable or if particles can be retained within quiescent pore spaces (Krone et al., 1958; Hunter and Alexander, 1963). Removal of of these smaller particles from suspension was empirically observed to be first order in suspended particle mass concentration, C, by Iwasaki (1937)

$$\frac{\partial C}{\partial x} = -\lambda C \qquad (2)$$

where x is migration distance and λ is called the filter coefficient. The integrated form of equation (2) that predicts the suspension concentration at a distance L into the clean porous media is

$$C(L) = C_o e^{-\lambda L} \qquad (3)$$

This exponential decay relationship only holds true when the porous media is clean over the distance L. Early research on filtration kinetics was devoted to determining empirical relationships for λ as a function of particle and media sizes and fluid flow rate (see Herzig et al., 1970; Ives, 1970). More recently a mechanistic approach to filtration kinetics has provided some success in predicting the filter coefficient through research by Yao et al. (1971), and Spielman and FitzPatrick (1973) with an overall summary given by Tien and Payatakes (1979).

Three dominant mechanisms have been recognized to control particle collisions with porous media. For particles smaller than a few micrometers, Brownian motion of the suspended particles dominates the collision process. For larger particles, particles moving with fluid streamlines can collide with media surfaces through interception, and particles having a density different than the fluid can move across fluid streamlines and collide through a gravitational sedimentation mechanism. Predictions of filter coefficients have been based on an analysis of fluid and particle flow past individual collectors and then corrected for the presence of multiple collectors within a porous media.

Particle collisions with a media surface do not necessarily result in attachment. The particle-media interactions must be favorable for attachment to occur, and these interactions are the result of hydrodynamic, London - van der Waals, and electrostatic forces. The hydrodynamic force results from squeezing out fluid as particles approach the media surface. The London - van der Waals force is an attractive force that operates among atoms and molecules, although only at very short range, less than 1 or 10 nm separations. Finally, particle surfaces in natural waters are electrically charged (Hunter and Liss, 1982), and if the media and the particles have the same charge, electrostatic repulsion is possible. The magnitude of electrostatic repulsion between particles and media is strongly dependent on the ionic composition of the water since high ionic strengths can compress the diffuse layer of counter ions and reduce the distance over which electrostatic repulsion forces act such that the attractive London - van der Waals force dominates at all separations and attachment is favored (see Spielman, 1977). Even when repulsive barriers exist due to electrostatic forces, particle capture is still possible in what is termed the "secondary minimum". Figure 2 plots the net interaction potential between a 1 μm particle and a much larger collector. Traditionally, repulsive energies are plotted as positive values, and the figure indicates a maximum energy barrier of 4×10^{-12} erg at a separation of 1 nm. For particle-collector separations greater than approximately 2 nm, an attractive interaction energy dominates with the secondary minimum at a separation of 4 nm. The primary minimum occurs at separations less than 1 nm. Theoretical predictions for capture in the secondary minimum by Spielman and Cukor (1973) have been applied to conditions likely in groundwater flows by McDowell-Boyer et al. (1985). The theory predicts particle retention over a wide range of ionic strengths when flows are at typical groundwater flow velocities. Due to the shallowness of the secondary minimum, higher flow velocities prevent particle capture. Such predictions have not been tested experimentally.

For the case of no electrostatic repulsion between particles and media surfaces the filter coefficient has been obtained from analysis of numerical simulation of particle trajectories. The

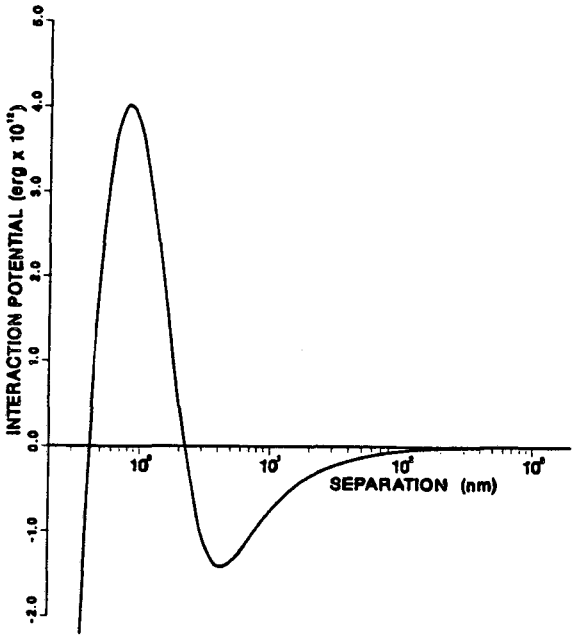

Figure 2. Net interaction potential for a 1 μm particle approaching a flat plate.

resulting empirical equation presented in Tien and Payatakes (1979) is

$$\lambda = \frac{3}{2}\frac{(1-p_o)}{d_m}\left[4A_s^{\frac{1}{3}}\left[\frac{3\pi\mu d_p d_m U}{kT}\right]^{-\frac{2}{3}} + 0.56A_s\left[\frac{A}{\mu d_p^2 U}\right]^{\frac{1}{8}}\left[\frac{d_p}{d_m}\right]^{\frac{15}{8}} + 0.0024\,A_s\left[\frac{v_s}{U}\right]^{1.2}\left[\frac{d_p}{d_m}\right]^{-0.4}\right] \quad (4)$$

where p_o is the clean bed porosity. The first term on the right hand side represents particle collection by Brownian motion and includes a particle size dependence of $d_p^{-2/3}$. Within the first term is the parameter A_s that depends only on porosity and corrects single collector capture for conditions in a packed bed (Tien and Payatakes, 1979). For example, when $p_o = 0.4$, then $A_s = 38$. Also appearing is μ, fluid viscosity, k, Boltzmann constant, and T, absolute temperature. The second term on the right hand side of equation (4) represents interception collision and includes a particle size dependence of $d_p^{15/8}$ and a very weak dependence on the Hamaker constant, A, that appears as a parameter in the London - van der Waals attractive force calculations. The final term accounts for gravitational sedimentation and includes the ratio of particle settling velocity, v_s, to fluid velocity, U, and when Stokes law applies

$$v_s = \frac{g}{18\mu}\left(\rho_p - \rho_f\right)d_p^2 \quad (5)$$

with g the gravitational acceleration constant, and ρ_p and ρ_f, the particle and fluid density, respectively. Their analysis of gravitational sedimentation was for fluid flow in the direction of gravity, typical of filter designs but not necessarily subsurface flows.

The predicted filter coefficient expression in equation (4) represents conditions where there is no electrostatic repulsion force. Experimentally measured filter coefficients are generally within a factor of two of the values predicted from equation (4) when either surface charges have been neutralized or the electrolyte concentration is high. Since many hydrogeological environments have sufficiently high ionic strengths to mask electrostatic

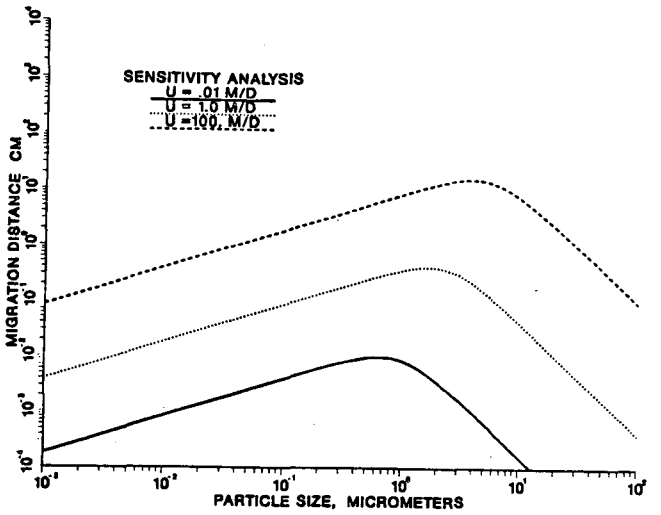

Figure 3. Sensitivity of particle migration distance, $1/\lambda$, to variations in approach fluid flow velocity, U, for $d_m = 0.1$ cm, $A = 10^{-13}$ erg, and $\rho_p = 1.5$ g/cm^3.

forces, equation (4) can be examined for its sensitivity to system conditions, particularly particle size and density, media size, and fluid flow velocity. While λ could be plotted directly, $1/\lambda$ is more useful as it provides a characteristic distance over which the particle concentration is reduced to $C_o e^{-1}$ or $0.37C_o$. Thus, $1/\lambda$ can be viewed as a migration distance for 63 percent removal by clean media. This migration distance roughly corresponds to the width of the mass transfer zone depicted in Figure 1.

In Figure 3 the inverse of the filter coefficient is plotted as a function of particle size for three approach velocities. The three curves have the same general shape of increasing migration distance with an increase in particle size up to 1 μm where Brownian collisions dominate. Then a steep decrease in migration distance is observed with increasing particle size when interception and gravitational sedimentation dominate particle-media collisions. Particles in the size range of 1 to 10 μm have the greatest mobility which increases with increasing flow velocity. For the condition of no electrostatic repulsion, particle capture within porous media at groundwater flow velocities up to 100 m/d is predicted to limit the effective mass transfer zone to less than 10 cm.

Sensitivity of particle migration distance to media size is shown in Figure 4. As in Figure 3 there exists a window of particle sizes near 1 μm with the greatest mobility when Brownian and gravitational sedimentation collisions tradeoff. At a particle density of 1.5 g/cm^3, interception dominated collisions are insignificant compared to gravitational sedimentation and this also explains why migration distance is relatively insensitive to media size at larger particle sizes. For the stated conditions, the third term of equation (4) dominates and predicts that

$$\lambda^{-1} \propto d_m^{0.6} \quad (6)$$

The curve for $d_m = 0.01$ cm terminates at $d_p = 10$ μm because straining is predicted through equation (1) to prevent all particles larger than that size from entering the porous media. Brownian particle capture is strongly dependent on media size. With a media of size 10 cm, an expected migration distance approaches a relatively short 100 cm, assuming laminar flow conditions continue to hold.

Figure 5 illustrates the sensitivity of migration distance to particle density under typical aquifer conditions of a 1 m/d flow velocity and a 0.1 cm media. Since gravitational sedimentation dominates over interception, except when $\rho_p = \rho_f = 1.0$ g/cm^3, large particle migration is strongly dependent on the density difference. Brownian particle capture is insensitive to particle

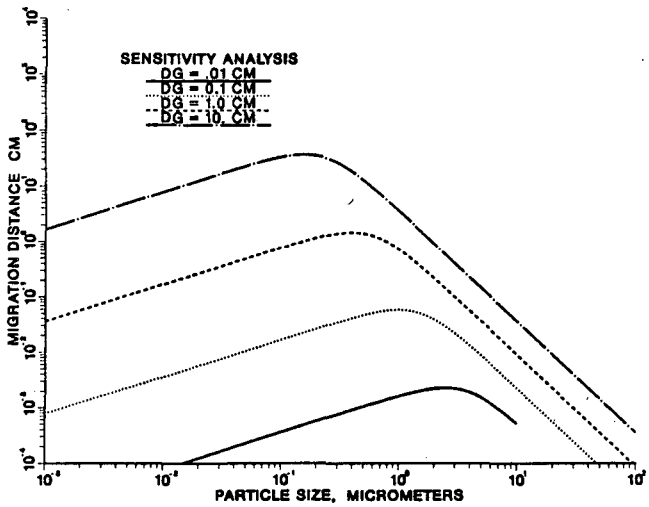

Figure 4. Sensitivity of particle migration distance, $1/\lambda$, to variations in media size, d_m, for U = 1 m/d, A = 10^{-13} erg, and ρ_p = 1.5 g/cm^3.

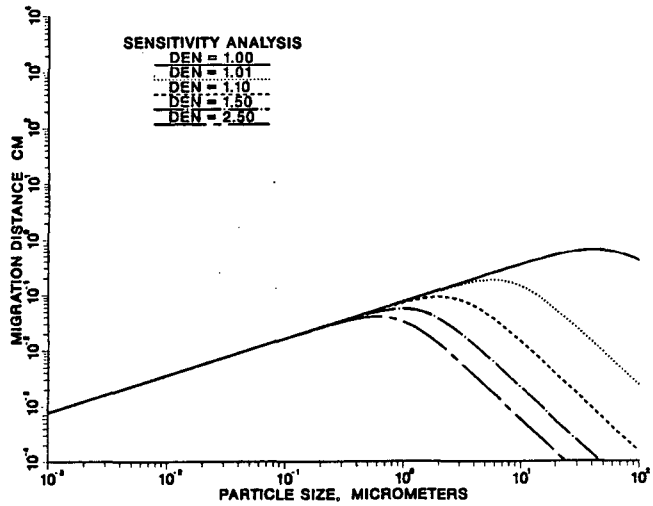

Figure 5. Sensitivity of particle migration distance, $1/\lambda$, to variations in suspended particle density, ρ_p, for U = 1 m/d, d_m = 0.1 cm, and A = 10^{-13} erg.

density. In general, destabilized particles, those that stick when they collide with particle or media surfaces, are predicted through equation (4) to have relatively limited migration. Greatest mobility is expected for low density particles within the size range of 0.1 to 10 μm at high flow rates in porous media composed of large grains.

When the suspended particles are not completely destabilized, that is, dispersed such that electrostatic forces exist during particle-media collisions, theoretical predictions and experimental data differ by orders of magnitude. The theory predicts that the filter coefficient is extremely sensitive to electrostatic forces such that small changes in surface charges are predicted to essentially stop particle attachment during Brownian collisions (Ruckenstein and Prieve, 1973; Spielman and Friedlander, 1974) and during interception collisions (Spielman and Cukor, 1973). Experimental data show a relatively weak dependence of the filter coefficient on particle and media surface charges with variations in filter coefficients from 1 to 3 orders of magnitude (Ives and Gregory, 1966; FitzPatrick and Spielman, 1973; Jordan et al., 1974). Hogg and Yang (1976) have show theoretically that particle attachment in the secondary minimum is much less sensitive to particle surface charge and aqueous chemistry compared to capture in the primary minimum. However, Bowen and Epstein's (1979) experimental data on particle capture by a flat plate cannot be described by collection in a secondary minimum.

Equilibrium Deposition And Permeability Reduction

If particle-media attachment and/or particle-particle attachment are energetically favorable, then particles will accumulate as a deposit occupying part of the available pore space. This deposit causes a decrease in media permeability resulting in either lower fluid flow rates if the driving pressure is constant, or higher pressure losses for a constant flow rate. This coupling between particle deposition and permeability reduction controls particle accumulation and possible nuclide isolation within the porous media.

For particle surfaces that have an electrical charge opposite that of the media, at most a monolayer of deposit is expected. Rajagopalan and Chu (1982) modeled particle accumulation by assuming a deposition rate and a release rate from the media surface such that an equilibrium in particle deposit resulted. While the authors acknowledged that particle release does not actually occur from the deposit, the assumed kinetic expressions provided a convenient method of modeling the experimental observations. For small particles dominated by Brownian deposition, Heertjes and Lerk (1967) did not detect a reduction in permeability following attainment of an equilibrium deposit. The filtration model of Wnek et al. (1975) incorporated a charge balance for the filter media so that the electrostatic force between particles and coated media was continuously updated during particle deposition. Their model was successfully fit to Heertjes and Lerk's (1967) data. Adamczyk et al. (1983) have provided an extensive review of the literature on particle collection on single spheres, cylinders and flat plates. They showed that predictive theories for particle collection on oppositely charged surfaces are within 20 percent of theoretical predictions.

If particle-media and particle-particle attachments are energetically favorable, then particle deposits accumulate within media pores and substantially alter media permeability to fluid flow. The rate of deposit accumulation is equal to the rate of removal of particles from solution, which under steady flow conditions is represented by

$$\frac{\partial \sigma}{\partial t} = -U \frac{\partial C}{\partial x} \tag{7}$$

where σ is the deposit in units of mass of particles retained per fluid volume of bed. Since deposited particles act as collectors for other particles, the kinetic expression in equation (2) must acknowledge that the filter coefficient depends on the deposit

$$\frac{\partial C}{\partial x} = -\lambda(\sigma)\, C \tag{8}$$

There are many proposed expressions for the functional dependence of the filter coefficient on the deposit, and all contain one or more parameters that must be determined by fitting the expression to experimental data. Tien and Gimbel (1982) summarize a number of the proposed expressions. In general, the presence of some deposit on the media surface increases the filter coefficient over the clean bed value because of the greater surface area available on the dendritic deposits that are formed (O'Melia and Ali, 1978). Further increases in the particle deposit results in pore space restriction and greater pore space restriction with increasing pore fluid velocity that hinder particle collisions. At some level of particle deposit accumulation, no further deposition takes place and an equilibrium is established.

A number of researchers have approached particle accumulation within filters as a chromatographic front as Figure 1 might suggest. Ives (1963) and Herzig et al. (1970) have derived the following relationship between suspended particle concentration and particle deposit

$$\frac{C(x,t)}{C_o} = \frac{\sigma(x,t)}{\sigma(x=0,t)} \quad (9)$$

When the particle deposit reaches a maximum deposit of σ_{max}, the equilibrium zone is predicted to migrate at a reduced velocity U_c, according to

$$U_c = U \frac{C_o}{\sigma_{max}} \quad (10)$$

While equations (9) and (10) are frequently assumed to hold for operating filters, experiments generally do not observe attainment of a uniform equilibrium deposit with depth (Ives, 1961; Cleasby, 1969; Adin and Rebhun, 1977; Letterman et al., 1979; Sandza, 1981; Rebhun et al., 1984). There are a few studies that have found experimental data that are in agreement with equation (9) (Srinivasan, 1981; Soo et al., 1985a, 1985b). The major difficulty in extrapolating linear chromatography theory to particle collection is that the retained particles can drastically alter the media permeability.

For clean porous media, the hydraulic gradient can be represented by the Carmen-Kozeny equation for a packed bed of irregular particles

$$i_o = -\frac{dh}{dx} = \frac{150\nu U}{g d_m^2} \frac{(1 - p_o)^2}{p_o^3} \quad (11)$$

where h is the hydraulic head, or fluid energy per unit mass, and i_o, the hydraulic gradient for the clean bed. The media permeability, k, as used in equation (11) is given by

$$k = \frac{d_m^2}{150} \frac{p_o^3}{(1 - p_o)^2} \quad (12)$$

and the frequently used hydraulic conductivity, K, of Darcy's Law is included as $K = gk/\nu$.

As particles accumulate within media pores, equation (11) does not apply because the deposited particles roughen the surface and decrease the porosity. Many researchers have attempted to model the increase in hydraulic gradient as particles deposit; for summaries of proposed models, see Herzig et al. (1970), Sakthivadivel et al. (1972) and Tien and Gimbel (1982). The analysis of Sakthivadivel et al. (1972) concluded that the available models could each be fitted to experimental data, but the semi-empirical correlations could not be applied to new situations.

SUMMARY

The simultaneous analysis of particle capture and permeability reduction has been extensively researched but predictive models are not available that can be generalized. An examination of some of the available data on particle accumulation and permeability reduction arrived at the following qualitative concepts for constant flow conditions (McDowell-Boyer et al., 1985).

1. Actual measurements of equilibrium deposit and permeability reduction are difficult to acquire due to substantial variations occurring over relatively short distances (centimeters). Simultaneous measurements of deposit and permeability or hydraulic gradient are rarely taken simultaneously over centimeter sized intervals. Deposit profiles can be recorded by using X-ray absorbing materials that provide spatial resolution down to a centimeter (Stanley, 1955; Ives, 1961; Sandza, 1981; Srinivasan, 1981). The alternative is to determine deposit accumulation through integration over time of equation (7) from discrete measurements of suspended particle concentration at various depths and times (Camp, 1964; Wright, 1983).

2. The mass of deposit in the equilibrium zone can be fairly small in comparison to the pore volume available. For example, Cleasby's (1969) data indicate that approximately 2.5 grams of clay was retained per liter of bed. For a clay particle density of 2.5 g/cm^3 and an initial porosity of 0.4, this amount of clay represents only 0.25 percent of the pore volume. Such maximum loadings are typical and explained by the highly porous nature of aggregates. A similar retention of clay particles was reported by Hunter and Alexander (1963) along with only a 10 to 20 percent decrease in permeability. Somewhat greater deposits are reported when coagulants are added resulting in deposits that occupy 1 to 10 percent of the pore volume and reduce the permeability by one to two orders of magnitude (Cleasby, 1969).

3. Simple two dimensional filters composed of cylinders have allowed observations of particle capture and of deposit morphology (Camp, 1964; Payatakes et al., 1982). As particles accumulate, some pores become plugged by a porous and permeable deposit that continues to collect particles. As flow through the deposit is restricted through plugged pores, the interstitial velocity increases in the remaining pores that remain open since the shear stress exceeds some critical value as discussed below. The fluid flow path through open pores can become very tortuous as fluid streamlines avoid clogged pores.

4. A critical flow velocity exists for a particle suspension such that no particles will accumulate above that velocity. At fluid velocities below the critical velocity, particle deposits accumulate up to the level that qualitatively corresponds to the interstitial velocity that gave no deposition (Hunter and Alexander,1963; Maroudas and Eisenklam, 1965a, 1965b; Kreissel et al., 1968). The amount of material deposited in the equilibrium zone is a function of the pore size and the poorly defined concept of aggregate strength (Hudson, 1948; Adin and Rebhun, 1977).

5. The actual mechanisms that maintain an equilibrium deposit are not agreed upon. Some explanations are based on erosion as a linear function of amount deposited, although this assumption conflicts with experimental measurements that show there is no erosion when clean water flows through a filter at the identical velocity used for particle deposition (Ives, 1970). Conversely, particle size distributions exiting the equilibrium zone are about an order of magnitude greater in size than the influent particles (Sandza, 1981). A photographic study of deposit accumulation by Payatakes et al. (1981) showed that the equilibrium is a dynamic process with accumulation of individual particles or small aggregates followed by aggregate erosion and later capture downstream.

6. For an existing deposit of fine particles, a critical velocity exists that will initiate erosion of the deposit into the flowing fluid. This critical velocity, acting as a surface shear stress, is a function of particle aggregate characteristics. Most of the research in this area has been done on erosion of clay particles where the strength of the clay mineral deposit strongly depends on clay mineralogy and aqueous chemistry (Khilar et al., 1985). Clay minerals within media pores can undergo swelling and erosion in response to changes in electrolyte composition. When saline water within an aquifer is replaced by freshwater, the permeability can decrease by orders of magnitude as either the clay swells or the clay disperses and blocks pores (Hardcastle and Mitchell, 1974; Goldenberg et al., 1983, 1984; Khilar and Fogler,1983, 1984). This phenomenon is termed "water sensitivity" by the petroleum engineers and is observed during water flooding operations used in secondary oil recovery.

7. The summary thus far has been limited to considering particle deposition under constant flow conditions where particle accumulation causes a reduction in permeability and an increase in pressure drop across the media. Natural and altered subsurface flows are driven by constant pressure gradients that result in declining flow velocities as permeability is reduced by particle accumulation. Experiments that measure particle accumulation within a column under constant pressure conditions, while typical of natural conditions, are very difficult to generalize. For example, Gruesbeck and Collins (1982) showed that a slight increase in media size in a 20 cm column resulted in the column going from completely plugged to only a slight decrease in permeability. Another problem of interpretation is that an average permeability is calculated for the column when the deposited particles are observed to accumulate near the entrance (Gruesbeck and Collins,

1982). Thus, the experiments become a function of the column length and generalization is hindered.

8. Besides the coupling between the flow, the aqueous chemistry, and the particle deposition, thermal gradients produced by waste canisters can alter particle deposition. The geothermal literature has recognized that cooling fluids can result in precipitation of particles either in solution or attached to media surfaces. These particles can plug formations if they are reinjected (Weres and Apps, 1982). Palmer and Cherry (1984) discuss similar, anticipated problems of precipitate accumulation when aquifers are used for heat storage.

CONCLUSIONS

Colloidal matter and particles are transported by fluid flows through porous and fractured media. The factors that control mobility are varied and include size, surface chemistry, aqueous chemistry, and fluid flow rate. While the filtration literature contains extensive theoretical developments, the conditions in natural and altered subsurface environments preclude predictive modeling of particle capture, subsequent permeability reduction, and deposit resuspension. Experimental investigations guided by developments in colloidal science and the filtration literature are needed to understand the processes occuring within porous and fractured media. With an understanding of the fundamental processes, prediction of particle and radionuclide migration can be attempted over time scales of thousands of years as is needed in evaluating nuclear waste disposal options.

REFERENCES

Adamczyk, Z., T.Dabros, J. Czarnecki, and T. G. M. van de Ven (1983). "Particle transfer to solid surfaces," Adv. Colloid Interface Sci., 19, 183-252.

Adin, A., and M. Rebhun (1977). "A model to predict concentration and head-loss profiles in filtration," J. Amer. Water Works Assoc., 69 (7), 444-453.

Avogadro, A., G. de Marsily (1983). "The role of colloids in nuclear waste disposal," in, Scientific Basis for Nuclear Waste Management VII, edited by G. L. McVay, Materials Research Society Symposia Proceedings, vol. 26, pp 495-505, Elsevier, New York, 1983.

Bowen, B. D., and N. Epstein (1979). "Fine particle deposition in smooth parallel-plate channels," J. Colloid Interface Sci., 72 (1), 81-97.

Camp, T. R. (1964). "Theory of water filtration," Amer. Soc. Civil Eng., J. Sanit. Eng. Div., 90 (SA4), 1-30.

Champlin, J. B. F., and G. G. Eichholz (1968). "The movement of radioactive sodium and ruthenium through a simulated aquifer," Water Resour. Res., 4 (1), 147-158.

Champlin, J. B. F., and G. G. Eichholz (1976). "Fixation and remobilization of trace contaminants in simulated subsurface aquifers, Health Phys., 30, 215-219.

Cleasby, J. L. (1969). "Approaches to a filterability index for granular filters," J. Amer. Water Works Assoc., 61 (8), 372-381.

Cleveland, J. M., and T. F. Reeves (1981). "Characterization of plutonium in Maxey Flats radioactive trench leachates," Science, 212 (26 June), 1506-1509.

Coles, D. G., and L. D. Ramspott (1982). "Migration of ruthenium-106 in a Nevada test site aquifer: discrepancy between field and laboratory results," Science 215, 1235-1237.

FitzPatrick, J. A., and L. A. Spielman (1973). "Filtration of aqueous latex suspensions through beds of glass spheres," J. Colloid Interface Sci. 43 (2), 350-369.

Goldenberg, L. C., M. Magaritz, A. J. Amiel and S. Mandel (1984). "Changes in hydraulic conductivity of laboratory sand-clay mixtures caused by a seawater-freshwater interface," J. Hydrol., 70, 329-336.

Goldenberg, L. C., M. Magaritz, V. S. Mandel (1983). "Experimental investigation on irreversible changes in hydraulic conductivity in seawater - freshwater interface in coastal aquifers," Water Resour. Res., 19, 77-85.

Gruesbeck, C., and R. E. Collins (1982). "Entrainment and deposition of fine particles in porous media," Soc. Pet. Eng. J., 22 (6), 847-856.

Hardcastle, J. H., and J. K. Mitchell (1974). "Electrolyte concentration-permeability relationships in sodium illite - silt mixtures," Clays Clay Minerals, 22, 143-154.

Heertjes, P. M., and C. F. Lerk (1967). "The function of deep-bed filters: Part I: The filtration of colloidal solutions," Trans. Inst. Chem. Engs. 45, T129-T137.

Herzig, J. P., D. M. Leclerc, P. Le Goff (1970). "Flow of suspensions through porous media - application to deep filtration, Ind. Eng. Chem., 62 (5), 8-35.

Hogg, R., and K. C. Yang (1976). "Secondary coagulation," J. Colloid Interface Sci., 56 (3), 573-576.

Hudson, H. E.,Jr. (1948). "A theory of the functioning of filters," J. Amer. Water Works Assoc., 40, 868-873.

Hunter, K. A., and P. S. Liss (1982). "Organic matter and the surface charge of suspended particles in estuarine waters," Limnol. Oceanogr., 27 (2), 322-335.

Hunter, R. J., and A. E. Alexander (1963). "Surface properties and flow behavior of kaolinite, part III. Flow of kaolinite solutions through a silica column," J. Colloid Sci., 18, 846-862.

Ives, K. J. (1961). "Filtration using radioactive algae," Proc. Amer. Soc. Civil Eng., J. San. Eng. Div., 87 (SA3), 23-37.

Ives, K. J. (1963). "Simplified rational analysis of filter behaviour," Proc. Inst. Civil Engs., 25, 345-364.

Ives, K. J. (1970). "Rapid filtration (review paper)," Water Res. 4, 201-223.

Ives, K. J., and J. Gregory (1966). "Surface forces in filtration," Proc. Soc. Water Treat. Exam., 15, 93-115.

Iwasaki, T. (1937). "Some notes on sand filtration," J. Amer. Water Works Assoc., 29, 1591-1597.

Jordan, T. A., M. M. Ghosh, and R. H. Boyd, Jr. (1974). "Physico-chemical aspects of deep-bed filtration," J. Water Pollution Control Fed., 46 (12), 2745-2754.

Khilar, K. C. and H. S. Fogler (1983). "Water sensitivity of sandstones," Society Petrol. Eng. J., 23 (1), 55-64.

Khilar, K. C., and H. S. Fogler (1984). "The existence of a critical salt concentration for particle release," *J. Colloid Interface Sci., 101* (1), 214-224.

Khilar, K. C., H. S. Fogler, and D. H. Gray (1985). "Model for piping-plugging in earthen structures," J. Geot. Eng., 111 (7), 833-847.

Kreissl, J. F., G. G. Robeck, and G. A. Sommerville (1968). "Use of pilot plant filters to predict optimum chemical feeds," J. Amer. Water Works Assoc., 60 (3), 299-314.

Krone, R. B., G. T. Orlob, and C. Hodghinson (1958). "Movement of coliform bacteria through porous media," *Sewage Ind. Wastes, 30,* 1-13.

Le Bell, J. C. and P. Stenius (1980). "The influence of cations on particle interactions and particle release form aqueous bentonite gels," Powder Technol., 26 (1), 17-27.

Letterman, R. D., R. R. Sama, and E. J. Didomenico (1979). "Direct filtration using polyelectrolyte coagulants," J. Amer. Water Works Assoc., 71 (6), 332-338.

Maroudas, A., and P. Eisenklam (1965a). "Clarification of suspensions: a study of particle deposition in granular media, part I. Some observations on particle deposition," Chem. Eng. Sci., 20, 867-873.

Maroudas, A., and P. Eisenklam (1965b). "Clarification of suspensions: a study of particle deposition in granular media, part II. A theory of clarification," Chem. Eng. Sci., 20, 875-888.

McDowell-Boyer, L. M., J. R. Hunt, and N. Sitar (1985). "Particle transport through porous media," in preparation, 1985.

Nelson, D. M., W. R. Penrose, J. O. Karttunen, and P Mehlhaff (1985). "Effects of dissolved organic carbon on adsorption properties of plutonium in natural waters," Environ. Sci.

Technol., 19 (2), 127-131.

O'Melia, C. R., and W. Ali (1978). "The role of retained particles in deep bed filtration," Prog. Water Tech., 10 (5/6), 167-182.

Palmer, C. D., and J. A. Cherry (1984). "Geochemical reactions associated with low-temperature thermal energy storage in aquifers," Can. Geotech. J., 21 (3), 475-488.

Payatakes, A. C., H. Y. Park, and J. Petrie (1981). "A visual study of particle deposition and reentrainment during depth filtration of hydrosols with a polyelectrolyte," Chem. Eng. Sci., 36 (8), 1319-1335.

Rajagopalan, R., and R. Q. Chu (1982). "Dynamics of adsorption of colloidal particles in packed beds, J. Colloid Interface Sci., 86 (2), 299-317.

Reardon, E. J. (1981). "K_d's - can they be used to describe reversible ion sorption reactions in contaminant migration," Groundwater, 19 (3), 279-286.

Rebhun, M. Z. Fuhrer, and A. Adin (1984). "Contact flocculation-filtration of humic substances," Water Res., 18 (8), 963-970.

Reynolds, W. D., R. W. Gillham, and J. A. Cherry (1982). "Evaluation of distribution coefficients for the prediction of strontium and cesium migration in a uniform sand," Can. Geotech. J., 19, 92-103.

Ruckenstein, E., and D. C. Prieve (1973). "Rate of deposition of Brownian particles under action of London and double-layer forces," J. Chem. Soc.: Faraday Trans. 2, 69 (10), 1522-1536.

Sakthivadivel, R. (1969). "Clogging of a granular porous medium by sediment," HEL 15-7, Hydraulic Engineering Laboratory, Univ. of Calif. Berkeley, 106 pp.

Sakthivadivel, R., Thanikachalam, V., and S. Seetharaman (1972). "Headloss theories in filtration," J. Amer. Water Works Assoc., 64 (4), 233-38.

Saltelli, A., A. Avogadro, and G. Bidoglio (1984). "Americium filtration in glauconitic and columns," Nuclear Technol., 67, 245-254.

Sandza, W. F. (1981). "An experimental study of solids accumulation in deep granular filters," M.S. thesis, 108 pp., Univ. of Delaware, Newark, 1981.

Shade, J. W., L. L. Amers, and J. E. McGarrah (1984). "Actinide and technetium sorption on iron-silicate and dispersed clay colloids," in, Geochemical Behavior of Disposed Radioactive Waste, edited by G. S. Barney, J. D. Nauratil, W. W. Schulz, Amer. Chem. Soc. Symp. Series 246, pp. 67-77.

Sheppard, J. C., M. J. Campbell, T. Cheng and J. A. Kittrick (1980). "Retention of radionuclides by mobile humic compounds and soil particles," Environ. Sci. Technol., 14 (11), 1349-53.

Sherard, J. L., L. P. Dunnigan, and J. R. Talbot (1984). "Basic properties of sand and gravel filters," J. Geot. Eng., 110 (6), 684-700.

Soo, H., and C. J. Radke (1985a). "A filtration model for the flow of dilute, stable emulsions in porous media Part I: Theoretical," *Chem. Eng. Sci.*, submitted.

Soo, H., M. C. Williams, and C. J. Radke (1985a). "A filtration model for the flow of dilute, stable emulsions in porous media Part II: Parameter evaluation and estimation," Chem. Eng. Sci., submitted.

Spielman, L. A. (1977). "Particle Capture from low-speed laminar flows," Ann. Rev. Fluid Mech., 9, 297-319.

Spielman, L. A., and P. M. Cukor (1973). "Deposition of non-Brownian particles under colloidal forces," J. Colloid Interface Sci., 43 (1), 51-65.

Spielman, L. A., and J. A. FitzPatrick (1973). "Theory for particle collection under London and gravity forces," J. Colloid Interface Sci., 42 (3), 607-623.

Spielman, L. A., and S. K. Friedlander (1974). "Role of electrical double-layer in particle deposition by convective diffusion," J. Colloid Interface Sci., 46 (1), 22-31.

Srinivasan, K. (1981). "Granular media filtration: unified theory and design," M.S. thesis, 119 pp. Univ. of Delaware, Newark, DE 1981.

Stanley, D. R. (1955). "Sand filtration studied with radiotracers," Proc. Amer. Soc. Civil Eng., 81(592), 1-23.

Tien, C., and R. Gimbel (1982). "On the development of a comprehensive model of deep bed filtration," Proc. Intern. Symp. on Water Filtration, edited by R. Weiler and J. G. Janssens, pp 1.1-1.13, Koninklijke Vlaamse Ingenieursvereniging, Antwerp.

Tien, C., and A. C. Payatakes (1979). "Advances in deep bed filtration," AIChE J., 25 (5), 737-759.

Valocchi, A. J. (1984). "Describing the transport of ion-exchanging contaminants using an effective K_d approach," Water Resour. Res., 20 (4), 499-503.

Weres, O., and J. A. Apps (1982). "Prediction of chemical problems in the reinjection of geothermal brines," Geological Society of Amer. Spec. Paper 189, pp 407-426.

Wnek, W. J., D. Gidaspow, and D. T. Wasan (1975). "The role of colloid chemistry in modeling deep bed filtration," Chem. Eng. Sci., 30 (9), 1035-1047.

Wright, A. M. (1983). "Filtration modelling," Ph.D. thesis, 181 pp., University of California, Berkeley.

Yao, K., M. T. Habibian, and C. R. O'Melia (1970). "Water and wastewater filtration: Concepts and applications," Environ. Sci. Technol., 5 (11), 1105-1112.

MULTIPARAMETER TESTING OF PERMEABILITY BY THE TRANSIENT VACUUM TECHNIQUE

A.T. Jakubick and R. Klein

Ontario Hydro
800 Kipling Avenue
Toronto, Canada, M8Z 5S4

ABSTRACT

This method measures media permeability under unsaturated conditions by radial air withdrawal rather than by axial injection of air. Therefore, large-size specimens or entire models of rock or concrete can be tested without leakage and confinement complications. The identical equipment and technique can also be used to measure rock or concrete under in-situ conditions. Using high-sensitivity vacuum transducers and fast data acquisition it was possible to estimate permeability not only from steady-state measurements but also from the late time portion of the pressure recovery curve even at high values of dimensionless storage constants. The transient vacuum evaluation is especially useful under field conditions because it does not require knowledge of drainage area. The technique proved to be a highly responsive fracture indicator. An increase of permeability with decreasing humidity was observed during tests performed under various humidity conditions.

INTRODUCTION

The vacuum permeability technique is a further development of the permeability measuring technique used at Ontario Hydro Civil Research by Loughborough (1966). A similar technique based on evacuation of concrete was later used by Figg (1973). To interpret measurements under field conditions a better understanding of the combined effect of humidity and temperature on the measurements was needed. Therefore, vacuum permeability tests on models made of concrete of various composition and size were carried out in the laboratory under controlled humidity and temperature conditions. The vacuum permeability technique lends itself to testing of dry or partially-saturated porous or fractured media.

TESTING PROCEDURE

In order to induce airflow in the tested medium, a hole of 1.3 and 1.5 inches in diameter was drilled through the medium; it was then sealed off and evacuated. Pumping of the tested hole was continued until steady-state conditions of flow were reached. (Sar Vac Vacuum Pump 8804 was used for the experiments). When steady-state conditions were established, the evacuation was stopped, and the response of the medium was observed. The pressure, air flow, humidity and temperature of the medium and of the ambient air were recorded. The required draw-down and recovery times depended on the permeability of the medium: in high permeability concrete the recovery was completed within a few minutes; in very low permeability concrete the recovery took several weeks (up to 30,360 minutes). The lowest level of permeability detection was controlled by the leakage of the vacuum system. This leakage rate was 0.01 torr/min at the 4 to 50 torr level, 0.005 torr/min at the 100 torr level, 0.003 torr/min at the 150 torr level and negligible above 150 torr.

The pressure was measured by high-precision sensors in a range from 0 to 1000 torr with a full-scale accuracy of 0.05% (1 torr = 0.0193 psi). The air flow from the tested medium was measured using hot-wire mass flow transducers in three ranges: 0 to 50 cm^3/min, 0 to 500 cm^3/min and 0 to 10 000 cm^3/min. The full-scale accuracy was 1%. Flow rates below detection limit can be calculated using Boyle's law as demonstrated by Bordman et al (1966). Although the analog recording of slow recovery processes can be done directly from the signal conditioning unit (Dicon DI 1000), we found it necessary to use a data acquisition system (Daytronic Model 10K7 Data Pac). For convenience an on-line computer was used for immediate evaluation.

The following example illustrates the evaluation of the test results using experiment 211A (concrete cylinder material B, r_e/r_w = 13.85). In the test chart (Fig 1), the pressure decreased during evacuation

until the ultimate pressure of 9.75 torr was achieved after 49.62 minutes. The stabilized flow was $\bar{q}$ = 10.9 cm^3/min with a standard deviation of ± 0.066 cm^3/min (Fig 2). A corresponding steady-state relative humidity of 43.7% was achieved at 25.1°C (Fig 3 and 4). After 60 minutes evacuation the test hole was shut off and the pressure and humidity build-up recorded.

Figure 1. Transient vacuum test.

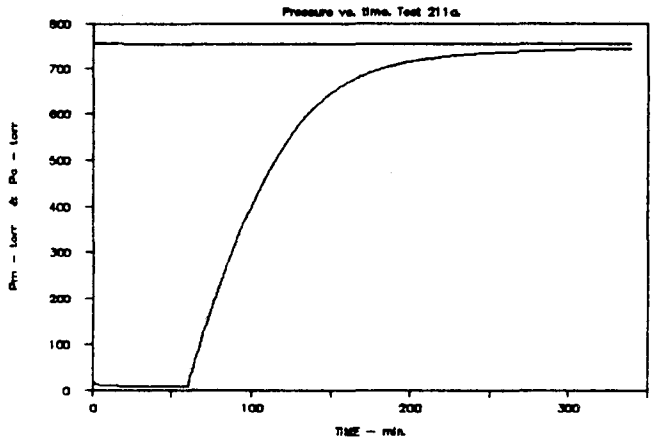

Figure 2. Transient vacuum test.

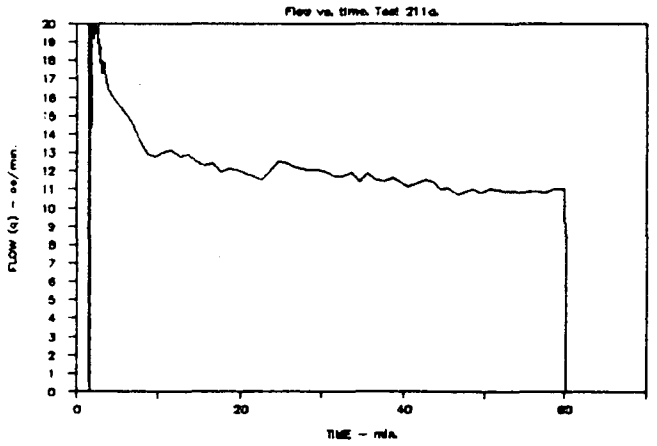

Figure 3. Transient vacuum test.

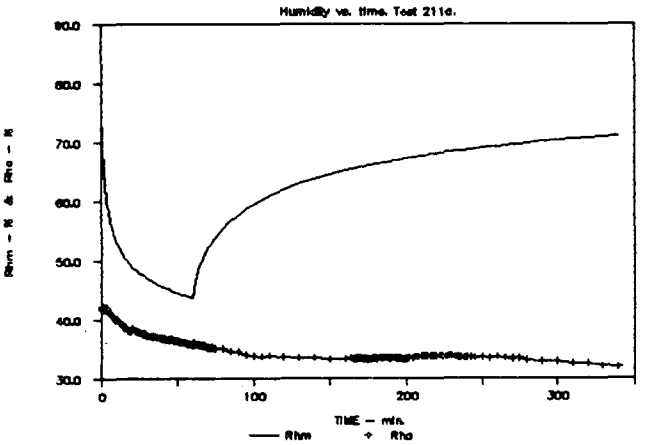

Figure 4. Transient vacuum test.

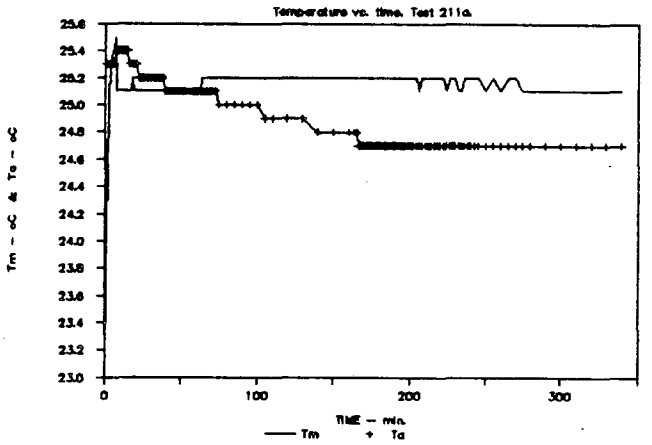

Using the recorded data, either the steady-state or the transient pressure section of the curve can be evaluated. While under field conditions, the extent of the drainage area is usually not precisely known and therefore steady-state evaluations are problematic, both approaches are possible under laboratory conditions where the outer

boundary of the tested medium is known. The steady-state permeability was calculated from:

$$k = 5{,}885 \frac{\mu \ln(r_e/r_w)T_f}{h(P^2_e - P^2_w)} Q_{sc}$$

k = permeability in mD; μ = viscosity in cp;
r_e = radius of the drainage area;
r_w = radius of the test hole;
T_f = temperature in ^{o}R; h = thickness of the the tested zone in cm;
P_e = pressure at the outer boundary; in torr;
P_w = pressure in the test hole; in torr;
Q_{sc} = flow in cm^3/min at standard conditions.

The domains of storage effect (slope = 1) and linear flow (slope = 0.5) were numerically identified as lasting for 112.58 minutes of the recovery time (log recovery time = 2.0515 on the type curve in Fig 5). It was then numerically established that radial flow existed between Horner times from 0.1303 to 0.1071 (corresponding recovery time from 171.58 to 214.58 minutes).

Figure 5. Type curve. Test 211a.

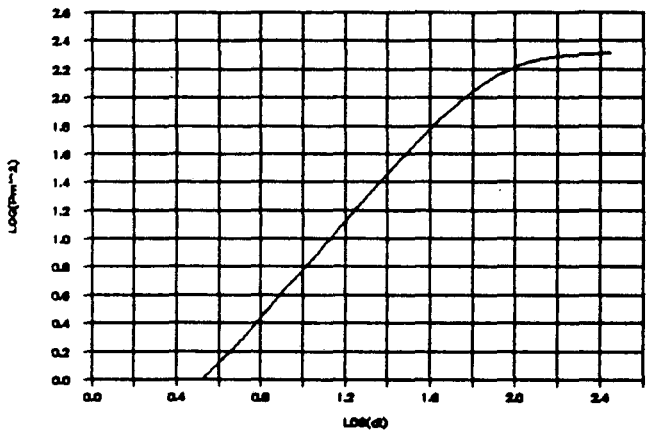

The permeability was calculated according to the simplified equation for pressure build-up:

$$k = 2{,}537 \frac{\mu TZ}{h\,m} Q_{sc}$$

k, μ, T, Q_{sc}, h as previously defined and Z = gas factor.

$$m = \frac{p^2_e - p^2_w}{\log \frac{t_p + \Delta t}{\Delta t}}$$

p_e = pressure at the outer boundary in psi
p_w = pressure in the test hole in psi
t_p = pumping time; Δt = time increments of the recovery phase.

The Horner plots for the concrete cylinders resembled those of gas wells in tight formations with a constant pressure outer boundary. The dimensionless storage constants of the cylinders were high:

$$Cd = \frac{C}{2\pi h \phi C_t r^2_w} = 10^3 \text{ to } 10^4$$

ϕ = porosity; C_t = effective isothermal compressibility of the system.

In such cases the storage and boundary effects are not sufficiently distanced on the Horner plot for reliable interpretation and the identification of the slope m is unreliable (Chen et al, 1978). This problem was circumvented by the use of transducers sensitive to minute changes of pressure and by fast data acquisition to obtain a large number of readings. By these means, sufficient data were collected and the straight plot was identified before distor-

tion due to the boundary effect. Numerical differentiation of the Horner plot provided the slope m. In the specific case of test No. 211A, 570 pressure readings collected within 4353 minutes proved to be sufficient. An amplified view of the Horner plot shows the late time part of the curve from which the average slope $\bar{m}$ = 201.5 (standard deviation ±39) was calculated (Fig 7).

Figure 7. Horner plot. Test 211a

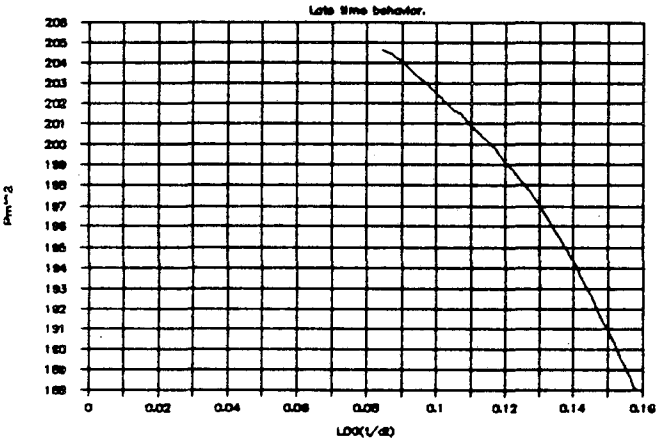

The steady-state permeability values compared well with permeabilities obtained from the pressure transient analyses within 15% to 20% of the standard deviation of m, the latter being consistently lower than the former.

RESULTS

Three sizes of concrete cylinders (diameter = 45.72 cm, 30.48 cm, 15.24 cm; with 3.3 cm and 3.81 cm centre holes; height = 53.0 cm) were tested. They were of four compositions each:

A - Normal Weight Concrete
Cement Type 40 270 kg/m^3
Fly Ash 13 kg/m^3
Coarse Aggregate Maximum Size 40 mm
W/C + FA ratio 0.50
(Material No. 3874)

B - Normal Weight Concrete
Cement Type 40 380 kg/m^3
Coarse Aggregate Maximum Size 20 mm
W/C Ratio 0.41
(Material No. 3870)

C - High-Density Concrete
Cement Type 40 405 kg/m^3
Coarse Aggregate: Magnetite Maximum Size 20 mm
W/C Ratio 0.37
(Material No. 13454)

D - High-Density Concrete
Cement Type 50 328 kg/m^3
Silica Fume 82 kg/m^3
Coarse Aggregate: Magnetite Maximum Size 20 mm
W/C + SF Ratio 0.35
(Material No. 13453)

Details of the composition of the high-density concrete are given by Hooton (1985). The permeability results are shown in Table I.

TABLE I

	Material			
	A	B	C	D
r_e/r_w	Permeability [μD]			
4.61	8	15	1580	9920
9.23	296	41	10	175
13.85	355	22.7	235	31

Duplicate tests were carried out for each of the values. There was no obvious relationship between change in materials and variation in permeabilities. This implied that it was the micro-fractures rather than matrix properties that controlled the permeability of concrete.

In order to determine the sensitivity of the technique, two very fine radial fractures were induced in one of the cylinders (material B) by means of an automated borehole dilatometer (Koopmans and Hughes, 1984). As an impression packer test showed, two fractures in the micron size range were created at an angle of 45° (Fig 8).

Fig 8 Dilatometer induced fractures

The r_e/r_w ratio of the cylinder was 13.85; the fractures remained internal only, not reaching the surface. Re-testing the cylinder after fracturation, we observed a decrease of the pressure recovery time from 18,240 minutes to 280 minutes and a doubling of permeability from 22.7 μD to 46 μD. The marked response to discontinuous fractures of such a small size confirmed the high fracture detection sensitivity of the testing technique.

Because of the frequent presence of water in concrete below 50°C, the effect of the water vapour on the pressure recovery process was investigated. Under the effect of evacuation (to about 1 torr), the water present in the fractures and pores evaporated as the previously balanced water vapour saturation was disturbed. As the water vapour was pumped out along with the air, the water in the tested media continued to evaporate into the evacuated hole until its partial pressure constituted a large portion of the total pressure at the steady-state vacuum. This effect was previously observed during in-situ vacuum testing of rock (Jakubick, 1984).

The following humidity conditions were tested in the lab for effect on permeability (Table II):

1) outside boundary humidity, RH_e, higher than in the test hole, RH_w, (at laboratory temperature in a humidity-controlled environment);

2) outside boundary humidity comparable to test hole humidity (at laboratory temperature);

3) outside boundary humidity lower than test hole humidity (at elevated temperatures).

Before the test, the temperature of the concrete cylinders was equilibrated with that of the ambient air.

TABLE II

T [°C]	RH_e [%]	Δe [torr]	k [μD]
24.2	95.0	16.40	27.4
24.2	95.0	15.51	27.4
25.6	55.0	6.78	38.7
24.2	41.7	2.85	35.0
30.2	20.6	-2.12	38.0
35.8	11.0	-5.60	37.6
40.8	4.3	-9.98	38.1
44.8	0.0	-16.40	44.9
50.0	0.0	-18.69	40.5

Δe = water vapour pressure gradient

At ambient temperatures there was a discernable permeability increase with decreasing media humidity. At elevated temperatures and at decreased humidity the permeability further increased.

CONCLUSIONS

Although it was previously shown that the transient vacuum analysis provided satisfactory results when used for measurements of in-situ permeabilities (Jakubick, 1983), testing under all conceivable field conditions is needed in order to interpret complex fracture systems. In conjunction with nuclear waste disposal, the evaluation of the technique at temperatures above 50°C is required. Finally, the combined effect of thermal, pressure and hygrometric conditions on permeability warrants additional research.

REFERENCES

Bordman, C.R., Skrove, J.W. (1966). "Distribution in Fracture Permeability of a Granitic Rock Mass Following a Contained Nuclear Explosion", Journal of Petroleum Technology, Vol. 18, No. 5, pp. 619-623.

Chen, H.K., Brigham, W.E. (1978). "Pressure Buildup for a Well With Storage and Skin in a Closed Square", Journal of Petroleum Technology, January, pp. 141-146.

Figg, J.W. (1973). "Methods of Measuring the Air and Water Permeability of Concrete", Magazine of Concrete Research, Vol. 25, No. 85, pp. 213-219.

Hooton, R.D. (1985). "Concrete Integrated Cask Program, Development of High-Strength, High-Density Concrete Mixes", Ontario Hydro Report No. 85-132-H.

Jakubick, A.T. (1984). "Vacuum Logging for Measurement of the Integrity of the Near-Excavation Zone", Field Measurements in Geomechanics, Proceedings of the International Symposium, Zurich, pp. 163-175.

Koopmans, R., Hughes, R. (1984). "An Automated and Computerized Dilatometer System to Measure Deformation Modulus of Rock", Ontario Hydro Report No. 84-330-K.

Loughborough, M.T. (1966). "Permeability of Concrete to Air", Ontario Hydro Research Quarterly, Vol. 18, No. 1, pp. 14-16 and p. 25.

POSTCLOSURE COUPLED GEOHYDROLOGICAL PROCESS ON TOP OF A REPOSITORY

by

VIETCHAU V. NGUYEN
EWA, INCORPORATED
12800 INDUSTRIAL PARK BOULEVARD
MINNEAPOLIS, MN 55441

ABSTRACT

Performance assessment of the conceptual design of a nuclear waste repository involves the evaluation of various coupling modes within the basic flow and transport processes. The coupling modes of interest induce the onset of thermohaline currents in the saturated domain on top of the repository. Once this convective pattern is formed, continuous circulation of the bulk fluid may give rise to the multiple steady states of the chemically reactive species in motion. In this technical communication we present a synthesis of the state-of-the-art knowledge of this problem, propose an approach to subsequently study the data uncertainty effects on numerical simulation schemes, and illustrate the derived results with a Basalt Waste Isolation example.

I. INTRODUCTION

Singularity theory, linear perturbation analysis, and the method of energy can be combined to study the various coupling modes of hydrogeological processes extant near a nuclear waste repository. Directly above the repository, possible postclosure scenarios under investigation resemble that of a thermally induced continuous stirred tank reactor. In this situation, it is shown that effective permeability and bulk decay-reaction rate can play a dominant role in the stability of the multiple steady states of a coupled velocity (V)-concentration (C)-temperature (T)-field. Consequently, the nonlinear behavior of the (V,C,T)-field governed by the scaled transport operators and the equation of state is highly sensitive to certain disturbances to the in-situ conditions and the chemical parameters.

As a result, knowledge of the Rayleigh (R_a) and the Damköhler (D_a) numbers for a fractured porous medium may be used to select suitable methods of solution for the (V,C,T)-field simulation.

On the other hand, uncertainty in the data base and errors incurred by parameter identification procedures may be regarded as stochastic disturbances of the above dimensionless numbers. This allows assignment of physically reasonable probability distributions to a class of characteristic parameters involved in the dimensional analysis. In this sense, the resulting mean values of these two numbers and their associated variances are found to form a set of criteria for the statistical classification of the coupling modes. Such criteria can be used to examine the validity of the application of predictive models by a comparison to the critical values derived independently from the stability analysis. Near the bifurcation threshold, numerical approximation assumptions, geometry of the grid mesh, and convergence to the steady state solutions must be carefully examined to ensure the accuracy of the simulation.

II. REVIEW AND SUMMARY OF EXISTING RESULTS

A. GOVERNING EQUATIONS :COUPLED SYSTEM I [1,2,4,6]

The conservation mathematical statements are well known and summarized as follows:

1. Conservation of fluid mass:
$$\nabla . u = 0$$

2. Conservation of momentum with Boussinesq's approximation (Darcy's law):
$$u = - K/\phi\mu (\nabla p - \rho g)$$

3. Conservation of energy:
$$\rho C_p V(\partial T/\partial t + u.\nabla T - \kappa\nabla^2 T) = -\Delta H V k_0 \exp\{-E/RT\} c - h A \{T - T_a\}$$

4. Conservation of species mass:
$$\partial c/\partial t + u.\nabla c - D\nabla^2 c = -k_0 \exp\{-E/RT\} c$$

5. Equation of state for the bulk fluid density:
$$\rho = \rho_0 [1 - \alpha(T-T_0) - \alpha_c (c - c_0)]$$

B. THERMOHALINE STABILITY CONDITIONS [4,5]

Using linear perturbation analysis and the method of energy, it can be shown that the onset of instability of convection is the violation of the following inequalities:

1. Monotonic stability:

$$R_a + S < 4\pi^2$$

2. Dual Stability:

$$(sR_a + rS)/(r+s) < 4\pi^2$$

The onset of free convection is independent of the magnitude of the horizontal fluid current. This is due to the fact that a translational moving reference frame may be attached to the lateral flow to preserve the validity of the stability analysis.

C. GOVERNING EQUATIONS : COUPLED SYSTEM II

Under the thermohaline convection mode, by integration over the saturated volume of influence and by first-order approximation, the involved conservation laws may be written as:

1. Conservation of energy:

$$\rho C_p V\{dT/dt - U(T_0 - T)\} = -\Delta H\, Vk_0 \exp(-E/RT)c - hA(T-T_a)$$

2. Conservation of species mass:

$$dc/dt - U(c_0 - c) = -k_0 \exp(-E/RT),$$

where $U = F/V$.

These equations are similar to those pertinent to a continuous stirred tank reactor system.

D. NONDIMENSIONALIZATION OF SYSTEM II [6]

By appropriate redefinition of the independent variables, system II of coupled transport equations may be written as:

1. $dX_1/dt = -X_1 + D_a(1 - X_1) \cdot \exp(X_2/(1 + (X_2/\gamma)))$

2. $dX_2/dt = -X_2 + B D_a(1 - X_1) \cdot \exp(X_2/(1 + (X_2/\gamma))) - \beta(X_2 - X_{2a})$

where

3. $X_1 = (c_0 - c)/c_0$,

4. $X_2 = \gamma(T - T_0)/T_0$,

5. $\tau = t_R/U$,

6. $\gamma = E/RT_0$,

7. $B = (-\Delta H)\, c_0 \gamma/\rho C_p T_0$,

8. $D_a = (k_0 e^{-\gamma} t_R)\tau$, and

9. $\beta = (h A t_R/V\rho C_p)\tau$.

E. SINGULARITY ANALYSIS OF SYSTEM II AND CLASSIFICATION OF MULTIPLE STEADY STATES [6]

Let X_{1s} and X_{2s} be the steady state solutions of D.1 and D.2. Then

1. $G(x_{1s},\tau) = Da_0\tau - (x_{1s}/(1 - X_{1s})) \cdot \exp\{-(BX_{1s} + \beta_0\tau X_{2a}) /[(1+\beta_0\tau) + (Bx_{1s} + \beta_0\tau X_{2a})/\gamma]\} = 0$,

and

2. $x_{2s} = (B X_{1s} + \beta_0\tau X_{2a})/(1 + \beta_0\tau)$,

where

3. $Da_0 = k_0 e^{-\gamma} t_R$

and

$\beta_0 = h A t_R/V\rho C_p$

are reference values of D_a and β , i.e., $D_a = Da_0\tau$ and $\beta = \beta_0\tau$.

4. Let m_1, m_2 be the solutions of

$$(\partial G/\partial X_{1s}) = 0,$$

then multiple steady states occur for

5. $m_1 < x_{1s} < m_2$,

and for Damköhler numbers in the range

6. $D_a(m_2) < D_a < D_a(m_1)$,

which correspond to E.3, E.4 and E.5. Details of singularity analysis of system II are given in [6].

III. STATISTICAL CONSIDERATIONS FOR NUMERICAL SIMULATION OF COUPLED HYDROGEOLOGICAL PROCESSES [1,3]

A. ENGINEERING APPROACH TO UNCERTAINTY ANALYSIS

In the postclosure performance assessment of the engineered barrier systems for a high level waste (HLW) repository, we are interested in the numerical solution of the coupled transport equations. The accuracy of the simulated processes and their sensitivity to the variation of the physical parameters depend strongly on the coupling modes, based on the knowledge of the dimensionless numbers R_a, S, r, s, m_1, m_2, $D_a(m_1)$ and $D_a(m_2)$. The dominant factors for monotonic instability are:

1. $R_a = (\alpha \beta_T g/\nu)(Kd^2/\kappa)$, and

2. $S = (\alpha_c \beta_c g/\nu)(K d^2/D)$.

Estimates of the first factor can be reasonably accurate. Consequently, the engineering design procedure would involve the statistical assessment of K, d, κ and D.

Once the uncertainty effect of the data base is known to the second factors, mean and variance of R_a and S can be estimated. The multiplicity of the steady states of the concentration field will be evaluated by means of variance analysis of the Damkohler numbers or the associated dominant factors arising from II.E.1. A sketch of the procedure for such statistical analysis has been given in [3].

B. ILLUSTRATION PROBLEM

An illustration of the proposed approach for the transport of uranium (U^{4+}) in the uranite oxidized state is given for the Basalt Waste Isolation Project (BWIP). The hypothetical repository is located within the Cohasset Flow, and the affected saturated zones are assumed to be defined from above by the Vantage Interbed, or the Mabton Interbed.

TABLE 1: Data for the Uranium Transport Problem in Basalt and Other Assumptions

Parameters	Values
Circular Repository, r	1,500m
Heights of Affected Saturated Zone, d	50m, 500m
Arrhenius 1st-Order Reaction	
-Frequency Factor, k_0	10^{-1} sec.$^{-1}$
-Activation Energy, E	5.85×10^4 J/mole
-Thermodynamic Constant, R	8.134 J/^{o}K-mole
-Field Temperature	350^{o}K
Heat of Decay-Reaction, ΔH	2.5×10^6 J/mole
Specific Heat for Saturated Basalt, C_p	1,200. J/Kg-^{o}K
Thermal Conductivity, K_T	1.62 W/m-^{o}K
Thermal Diffusivity, κ	0.16×10^{-6} m^2/sec.
Thermal Expansion Coefficient, α	3.7×10^{-4} ^{o}K
Upward Temperature Gradient, β_T	4.75×10^{-2} ^{o}K/m
Bulk Vertical Hydraulic Conductivities, K	10^{-4}, 10^{-6} m/sec.
Effective Porosity, ϕ	10^{-3}
Fluid Density, ρ	1,100. Kg/m^3

TABLE 2: Some Possible Coupling Modes Affecting the Transport of Uranium (U^{4+}) for BWIP Site

	Mean	Variance	Critical Values or Range	Coupling Modes	Numerical Problems
R_a	27.5	$Var(\log R_a) \pm 4$	$4\pi^2$	Cells or Rolls of Bénard Convection	Numerical Dispersion & Design of Grid Geometry
D_a	2.28×10^{-2}	$Var(\log D_a) \pm 4$	$[D_{a1}\pm10^{-2}, D_{a2}\pm10^{-1}]$	Multiple Steady States in $[D_{a1}, D_{a2}]$	Nonconvergence & Instability near or in $[D_{a1}, D_{a2}]$

Comprehensive numerical results of the uncertainty analysis tabulated above will be documented in a forthcoming technical report.

IV. REFERENCES

1) M.A. Combarnous and S.A. Bories (1975) "Hydrothermal Convection in Saturated Porous Media", in Adv. in Hydroscience X, V.T. Chow ed., Academic, New York, pp. 231-307.

2) V.V. Nguyen, G.F. Pinder, W.G. Gray and J.F. Botha (1983) "Numerical Simulation of Uranium In-Situ Mining", Chem. Eng. Sci., 38 (11): 1855-1862.

3) V.V. Nguyen and L. Lehman (1985) "Interscale Transfer of Information in Nuclear Waste Repository Multibarrier Systems", Proc. of NWWA Western Regional Groundwater Conf.,Reno, Nevada,pp41-51.

4) D.A. Nield (1968) "Onset of Thermohaline Convection in a Porous Medium", WRR, 4 (3): 553-560.

5) M. Prats (1966) "The Effect of Horizontal Fluid Flow on Thermally Induced Convection Currents in Porous Media", J. Geophys. Res., 71 (20): 4835-4838.

6) A. Uppal, W.H. Ray and A.B. Poore (1976) "Classification of the Dynamic Behavior of Continuous Stirred Tank Reactors", Chem. Eng. Sci., Vol. 31, pp. 205-214.

ACKNOWLEDGMENT

Dr. Georges Abi-Ghanem assisted in the multiple steady states analysis of the BWIP problem.

NOTATION

A virtual heat transfer area
B adiabatic temperature rise
c species concentration
C_p specific heat
d depth of affected saturated porous medium
E activation energy
F effective influx rate of fluid bounded by V
g gravitational acceleration
h heat transfer coefficient
ΔH heat of reaction
k_0 reaction constant
K permeability of porous medium
R thermodynamic constant
t time
t_R reference time
T temperature
T_a ambient temperature
T_0 temperature of repository top
u velocity of fluid phase
U F/V
V saturated volume of influence above the repository
X_{2a} normalized ambient temperature

Dimensionless Numbers

D_a Damkohler number, $k_0 e^{-\gamma} t_R$
R_a thermal Rayleigh number, $\alpha \beta_T g K d^2/\kappa\nu$
S solute Rayleigh number, $\alpha_c \beta_c g K d^2/D\nu$
r Prandtl number, ν/κ
s Schmidt number, ν/D

Greek Symbol

α thermal expansion coefficient
α_c solute expansion coefficient
β_T upward temperature gradient
β_c upward concentration gradient
γ dimensionless activation energy, E/RT.
ρ bulk fluid density
κ thermal diffusivity
D_μ dispersion coefficient
μ fluid viscosity
ν kinematic viscosity, μ/ρ
ϕ porosity
τ resident time in V, t_R/V
∇ del operator
∇^2 Laplacian operator

HYDRODYNAMIC DISPERSION

M.H.L.Pryce

Physics Department
University of British Columbia
Vancouver, B.C., Canada, V6T 2A6

ABSTRACT

A dominant mechanism contributing to hydrodynamic dispersion in fluid flow through rocks is variation of travel speeds within the channels carrying the fluid, whether these be interstices between grains, in granular rocks, or cracks in fractured crystalline rocks. The complex interconnections of the channels ensure a mixing of those parts of the fluid which travel more slowly and those which travel faster. On a macroscopic scale this can be treated statistically in terms of the distribution of times taken by a particle of fluid to move from one surface of constant hydraulic potential to another, lower, potential. Over distances large compared with a grain size in the one case, or the microcrack length in the other, correlations become lost, and one can then trace the spatial development of the time-distributions as though they were convolutions of independent probabilities.

The distributions in the individual channels are such that very long travel times make a very important contribution. Indeed, while the mean travel time is related to distance by a well-defined transport speed, the mean square is effectively infinite. This results in an asymmetrical plume which differs markedly from a gaussian shape.

The distribution of microscopic travel times is related to the distribution of apertures in the interstices, or in the microcracks, which in turn are affected in a complex way by the stresses acting on the rock matrix.

DISPERSION

Consider a situation in which a fluid (groundwater) flows through a permeable medium such as sand, sandstone or igneous rock permeated by fractures of various sizes. For simplicity I shall assume that the physical conditions governing the flow are independent of time. Transient conditions can be dealt with later. Again, for simplicity of exposition, I shall suppose that the flow is in a certain sense one-dimensional. Again, three-dimensional flow can be dealt with later, though it it requires making more careful distinctions than I can do here without diverting from the salient features of what I want to discuss.

The topic is hydrodynamic dispersion, namely the phenomenon that different elements of fluid crossing the same hypothetical surface drawn inside the medium may travel at different speeds. Consequently, the time taken by elements of the fluid which cross one surface at the same time to travel downstream to another surface is not the same for all the elements. When I speak of "elements of the fluid" in the context of a nuclear waste repository, I am mainly referring to dissolved molecules or ions of radioactive species, because it is their transport through the rock which is of concern. Since these are carried by the fluid, it is basically the flow of water molecules which governs the process. So, for the purpose of exposition, let me refer to the elements as "molecules".

In the context of nuclear waste disposal, the time taken by radioactive substances to travel from the repository to the biosphere is of central importance. Insofar as this may be affected by hydrodynamic dispersion, we need to understand the process of dispersion. Personally, I think that the effects of dispersion are unimportant - but one has to be sure.

Since, on a microscopic scale, the flow follows tortuous paths, encountering many stagnant regions, different molecules will have a wide diversity of transit times in going from one plane transverse to the flow, to another plane further downstream. Although there will exist a shortest time (greater than zero), corresponding to the fastest path, for practical purposes there will be no upper limit to the transit time. This is because molecules may get trapped for indefinitely long times in stagnant regions. Although infinitely long times will not really occur, since diffusion will eventually allow any molecule to get back into the stream, for the purposes we have in mind, the upper limit to the travel time is effectively infinite.

The crucial point is that the mean square of the time required to travel from one plane to another is for all practical purposes infinite. So, although there is a well-defined mean travel time, which is proportional to the distance between the planes, and whose coefficient of proportionality defines an effective mean transport speed, the variance is infinite.

This implies that the statistical distribution of the travel times does not approach a normal distribution as the distance of travel increases indefinitely. Much of simple statistical theory relies on the central limit theorem, but the conditions for its validity are not fulfilled here.

Nevertheless it is possible to work out a useful stochastic description of dispersion. Let us start by analyzing a simple situation in which the microscopically randomly distributed flow channels through the medium are, on a macroscopic scale, statistically uniformly distributed. Assume that the flow is in the x-direction, and that the average transport speed is V. The precise definition of V will become clear as we develop the analysis.

We wish the analysis to be applicable to the response to different hydraulic gradients. This implies that the local velocities will be different in different hydraulic gradients. In the present applications the Reynolds numbers are very small, so that the local velocities are all proportional to the hydraulic gradient, and scale linearly with V.

Let us consider two planes, $x = a$ and $x = a + b$, and let us study the distribution of times taken for molecules to travel from one plane to the other. The mean time is b/V. To exploit the way in which the local velocities scale with V, we introduce a variable, s, with the dimensions of a length, such that the time taken by a selected molecule to travel from one plane to the other is s/V.

If we now study the statistical distribution of the transit times, this can be conveniently replaced by the distribution of the variable s, in terms of a probability distribution $p(b;s)\,ds$ for s to lie in an interval ds. The distribution is normalized by

$$\int_0^\infty p(b;s)\,ds = 1 \quad . \tag{1}$$

The transport speed V is implicitly defined by the relation

$$\int_0^\infty s\,p(b;s)\,ds = b \quad . \tag{2}$$

The distribution $p(b;s)$ depends on b. We can comment on two extremes. When b is small in comparison with the scale of the microstructure of the medium (e.g. the grain size), the distribution in s/b becomes the distribution in the product of V and the reciprocal of the x-component of the local velocity field. For the present investigation this is of no interest. When b is large in comparison with the scale of the microstructure, the distribution in velocities (more strictly in their reciprocals) on the planes $x = a$ and $x = a + b$ become more and more statistically uncorrelated as b increases. We shall henceforth concentrate on distances sufficiently large that we can assume total loss of correlation.

We now consider three successive planes, with coordinates a, $a + b$ and $a + b + c$, and enquire about distribution in times taken to travel 1) from the first to the second, 2) from the second to the third, and 3) from the first to the third. Call these times respectively $t_1 = s_1/V$, $t_2 = s_2/V$ and $t = t_1 + t_2 = s/V$. Then the probability distribution for s_1 is

$$p(b;s_1)\,ds_1 \ ,$$

for s_2 it is

$$p(c;s_2)\,ds_2 \ ,$$

and for s it is

$$p(b + c;s)\,ds.$$

Since $s = s_1 + s_2$, and the probabilities are uncorrelated, we have

$$p(b+c;s) = \int_0^s p(b;s_1)\,p(c;s-s_1)\,ds_1 \tag{3}$$

This convolution relation is more easily handled in terms of Laplace transforms with respect to the variable s. To this end we introduce a variable w, conjugate to s, and whose dimensions are those of a reciprocal length, and define the Laplace transform $q(b;w)$ by

$$q(b;w) = \int_0^\infty e^{-ws}\,p(b;s)\,ds \tag{4}$$

The relationship (3) then implies

$$q(b + c;w) = q(b;w)\,q(c;w). \tag{5}$$

The convolution relationship is valid provided that b and c are larger than the correlation length scale of the flow channels. For granular rocks this means something larger than a few times the grain size. For fractured igneous or metamorphic rock it is more difficult to give a clean interpretation.

In most situations it can be regarded as "greater than the scale of the most important water-bearing fractures", leaving open the vexed question of which those are. For the present discussion I will suggest, very tentatively, that 10 meters is sufficiently large; and that we are going to be interested in the effects of dispersion over distances in excess of 100 meters, so that the present analysis does have a range of applicability.

The solution to (5) is

$$q(x;w) = \exp(-xf(w)) , \quad (6)$$

where $f(w)$ is a function of the complex variable w . which is well-defined and analytic for all values of w whose real part is greater than zero. It has a branch-point type of singularity at w 0.

The normalizing relations (1) and (2) imply that f and its first derivative tend to 0 and 1 respectively as w approaches 0 from the allowed domain. The fact that the second moment of the travel time is infinite indicates that the second derivative of f tends to infinity as w approaches 0 .

I have studied a few simplified models of microscopic flow paths, to guide me in understanding the nature of the function $f(w)$, and these suggest that for small values of the complex variable w , the function has the form

$$f(w) = w - B w^{\alpha} + \text{smaller}, \quad (7)$$

where the power index α lies between 1 and 2. The variable w and the function f both have the dimensions of an inverse length. The coefficient B has the dimensions of a length raised to the power $\alpha-1$.

As the distance travelled gets longer and longer, it is the behavior of $f(w)$ in a smaller and smaller region near w 0 which determines the travel-time probability distribution. For very long distances it is adequate to replace (7) by the approximation

$$f(w) = w - Bw^{\alpha} . \quad (7a)$$

If one substitutes the corresponding Laplace transform into the standard inversion formula, one finds that the distribution function for the travel time, $P(x;t)\,dt$, can be expressed in terms of an index β , equal to the reciprocal of α , and a function of a non-dimensional variable u , defined by

$$u = (Vt-x)/(Bx)^{\beta} , \quad (8)$$

in the form

$$P(x;t)\,dt = (V/(Bx)^{\beta})\, F(\beta,u)\,dt \quad (9)$$

where $F(\beta,u)$ is a nondimensional real function of the index β and the non-dimensional real variable u . The latter can be looked upon as a scaled measure of the arrival time, measured from the arrival time of a hypothetical element of fluid travelling at the mean transport speed V .

The index β is a characteristic of the structure of the medium. It lies between 0.5 and 1.0. A plausible model for flow through fractured crystalline rock suggests $\alpha = 7/4$, i.e. $\beta = 4/7$.

For a given value of β , the function F, looked on as a function of u , the scaled time deviation, is asymmetrically peaked. The maximum is reached at a slightly negative value of u. In other words, the peak breakthrough occurs a little before the arrival of fluid travelling at the mean speed. From the early side the peak rises very steeply. On the late side it falls off more gently.

F can be expressed as a power series in u , namely

$$F(\beta,u) = \frac{\beta}{\pi} \sum_{n=1}^{\infty} u^{n-1} \Gamma(n\beta) \sin(n\pi\beta)/\Gamma(n). \quad (10)$$

About twelve terms of this series are adequate to give convergence over the range covering the peak and down to 5% on both sides. Beyond this, asymptotic expressions are available to calculate the tails.

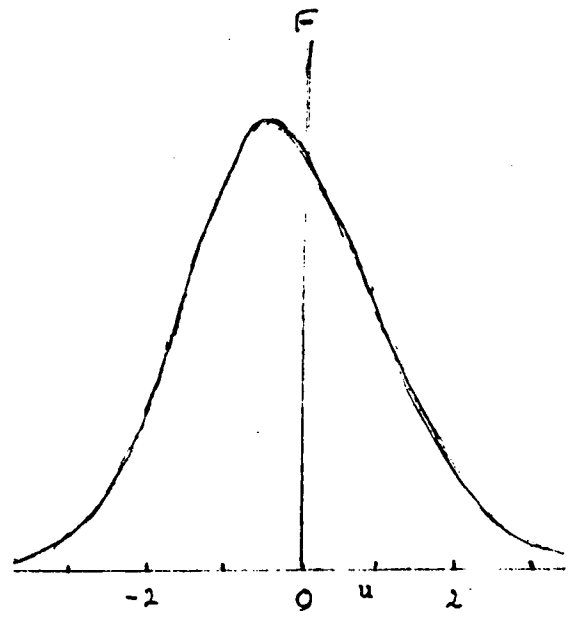

Figure 1. Breakthrough curve for 4/7

Figure 1 shows a plot of $F(4/7,u)$. This could be appropriate for the behavior of fractured crystalline rock. It can be interpreted in terms of a situation where some chemical species is injected uniformly over a plane $x=0$ over a short time interval, and one is monitoring the concentration as a function of time on a plane some large distance x downstream.

One could also ask the closely related question about the spatial distribution of the dissolved species at some fixed, large, time after injection. I shall not enter into the details here. It is fairly obvious how to connect the two questions.

What this analysis suggests is that hydrodynamic dispersion should be characterized by two quantities :- an index β (or its reciprocal α), and a coefficient B , with the dimensions of a length raised to the power $\alpha-1$.

It is common engineering practice to fudge dispersion as though it mimicked the effects of diffusion, by adding the product of the transport speed and the "diffusivity" to the true diffusion coefficient (which is generally small in comparison), and treating the sum as an effective diffusion coefficient. It corresponds to the limiting case $\alpha = 2$, $\alpha = 0.5$ of the present analysis, where the coefficient B is closely related to the diffusivity. It is not a very satisfactory representation of dispersion, though it does give some useful insights. One of its attractions is that it can be represented by a partial differential equation, for which computer routines exist. This attraction is somewhat illusory, for the particular differential equation is troublesome in regard to numerical stability.

In the applications to nuclear waste disposal, what is mainly required is a response function to the injection of solutes at the boundary of the repository. The present analysis is capable of furnishing this.

This account is necessarily greatly simplified. It has not touched on transverse dispersion; nor on flow which is not "one-dimensional"; nor on the effects of time-dependent rock properties; nor on the effects of spatial variations in rock properties; nor on the effects of dispersion at less extreme distances, where the approximation (7a) is inadequate, but where there are very interesting effects. I believe that all of the above topics can be dealt with rationally by refinements of the present analysis.

In closing, I would like to pay lip service to the central theme of this symposium by remarking that the different stresses in the rock at different depths will modify the geometry of the channels through which the groundwater flows. There should be some interesting research to be done on how β and B are affected by in situ stresses. Though I have been emphasizing the hydraulic aspects of the phenomenon, it should be evident that it is strongly affected by mechanical factors.

SLIP-FLOW EXPERIMENTS IN WELDED TUFF: THE KNUDSEN DIFFUSION PROBLEM

Daniel C. Reda
Fluid and Thermal Sciences Department
Sandia National Laboratories
Albuquerque, NM 87185

ABSTRACT

Gas-phase permeability experiments, using nitrogen, were conducted on a sample of densely welded tuffaceous material from the Nevada Test Site. The primary independent variable was the average pore pressure, which was systematically varied from 13.1 to 0.1 MPa; net circumferential stress was maintained constant at 4.3 MPa. Gas permeability was found to be a strong function of pore pressure, undergoing an order-of-magnitude increase as pore pressure was reduced over the stated range. Based on these measurements, the Knudsen diffusion coefficient for water vapor, at 296 K, was calculated to be $\approx 3.2 \times 10^{-7}$ m^2/s and the material's average pore diameter was estimated to be $\approx 8 \times 10^{-9}$ m. Comparison of this length scale with mercury intrusion porosimetry results showed agreement to within one order of magnitude.

NOMENCLATURE

A	=	core cross-sectional area
b	=	Klinkenberg constant
D_K	=	Knudsen diffusion coefficient
$\bar{d}_p$	=	average pore diameter
d_{mol}	=	diameter of molecule
k_G	=	absolute gas-phase permeability
k_L	=	absolute liquid-phase permeability
L	=	core length
M_G	=	gas molecular weight
m_{mol}	=	mass of molecule
P	=	pressure
P_c	=	confining pressure
$\bar{P}_p$	=	average pore pressure, $(P_1 + P_2)/2$
ΔP	=	pressure drop along core, $(P_1 - P_2)$
Q	=	volumetric flow rate
R	=	universal gas constant
R_G	=	gas constant
T	=	temperature

Greek

λ	=	gas mean free path length
μ_G	=	gas viscosity
τ	=	tortuosity factor
ϕ	=	porosity

Subscripts

atm	=	at atmospheric pressure
H_2O vapor	=	water vapor
max	=	maximum
min	=	minimum
N_2	=	nitrogen
p	=	at average pore pressure
$1, 2$	=	upstream, downstream of core

INTRODUCTION

Experimental and theoretical efforts are under way to investigate the technical feasibility of nuclear waste isolation within proposed geologic repositories. The Nevada Nuclear Waste Storage Investigations (NNWSI) Project is addressing the feasibility of isolating heat-producing waste canisters within welded tuffaceous rocks located above the water table. In order to accomplish this task, the physics of two-phase flows (of water and water vapor) through partially saturated tuff, driven by coupled thermal/ hydrological effects, must be understood (see Tsang, 1984). In addition, the impact of these coupled thermal/hydrological processes on repository design must then be evaluated.

One such coupled thermohydrological process encountered in low permeability tuff is the Knudsen diffusion of water vapor, driven by temperature-induced vapor pressure gradients. Whenever the mean free path length of any gas approaches the same order of magnitude as the pore dimensions of the permeable medium through which it flows, noncontinuum gas dynamic effects become important. Gas molecules adjacent to pore boundaries no longer adhere to these boundaries and "slip-flow" phenomena are encountered. Klinkenberg (1941) has shown that this re-

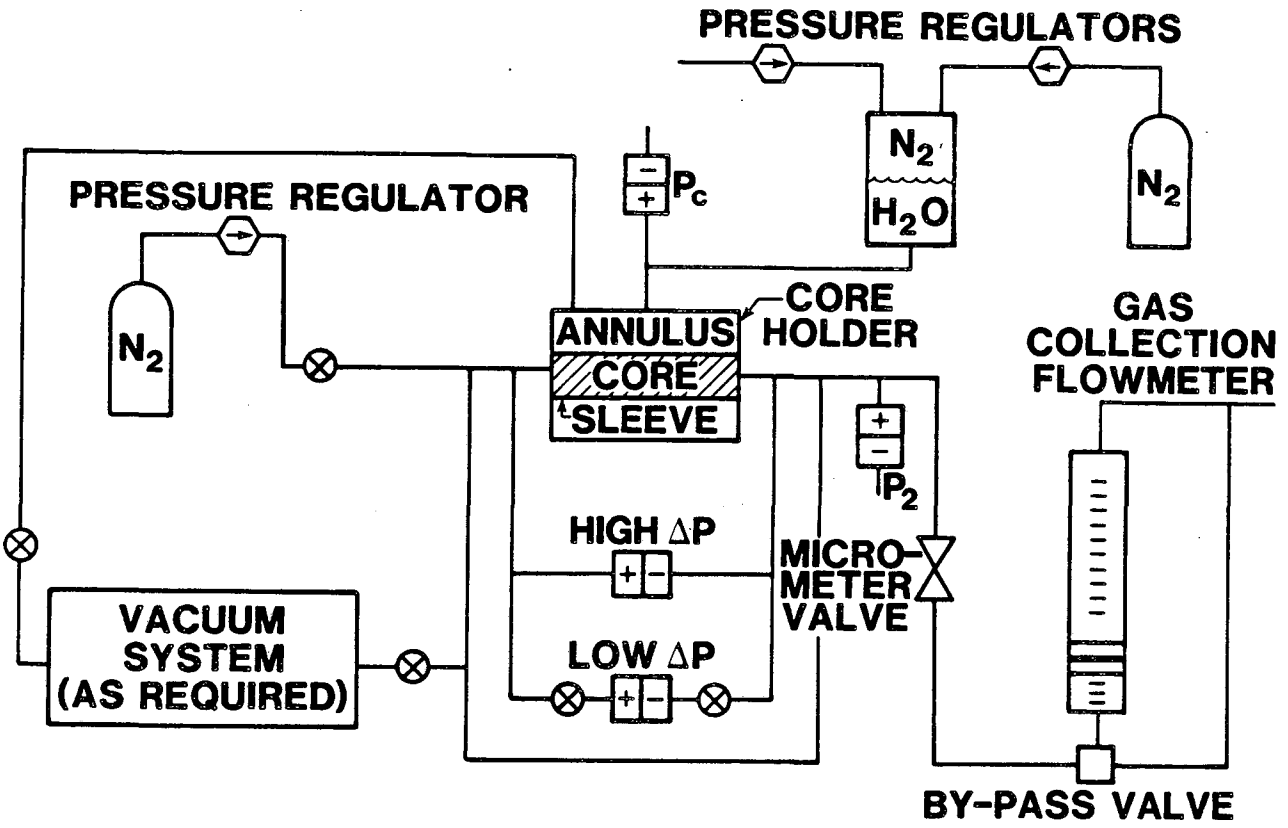

FIG. 1: Schematic of Apparatus

duced resistance to gas flow, which occurs on a microscopic level, can be quantified by the measurement of a macroscopic parameter, the gas-phase permeability (k_G). His laboratory results showed that k_G scales with the average pore pressure of the gas ($\overline{P}_p$) in the following manner:

$$k_G = k_L \left[1 + \frac{b}{\overline{P}_p}\right] \qquad (1)$$

where k_L is the single-phase liquid permeability and b is a constant of proportionality dependent on the gas/medium combination under study. In the limit of infinite gas pressure, k_G approaches k_L.

The objective of the present research was to investigate the Knudsen diffusion regime for gas flows in welded tuff. Results of these experiments were then used to determine values for the Knudsen diffusion coefficient as well as the average pore diameter of the material.

EXPERIMENTAL APPROACH

Experiments were conducted on a cylindrical core sample of unfractured welded tuff taken from the Busted Butte outcrop of the Topopah Spring Member of the Paintbrush Tuff on the Nevada Test Site. This core had a diameter of 5.54 cm and a length of 6.36 cm. Material effective porosity, determined in previous liquid-permeability experiments (Reda, 1985) was 0.106. The core was dried in an oven at 70°C for 4 days prior to mounting in the core holder. This procedure, plus the subsequent passage of dry gas through the core, ensured that the core was in a fully dried state prior to the gas-phase permeability measurements.

Figure 1 shows a schematic of the test apparatus. Net circumferential stress on the core ($P_c - \overline{P}_p$) was maintained constant at 4.3 ± 0.2 MPa. All experiments were run at a temperature of 296 K.

Dry nitrogen gas was used as the working fluid. Average pore pressure ($\overline{P}_p$) was systematically varied from a maximum value of 13.1 MPa to a minimum

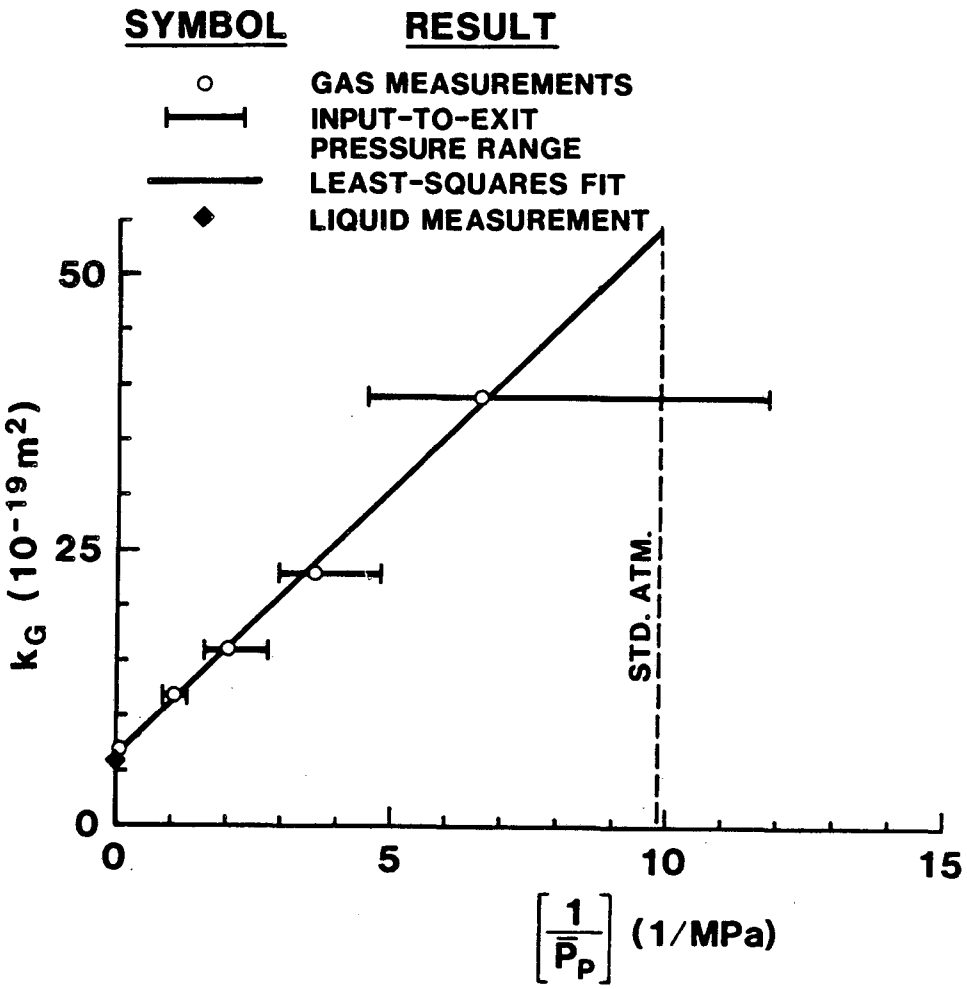

FIG. 2: Gas Permeability versus Inverse Pore Pressure

value of 0.15 MPa through utilization of a pressure regulator upstream of the core and a dual-micrometer flow control valve downstream of the core. Upon the attainment of a steady-state pressure drop (ΔP) across the core, the gas volumetric flow rate through the core at atmospheric pressure (Q_{atm}) was measured. (The instrument used for this purpose was a gas-collection device incorporating a sliding-seal piston in a graduated glass cylinder.) For the isothermal flow of an ideal gas, it can be shown that

$$PQ = constant \tag{2}$$

Hence,

$$Q_p = \left[\frac{P_{atm}}{\bar{P}_p}\right] Q_{atm} \tag{3}$$

Darcy's law was then used to calculate the gas-phase permeability

$$k_G = \left[\frac{Q_p \mu_G L}{A \Delta P}\right] \tag{4}$$

RESULTS

Measurements of gas permeability as a function of inverse pore pressure are shown in Figure 2. Gas permeability was found to increase by an order of magnitude, from $\approx 5 \times 10^{-19}$ m^2 to $\approx 50 \times 10^{-19}$ m^2, over the pore pressure range $13.1 \geq \bar{P}_p \geq 0.1$ MPa. A linear, least squares fit of the data, extrapolated to infinite pore pressure, yielded an intercept (inferred permeability to liquid) of 6.3×10^{-19} m^2, within 13 percent of the previously measured k_L value of 5.6×10^{-19} m^2 (Reda, 1985). The value for the Klinkenberg constant (b) was 0.76 MPa.

Hadley (1982) has shown that the Knudsen diffusion coefficient (D_K) can be calculated from the Klinkenberg constant in the limit of zero liquid saturation

$$D_K = \left[\frac{b k_L}{\phi \mu_G}\right] \tag{5}$$

The Knudsen diffusion coefficient for nitrogen, at 296 K, was thus calculated to be

$$D_{K,N_2} = 2.6 \times 10^{-7} \quad \mathrm{m^2/s} \tag{6}$$

Dullien (1979) has shown that D_K scales with the inverse square root of gas molecular weight

$$D_K = \frac{\bar{d}_p}{3\tau}\sqrt{\frac{8RT}{\pi M_G}} \tag{7}$$

Converting the nitrogen result of Eq. (6) to the molecular weight of water vapor, at 296 K, yields

$$D_{K,H_2O\ vapor} = 3.2 \times 10^{-7} \quad \mathrm{m^2/s} \tag{8}$$

Equations (6) and (7), or Eqs. (7) and (8), can then be combined to solve for the average pore diameter of welded tuff ($\bar{d}_p$). Assuming a value of 5 for the tortuosity factor τ yields

$$\bar{d}_p \cong 8 \times 10^{-9} \quad \mathrm{m} \tag{9}$$

A self-consistency check on these empirical results was then made. The estimated pore diameter of Eq. (9) was compared to the range of gas mean free path lengths (λ) experienced under present test conditions (see Vincenti, 1965):

$$\lambda = \left[\frac{m_{mol} R_G T}{\sqrt{2}\pi d_{mol}^2 P}\right] \tag{10}$$

where $\lambda_{min} \approx 5 \times 10^{-10}$ m and $\lambda_{max} \approx 4 \times 10^{-8}$ m. Results showed $\lambda_{min} < \bar{d}_p < \lambda_{max}$, consistent with the experimental observations of Knudsen diffusion effects shown in Figure 2. (Note: This observation would still hold for an assumed tortuosity factor of 10.)

Another experimental method which can be used to estimate pore size distributions is mercury intrusion porosimetry. In this technique, measurements are made of the pressure increases required to force additional volumes of a nonwetting liquid (mercury) into the pore space. In order to convert such pressure/volume measurements into pore size information, one must invoke the "bundle of capillary tubes" model (see Dullien, 1979). In this model, the pore volume is assumed to be a bundle of parallel capillary tubes of different diameters and equal lengths; every capillary tube is assumed to have a uniform diameter along its entire length.

Given these assumptions, it is apparent that mercury intrusion does not reveal the presence of the larger internal pores that are separated from the sample exterior by smaller diameter necks or restrictions. As pressure is increased, mercury is ultimately forced through these restrictions and into adjacent (larger) pores which lie beyond; the incremental volume associated with this penetration is then assigned to capillary tubes of diameter equivalent to that of the restrictions. Dullien (1979) has discussed the caveats of this method in some detail. In summary, he notes,

> "The danger inherent in such models is that, owing to their simplicity, they become popular and some people may believe that they closely approximate reality, in this case, the actual pore structure. In fact, nothing could be farther from the truth."

Nevertheless, since the mercury intrusion technique is one of the methods commonly used to assist in the overall characterization of geologic materials, it was felt that a comparison of pore sizes determined from mercury-intrusion and Knudsen-diffusion experiments would be informative. Such a comparison is shown in Figure 3.

No mercury intrusion data were available for welded tuff from the Busted Butte outcrop. However, such results were available for a sample of densely welded tuff taken from the same geologic unit: Topopah Spring Member of the Paintbrush Tuff, Yucca Mountain, Nevada Test Site, borehole USW G-4 1158 feet (353 meters). The liquid permeability of this sample (1.9×10^{-18} m^2) was comparable to that of the material tested herein (see Peters, et al., 1984).

As can be seen in Figure 3, the fifty-percentile value determined by the mercury intrusion technique was $\approx 6\times$ the "average" value ($\bar{d}_p$) determined from the Knudsen diffusion results. The "average" pore diameter determined from the mercury intrusion results (i.e., the mean hydraulic diameter, defined as four times the ratio of pore volume to pore surface area) was found to be $\approx 4\times$ the Knudsen diffusion value. Given the uncertainties in the tortuosity factor for welded tuff, this comparison showed that the two techniques yielded comparable estimates (within one order of magnitude) for the average pore diameter.

Present results have been input to the multiphase flow code NORIA of Bixler (1985) and numerical calculations are under way to determine the importance of Knudsen diffusion effects on repository design.

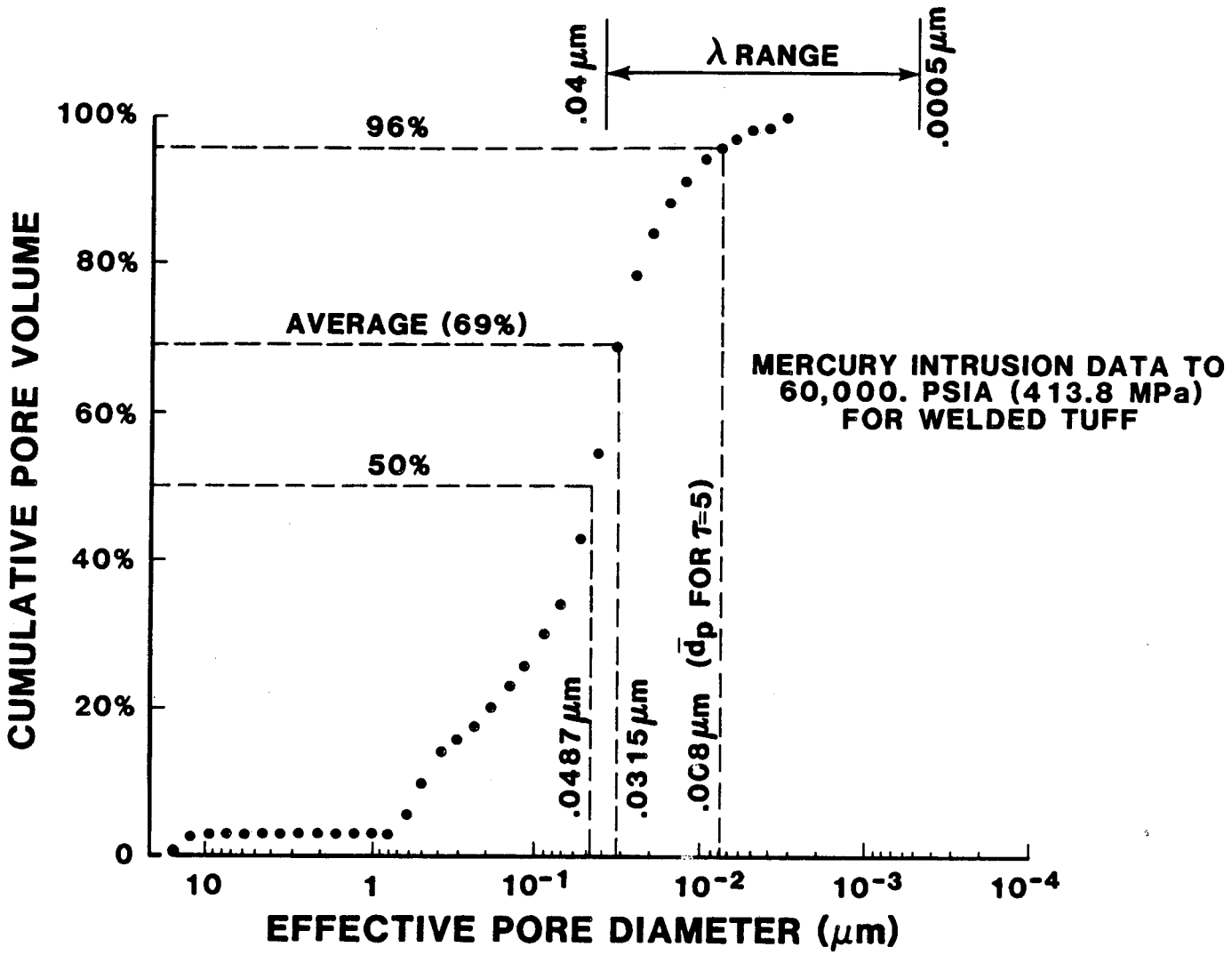

FIG. 3: Pore Diameter Comparison, Mercury Intrusion versus Knudsen Diffusion Results

SUMMARY

Gas-phase permeability experiments were conducted on a sample of densely welded tuff, with average pore pressure being the primary independent variable. Based on these measurements, and on analyses of results, the following observations were made:

1. Gas-phase (nitrogen) permeability was found to be a strong function of pore pressure, undergoing an order-of-magnitude increase as pore pressure was systematically reduced from 13.1 to 0.1 MPa. The value for the Klinkenberg constant was found to be 0.76 MPa.
2. The Knudsen diffusion coefficient for water vapor, at 296 K, was calculated to be 3.2×10^{-7} m^2/s.
3. The average pore diameter for densely welded tuff was estimated to be 8×10^{-9} m based on an assumed tortuosity factor of 5.
4. Calculated gas mean free path lengths for this experiment were found to bracket the estimated average pore diameter, consistent with the observations of conclusion (1).
5. Mercury intrusion data to ≈ 400 MPa on a similar sample of densely welded tuff yielded an estimate for the material's average pore diameter ≈ 4× larger than the Knudsen diffusion result.

ACKNOWLEDGEMENTS

This work was performed at Sandia National Laboratories supported by the U. S. Department of Energy under contract number DE-AC04-76DP00789.

REFERENCES

Bixler, N. E., (1985), "NORIA-A Finite Element Computer Program for Analyzing Water, Vapor, Air, Energy Transport in Porous Media," Sandia National Laboratories, Technical Report SAND84-2057.

Dullien, F. A. L., (1979), Porous Media: Fluid Transport and Pore Structure, Academic Press, New York, NY.

Hadley, G. R., (1982), "Theoretical Treatment of Evaporation Front Drying," Int. J. Heat and Mass Transfer, Vol. 25, pp. 1511-1522.

Klinkenberg, L. J., (1941), "The Permeability of Porous Media to Liquids and Gases," American Petroleum Inst., Drilling and Production Practice, pp. 200-213.

Peters, R. R., Klavetter, E. A., Hall, I. J., Blair, S. C. , Heller, P. R., and Gee, G. W., (1984), "Fracture and Matrix Hydrologic Characteristics of Tuffaceous Materials from Yucca Mountain, Nye County, Nevada," Sandia National Laboratories, Technical Report SAND84-1471.

Reda, D. C. and Hadley, G. R., (1985), "Saturated Permeability Measurements on Pumice and Welded-Tuffaceous Materials," Proceedings 17th International Congress, International Assoc. of Hydrogeologists, Hydrogeology of Rocks of Low Permeability, Tucson, AZ.

Tsang, C. F. and Mangold, D. C., editors, (1984), "Panel Report on Coupled Thermo-Mechanical-Hydro-Chemical Processes Associated with a Nuclear Waste Repository," Lawrence Berkeley Laboratory, Report LBL-18250, Univ. of California.

Vincenti, W. G. and Kruger, C. H., Jr., (1965), Introduction to Physical Gas Dynamics, John Wiley and Sons, Inc., New York, NY.

THEORY AND APPLICATION OF THE PORFLOW MODEL FOR ANALYSIS OF COUPLED FLOW, HEAT AND RADIONUCLIDE TRANSPORT IN POROUS MEDIA

Akshai K. Runchal

Analytic & Computational Research, Inc.
3106 Inglewood Boulevard
Los Angeles, CA 90066

ABSTRACT

This paper describes the theory and application of the PORFLOW model for analysis of coupled flow, heat and species transport processes in saturated, porous or equivalent porous media. The model is based upon the nodal point integration method. It inherently conserves mass and energy at both local and global scales. It provides for inhomogeneous, anisotropic and time-dependent properties and accounts for buoyancy effects due to density changes. It has been in development for over 9 years and its applications have included nuclear waste disposal, geothermal storage, ground water resource management, chemical pollution of aquifers, and others. Two applications of the model to problems related to disposal of high level waste are described in this paper.

INTRODUCTION

The coupled fluid flow, heat and mass transport processes in geologic materials have become a subject of considerable interest in recent years. Though such processes play an important role in nuclear, petroleum and reservoir engineering, the most recent expansion in the interest lies in the disposal of high and low level nuclear waste. Of all the suggested methods for disposal of this waste, that of deep underground burial in geologic formations has so far been recognized as the most economical and technically feasible.

The most important problem associated with the disposal of nuclear waste in geologic formations is the isolation of radioactive elements and their daughter products from the accessible environment over a time span of tens to hundreds of thousands of years. Physical processes, human intervention, and natural events and episodes may all contribute to the movement of radioactive material. However, transport by ground water is the most probable of all mechanisms for potential movement of significant radioactivity to the accessible environment. This transport may be considerably influenced by the heat released from the decay of nuclear waste. Thus, the coupled processes of flow, heat, and species transport must be considered in any credible analysis of nuclear waste disposal. The PORFLOW provides a tool for such analyses.

The general methodology of the PORFLOW models, and the specifics of some of the versions, have been extensively verified against a number of analytic solutions, experimental and field data, and other numerical models (Runchal and Sagar, 1985; Eyler and Budden, 1984; Fujioka and Runchal, 1983; Kline et al., 1983; Runchal and Hocking, 1981; Runchal et al., 1979, 1980, 1981). This paper describes the essentials of the mathematical and numerical basis of the model and two of its applications.

THE MATHEMATICAL BASIS

The Momentum Balance Equations. The momentum balance for a porous medium is expressed by a generalized Darcy's Law which, for non-isothermal conditions, is written as (Bear, 1972):

$$U = - K_x \partial_x P \quad , \tag{1}$$

$$V = - K_y (\partial_y P + R) \quad , \tag{2}$$

where:

$$P = p/(\rho^* g) + y - Y \quad , \tag{3}$$

$$K_x = k_x g \rho^*/\mu \quad , \tag{4}$$

$$K_y = k_y g \rho^*/\mu \quad , \text{ and} \tag{5}$$

$$R = \rho/\rho^* - 1 \quad . \tag{6}$$

In the above equations:

U, V	are the specific discharge or Darcy velocity components in the x- and y-directions, respectively,
K_x, K_y	are, respectively, the principal x- and y-directional components of the hydraulic conductivity tensor,
∂x, ∂y	denote partial differentiation with respect to x and y, respectively,
P	is the pressure head at reference density,
x, y	are mutually orthogonal coordinates,
R	is a density-deficit parameter,
p	is the thermodynamic pressure,
ρ	is the mass density of fluid,
g	is the gravitational acceleration constant,
Y	is a datum for the vertical (y) coordinate,
k_x, k_y	are, respectively, the x- and y- components of the intrinsic permeability tensor,
μ	is the molecular viscosity of fluid, and
*	denotes a reference value.

The Pressure Equation. The governing equation for pressure is obtained by substituting the Equations 1 and 2 in the mass conservation equation for a compressible porous media. This equation may be written as (Runchal & Sagar, 1985):

$$S_s \partial_t P = r^{-1} \partial_x(r K_x \partial_x P) + \partial_y(K_y \partial_y P) + \partial_y(K_y R) + S_p \quad , \tag{7}$$

with:

$$S_s = \alpha + n \alpha_f \quad , \tag{8}$$

$$S_p = m_v + n \beta_f \partial_t T \quad , \tag{9}$$

$$\alpha_f = \rho^{-1} (\partial \rho/\partial P)_T \quad , \text{ and} \tag{10}$$

$$\beta_f = - \rho^{-1} (\partial \rho/\partial T)_P \quad . \tag{11}$$

In the Equations 7 through 11 above:

S_s	is the specific storativity,
t	is the time coordinate,
r	is the radius of curvature which is assumed to be coincident with the x-direction for axially symmetric problems,
Sp	is the source term for pressure.

n is the effective porosity,
α is the soil compressibility divided by specific weight of water,
α_f is the compressibility of fluid divided by its specific weight.
m_v is the volumetric injection (+) or withdrawal (-) rate per unit volume of the porous matrix,
β_f is the expansion coefficient of fluid, and
T is the temperature, and

The Temperature Equation. The temperature equation for PORFLOW is written as (Bear, 1972):

$$\partial_t (C_e T) + r^{-1} C_f \partial_x (rUT) + C_f \partial_y (VT) = r^{-1} \partial_x (rk_e \partial_x T) + \partial_y (k_e \partial_y T) + S_T \quad (12)$$

The C_e, C_f, k_e and, S_T, terms are given by:

$$C_e = n \rho c_f + (1 - n) \rho_s c_s \quad (13)$$
$$C_f = \rho c_f \quad (14)$$
$$k_e = n k_f + (1 - n) k_s \quad (15)$$
$$S_T = s_T + c_f T \partial_t (n \rho) \quad (16)$$

In the Equations 12 through 16:

C_e is the effective specific heat of the porous matrix per unit volume,
T is the temperature,
C_f is the fluid specific heat per unit volume,
k_e is the effective thermal conductivity,
S_T is the rate of heat source (+) or sink (-) per unit volume,
s_T is the rate of heat generation (+) or absorption (-) per unit volume,
c_f is the specific heat of water,
c_s is the specific heat of the solid, and
ρ_s is the density of the solid.

The Species Concentration Equation. The concentration equation for a chemical species can be written as (Freeze and Cherry, 1979):

$$\partial_t (n R_d C) + r^{-1} \partial_x (rUC) + \partial_y (VC) = r^{-1} \partial_x (rnD_x \partial_x C) + \partial_y (nD_y \partial_y C) + SC - nR_d R_C C \quad (17)$$

with:

$$R_d = 1 + (1-n) \rho_s k_d / n \quad (18)$$
$$D_x = D_M + \alpha_L u + \alpha_T v \quad (19)$$
$$D_y = D_M + \alpha_T u + \alpha_L v \quad (20)$$
$$u = U^2/(n \bar{V}) \quad (21)$$
$$v = V^2/(n \bar{V}) \quad (22)$$
$$\bar{V} = \sqrt{U^2 + V^2} \quad (23)$$

In the Equations 17 through 23 above:

R_d is the retardation factor,
C is the concentration of the species in the fluid phase,
D_x, D_y are ,respectively, the x- and y- directional components of the total molecular and hydrodynamic dispersion,
S_C is the source of the species,
R_C is the radioactive decay or chemical reaction constant,
k_d is the distribution coefficient.
D_M is the molecular diffusivity of water,
α_L is the longitudinal dispersivity,
α_T is the transverse dispersivity coefficient,
u, v are respectively, the particle velocity components in the x- and y-directions, and
$\bar{V}$ is the magnitude of the local particle velocity vector.

THE AUXILIARY RELATIONS

A number of auxiliary relations are required to solve the set of governing transport equations described above. These pertain to the specification of the fluid and host matrix properties and the source terms. The mathematical framework of PORFLOW is general enough to accommodate virtually any of the available relations for these quantities and, many options are continually being added to various versions of the PORFLOW model. Some of the built-in options are described below.

The Fluid Density. The density of most liquids is generally a much stronger function of temperature and concentration of dissolved species than that of pressure. In PORFLOW, the density changes due to pressure are ignored except in the compressibility term associated with specific storativity. The model provides three options for calculation of fluid density; these are:

$$\rho = \rho^* [(T_C - T)/(T_C - T^*)]^a \text{ ,and} \quad (24)$$
$$\rho = a + b T - c T^2 + d T^3 \quad (25)$$
$$\rho = \rho^* [1 + a (T^* - T) + b(C^* - C)] \quad (26)$$

where a, b, c and d are empirical constants, T_C is the critical temperature, and * denotes a reference value of the corresponding quantity.

The Fluid Viscosity. In general, the liquid viscosity is a much stronger function of temperature than that of pressure. The PORFLOW, provides three different options for calculation of the fluid viscosity; these are:

$$\mu = a \exp [b /(T + T_A)] \quad (27)$$
$$\mu = a + b T + c T2 + d T3 \quad (28)$$
$$\mu = \mu^* \exp[a (T^* - T) - b (T^* - T)^2] \quad (29)$$

where a, b, c, d, are empirical constants, T_A is the base temperature for conversion to absolute units, and * denotes a reference value.

The Source and Sink Terms. The source terms, m_v (Equation 9), s_T (Equation 16) and, S_C (Equation 17) may be either constant or functions of time. In the latter case. these may be either tabulated or analytic functions of time. The tabulated values of the source terms may vary arbitrarily with time. The analytic options provide for two formulations: an exponential decay with time and a solubility-limited option.

The built-in exponential decay formulation, for a source comprised of I components, is:

$$S = \sum_{i=1}^{I} s_i \exp [- f_i t] \quad (30)$$

where S is any of m_v, s_T or S_C, s_i is the strength of the i-th component of source, f_i is the characteristic time constant, t is the time

The solubility-limited option is only available for the S_C term where it is assumed that a finite inventory of the source material is initially present. This material is then dissolved by the fluid such that the maximum concentration in the fluid phase does not exceed the solubility of the

species. Specifically, the rate of dissolution of the species per unit width, m_C, is given by:

$$m_C = \int V_{in} (C_{in} - C_s) \, dN, \qquad (31)$$

where:

m_C is the mass of species dissolved by the fluid per unit width of the source zone normal to the plane of simulation,
V_{in} is the specific flux (darcy velocity) of the incoming fluid,
C_{in} is the concentration of the species in the incoming fluid,
C_s is the saturation limit of the species, and
N is the coordinate normal to the direction of flow.

The only decay term explicitly accommodated in PORFLOW is the term R_C in the Equation 17. This term represents the exponential decay of a radioactive species or chemical reaction rate through a simple Arrhenius reaction. With t* as the half life of the species, the decay rate is given by:

$$R_C = \ln(1/2)/t^* \, . \qquad (32)$$

BOUNDARY AND INITIAL CONDITIONS

Well-posed boundary and initial conditions must be specified for successful solution of the governing equations. The built-in options in PORFLOW consist of the Dirichlet, Neuman and mixed kind of boundary conditions. The initial conditions may be specified explicitly or they are taken to be zero by default.

THE NUMERICAL BASIS

The General Transport Equation. The transport Equations 7, 12 and 17, all have similar mathematical form and therefore can all be represented by a general equation of the form:

$$a \, \partial_t F + r^{-1} \partial_x (brUF - c_x r \, \partial_x F) + \partial_y (bVF - c_y \, \partial_y F) = S_F - S_m F \, , \qquad (33)$$

where F is the transported property, a, b, and c are the fluid or host media property coefficients, S_F is the source term of F and S_m is the rate constant for reaction or removal of property F.

An Outline of the Numerical Method. The PORFLOW employs a combination of the Nodal Point Integration (NPI) and the Alternating Direction Implicit (ADI) methods for transforming the governing differential equations into linearized algebraic equations. Some models of the PORFLOW series also provide for a combination of the NPI with one of the Successive-Over-Relaxation, the Strongly-Implicit-Procedure, the iterative-ADI and, the Cholesky decomposition methods. A discussion of these, including that of the ADI is given, for example, in Varga (1962) and Yanenko (1971).

The Nodal Point Integration Method. Though the NPI method bears some resemblance to the finite-element methods, it is simpler and more economical. A major advantage of this method, over the finite-difference and finite-element methods, is that it intrinsically preserves the material and energy fluxes both at local and global scales. It thus leads to more accurate formulations. The details of the NPI method are given by Runchal (1969) and Gosman et al. (1969). For integration by NPI, the field of interest is divided into a number of contiguous elements each of which acts like an individual control volume (Figure 1). A nodal point is associated with each of these volumes or elements. The governing differential equation is then integrated individually for each control volume.

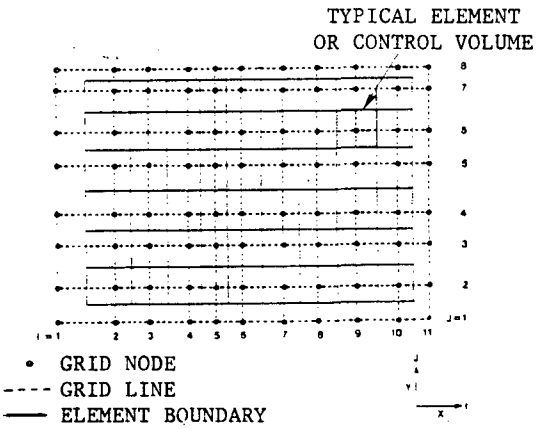

FIGURE 1. GRID AND CONTROL VOLUME ARRANGEMENT.

The PORFLOW series of programs employ a sophisticated numerical approach for spatial integration to ensure unconditional (linear) stability. The spatial variation of state variables, P, T and C, is approximated by appropriate profiles to ensure accuracy and stability. The governing transport equation (Equation 33) consists of four types of terms: the accumulation terms, the convective terms, the diffusive terms and the source terms. The NPI treats the convective and diffusive terms in a unified manner; the other terms are treated individually. The manner of integration of these terms is explained below.

Consider the x-directional convective and diffusive flux terms appearing in Equation 33. The integral of these terms over the volume of a single element shown in Figure 2, $r \, \delta x \, \delta y$, is given by:

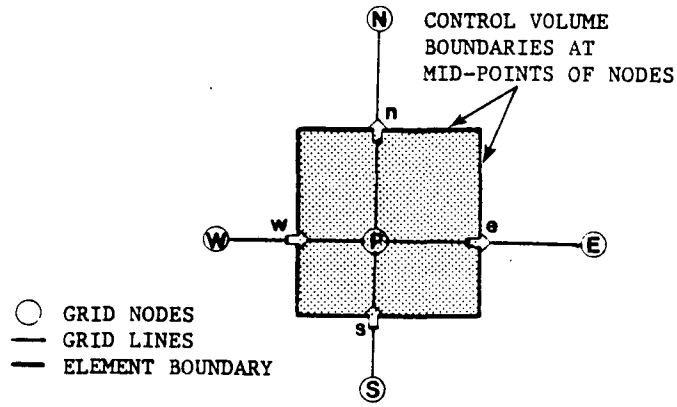

FIGURE 2. A TYPICAL INTEGRATION CONTROL VOLUME.

$$I = \int_y \int_x r^{-1} \partial_x(rbUF - rc_x \partial_x F)\, r\, dxdy, \quad (34)$$

Integrating once:

$$I = I_e - I_w , \quad (35)$$
$$I_e = \int_y [(rbUF - rc_x \partial_x F)_e]\, dy , \quad (36)$$
$$I_w = \int_y [(rbUF - rc_x \partial_x F)_w]\, dy , \quad (37)$$

where the subscripts 'e' and 'w' denote, respectively, the average values for the 'e' and 'w' faces of the element shown in Figure 2. The integrand of I_e may be written as:

$$r\, b\, U\, F - r\, c_x\, \partial_x F = r\, f(x,y,t) , \quad (38)$$

where f is a so-far undetermined function of x, y and t. An exact solution to this equation is:

$$F = (1/A)\ (\int A\, B\, dx + C\ ), \quad (39)$$
$$A = \exp \int(-D)\, dx , \quad (40)$$
$$B = f / c_x , \text{ and} \quad (41)$$
$$D = bU / c_x . \quad (42)$$

If it is assumed that, in the interval between $x=x_P$ and $x=x_E$, the U, c_x, f and D can all be replaced by some representative values, u*, c*, f* and D*, then Equations 39 through 42 yield:

$$F = - f^*/bU^* + C \exp(D^* x). \quad (43)$$

The two 'constants', f* and C, are obtained by recourse to the values of the variable F at the two nodes P and E. With reference to Equation 43:

$$F_P = - f^*/bU^* + C \exp(D^* x_P), \text{ and} \quad (44)$$
$$F_E = - f^*/bU^* + C \exp(D^* x_E). \quad (45)$$

Rearrangement then yields:

$$C = \delta F \exp(-D^* x_P) / (\exp P^* - 1), \quad (46)$$
$$\delta F = F_E - F_P , \text{ and} \quad (47)$$
$$P^* = D^* (x_E - x_P) , \quad (48)$$

where P* is a Peclet number based on grid interval. Substitution of Equation 46 in 45 then leads to:

$$f^* = bU^* [\delta F / (\exp P^* - 1) - F_P] . \quad (49)$$

The variation of the dependent variable F, between the nodes P and E is now obtained from Equations 43, 46 and 48 as:

$$F = F_P + \delta F[\exp(D^*(x-x_P)) - 1]/(\exp P^* - 1). \quad (50)$$

The integral I_e can now be evaluated from the known distribution of F and the further assumption that within the domain of integration the average values of all quantities at the element face 'e' are represented by their respective values at $y=y_e$. It is seen that if y_e is located at the middle of the range of integration in the y-direction, then this leads to a second-order approximation. The integral in Equation 36 is now given by:

$$I_e = r_e bU^* [\delta F/(\exp P^* - 1) - F_P]\, \delta y . \quad (51)$$

The integrals for the other convective and diffusive terms are obtained in a similar manner.

The Accumulation Term. The accumulation term is integrated by assuming that the values of the variables for whole of the element are represented by the nodal values. The integral of the accumulation term of Equation 33 is thus written as:

$$I_{acc} = \int_t \int_V a(\ _tF)\, dV\, dt ,$$
$$= a_P (F_P^n - F_P^o)\, \delta V_P , \quad (52)$$

where the superscripts n and o denote, respectively, the "new" and "old" values.

The Source Terms. The integral of the source terms is given by:

$$I_{sor} = \int_t \int_V (S_F - S_m F)\, dV\, dt ,$$
$$= (S_F - S_m F)_P\ \delta V\, \delta t . \quad (53)$$

The Algebraic Analogue of the Differential Equation. An algebraic analogue of the general transport equation (Equation 33) can now be written in terms of the nodal values. With reference to Figure 2, this analogue is:

$$C_P (F_P^n - F_P^o) + \sum_{K=E,W,N,S} A_K (F_P - F_K) + \delta V\, S_{m,P} F_P^n = \delta V S_{F,P}, \quad (54)$$

where the subscripts P and K denote, respectively, the representative values for the grid cell P (in Figure 2) and any of the values for the four neighboring grid cells (E,W,N, and S). Some further details concerning the coefficients of this analogue are given by Runchal and Sagar (1985).

Polynomial Approximation. The exponential profile (Equation 43) forms the cornerstone of the PORFLOW discretization. However, the computation of exponentials can be expensive. The PORFLOW therefore provides alternative methods to evaluate the integrals. The exponential term of Equation 49 can be expanded in power series to obtain:

$$f^* = bU^* [\delta F/(P^* + P^{*2}/2 + \ldots) - F_P] , \quad (55)$$

If only the first term in the denominator is retained, then from Equations 48 and 55:

$$f^*_1 = c^*\ \delta F/(x_E - x_P) - b\, U^*\, F_P , \quad (56)$$

where f^*_1 is a first-order approximation to f*. It can be shown that, in the above expression, the diffusion terms are still being approximated in a second-order manner. A second order approximation is obtained as:

$$f^*_2 = c^*\ \delta F/(x_E - x_P) - b\, U^*\, (F_E + F_P)/2 . \quad (57)$$

Equation 56 and 57 are also obtained from first and second degree polynomial assumptions for variation of F. These, respectively, correspond to the more familiar 'upwind' and 'central-difference' discretization approaches (Roache, 1972).

The PORFLOW provides for all three, the exponential, the first order, and the second order, approximations. The second order approximation, however, may lead to numerical instabilities if the value of P*, the local Peclet number, exceeds 2 (Roach, 1972). In PORFLOW, therefore, the P* is

constantly monitored and if its value exceeds 2, then an automatic shift to the 'upwind' formulation is made. This method of enhancing stability is known as the hybrid scheme (Runchal, 1972). For computational economy, the PORFLOW provides an option to approximate the exponential term in the range between 0.1 and 10 by the formulae:

$$EXP(-P^*)=1-P^*/(1+0.1661P^*)^3;\ 0.1<P^*<1, \quad (58)$$

$$EXP(-P^*)=1-1/[1+3.60344/(1+0.44P^*)^5];\ 1<P^*<10. \quad (59)$$

APPLICATIONS

The PORFLOW model, or its versions, have been extensively used for a large number of problems; a list of some of these problems, along with the references which provide the details of the applications, are given in Runchal (1985). Two of the applications related to high level nuclear waste disposal are described below.

Heat Transfer from A Waste Canister. This test case concerns heat transfer in the vicinity of a buried spent-fuel canister. A number of canisters are buried at a uniform pitch in holes drilled from the floor of a series of uniformly spaced excavations (drifts) in a geologic formation. The geometry of a typical canister emplacement is illustrated in Figure 3. Due to symmetry, only one-half of a canister was considered. The heat capacity of the host rock was taken as 2.17 MJ/m^3K and the thermal conductivity as 1.80 W/mK. The initial rock temperature was 26 °C and the heat release rate from the waste canister was defined by a three component exponential decay of the form given by Equation 30; the s_i and f_i of this equation are given in Table 1. Further details of this application are given by St. John (1985).

TABLE 1. CONSTANTS FOR EXPONENTIAL HEAT DECAY

COMPONENT, i	si (kW/cubic m)	fi (1/year)
1	1.28210	2.626E-2
2	0.33796	2.068E-3
3	0.04067	5.222E-5

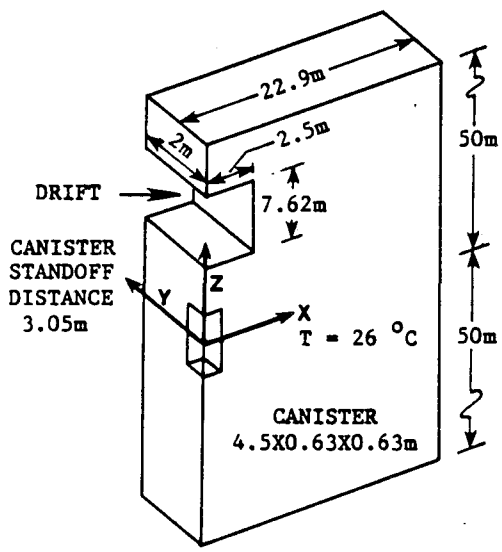

FIGURE 3. THE SCHEMATIC OF BURIED WASTE CANISTER.

The PORFLOW was used to obtain temperature distribution in the x-z plane (Figure 3. Due to the narrow canister spacing, the temperature variation in the y-direction was assumed to be negligible. This introduces some errors in the immediate vicinity of the canister; however a few canister diameters away, this approximation is expected to be adequate. The temperature distribution was obtained for two scenarios. In the first, the drifts were assumed to be ventilated at a constant temperature of 30 °C. In the second, the drifts were unventilated; in this case the effects of natural convection were ignored but those of radiation were accounted for by enhanced diffusivity for the room air. These results were compared with those obtained from an analytical model, TEMP3D, and a three-dimensional numerical model, THERM3D (St. John, 1985). The TEMP3D is based on the analytic solutions for constant or exponentially decaying point sources in an infinite region. The THERM3D is a finite difference heat transfer model. The numerical results for the ventilated and the unventilated drift are compared with the analytic results in Figure 4.

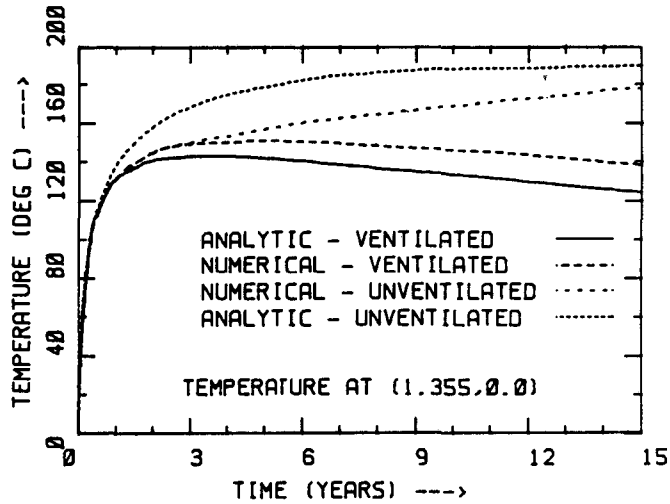

FIGURE 4. COMPARISON OF THE NUMERICAL AND ANALYTIC RESULTS FOR THE BURIED WASTE CANISTER PROBLEM.

The numerical results lie within the bounds predicted by the analytical model. In the analytic model, the ventilated drift was approximated by a fixed temperature boundary at the floor of the drift within a semi-infinite region. Since most of the heat transfer occurs at this boundary, these results are a good approximation to the ventilated drift. The unventilated drift was treated as an infinite region where the thermal properties of the drift were the same as those of the host rock. Given the approximations inherent in the analytical solution and in the numerical method, the two sets of results are in good agreement with each other.

The PORFLOW results were also compared with those obtained from the three-dimensional model THERM3D. The canister centerline temperature and the heat loss to the ventilation air for the two models are compared in Tables 2 and 3. For the results shown in Table 2, the THERM3D was employed in a two-dimensional mode with the heat source uniformly distributed in the y-direction.

TABLE 2. PORFLOW AND THERM3D RESULTS FOR CANISTER CENTERLINE TEMPERATURE.

Time (years)	Temperature (oC)	
	THERM3D	PORFLOW
0.10	94.0	93.7
0.20	114.2	113.9
0.30	126.5	126.0
0.40	135.1	134.4
0.50	141.7	140.7

TABLE 3. PORFLOW AND THERM3D RESULTS FOR HEAT LOSS TO VENTILATION AIR.

Time (years)	Heat Loss (W/m of drift)	
	THERM3D	PORFLOW
0.10	-3.1	-45.9
0.20	11.2	13.3
0.30	51.5	55.4
0.50	107.5	115.8
1.00	184.0	196.7
2.00	253.1	266.0
5.00	330.4	328.7

The two sets of results in Tables 2 and 3 are in good agreement with each other. It is of special interest to note that the heat loss to the ventilation air in the drift calculated by the two-dimensional PORFLOW model is very close to that calculated by the three-dimensional THERM3D model. This shows that the temperature distribution has acquired a dominantly two-dimensional nature at the floor level of the drift.

Hypothetical Nuclear Waste Repository

The stratigraphy and the geometrical arrangement for this problem is illustrated in Figure 5. The hypothetical repository is assumed to be located in a crystalline rock which is overlain by sedimentary deposits. A relatively less permeable rock formation is located to the east and downstream of the proposed repository horizon. The hydrothermal properties of the three formations and the thermal loading history for the repository are summarized in Tables 4 and 5, respectively. The radionuclide release is assumed to be constant at a rate of 0.01kg/year-/m^3 for the first 500 years and zero thereafter. The mass diffusivity is taken to be 1.E-5 m^2/year.

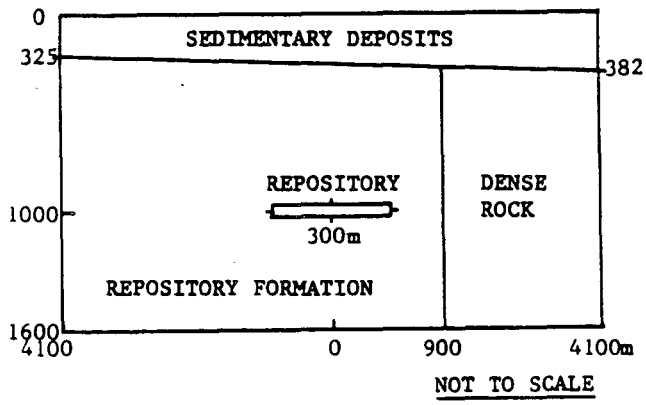

FIGURE 5. SCHEMATIC OF THE STRATIGRAPHY AND REPOSITORY LOCATION.

TABLE 4. PROPERTIES OF GEOLOGIC FORMATIONS.

Member Property	Sedimentary Formation	Dense rock Formation	Repository Formation
Hydraulic conductivity (m/yr)	7.8868E+2	1.5774E-2	3.1547E-1
Thermal conductivity (J/m yr oC)	1.1290E+8	6.7911E+7	8.5231E+7
Specific Heat (J/kg/m3)	665.28	749.40	957.55
Distribution Coefficient	1.1111E-3	1.2758E-3	0.00
Porosity	0.40	0.03	0.001
Density (kg/m3)	2400	2400	2400

TABLE 5. HEAT RELEASE RATE FOR THE REPOSITORY.

Time (years)	Source strength (J/year/m3)
0.0	5.0E+7
10.0	4.5E+7
50.0	2.0E+7
100.0	1.0E+7
490.0	1.0E+6
1,000.0	1.0E+5
50,000.0	1.0E+4

The density and viscosity changes for water were calculated according to the Equations 24 and 27, respectively. The hydrologic conditions consisted of an impermeable top and bottom, and a regional flow from left to right with a pressure gradient of 0.673 meters per kilometer. The thermal boundary conditions consisted of a constant temperature of 0 °C at top, and a vertical temperature gradient of 14.6 °C per kilometer. The initial conditions for pressure (flow) and temperature were calculated from these specified gradients. The temperature at all four boundaries was assumed to be constant over the time period of simulations. The initial values of the radionuclide concentration were assumed to be zero everywhere. The boundary conditions were also assumed to be zero except at the downstream boundary where a condition of zero normal gradient was imposed.

Typical velocity patterns and flow paths, as shown by the stream lines, in the vicinity of the repository are shown in Figures 6 and 7. These indicate a net upwards flow in the immediate vicinity of the repository and a near horizontal flow in the upper sedimentary formation. The relatively impermeable formation downstream of the repository, in combination with the net upwards buoyancy due to the heat release, causes the flow in the repository horizon to be deflected upwards. However, the net upward flux, as seen from the streamline contours, is small in comparison to the stronger horizontal flow in the upper sedimentary formation. A small downward deflection of the flow upstream of the repository and an upward deflection downstream of the repository is also evident from these figures. All these results are in accord with intuitive and physical understanding of the flow under these circumstances.

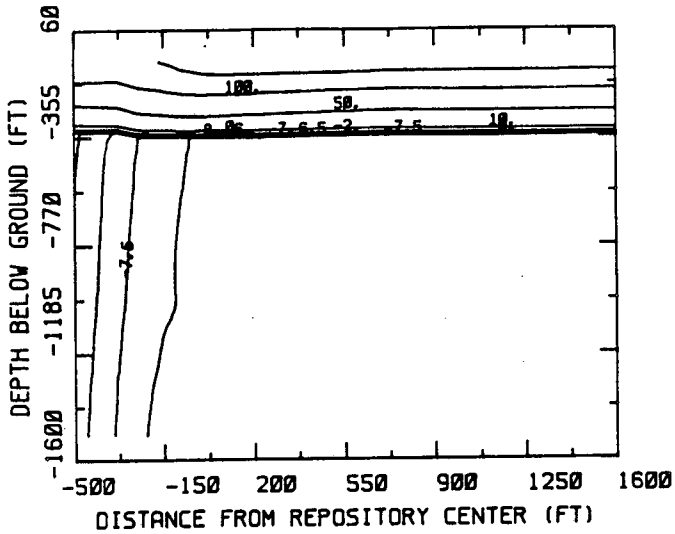

FIGURE 6. STREAM LINE PATTERN AFTER 250 YEARS.

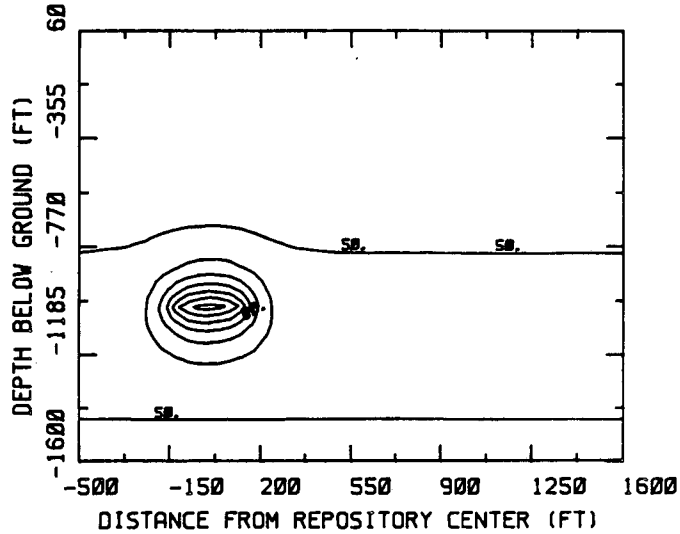

FIGURE 8. TEMPERATURE CONTOURS AFTER 250 YEARS.

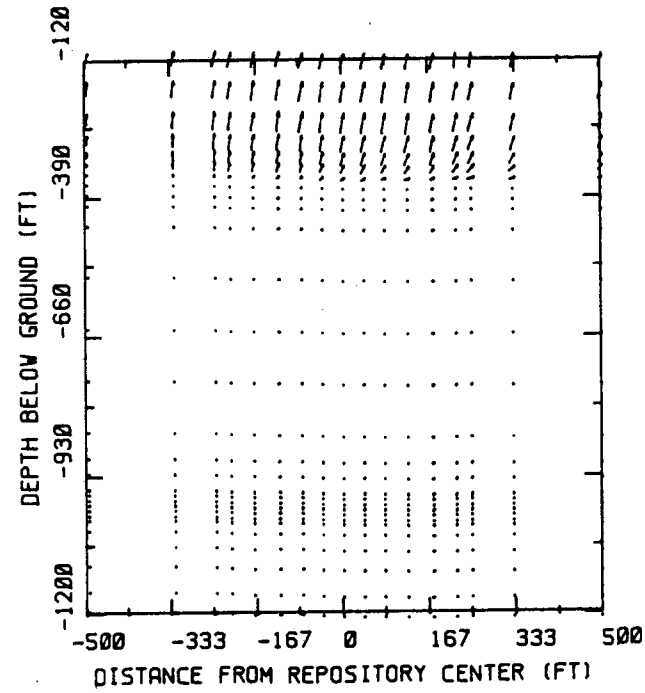

FIGURE 7. VELOCITY VECTORS AFTER 250 YEARS.

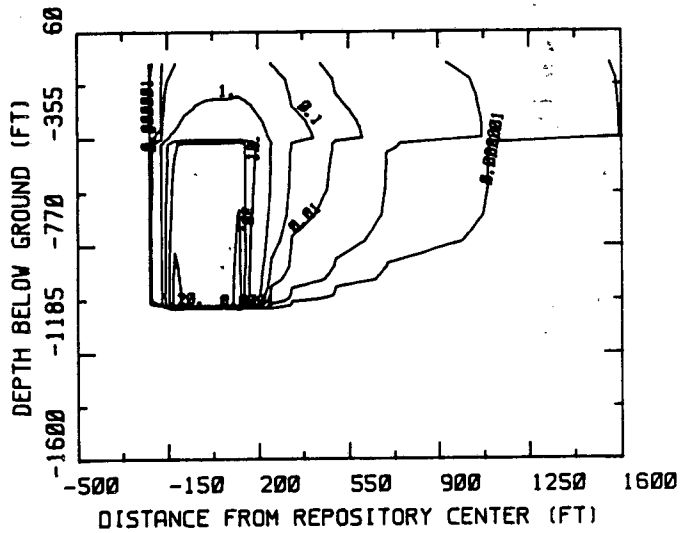

FIGURE 9. CONCENTRATION CONTOURS AFTER 250 YEARS.

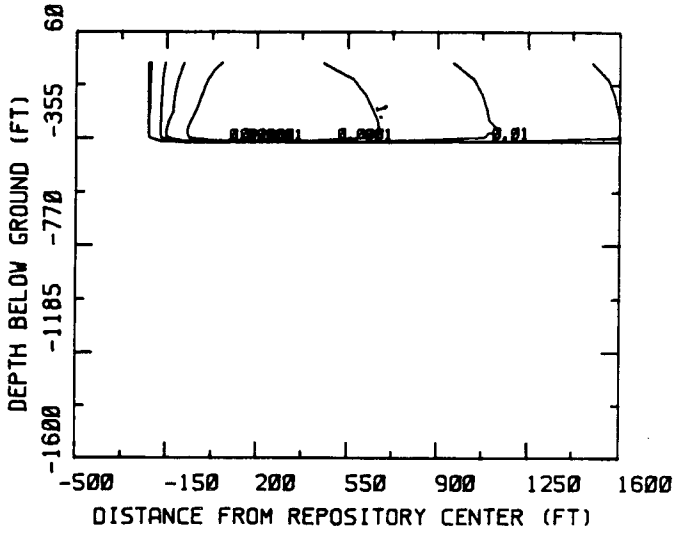

FIGURE 10. CONCENTRATION CONTOURS AFTER 1,000 YRS.

The predicted temperature distribution after 250 years, and the radionuclide concentration 250 and 1,000 years after emplacment of nuclear waste are shown in Figures 8 through 10. The temperature distribution is dominated by conduction. This is expected since the fluid flux in the relatively low permeability host rock is small. The radionuclide transport, in contrast, is governed by fluid particle velocity rather than the fluid flux which is high due to the low porosity of the host rock. In 1,000 year, the nuclide cloud has travelled to the highly permeable sedimentary formation and its center is located a few hundred meters downstream of the repository. The maximum concentration at 1,000 years in this cloud is over three orders of magnitude lower than that at 250 years.

CONCLUSIONS

1. The coupled processes which govern the flow, heat and nuclide transport in geologic media of practical interest can be adequately modelled by the use of numerical techniques.

2. The PORFLOW results for heat transfer from a buried waste canister compare well with those from an analytic method and another numerical model.

3. The PORFLOW model is shown to be applicable to the prediction of coupled processes which govern the transport of radionuclides from a geologic repository.

ACKNOWLEDGEMENT

A part of this work, dealing with buried waste canister was funded by Sandia National Laboratories (SNL), Contract No. 52-3876. Dr. A.J. Mansure of SNL was project Technical Monitor. The analytic solutions for this problem were obtained at Agbabian Associates, El Segundo, CA, under the same contract with Dr. Christopher St. John as the Principal Investigator.

REFERENCES

1. Bear, J. (1972). Dynamics of Fluids in Porous Media, American Elsevier, New York.

2. Eyler, L.L. and M.J. Budden (1984). "Verification and Benchmarking of PORFLO: An Equivalent Porous Continuum Code for Repository Scale Analysis," Report No. PNL-5044, UC-70, Battelle Pacific Northwest Laboratory, Richland, WA 99352.

3. Freeze, R.A., and J.A. Cherry (1979). Groundwater, Prentice-Hall, Englewood Cliffs, New Jersey.

4. Fujioka, M.R. and A.K. Runchal (1982). "Cooling Water Supply Disposal in Coastal Aquifer," ASCE, J. Energy Engg., Vol. 109, No. 2, June 1982, pp.88-102.

5. Gosman, A., W. Pun, A.K. Runchal, D.B. Spalding and M. Wolfshtein (1969). Heat and Mass Transfer in Recirculating Flows, Academic Press, London.

6. Kline, N.W., A.K. Runchal and R.G. Baca (1975). "PORFLO Computer Code: Users Guide," RHO-BW-CR-138P, Rockwell Hanford Operations, Richland, WA. 99352.

7. Roache, P.J. (1972). Computational Fluid Dynamics, Hermosa Publishers, Albuquerque, New Mexico.

8. Runchal, A.K. (1969). Transfer Processes in Steady Two-Dimensional Separated Flows, Ph.D. Thesis, London University, U.K.

9. Runchal, A.K. (1972). "Convergence and accuracy of three finite Difference Schemes for a Two-Dimensional Conduction and Convection Problem," Int. J.Num. Methods Eng., 4, p. 541-550.

10. Runchal, A.K. (1985). "PORFLOW: A General Purpose Model for Fluid Flow, Heat Transfer and Mass Transport in Anisotropic, Inhomogeneous, Equivalent Porous Media," Technical Note TN-011, Analytic & Computational Research, Inc., Los Angeles, CA 90066.

11. Runchal, A.K., P. Bardey and R.G. Baca (1981). "An Equivalent Continuum Model for Flow and Transport in a Basalt Medium: Model Theory and Verification," ACRI Job 007-01.

12. Runchal, A.K. and G. Hocking (1981). "An Equivalent Continuum Model for Fluid Flow, Heat and Mass Transport in Geological Materials," Paper 81-HT-54, ASME, 20th Joint ASME/AIChE National Heat Transfer Conference, Milwaukee, Wisconsin, Aug. 2-5.

13. Runchal, A.K. and B. Sagar (1985). "PORFLO - A Continuum Model for Fluid Flow, Heat Transfer and Mass Transport in Porous Media: Model Theory and Benchmarking," RHO-BW-CR-150, Rockwell Hanford Operations, Basalt Waste Isolation Project, Richland, WA 99352.

14. Runchal, A.K., B. Sagar, J. Treger, R.G. Baca and R.C. Arnett (1980). "Theoretical Analysis of Waste Isolation in a Basalt Media: An Evaluation of Postulated Release Scenarios," Rockwell Hanford Operations, Basalt Waste Isolation Project, Richland, WA 99352.

15. Runchal, A.K., J. Treger, and G. Segal (1979). "Two-Dimensional Fluid Flow, Heat, and Mass Transport in Porous Media," Dames and Moore, Advanced Technology Group, Technical Note, TN-LA-3.

16. St. John, C. (1985). "Thermal Analysis of BWR - Spent Fuel Vertical Emplacement Scheme," Sandia National Laboratory, R-8327-5913, SAND 84-7207.

17. Varga, R.S. (1962). Matrix Iterative Analysis, Prentice-Hall, Englewood Cliffs, New Jersey.

18. Yanenko, N.N. (1971). The Method of Fractional Steps, Springer-Verlag, New York

ANALYSIS OF COLLOID TRANSPORT

B. J. Travis* and H. E. Nuttall**

*Earth and Space Sciences Division
Los Alamos National Laboratory
Los Alamos, New Mexico 87545
**Nuttall and Assoc., Inc.
1445 Honeysuckle, Dr., NE
Albuquerque, NM 87122

ABSTRACT

The population balance methodology is described and applied to the transport and capture of polydispersed colloids in packed columns. The transient model includes particle growth, capture, convective transport, and dispersion. We also follow the dynamic accumulation of captured colloids on the solids. The multidimensional parabolic partial differential equation was solved by a recently enhanced method of characteristics technique. This computational technique minimized numerical dispersion and is computationally very fast. The FORTRAN 77 code ran on a VAX-780 in less than a minute and also runs on an IBM-AT using the Professional FORTRAN compiler. The code was extensively tested against various simplified cases and against analytical models.

The packed column experiments by Saltelli et al. were re-analyzed incorporating the experimentally reported size distribution of the colloid feed material. Colloid capture was modeled using a linear size dependent filtration function. The effects of a colloid size dependent filtration factor and various initial colloid size distributions on colloid migration and capture were investigated. Also, we followed the changing colloid size distribution as a function of position in the column.

Some simple arguments are made to assess the likelihood of colloid migration at a potential NTS Yucca Mountain waste disposal site.

INTRODUCTION

To date both laboratory (Saltelli et al. 1984; Freid et al. 1976) and site studies (Champ et al. 1982; Travis and Nuttall 1985) have demonstrated the existence and in some cases the accelerated transport of colloids. Nuttall, Hart, and Travis (1985) developed a theory for colloid transport using the population balance concept. Travis and Nuttall (1985) applied the population balance theory and the TRACR3D computer code to study the hydrology and transport of radiocolloids at a Los Alamos waste disposal site. Saltelli et al. (1984) derived and tested a one-dimensional filtration model and applied it to transient column profile data obtained by injecting ^{241}Am contaminated waste-glass colloids into a 26 mm by 180 mm sand packed column. They measured the size distribution of feed colloids and attempted to model the effects of the polydispersed colloids on the capture profile by assuming a distribution for the filtration factor. This approach did not yield a fundamental understanding of the effect of colloid size, but they did show that one must consider the size distribution in treating the experimental data.

In the following analysis of colloid transport, we used the multidimensional form of the population balance equation to analyze directly the effects of polydispersed colloids. The theory is developed for the transport of polydispersed colloids through a one-dimensional porous region. Conversion from a weight distribution to the corresponding number density function and back to a weight distribution after solution of the population balance equation is treated. We used the model to investigate the effect of two size distributions and to compare the effect of a constant versus size dependent filtration type colloid capture model.

THEORY

Randolph (1962) derived the general form of the population balance model in 1962. The population balance theory was derived at about the same time by Hulburt and Katz (1964). The population balance is a number continuity equation which has been applied successfully to crystallization, aerosols, and biological processes. Recently Travis and Nuttall (1985) applied this methodology to the problem of colloid transport. In this study, we apply the dynamic microscopic form of the population balance model with convective transport in one spatial dimension and particle growth along a colloid size axis to the problem of radiocolloid transport in nuclear waste disposal.

The colloid population density function, $P(t,z,L)$, is dependent on time, space and the colloid characteristic size which we assume to be the colloid diameter. $P(t,z,L)$ is the number of colloids of a particular size L at a point z in space and time t per unit volume of solution. When P is integrated over the colloid size range we have the total number of colloids per unit volume. In general, colloid charge or any other useful colloidal properties could be modeled by simply adding the appropriate property axes. The population balance also includes a birth/death term $f(P,t,z,L)$ which again accounts for the birth of new colloids as well as the adsorption and release of colloids by the rock matrix. The adsorption and release function treats colloids of arbitrary size. In this study we do not treat the adsorption of radionuclides on the colloids nor are we investigating the growth of colloids. To model colloids of the same size but with differing amounts of radionuclides would require an additional property axis for concentration.

Under these assumptions the population balance is:

$$\frac{\partial P}{\partial t} + v\frac{\partial P}{\partial z} - D\frac{\partial P^2}{\partial z^2} + u\frac{\partial P}{\partial L} = -f \qquad (1)$$

The filtration term is

$$f = \lambda(L)\, v\, P(t,z,L) \quad . \qquad (2)$$

It is sometimes desirable to work with a dimensionless form of the population balance. Carrying out the transformation of Eq. (1) using the dimensionless variables defined in the notation section leads to:

$$\frac{\partial \psi}{\partial \tau} + \phi\frac{\partial \psi}{\partial \beta} - \frac{D}{\bar{z}\,\bar{v}}\frac{\partial^2 \psi}{\partial \beta^2} + \upsilon\frac{\partial \psi}{\partial \rho} = \frac{\bar{z}}{P_i \bar{v}}\, f(\phi,\tau,\beta,\rho) \qquad (3)$$

Adsorption of colloids onto the surrounding matrix is assumed to follow the filtration model where the rate of mass accumulation is proportional to the concentration of colloids in the solution. In our model the colloids concentration in solution must be expressed in terms of the population distribution function. The mass concentration c(t,z) of colloids in the fluid is

$$c = \int_0^\infty c(L)dL \qquad (4)$$

where

$$c(L) = \rho\, K_v\, P(t,z,L)\, L^3 \quad , \qquad (5)$$

and K_v = volumetric shape factor, $\pi/6$ for a sphere.

The rate of mass build up on the matrix at a point in space for each colloid size is

$$\frac{d\sigma_i}{dt} = \varepsilon\, \lambda(L)\, v\, c(L) \qquad (6)$$

The total rate of mass accumulation for all colloid sizes is equal to the integral of Eq. (6) over the colloid size range.

$$\frac{d\sigma}{dt} = \varepsilon\, \rho\, v\, k_v \int_0^{L_m} \lambda(L)\, P(t,z,L)\, L^3\, dL \qquad (7)$$

In the general case $\lambda(L)$ will be some function of colloid size. However, if $\lambda(L)$ is size independent then the filtration follows the conventional form showing a straight line profile for the concentration of colloids captured on the sand packing when plotted on semilog paper.

To treat experimental data, it is often necessary to convert between weight distributions and number distributions. In terms of the number density function the distributed weight function is (Randolph and Larson 1971):

$$w(L) = \rho K_v L^3 P(L)/M_T \qquad (8)$$

The population balance, Eq. 3, was solved numerically by an improved method of characteristics technique presented by Douglas and Russell (1982). The buildup of colloids on the porous matrix is described by Eq. 7 which was coupled to the population balance and solved as a series of ODEs using the 4th order Runge-Kutta method. Note that σ is a function of column position, z, and time.

In our studies we tested both a gamma and a log-normal distribution to model the initial weight distribution of radiocolloids. The log-normal distribution gave a better fit to the measured feed distribution. The cumulative and distributed forms for the log-normal distribution are respectively: (Randolph and Larson 1971, p. 32)

$$W(L) = 0.5 + 0.5\, \mathrm{erf}(z) \qquad (9)$$

$$z = [\ln(L/\bar{L}')]/2^{1/2} \ln \sigma'$$

where $\bar{L}'$ = geometric mean size, μm; σ' = width parameter, (geometric STD), μm and the distributed form of the log-normal function is

$$w(L) = \frac{1}{(2\pi)^{1/2} \ln \sigma'} \exp\left[\frac{-\ln^2(L/\bar{L}')}{2\ln^2 \sigma'}\right] \qquad (10)$$

CASE STUDIES

Packed Column Simulations

Saltelli, et at. (1984) investigated the migration of polydispersed ^{241}Am colloids through a packed column of glauconitic sand. Colloidal ^{241}Am, leached from a simulated waste glass, was injected into a column. Three experiments of 28, 80, and 170 day duration were run. At the end of each test the column was dismantled, sectioned, and the ^{241}Am profile analyzed. Those authors analyzed their data using the filtration capture model and found that the column profiles could not be matched using the conventional constant parameter filtration model. To fit the profile curves they assumed that the colloid feed exhibited a distribution of filtration coefficients. In this way they hoped to approximate size dependent filtration and by adjusting the filtration distribution parameters they did fit the shape profile curves. Their model also included a Langmuir isotherm model to treat the observed early adsorption of ^{241}Am which occurred throughout the length of the column. This rapid adsorption of ^{241}Am on the porous matrix was at a very low concentration level and the mechanism for this phenomenon has not been directly investigated; therefore, we did not choose to include this mechanism in our model. To match the experimental data we simply assumed an initial adsorbed ^{241}Am concentration of 10^{-10} moles/liter.

The size distribution of the colloid feed was measured by filtration and represented in our analysis by a log-normal distribution. The measured ^{241}Am colloid distribution along with our curve-fitted distributed and cumulative log-normal distributions are illustrated in Fig. 1. The measured range of the feed colloids was from approximately .05 μm to a maximum of 10 μm. Our

curve-fit parameters for the log-normal distribution were $\bar{L}$ = 0.45 μm and σ = 7.39 μm.

The upper colloid size was experimentally controlled by passing the feed solution through a 10 μm filter prior to entering the column. The experimental conditions are give in Table I.

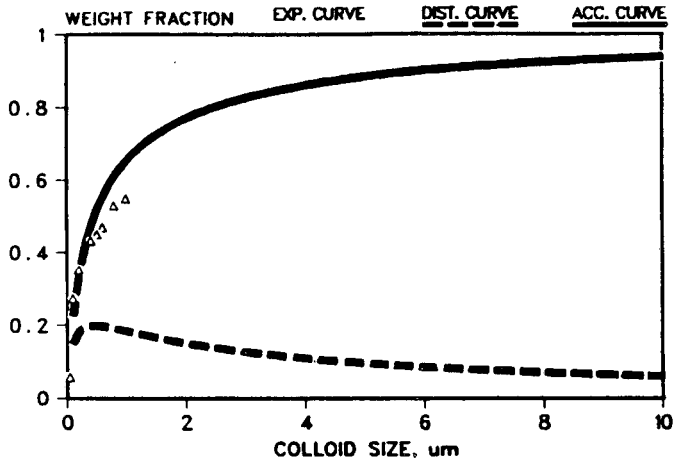

Figure 1. Colloid feed size distribution.

TABLE I - Experimental Parameters

Column Dimensions:	18 cm X 2.6 cm
Porosity:	0.38
Dispersion Coefficient:	62.6 cm^2/d
Darcy Velocity:	20.9 cm/d
Inlet Concentration:	3.8×10^{-10} M
Exit Concentration:	$3.5\text{-}6.5 \times 10^{-13}$ M
Feed Concentration Correction at 170 d:	0.242
Column Packing:	Sand with 20% clay

We solved the population balance model for the above conditions and used the log-normal distribution to represent the colloid feed. We also found that a size dependent λ was required. In our analysis, however, λ represents the actual capture mechanism whereas in Saltelli et al. (1984), λ represented capture mechanism and size distribution effects together. The resulting concentration profile for ^{241}Am on the porous matrix is compared with the experimentally measured profile after 170 days of continuous column operation and shown in Fig. 2 . The strong curvature in the calculated profile is created by the linear size dependent filtration function, $\lambda = 2_{-}L_{10}$ The asymptotic level of concentration at 10^{-10} shown on the far right of the curve was modeled by arbitrarily setting this level of concentration as an initial condition in the column. The mechanism for this early low level of concentration is still speculative and can be modelled in several ways; however, the true physical mechanism has not been identified.

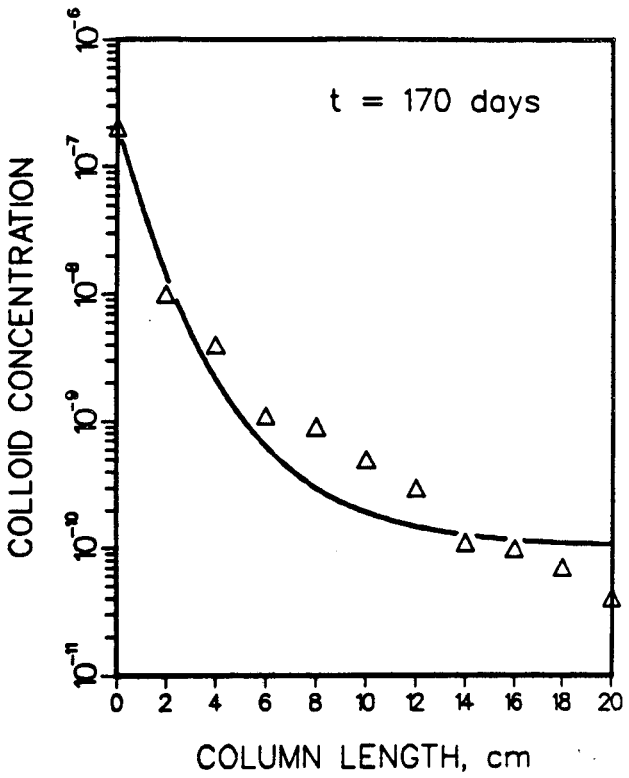

Figure 2. Measured and calculated solid concentration profile for ^{241}Am. (concentration, moles/liter of column.)

The numerical solution of the population balance also provides some interesting information on the change in the fluid phase colloid size distribution as a function of position down the vertical column. Fig. 3 illustrates in three dimensions the position varying colloid weight distribution in the liquid. The surface shows both the rapid decrease in the mass of colloids in solution and the shift in the mode of the distribution to small sizes. Because of the size dependent filtration coefficient the larger colloids are preferentially removed early at the top of the column leaving the smaller particles to transport downward through the porous medium. In the case of a constant filtration factor, λ, the nature of the colloid size distribution has no effect on the solid concentration profile since then each particle has the same capture probability independent of size.

The calculated ^{241}Am concentration profile in Fig. 2 follows the trend of the experimental data but does not agree equally well at every point. A major cause of this is the uncertainty in the true form of the filtration function λ(L). An alternative approach to analyzing this experiment is to consider it an inverse problem for λ(L). That is, instead of estimating λ(L) and then calculating colloid transport, we could solve Eqs. (1) and (7) directly for λ(L). That is, we could solve the minimization problem

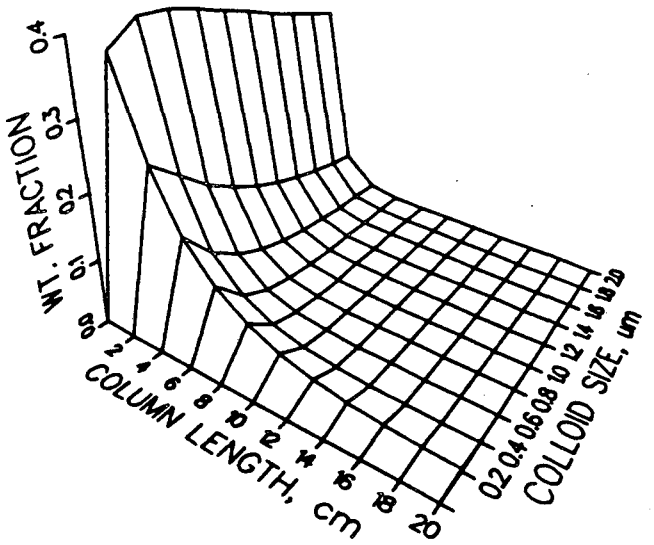

Figure 3. Liquid phase colloid weight distribution versus position along column.

$$\min \sum_i \sum_j (\sigma_o(t_i,z_j) - \sigma_m(t_i,z_j))^2 \qquad (11)$$

subject to

$$\frac{d\sigma_m}{dt} = \varepsilon \rho v K_v \int_0^{L_m} \lambda(L)\, P(t,z,L)\, L^3\, dL \qquad (12)$$

and

$$\frac{\partial P}{\partial t} + v\frac{\partial P}{\partial z} - D\frac{\partial^2 P}{\partial z^2} = -v\,\lambda(L)\,P, \qquad (13)$$

$$P(t,o,L) = g(L),\ P(o,z,L) = 0 \qquad (14)$$

where $\sigma_o(t_i,z_j)$ is the observed mass accumulation at time t_i and location z_j and σ_m is the calculated value. The solution can be obtained by nonlinear optimization techniques, such as the adjoint method. The solution will be the most likely form for $\lambda(L)$. We plan in fact to solve the equation set (11) to (14) in the near future. This analysis points out a problem frequently encountered--incomplete data. In this case, a set of experiments, each using a different but uniform colloid size, would allow independent determination of $\lambda(L)$.

NTS YUCCA MOUNTAIN SITE

Colloids may originate in a waste repository from several sources: by the corrosion of waste glass and canisters, by degradation of the engineered backfills, and by erosion from naturally occurring clays. Hence, there is a reasonable likelihood that colloids will exist; however, the important consideration is whether the geological medium is conducive to colloid transport or whether colloid migration and capture will retard their transport. Colloid transport depends on at least four factors: filtration, pH of the solution, water velocity, and diffusion.

At Yucca Mountain filtration will be an effective barrier in the tuff matrix. Pore size is an important element in filtration. Pseudocolloids will obviously not flow through pores that are smaller than the pseudocolloids themselves. Pore size distributions have been measured for several Yucca Mountain tuff samples. Mercury porosimetry data, measured by Quantachrome Co., on a sample of Topopah Spring tuff showed that most of the pores are less than 1 μm and approximately 50% are smaller than 0.1 μm. Even though a small percentage of pores are larger than 1.0 μm these large pores will not transport colloids because they will be dry. In the Topopah Spring formation at NTS, the saturation is less than 90% and large pores are the last to become saturated. In another NTS site formation, Calico Hills, approximately 50% of the pores are smaller than 0.06 μm. Hence colloids must be on the order of 0.1 μm in diameter or less to pass through the NTS tuff.

Pore water velocities, assuming matrix flow, are estimated at less than 2.0 cm/yr. These low velocities are on the order of molecular diffusion rates thus greatly limiting the migration of colloids within the tuff matrix. Transport of colloids through fractures is possible; however, for the measured fracture apertures of 50 to 250 μm in Topopah Spring tuff the water flow rate would only be about 2 m/yr or still not much greater than molecular diffusion transfer rates. If fracture flow were episodic, corresponding to a few intense rainfalls per year, flow rates in fractures might be much larger but for only very short times.

Colloids greater than 0.1 μm in diameter will likely be removed by gravitational settling (Apps, et al. 1983). The transporting ability of very small colloids may be diminished by diffusion of radionuclides out of the particles and subsequent adsorption of the nuclides onto the tuff matrix. Diffusivities for some nuclides in some clays have been measured at 10^{-13} to 10^{-16} cm^2/s. Characteristic diffusion times for 0.1 μm particles are consequently only a few days. Migration of small colloids may be possible in a fracture flow regime. Work is continuing to understand the migration mechanisms of the very small colloids.

SUMMARY

The population balance methodology which operates on a number continuity approach is well suited for describing the complex phenomena of colloid transport. In the present study the problem of polydispersed colloid transport in a porous medium was successfully modeled and agreement was found between model results and data. The advantages of this methodology are that it provides a comprehensive and fundamental tool for analyzing the complex mechanisms of colloid migration. The approach requires conversion back and forth between the weight and number distributions; however, this conversion is a straight forward process. In this study, the colloid size distribution had a significant effect on the migration and capture process when a size dependent filtration capture model was

used. In the case of size dependent filtration, the larger colloids were rapidly captured while the smaller ones migrate much further through the porous medium. Both a constant and a linear size dependent filtration type capture model were tested. The size dependent model was required to match the measured column profile data. The experimental data was modeled successfully with only one adjustable parameter, s, the slope of the filtration coefficient function. If λ, the filtration factor, is constant then the colloid size distribution has no effect on transport or capture.

A limited study of parameter sensitivity showed that the width of the colloid feed distribution influenced the curvature on a semilog plot of the solid phase concentration profile with narrowing of the distribution converging to the monodispersed model and producing a linear concentration profile on a semilog plot.

In light of our findings, we made a preliminary review of some colloid transport characteristics for a potential NTS nuclear waste disposal site. We found geological factors favorable for retarding colloid migration. However, the potential for very small colloids to migrate in fractures with episodic flow characteristics may be significant and therefore requires further study and analysis.

NOTATION

c	Colloid Concentration in fluid	gm/cm^3
n	Hydrodynamic Dispersion Coefficient	cm^2/d
f	Birth/Death Rate Function	$\#/cm^3\mu md$
L	Colloid Size Dimension	μm
M_T	Initial Mass Concentration of Colloids	gm/cm^3
P	Population Density Function	$\#/cm^3\mu m_l$
s	Slope of Filtration Function	$cm^{-1}\mu m^{-1}$
t	Time	d
u	Growth Rate Along the Size Axis	$\mu m/d$
v	Darcy Water Velocity	cm/d
w	Weight Distribution Function	$gm/cm^3\mu m$
W	Cumulative Weight Distribution	gm/cm^3
z	Space Dimension	cm

Greek Symbols

ψ	Population Density Function (P/P_t)	dimensionless
ϕ	Velocity $(v/\bar{v})$	dimensionless
ν	Growth Date $(u\bar{z}/\bar{v}\bar{L})$	dimensionless
β	Space $(z/\bar{z})$	dimensionless
ρ	Colloid Size $(L/\bar{L})$	dimensionless
λ	Filtration Coefficient	cm^{-1}
σ	Mass Concentration of Colloids on the Matrix	gm/cm^3
σ_i	Mass Concentration of Colloids at Size L on the Matrix	$gm/cm^3\mu m$
τ	Time $(t\bar{v}/\bar{z})$	dimensionless
-	Average Properties or Limiting Properties	
ε	Porosity	

ACKNOWLEDGEMENT

"Prepared by Nevada Nuclear Waste Storage Investigations (NNWSI) Project participants as part of the Civilian Radioactive Waste Management Program (CRWM). The NNWSI Project is managed by the Waste Management Program Office (WMPO) of the U. S. Department of Energy, Nevada Operations Office (DOE/NV). NNWSI Project work is sponsored by the Office of Geologic Repositories (OGR) of the DOE Office of Civilian Radioactive Waste Management (OCRWM)."

The authors express their sincere appreciation to Mabel P. Grey for typing this paper and to M. A. Olson for preparing illustrations and graphic presentation.

REFERENCES

Apps, J.A. et al. (1983), "Status of Geochemical Problems Relating to the Burial of High-Level Radioactive Waste," prepared for U.S. NRC, NUREG/CR-3062.

Champ, D.R., Merritt, W.F. and Young, J.L. (1982). "Potential for the Rapid Transport of Plutonium in Groundwater as Demonstrated by Core Column Studies," Scientific Basis for Nuclear Waste Management, Vol. 5, pp. 745-754.

Douglas Jr., J. and Russell, T.F. (1982). "Numerical Methods for Convection Dominated Diffusion Problems Based on Combining the Method of Characteristics with Finite Element or Finite Difference Procedures," SIAM Journal of Numerical Analysis, Vol. 19, No. 5, pp. 871-885.

Fried, S.M. et al. (1976). "Annual Report for FY 1976 on Project AN0115A: The Migration of Plutonium and Americium in the Lithosphere," Argonne National Laboratory report ANL-76-127.

Hulburt, H.M. and Katz, S. (1964). "Some Problems in Particle Technology," Chemical Engineering Science, Vol. 19, pp. 555-574.

Nuttall, H.E., Hart, R. and Travis, B.J. (1985). "Population Balance Model for Colloid Transport," submitted to Nuclear Technology.

Randolph, A.D. (1962). "A Population Balance for Countable Entities," Can. J. Chem. Eng. Vol., 42, pp. 280-281.

Randolph, A.D. and Larson, M.A. (1971). "Theory of Particulate Processes," Academic Press.

Saltelli, A., Avogadro, A. and Bidoglio, G. (1984). "Americium Filtration in Glauconitic Sand Columns," Nuclear Technology, Vol. 67, pp. 245.

Travis, B.J. and Nuttall, H.E. (1985). "A Transport Code for Radiocolloid Migration: With an Assessment of an Actual Low-Level Waste Site," Materials Research Society, Symposia Proceedings, Vol. 44, Scientific Basis for Nuclear Waste Management VIII, pp. 969-976.

ANALYSIS OF PERMEABILITY REDUCTION DURING FLOW OF HEATED, AQUEOUS FLUID THROUGH WESTERLY GRANITE

Peter J. Vaughan

Dept. of Computer Science
SUNY Plattsburgh
Plattsburgh, NY 12901

ABSTRACT

The permeability of intact granite is known to be controlled by low aspect ratio cracks. A substantial reduction of permeability occurred in experiments in which a heated, aqueous fluid was passed through Westerly Granite down a temperature gradient. Scanning electron microscopy of the sample from this experiment indicated that deposition of material in small cracks (1 μm wide) was the probable cause of the permeability reduction. Much of the deposited material was Si-rich and the fluid discharged from the sample was supersaturated with respect to quartz suggesting that the deposit was quartz. Rate equations for dissolution and precipitation of quartz have been integrated to calculate the concentration of silica in pore fluid moving through the sample. These calculations also predict the concentration of silica in the discharged fluid for comparison with measured values. The comparison indicates that an effective A/M ratio of about 10000 is a reasonable value for Westerly Granite under the conditions of the experiment. The integration of the rate equations also permitted a determination of the volume of quartz dissolved and precipitated in the sample as a function of radius and elapsed time from the start of the experiment. The maximum, calculated decrease in porosity was 8% which would account for about 22% reduction in permeability assuming homogeneous precipitation. However, the observed permeability reduction was 96%. Two possible causes of this discrepancy are; (1) nonhomogeneous precipitation causing a greater rate of permeability reduction, or (2) the precipitation of minerals other than quartz is a contributing factor to the permeability reduction. SEM observations would tend to support either of these possibilities.

INTRODUCTION

The permeability of intact granite is controlled by low aspect ratio cracks (Brace, 1977). Several types of cracks occurring in granite include; (1) intragranular cracks in all three major minerals, (2) coincident grain boundary cracks, and (3) transgranular cracks (for definitions see Simmons and Richter, 1976). Cracks in Westerly Granite include all three types (Sprunt and Brace, 1974; Hadley, 1976; Vaughan et al., 1985) and are always present in intact granite although their length rarely exceeds the grain size. In addition to these small cracks, larger fractures are also present in most granites. These latter could be very important to the permeability of large volumes of rock. However, the present work considers only the permeability of small, intact samples and the cracks present in them.

The various types of cracks join together to form networks that provide pathways for fluids flowing through the rock. Thus, the specific geometrical characteristics of individual cracks and the geometry of the networks are both significant in controlling permeability. Cracks in quartz are especially important to the permeability of Westerly Granite because quartz grains are generally surrounded by grain-boundary cracks (Vaughan et al., 1985). Fluid moving along intragranular cracks within a quartz grain can be expected to flow along grain boundary cracks at the edge of the grain. In the case of feldspars, this is a less likely possibility because grain boundaries between the two feldspars are not normally cracked. Thus, intragranular cracks in feldspars frequently meet closed grain boundaries which are dead ends.

If heated aqueous fluids are pumped through granite, the chemical interaction of the heated fluid with its surroundings in the rock can cause changes in the physical characteristics of the cracks. As an example, if fluids are undersaturated with respect to quartz, then cracks in quartz will be enlarged as material is dissolved away from crack faces. The enlarged cracks will cause increased permeability. By contrast, supersaturated fluids may precipitate quartz on crack faces causing substantial reductions in permeability. The rapid rates of dissolution and precipitation reactions for quartz (Rimstidt and Barnes, 1980) tend to enhance these effects.

PERMEABILITY EXPERIMENTS

Permeability experiments in which a heated, aqueous fluid was passed through rock samples have demonstrated substantial decreases in permeability with time (Morrow et al., 1981; Moore et al., 1983). These experiments were conducted on cylinders of rock with axial boreholes. The fluid flowed radially outwards from the borehole to the outer edge of the sample down a radial temperature gradient. These experiments were run for periods of 2-3 weeks with the following physical conditions maintained constant; (1) confining pressure, (2) temperature in the borehole, (3) pore pressure at the outer edge of the sample, and (4) pore pressure difference between the borehole and the outer edge of the sample. The volume of fluid pumped into the sample was recorded continuously during the experiment and the flow rate, Q, within the sample was calculated from these measurements. Permeability was obtained from the equation,

$$k = \frac{Q\int(\nu(r)/r)dr}{2\pi l\Delta P} \qquad (1)$$

where l is the length of the sample, ΔP is the pore pressure difference and ν is the dynamic viscosity of water which is a function of radius in these experiments because of the radial temperature gradient.

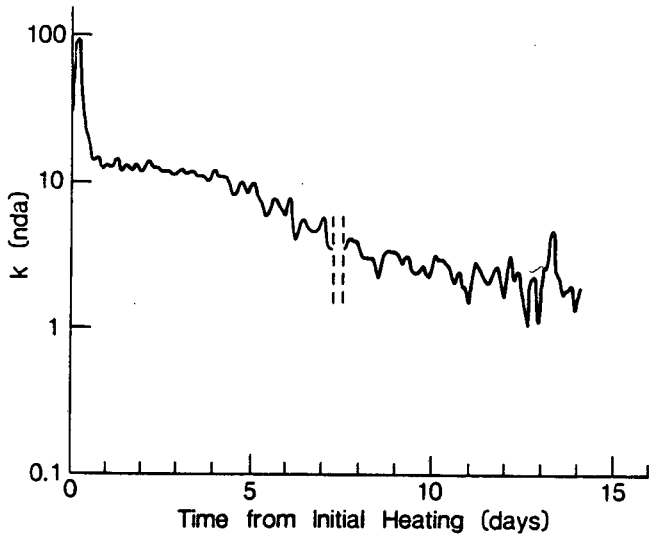

Figure 1. Permeability (nda) as a function of time from initial heating for experiment W300 (Moore et al., 1983). The vertical dashed lines represent a time when the pore pressure fluid pump was being recharged.

In experiment W300 (Moore et al., 1983) permeability dropped by a factor of 25 during a two-week period (Figure 1). Conditions of this experiment were; (1) temperature in the borehole - 300 °C, (2) temperature at the outer edge - 92 °C, (4) confining pressure - 60 MPa, and (5) pore pressure - 20 MPa. Cracks in the sample from this run were examined using a scanning electron microscope (Vaughan et al., 1985). They determined that about half the cracks near the borehole became filled with either a Si-rich or Ca-rich massive deposit. Other cracks, also near the borehole, were open and had rough surfaces suggesting dissolution. A platy texture was developed for Si-rich fillings near the outer edge of the sample. The presence of dissolution features and fillings in cracks in the experimentally altered sample is evidence that chemical interaction between the fluid and the rock has occurred. Furthermore, since narrow cracks are known to control the permeability of granite, the fillings are very likely to be significant to the permeability reduction. The ubiquitous presence of Si-rich fillings and the high concentration of dissolved silica in fluid discharged from the sample during the experiment (Moore et al. 1983), suggest that dissolution and precipitation of quartz are causing the permeability reduction (Morrow et al., 1981; Moore et al., 1983).

SILICA CONTENT OF THE DISCHARGED FLUID

In the present work, the rate equations for dissolution and precipitation of quartz (Rimstidt and Barnes, 1980) are integrated to predict silica concentrations of discharged fluids obtained during permeability experiments on granite (Morrow et al., 1981; Moore et al., 1983). Reactions of the fluid with minerals other than quartz also occurred and the discharged fluids contained the cations Na, Ca and K as well as the anions Cl, SO_4 and HCO_3 in the concentration range of 10-350 mg/L (Moore et al., 1983). However, the results reported here are only for quartz.

In order to calculate the silica content of the discharged fluid one must calculate the evolution of silica concentration in the fluid as it is pumped outwards through the sample. The rate of change of silica concentration in a solution in contact with solid quartz is

$$dm/dt = (A/M)(k_+ - k_-m) \qquad (2)$$

where m is the molality of H_4SiO_4; k_+ and k_- are the constants for dissolution and precipitation of quartz and A/M (area of reacting surface/mass of water) is a measure of the specific amount of reacting surface area for a given geometrical form. For a narrow flat crack, A/M is large; whereas for a tube or sphere, A/M will be less. The rate constants are given by Rimstidt and Barnes (1980),

$$\log_{10}k_+ = 1.174 - 2.028e\text{-}03T - 4156/T \qquad (3)$$

and

$$\log_{10}k_- = -.707 - 2598/T \qquad (4)$$

where T is the temperature in degrees Kelvin. Temperatures for fluid moving through the sample can be expressed as a function of time using

$$T(t) = T_a + \frac{(T_b - T_a)}{\ln(b/a)}\ln\{[(b^2-a^2)(t/t_r)+a^2]^{\frac{1}{2}}/a\} \qquad (5)$$

where T is the temperature at the borehole, T is the temperature at the outer edge, a is the borehole radius, b is the outer edge radius and t is the residence time in the sample. Equations (2) through (5) were integrated numerically using the Runge-Kutta technique to calculate silica concen-

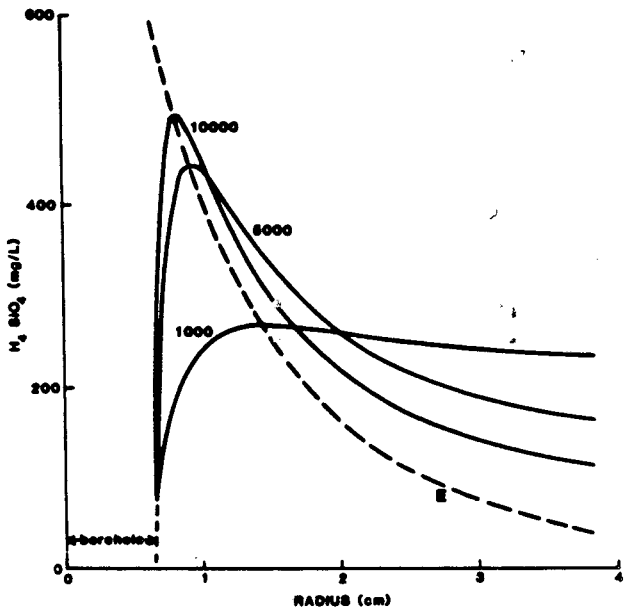

Figure 2. Concentration of dissolved silica in the pore fluid during the early portion of experiment W300 (Moore et al., 1983) as computed from rate equations for dissolution and precipitation of quartz. Computations are for three values of the A/M ratio printed on the graph. The dashed line is the equilibrium silica concentration.

tration as a function of radius in the sample. Figure 2 gives the resulting concentrations for the conditions of W300 (Moore et al., 1983). The total residence time for fluid in the sample was one hour which corresponds approximately to residence times expected for the early portion of W300. As the fluid enters the sample from the borehole, the silica content increases until it crosses the dashed equilibrium curve. Beyond this crossing point, the fluid is supersaturated with respect to quartz and the silica content decreases as quartz precipitates. Three curves are shown for different A/M ratios representing the range of reasonable values from 1000 to 10000. The degree of deviation from the equilibrium curve is greater for lower values of the A/M ratio corresponding to wider cracks. For the lowest A/M ratio (1000), the fluid becomes supersaturated at a relatively low value of 230 mg/L but it is moving rapidly enough that significant precipitation does not occur. The silica content of the solution in the outer portion of the sample is thereby stabilized under these conditions. For greater A/M ratios, the silica content decreases more rapidly resulting in a lower concentration in the discharged fluid.

The three curves for different A/M ratios (Figure 2) demonstrate that the silica content of the discharged fluid is quite sensitive to the A/M ratio. Thus, one can estimate the effective A/M ratio for Westerly Granite under the conditions of the experiment by measuring the silica content of

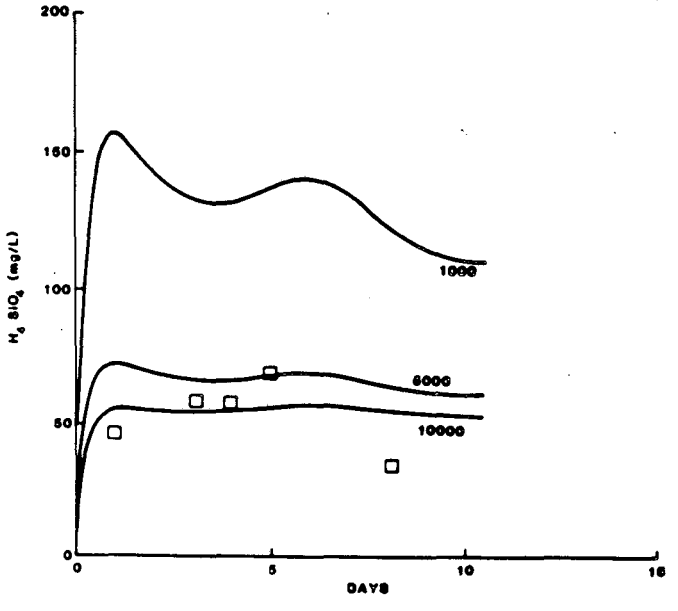

Figure 3. Silica concentration of the discharged fluid from experiment W300 (Moore et al., 1983). The three curves are calculated for three A/M ratios, the squares are measured concentrations.

the discharged fluids. Figure 3 is a comparison of calculated and observed silica concentrations for discharged fluids from run W300. In the early stages of the experiment, fluid initially present in the porous sample jacket diluted the discharged fluid. This effect has been accounted for in the calculation and, initially, the silica content of discharged fluid is always zero (Figure 3). However, after one day this dilution effect becomes insignificant. Each curve represents the silica content of the discharged fluid plotted against time from the start of the experiment.

The numbers at the end of each curve in Figure 3 are the presumed A/M ratios. For A/M=1000, the curve lies significantly above the data points indicating that this value of A/M is too low. Among the three values chosen, the best fit is for A/M=10000 corresponding to an average crack width of 0.2 μm. Brace (1977) calculated a value of 0.2μm as the geometric mean width of cracks in Westerly Granite. However, the A/M ratio will be influenced by crack surface roughness as well as crack width. Since crack surface roughness was greater in the altered sample than in the starting material (Vaughan et al., 1985), the crack width estimated from the A/M ratio is likely to be a lower bound. The last data point in Figure 3 lies considerably below the trend of the other data points and the calculated curve. This could be caused by an increasing A/M ratio related to the increasing roughness of crack surfaces as the experiment progressed.

MODEL OF PERMEABILITY REDUCTION

Precipitation of minerals in cracks during the permeability experiments of Morrow et al. (1981) probably caused local reductions of crack porosity in the sample. These crack porosity changes altered the permeability of the rock as open cracks became sealed.

If homogeneous precipitation occurs, the mineral being formed coats cracks uniformly. This is the simplest case for analysis because of its geometrical similarity to closing open cracks by forcing their faces closer together through increased confining pressure. Brace (1977) showed that the reduction in permeability that occurs with increasing confining pressure in Westerly Granite can be attributed to reduction in the crack porosity only. In other words, using

$$k = (m^2/A)\phi^3 \qquad (6)$$

(where A is a shape factor, m is hydraulic radius and ϕ is crack porosity) Brace found that changes in confining pressure caused changes in permeability by influencing only the crack porosity. The hydraulic radius was unaffected. This behavior is peculiar to Westerly Granite because of specific characteristics of the distribution of crack dimensions (Brace, 1977). The implication, however, is that equation 6 can be used to express the variation in permeability due to overall narrowing of the cracks by either application of confining pressure or homogeneous precipitation on the crack faces.

Using the A/M ratio of 10000, I calculated the variation in crack porosity in the sample due to dissolution and precipitation of quartz. In this calculation, small volume increments of fluid were passed along temperature-time paths specified by equation 5. In order to determine local porosity changes, the sample was divided into a series of hypothetical concentric cylinders. A running sum of the volume of quartz dissolved or precipitated in each cylinder was calculated for successive increments of fluid that passed through the sample. Local changes in porosity were then determined from the pore volume changes in each cylinder.

The total residence time varied for each

increment of fluid moving through the sample because the permeability decreased as the experiment progressed. The variations in residence time were computed from a sixth degree polynomial that expressed flow rate as a function of time. This polynomial was obtained by a least squares fit to the data.

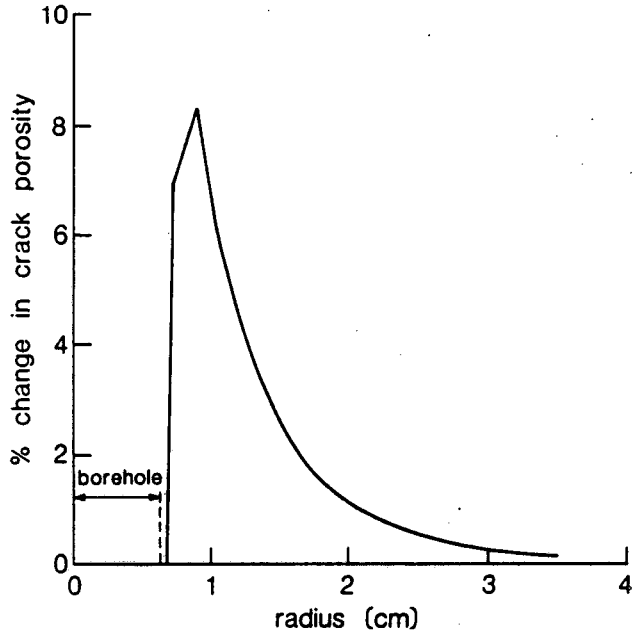

Figure 4. The calculated change in crack porosity due to precipitation of quartz in experiment W300. The maximum change in porosity is less than 10%.

The calculated variation in crack porosity for run W300 (Moore et al, 1983) is given in Figure 4. The maximum change in crack porosity is about 8% at a distance of 3 mm from the borehole. Using equation (6), the calculated reduction in permeability is 22% whereas the measured overall reduction in permeability for experiment W300 was 96%. Two possible causes of this discrepancy are; (1) equation 6 implies that porosity is being changed by homogeneous precipitation, whereas observations of discontinuous crack fillings (Vaughan et al., 1985) suggest that homogeneous precipitation is a poor assumption, and (2) precipitates other than quartz, particularly a Ca-rich filling, were found in the W300 sample.

CONCLUSION

A permeability experiment in which a heated aqueous fluid was passed down a temperature gradient through Westerly Granite showed a reduction in permeability of 96% over a two-week period (Morrow et al., 1981; Moore et al., 1983). At various times during the experiment the discharged pore fluid was chemically analyzed (Moore et al., 1983). They determined that silica concentrations of the order of 100 mg/L were present in these fluids. In the present work, I have calculated the silica content of fluids within the sample from the W300 experiment (Moore et al., 1983) utilizing rate equations for dissolution and precipitation of quartz (Rimstidt and Barnes, 1980). A comparison of the measured silica content of the discharged fluid with the calculated values for different A/M ratios indicates that silica content is a sensitive function of the A/M ratio. A/M is the ratio of reacting surface area to mass of water. The effective A/M ratio for the W300 sample under the conditions of this experiment is 10000. However, the silica concentration data indicate that A/M may have been increasing with time during the experiment.

The A/M ratio of 10000 has been used to obtain the variation in crack porosity in the sample due to dissolution and precipitation of quartz. The maximum deposition occurs around 3 mm from the borehole but only represents about 8% of the original crack porosity. Assuming homogeneous precipitation on cracks, this porosity reduction can account for a 22% reduction of permeability as compared to the observed 96% reduction. The discrepancy could be caused by; (1) non-homogeneous precipitation of quartz, or (2) precipitation of other minerals, particularly a Ca-rich crack filling which was observed near the borehole.

REFERENCES

Brace, W.F. (1977). Permeability from resistivity and pore shape, Jour. Geophys. Res., 82, 3343-3349.

Hadley, K. (1976). Comparison of calculated and observed crack densities and seismic velocities in Westerly Granite, Jour. Geophys. Res., 81, 3483-3494.

Moore, D.E., C.A. Morrow and J.D. Byerlee (1983). Chemical reactions accompanying fluid flow through granite held in a temperature gradient, Geochim. Cosmochim. Acta, 47, 445-453.

Morrow, C.A., D. Lockner, D.E. Moore and J.D. Byerlee (1981). Permeability of granite in a temperature gradient, Jour. of Geophys. Res., 86, 3002-3008.

Rimstidt, J.D. and H.L. Barnes (1980). The kinetics of silica-water reactions, Geochim. Cosmochim. Acta, 44, 1683-1699.

Simmons, G. and D. Richter (1976). Microcracks in rocks, in: The Physics and Chemistry of Minerals and Rocks, R. Strens (Ed.), Interscience, New York, 105-137.

Sprunt, E. and W.F. Brace (1974). Direct observation of microcavities in crystalline rocks, Int. J. Rock Mech. Min. Sci. & Geomech. Abstr., 11, 139-150.

Vaughan, P.J., D.E. Moore, C.A. Morrow and J.D. Byerlee (1985). The mechanism of permeability reduction during flow of heated, aqueous fluids through Westerly Granite, USGS Open File Report #85-262.

THE EFFECTS OF SILICA REDISTRIUBTION ON THE PERFORMANCE OF HIGH-LEVEL NUCLEAR WASTE REPOSITORIES

by

A. Verma and K. Pruess

Evaluation of the thermohydrological conditions near high-level nuclear waste packages is needed for the design of the waste canister and for overall repository design, as well as for performance assessment. Most available studies in this area have assumed that the hydrologic properties of the host rock are not changed in response to the thermal, mechanical, or chemical effects caused by waste emplacement.

We have studied dissolution and precipitation of silica in thermally driven flow systems, including changes in formation porosity and permeability. Using numerical simulation, we compare prediction of thermohydrological conditions with and without inclusion of silica redistribution effects. Two cases were studied, namely, a canister-scale problem, and a repository-wide thermal convection problem. We find that silica redistribution can have sizable effects on pore pressures, and on flow velocities. We also present results showing the sensitivity of those effects to the (hypothetical) pore model of the permeable medium (fractures versus capillary tubes).

COUPLING OF THERMO-PLASTIC AND HYDRAULIC EFFECTS IN CLAY REPOSITORY NEAR-FIELD ANALYSIS

G. Baldi, M. Borsetto, T. Hueckel, A. Peano

ISMES
V.le G. Cesare, 29
24100 Bergamo, Italy

ABSTRACT

Clay thermomechanical properties are studied experimentally in the range of temperatures till 120° C and of isotropic pressures till 8 MPa. Particularities of water-solid skeleton interaction in heating conditions are pointed out and a novel mathematical model of coupled hydraulic thermo-elastoplastic response is presented. Thermal compaction of clay skeleton both in elastic (overconsolidation) range and in plastic (normal consolidation) range together with significant pore water pressure build up are the principal peculiarities of clay behaviour with respect to other geomaterials.

1. INTRODUCTION

The prominent feature of clay as a nuclear waste storage medium is its low permeability ranging from 10^{-8} m/sec to 10^{-12} m/sec. It offers an effective barrier to far field water migration and possible radionuclides proliferation toward the human environment.

In the vicinity of the repository however the decay heat of the waste may affect significantly water-soil equilibrium and give rise to undesired pore water pressure build up and/or water flow off and toward the repository.

Thermal changes in the water-solid interaction affect clay behaviour on the level of the boundary value problem, on the level of the phenomenological material properties and finally on microstructural level, or briefly on mega -, macro - and micro-levels.

In the paper some macroscopic experimental observations are presented concerning mostly the thermomechanical effects in clays. Some comments on the microstructural interpretation especially of thermal shrinkage of clay are given afterwords. Then a macroscopic model is developed. On this basis prospective scenarios of the clay repository performance are discussed, resulting from hydraulic-thermo-mechanical coupling on mega-level. An example of a near field numerical analysis is given.

2. MACROSCOPIC EFFECTS OF WATER-SOLID THERMOMECHANICAL COUPLING IN CLAYS

At depths suitable for nuclear waste repositories clays are fully saturated with water under a high hydrostatic pressure . For the latter reason no water vaporisation at temperatures below 150° C may be expected as seen from a one year test at 160° C under 0.6 MPa of confinement stress [1].

For this reason clay is considered in what follows as a two-phase medium comprised of a solid mineral phase and water.

The mechanical behaviour of a porous medium fully filled with a fluid is governed by the equations of the fluid flow continuity and of the solid skeleton deformation.

The attention here is focused on the skeleton deformation.

The experiments have been performed in the high temperature, high pressure triaxial apparatus implemented at ISMES in a controlled temperature room. Loads are applied via a high pressure system. Heat is generated by a system of resistences attached to the cell and embeded in the apparatus cell [2]. Two materials were tested: a remoulded Pontida Silty Clay and indisturbed Boom Clay from Mol site.

A closed cycle of isotropic pressure and temperature has been first performed in drained conditions on Boom Clay, Fig. 1a. It consisted of loading (0-1) at room temperature, heating under constant isotropic pressure (1-2) at overconsolidation ratio, OCR = 1.8, further loading (2-3) and unloading (3-4) at constant elevated temperature and finally cooling at constant, low pressure (4-5) followed by an isothermal reloading (5-10) involving normal consolidation.

Consider first constant isotropic pressure heating tests. Typical experimental curves of volume of water expelled from the specimen in function of time show similarity to the mechanical consolidation curves. Therefore the classical technique has been adopted for defining the termination of the non-viscous part of the process (thermal primary consolidation). Further elaboration of the curves consisted in cor-

recting the obtained volumes for the expansion of water contained in the testing system outside the specimen (porous stones, tubes etc.). The expansion of pore water contained in the specimen itself was estimated then on the basis of the standard formula for nonlinear thermal expansion of pure water and subtracted from the corrected volume of expelled water. The resulting clay solid phase volumetric strain in function of temperature is presented in Fig. 1b,

It should be noted first of all, that the thermally induced volume changes are compactive. Therefore the ratio of the volume change to the temperature difference, referred to as effective coefficient of thermal expansion of clay solid results negative, see also [3-6]. On the other hand there is a remarkable influence of the effective isotropic stress on thermal strain. A comparison of unloading (3-4) of heated material and cool loading (5-6), Fig. 1a, shows that the bulk compliance modulus of clay is reduced by heating.

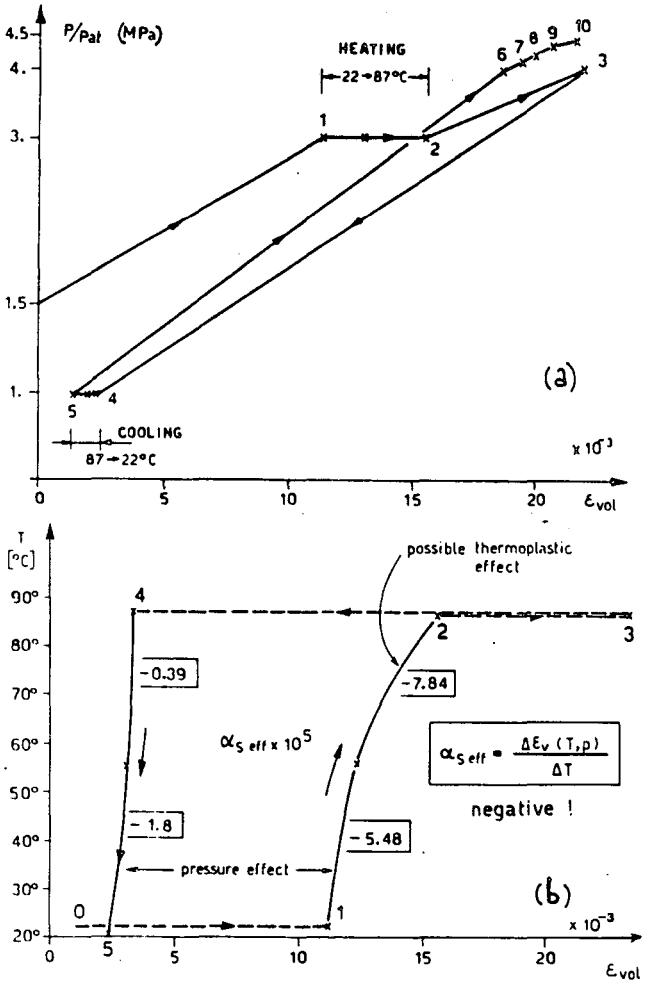

Figure 1. Volumetric strain in (a) - isotropic pressure and (b) - temperature cycle. Overconsolidated Boom Clay.

Under loading at constant temperature, additional strains of the order of heating strains, are seen when comparing the residual strains between points 4 and 5 with those between points 6 and 3 in Fig. 1a.

In normal consolidation states the thermal compaction strains are almost entirely irreversible. They are much higher than in the overconsolidation range. Results for the remoulded material (Pontida Silty Clay) under heating in the range 20°- 87° C, Fig. 2a show that about 60% percent of the final strain is irreversible upon cooling. A further mechanical loading has been undertaken after completion of cooling in order to investigate the normal consolidation range sensitivity to cooling, Fig. 2b. In fact, a localized modulus increase is seen at the first reloading step followed by a decrease to the value of hardening modulus measured in the plastic loading before heating.

The above experiments are sufficient for conceptual development and calibration of a simple thermomechanical model. The main conclusions to be drawn from the above tests are the following: thermally induced strains in clay are compactive; there is a strong effective stress dependence of the thermal expansion coefficient (negative), a temperature dependence is also observed; thermal volume strains in the normal consolidation range are much larger than those in the overconsolidation range; the normal consolidation range limit is sensitive to the heating-cooling cycle.

3. MICROSTRUCTURAL ASPECTS OF WATER-SOLID THERMAL COUPLING IN CLAY

The macroscopic experiments presented indicate that heating causes a shrinkage rather than an expansion of the clay skeleton. This is a well known effect at much higher temperatures in brick technology. However, the mechanism of dehydration due to evaporisation typical for ceramics in contact with air at free surface [3] is not likely to occur in immersion conditions at depth of interest here. Any way, the principal microstructural mechanism of heating shrinkage in immersion seems to be the water phase exchange. Of the four phases of water in clay i.e. structural, firmly adsorbed, loosely adsorbed and pore water [8] only the two last can leave the soil when heated. It is most probable that shrinkage is caused by changes of configuration of the loosely adsorbed water [4-6] due to a reduction of its density and its partial transformation into pore water.

A generation of irreversible stra-

ins by heating confirms this hypothesis. In fact, the straining of clays under isotropic consolidation is attributable on microstructural level to the formation of contacts between mutually attracting grains of clay solid mineral [10]. The contacts are of two types, i.e. mineral-to-water-to-mineral (M-W-M) and mineral-to-mineral (M-M). In the latter contacts, grain may glide in direct touch with respect to others due to irreversible shear of thin films of the firmly adsorbed highly viscous water. These contacts an considered as not removable with a decrease of pressure [8]. In the (M-W-M) contacts the grains are separated by large cushions of loosely adsorbed water which deform reversibly under loading, giving rise to global elastic strains. Plastic deformation of clays are considered as the increase of number of (M-M) contacts instead of (M-W-M) contacts. Heating reduces specific density and thus viscosity and stiffness of loosely adsorbed water cushions. This facilitates formation of (M-M) contacts, and thus globally produces irreversible strains.

The above considerations are purely qualitative at the moment and call for systematic experimental and theoretical studies. They are not only of theoretical interest but would be utmost useful for adequate evaluation of the volume of expanded clay water and thus of the skeleton deformability.

4. MACROSCOPIC COUPLED THERMO-ELASTO-PLASTICITY MODEL FOR CLAY SKELETON BEHAVIOUR

The model is limited to small strains and refers to the deformability of clay skeleton alone. Thus effective stresses are introduced as acting on the skeleton defined via Terzaghi principle $\underline{\sigma} = \underline{\sigma}' + u \cdot \underline{m}$, where the vector $\underline{m}$ is composed of units for normal strain components and of zeros for shear components. Extension is taken as positive.

Strains are supposed to depend on effective stress and pore water pressure as well as on temperature and on a number of hidden variables like plastic volumetric strain ε_v^p; geostatic strain, ε_g, referred to the in situ situation prior to the application of loading; and e_g being a void ratio connected with the geostatic stress state. The latter two are dead variables for a given geostatic situation.

$$\underline{\varepsilon} = \underline{\varepsilon}\,(\underline{\sigma}', u, T, \varepsilon_v^p, \varepsilon_g, e_g) \qquad (1)$$

Strain is decomposed into reversible and irreversible part

$$\underline{\varepsilon} = \underline{\varepsilon}^r + \underline{\varepsilon}^i \qquad (2)$$

Reversible deviatoric strain is thermally insensitive, while the volumetric reversible strain reads:

$$\varepsilon_v^r = K \ln \frac{tr\underline{\sigma}'}{tr\underline{\sigma}_g'} + \alpha \Delta T - C^* u - \varepsilon_g \qquad (3)$$

$$K = [K_i/(1+e_0)](1 + \beta\Delta T + \gamma\Delta T^2); \qquad (4)$$

$$\alpha = \alpha^* + \alpha_0 + (\alpha_1 + \alpha_3 \Delta T) \ln \frac{tr\underline{\sigma}'}{tr\underline{\sigma}_g'} + \alpha_2 \Delta T$$

where: ΔT is the actual temperature difference with reference to a laboratory temperature To; Ki is the isothermal bulk compliance modulus, α^*, C* are the thermal expansion coefficient and bulk compliance modulus of the mineral solid, $\beta, \gamma, \alpha_0, \alpha_1, \alpha_2, \alpha_3$ are constants.

The irreversible strain due to path dependence is defined incrementally via a plastic flow rule.

$$d\underline{\varepsilon}^i = d\hat{\lambda}\,(d\underline{\sigma}', du, dT)\,\frac{\partial f}{\partial \underline{\sigma}'}; \quad d\hat{\lambda} \geq 0,\ df \leq 0;\ df\, d\hat{\lambda} = 0 \qquad (5)$$

The plastic multiplier $d\hat{\lambda}$ defines the entity of the irreversible strain increment. Its direction is assumed as normal to a yield surface defined as a limit of purely elastic response of overconsolidated material. The normality rule implies therefore the presence of a deviatoric thermal irreversible strain.

The elliptic yield sufaces is that of modified Cam Clay generalized to the temperature dependence. Due to temperature rise the overconsolidation domain shrinks in the hardening range, OCR<2, while in the softening range its necessary shrinking for mechanical reasons is mitigated by the temperature. As a result one obtain a thermally induced increase of ductiliy. In the softening range it requires a coupling between strain and thermal hardening.

After some algebra the total response is obtained in the following form:

$$d\underline{\sigma} = \underline{\underline{D}}\, d\underline{\varepsilon} + \frac{1}{3}\left[(\underline{\underline{D}}\,\underline{m}\,C^* - \underline{m})\,du + (\alpha_T \underline{\underline{D}}\,\underline{m} - \underline{q}^{pl})\,dT\right] \qquad (6)$$

in which $\underline{\underline{D}}$ is the thermo-elasto-plastic incremental matrix defined as follows

$$\underline{\underline{D}} = \underline{\underline{C}} - \frac{1}{\Delta H}\,\underline{M}\,\underline{M}^T; \quad \underline{M} = \underline{\underline{C}}\,\frac{\partial f}{\partial \underline{\sigma}'}, \qquad (7)$$

where ΔH is the brittleness index which defines an incremental compliance (strain-stress invariant curve slope). The behaviour is perfectly brittle if $\Delta H \to 0$. $C = C\,(\Delta T, tr\underline{\sigma}')$ is the inverse incremental elasticity matrix; α_T is a combination of thermal expansion coefficients of skeleton, water and mineral solid, while

thermal plastic strains are defined through, [11]

$$\underline{q}^{pl} = \frac{1}{\Delta H} \frac{\partial f}{\partial T} \underline{C} \frac{\partial f}{\partial \underline{\sigma}}, \qquad (8)$$

Account taken of the water and mineral solid compressibility and their thermal expansion together with the pore volume changes due to skeleton deformation described in (6), the water outflow per unit volume may be determined. Combining it with the Darcy equation a governing system is reached describing coupled hydraulic mechanical response of the clay-water medium to a given temperature

$$\begin{bmatrix} 0 & 0 \\ 0 & K\frac{\partial^2}{\partial \underline{x}} \end{bmatrix} \begin{Bmatrix} \underline{\varepsilon} \\ u \end{Bmatrix}^{\cdot} + \begin{bmatrix} \underline{D} & \frac{1}{3}\underline{D}\,\underline{m}\,C^{*} - \underline{m} \\ -\underline{m}^{T} + \frac{1}{3}C^{*}\underline{m}^{T}\underline{D} & C^{**} + \frac{1}{9}C^{*2}\underline{m}\,\underline{D}\,\underline{m} \end{bmatrix} \begin{Bmatrix} \dot{\underline{\varepsilon}} \\ \dot{u} \end{Bmatrix} +$$

$$+ \begin{Bmatrix} -\frac{1}{3}\alpha_T \underline{D}\,\underline{m} + \underline{q}^{pl} \\ \frac{1}{3}C^{*}\underline{m}^{T}\underline{q}^{pl} + \alpha_v - \frac{1}{3}\alpha_T C^{*}\underline{m}^{T}\underline{D}\,\underline{m} \end{Bmatrix} \dot{T} = \begin{Bmatrix} \dot{\underline{\sigma}} \\ 0 \end{Bmatrix}; \quad C^{**} = (1-n)C^{*} + nC_w \qquad (9)$$

$$\alpha_v = (1-n)\alpha^{*} + n\alpha_w$$

n - is the current porosity.

In short term analysis, in which in the presence of the extremely low permeabilities of clay $K \to 0$ no flow virtually occurs, it is useful to develop a decoupled hydrostatic thermo elasto-plastic system which reads

$$d\underline{\sigma} = \left(\underline{D} + C^{pu}\underline{Q}\,\underline{Q}^{T}\right) d\underline{\varepsilon} + \underline{Q}^{\alpha} - \frac{1}{\Delta H}\frac{\partial f}{\partial T}\underline{M}\,dT; \qquad (10)$$

$$du = C^{pu}\underline{Q}^{T} d\underline{\varepsilon} + \left(\alpha_q + \frac{1}{C^{*}}\alpha_T\right) dT, \qquad (11)$$

where:

$$\underline{Q} = \left(\frac{1}{3}C^{*}\underline{D} - \underline{I}\right)\underline{m}\,; \quad \underline{Q}^{\alpha} = \left(\frac{1}{3}C^{*}\alpha_q\,\underline{D} - \underline{I}\right)\underline{m}$$

$$\alpha_q = -\frac{\alpha_T}{C^{*}} + C^{pu}\left[(n\alpha_w + (1-n)\alpha^{*} - \frac{1}{9}C^{*}\alpha_T\,\underline{m}^{T}\underline{D}\,\underline{m} - \frac{1}{3\Delta H\dot{T}}C^{*}\frac{\partial f}{\partial T}\underline{m}^{T}\underline{M}\right.$$

$$C^{pu} = \left[(1-n)C^{*} + n\,C_w - \frac{1}{3}C^{*2}\,\underline{m}^{T}\underline{D}\,\underline{m}\right]^{-1} \qquad (12)$$

In the above, temperature is considered as known. It means that heat diffusion is assumed to be decoupled from the hydraulic and deformational fields.

Both undrained and transient models have been implemented into a finite element computer code, see [11].

5. SCENARIOS OF REPOSITORY PERFORMANCE DUE TO COUPLED PROCESSES IN CLAYS

Three possible scenarios may be envisaged on the mega-scale level. In the first scenario pore pressure gradients due to the temperature space distribution produce a slow but long term water out flow. In adverse circumstances it may enhance nuclear pollutant migration toward human environment (see e.g. [12]). Novel points in this problem arise from the particular properties of clays expounded in sec. 3 and 4.

The second scenario consists in such thermally induced build up of the pore pressure that the clay skeleton reaches a failure state. In fact, due to water pressure build up, the effective isotropic stress in the skeleton reduces. Thus even at constant shear stress a failure may occur due to lack of skeleton confinement stress.

The plausibility of such occurrence has been confirmed experimentally in laboratory tests on homogeneous specimens for two kinds of clay. For a remoulded Pontida Silty Clay Fig. 3a shows the stress path composed of an undrained shear loading up to conditions simulating a normally anisotropically consolidated clay state. After having allowed material to creep till stabilization, heating has been performed under constant total stress. Correction for the water expansion in the apparatus, porous stones and tubes has been applied. As the result a net pore water pressure development in the specimen has been obtained as a function of the specimen vertical deformation, Fig. 3b. Failure has been reached at 92° C, and has been accompanied by a pore pressure slight regression and then stabilization. No localized shear band has been observed in this test, while it was present for the Boom Clay.

The stress path may be interpreted as purely elastic, what has been confirmed in a similar test with local unloadings. In the final phase however, the thermally reduced yield surface is reached in its softening range. Then the yield surface shrinks and "forces" the effective isotropic stress to increase again a little and thus the pore pressure to decrease until the critical state is reached and plastic skeleton residual flow is activated.

The third scenario is a combination of the former effect developed partially with a subsequent or simultaneous deviatoric loading induced by construction or emplacement. It is in fact sufficient to diminish only in part the effective stress to promote a significant reduction of the "undrained shear strength", C_u of clay. Therefore clay is more susceptible to failure after heating even under moderate shear loading.

It is important to point out that in actual in situ conditions there are usually several stabilizing effects. Initial pore pressure excess is normally zero or small. Secondly, a locally induced instability needs not mean an overall instability, because of the stabilizing contribution of adjacent zones

[14]. However numerical and experimental studies are required to prove that the above scenarios cannot occur in real repository situations.

Preliminary computations have been undertaken by means of the mathematical models developed in sec. 4. An axisymmetrical Pontida silty clay column 90 m high and 37 m in radius has been simulated in plane strain. The column has been heated by a centrally placed heater of 15 cm radius emitting to 224 W/m constant in time. The heater simulates a series of alternating HLW and CH containers 1.5 m high, emplaced 30 years after disposal from the reactor.

Fig. 4a presents the distribution in the radial direction of temperature and excess pore pressure developed after one year and after ten years from the beginning of heating, for three cases of clay permeability, $K_1 = 1.10^{-8}$ m/sec, $K_2 = 1.10^{-10}$ m/sec, $K_3 = 0$. The first two cases have been studied with the "Transient flow" option, while the latter with the option "Undrained".

Note first that the distribution of the pore pressure for $K_2 = 1.10^{-10}$ m/sec. is almost identical to the "undrained" solution both in the 1 year and in the 10 year analysis. Secondly, in the central, most heated zone the pressure is almost double for K_2 with respect to K_1. At greater distances the difference diminishes. The vertical effective and total stress distribution, as well as flow velocities, fig. 4b show quite significant effects in the range of about 18 m. The results obtained for 50 years, not reported in figures, indicate a fairly extended zone of alteration of natural conditions. In fig. 4c the effective stress path is shown for the element closest to the heater, in analogy with the test result from the fig. 3a. Although the stress does not reach the failure envelope, it markedly approaches it.

6. CONCLUSIONS

Above results indicate a relevance of heat induced variations of the hydrological and mechanical original conditions of clay in the near field. This refers both to the extension of the zone affected and to the intensity of the phenomena. Thermally induced nonlinear mechanical behaviour of clay has to be taken into account during repository design both in order to avoid negative effects by appropriate spacing of the canisters and in order to exploit beneficial effects, such as improved self sealing due to enhanced plastic behaviour. Clearly, both tests and computations are a very simplified approximation of the real effects in situ. Further laboratory and numerical work is under way at ISMES in order to perform a more realistic simulation.

ACKNOWLEDGEMENTS

The work described has been carried out at ISMES as a part of a research programme supported by ENEA (National Board of Alternative Energies of Italy) and by the Commission of European Communities.

REFERENCES

1. Heremans R., (1981). in: Near-field phenomena in geologic repositories for nuclear waste, Proc. of Workshop Seattle, WA, ECD/NEA, Paris.
2. Baldi G., Hueckel T, Tassoni E, (1985). presented for Int. Symp on Environmental Geotechnology, Allentown, PA, (to be published)
3. Campanella R.G., Mitchell J.K., (1968). J. SMFE Proc. ASCE, 94, 3, 709
4. Silva A.J. et al (1981), "Geotechnical aspects of suseabed disposal of high level radioactive waste", University of Rhode Island.
5. Passwell R.E. (1967). ASCE, SM8, 9-21.
6. Deamars K.R. and Charles R.D. (1982). Canadian Geotech. J., 188-194.
7. Weaver Ch. E., (1976). "Thermal properties of clays and shales", Union Carbide, Rep. Y/OWI/SUB-7009/1.
8. Rosenquist T., (1959). Proc. ASCE, SM2, 31-53.
9. Resendiz D., (1965). On the strength of clayey soils, Univ. Nac. Autonoma de Mexico.
10. Murayama S., Shibata T., (1966). Proc. REMESO Grenoble, 1964, Springer Berlin p. 99.
11. Borsetto M., Cricchi D., Hueckel T., Peano A., (1984) in "R.W. Lewis et al", "Numerical Methods for Transient and Coupled Problems", Pineridge Press, Swansea UK.
12. Burke P.J. and Hodgkinson D.P., (1979). Proc. of workshop Low-flow, low-permeability measurements in largely impermeable rocks, Paris, pp. 221-234.
13. Davis T.G., Banerjee P.L., (1980). "Constitutive relationships for ocean sediments subjected to stress and temperature gradients, AERE Harwell, Report No HL 80/2609 (C.22).
14. Hueckel T., Maier G., (1977). Int. J. Solids and Structures, 13, 1, pp. 1-15.

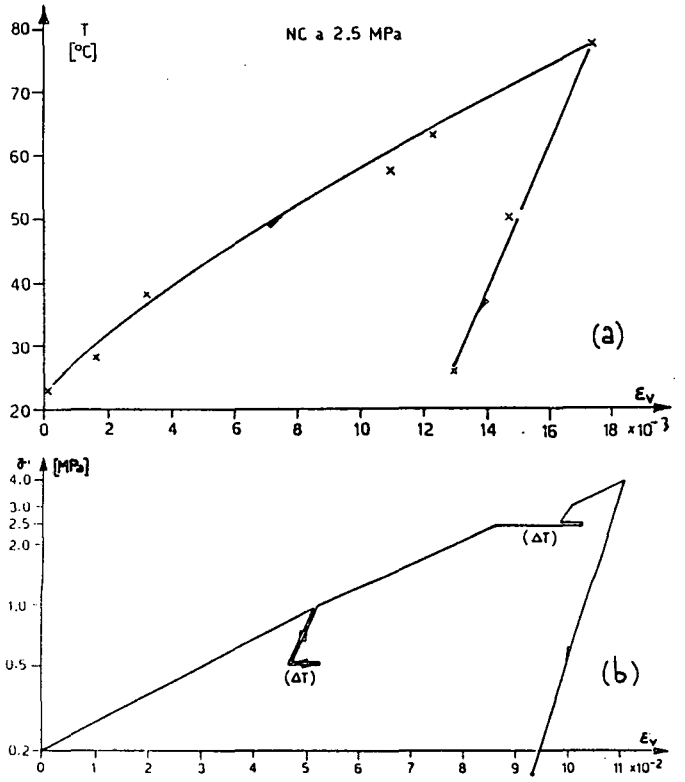

Figure 2. Volumetric strain in (b) - pressure and (a) - temperature cycle. Normally consolidated Pontida Clay.

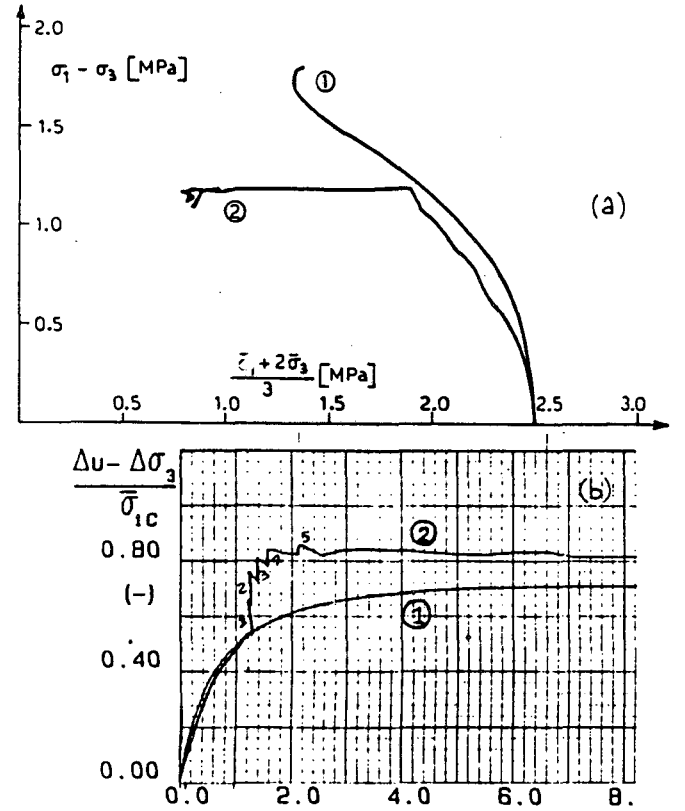

Figure 3. (a) - Stress path and (b) - water excess pressure vs. vertical strain in undrained constant loading heating.

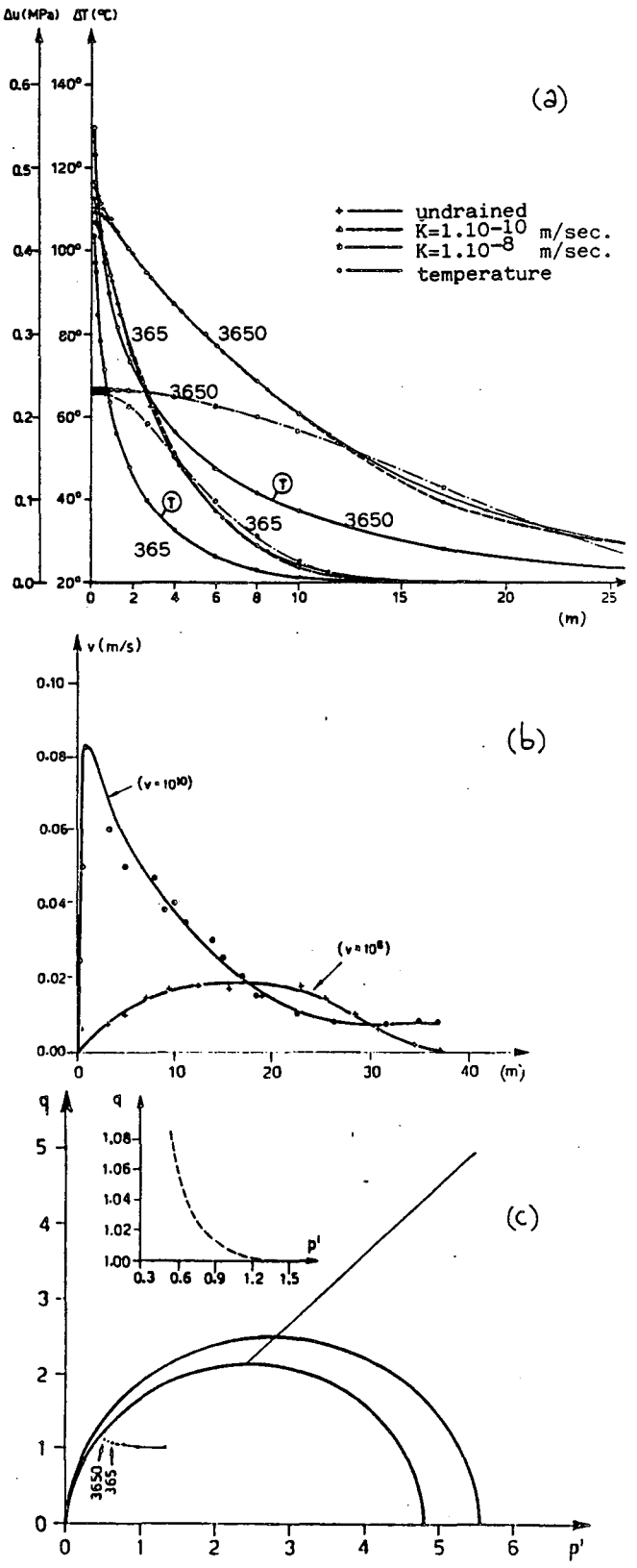

Figure 4. (a) - Pore pressure and temperature distribution around the canister, (b) - water flow velocities, (c) - effective stress path.

MODELLING OF PERVIOUS FAULT GENERATION IN CLAY HOST FORMATION

M. Borsetto*, T. Hueckel*, A. Peano*, E. Tassoni**

* ISMES, v. G. Cesare 29, Bergamo, Italy
** ENEA, Casaccia, Rome, Italy

ABSTRACT

Some aspects are presented of mathematical simulation of a generation in clay formation of discontinuities propagating from a moving bed-rock. Modelling of pre-critical and post-critical behaviour of clay together with discontinuity generation conditions are discussed.

INTRODUCTION

The concept of radioactive waste disposal in deep continental clay formations is based on their high efficiency as a radionuclide migration barrier. It offers the possibility of a very limited effort required for backfilling of repositories and of emplacement of canisters directly into clay.

The quality of clay as a barrier against migration relies on its extremely low permeability ranging between 10^{-9} m/sec and 10^{-12} m/sec as well on its high ductility which mitigates effects of possible fractures of thermal or mechanical origin. A relatively high retaining capacity of radionuclides through geochemical processes is also associated with the low permeability.

However, due to the required extremely long durability of the repository it is necessary to study all possible adverse phenomena which could alter the original integrity of the geological formation of interest.

In this paper, attention is focused on a possible dislocation of the bed-rock underlying the repository. Consequences of such event to the clay formation continuity (such as formation of a fracture) should be evaluated.

In particular two principal areas should be investigated. The first one regards conditions of generation of the phenomenon in clay, its extent and propagation. The second one is related to the characterization of potential water flow through a discontinuity in clay. In particular, the fracture enhanced permeability of clay should be quantified in order to understand whether the natural water circulation towards human environment could become critical.

Bed-rock movements can differentiate significantly among them. In consequence, also the mechanical reactions of the clay formation to them would be different. Normal or reversed faults may propagate into the clay strata causing its intense shearing. The normal faults heading towards one another produce "trough faulting" or sunken block, or "graben", all causing partial relief of stresses in clay and zonal tensions.

The bed-rock intense shear or partial removal of compression stress can give rise or not to respectively shear fractures or tension fractures in clay depending on the type of clay and on the depth of the deposit.

To begin with, only shear fractures will be dealt with in what follows. It is well known in surface geotechnics that for example at landslide tips, zones of intense shear composed of numerous, evolving fractures occur exhibiting substantial dilatancy. Often, even partial fractures degenerate and progress due to water percolation and produce finally collapse mechanisms. On the other hand, it is known that the confining isotropic pressure is a highly stabilizing effect and may moderate or even suppress formation of fractures.

Therefore due to the presence of confining effective stress of several Megapascals, the generation of shear fractures at depth in the clay of different plasticity is not a straightforward problem and requires ad hoc experimental and theoretical studies.

For hard clays there exists an evidence from an open lignite mine (Santa Barbara, Italy) of the presence of numerous well exposed discontinuites. Some of the discontinuities are accompanied by a yellowing of the adjacent zones up to 50 meters deep, what indicates a possible past water circulation.

Plastic clays on the other hand, and especially at high confining pressures, may exhibit large ductile strains due to bed-rock fault propagation. This may lead to the formation of either extensive zones of diffused plastic strains or shear bands of a certain width, running even through the whole clay formation. The crucial question arises now concerning volumetric strains (dilatan-

cy) and thus permeability changes at such phenomena.

Answers to the above queries should be looked for on three parallel ways: by searching for natural analogs, like recent earthquake formed on-surface cracks of assurred depth or undergroung mine fractures; via laboratory studies both on small homogeneous and large samples as well as on samples with variable centrifugal gravity fields; and finally by numerical simulations employing adequate constitutive models.

In order to approach these problems a comprehensive research programme has been undertaken at ISMES encompassing both in situ and laboratory studies as well as mathematical simulations.

In this paper several aspects of mathematical modelling are discussed. In the matter of fact, to the best of our knowledge the problem of fault propagation in clays at such depth has not been tackled till now in sufficiently complete manner as to give meaningful results. The discussion presented concerns methods of describing the formation of a fracture in clay medium and its propagation, i. e. pre-critical and post-critical constitutive law, as well as an inception criterion.

Questions connected with the finite element treatment of the above phenomena are also discussed.

GENERAL ASPECTS OF MATHEMATICAL MODELLING OF FRACTURES IN CLAY

Penetration of a pratically rigid rock into clay stratum produces in clay a stress field, which almost immediately ceases to be elastic at least in singularity points. Stress in fact soon reaches critical values giving rise to inelastic deformations which may be either highly localized or diffused depending both on material properties and on boundary conditions.

The localized shear deformation in clays may take on three different forms, Fig. 1. First of all, an actual discontinuity within the medium can take place involving relative displacements of two parts of originaly unique material elements, Fig. 1a. Such phenomena is treated by methods of fracture mechanics.

Secondly, there is a possibility of formation of a narrow zone of advanced ductile shear deformations, Fig. 1b. Such effects are modelled via plasticity models.

Finally, one may have a narrow zone of material suffering an oriented or isotropic damage in the form of growing defects like microcracks or voids, Fig. 1c. These effects are modellable by means of inelastic damage theories.

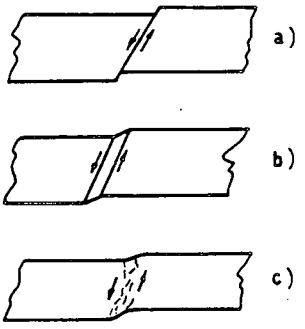

Figure 1. Typical forms of localized shear deformation in clay.

Physically, the above effects often follow each other either in time or in space (Morgenstern, Tchalenko, 1967).

From the simulation point of view the above three forms of the deformation localization can sometimes be used to represent a different scale vision of the same physical fact for a numerical convenience. It is possible on the other hand, that in the finite element calculations the differences between the approaches become immaterial computationally. The choice of the approach is however not indifferent from the conceptual point of view for interpretations of the numerical results.

Mathematical description of the localized deformation simulating a fault propagation into a clay stratum requires first of all a description of the behaviour of clay continuous element by itself, i. e. prior to any critical state.

Mathematical modelling of clay behaviour for surface geotechnical application is a topic of intensive studies, both from the points of view of constitutive laws and numerical methods. The most advanced studies have been made in the framework of the theory of plasticity.

Plastic behaviour of materials is insensitive to the time scale, in contrast to viscous or viscoplastic behaviour. In the present application the real time elapses are insignificant, therefore the sole dependence of the behaviour on the sequence of events, well described by the rate insensitive plasticity theory is here a sufficiently good approximation of the actual material memory.

An archetype of studies on the fracture propagation is the rigid perfectly-plastic solution of boundary value probem, admitting discontinuity in the velocity field. Such solution, besides the highly idalized behaviour of

the material is connected with the concept of full plasticization of the continuum and requires the development of a complete failure machanism.

Therefore effects of the primary interest for the present application like kinematics of propagation, including variable dilatancy and, first of all partial localizations which do not develop any failure mechanism cannot be described by perfect plasticity.

The interest is therefore concentrated on more sophisticated models of hardening and softening incremental plasticity or damage theories. These models describe gradual loss of incremental stiffness together with accumulation of inelastic deformation till the peak state is reached at zero incremental stiffness. The peak is followed by a smooth stress reduction at continuous homogeneous straining. It corresponds to a uniform degradation of the material with a negative incremental stiffness till an ultimate resistance state of unlimited plastic flow is reached. Such models are now fairly developed for geomaterials.

The actual behaviour of clay may exhibit several departures from these models. One of principal departures of relevance here consists in a possibility of the formation in a homogeneously strained specimen of a localized discontinuity of shear or extension kind at, or before the peak state is reached. Further deformation is then concentrated at such discontinuity to which often also all degradation or softening effects are circumscribed. Moreover, such effects, if referred to the whole elemental volume give the elemental softening much underestimated or inexistent. The main consequence of the localization is that an actual post-critical deformation mechanism drastically changes and variables controlling it become discrete i.e. referred to the interface.

In the framework of the theory of plasticity two approaches are developed dealing with strain localization, treating it on a global or local scale. In the first option the localization is conceived as an effect of the solution of a boundary value problem in which a zone of high strain gradients is formed in the strain field.

In the other approach, the localization of deformation is postulated at an infinitesimal element as a generation of an admissible discontinuity within the elemental strain field. The generation is triggered by a loss of stability of the material locally. A growing sequence of material elements in which it occurs simulates the propagation of the localization in the medium.

MODELLING OF PRE-CRITICAL BEHAVIOUR

In the both approaches to localization, the modelling of the pre- critical behaviour plays an important role. A model of the type of Cam Clay developed for surface geotecnics may be used for the present purpose after some modifications, Schofield and Wroth (1968). There are in fact several requirements which such model should meet.

First, a possibility of modelling of plastic dilatancy prior to critical states both for overconsolidated and normally consolidated stress paths should be assurred, Nova (1982). Indeed a correct modelling of the dilatancy is a necessary element of adequate evaluation of permeability changes.

Secondly, the ultimate state locus being a non-linear shear stress invariant function of effective isotropic stress, characteristic for clay behaviour at depths should be simulable. Thirdly, a possibility of low cyclic pore water pressure build up in the overconsolidation range due to seismic wave induced motion prior to the local generation of discontinuity is an important effect to be taken into account Hueckel and Nova (1981). In fact, such effect is known to lead to a reduction of undrained shear strength.

Finally, it must be stressed that there exists a coupling between the pre-critical behaviour and the mode and the stress level of the critical state itself. In other words, the critical state understood as bifurcation is highly sensitive to the pre-critical model. It refers in particular way to the flow rule defining plastic strain rate direction, which deviation from the yield surface normal is considered as a major factor promoting bifurcation.

One of the causes of the non- normality of clay flow rules is the elasto-plastic coupling which models the well known strong elastic anisotropy due to plastic non-isotropic pre- consolidation.

This and/or other sources of phenomenological non-normality should be carefully analyzed in the model for deep clays.

MODELLING OF FAULTS VIA LOCALIZATION OF SHEAR STRAIN

As already mentioned there are two options in modelling the strain localization of plasticity.

In the first one, referred to the boundary value problem treated with the finite element method no local bifurcation occurs. The localization occurs due to formation in the strain field of a band of high shear strain gradients in

concommitance with a transition from the elliptic range to hyperbolic range of partial derivative differential equation system describing the medium behaviour, Hill and Hutchinson (1975), Vardoulakis (1981). In the models for geomaterials it coincides with or precedes the shear stress strain characteristics peak point. It is equivalent to local loss of stability, Maier and Hueckel (1979), in the sense of Hill (1958), but no further consequence to the deformation mode is considered. It means that in this approach the pre-critical homogeneous elemental deformation mode is maintained.

Note moreover, that despite local instabilities not necessarily global instability occurs due to the stabilizing contribution of the adjacent volumes, Hueckel and Maier (1977). If the global instability is reached, coincident with loss of positive definiteness of the boundary value problem incremental matrix, a global bifurcation occurs and thus an alternative kinematic configuration can be generated. This stage hovever is rarely considered in the geotechnical applications since such advanced failure is usually out of the range of small strains and of the validity of constitutive models for clays.

Clearly, any numerical result in this approach depends on the refinement of the finite element mesh. It may therefore happens that due too coarse mesh the localization is excessively smoothened and the dilatancy associated with it is underestimated.

One of the ways to avoid such occurrence is to choose the other mentioned option in which the local bifurcation is taken into account. In this approach limited to plane cases only a bifurcation point in elemental behaviour is looked for by considering an elemental admissibly discontinuous strain field, following Rudnicki and Rice (1975) and Vardoulakis (1981). As a result one obtains not only the stress level at which the bifurcation occurs, but also an inclination of the discontinuity plane.

Crucial role in the assessing of the stress level and discontinuity direction is played by the form of non-normality of the flow rule. The deviation from the normality in fact implies a strong decrease of the bifurcation level as discussed in the preceding sections. The bifurcation criterion coincides with the condition of a loss of positive definiteness of the incremental constitutive plane strain matrix with reduced degrees of freedom imposed by discontinuity admissibility requirements.

Further irreversible process localizes at the discontinuity plane at which a particular form of the constitutive law must be determined.

POST-CRITICAL BEHAVIOUR MODELS

In the first approach, with the Cam- Clay laws, models the post-critical behaviour is an intrinsic part of the model.

It is defined via softening behaviour for strongly overconsolidated states, while it coincides with perfectly plastic flow for normal consolidation range. Therefore the main three element of post-critical behaviour of the localization, i.e.

(a) criterion for propagation of discontinuity
(b) direction of the propagation
(c) relationship for plastic flow and dilatancy at the discontinuity.

are the result of the boundary value problem.

The three point indicated above are however an almost completely open problem for the second approach.

First, the only known propagation criterion based on the J-integral approach as proposed by Palmer and Rice (1973) is valid for a very simple non-incremental deformational plasticity laws.

Then, the direction of the propagation is determined by the discontinuity inclination of neighbouring elements and there is no a priori indication that the bifurcation is reached in the neighbourhood.

Finally, the relationship between surface traction at the discontinuity boundary and relative displacement is an unsettled question. There is some preliminary works concerning general conditions of friction between two mineral surfaces, Mroz (1980), but behaviour at a surface internal to the element is in some aspects considered as not measurable. Several as hoc techniques for determining constitutive law may be adopted by a back analysis of numerical solutions employing hypothetic laws.

FINITE ELEMENT DISCONTINUITY SIMULATIONS

An implementation of the above approaches into a computer finite element code may be performed in two different ways in which particular forms of finite element mesh should be elaborated.

In the first option the emphasis is put on a zonal refinement of the mesh of usual elements and its stepwise remaking, while in the second one a special kind of joint elements are introduced in order to simulate explicitly the discontinuities. The central conceptual prob-

lem any way consists in a conditioning of the solution by a priori choice of the f.e. mesh. It refers both to the degree of the refinement and to the location of the zone of the refinement.

Both elemental and boundary value problem localization approaches are tractable by the first option. The elemental localization is approached by smearing the effects of the discontinuity over the element by modifying the stress- strain relationship in such a way that the dissipated energy of the cracked and fictitiously continuous element remains the same, Cedolin and Dei Poli (1979), Bazant and Oh (1981).

In the second option the joint elements require a special kind of stress-strain law describing the material behaviour at the discontinuity interface as well as a finite element criterion for formation of a descontinuity derived from a criterion for continuum bifurcation mentioned in preceding sections.

Further discretization problems arise in the vicinity of the fracture tip, see Peano et al. (1979). For a limited number of loading steps the same mesh may employed in a deformed configuration until the aspect ratio of elements remains acceptable. Than a complete reset of the mush must be undertaken.

As seen from the above consideration several numerical technique problems have to be takled with in order to simulate succesfully the discontinuity propagation. Efforts in this direction are under way at ISMES with special application to the discontinuity propagation within the clay formations.

CONCLUSIONS

In this paper we discussed several aspects of mathematical modelling of the propagation of a bed-rock dislocation into clay formation. A general scheme for tackling its adequate mathematical simulation was presented, including various options in dealing with particular problems in the framework of the plasticity theory. Some queries are also risen concerning both theoretical and numerical problems of the simulation of discontinuity generation and propagation by means of the bifurcation approach. They are either common to crack propagation problems in other materials or are particularly referred to the behaviour of clays at significant depths.

Several other important factors concerning pervious fault in clays are not treated herewith, while easily implementable in the general scheme presented. It refers for example to a possibility of drastic increase of dilatancy and permeability in an already fractured zone in clay in the post- critical deformational range due to low cyclic loading, Zoback and Byerlee (1975).

Work is in progress in the above described areas both on theoretical, numerical an experimental aspects.

ACKNOWLEDGMENTS

The work described has been carried ont at ISMES as a part of a research programme supported by ENEA (National Board for Alternative Energies of Italy) and by the Commission of European Comunities.

REFERENCES

Bazant Z.P. and Oh B.H. (1981), Concrete fracture via stress-strain relations, Rep. No 81-10/665c, Northwestern University, Evanston, Illinois.

Cedolin L., and Dei Poli S. (1977), Finite Elements studies of shear critical R/C Beams, ASCE, EM3, vol 103, 395-410.

Hill R., (1958), A general theory of uniqueness and stability in elastic- plastic solids, J. Mech. Phys Solids, 6, 236-249.

Hill R. and Hutchinson J.W. (1975), Bifurcation phenomena in the plane tension test, J. Mech. Phys. Solids 23, 239-264.

Hueckel T. and Maier G. (1977) Incremental boundary value problems in the presence of coupling of elastic and plastic deformations; a rock mechanics oriented theory, Int. J. Solids and structures, 1, 1-15.

Hueckel T. and Nova R. (1981), On cyclic degradation of clays. Rivista Geotecnica Italiana, 15, 1-12.

Maier G. and Hueckel T. (1979), Non-associated and couppled flow rules of elasto-plasticity, Int. J. Rock. Mech. Min. Sci., 16, 77-92.

Morgenstern N.R. and Tchalenko J.S., (1967), Microscopic structures in kaolin subjected to direct shear, Geotechnique, 17, 309-328.

Mroz Z. (1980), Deformation and flow of granular materials, Proc, IUTAM Congress 1980, 119-132.

Nova R. (1982) A constitutive model for soil under monotonic and cyclic loading, n; 13, Soil Mechanics. Transient and

cyclic loads, G.N. Pande and O.C. Zienkiewicz eds., Wiley.

Palmer A.C. and Rice J.R. (1973) The growth of slip surfaces in the progressive failure of over-consolidated clay, Proc. Royal Soc. London, A. 332, 527-548.

Peano A., Pasini A., Riccioni R., and Sardella L., (1979), Adaptive approximations in finite element structural analysis, Computer and Structure, 10, 332-342.

Rudnicki J.W. and Rice J.R. (1975), Conditions for the localization of deformation in pressure sensitive dilatant materials, J. Mech. Phys. Solids, 23, 371-394.

Vardoulakis J. (1981) Bifurcation analysis of the plane rectilinear deformation on sand samples, I.J. Solids Structures, 17, 1085-1101.

Zoback M.O. and Byerlee J. D., (1975) The effect of microcrack dilatancy on the permeability of wester by Granite, J. Geophys. Res. 80., 752-755.

COUPLED PROCESSES IN REPOSITORY SEALING

John B. Case and Peter C. Kelsall

IT Corporation
2340 Alamo SE, Suite 306
Albuquerque, New Mexico 87106

ABSTRACT

The significance of coupled processes in repository sealing is evaluated. In most repository designs, shaft seals will be located in areas of relatively low temperature perturbation, in which case the coupling of temperature with stress and permeability may be less significant than the coupling between stress and permeability that occurs during excavation. Constitutive relationships between stress and permeability are reviewed for crystalline rock and rocksalt. These provide a basis for predicting the development of disturbed zones near excavations. Field case histories of the degree of disturbance are presented for two contrasting rock types - Stripa granite and Southeastern New Mexico rocksalt. The results of field investigations in both rock types confirm that hydraulic conductivity or permeability is stress dependent, and that shaft seal performance may be related to the degree that stresses are perturbed and restored near the seal.

INTRODUCTION

The development of shafts and ramps accessing an underground nuclear waste repository poses the potential problem of creating preferred pathways for radionuclide migration. While plug materials used in sealing may have low permeability, disturbed zones may develop in the adjacent rock as a result of fracturing or stress relief across existing fractures. Over the long term, further disturbance may result from alteration of the thermal, hydrologic and stress regimes. The interface zone between the plug and the rock may also be altered in the long term.

An understanding of coupled processes is necessary to identify technical issues, to perform geologic characterization and laboratory or field testing of constitutive properties, to evaluate performance, and to design seals. This paper presents a discussion of the coupled processes that result in rock disturbance, and describes two field case histories of the degree of disturbance in two contrasting rock types - Stripa granite and Southeastern New Mexico rocksalt. These case histories provide a basis for identifying and resolving technical issues for future work on coupled processes in repository sealing.

During excavation, the state of stress around a shaft or drift will be altered with stress redistribution to the surrounding rock mass. Temperatures in the surrounding rock mass may also be altered as underground forced air ventilation is established. Pore pressures may be reduced if water flow is induced towards the excavation. Following seal construction, the temperature and pore pressure fields may be fully reestablished, and stress fields may be partially reestablished. During repository operation, the temperature, pore pressure, and stress fields are again perturbed with the response of the seal system dependent on proximity to the waste.

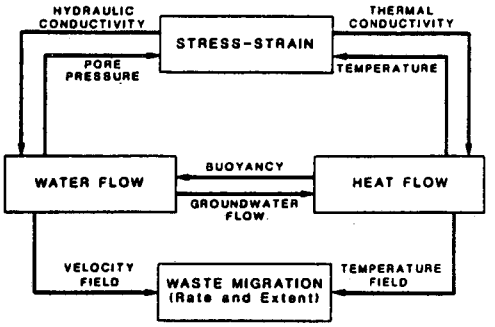

Figure 1. Interrelationship of coupled processes.

The change in field variables (temperature, pore pressure and stress) during the several phases of repository development and operation will result in a general intercoupling of phenomena (Figure 1). The degree of intercoupling will depend principally on the perturbation of field variables and secondarily on coupled constitutive relations. In the very near field (canister scale) or near field (room scale), the degree of coupling between water flow and heat flow during repository operation may be significant. In contrast, the degree of coupling at key seal locations may be less significant during repository operation if the seal components are located further from the waste where there is lower temperature perturbation. Heat transfer analyses have been conducted to predict the rise in temperature at potential seal locations for preliminary repository layouts in crystalline rock and salt (Kelsall et al., 1982a). As illustrated in Figure 2, the rise in temperature at several potential seal locations ranges from 10 to 50°C. At key shaft seal locations the rise in temperature is as small as 10°C when the shafts are located within a shaft pillar away from the waste.

Small temperature rises would be expected to cause small stress and pore pressure perturbations. In contrast, the stress relief occurring during shaft excavation is significant, and affects fundamental constitutive properties for fluid flow (Kelsall et al., 1982b; 1984). Relatively strong crystalline rocks at shallow depths behave essentially elastically, whereby deformations are reversible and there is no failure. At greater depths, the same rock might respond with proportionally greater deformation due to slippage along fractures. In salt, time-dependent inelastic deformations occur and a zone of stress relaxation extends some distance from the excavation. In both cases, constitutive properties that relate stress to permeability may be used to predict the increase

in permeability and the extent of the disturbed zone.

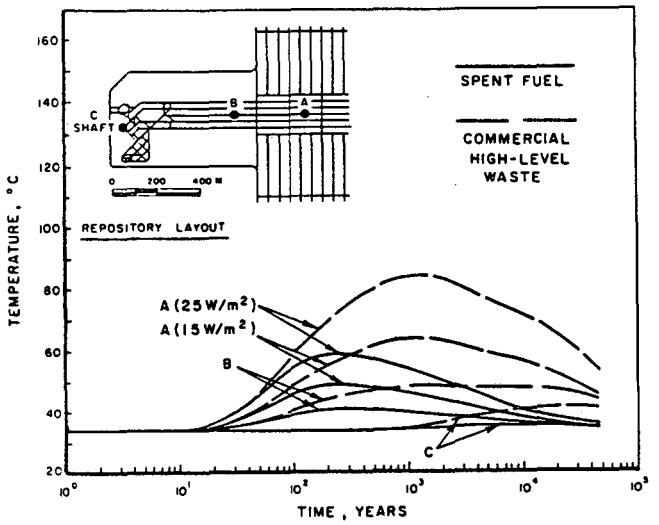

Figure 2. Approximate temperature histories.

In summary, for repository sealing applications, the intercoupling between the various phenomena presented in Figure 1 is dominated by the coupling between stress-strain and water flow that occurs principally during excavation. Stress analysis and coupled stress-permeability relationships may be used to predict the zone of increased permeability.

CONSTITUTIVE RELATIONSHIPS BETWEEN STRESS AND PERMEABILITY

The change in stress state around an opening might affect the permeability of a rock mass in one of three ways: (1) fracturing of originally intact rock due to excessive compressive or tensile stresses; (2) opening or closing of pre-existing fractures due to changes in the normal stresses acting across the fractures or to shearing along the fractures; and (3) loosening of the crystal structure in response to reduced confining stresses. The relative influence of these three processes on the disturbed zone permeability will vary according to parameters such as the size of the opening relative to the fracture spacing, the strength of the intact rock, the in situ stress field, and the shape of the opening. Loosening of the crystal structure may be significant only in relatively weak rocks such as salt.

In strong crystalline rocks such as basalt or granite, consideration is given to the effects on preexisting fractures since it has been found that stress perturbation due to excavation is not sufficient to fracture intact rock at proposed repository depths (Kelsall et al., 1984). The degree to which flow through a fracture will be influenced by stresses acting on the fracture is determined by how the fracture aperture is influenced by stress or, in other words, by the deformability of the fracture. Iwai (1976) proposed the following model for the influence of effective normal stress on flow rate, based on a model for non-linear deformability of a fracture originally proposed by Goodman (1976):

$$\frac{(Q/\Delta h)}{(Q/\Delta h)_0} = \frac{1}{\left[A\left(\frac{\sigma_e}{\xi}\right)^t + 1\right]^3} \qquad (1)$$

where

$Q/\Delta h$ = flow rate divided by head difference at an effective stress σ_e;

$(Q/\Delta h)_0$ = flow rate divided by head difference at zero effective stress; and

A, ξ, t = empirical constants.

Kelsall et al. (1984) evaluated this relationship through the use of the cubic law (Witherspoon et al., 1980) and other relations to obtain a rock mass conductivity relation:

$$\frac{K_e}{K_o} = \frac{1}{\left[A\left(\frac{\sigma_e}{\xi}\right)^t + 1\right]^3} \qquad (2)$$

where

K_e = hydraulic conductivity of the rock mass at effective stress σ_e, and

K_o = hydraulic conductivity at zero effective stress.

The similarity between equations (1) and (2) suggests that the relation K_e/K_o for the hydraulic conductivity of a system of parallel fractures may be obtained from laboratory tests on a single fracture (assuming that all the fractures have the same deformability). Kelsall et al. (1982b, 1984) used Equation (2) to predict changes in hydraulic conductivity near a shaft excavated in basalt. Two models were used for calculation of the stress redistribution. The first model assumed that the rock responds elastically as might occur at shallow depth. In this zone, permeability is expected to increase in the axial direction but reduce in the radial direction. The second model assumed that the rock responds elastoplastically where there is permanent deformation by slippage along fractures in a failed zone adjacent to the penetration. In this zone, permeability is expected to increase in both the axial and radial directions. For a circular shaft at a depth of 1000 m, the permeability parallel to the shaft axis is predicted to increase by one to two orders of magnitude within 1 to 1.5 radii of the wall.

For salt, a number of investigators have examined the relationship between effective stress and permeability (Isherwood, 1981). Lai (1971) presented laboratory data that relate salt permeability to mean confining stress and octahedral shear stress. These tests were conducted in a high pressure triaxial cell, which allowed axial loads and lateral confining pressures to be applied independently. These measurements indicate permeabilities from 10^{-4} to 10^{+2} milldarcy (md) over a range of confining stress between 0 and 40 MPa.

Sutherland and Cave (1980) measured the permeability of Southeastern New Mexico rocksalt using a transient method. They investigated the effects of confining pressure and time and reported permeabilities of between 10^{-2} and 10^{-4} md. They found that permeability decreased with time, even after 500 hours of load application, but they were not certain if the measured reduction represented fracture healing or a reduction of porosity. They suggested that the most representative value for in situ permeability would be obtained from specimens subjected to long-term pressure application.

FIELD INVESTIGATIONS OF ROCK MASS DISTURBANCE

Granite - Evidence regarding changes in permeability around a tunnel in granitic rock was obtained from the macropermeability test conducted at Stripa, Sweden (Wilson et al., 1983). This test was designed to measure the permeability of a large volume of low-permeability, fractured rock by monitoring water inflow into a 33 m long section of a tunnel. Hydraulic gradients around the tunnel were determined by monitoring groundwater pressures in piezometers installed in a total of 90 isolated intervals in 15 radial boreholes drilled from the tunnel. The tunnel was excavated using smooth-blasting techniques at a depth of about 340 m. Fracture frequency measured in holes drilled from the tunnel ranged from 2.9 joints/m to 4.5 joints/m.

Figure 3 shows the hydraulic heads measured in the boreholes plotted vs radial distance from the wall of the tunnel. Nelson and Wilson (1980) calculated an average rock mass hydraulic conductivity from the observed gradient (the slope of the head vs. log-distance plot) and the water inflow monitored in the tunnel. If the weighted average line shown in Figure 3 is projected to the drift wall, it indicates a higher water head than can exist in practice. This indicates that there is a zone approximately 2.5 m thick adjacent to the walls of the tunnel, in which the hydraulic conductivity is reduced by a factor of approximately three relative to the far-field value.

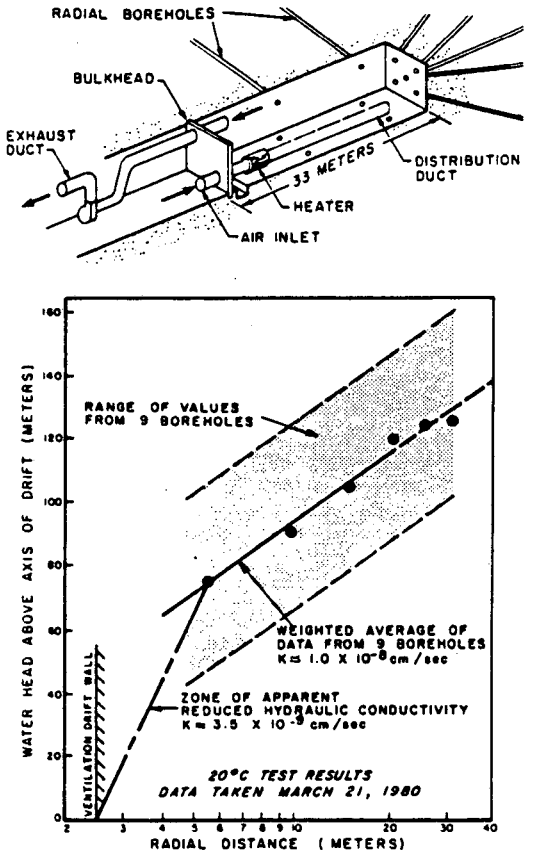

Figure 3. Macropermeability test, Stripa (Nelson and Wilson, 1980). (a) test arrangement; (b) distance drawn on plot at end of 20°C temperature experiment.

Wilson et al. (1983) attributed the apparent zone of lower conductivity at the excavation to compressive rock stresses around the drift, chemical precipitates left in the rock by evaporating water, or two-phase flow from gases coming out of solution. The first hypothesis is tested by comparing the observed changes with those predicted using an analytical approach described by Kelsall et al. (1984). The predicted hydraulic conductivity is derived from the stress-hydraulic conductivity relationship presented earlier and an elastic stress distribution derived from the Kirsch solution. The far-field hydraulic conductivity away from the influence of the room is set as 10^{-8} cm/sec at 20°C. Assumptions made are that the flow to the tunnel is determined largely by radial fractures, and the rock behaves essentially elastically. These assumptions are considered reasonable given that the dominant fractures strike obliquely to the tunnel and that the tunnel is located in good quality rock at relatively shallow depth. Figure 4 shows that the predicted reduction in radial hydraulic conductivity close to the tunnel wall is consistent with the reduction inferred from the macropermeability test. The results apparently validate the hypothesis that increased tangential stresses may reduce hydraulic conductivities in the radial direction although it is noted that the analysis involved several assumptions. The analysis may be extended to predict the increase in permeability that should occur in the disturbed zone in the axial direction.

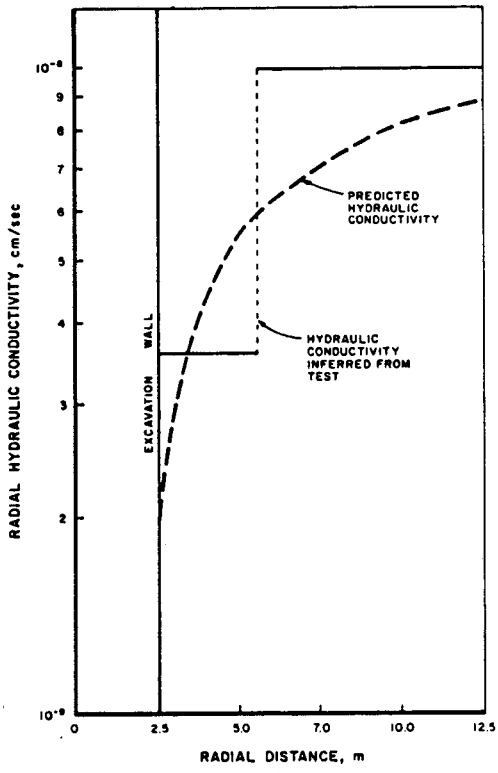

Figure 4. Comparison of hydraulic conductivities predicted by analysis and inferred from field measurements, Stripa macropermeability test.

Further confirmation of the influence of the tangential stress around the opening is obtained by considering the effects of temperature on flow rate into the tunnel. Theoretically, the effect of

heating the tunnel should be to increase the tangential stress and, thereby, to reduce the rate of inflow. A simple analysis of thermal stresses around a tunnel was performed to demonstrate this effect. Temperature distributions around the tunnel were calculated using a closed-formed solution given by Carslaw and Jaeger (1959) for transient heat conduction through a region bounded internally by a cylinder. Thermoelastic stresses were calculated using the relation for tangential stress given by Carlsson (1978) for a temperature rise from 20°C to 30°C. The analysis predicted that increased tangential stress should reduce flow through the disturbed zone by approximately 30%. The observed flow rates (Nelson and Wilson, 1980) were 50 ml/min at 20°C and 42 ml/min at 30°C, a difference of 16%.

Recently, Barton et al. (1985) proposed a joint constitutive model which describes the coupling of conductivity with both shear and normal stress. Their model is based upon simple estimates of the joint roughness coefficient (JRC), the wall strength (JCS), the residual friction angle, and the conducting smooth wall aperture. Empirical relationships were also developed to account for sample size and joint spacing since it has been found that fundamental joint properties are subject to scalar effects. Their analysis indicates that strong rocks, such as basalt or granite, with rough joints typically have high joint normal stiffness and high shear strength leading to strong coupling between shearing and conductivity. These constitutive models (which can be developed without extensive laboratory or field testing) could be used to refine predictions of the increase in permeability in the disturbed zone in crystalline rock.

Salt - Evidence regarding changes in permeability around an entry in salt is obtained from in situ permeability measurements made with a guarded straddle packer system at a depth of approximately 610 m at the WIPP (Peterson et al., 1985). The test horizon is located in a horizontal bed of halite that contains clay and anhydrite layers. The tests were performed to determine the permeability of salt and its variation with distance from the mined surface, and the influence of the interspersed anhydrite and clay seams.

The tests were conducted in vertical boreholes drilled into the roof and floor, and horizontal boreholes drilled into the sidewall, all in a 10 m wide by 4 m high rectangular entry. The guarded straddle packer test system and data reduction technique were designed to measure the low permeability of salt. The downhole measurement system consisted of a dual packer assembly which isolated a test interval at the end of a borehole (1 to 2 m in length) and an adjacent guard interval. Any leakage that occurs near the packer-salt interface is accounted for in the permeability measurements. The combined permeability measurements near the entry are shown in Figure 5, and apparently indicate that there is a relationship of permeability with test interval depth. The data indicate that permeability is reduced by two orders of magnitude (10^{-4} md to 10^{-6} md) over depths of 1 to 14 m. This trend is similar to that predicted by Kelsall et al. (1982b). Since measurements are made for flow in a direction parallel to the drift

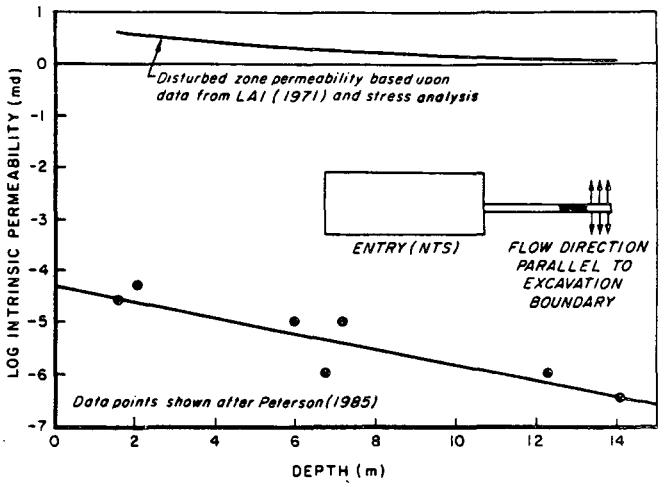

Figure 5. Relationship of salt permeability with depth near an excavation.

excavation surface (Figure 5) and normal to the direction of stress relief, this result is not unexpected.

Predictions of the zone of increased permeability at WIPP are made using the stress permeability relations presented by Lai (1971). Estimates of the amount of stress relief as a function of depth from the rectangular entry may be made using relationships developed by Chabannes (1982). Assumptions or simplifications include that the stress distribution is steady state and based on a secondary creep law, that the excavation is circular in a homogenous salt medium, and that the farfield stress is hydrostatic. The predicted results (Figure 5) show a similar trend to the in situ data, but the absolute values are 4 to 5 orders of magnitude higher. The in situ test results indicate steeper changes in permeability with depth than the predictive analysis. This might indicate that the actual stress distribution is not steady state.

The range of salt permeabilities from laboratory and field tests from several sources is presented in Figure 6. A test conducted on a single crystal by Shelby, as reported by Sutherland and Cave (1980), is also shown. Measured permeabilities reflect a wide variability attributable to a combination of constitutive and experimental/environmental factors. Constitutive factors include differences in salt properties (especially porosities; see Kelsall and Nelson, 1983), the dependence of permeability on stress and time, and stress history (loading and unloading during sample recovery or borehole drilling). Experimental factors include limitations in the resolution of test method and test technique. For in situ tests, Peterson et al. (1985) have cited the importance of testing with a guard zone.

It is interesting to note that sample or test interval disturbance results in a loosening of crystal structure which would increase the measured permeability in both field and laboratory tests. In laboratory testing, stresses are relieved in sample recovery and reapplied during testing. In field testing, stresses are partially relieved in the vicinity of the test zone and partially reapplied during pressure testing. Since laboratory

specimens are subject to more disturbance, laboratory measured values might be expected to be higher than field measured values, except where the latter are influenced by discontinuities. The results of permeability testing illustrated in Figure 6 are consistent with this observation.

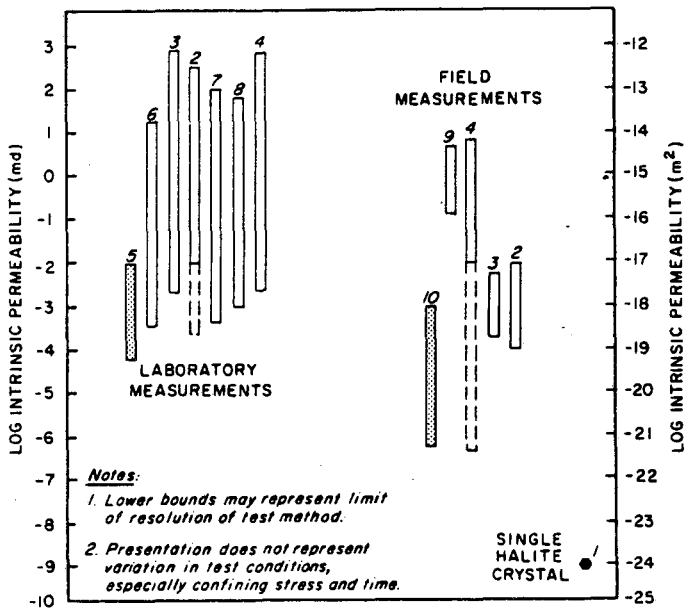

Legend:
1. Shelby, as reported by Sutherland and Cave (1980)
2. Acres (1979)
3. Golder (1977)
4. Aufricht and Howard (1961)
5. Sutherland and Cave (1980)
6. Core Labs (1977)
7. Reynolds and Gloyna (1960)
8. Lai (1971)
9. Thoms and Gehle (1982)
10. Peterson et al. (1985)

Figure 6. Comparison of field and laboratory measurements of permeability of rock salt.

This discussion has been presented to show that the use of values for salt permeability measured by laboratory or in situ testing in performance assessment might overestimate true in situ permeability, and thus underestimate geologic containment in salt, provided that discrete fracture systems are not a dominant flow regime. A further caution regarding interpretation of laboratory and field tests, and application of conventional flow analysis in salt is made by Remson (1984). He cites evidence of non-Newtonian flow where all flow occurs sufficiently close to mineral surfaces to be affected by surface forces. Flow rates are lower than those predicted on the basis of Darcy's Law.

CONCLUSIONS

Stress analysis and constitutive relations derived from laboratory testing can be used to develop disturbed zone models. In crystalline rock, there is reasonable agreement for relatively shallow excavations where the rock behaves elastically. Further validation is required for deeper rocks which might deform inelastically. The effects of shear stress in increasing conductivity in the disturbed zone needs further evaluation.

In salt, current disturbed zone models (Kelsall et al., 1982b) appear to predict the correct relative change in permeability occurring near an excavation. Prediction of absolute permeability is complicated, however, because both in situ and laboratory measurements may be subject to disturbance due to stress relief and the loosening of crystal structure. Measurement of the permeability of salt in the laboratory is not likely to provide results representative of in situ values unless tests are conducted under high confining stress over periods of at least several months. In situ testing methods are preferred because disturbance is less severe and because of the ability to detect fracture anomalies.

In the long-term isolation of nuclear waste in fractured rock, the disturbed zone may represent a significant flow path, and site-specific evaluations of groundwater flow near seal systems such as those carried out by Lundstrom et al. (1985) are required. In salt, fracture healing processes may be important and result in a reduction in permeability. Analyses conducted by Kelsall et al. (1982a) indicate that stresses at the interface of an excavation in salt sealed with a plug will be restored to the far-field stress after 100 years. This stress buildup will reduce the permeability near the excavation by reducing shear stress and increasing mean stress.

The results of field investigations in both crystalline rock and rocksalt confirm that hydraulic conductivity or permeability is stress dependent. Shaft seal system performance is related to the degree to which stresses are perturbed near the seal system. In the adjacent disturbed zone, small changes in stress may be significant in increasing or reducing hydraulic conductivity or permeability. The effects of temperature in seal zones are less significant provided that the seals are isolated from the waste by pillars.

REFERENCES

Acres (1979). "Weeks Island Mine Additional Geotechnical Studies," Acres American, Inc., Buffalo, NY (unpublished report).

Aufricht, W. R., and K. C. Howard (1961). "Salt Characteristics as they Affect Storage of Hydrocarbons," J. Pet. Tech., Vol. 13, pp. 730-738.

Baca, R. G., J. B. Case, and J. G. Patricio (1980). "Coupled Geomechanical/Hydrological Modeling: An Overview of BWIP Studies," Proceedings, Workshop on Thermomechanical-Hydrochemical Modeling for a Hardrock Waste Repository, LBL-11204, Berkeley, CA., pp. 70-80.

Barton, N., S. Bandis, and K. Bakhtar (1985). "Strength, Deformation and Conductivity Coupling of Rock Joints," Int. J. Rock Mech. Min. Sci. & Geomech. Abstr., Vol. 22, No.3, pp. 121-140.

Carlsson, H. A. (1978). "A Pilot Heater Test in the Stripa Granite," LBL-7086, Lawrence Berkeley Laboratory, Berkeley, CA.

Carslaw, H. S., and J. C. Jaeger (1959). "Conduction of Heat in Solids," Clarendon Press, Oxford, England.

Chabannes, C. R. (1982). "An Evaluation of the Time-Dependent Behavior of Solution-Mined Cavities in Salt for the Storage of Natural Gas," M.S. Thesis, Department of Mining, Pennsylvania State University, State College, PA, 150 pp.

Core Laboratories (1977). "Permeability and Porosity Determinations, Cote Blanche Salt Core," prepared by Core Laboratories, Inc., for RE/SPEC Inc., Rapid City, SD (unpublished report).

Golder (1977). "Geotechnical Study of Cote Blanche Island Salt Mine," Vol. 1, Golder Associates, Kirtland, WA (unpublished report).

Goodman, R. W. (1976). "Methods of Geological Engineering in Discontinuous Rocks," West Publishing Co., St. Paul, MN.

Isherwood, D. ed. (1981). "Geoscience Data Base Handbook for Modeling a Nuclear Waste Repository," Vol. 1, NUREG/CR-0912, Lawrence Livermore Laboratory, Livermore, CA.

Iwai, K. (1976). "Fundamental Studies of Fluid Flow Through a Single Fracture," Ph.D. Dissertation, University of California, Berkeley, CA, 208 pp.

Kelsall, P. C., J. B. Case, D. Meyer, and W. E. Coons (1982a). "Schematic Designs for Penetration Seals for a Reference Repository in Bedded Salt," ONWI-405, Office of Nuclear Waste Isolation, Columbus, OH.

Kelsall, P. C., J. B. Case, and C. R. Chabannes (1982b). "A Preliminary Evaluation of the Rock Mass Disturbance Resulting from Shaft, Tunnel, or Borehole Excavation," ONWI-411, Office of Nuclear Waste Isolation, Columbus, OH., 132 pp.

Kelsall, P. C., and J. W. Nelson (1983). "Geologic and Engineering Characteristics of Gulf Region Salt Domes Applied to Underground Storage and Mining," Sixth International Symposium on Salt, Toronto.

Kelsall, P. C., J. B. Case and C. R. Chabannes (1984). "Evaluation of Excavation-Induced Changes in Permeability," Int. J. Rock Mech. Min. Sci. & Geomech. Abstr., Vol. 21, No. 3, pp. 123-135.

Lai, C. S. (1971). "Fluid Flow Through Rock Salt Under Various Stress States," Ph.D. Dissertation, Michigan State University, East Lansing, MI.

Lundstrom, R. A., J. B. Case, P. C. Kelsall, and S. R. Cullinan (1985). "The Influence of the Damaged Zone, Interface, and Various Sealing Components on Shaft Seal Performance for a Repository in Basalt," paper presented at the American Nuclear Society International Topical Meeting on High Level Nuclear Waste Disposal, Pasco, WA.

Nelson, P., and C. Wilson (1980). "Thermo-mechanical and Macropermeability Experiments in the Stripa Granite - Status Report," Proceedings, Workshop on Thermomechanical-Hydrochemical Modeling for a Hardrock Waste Repository, LBL-11204, Berkeley, CA., pp. 45-55.

Peterson, E., P. Lagus, J. Brown, and K. Lie (1985). "WIPP Horizon In Situ Permeability Measurements Final Report," SAND85-7166, Sandia National Laboratories, Albuquerque, NM.

Remson, I. (1984). "Hydrogeologic Overview of the Nuclear Waste Isolation Program," 25th U.S. Symposium on Rock Mechanics, Evanston, IL, pp. 1177-1187.

Reynolds T. D., and Gloyna, E. F. (1960). "Reactor Fuel Waste Disposal Project - Permeability of Rock Salt and Creep of Underground Salt Cavities," prepared by the University of Texas for the U.S. Atomic Energy Commission, Washington, D.C.

Sutherland, H. J., and S. P. Cave (1980). "Argon-gas Permeability of New Mexico Rock Salt Under Hydrostatic Compression," Int. J. Rock Mech. Min. Sci. & Geomech. Abstr., Vol. 17, pp. 281-288.

Thoms, R. L., and R. M. Gehle (1982). "Experimental Study of Rocksalt for Compressed Air Energy Storage," ISRM Symposium, Aachen, May, 1982.

Wilson, C. R., P. A. Witherspoon, J. C. S. Long, R. M. Galbraith, A. O. Dubois, and M. J. McPherson (1983). "Large-scale Hydraulic Conductivity Measurements in Fractured Granite," Int. J. Rock Mech. Min. Sci. & Geomech. Abstr., Vol. 20, No. 6, pp. 269-276.

Witherspoon, P. A., J. S. Y. Wang, and J. E. Gale (1980). "Validity of Cubic Law for Fluid Flow in a Deformable Rock Fracture," Wat. Resour. Res., Vol. 16, No. 6, pp. 1016-1024.

NUMERICAL MODELLING OF COUPLED THERMO-HYDRO-MECHANICAL PROCESSES IN NUCLEAR FUEL WASTE DISPOSAL

T. Chan, V. Guvanasen* and J.A. Keith Reid

Atomic Energy of Canada Limited
Whiteshell Nuclear Research Establishment
Pinawa, Manitoba R0E 1L0
Canada

A three-dimensional (3D) finite-element code, MOTIF (Model of Transport In Fractured/Porous Media), has been developed to model the coupled processes of groundwater flow, heat transport, brine transport, and one-species radionuclide transport in geological media. Three types of elements are available: (1) a 3D continuum element, (2) a planar "fracture" element that can be oriented in any arbitrary direction in 3D space, and (3) a line element for simulating fracture flow in 2D space or pipe flow in 3D space.

As a quality-assurance measure, the MOTIF code was verified by comparison with analytical solutions or other published numerical solutions. These verification problems included: (1) transient flow from a borehole in a fractured porous medium, (2) steady-state flow in a rock mass intersected by fracture zones, (3) free thermal convection in a saturated porous medium, (4) free thermal convection in a Hele-Shaw cell, (5) concentration-driven brine transport in a 2D porous medium, and (6) one-species radionuclide transport along a discrete fracture in a porous rock matrix.

To evaluate the validity of the MOTIF code, it was applied to predict the drawdown and water inflow caused by excavation of the shaft at the Underground Research Laboratory in a granitic pluton on the Canadian Shield. The predictions compared favorably with subsequent field measurements.

Further development is being carried out by enhancing MOTIF into a coupled thermo-hydro-mechanical model. Field evidence and preliminary calculations illustrate the need for developing the 3D coupled hydro-mechanical modelling capability.

*Current Address: GEOTRANS, Inc., Herndon, Va. 22070

COUPLED TRIAXIAL TESTING OF ROCK SALT SPECIMENS

Fred A. Donath, The Earth Technology Corporation, Long Beach, CA 90807
Jon T. Holder, CGS, Inc., Austin, TX 78704
Lester S. Fruth, CGS, Inc., Urbana, IL 61801

ABSTRACT

This paper describes an apparatus that permits simultaneous measurement of several coupled geo-mechanical and geophysical parameters on intact specimens of rock salt saturated with brine and subjected to triaxial test conditions. Representative experimental results are presented for hydraulic permeability, electrical resistivity, and p-wave velocity which were determined while the test specimen equilibrated at a confining pressure of 6.2 MPa (900 psi) and a pore pressure of 2.75 MPa (400 psi), during axial loading and deformation to a total axial strain of 5 percent, and subsequent to the deformation. The results are cross-correlated with the applied (differential) axial stress. The extremely low permeability of rock salt and corrosive nature of saturated brine required development of special sample preparation and jacketing techniques, as well as wetted apparatus parts made from Hastalloy, and the use of the transient pulse technique for permeability determinations.

Measurement of permeability as low as 10 nanodarcy (10^{-20} m^2) were successfully made. Measured pore pressure variations caused by either a pressure step increase or decrease showed excellent reproducibility and agreement with calculated curves. During the last 12 hours of equilibration under confining pressure, the permeability of the salt specimen decreased from slightly more than 1 microdarcy to about 500 nanodarcy; permeability increased to approximately 70 microdarcy after deformation to 5 percent strain. The increase in permeability caused by deformation was accompanied by a decrease in electrical resistivity. Porosity also increased with deformation, as indicated by dilatancy measurements. These observations indicate microfracturing to be occurring for strains above 1.5 percent. The electrical resistivity measurements involved phase-sensitive detection with a 4-terminal electrode configuration, thus permitting determination of absolute values as well as relative changes in electrical resistivity of the salt. Little variation in compressional wave velocity was observed in the brine-saturated salt, in contrast to observations in dry and partially saturated salt specimens.

INTRODUCTION

The laboratory characterization of geologic materials is considerably enhanced by simultaneous measurements of several coupled geomechanical and geophysical parameters in realistic simulations of in-situ conditions. The consideration of salt as a medium for the storage of high-level radioactive wastes has placed particularly high demands on the quality of laboratory data, while many of the geomechanical properties of salt—including those which make it attractive as a storage medium—complicate the laboratory study of its behavior. In particular, salt is very impermeable and the natural pore fluid, brine, is very corrosive. Laboratory deformation studies (e.g., Pfeifle et al, 1984) have been conducted on dry samples, and laboratory permeability measurements (Sutherland and Cave, 1980) have used various gases as the pore fluid. The absence of an electrically conductive pore fluid precludes resistivity studies, but pore water is known to influence the mechanical properties of salt (Horseman, 1983). Few laboratory studies of salt in its natural saturated state have been carried out.

The apparatus described in this paper has been designed to simultaneously measure the axial load, axial strain, volumetric strain, permeability, axial p-wave transit time, and electrical resistance of jacketed 10 cm by 20 cm cylindrical test specimens of salt saturated with brine, during triaxial deformation in simulated geologic environments. The collar-coupled loading column facilitates sample installation and minimizes system complexity, and the compact system has been used to carry out measurements in remote field as well as laboratory locations.

APPARATUS DESCRIPTION

The test apparatus used for this study consists of a triaxial pressure vessel coupled to a 150-ton hydraulic ram by means of a steel collar. The basic design was first introduced some years ago and a description can be found in Donath (1966). The collar-coupling type of loading press is more compact than the tie-bar type and, because it is mobile, can be easily moved to remote locations if desired. The test specimen is jacketed in a flexible rubber membrane and sealed to an upper end cap and piston and to a lower end cap and anvil by o-rings. The specimen assembly is inserted into the top of the triaxial vessel and retained by a top plug screwed into place. The Hastalloy end caps contain the wave velocity

transducers and diffuser plates for pore fluid spreading at the specimen ends. Pressure transducers monitor the pore-fluid pressures, both up- and downstream from the specimen, and the confining pressure. A load cell is placed in series between the ram and the loading piston which enters the bottom of the pressure vessel. Linear displacement transducers monitor the vertical displacement of the loading piston and the piston of the confining pressure syringe-type pump used as a dilatometer by determining fluid displaced from the pressure vessel. The test apparatus can be manually operated or placed under automated control. Electrical outputs of the pressure transducers are amplified by a signal conditioning unit, which also supplies their dc excitation voltage. The amplified outputs, along with the confining fluid and axial displacement signals, are monitored and stored by a microcomputer-controlled data acquisition system. In addition, up- and downstream pore pressure transducer outputs are recorded on a strip chart recorder; axial load and displacement are recorded on an x-y recorder; and analog readouts are provided for ram pressure, confining pressure, and pore fluid pressure.

EXPERIMENTAL PROCEDURES

The preparation of test specimen end surfaces must be carried out with extreme care because large salt grains can be easily dislocated along the edges of the end surfaces. For our test specimens, the specimen surface next to the end is coated with silicone adhesive and a one-half to one-inch length of heat-shrink teflon jacket (preshrunk to the specimen diameter) is placed over the specimen end and secured with a jacket clamp prior to all end cuts. This procedure eliminates almost all grain-scale chipping along the end surface edges.

Because of the low permeability of the salt it is essential that all pore fluid flow between the specimen and the jacket be eliminated. If the outer surface of the test specimen is smooth, soft jacketing material such as viton or rubber membrane conform to the surface well enough to prevent by-pass flow. Most of the cored salt specimens used for our studies have surface variations on the order of a few tenths of a millimeter, and a rubber membrane jacket is not adequate by itself if specimen permeabilities are less than a microdarcy. For our specimens a thin, even coat of silicone adhesive is applied to the specimen surface and allowed to set for one hour before jacketing. A rubber membrane jacket is then mounted, and the assembly is allowed to set for 8 to 12 hours before installation in the test vessel. Pore fluid equilibration times that exceed those corresponding to permeabilities of 10 nanodarcy have been observed with this configuration.

Test specimen deformation properties are determined in this system from the measured axial load, loading-piston displacement, and the volume of confining fluid displaced from the vessel chamber. Procedures and apparatus distortion corrections for the calculation of axial stress and strain are described by Donath and Guven (1971). Volumetric strain is calculated from the confining fluid displacement volume, after correction for the vessel chamber volume change caused by the applied axial load.

Axial p-wave velocities are determined from measured transit times of pulses traveling between transducers located in the end caps, after a correction for the transit time within the end caps (ASTM, 1984).

A uniform axial current density is generated by using the two end caps as current electrodes. The in-phase voltage difference between two (Hastalloy) potential electrodes located along the length of the specimen, one-third the distance from the top and bottom, respectively, is measured with a phase sensitive lock-in amplifier operating at 20 Hertz. Voltage readings are translated directly to corresponding electrical resistances of the specimen region between the potential electrodes by using the voltage across a calibrated decade resistance box in series with the test specimen as the reference signal. This configuration effectively eliminates effects caused by non-ohmic processes within the specimen and by contact potentials at sample-electrode interfaces, and provides a reliable measure of the absolute values of electrical resistivity as well as relative changes in specimen resistivity.

Transient pulse techniques (Brace et al, 1968) must be used to determine the permeability of the salt specimens, which have permeabilities in the range of 10 nanodarcy to 100 microdarcy. Because of the relatively large specimen—and corresponding pore volume—size, the storage capacity of the pore-fluid volume (change in pore fluid volume with pore pressure) must be included

in the analysis of the pore pressure decay. The set of coupled differential equations for the pressure decay has no closed-form analytical solution, but finite difference and series solutions have been developed (Lin, 1977; Trimmer et al, 1980; Hsieh et al, 1981; Trimmer, 1982). Specimen permeability can be determined by fitting measured pore pressure decay curves to the calculated curves.

This procedure is complicated somewhat by the fact that neither the permeability nor the pore-volume storage capacity is generally known prior to a test. However, because the specimen permeability appears in the differential equations only as a linear product with time, a single family of curves of pore pressure vs. logarithm of time can be calculated for different pore-volume storage capacities that can be used for all permeabilities. The calculated curves for a single value of specimen permeability can be translated from their original position along the time axis until they match the measured pore pressure decay curves. The magnitude of the displacement vector is equal to the logarithm of the permeability being measured minus the logarithm of the permeability used for the calculated curves.

The finite difference solution of Trimmer et al (1980), modified to operate with Microsoft Mbasic on a microcomputer, is used to calculate the family of type curves for our permeability determinations. The parameter 'effective porosity' is here defined as $\phi = S/\beta V$ and is used to represent the specimen pore-fluid storage capacity, where S is the storage capacity, V is

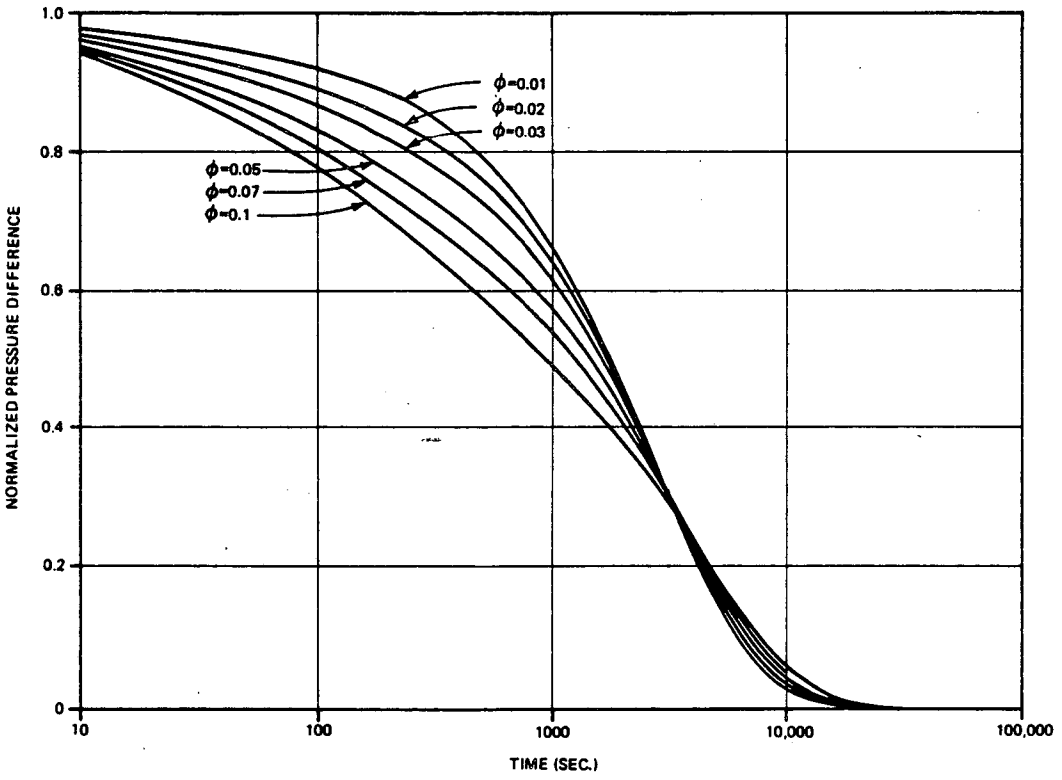

Figure 1. Calculated curves of normalized pressure differences versus log time for the system parameters noted in the text, a specimen permeability of 100 nanodarcy, and the indicated values of effective porosity.

specimen volume, and β is the compressibility of water. The reader is referred to the articles by Trimmer for more detailed discussion of the parameters and relevant expressions.

Although pressure variations in both the up- and downstream pore fluid reservoirs are measured in the testing system, and both should conform to calculated variations, several factors can affect the behavior in each reservoir. For example, fracture porosity and permeability in the test specimens, particularly in freshly cored salt specimens, can be nonuniform over sample dimensions, and temperature variations on the order of $1^{\circ}C$ in the measurement system can generate pore pressure variations on the same order (a few tenths MPa) as those measured in the permeability determinations. However, these factors do not significantly affect the measured differences between up- and downstream pressures, and pressure differences are used for the permeability determinations in our studies.

Figure 1 shows calculated variations in normalized pressure differences for brine flow in 10 by 20 cm cylindrical specimens with a range of effective porosities and a permeability of 100 nanodarcy, for our test vessel which has equal up- and downstream storage capacities of 0.19×10^{-4} l/MPa. Trimmer et al (1980) note that the region between normalized pressure differences of 0.1 and 0.6 is much less affected by differences in the effective porosity, and should therefore be most heavily weighted in the fit to experimental data.

TEST MEASUREMENTS

The following set of measurements on a test specimen from the initial stage of a study of domal salt are presented to illustrate the operation of the test system. The test specimen was cored with brine and maintained in a near-saturated state by waxing the core for shipment. Brine was also used as a lubricant for specimen preparation, and specimen preparation was completed within 24 hours of extraction from the site.

After jacketing the specimen and installing it in the pressure vessel, the pore fluid system was evacuated for a period of one hour. A pore pressure of 2.75 MPa was applied while maintaining an effective pressure of approximately 0.35 MPa; the confining pressure was then raised to 6.2 MPa. The system was allowed to equilibrate for approximately 24 hours.

The electrical resistance and the specimen pore pressure were periodically monitored during the equilibration period. A constant resistance reading indicates specimen saturation and pore fluid equilibration (Trimmer et al, 1980), as well as specimen mechanical stability. The pore pressure variations stabilized to within the range of temperature-induced changes (less than 0.02 MPa per hour) within a few hours, but the specimen resistivity continued to increase in a steady fashion. The resistance across the specimen region between the potential electrodes increased from approximately 2 Kohm to over 10 Kohm in the 24 hour period.

Figure 2 shows pore pressure variations for three sets of measurements on the undeformed specimen. The pressure differences are normalized to the initial pressure step (decreases for curves a and c, increase for curve b) of approximately 0.28 MPa in the upstream pore fluid reservoir, and plotted as a function of the logarithm of time after the step in pore pressure. Data for curve (a) were measured after the specimen had equilibrated for only 12 hours at the test conditions. Measurements corresponding to curves (b) and (c) were carried out within a short period (10 minutes) of one another after the specimen had equilibrated an additional 12 hours. The calculated curves that best fit the data are also shown; both were computed for a permeability of 100 nanodarcy and translated backward (-) along the abscissa to their indicated positions.

The measured variations for the two closely spaced tests are nearly identical, particularly in the 'critical region'. The widely spaced tests indicate that permeability decreased from $1.18 \pm .05$ microdarcy to 500 ± 20 nanodarcy during the last 12 hours of specimen equilibration, while the effective porosity increased from 2 to 3 percent. During this same time period the confining fluid displacement volume indicated a total specimen volume increase of approximately 0.1 percent and the electrical resistivity slightly more than doubled.

The relatively high permeability in the unstressed specimen reflects coring-induced microfracture, which was also apparent from visual observation of the cores. The contrasting porosity and permeability behavior during equilibration indicates that low-asperity microfractures (which limit pore-space interconnectivity) are healing while the larger pore spaces (which contribute most of the specimen porosity) are increasing in size because of pore fluid infiltration during equilibration and/or ambient temperature variation.

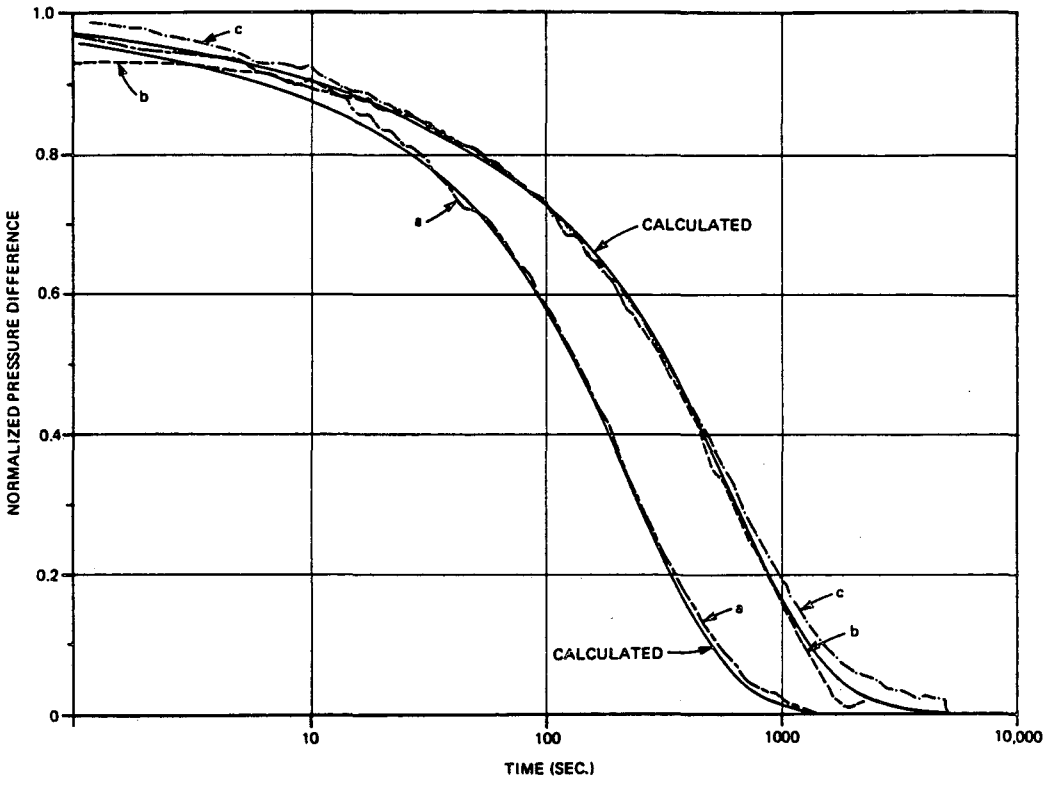

Figure 2. Measured pressure differences, normalized to the initial pore pressure change, versus log time. The solid curves are the best-fit calculated variations; refer to the text for an explanation of measurement curve designations.

The variations in axial (differential) stress, volumetric strain, electrical resistivity, and compressional wave velocity are shown in Figure 3 as a function of axial strain during the triaxial deformation of the specimen at a constant strain rate of 10 per second.

Data for the axial stress and volumetric strain curves were collected automatically at axial strain intervals of 0.02 percent and contributed to the high resolution of the calculated curves (less than 0.01 percent for the volumetric strain). The Young's modulus of 28 GPa and Poisson's ratio of 0.31, calculated from the slopes of the unloading regions of the axial stress and volumetric strain curves, are in the same range as values reported for dry domal salt specimens (Pfeifle et al, 1984).

The electrical resistivity and compressional wave velocity measurements must be made manually; 12 measurements of each were carried out during the deformation to 5 percent total strain. In contrast with the equilibration data, the changes in electrical resistivity and volumetric strain during deformation are opposite in sign, indicating that changes in porosity and permeability are of the same sign. This indicates substantial microfracturing for axial strains above 1.5 percent. Little variation in compressional wave velocity is observed in these saturated salt specimens, in contrast with observed increases on the order of 10 percent for dry and partially saturated specimens during initial deformation (strains below 1 percent). The sensitivity of variations of compressional wave velocity during loading to the degree of saturation is consistent with observations in other rock systems (Johnston and Toksoz, 1980), but the variation in the saturated salt is lower because of its lower porosity.

Transient pulse measurement carried out 24 hours after the deformation indicate a permeability of 70 $\pm$ 10 microdarcy. The permeability increase of almost two orders in magnitude is consistent with the observed resistivity decrease and volumetric strain increase associated with deformation-induced dilatancy. The large uncertainty in the measured permeability reflects the difficulty in fitting the pressure decay curves,

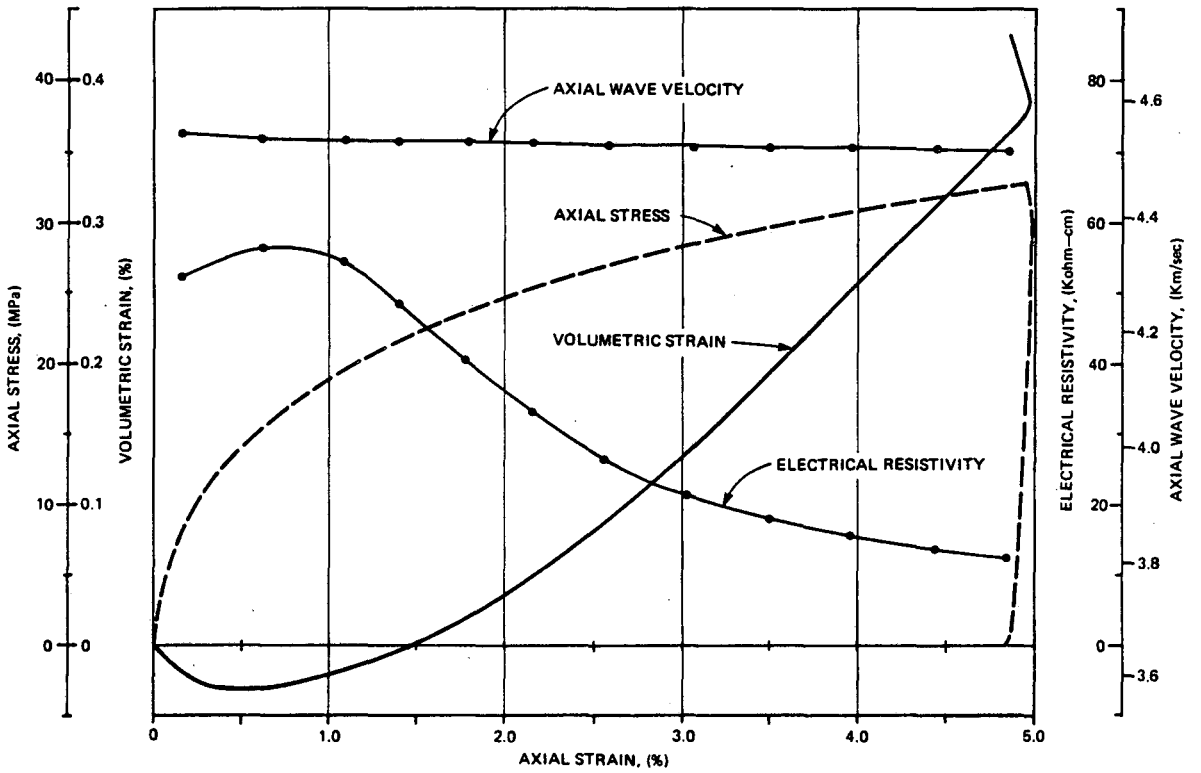

Figure 3. Measured variation in axial stress, volumetric strain, electrical resistivity, and compressional wave velocity as a function of axial strain during triaxial deformation to 5 percent total strain. Confining pressure is 6.2 MPa and pore pressure is 2.75 MPa.

and indicates that this permeability is near the upper limit of the permeability range for which transient pulse techniques can be used in this system.

REFERENCES

ASTM (1984). "Lab determination of pulse velocities and ultrasonic elastic constants of rock". Annual ASTM Standards Book Part 19, 425-432.

Brace, W. F., J. B. Walsh, W. T. Frangos (1968). "Permeability of granite under high pressure". Geophys. Res. 73, 2225-2236.

Donath, F. A. (1966). "A triaxial pressure apparatus for testing of consolidated or unconsolidated materials subjected to pore pressure." Testing Techniques for Rock Mechanics, Am. Soc. Testing Materials Special Publication No. 402, 41-51.

Donath, F. A. and N. Guven (1971). "Data reduction in experimental rock deformation". Contrib. to Geology 10, 89-123.

Horseman, S. T. (1984). "Moisture content--a major uncertainty in storage cavity closure prediction." 2nd Conference on Mechanical Behavior of Salt. Pennsylvania State University, University Park, PA.

Hsieh, P. A., J. V. Tracy, C. E. Neuzil, J. D. Bredehoeft, S. E. Silliman (1981). "Lab method for determining hydraulic properties of tight rocks-I. Theory". Int. J. Rock. Mech. Min. Sci. Geo. Abst. 18, 245-252.

Lin, W. (1977). "Compressible fluid flow through rocks of variable permeability". UCRL-52304 LLNL.

Pfeifle, T. W., K. D. Mellegare, P. E. Senseny (1983). "Constitutive properties of salt from four sites." ONWI-314, 84p.

Sutherland, H. J. and S. P. Cave (1980). "Argon gas permeability of New Mexico rock salt under hydrostatic compression". Int. J. Rock. Mech. Min. Sci. Geo. Abst. 17, 281-288.

Trimmer, D. (1982). "Laboratory measurements of ultra low permeabilities of geologic materials". Rev. Sci. Inst. 53, 1246-1254.

Trimmer, D., B. Bonner, H. C. Heard, A. Duba, (1980). "Effect of pressure and stress on water transport in intact and fractured granite and gabbro". J. Geophys. Res. 85, 7059-7071.

HYDROMECHANICAL MODELLING OF FRACTURED ROCK MASSES USING COUPLED NUMERICAL SCHEMES

Derek Elsworth* and Richard E. Goodman**

*The Pennsylvania State University, University Park, PA 16802
**University of California, Berkeley, CA 94720

ABSTRACT

Coupled boundary element-finite element procedures are presented for the hydraulic analysis of discretely fractured rock masses. The respective analyses evaluate flow in three dimensional, rigid fractured media in the time domain and two dimensional porous-fractured deformable media. For flow analysis, a direct boundary element procedure is invoked to yield the elemental geometric conductance of an individual fissure disc with reduced degrees of freedom. The global matrices are cast in finite element format and extended to the transient domain. Coupled analysis for deformation utilizes an indirect displacement discontinuity formulation to represent the behavior of the fractured elastic continuum. Flow within both fissures and blocks is achieved using a revised boundary element-finite element procedure. The numerical formulations are illustrated, in all cases, to provide a tractable and computationally efficient means of handling spatially large systems of fractures in either two or three dimensional space. Illustrative examples are included to emphasise the capabilities of the methods presented.

INTRODUCTION

The safe immobilisation of radioactive waste in geologic formations requires that predictive techniques and analyses must be capable of extending to time spans of the order of tens of hundreds of years. The most favored host rocks for a repository comprise low permeability formations about which little field and design data are presently available. The very nature of these low permeability and sparsely fractured rock formations negates the application of well tested homogenisation techniques in attempting correlations with "equivalent" continua. This observation is equally valid with regard to both uncoupled flow characterisation and with respect to coupled rock mass deformations. The discrete nature of fracturing within the masses require that revised numerical formulations are available that are capable of efficiently evaluating both uncoupled and coupled flow-deformation behavior.

Consideration within the following will be limited to evaluation of the response of sparsely fractured masses. Representative elemental volume considerations require that, at a certain scale, individual fissures must be modelled discretely (Long, 1983). The large number of fissures comprising a typical section of the rock mass requires that numerical models appropriate to the problem geometry reflect the utmost in computational efficiency. This is necessary if the capacity of currently available hardware is not to be exceeded for even relatively modest realizations of fissure density. Fractured rock masses are genuinely three dimensional with a compatible two dimensional idealisation being difficult to either determine or justify. This situation is further compounded on realizing that any two dimensional analogy of a three dimensional system will always underestimate potential hydraulic conductivity. Two dimensional analyses will, therefore, be expected to err on the unsafe side for the specific task of waste immobilisation predictions.

While discrete modelling of individual rock fissures may be desirable in the near field, the domain external boundaries must also be appropriately represented. For the effective infinite or semi-infinite extent of the mass surrounding a repository, arbitrary truncation of the discretised domain may result in incorrect evaluation of fluid flow or mass displacement fields. It is important that these external boundaries are correctly represented as the radius of influence increases with elapsed time.

For modelling of flow in sparsely fractured rock masses it is convenient if domain discretisation is restricted purely to individual fractures. Boundary element techniques may be invoked, based on a restricted discretisation, to evaluate linear flow and linear elastic deformation of the surrounding body. Nonlinearities with regard to flow turbulence within and inelastic stress-displacement across the individual fissures may be adequately accommodated. For likely repository scenarios, flow turbulence is not considered a major concern although nonlinear rock joint response may be shown to be an important factor.

STEADY ANALYSIS

For an array of randomly distributed fissure discs in three dimensional space, a single fissure disc may be isolated as the basic geometric conduit. An array of three discs is illustrated in Figure 1. The central disc is isolated with appropriate hydraulic connections in two dimensional space in Figure 2. The direct boundary constraint equation for steady linear

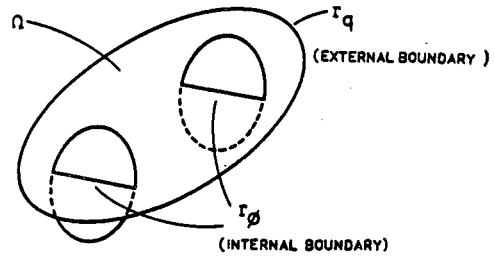

Figure 1. Perspective view of three intersecting fissure discs.

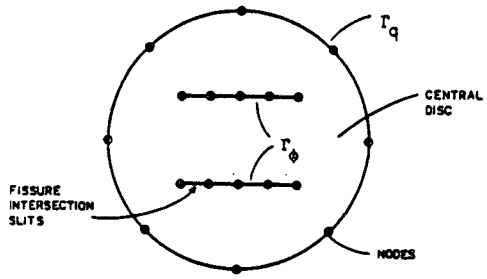

Figure 2. Boundary element representation of the central disc of Figure 1.

potential flow may be stated as (Jawson, 1977; Bannerjee, 1980)

$$c(p)\phi(p) + \int_\Gamma V(p,q)\phi(q)\, d\Gamma = \int_\Gamma \Phi(p,q)v(q)\cdot\bar{n}\, d\Gamma \qquad \ldots(1)$$

where $V(p,q)$, $\Phi(p,q)$ are kernels describing, respectively, induced velocity and total hydraulic potential at point q due to a unit source at point p. The parameters of boundary potential (ϕ) and normal to the boundary velocity ($v\cdot\bar{n}$) are either supplied as boundary conditions or solved for as unknowns. All integrations are evaluated over the surface of the body (Γ) which, for the case of a two dimensional disc, comprises a line segment of closed contour. Intersections within the disc interior may be accommodated where integrations are evaluated taking due account of the free term c(p). Where the source point is present on the smooth boundary, the free term is equal to ½ δpq where δ is the Kroncker delta. For internal elements, the free term is equal to unity.

The integrals of equation (1) may be evaluated either in closed form or numerically. For the isoparametric representation of fissure edge contour and singularity distribution used in this work, numerical integration is necessary. A typical three noded curved element is illustrated in Figure 3. Consistent with the representation of geometry, quadratic basis functions are used in the evaluation of integrals to yield the boundary constraint equation in matrix form as

$$\underset{nxn}{\underline{\Phi}}\ \underset{nx1}{\underline{v}} = \underset{nxn}{\underline{V}}\ \underset{nx1}{\underline{\phi}} \qquad (2)$$

where $\underline{\Phi}$ and $\underline{V}$ are fully populated tensors of integrated kernel functions for potential and velocity, respectively, and $\underline{v}$ and $\underline{\phi}$ are the nodal values of normal velocity and total hydraulic potential. A total of n nodes comprise the external domain boundary. In a well posed problem either boundary nodal velocity or boundary head will be prescribed and equation (2) may be rearranged to solve for the unknowns at respective nodes. For the case of the fissure disc the external normal boundary velocity is zero although no prescribed conditions are set at the internal nodes. Symbolic rearrangement of equation (2) yields (Zienkiewicz, 1977b)

$$\underline{v} = [\underline{\Phi}^{-1}\ \underline{V}]\ \underline{\phi} \qquad (3)$$

which, for the case of m internal nodes, is equivalent to solving n + m simultaneous equations for m load cases. The resulting matrix is m x m in dimension and bears a basic facsimile to finite element format being symmetric and positive definite. Thus

$$\underline{q} = \underline{f}\ [\underline{\Phi}^{-1}\ \underline{V}]\ \underline{\phi} \quad \equiv \underline{q} = \underline{k}\ \underline{\phi} \qquad (4)$$

where $\underline{q}$ is a vector of nodal discharges and $\underline{f}$ is a vector of integrated basis functions relating nodal velocities to discharge. In the condensation procedure the external edge degrees of freedom are redundant and the internal degrees of freedom may be reduced to a minimum of one per intersection. Global assembly may be completed in standard finite element fashion to yield a reduced degree of freedom system.

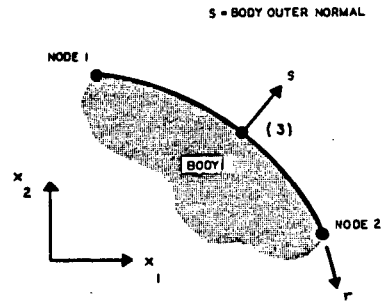

Figure 3. Isoparametric form of a single three-noded line element.

APPLICATION

To emphasize the potential of the proposed formulation, consider the network illustrated in Figure 4(a). The system comprises a total of six circular fissure discs and a single vertical square fissure. All circular disc sets are arranged with equal separation in their respective orientations. The single rectangular disc intersects all circular fissure discs and provides hydraulic connection between them in addition to the horizontal trace intersections between the circular discs. The discretised forms of two typical discs are illustrated in Figure 4(b), the full network comprising 57 nodal degrees of freedom. Although it is possible to further condense the system degrees of freedom, accurate mapping of potential gradient within the system requires that sensible nodal density be retained.

For the 57 node system it is possible to rapidly analyse a number of different hydraulic scenarios for contrasting relative conductivities of the discs. The parallel plate analogy in any convenient linear form may be used to obtain suitable values for disc hydraulic conductivity from fissure aperture and roughness. Nodal meshing input data preparation is not excessive. Matrix reduction to obtain the reduced degree of freedom system took 50 CPU seconds on a DEC Vax 11/780. This step has only to be completed once, the tensors for increased fissure conductivity being scalar multiples of the original disc tensors. Global matrix assembly and LU factorization took 13 CPU seconds with an additional 3 CPU seconds required per additional execution case.

The results for sample runs on the fissure geometry illustrated in Figure 4(a) are illustrated in Figure 5. A unit drop in hydraulic potential is applied between the intersection traces identified in Figure 4(a). Transmissivities (K_h, K_v) for the circular discs are arranged for two comparative cases as both isotropic (K_h, K_v = 1.0) and horizontally dominant (K_h/K_v = 100.0). The transmissivity of the backing square fissure is varied throughout.

Under the unit head differential, the importance of accommodating the truly three dimensional nature of the fissure geometry is illustrated. The baseline characteristics for the hydraulic behavior of both a two-dimensional lattice and the vertical square fissure are illustrated. Where the square fissure provides poor hydraulic connectivity (K_h/K_v < 0.1) the assemblage behaves in an essentially two-dimensional manner. As the hydraulic conductivity of the backing disc is increased, the performance of the system is dominated by this major structural feature. Lack of account for the influence of this feature in evaluating the hydraulic response of the medium would clearly be inappropriate. The errors that this neglect may entrain into the analysis could clearly overshadow the applicability of a more complex two dimensional analysis accounting for the hydromechanical behavior of rock fissures. An important consideration in selection of an

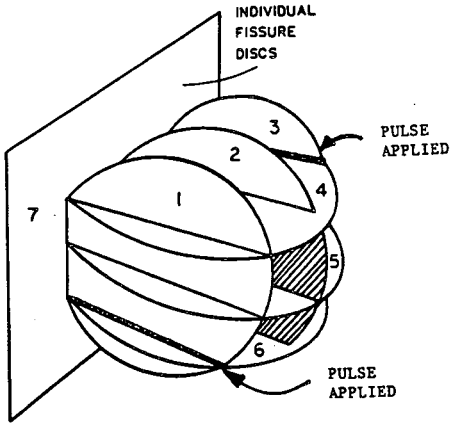

Figure 4(a). Perspective view of seven disc assemblage.

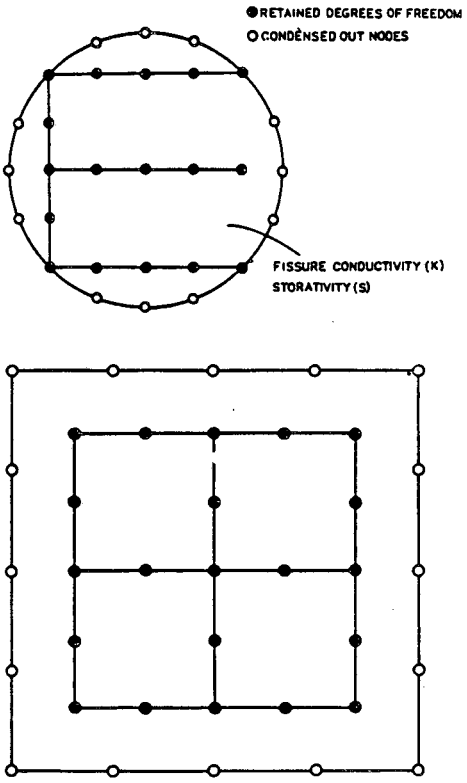

Figure 4(b). Representative constituent discs.

appropriate level of modelling "sophistication" might therefore include spatial dimentionality of the analysis.

TRANSIENT ANALYSIS

In finite element form, the transient response of a system at any moment in time (t) may be represented by the matrix identity.

$$\underline{K}\,\underline{\phi}_t + \underline{S}\,\dot{\underline{\phi}}_t = \underline{q}_t \qquad (5)$$

where $\underline{\phi}_t$ and $\dot{\underline{\phi}}_t$ are respectively vectors of total head and time derivative of head. Prescribed nodal discharges (q_t) are known boundary conditions and $\underline{K}$ and $\underline{S}$ are tensors of geometric conductance and storativity. Stability

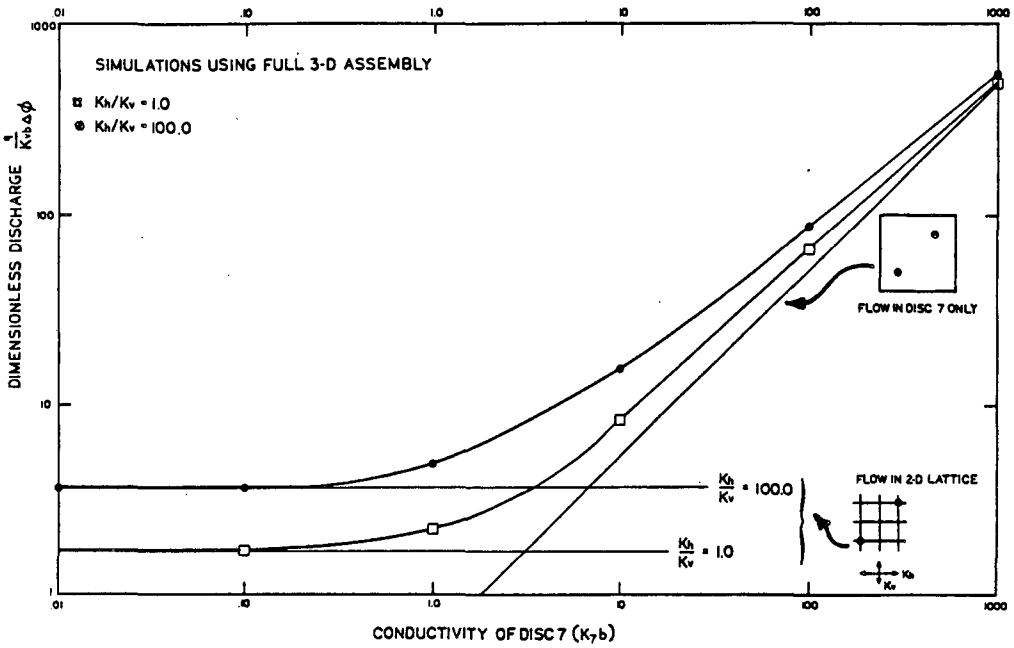

Figure 5. Variation in steady discharge through the fissure assemblage with varied component conductivities.

considerations dictate that a lumped vector of storativity terms (Newman, 1977) is used whereby equation (5) may be rearranged to yield

$$\underline{K}^* \underline{\phi}_{t+\Delta t} = \underline{q}^*_{t+\Delta t} \qquad (6)$$

where $$\underline{K}^* = (\underline{K} + \underline{S}/\Delta t) \qquad (7)$$

$$\underline{q}^*_{t+\Delta t} = q_{t+\Delta t} + \underline{\phi}_t \underline{S}/\Delta t \qquad (8)$$

Linear variation in nodal head within a single time step is assumed, the integration scheme being unconditionally stable for any time increment Δt (Polivka, 1976).

The sum of entries within the elemental storativity vector must equal the total domain storativity. For closed contour problems, such as the fissure disc application, the total storativity for the domain is the product of area integral, mean fissure aperture and specific storage. This total must then be distributed between nodes in any acceptable fashion. Nodal weighting of the storativity terms may be achieved using finite element basis functions if elements are meshed throughout the disc (Zienkiewicz, 1977a). This would, however, be counterproductive in that development of the solution procedure is motivated by the ease with which element meshing may be achieved. Any tributary area distribution technique may be adopted. It has been found satisfactory to distribute the total storativity between nodes based on the magnitude of the diagonal terms of the elemental geometric conductivity matrix, $\underline{K}$ (Elsworth, 1985). Since the nodal weightings used in finite element analysis are somewhat arbitrary, the consequences of the chosen distribution procedure are minimised providing large numbers of discs comprise a complete network.

The matrix identity in equation (6) requires that the $\underline{K}^*$ matrix is factored only once. The variable form of the prescribed discharge vector ($\underline{q}^*$) represents successive loading cases for which backsubstitition yields the time-updated magnitudes of nodal potentials ($\underline{\phi}_{t+\Delta t}$).

APPLICATION

For the model network illustrated in Figure 4(a), the transient performance is gauged using this compacted scheme. The execution times quoted in the previous section for steady flow are representative for the transient condition with solution for a single additional load case being equivalent to integrating forward a single time step. The time marching scheme has been shown capable of representing the transient performance of a single disc with only one degree of freedom retained per intersection (Elsworth, 1985). For the model geometry of Figure 4(a), a distinct advantage is obtained in accurately mapping changes in domain potential if multiple nodes are retained. The reduced system is retained at 57 nodes with a unit pulse applied at the basal intersection (Figure 4(a)) and all other outlets sealed.

Transient response curves for the sealed domain are shown in Figures 6 and 7 for the variety of mixed conductivity conditions of the steady analyses. The transient hydraulic response of the system for homogeneous conductivity in the six circular discs is shown in Figure 6. Curves A through C are respectively for the behavior of the lattice only, the square disc only and the combined lattice and square disc. The highest initial time history of

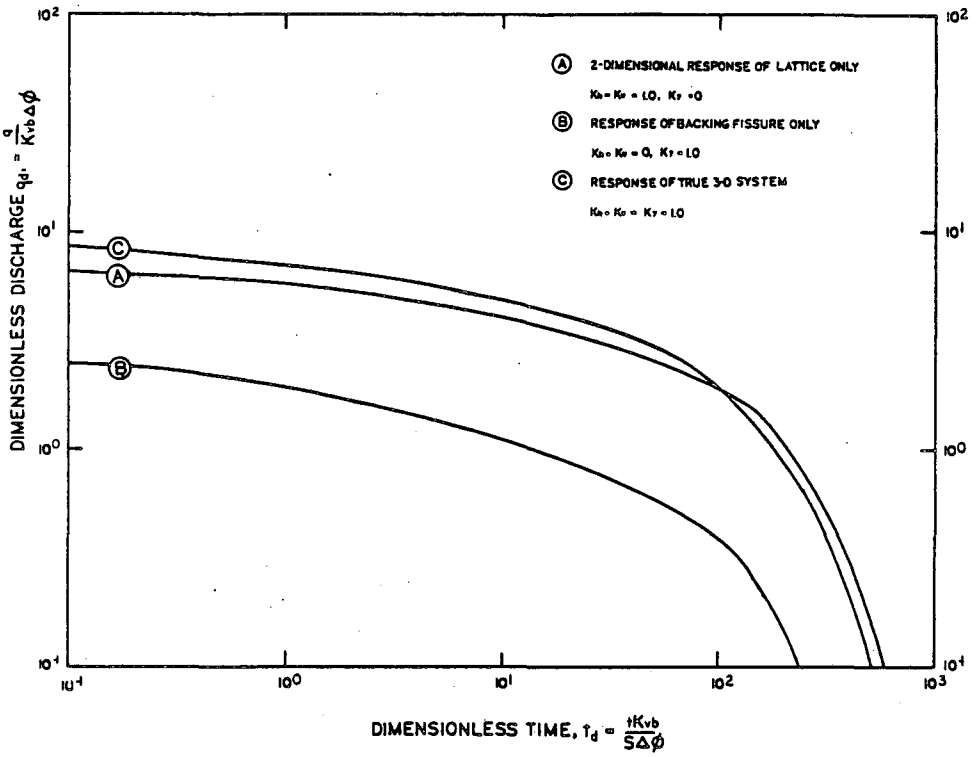

Figure 6. System transient response for two and three dimensional analyses.

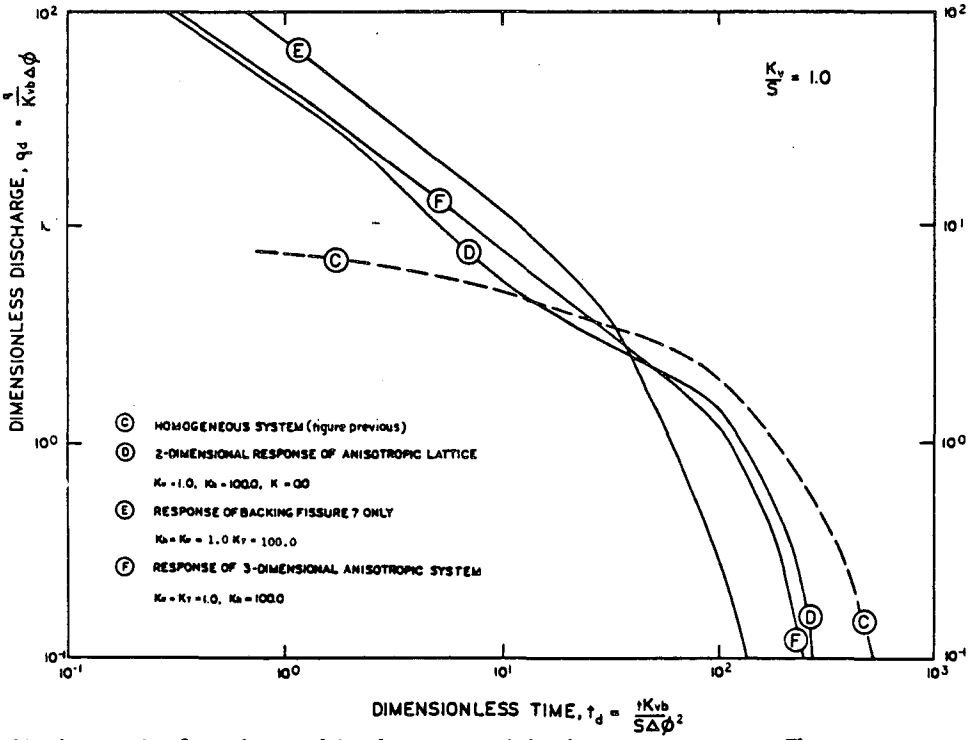

Figure 7. System transient response for anisotropic domain analyses.

discharge is for the combined system with the next highest being for the two dimensional lattice alone. This behavior might be expected if it is noted that discharge from the crossed lattice is along a specific length. The lowest of the discharge histories is for the single square disc alone. The sluggish response of the system at early dimensionless times (t_d < 1.0) is a facet of the numerical analysis. The initial perturbation gradient within the disc system is controlled, to great extent, by the nodal spacing within discs. Hence, the early time performance is strongly controlled by this factor.

The response scenarios are investigated for non uniform conductivity within discs in Figure 7. Curves D through F represent the behavior of the system with; (D) high conductivity of the horizontal discs (K_h/K_v = 100, K_7/K_v = 0.0) with no backing square fissure, (E) uniform conductivity of the lattice with the backing disc of much higher conductivity (K_h/K_v = 1.0, K_7/K_v = 100.0), and (F) high conductivity of the horizontal discs with the backing fissure of unit conductivity (K_h/K_v = 100, K_7/K_v = 1.0). The presence of a highly conductive backing fissure is shown to accelerate drainage and ultimate depletion of the system. A similar effect is

evident where high horizontal conductivity is apparent. With no backing fissure, the system response exhibits a definite discontinuity at dimensionless time of $t_d = 10$. This represents full drainage of the horizontal fissures with the low conductivity vertical system beginning to contribute to the supply. This discontinuity in behavior is masked where the backing fissure is present to aid discharge.

For curves D through F of Figure 7 the spurious numerical response in the initial drainage period (small t_d) is not evident. This factor is as a result of the high conductivity of single network components giving a lateral shift to these data. The restriction of accurate modelling at small dimensionless times is not considered a serious detraction from the practical applicability of an otherwise promising technique. If the response of a large volume of rock mass is required then, by definition, the finite transit velocity of the perturbation pulse infers that the late behavior is of most significance. The generality of formulation further allows increased meshing density in regions where transient gradients are likely to be excessive. Refinements of this nature are only relevant if viewed relative to the quality of geologic data available.

COUPLED FLOW-DETERMINATION ANALYSIS

Emphasis within the previous has been to illustrate the applicability of boundary element formulations in reducing system degrees of freedom to a minimum. Where the analysis is extended into the realm of rock mass deformation this basic premise may be adhered to if the nonlinear rock fissure deformation response is restricted only to the discontinuity traces in two dimensions.

Of the available point force and point displacement formulations available the displacement discontinuity method is most applicable. The basic kernel function is a point discontinuity in displacement from which the induced stresses and displacements in the surrounding medium may be determined (Wiles, 1982). The method is particularly suited to analysis of fissured media in that the point shear and normal singularities represent the physical properties of shear displacement and aperture change across individual joints. The basic matrix identity for two dimensional analysis is (Crouch, 1976)

$$\begin{bmatrix} \sigma_n \\ \tau \end{bmatrix} = \begin{bmatrix} A_{nn} & A_{ns} \\ A_{sn} & A_{ss} \end{bmatrix} \begin{bmatrix} D_n \\ D_s \end{bmatrix} \qquad (9)$$

where σ_n, τ are total normal and shear stresses induced in the medium by unit nodal normal and shear displacement discontinuities D_n, D_s. The linking $\underline{A}$ matrix contains the appropriate integrals of kernel functions. Appropriate magnitude of the stress vector terms may be obtained from the known field stresses and required boundary conditions. Where linear joint stiffness in closing is accommodated a further solution constraint is added such that

$$\begin{bmatrix} \sigma_n \\ \tau \end{bmatrix} = \begin{bmatrix} K_n & 0 \\ 0 & K_s \end{bmatrix} \begin{bmatrix} D_n \\ D_s \end{bmatrix} \qquad (10)$$

where K_n, K_s are the linear fissure stiffnesses under normal and shear loading. Solution of (9) subject to (10) yields a distribution of fissure apertures for which the flow field may be evaluated. Linearly varying displacement discontinuities and linearly tapering fissure finite elements are used in the analyses presented. Previous analysis using constant displacement discontinuities and constant fissure flow elements within impermeable wall rock has been reported (Cruikshank, 1979).

For two dimensional analysis an example porous flow domain containing a single, centrally discharging fracture is illustrated in Figure 8. The formation hydraulic conductivity (K_m) is set to unity. A unit head differential is set between the producing wellbore at the fissure centre and the outer boundary at radius 50 meters. The porous domain is represented exclusively by boundary elements. Dipole flow elements are meshed on the internal fracture extent to which linearly tapering line flow elements are connected. Linear displacement discontinuity elements are meshed along the fracture length.

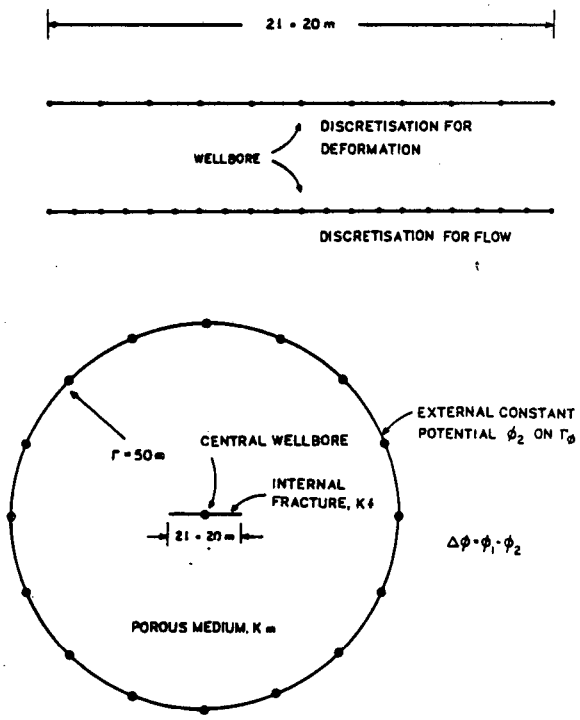

Figure 8. Discretisation for deforming fracture flow. Central fissure discretisation above.

For uncoupled solution, the variation in potential head with length along the fissure is illustrated for different apertures and hence conductivity in Figure 9. For an impermeable fissure ($K_f = 0$), the head variation corresponds to radial, porous media flow. For increased conductivity of the fissure, the flow patterns are increasingly dominated by the presence of the conduit. Where the equivalent fissure conductivity exceeds formation conductivity by a factor of 10^4, the fracture acts as a conduit of infinite conductivity.

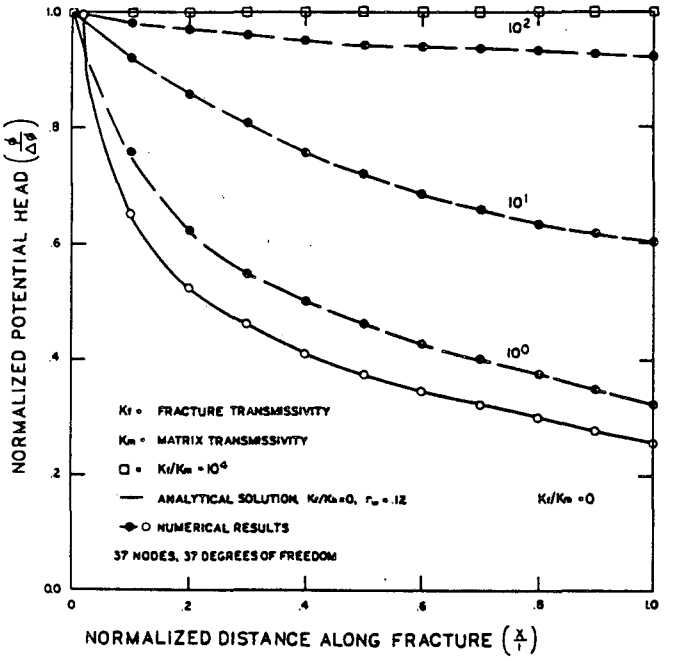

Figure 9. Variation in potential along the fracture of Figure 8, for different fracture conductivities.

The effect of including rock mass deformability within the analysis is illustrated for the single fissure geometry in Figure 10. For fluid injection, hydraulic opening of the fissure is illustrated to have a profound effect on the head distribution along the feature. The aperture distribution in opening is controlled by the elastic parameters of the intact rock. The resistance to opening under a prescribed increase in fluid pressure is increased with increased stiffness of the surrounding mass. All solutions were completed retaining 37 flow and 22 displacement degrees of freedom. Coupled solutions were completed in under 60 seconds CPU time on a DEC Vax 11/780.

DISCUSSION AND CONCLUSIONS

A variety of coupled models are presented that are capable of efficiently analysing two and three dimensional flow problems in porous and fractured media. Coupling of boundary element and finite element procedures are shown to provide optimisation in solution efficiency where the innate advantages of each formulation are emphasised. Consistent use of appropriate element basis functions provides compatibility between all formulations presented and the

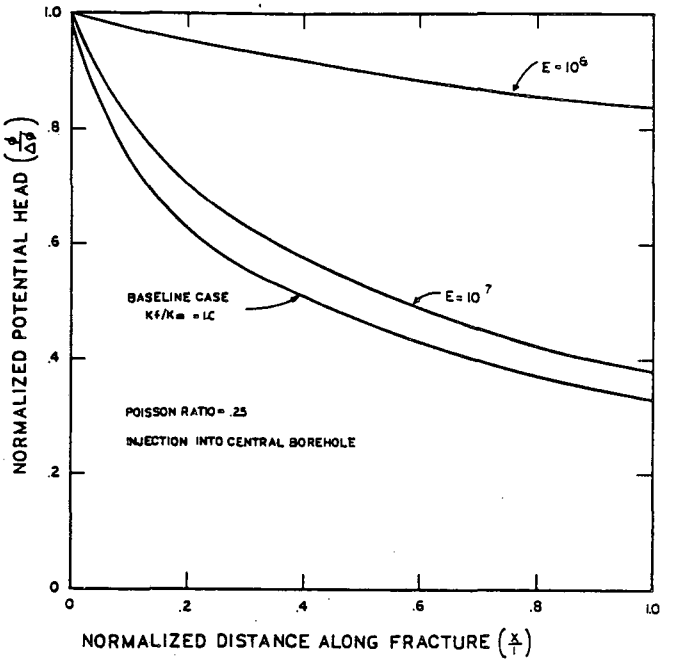

Figure 10. Variation in normalised potential along the fracture of Figure 8 for coupled hydromechanical analysis.

coupled flow deformation analyses. Ease of data input and minimised global equation size is maintained using the boundary element procedures. The displacement discontinuity matrices are in all cases fully populated. Where coupled procedures are used to condense the elemental conductivity matrices for individual fissure discs, the resulting matrices are, in all cases, positive definite, symmetric and sparsely populated. The reduction procedure retains computations at an elemental or disc level prior to global matrix assembly. As such, the procedure is ideally suited to mini or micro-computer implementation.

Considerable insight into the projected hydromechanical behavior of rock masses may be afforded by coupled numerical models. Coupled numerical schemes offer strong computational advantages over more generally used methods. The complexity of rock masses and truly three dimensional extent of the structural features dictate that truly three dimensional models should be employed. Extension into the third dimension requires that maximum coding and formulation efficiency is maintained. Coupled finite element-boundary element procedures have the potential to achieve this goal.

The example results for three dimensional analysis in a rigid fractured rock mass illustrate the importance of considering out of plane features. Both steady discharge and the transient response are influenced by a major throughgoing feature. Behavior is truly three dimensional and does not readily conform to a two dimensional analogue. The errors that may be entrained by not considering the true extent of the structural features may possibly outweigh the advantages of completing coupled analyses in two

dimensions. Judicious use of all available techniques is clearly desirable to aid successful location and commissioning of a terminal waste facility.

ACKNOWLEDGEMENTS

The work was supported by the Director's Fund of Lawrence Berkeley Laboratory under contract DE0AC03-76SF00098 and by the National Science and Engineering Research Council of Canada under grant A4762.

REFERENCES

Bannerjee, P. K. and Butterfield, R. (1981) "Boundary Element Methods in Engineering Science," McGraw-Hill (U.K.).

Crouch, S. L. (1976) "Analysis of Stresses and Displacements Around Underground Excavations: An Application of the Displacement Discontinuity Method," RANN Program, National Science Foundation.

Cruickshank, D. J. and Curran, J. H. (1979) "A B.I.E. Approach to Modelling Fluid Flow in Discontinuous Rock Masses," Proceedings of the Seventh Canadian Congress of Applied Mechanics, Sherbrooke, 887-888.

Elsworth, D. (1985) "The Transient Hydraulic Response of Three Dimensional Sparsely Fractured Rock Masses," University of Toronto, Department of Civil Engineering, Internal Report.

Jawson, M. A. and Sym, G. T. (1977) "Integral Equation Methods in Potential Theory and Elastostatics," Academic Press.

Long, J. C. S. (1983) "Investigation of Equivalent Porous Medium Permeability in Networks of Discontinuous Fractures," Ph.D. Thesis, University of California, Berkeley.

Neuman, S. P. and Narasimhan, T. N. (1977) "Mixed Explicit-Implicit Iterative Finite Element Scheme for Diffusion Type Problems: I. Theory," Int. Journ. for Num. Meth. in Eng., VII, 309-323.

Polivka, R. M. and Wilson, E. L. (1976), "Finite Element Analysis of Nonlinear Heat Transfer Problems," Department of Civil Engineering, University of California, Berkeley, UCSESM 76-2.

Wiles, T. D. and Curran, J. H. (1982) "A General 3-D Displacement Discontinuity Method," Proc. 4th Int. Conference on Numerical Methods in Geomechanics, Edmonton, 103-111.

Zienkiewicz, O. C. (1977) "The Finite Element Method," Third Edition, McGraw-Hill (U.K.).

Zienkiewicz, O. C., Kelly, D. W. and Bettes, P. (1977), "The Coupling of the Finite Element Method and Boundary Element Procedures," Int. J. for Num. Meth. in Eng., VII, 355-375.

A COUPLED MODEL FOR FLUID-DRIVEN FRACTURES

F. E. Heuze, R. J. Shaffer and A. R. Ingraffea*

Lawrence Livermore National Laboratory
Livermore, CA

Cornell University*
Ithaca, NY

ABSTRACT

The Unconventional Gas Program at Lawrence Livermore National Laboratory [1] is pursuing research in the stimulation of tight gas reservoirs. The enhancement of gas recovery is based on creating large induced fractures in an otherwise naturally jointed medium. The mechanics of stimulation involve the coupling of fluid flow, rock deformation, non-linear joint behavior and mixed-mode fractures mechanics. We have developed a finite element model, FEFFLAP [2-4] which accounts for the coupling of these various mechanics and we have verified it on physical experiments.

INTRODUCTION

Considerable quantities of natural gas are locked tightly into gas formations in the Western Gas Sands and the Eastern Devonian Shales of the U.S. In the Western Gas Sands, the gas is localized in sandstone lenses that are embedded in shale. Figure 1 is an aerial view of an area near Glenwood Springs, Colorado, where deep formations outcrop; the demarcation between sandstone lenses and shale is clearly visible. This formation is typical of geology at depth in the tight gas sands of western Colorado.

To recover this gas, it is necessary to "stimulate" the rock reservoirs, that is, to produce large, man-made fractures that penetrate the reservoirs and drain the gas toward wells. Fractures can be created either by injecting fluids under pressure (hydrofracturing) or by burning solid propellants in the wells. To use either technique effectively, one must be able to predict how the rock will fracture.

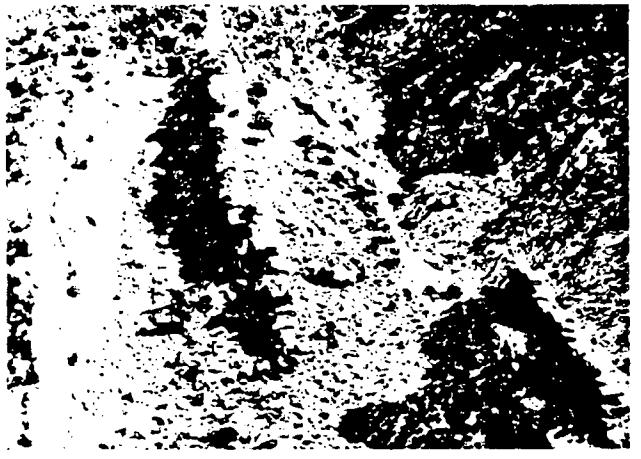

Figure 1. Aerial view of a gas-bearing sandstone lens embedded in nonproductive shales near Glenwood Springs in western Colorado.

Rock reservoirs contain extensive natural fractures and joints, making it difficult to predict the effects of induced fracturing. An analysis of fracturing in such a medium must include a realistic characterization of the joint systems and preexisting cracks that are packed with infill material. The joints are subject to compressive and shear forces; when compression increases, the joints become stiffer, and if shearing becomes too large, slippage occurs. Consequently, in a realistic model, joint properties must change with applied stress. In the Western Gas Sands, interfaces are the regions where shales and sandstones meet, and these interfaces can be treated like joints.

FINITE ELEMENT MODEL

We have developed a computer code, FEFFLAP (Finite-Element Fracture and Flow Analysis Program), that has enabled us to make great progress in describing the complex physics of fluid-driven fracture propagation in jointed media. The coupled FEFFLAP model includes solid mechanics, fracture mechanics, and fluid mechanics. FEFFLAP has been developed from three main sources: FEFAP, an elastic finite element model that has sophisticated fracture mechanics and computer interactivity with the user, [5], JPLAXD for the nonlinear joint elements [6], and JTFLOW, an LLNL enhanced version of an earlier model for fluid flow in rocks [7]. FEFFLAP treats one dimensional, viscous, aperture-dependent flow through cracks and joint systems. The fluid mechanics and the solid/fracture mechanics are coupled in the code. Fluid flow provides pressures that are used as boundary conditions in the solid/fracture model and the solid/fracture model provides apertures that are needed to determine fluid flow.

Whereas in many hydrofracture models, the cracks are assumed to go straight, in FEFFLAP the cracks are allowed to curve according to any one of three mixed-mode fracture-mechanics theories. In standard numerical models, sequential cracks are difficult to handle because the zoning must be manually changed to accommodate each new crack increment. In our model, this rezoning is done automatically and so is nodal renumbering, to conserve computation time.

VERIFICATION AND RESULTS

The fracture mechanics in FEFFLAP have been tested with analytic solutions [3]. We also performed laboratory experiments to verify our model [4,8]. We used steel platens to compress

cubes constructed of two hydrostone materials separated by a slanted interface. The blocks were then fractured by pressurizing oil in a borehole (Fig. 2). The induced fractures sometimes crossed the interface and sometimes stopped at it. We have reproduced both results with FEFFLAP.

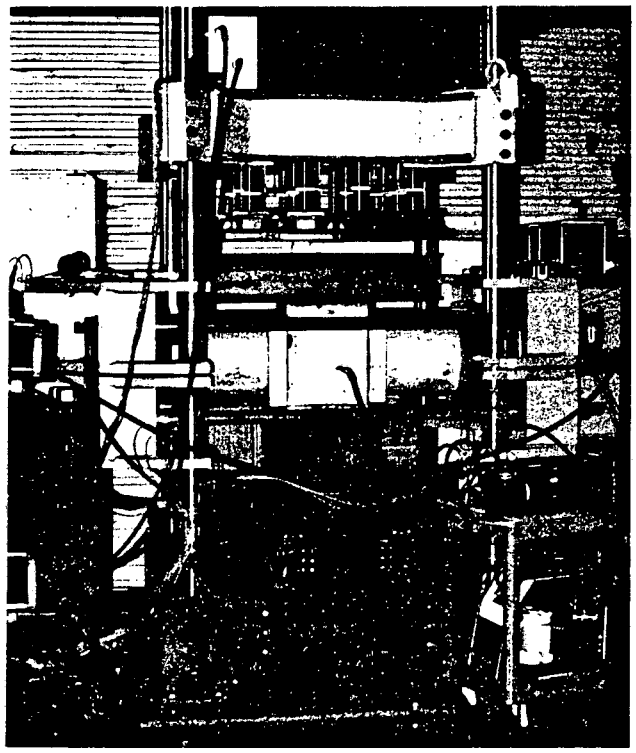

Figure 2. Typical LLNL experiment designed to test our FEFFLAP model. The two hydrostone blocks were compressed with steel platens and fractured by pressurizing oil in a borehole. Some induced fractures crossed the interface of the blocks.

Figure 3 shows the kind of realistic field problem FEFFLAP was designed to solve. In this case, there is a joint system (heavy lines) around a borehole, and the ends of the two discontinuous joints are treated as points of possible crack extension. The sequence illustrates successive steps in the analysis. In this example, the fluid flows into a preexisting joint system; in other cases, the induced crack may cross the first interface. This numerical calculation also showed, for the first time, a phenomenon that had been predicted only analytically: the advancing crack front tends to open the natural fracture by inducing tensile stresses ahead of itself.

Sandia National Laboratories, Albuquerque, is currently conducting the Multi-Well Experiment in the Western Gas Sand formations near Rifle, Colorado, at a depth of several thousand feet. Three proximate wells have been drilled, and one has been hydraulically fractured. The progress of a hydrofracture in one well was monitored from a second well by passive seismic means. Sandia found that the seismic noises originated from a zone between 6 and 24 m wide, considerably greater than the original fracture width (about 2.5 cm). FEFFLAP can demonstrate (see Fig. 3) how a large volume of rock may react to a single hydrofracture injection, and we are using it to help explain the above observations at the Multi-Well Experiment.

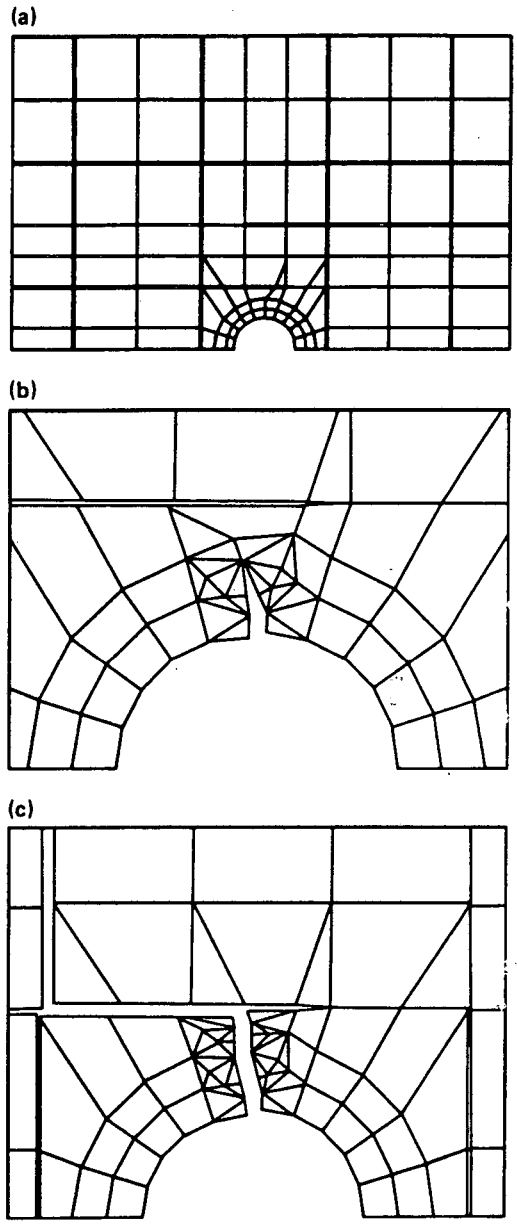

Figure 3. Successive stages in a typical FEFFLAP analysis of a realistic field condition. (a) The heavy lines around the borehole represent joints; the two discontinuous joints are points of possible crack extension. (b) Fluid pressure initiates a crack that propagates toward the nearest joint. (c) The fracturing fluid opens up the joint system, promoting gas recovery.

SUMMARY

We have developed a state-of-the-art model to describe fluid-driven fracture propagation in naturally jointed gas-bearing rock formations. It is a finite element code, named FEFFLAP (Finite Element Fracture and Flow Analysis Program). The program is highly interactive, with extensive graphical displays of the fracture behavior. Many automatic features for input generation, zoning, and rezoning make the code particularly efficient. The fracture mechanics, solid mechanics, and fluid mechanics are fully coupled. Model verification has been performed against analytical solutions and physical experiments.

REFERENCES:

1. Heuze, F. E., (1985). "LLNL Unconventional Gas Program," Director's Annual Review of Energy and Resources Programs, Lawrence Livermore National Laboratory, UCIR-1562, January.

2. Ingraffea, A. R., Shaffer, R. J., and Heuze,F. E., (1985). "FEFFLAP: A Finite Element Program for Analysis of Fluid-Driven Fracture Propagation in Jointed Rock, Vol. 1: Theory and Programmer's Manual," Lawrence Livermore National Laboratory, UCID-20368, March.

3. Shaffer, R. J., Ingraffea, A. R., and Heuze, F. E., (1985). "FEFFLAP: A Finite Element Program for Analysis of Fluid-Driven Fracture Propagation in Jointed Rock, Vol. 2: User's Manual and Model Verification," UCID-20369, Lawrence Livermore National Laboratory, March.

4. Shaffer, R. J., Thorpe, R. K., Ingraffea, A. R., and Heuze, F. E., (1984). "Numerical and Physical Studies of Fluid-Driven Fracture Propagation in Jointed Rock," 25th Rock Mechanics Symposium, (SME, Littleton, CO), pp 117-126.

5. Ingraffea, A. R., Saouma, V., (1984). "Numerical Modeling of Discrete Crack Propagation in Reinforced and Plane Concrete," Application of Fracture Mechanics to Concrete Structures, G. C. Sih and A. DiTommaso, editors, Martinus Nijhoff Publishers.

6. Heuze, F. E., (1981). "JPLAXD: A Finite Element Program for Static, Plane and Axisymmetric Analysis of Structures in Jointed Rock," Lawrence Livermore National Laboratory, UCID-19047.

7. Noorishad, J., Witherspoon, P. A., and Brekke, T. L., (1971). "A Method for Coupled Stress and Flow Analysis of Fractured Rock Masses," Publ. No. 71-6, University of California, Berkeley, March.

8. Thorpe, R. K., Heuze F. E., and Shaffer, R. J., (1984). "An Experimental Study of Hydraulic Fracture-Interface Interaction," UCID-20114, Lawrence Livermore National Laboratory, Livermore, July.

Acknowledgments

This work was performed as part of the Unconventional Gas Program at Lawrence Livermore National Laboratory. Funding was obtained from the U.S. Department of Energy, through the Morgantown Energy Technology Center, under Contract W-7405-ENG-48.

SHEAR-FLOW COUPLING IN NON-PLANAR ROCK JOINTS

Axel Makurat and Nick Barton,
Dam, Rock and Avalanche Division
Norwegian Geotechnical Institute, Oslo, Norway.

ABSTRACT

Crystalline rock masses are regarded as a possible host rock for permanent nuclear waste disposal. Already during the excavation of the required shafts and tunnels the initial state of stress will be changed and cause a deformation of the rock mass and discontinuities. Under the lifetime of the nuclear repository joint apertures may change due to thermally induced stress variations during the heating and the cooling phase.

As the conductivity of a joint is very sensitive to its aperture, fluid flow from and towards a repository, as well as the potential transport times of radionuclides are highly dependent on the deformability of the joints.

Theoretical calculations of coupled flow in rock joints (Barton et al. 1984) predict an increase of conductivity of several orders of magnitude for the first few millimeters of shear displacement. Figure 1 shows the shear-dilation-conductivity coupling for two block sizes at two effective stress levels.

A coupled shear displacement-flow test (Makurat, 1985) showed good agreement with these model calculations. The test was run on a natural joint in granite, using a 150 mm diameter core sample. A specially designed biaxial cell allows maximum shear displacements of 5 mm, and effective confining pressures of up to 20 MPa (see Figure 2).

NGI

The first test showed an increase in flow rate of two orders of magnitude under a normal stress of 5 MPa after a shear displacement of only 1-2 mm (see Figure 3). Another test, which was conducted on a smoother foliation plane in schist showed a reduced conductivity during dilation. Repeated forward and reverse shearing had produced gouge which must have closed essential parts of the major flow paths.

Further tests on different types of joint samples are foregoing and the results will be presented.

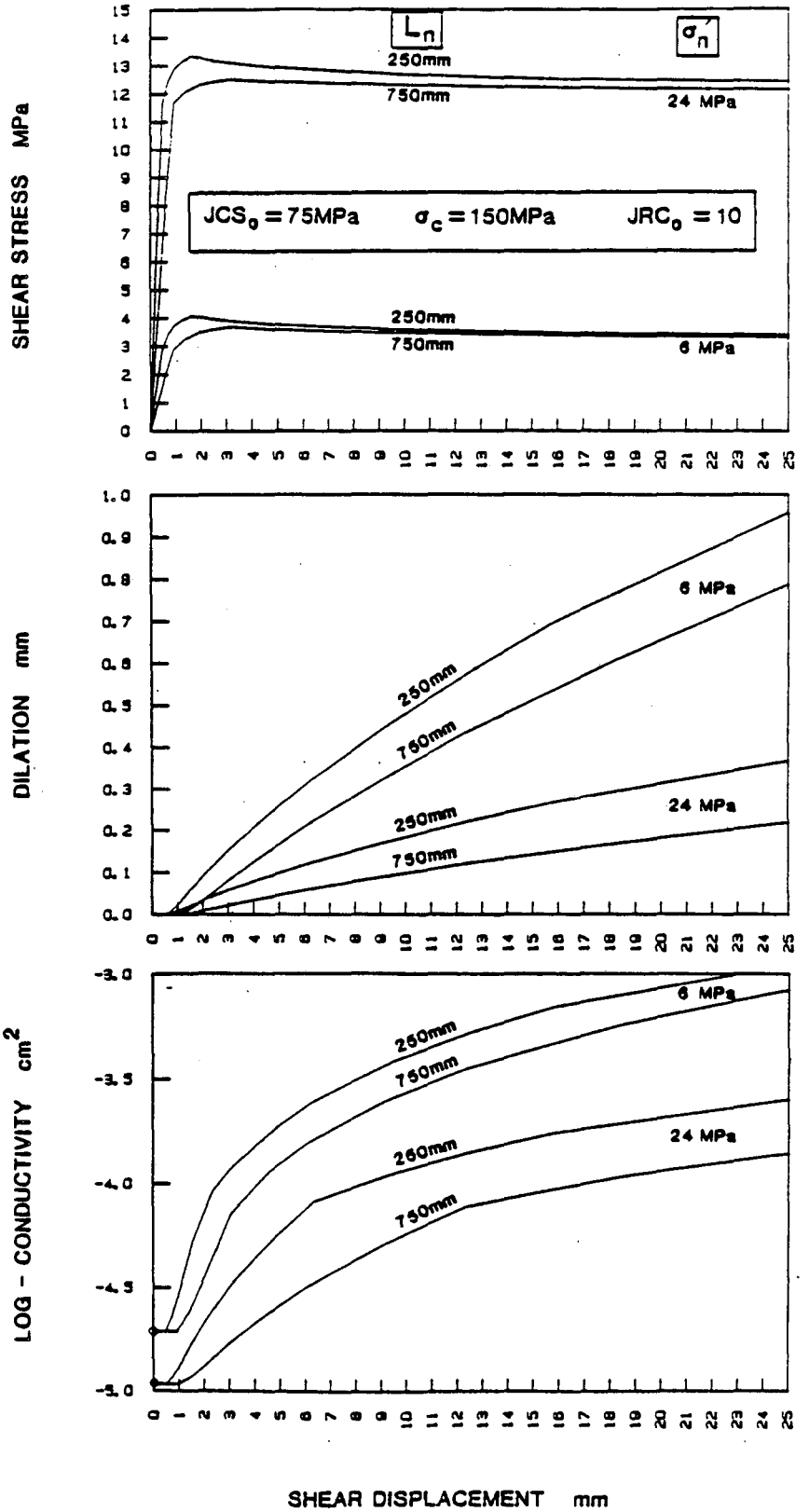

Figure 1. Shear, dilation and flow coupling for two block sizes at two different effective normal stress levels. After Barton et al. (1985).

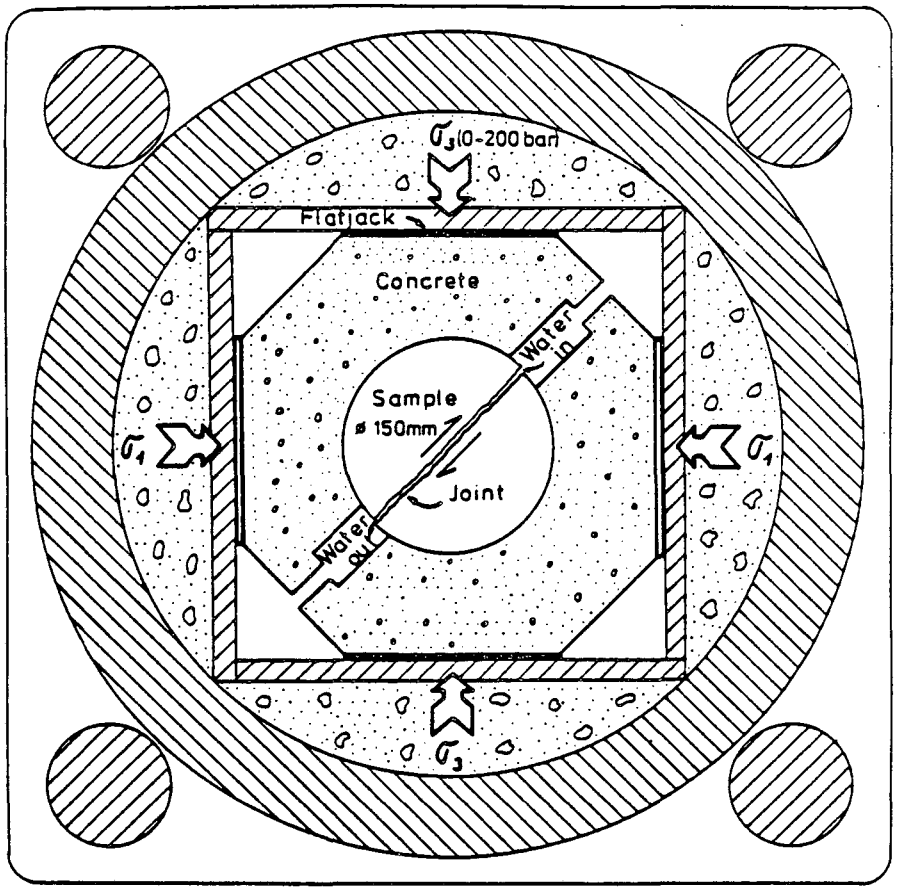

Figure 2. Cross section through the NGI biaxial press with joint sample mounted in test position.

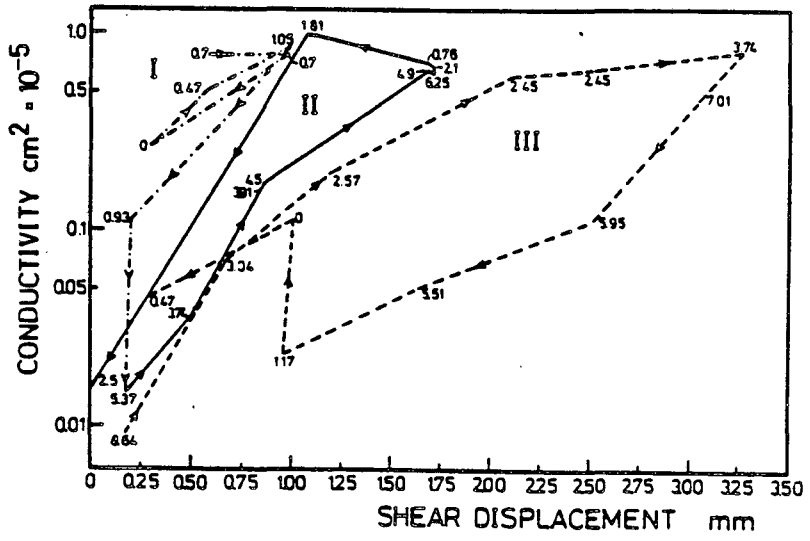

Figure 3. Coupled shear-flow tests performed on a joint in gneiss. Shear cycles I and II were in a forward direction, cycle III was in the reverse direction. The samll numbers appended to the curves indicate effective normal stress in MPa. After Makurat (1985).

STUDY OF THE INFLUENCE OF THERMOMECHANICAL AND HYDRAULIC COUPLING ON RADIONUCLIDE MIGRATION THROUGH MAJOR FRACTURES.

A. MILLARD - Ph. JAMET

M. DURIN - S. GOLDSTEIN.

CEA. DEMT. CEN-SACLAY 91191 GIF-SUR-YVETTE CEDEX.

In crystalline rock, performance of nuclear waste repository is strongly dependent upon fractures.

Indeed a major fracture will lead to a different behaviour of rock mass under thermal loading and thus to different values of stresses and displacements. Major fractures being preferential ways for ground water flow and thus radionuclide migration, the study of their hydraulic properties versus time with respect to thermal loading is the coupled process studied in this paper.

Calculations performed using CEA SEMT Finite Elements System are divided in three steps :

- thermal calculation in axisymetrical geometry.
- mechanical calculation in a vertical plane crossing the waste.
- hydraulics and migration calculations in the plane of the fracture.

For the thermomechanical calculations, the fracture is represented by special "joint-elements", which have only compression and shear resistances. Their axial strain is assumed to be negligible. The material behaviour is depicted by a COULOMB yield criterion and a non associated flow rule, in the plastic regime, giving way to dilatancy. In the elastic regime, the compression and shear behaviour are uncoupled.

The variation of the crack thickness versus time is used as imput into the thermohydraulical and migration computer code TRASH.

It is assumed that there is no back coupling of thermohydraulics on thermal and mechanical behaviour.

For the hydraulic calculation, we are looking at a simple case where the conection between fracture and rock is arbitrarily fixed. The flow rate crossing the fracture is prescribed by a regional head distribution independant of time. For the machanical calculation, average material properties derived from the litterature are used.

The comparaison between calculation with and without fracture show the influence of the fracture on the stess distribution and ground displacements. The hydraulical and migration calculations were made with and without taking into account thermal and thickness variation effects.

COUPLED HYDROLOGICAL-MECHANICAL EFFECTS DUE TO EXCAVATION OF UNDERGROUND OPENINGS IN UNSATURATED FRACTURED ROCKS

By
Parviz Montazer

U.S. Geological Survey
Denver, Colorado

One of the effects of excavating an underground opening in fractured rocks is a modification of the state of the stress in the rock mass in the vicinity of the opening. This effect causes changes in the geometry of the cross sections of the fracture planes, which in turn results in modification of the hydrologic properties of the fractures of the rock mass. The purpose of this paper is to demonstrate the significance of the orientation of the fractures and their stiffness on the extent of the modification of the hydrologic properties as a result of excavation of underground openings. A conceptual model is presented to illustrate the complexity of the coupled hydrological-mechanical phenomena in the unsaturated zone. This conceptual model is used to develop an investigative program to assess the extent of the effect at a proposed repository site for storing high-level nuclear wastes.

The effect of excavation of underground openings on permeability of a fractured rock mass that is saturated with a single component fluid may be considered as a sequentially or fully coupled phonomenon, depending on the initial state of the fluid potential field within the rock mass. The problem of analyzing such phenomena arises from the combination of the effects of the stress modification and the creation of new boundary conditions for the fluid potential field. If the effects of the new boundary conditions and the influence of the fluid potential field on the stress field can be ignored, the problem would become one of sequentially coupled phenomena and analysis would be greatly simplified. The concept of the sequentially coupled phenomena was used in a theoretical analysis of the effect of excavation on a single fracture intersecting an opening at various angles. The results were compared with actual field observations.

In fractured media containing multiphase fluids, interrelationships among permeabilities, fluid potentials, and saturations and their sensitivity to stress changes complicate the analysis. In this case, a fully coupled analytical technique would be needed to assess the significance of the effects of excavation on these hydrologic parameters. However, the validity of the numerical techniques in such an analysis would be questionable without a comprehensive field and laboratory experimental investigation. This phenomenon is planned to be investigated in conjunction with the site characterization effort that is underway at Yucca Mountain, Nevada. The research activity will involve evaluation of the coupled hydrologic-mechanical effects at various scales ranging in size from a single fracture sample to room scale. This investigation will provide an insight into the problem of coupled hydrological-mechanical effects in unsaturated fractured rocks.

DEVELOPMENT OF FINITE ELEMENT CODE FOR THE ANALYSIS OF COUPLED THERMO-HYDRO-MECHANICAL BEHAVIORS OF SATURATED-UNSATURATED MEDIUM

Yuzo Ohnishi, Hideaki Shibata and Akira Kobayashi

School of Civil Engineering
Kyoto University, Kyoto 606
Japan

ABSTRACT: A model is presented which describes fully coupled thermo-hydro-mechanical behavior of porous geologic medium. The mathematical formulation for the model utilizes the Biot theory for the consolidation and the energy balance equation. The medium is in the condition of saturated-unsaturated flow, then the free surfaces are taken into consideration in the model. The model, incorporated in a finite element numerical procedure, was implemented in a two-dimensional computer code. The code was developed under the assumptions that the medium is poro-elastic and in plane strain condition; water in the ground does not change its phase; heat is transfered by conductive and convective flow. Analytical solutions pertaining to conslidation theory for soils and rocks, thermo elasticity for solids and hydrothermal convection theory provided verification of stress and fluid flow couplings, respectively in the coupled model. Several types of problems are analysed. The one is a study of some of the effects of completely coupled thermo-hydro-mechanical behavior on the response of a saturated-unsaturated porous rock containing a buried heat source. Excavation of a underground opening which has radioactive wastes at elevated temperature is modeled and analysed. The results shows that the coupling phenomena can be estimated at some degree by the numerical procedure. The computer code has a powerful ability to know more about the complex nature.

1. INTRODUCTION

The problems of heat transfer in a geologic medium have recently become a subject of world attention in relation to geothermal energy production, usage of heat reservoir in an deep aquifer, underground disposal of radioactive waste, etc.. The geologic medium which is composed of a soil or rock mass is porous and is filled by water and/or air. It can be subjected to various types of loading conditions which are primarily due to a combination of three physical processes; mechanical, heat flow and fluid flow. The interdependence of each of these three phenomena leads to to a coupled behavior, whose mechanism is very complex and is not fully understood. However, recent progress in coupled analyses provides a basis for treating complex interdependence phenomena in a fully coupled manner.

The coupled analyses have been performed among pairs of the hydro-thermal-mechanical phenomena. For a long time, solution techniques for these coupled problems lagged behind analytical solutions and were restricted to simple geometries. Recent development of high speed digital computers advanced numerical techniques drastically in the field of coupled analyses. For coupled hydro-mechanical problems, Sandhu and Wilson applied a finite element method to the Biot's consolidation theory. Solution technique was extended to solve a consolidation problem which included an unsaturated region by using IFDM by Narasimhan and by using FEM by Ohnishi et al. For hydro-thermal problems, Lippmann et al introduced a model for mass and energy equation combined with the numerical solution of Terzaghi's consolidation equation. Witherspoon et al developed a model of two-phase steam-water saturated region. This model was extended to unsaturated region by Pruess et al. For thermo-mechanical problems, there are many solution techniques are known in the area of solid and structural mechanics.

In more recent studies, problems of coupled hydro-thermal-mechanical phenomena as shown in Fig.1 have been analysed. Bear and Carapcioglu derived the basic equations which described thermo-elastic behavior of a ground due to hot water injection into confined and leaky aquifers. Hart presented a model which described fully coupled thermal-mechanical-fluid flow behavior of highly nonlinear porous geologic systems and analysed the model by an explicit finite difference method. Noorishad et al applied a finite element method with joint elements to fully coupled phenomena for a saturated fractured porous rock mass.

This paper describes the developement of finite element code for the analysis of coupled thermal-hydraulic-mechanical behavior of saturated-unsaturated geologic medium. The mathematical formulation for the model utilizes the Biot's theory for the consolidation and the energy balance equation for the heat transfer. The geologic medium is in the condition of saturated-unsaturated flow, then the free surfaces are taken into consideration in the numerical model.

Several types of problems are analysed. the one is a study of some of the effects of completely coupled thermo-hydro-mechanical behavior on the response of a saturated-unsaturated porous medium which has an underground opening containing a heat source at an elevated temperature. Detailed discussion of validity and applicability of the developed code is given later.

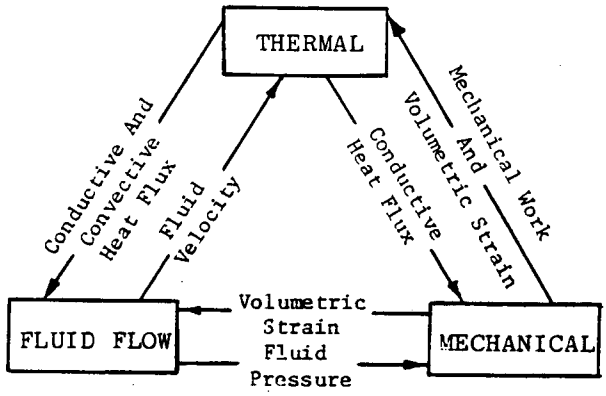

Figure 1. Interaction mechanisms in a fully coupled thermal-mechanical-fluid flow system (Hart, 1981)

2. GOVERNING EQUATIONS

The governing equations are derived under the following assumptions:

1) The medium is isotropic and poro-elastic.
2) Darcy's law is valid for flow of water in the saturated-unsaturated medium.
3) Energy flow occurs only in the solid and liquid phase. Energy transfer by gas, phase change between liquid and gas phases are not considered.
4) Heat transfers among three phases (solid, liquid and gas) are neglected.
5) Fourier's law holds for heat flux.
6) Water density varies depending upon the temperature and pressure of water.
7) The code is developed for the condition of plane strain.

Finite element formulation is performed by using the governing equations for coupled thermal-hydraulic-mechanical problems.

(1) Equilibrium Equation

Equation of motion for the medium in a static case is known as an equilibrium equation. It is written in total stress expression as follows:

$$\sigma_{ij,j} + \rho b_i = 0 \qquad (1)$$

where σij is the total stress, ρ is a density of the medium and bi is the body force.

Terzaghi defined the effective stress principle. Bishop and Blight extended his definition and proposed the following equation for a saturated-unsaturated medium.

$$\sigma_{ij} = \sigma'_{ij} + \chi\delta_{ij}\rho_f\psi \qquad (2)$$

where $\sigma'ij$ is the effective stress, δij is kronecker's delta, ρf is unit weight of water, ψ is the pressure head.

The parameter χ is defined as follows:

$$\chi = \begin{cases} 1 & : \text{saturated zone} \\ \chi(Sr) & : \text{unsaturated zone} \end{cases} \qquad (3)$$

χ is a nonlinear function of Sr (degree of saturation). It is usually determined by laboratory experiments.

Validity of Eq(2) is not definite and still now is under debate. However, we assume that χ approximately equal Sr.

Putting Eq(1) into Eq(2), we obtain the equilibrium equation for the effective stress in the saturated-unsaturated geologic medium.

$$(\sigma'_{ij} + \chi\delta_{ij}\rho_f\psi)_{,j} + \rho b_i = 0 \qquad (4)$$

where $(\chi\delta ij\rho f\psi),j$ is the term which means that the change of pressure head influences on the equilibrium equations.

Temperature effect can be implemented in the constitutive law for a solid medium. For an isotropic linear elastic material, Duhamel-Neuman relationship can be used and the following constitutive law is obtained.

$$\sigma'_{ij} = C_{ijkl}\varepsilon_{kl} - (3\lambda + 2\mu)\,\alpha\delta_{ij}(T-T_o) \qquad (5)$$

where Cijkl is a elastic matrix, εkl is the strain tensor, T is temperature, λ and μ are Lame's constants and α is the expansivity coefficient. Subscript 0 means that the parameters are in reference state.

Infinitesimal strain-deformation relationship is:

$$\varepsilon_{kl} = \tfrac{1}{2}(u_{k,l} + u_{l,k}) \qquad (6)$$

where ui is deformation vector.

Substituting Eq(5) and (6) into Eq(4), we get the stress equilibrium equation which takes into account the effects of heat transfer and pore pressure change.

$$\{\tfrac{1}{2}C_{ijkl}(u_{k,l} + u_{l,k}) - \beta\delta_{ij}(T-T_o) + \chi\delta_{ij}\rho_f\psi\}_{,j} + \rho b_i = 0 \qquad (7)$$

where $\beta = (3\lambda+2\mu)\alpha$

$(-\beta\delta ij(T-T0)),j$ is the term which means that heat transfer influences on the equilibrium equation.

(2) Continuity Equation for Groundwater

Equation of continuity for groundwater in the saturated-unsaturated zone is derived from Richards theory as follows:

$$\frac{\partial(\rho_f\theta)}{\partial t} = -(\rho_f v_i)_{,i} \qquad (8)$$

where θ is volumetric water content, t is time and vi is velocity vector.

Equation of motion for groundwater is similar to Darcy's law. That is:

$$v_i = -k(\theta)h_{,i} \qquad (9)$$

$k(\theta)$ is permeability which is a function of θ and h is total head.

The total head can be expressed as the sum of pressure head(ψ) and elevation head (z).

$$h = \psi + z \qquad (10)$$

Volumetric water content is a function of degree of saturation Sr and expressed as follows:

$$\theta = n\,S_r \qquad (11)$$

Substituting Eqs(9)(10)(11) for Eq(8) we obtain the following equation.

$$\{\rho_f k(\theta)(\psi+z)_{,i}\}_{,i} = \frac{\partial}{\partial t}(\rho_f n S_r) \qquad (12)$$

Considering the compressibility and expansivity of water, water density can be expressed as follows:

$$\rho_f = \rho_{fo}[1-\beta_t(T-T_o)+\beta_p(P-P_o)] \qquad (13)$$

where P is pore pressure, $\rho f0$ is a reference

density at P=P0 and T=T0. βT, βP are expansivity and compressibility of water respectively. They are defined as:

$$\beta_t = -\frac{1}{\rho_f}\frac{\partial \rho_f}{\partial T}\Big|_{p=\text{constant}} \quad (14)$$

$$\beta_P = \frac{1}{\rho_f}\frac{\partial \rho_f}{\partial P}\Big|_{T=\text{constant}} \quad (15)$$

Eaton assumed that buoyancy could be neglected in an unsaturated zone. Adopting this assumption we set $\beta T=0$ in the unsaturated zone. Then, the right hand side of Eq(12) is changed to:

$$\frac{\partial}{\partial t}(\rho_f n S_r) = nSr\frac{\partial \rho_f}{\partial t} + \rho_f S_r \frac{\partial n}{\partial t} + \rho_f n \frac{\partial S_r}{\partial t} \quad (16)$$

The first term represents the density change of pore water. The second term means the change of skeleton of the porous medium. The third one means the change of water storage capacity.

Combination of the first term of Eq(16) and Eq(13) gives rise to:

$$nS_r \frac{\partial \rho_f}{\partial t} = \rho_{fo} nS_r(-\beta_T \frac{\partial T}{\partial t} + \beta_P \frac{\partial P}{\partial t}) \quad (17)$$

The pressure head ψ is related to pore pressure as follows:

$$\psi = \frac{P}{\rho_f g} \quad (18)$$

Taking into account Eq(10) and (18), Eq(17) can be modified to:

$$nS_r \frac{\partial \rho_f}{\partial t} = \rho_{fo} nS_r(-\beta_T \frac{\partial T}{\partial t} + \rho_f g \beta_P \frac{\partial h}{\partial t}) \quad (19)$$

where the first and second terms of the right hand side of Eq(19) means the density change of pore water due to temperature change and due to total head respectively.

Assuming the strain is infinitesimal, the second and third terms of the right hand side of Eq(16) are expressed as follows:

$$\rho_f S_r \frac{\partial n}{\partial t} \cong \rho_f S_r \frac{\partial u_{i,i}}{\partial t}$$

$$\rho_f n \frac{\partial S_r}{\partial t} \cong \rho_f \frac{\partial (nS_r)}{\partial t} = \rho_f \frac{\partial \theta}{\partial t} = \rho_f \frac{\partial \theta}{\partial \psi}\frac{\partial \psi}{\partial t} \quad (20)$$

Eq(12) is modified by using Eqs(19)and (20).

$$\{\rho_f k(0)(\psi + z)_{,i}\}_{,i} = -\rho_{fo} nS_r \beta_T \frac{\partial T}{\partial t}$$

$$+ \rho_{fo} nS_r \rho_f g \beta_P \frac{\partial h}{\partial t} + \rho_f S_r \frac{\partial u_{i,i}}{\partial t} + \rho_f C(\psi)\frac{\partial \psi}{\partial t} \quad (21)$$

where $C(\psi)$ is a specific water content and is defined as:

$$C(\psi) = \frac{\partial \theta}{\partial \psi} \quad (22)$$

Eq(21) is the equation of continuity for groundwater, which takes into account the compressibility of the ground and density change by heat transfer.

(3) Energy Conservation Law

In general the ground consists of the materials with three phases; solid, liquid and gas. It is not so easy to analyse the behavior of heat transfer since the thermal process is different in each phase. We assume in this paper that the pore in the porous medium is filled by the material in liquid phase. It means that the groundwater does not change its phase from liquid to gas or vise versa. Heat transfer in the gas phase is not considered.

With the above assumptions, we derive the energy conservation law without the effects of viscous dissipation for groundwater, based upon the one proposed by Bear et al. It takes into account the existence of unsaturated zone and is written by the following equation.

$$nS_r \rho_f C_{vf} \left(\frac{\partial T_f}{\partial t} + V_f \cdot \nabla T_f\right) =$$

$$-\nabla \cdot nS_r J_f - \left(\frac{\partial P}{\partial T_f}\right)_{\rho_f} nS_r T_f \cdot \nabla \cdot V_f \quad (23)$$

where Cv is specific heat, J is heat flux by conduction. Subscript f means "fluid". In Eq(23), the first term in the left hand side shows the time dependency of energy, the second term shows the energy change due to heat convection. The first term in the right hand side expresses the energy change by heat conduction and the second term shows the reversible energy change caused by the compression.

Similarly the energy conservation law for a solid is written as:

$$(1-n)\rho_s C_{vs}\left(\frac{\partial Ts}{\partial t} + v_s \cdot \nabla Ts\right) =$$

$$-\nabla \cdot (1-n) J_s - (1-n)\beta T_s \frac{\partial \varepsilon_s}{\partial t} \quad (24)$$

where the subscript s means "solid". In Eq(24), the second term in the right hand side expresses the reversible energy change caused by deformation.

Faust and Mercer's proposal is that the movement of water through porous media is sufficiently slow and the surface areas of all phases are sufficiently large that it is reasonable to assume that local thermal equilibrium among phases is achieved instantaneously. If this assumption is permited, the following equations are formed.

$$T = T_s = T_f \quad (25)$$

With Eq(25), Eqs(23) and (24) can be united as the energy conservation law at a temperature.

$$\{nS_r \rho_f C_{vf} + (1-n)\rho_s C_{vs}\}\frac{\partial T}{\partial t}$$

$$+ \{nS_r \rho_f C_{vf} V_f + (1-n)\rho_s C_{vs} V_s\} \cdot \nabla T$$

$$= -\nabla \cdot \{nS_r J_f + (1-n) J_s\} - nS_r T\left(\frac{\partial P}{\partial T}\right)_{\rho_f} \cdot \nabla \cdot V_f$$

$$- (1-n)\beta T \frac{\partial \varepsilon_s}{\partial t} \quad (26)$$

When it is assumed that Fourier's law is valid for heat flux, the following equations are formed.

$$J_f = -K_{Tf} \nabla T$$

$$J_s = -K_{Ts} \nabla T \quad (27)$$

where KT is a coefficient of heat conduction.

The term $(\partial P/\partial T)$ in Eq(26) can be modified by using Eqs(14) and (15) as follows.

$$\left(\frac{\partial P}{\partial t}\right)_{\rho_f} = \frac{\beta_T}{\beta_P}\Big|_{\rho_f=\text{constant}} \quad (28)$$

Neglecting the velocity of the solid, Eq(26) is rewritten with the help of Eqs(6), (9), (27) and

(28) in the following form.

$$(\rho C_v)_m \frac{\partial T}{\partial t} + nS_r\rho_f C_{vf} V_f \cdot \nabla T =$$
$$\nabla \cdot K_{Tm} \nabla T - nS_r T \frac{\beta_T}{\beta_p} k(\theta) h_{,ii}$$
$$- 1/2(1-n)\beta T \frac{\partial}{\partial t} (u_{i,j} + u_{j,i})\delta_{ij} \quad (29)$$

where $(\rho C_v)_m$, K_{Tm} are expressed as follows:

$$(\rho C_v)_m = nS_r\rho_f C_{vf} + (1-n)\rho_s C_{vs} \quad (30)$$

$$K_{Tm} = nS_r K_{Tf} + (1-n)K_{Ts} \quad (31)$$

Eq(29) is the energy conservation law in which the stress-deformation and groundwater flow are considered. The first term in the left hand side shows time dependency of energy and the second term shows the energy change due to heat convection. The first , second and third terms in the right hand side express the energy change due to heat conduction, pore pressure change and reversible energy change caused by solid deformation, respectively.

(4) Governing Equation

Eqs(7), (21) and (29) represent the governing equation for the coupled thermo-hydro-mechanical problems. It should be noticed that pore pressure distribution is not known when the hydraulic boundaries move. In that case it is rational to use the total head expression in which the reference point for the elevation head is the lowest in the domain. That is:

$$[\ 1/2C_{ijkl}(u_{k,l} + u_{l,k}) - \beta\delta_{ij}(T-T_o) + \lambda\delta_{ij}\rho_f h\ ]_{,j} + \bar{\rho}_s b_i = 0$$

$$\{\ \rho_f k(\theta) h_{,i}\ \}_{,i} - \rho_{fo} nS_r \rho_f g\beta_p \frac{\partial h}{\partial t} - \rho_s C(\psi) \frac{\partial h}{\partial t}$$
$$- \rho_f S_r \frac{\partial u_{i,i}}{\partial t} + \rho_{fo} nS_r \beta_T \frac{\partial T}{\partial t} = 0$$

$$(\rho C_v)_m \frac{\partial T}{\partial t} + nS_r\rho_f C_{vf} V_{fi} T_{,i} - K_{Tm} T_{,ii}$$
$$+ nS_r T \frac{\beta T}{\beta_p} k(\theta) h_{,ii}$$
$$+ 1/2(1-n)\beta T \frac{\partial}{\partial t} (u_{i,j} + u_{j,i})\delta_{ij} = 0 \quad (32)$$

where $\bar{\rho}_s = \rho - \chi\delta_{ij}\rho_f\delta_{ij}$.

It is necessary to set the following initial and boundary conditions to solve Eq(32).

Initial Conditions

$$u_i(\underset{\sim}{x},t) = u_i(\underset{\sim}{x},0)$$
$$h(\underset{\sim}{x},t) = h(\underset{\sim}{x},0)$$
$$T(\underset{\sim}{x},t) = T(\underset{\sim}{x},0) \quad (33)$$

Boundary Conditions

displacement; $u_i(\underset{\sim}{x},t) = \hat{u}_i(\underset{\sim}{x},0)$

traction ; $\sigma_{ij}(\underset{\sim}{x},t)n_j(\underset{\sim}{x}) = \hat{T}_i(\underset{\sim}{x},t)$

hydraulic ; $h(\underset{\sim}{x},t) = \hat{h}(\underset{\sim}{x},t)$

flow rate ; $k(\theta)h_{,i}\, n_i = -\hat{Q}(\underset{\sim}{x},t)$

temperature ; $T(\underset{\sim}{x},t) = \hat{T}(\underset{\sim}{x},t)$

heat flow ; $K_{Tm}T_{,i}n_i = -\hat{Q}_T(\underset{\sim}{x},t)$ (34)

where $\underset{\sim}{x}$ is position vector, nj is unit normal vector, $\hat{u}$ is known displacement, $\hat{h}$ is known head, $\hat{T}i$ is known surface traction, $\hat{Q}$ is prescribed flow rate and $\hat{Q}T$ is prescribed heat flow.

(5) Finite Element Formulation

Several methods are well known to formulate the finite element descritization, such as variational method and weighted residual method. We used here the Galerkin type formulation. Linear quadrilateral isoparametric elements for h, T and a quadratic quadrilateral element for ui are employed in the code. In order to integrate time derivatives, an accelerater was introduced and then any type of finite difference scheme can be applied.

3. NUMERICAL ANALYSES

In order to demonstrate the function of this code and the possible effects of coupled behavior on the response of a geologic system, some example problems are solved by this code. They are a one-dimensional consolidation problem of saturated soil, a seepage problem in a saturated-unsaturated porous media, a thermo-hydro coupled problem in a saturated media, and a thermo-hydro-mechanical coupled problem. The result of the consolidation analysis is compared with the Terzaghi's theoreti-

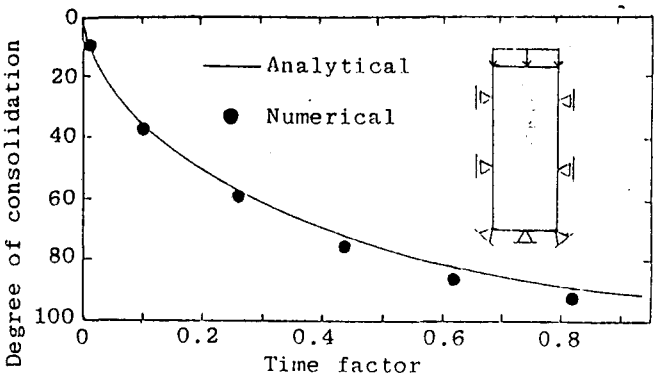

Figure 2. Comparison of numerical and analytical solution

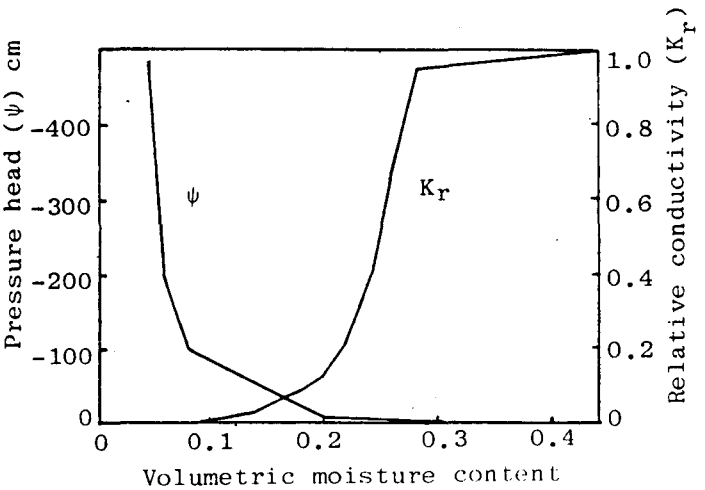

Figure 3. Unsaturated property

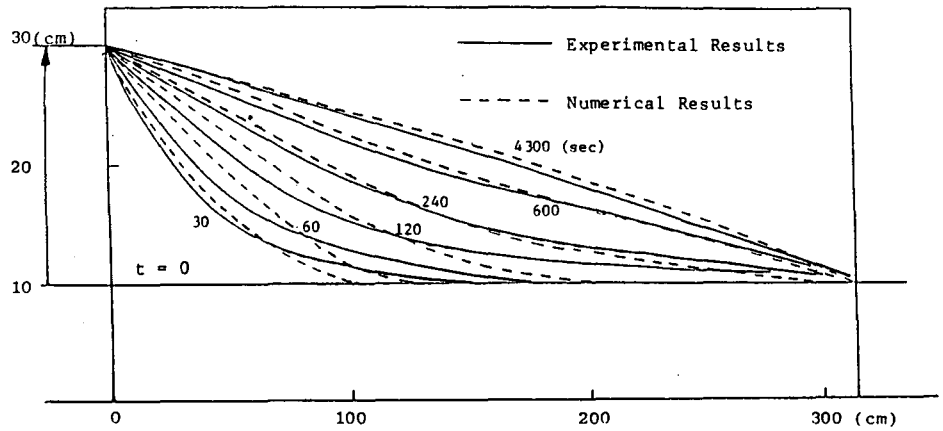

Figure 4. Comparison of numerical and experimental results (for wetting)

cal solution, and the results of the seepage analysis and the thermo-hydro-analysis are compared with the laboratory experimental results. The fourth problem, a thermo-hydro-mechanical coupled problem, is the most complicated one which this code can handle and is solved to show the versatility of the code.

3.1 Consolidation Analysis

For examination of the validity of this code to a coupled hydro-mechanical problem, a one-dimensional consolidation problem was solved by this code, and the numerical result was compared with the Terzaghi's solution. The comparison in the degree of consolidation is shown in Figure 2. It shows a very good agreement between the theory and the numerical calculation.

3.2 Seepage Analysis in Saturated-Unsaturated Porous Media

This code can also handle seepage problems in saturated-unsaturated media whether it has a free surface or not. Demonstranting the validity of this code to such a problem, a comaprison between the numerical solution by this code and the experimental result obtained by Akai et al on seepage in a sand box model is shown in Figure 4. In the experiment, the initial water level was kept at 10 cm from the inpermeable bottom, and the water level at the left side of the sand model was raised up to 30 cm from the bottom, instantly. The progress of the free surface observed in the experiment is well presented by the numerical solution by this code as shown in Figure 4. The unsaturated properties used in the analysis were empirically estimated as shown in Figure 3.

3.3 Coupled Thermal-Hydraulic Problem

Sato conducted a thermal-hydraulic test in a sand specimen which is shown in Figure 5. In the experiment, water at a temperature of 20 °C was supplied from the top of a saturated sand sample at 6.6 °C. The hydraulic gradient was kept constant between the top and bottom of the sample. The test was simulated by this code setting the same initial and boundary conditions. Figure 6 shows the comparison between the experimental and the numerical results in temperature distribution at different time stage. The numerical analysis using this code can represent the tendency of heat transfer with water flow observed in the Sato's experiment, though the transference of heat in the analysis is slower than that in the experiment.

3.4 Thermo-Hydro-Mechanical problem

The completely coupled thermo-hydro-mechanical problem in a saturated-unsaturated medium which has an underground opening containing a heat source at a temperature of 100°C was solved by the code. Since there is no underground research laboratory in Japan at this moment, this is only a conceptual

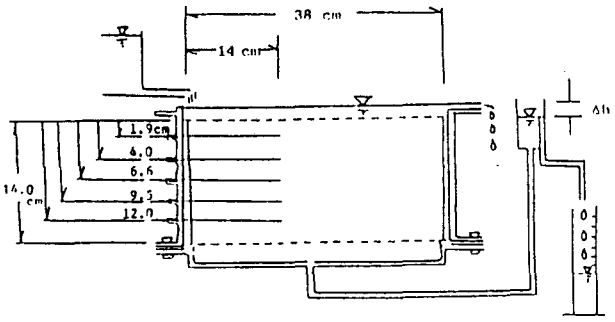

Figure 5. Testing Equipment

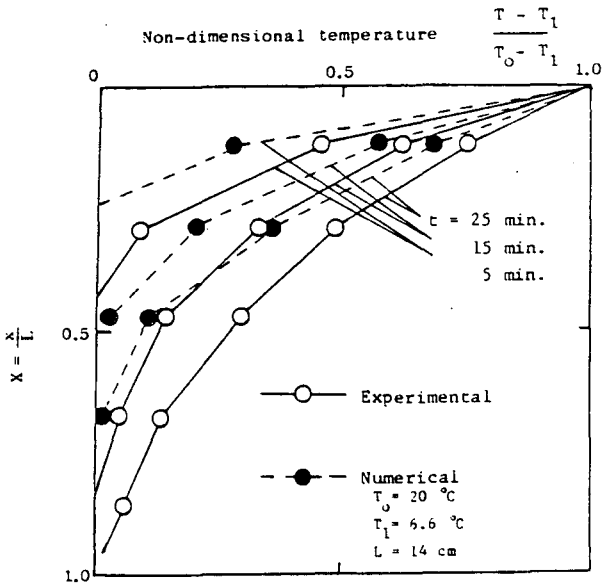

Figure 6. Comparison of numerical and experimental results

numerical model in relation to an underground nuclear waste disposal project. The properties used in this analysis is given in Table 1. Figure 7 shows the numerical results which are locations of free surfaces and distribution of temperature both at 2000000 sec. Interaction between water flow and temperature is apparently noticed. Figure 8 shows the displacement at the surface of the underground opening at different time stages. The opening settles down due to consolidation of the geologic medium. The effect of heat transfer is not shown clearly on deformation.

4. CONCLUSIONS

The work described in this paper provides a new technique for investigation of coupled thermo-hydro-mechanical behavior of the saturated-unsaturated porous medium. It is known that the coupling phenomena are very complex and it is not so easy to understand these phenomena theoretically or experimentally. The numerical tool such as presented in this paper is powerful and can be used for more detailed research on the behavior of geologic materials.

Unsaturated zone was considered for the first time in the fully coupled calculation. It was found that the unsaturated media has strong effects on the behavior of fluid flow and heat transfer. Research is required to know more the unsaturated properties of geologic media.

Nonlinear coupling effects should be investigated to increase the accuracy of calculation since we have been handling only some nonlinearities of parameters. There is a vast of nonlinearities left to be explored.

Table 1. Data Used for Analysis of Thermo-Hydro-Mechanical Problem

Property	Value
Prosity	2.5×10^{-1}
Young's modulus	1×10^{4} tf/m^2
Poisson's ratio	4.0×10^{-1}
Thermal expansion coef.	3.0×10^{-4}
Specific heat	8.37×10^{2} J/kg°C
Thermal conductivity	2.0 J/ms°C
Permeability	1.0×10^{-3}m/s

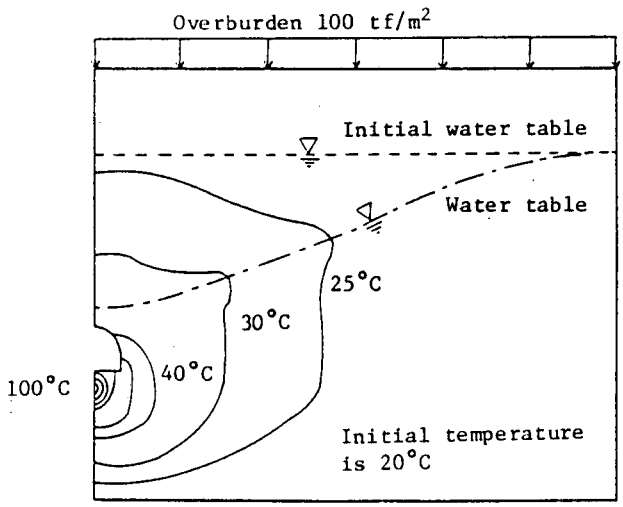

Figure 7. Water table and temperature distribution at 2×10^{6}sec.

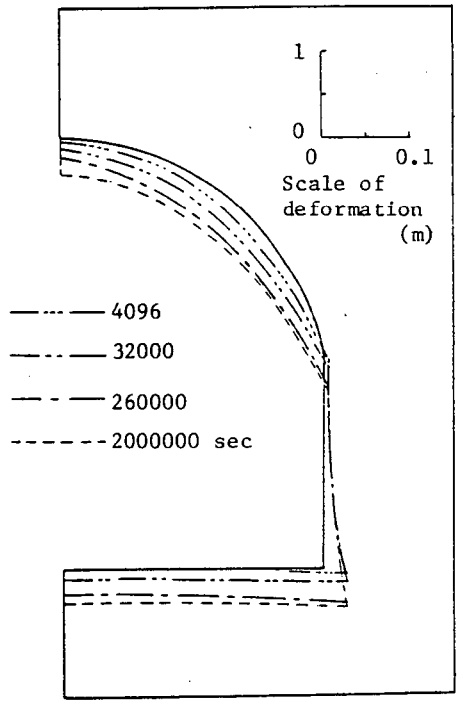

Figure 8. Deformation of the undergroud opening

REFERENCES

Akai, K.,and Uno, T. (1966),"Study on The Quasi-One-Dimensional, Non-Steady Seepage Flow through Soil", Transactims of The JSCE, No.125 pp.14-22

Bear, J.,and Corapcioglu, M.Y. (1981). "A Mathmatical Model for Consolidation in A Thermoelastic Aquifer Due to Hot Water Injection or Pomping",Water Resour. Res.,Vol.17, No.3, pp 723-736

Bishop, A.W.,and Blight, G.E. "Some Aspects of Effective Stress in Saturated and Pertly Saturated Soil", Giotechnique, Vol.13, No.3

Eaton, R.R. (1983). "A Numerical Method for Computing Flow through Pertially Saturated Porus Media", Numerical Methods in Thermal Problems, Vol.3, pp.911-920

Faust, C.R.,and Mercer, J.W. (1979). "Geothermal Reservior Simulation 1. Mathematical Models for Liquid- and Vapor- Dominated Hydrothermal Systems",Water Resour. Res., Vol.15, pp. 23-30

Hart, R.D. (1981). "A Fully Coupled Thermal-Mechanical-Fluid Flow Model for Nonlinear Geologic System", PH.D.Thesis, Univ. of Minesota

Nnarashimhan, Y.N. (1975)."A Unified Numerical Model for Saturated-Unsaturated Groundwater Flow" PH.D.Thesis, Univ. of California, Berkeley

Ohnishi, Y.,and Murakami, T. (1980)."Coupled Stress-Flow Finite Element Analysis of Soil", Transactims of the JSCE No.298, pp.87-96

Sandhu, R.S.,and Wilson, E.L. (1969)."Finite-Element Analysis of Seepage in Elastic Media", Journal of The Eng. Mech. Division, ASCE, Vol.95, No.EM-3, Proc. Paper 6615, pp.641-652

Sato, K. (1982)."Experimental Determination of Transfer Parameters of Heat Flow through Porous Media by means of A New-designed Apparatus in Laboratory", Transactims of The JSCE No.320, pp. 57-65

A FIELD STUDY OF COUPLED MECHANICAL-HYDROLOGICAL PROCESSES IN FRACTURED CRYSTALLINE ROCK

L.E. Sour *, A.M. Richardson*, S.M. Brown*, W.A. Hustrulid*, and E.N. Lindner**

* Colorado School of Mines
Mining Engineering Department
Golden, Colorado 80401

** Battelle Memorial Institute
Office of Crystalline Repository Development
505 King Avenue
Columbus, Ohio 43201

ABSTRACT

The Colorado School of Mines, with Battelle Memorial Institute, is conducting a series of experiments with a large in-situ cube of fractured metamorphic rock. The purpose is to better understand the response of jointed rock to loading.

One of the fundamental parameters which can be measured in any mechanical testing scheme is displacement. An instrumentation system was developed to measure absolute displacements in the interior of the block during loading, avoiding a suspected decoupled zone near the surface. The system is based on an array of inductive proximity transducers mounted on a rigid reference frame anchored to the mine roof above the block.

The stress field within the block during loading was monitored at several points with U.S.B.M. borehole deformation gages, using elastic moduli determined separately at each point with a borehole dilatometer. With these data the effect of fractures on the redistribution of stresses can be more readily understood.

Fracture conductivity affects the rate of contaminant migration from repositories to the biosphere. A multiple-zone borehole probe is being developed that simultaneously monitors fracture aperture and conductivity in each zone.

A two-dimensional computer model of the test block is being calibrated with the results of the deformation and stress studies. Successful application of such models would create confidence in using them to predict excavation performance.

INTRODUCTION

A series of mechanical and hydrological experiments is being conducted with an in-situ block of fractured crystalline rock at the Colorado School of Mines Experimental Mine. Sponsored by the Office of Crystalline Repository Development at Battelle Memorial Institute, this project includes studies of:

- applied stress vs. deformation of fractured rock
- applied stress vs. measured stress within fractured rock
- applied stress vs. fracture conductivity
- fracture deformation vs. fracture conductivity

The test block is a two-meter cube of Precambrian gneiss excavated by Terra Tek, Inc. in 1979 in the floor of a mine drift. After their program was completed (Hardin et al., 1981), C.S.M. began a second series of experiments with it. The block is defined by line-drilled slots which contain hydraulic flatjacks set up so that loading can be controlled separately in two directions. The top of the block is a free surface while the bottom is continuous with the surrounding rock mass.

Three major near-vertical fractures create four sub-blocks within the test block, and a strong foliation trend is evident that is also near-vertical. Figure 1 is a map of the surface geology with the instrument locations (boreholes) for the load-displacement and load-stress studies.

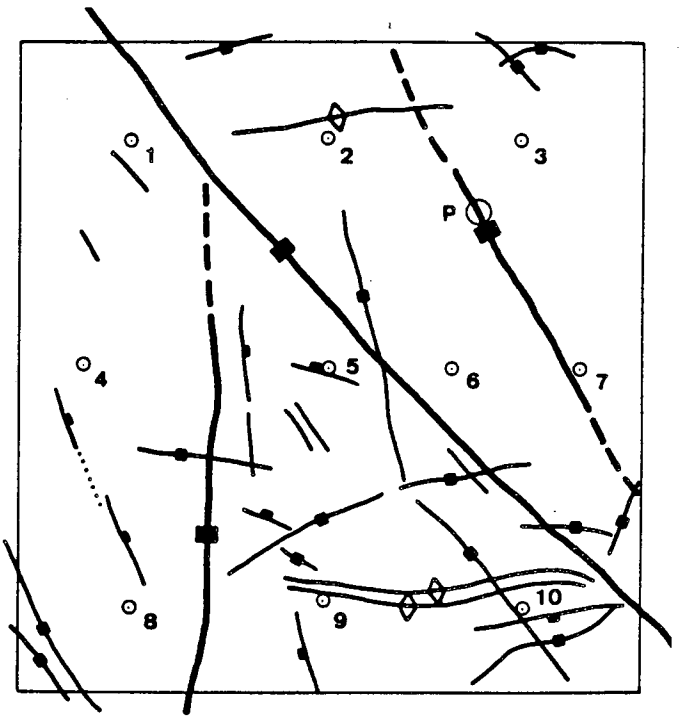

Figure 1. Surface geology, with major instrument locations. Test block is 2.0 m x 2.1 m x 2.0 m.

There are 24 open boreholes in the block, a legacy from the first experimental program. Ten of the EX size (3.2 cm diam.) were selected for the instrumentation. One of the NX size (7.6 cm diam.) holes is being used in the permeability program. These boreholes are all vertical.

Tests investigating the ambient temperature mechanical behavior of the block have been completed, and the hydrologic studies have progressed from prototype development to preliminary testing. A heated mechanical-hydrologic test series is in the planning stage.

MECHANICAL BEHAVIOR OF THE BLOCK

It was desired to measure the absolute displacements of points at various depths within the block during loading. With data of this type any form of relative displacements can be calculated, in addition to the advantage of knowing the movement vectors of discrete locations. An instrumentation system was designed for this purpose, and is described in detail by Richardson (1984) and Richardson et al. (1985a).

The test block was modeled with the boundary integral code BITEMJ developed by Janice Crotty of C.S.I.R.O. (Crotty, 1983). Although the program has the ability to model linear and nonlinear joint normal and shear behavior, the version used for the present effort was not designed to handle the interior joint intersection. Therefore, an elastic model was prepared using an equivalent modulus of 12 GPa and Poisson's ratio of 0.25 (Figure 2). A revised version of the code is currently available with increased capabilities for modeling fracture intersections within solids.

The elastic model was constrained by rollers on the left and bottom sides, with the lower left corner pinned. To compare the resulting displacements with the measured absolute vectors, the calculated values were re-referenced with respect to an arbitrarily fixed point at the center of the block. It is difficult to compare modeled and measured data in this fashion since, in this type of block test, there is no true fixed point. The block is constrained to some degree by the attached bottom, but a two-dimensional section can translate horizontally depending on the relative stiffnesses of the four flatjack reaction surfaces (the grout on the inner side, and the rock on the outside). It is therefore dangerous to draw conclusions from Figure 2, although it is likely that some of the deviation from elastic behavior exhibited in holes 6 and 7 results from normal closure of the two diagonal joints.

Figure 3 shows the displacement history of the monitored points within the block during equal biaxial compression to 5.17 MPa (750 psi) in 14 load steps. It is not a simple history; all stations move gradually but not immediately toward the block interior. The deformation mechanisms are quite complex, and include sub-block translations, rotations, and strains, which activate joint normal and shear deformations. When studying Figure 3 it should be remembered that the block geometry has been much simplified for this analysis (see Figure 1). A mathematical

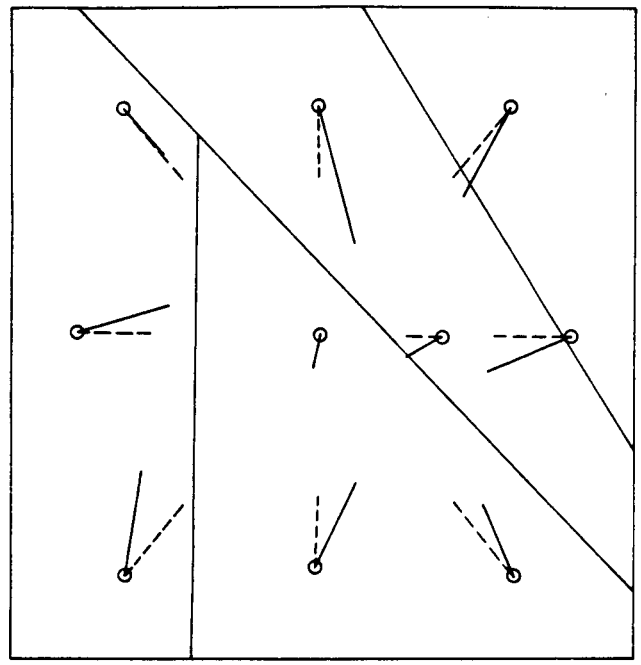

Figure 2. Measured (solid) and modeled (dashed) peak-load displacements from equal biaxial compression (5.17 MPa).

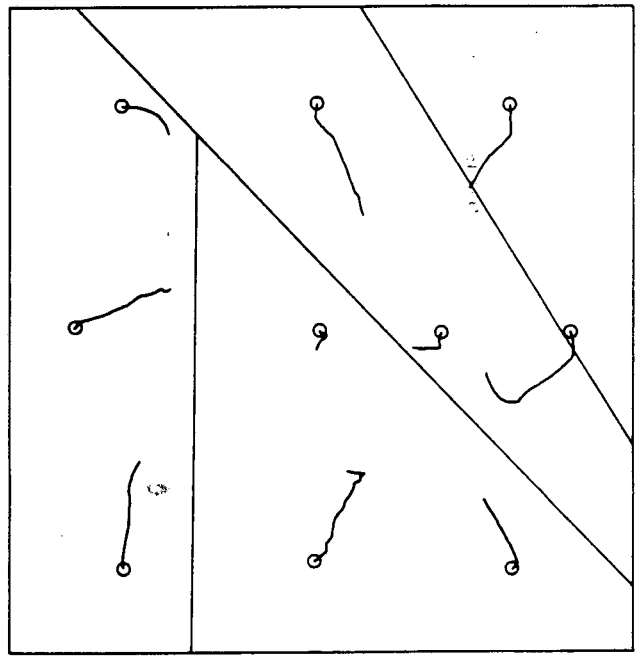

Figure 3. Displacement history during loading to 5.17 MPa (After Richardson, 1985b).

interpretation of this incremental behavior has been prepared by Richardson et al. (1985b) using the method developed by Shi and Goodman (1984). That analysis also concluded that the deformation mechanisms in a jointed block test are very difficult to interpret from even very careful displacement measurements, and that simple interpretations (such as rigid-body block motions and linear normal and shear strain) will explain some but not all of the total and incremental deformations. The total picture probably also

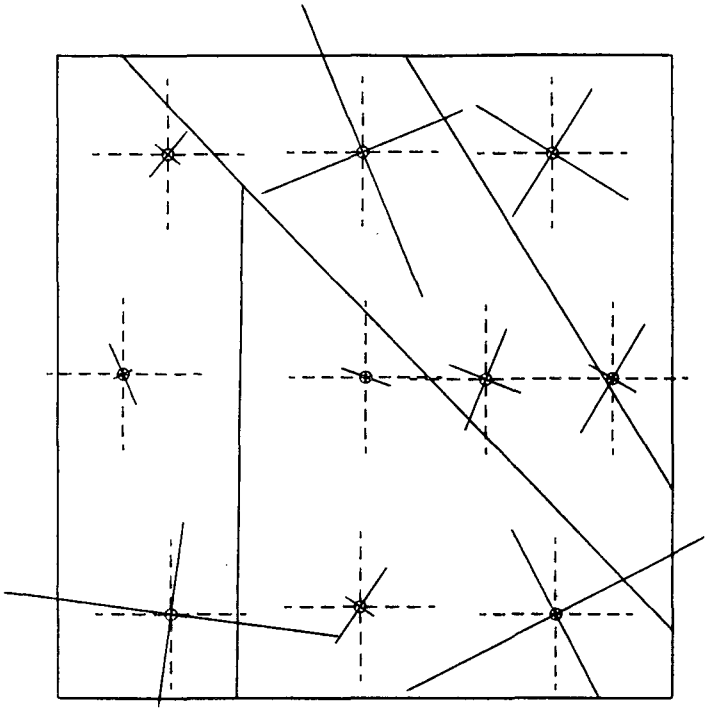

Figure 4. Measured (solid) and applied (dashed) peak-load stresses from equal biaxial compression.

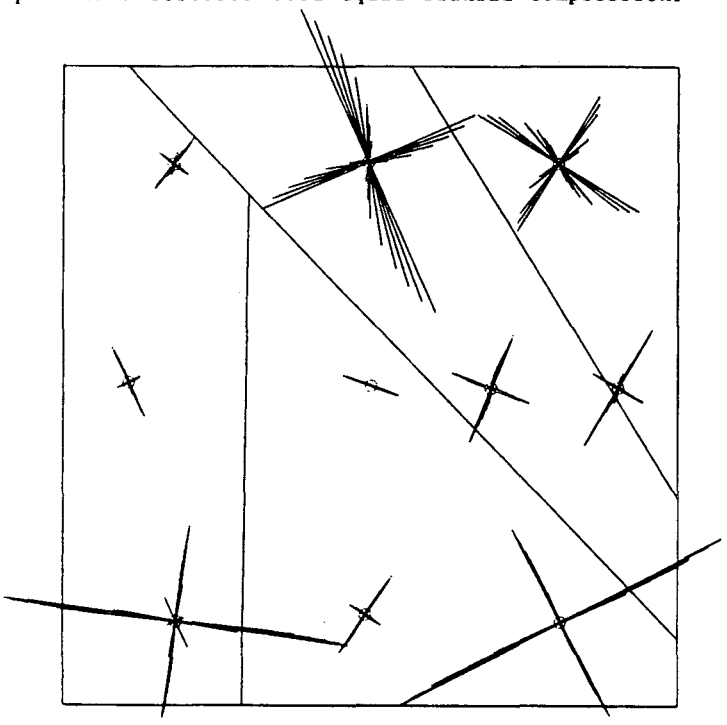

Figure 5. Stress history during loading.

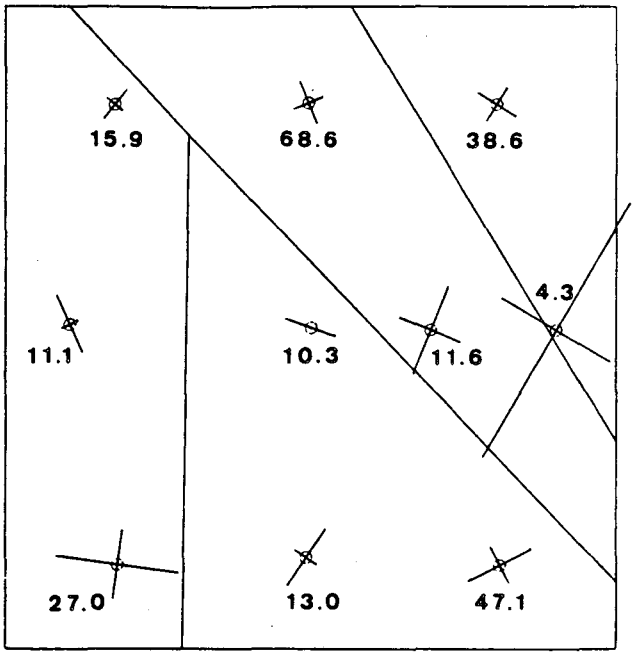

Figure 6. Major principal strains at peak load (5.17 MPa) during equal biaxial compression, and elastic moduli (GPa).

includes nonlinear normal and shear strain, bending, and anisotropic strain.

The principal horizontal stresses in the two upper right-hand sub-blocks are rotated counter-clockwise from the applied stress field (Figures 4 and 5). Progressive sinistral shear along the upper diagonal fracture would tend to produce this effect, and can also be seen in the incremental displacements (Figure 3), although here it is partially obscured by translation and rotation of the two upper sub-blocks as a unit (downward and clockwise, respectively). Closure of the upper diagonal fracture occurs only after the shear motion "sticks".

Measured stresses in the center of the block are lower than would be expected. This probably is due to a combination of structural and historical factors. The mid-strip has the highest density of surface-mapped major fracture planes, which would tend to isolate points there from applied loads. This appears particularly true for point 5, whose minor horizontal stress was tensile for the entire loading cycle. It is also somewhat the case for point 1, which is in very close proximity to three large boreholes drilled in the middle diagonal fracture. The joint has a relatively low normal stiffness, tending to decrease the elastic modulus as seen by the CSM Cell (Figure 6). In addition, the boreholes may create a stress "shadow" so that low strain is measured (Figure 6). Together these effects cause lower-than-expected stress magnitudes.

The boreholes in the mid-strip of the block (points 4 through 7) were sites for the heaters used by Terra Tek, Inc. during the previous testing program. These points also have the lowest elastic moduli, possibly a result of near-hole heat damage to the rock. The fact that the strains are not correspondingly large (point 7 is the exception to this; it is situated on the fracture) may be due to the fact that the modulus measurements probably are more sensitive to near-hole conditions than are deformations from externally-applied load, which involve a much larger volume of rock.

Note that the stresses in Figure 4 were calculated using the strains and elastic moduli from Figure 6. Data is from Brown (1985).

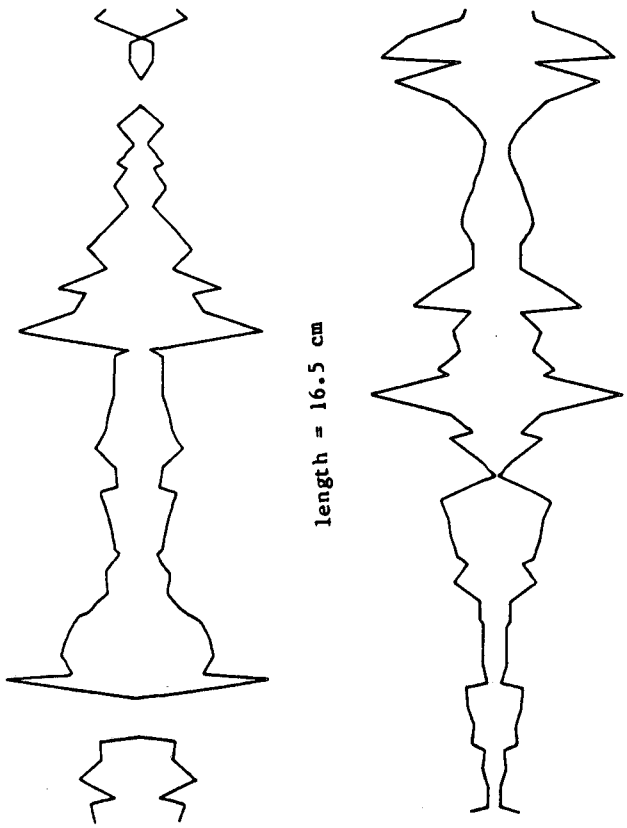

Figure 7. Example of aperture variation of both sides of test fracture (aperture exaggerated 30 times with respect to fracture length).

FRACTURE CONDUCTIVITY

The upper diagonal fracture was selected for the permeability study because it intersects a borehole longitudinally for almost 1.5 m, providing accessibility. Its aperture has been measured in detail for the entire length of its exposure in the borehole (Figure 7); it has a log-normal distribution with an average value of 0.5 mm (0.02 in.).

Figure 8 is a schematic drawing of part of the MZBP (multiple-zone borehole probe), which was built to monitor changes in borehole shape simultaneously with determination of permeability. Here, where the fracture plane is parallel to the borehole axis, change in borehole shape is largely equivalent to change in fracture aperture. Six inflatable packers in the probe create five separate test zones. FDG's (fracture deformation gages) designed from the U.S.B.M. borehole deformation gage except with four cantilever arms instead of six, are mounted on the ends of the packers in each zone. Each packer is coated with uncured rubber to obtain an impression of the fracture trace, allowing precise determination of the orientation of the fracture plane with respect to the FDG measurement axes (Figure 9). Thus displacement is monitored in areas of different initial aperture.

Concurrently with operation of the borehole probe, rock deformation and displacement will be monitored at six points surrounding the test

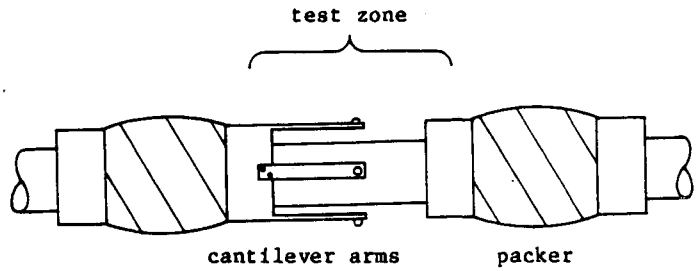

Figure 8. Schematic of part of multiple-zone borehole probe, showing packers and fracture deformation gage.

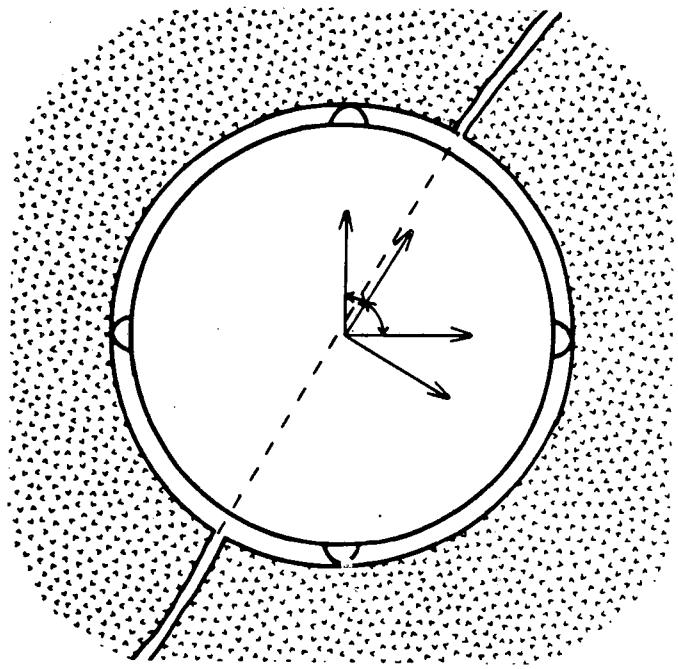

Figure 9. Cross-section of FDG in borehole, showing relationships between fracture plane and FDG measurement axes.

fracture (Figure 10). In each of these boreholes a U.S.B.M. borehole deformation gage will be placed slightly below the mid-depth of the permeability probe. Immediately above it will be set the anchor of a displacement-monitoring assembly. Information about the reaction of the rock mass in the immediate vicinity of the test borehole will supplement the in-hole data; for instance, test borehole deformation measured by the FDG's can be separated into components of fracture aperture change and rock deformation using the rock deformation measurements provided by the U.S.B.M. gages.

Preliminary tests have indicated that the fracture is highly conductive; consequently, steady-state injection tests will be performed. Nitrogen gas was chosen as the primary fluid.

The flowfield boundary conditions are not simple. The fracture plane can be thought of as a parallogram, with its upper side being the surface trace (venting to the mine drift), the lower side arbitrarily defined at the bottom of the block, and the vertical sides at the

intersections of the fracture with the flatjacks (venting to the atmosphere, more slowly, through the parting between the flatjacks and the enclosing grout). In addition, two additional boreholes intersect the fracture or branches of it; one of them is open to the atmosphere.

The multiple zones of the probe introduce further complications. Although cut off from each other in the borehole, they are not independent since the fracture connects them hydraulically. At equal injection pressures the zone of influence of each test zone is assumed to extend halfway to the next zone, and away from the borehole in a horizontal line. This simplification is complicated in reality by variations in fracture aperture, the sink effect of the mine drift, and the influence of the two boreholes mentioned above.

Figure 11 is a plot of the conductivity trend under low normal load determined from a preliminary series of experiments. In this instance, the middle zone was pressurized and the hydraulic gradient was calculated from pressures observed passively in the other zones. Lines connect points from individual loading cycles. The data are insufficient to do more than hint at trends, although permeability reduction with increased normal load on the fracture would be expected.

FUTURE WORK

The anisotropy of the rock in the test block is being studied in relation to stress field determination using the method synthesized by B. Amadei (1983).

The bulk of the permeability field experiments will be conducted this fall. The reaction of the fracture to both tension (provided by increasing the pressure in the packers) and compression (using the flatjack system) will be characterized. Equal biaxial loading of the test block, which closely approaches true normal loading of the fracture, will be conducted first in order that the effects of purely normal closure will be understood before undertaking the relatively more complex analysis of shear, which will be examined during a series of uniaxial loading cycles.

The data gained from monitoring the displacement and deformation of points elsewhere in the test block but bracketing the fracture will be compared to data collected from similar instrument configurations used during the previous load-displacement and load-stress phases of the research program. In this way a more comprehensive understanding of the interactions among stress, displacement, and conductivity in fractured crystalline rock can be obtained.

ACKNOWLEDGEMENTS

The authors thank the Colorado Engineering Experiment Station, Inc. and Rogers Arms and Machine Co. for their generosity and help with flow calibration and FDG construction.

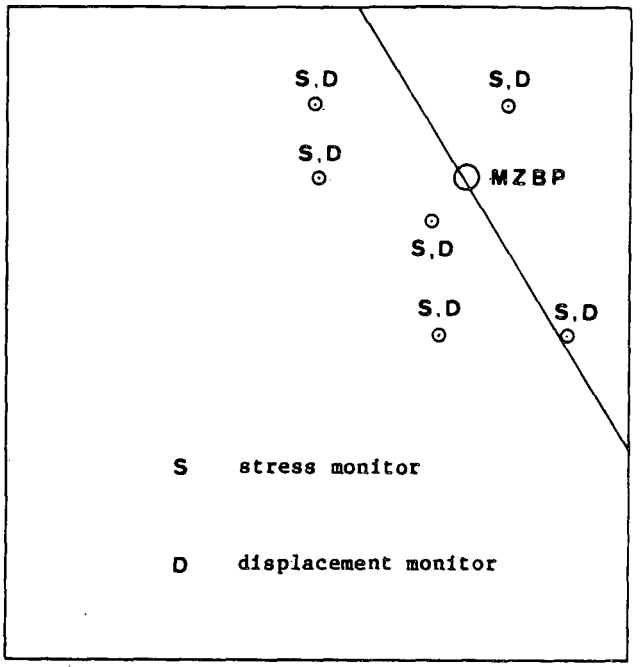

Figure 10. Instrument locations for permeability experiments.

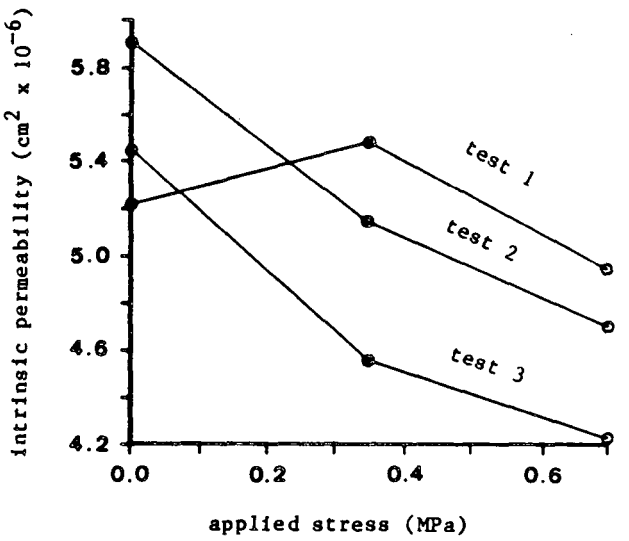

Figure 11. Preliminary permeability test results.

REFERENCES

Amadei, B., 1983. Rock Anisotropy and the Theory of Stress Measurements, Springer-Verlag, New York, 478 p.

Brown, S., Hustrulid, W., and Richardson, 1985. "A Study of the Validity of Stress Measurements in Jointed Crystalline Rock", Proceedings of the 26th U.S. Symposium on Rock Mechanics, Vol. 2, June 1985, Rapid City, South Dakota, p. 1247-1254.

Crotty, J., 1983. Program BITEMJ User's Manual, CSIRO Division of Applied Geomechanics, P.O.

Box 54, Mount Waverly, Victoria, Australia, 3149.

Hardin, E., Barton, N., Lingle, D., Board, M., and M. Voegele, 1981. "A Heated, Flatjack Test Series to Measure the Thermomechanical and Transport Properties of In Situ Rock Masses", prepared by Terra Tek Inc. for O.N.W.I., Battelle Memorial Institute, Columbus, Ohio.

Richardson, A., 1984. "In-Situ Load-Deformation Characterization of a Jointed Block of Crystalline Rock under Ambient Temperature Conditions", engineering test plan prepared by the Colorado School of Mines for O.C.R.D., Battelle Memorial Institute, Columbus, Ohio.

Richardson, A., 1985. "Ambient-Temperature Load-Deformation Response of the CSM/OCRD Test Block", technical report BMI/OCRD-4(18), prepared by the Colorado School of Mines for O.C.R.D., Battelle Memorial Institute, Columbus, Ohio.

Richardson, A., Hustrulid, W., Brown, S., and W. Ubbes, 1985a. "In-Situ Load-Deformation Characterization of the CSM/OCRD Jointed Block Test", Proceedings of the 26th U.S. Symposium on Rock Mechanics, Vol. 2, June 1985, Rapid City, South Dakota, p. 777-784.

Richardson, A., Hustrulid, W., Shi, G., and E. Lindner, 1985b. "A Mechanical Study of the Influence of Joints on Block Test Results", International Symposium on Fundamentals of Rock Joints, Sept. 1985, Bjorkliden, Lapland, Sweden.

Shi, G., and R. Goodman, 1984. "Discontinuous Deformation Analysis", Proceedings of the 25th U.S. Symposium on Rock Mechanics, June 1984, Evanston, Illinois, p. 269-277.

LAWRENCE BERKELEY LABORATORY
TECHNICAL INFORMATION DEPARTMENT
UNIVERSITY OF CALIFORNIA
BERKELEY, CALIFORNIA 94720

LAWRENCE BERKELEY LABORATORY
TECHNICAL INFORMATION DEPARTMENT
UNIVERSITY OF CALIFORNIA
BERKELEY, CALIFORNIA 94720